EDITOR'S PICK 2021: HIGHLIGHTS IN SIGNALING

EDITED BY: Ana Cuenda

PUBLISHED IN: Frontiers in Cell and Developmental Biology

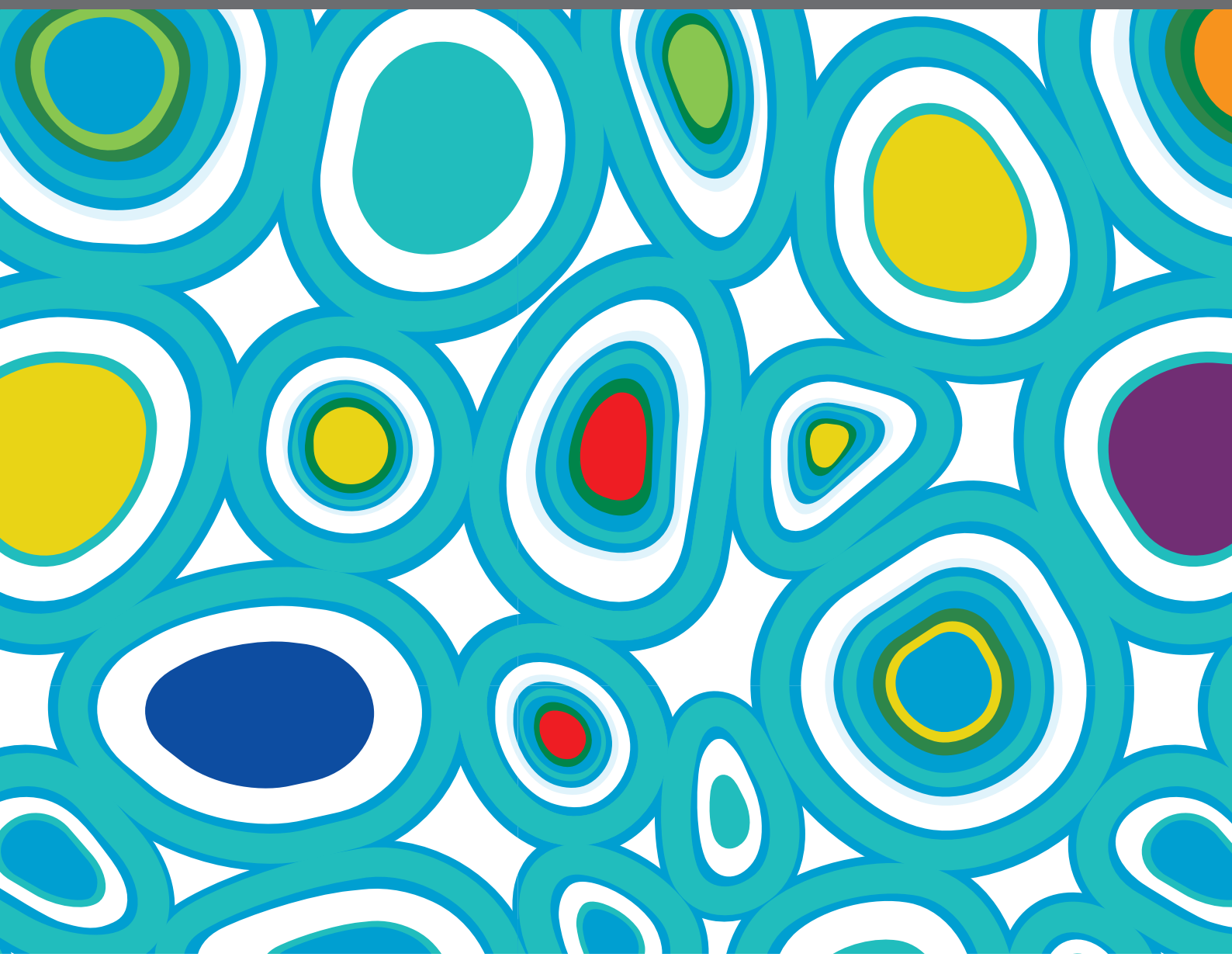

frontiers Research Topics

frontiers

ISSN 1664-8714
ISBN 978-2-88974-347-6
DOI 10.3389/978-2-88974-347-6

About Frontiers

Frontiers is more than just an open-access publisher of scholarly articles: it is a pioneering approach to the world of academia, radically improving the way scholarly research is managed. The grand vision of Frontiers is a world where all people have an equal opportunity to seek, share and generate knowledge. Frontiers provides immediate and permanent online open access to all its publications, but this alone is not enough to realize our grand goals.

Frontiers Journal Series

The Frontiers Journal Series is a multi-tier and interdisciplinary set of open-access, online journals, promising a paradigm shift from the current review, selection and dissemination processes in academic publishing. All Frontiers journals are driven by researchers for researchers; therefore, they constitute a service to the scholarly community. At the same time, the Frontiers Journal Series operates on a revolutionary invention, the tiered publishing system, initially addressing specific communities of scholars, and gradually climbing up to broader public understanding, thus serving the interests of the lay society, too.

Dedication to Quality

Each Frontiers article is a landmark of the highest quality, thanks to genuinely collaborative interactions between authors and review editors, who include some of the world's best academicians. Research must be certified by peers before entering a stream of knowledge that may eventually reach the public - and shape society; therefore, Frontiers only applies the most rigorous and unbiased reviews.
Frontiers revolutionizes research publishing by freely delivering the most outstanding research, evaluated with no bias from both the academic and social point of view. By applying the most advanced information technologies, Frontiers is catapulting scholarly publishing into a new generation.

What are Frontiers Research Topics?

Frontiers Research Topics are very popular trademarks of the Frontiers Journals Series: they are collections of at least ten articles, all centered on a particular subject. With their unique mix of varied contributions from Original Research to Review Articles, Frontiers Research Topics unify the most influential researchers, the latest key findings and historical advances in a hot research area! Find out more on how to host your own Frontiers Research Topic or contribute to one as an author by contacting the Frontiers Editorial Office: frontiersin.org/about/contact

EDITOR'S PICK 2021: HIGHLIGHTS IN SIGNALING

Topic Editor:
Ana Cuenda, Spanish National Research Council (CSIC), Spain

Citation: Cuenda, A., ed. (2022). Editor's Pick 2021: Highlights in Signaling. Lausanne: Frontiers Media SA. doi: 10.3389/978-2-88974-347-6

Table of Contents

frontiers in Cell and Developmental Biology

REVIEW
published: 04 March 2020
doi: 10.3389/fcell.2020.00110

Wnt5a Signaling in Gastric Cancer

*Pablo Astudillo**

Instituto de Ciencias Biomédicas, Facultad de Ciencias de la Salud, Universidad Autónoma de Chile, Santiago, Chile

Gastric cancer remains an important health challenge, accounting for a significant number of cancer-related deaths worldwide. Therefore, a deeper understanding of the molecular mechanisms involved in gastric cancer establishment and progression is highly desirable. The Wnt pathway plays a fundamental role in development, homeostasis, and disease, and abnormal Wnt signaling is commonly observed in several cancer types. Wnt5a, a ligand that activates the non-canonical branch of the Wnt pathway, can play a role as a tumor suppressor or by promoting cancer cell invasion and migration, although the molecular mechanisms explaining these roles have not been fully elucidated. Wnt5a is increased in gastric cancer samples; however, most gastric cancer cell lines seem to exhibit little expression of this ligand, thus raising the question about the source of this ligand *in vivo*. This review summarizes available research about Wnt5a expression and signaling in gastric cancer. In gastric cancer, Wnt5a promotes invasion and migration by modulating integrin adhesion turnover. Disheveled, a scaffolding protein with crucial roles in Wnt signaling, mediates the adhesion-related effects of Wnt5a in gastric cancer cells, and several studies provide growing support for a model whereby Disheveled-interacting proteins mediates Wnt5a signaling to modulate cytoskeleton dynamics. However, Wnt5a might induce other effects in gastric cancer cells, such as cell survival and induction of gene expression. On the other hand, the available evidence suggests that Wnt5a might be expressed by cells residing in the tumor microenvironment, where feedback mechanisms sustaining Wnt5a secretion and signaling might be established. This review analyzes the possible functions of Wnt5a in this pathological context and discusses potential links to mechanosensing and YAP/TAZ signaling.

Keywords: Wnt5a, gastric cancer, Disheveled, adhesion, invasion, metastasis, mechanosensing

OPEN ACCESS

Edited by:
Jose Maria Carvajal-Gonzalez, University of Extremadura, Spain

Reviewed by:
Hyun Woo Park, Yonsei University, South Korea
Mariaceleste Aragona, Université libre de Bruxelles, Belgium

***Correspondence:**
Pablo Astudillo
pablo.astudillo@uautonoma.cl

Specialty section:
This article was submitted to Signaling, a section of the journal Frontiers in Cell and Developmental Biology

Received: *13 December 2019*
Accepted: *10 February 2020*
Published: *04 March 2020*

Citation:
Astudillo P (2020) Wnt5a Signaling in Gastric Cancer. Front. Cell Dev. Biol. 8:110. doi: 10.3389/fcell.2020.00110

THE WNT SIGNALING PATHWAY: AN OVERVIEW

The Wnt signaling pathway plays fundamental roles in the context of embryonic development and adult homeostasis (Logan and Nusse, 2004). This pathway is composed of a family of secreted Wnt ligands, Frizzled receptors, and several co-receptors, intracellular adaptors, and scaffolding proteins, and is commonly divided into two main branches.

The "canonical" (or "Wnt/β-catenin") pathway depends on the stabilization of β-catenin, a protein that acts both at cell-cell interactions and as a transcription factor (Valenta et al., 2012). In the absence of a canonical Wnt signal, the pathway is inactivated through a negative feedback mechanism, which includes both a β-catenin destruction complex, which targets β-catenin for proteasomal degradation, and the plasma membrane ZNRF3/RNF43 ubiquitin ligases. Upon

binding of a canonical Wnt ligand to a Frizzled receptor, several processes are triggered at the plasma membrane. First, binding of canonical Wnt ligands to Frizzled receptors leads to phosphorylation of the cytoplasmic domain of LRP5/6. Subsequently, intracellular components translocate to the cytosolic side of the membrane, followed by clustering and formation of a so-called "signalosome" (Davidson et al., 2005; Zeng et al., 2005; Gammons and Bienz, 2018). These events lead to direct inhibition of GSK-3β and internalization of the signalosome (Taelman et al., 2010). Consequently, the β-catenin degradation complex becomes inhibited, and newly synthesized β-catenin can translocate to the nucleus to exert its transcriptional role (Li et al., 2012). Other ligands and proteins also modulate this pathway. For instance, secreted R-spondin proteins have been shown to cooperate with Wnt ligands, potentiating the activation of the pathway (Binnerts et al., 2007; Wei et al., 2007; Kim et al., 2008). R-spondins bind to LGR4/5/6 receptors (de Lau et al., 2011; Glinka et al., 2011), leading to inactivation of the ZNRF3/RNF43 ubiquitin ligases and stabilization of Frizzled receptors (Hao et al., 2012; Koo et al., 2012).

On the other hand, there is a collection of "non-canonical" Wnt signaling pathways, which are independent of β-catenin stabilization. These non-canonical pathways also depend on the activation of intracellular proteins, including small GTPases RhoA, Rac1, and Cdc42, which activate downstream effectors such as DAAM1 and JNK (Schlessinger et al., 2009). Non-canonical Wnt signaling also depends on Wnt ligands, Frizzled receptors, and several co-receptors. These co-receptors include Ror1/2, Strabismus, Ryk, Vangl2, and heparan sulfate proteoglycans, among others (Niehrs, 2012). Depending on the available receptors, co-receptors, and intracellular effectors, several non-canonical pathways are defined (Semenov et al., 2007). Among these, two well-studied pathways are the planar cell polarity (Wnt/PCP) pathway and the Wnt/Ca^{2+} pathway (Veeman et al., 2003). Collectively, non-canonical Wnt pathways modulate different aspects of cell behavior, such as cell shape and migration. Of note, Disheveled acts as an intracellular scaffolding protein with roles in both canonical and non-canonical pathways (reviewed by Sharma et al., 2018).

Wnt ligands are typically classified as either canonical or non-canonical. This classification initially stemmed from the ability of ligands to induce the transformation of the C57MG cell line (Shimizu et al., 1997; Chien et al., 2009). For instance, Wnt3a and Wnt1 are classified as canonical ligands, whereas and Wnt5a and Wnt11 are considered non-canonical ligands. However, the specific pathway activated by a given Wnt ligand depends on the cellular context, such as the availability of co-receptors. Wnt5a provides an outstanding example of this complexity: besides activating non-canonical Wnt signaling, Wnt5a can both activate and repress Wnt/β-catenin signaling (Torres et al., 1996; Mikels and Nusse, 2006).

Given the multiple processes that follow Wnt stimulation, signaling levels must be tightly regulated, and proper termination mechanisms must be employed to dampen the signal when needed. In the case of the Wnt/β-catenin pathway, it is well known that several Wnt target genes (such as *AXIN2*, *NAKED1*, and *DKK1*) encode for proteins that inhibit the pathway, thus providing a negative feedback loop (Filipovich et al., 2011). Therefore, activating mutations in Wnt components, as well as persistently high levels of Wnt ligands, might lead to the establishment of diseases, including cancer (Logan and Nusse, 2004).

In this regard, the relationship of the Wnt/β-catenin pathway with cancer is well established, and several excellent reviews have been published recently (Anastas and Moon, 2013; Zhan et al., 2017). However, the role of the non-canonical Wnt pathway and its ligands in cancer is somewhat less understood. Once again, a remarkable example is Wnt5a. This ligand has been detected in several cancer types, and it is believed to play an essential role in both cancer cell migration and tumor suppression. However, the precise molecular role of Wnt5a in cancer has not been fully clarified. Therefore, a deeper understanding of the biological functions of Wnt5a in cancer is highly desirable. Comprehensive overviews of Wnt5a in cancer have been published elsewhere (Kikuchi et al., 2012; Endo et al., 2015; Asem et al., 2016). Instead, this review focuses on the specific role of Wnt5a in gastric cancer.

WNT5A EXPRESSION IN GASTRIC CANCER

Gastric cancer (GC) is typically diagnosed at advanced stages, impairing adequate treatment, and leading to elevated mortality rates (Van Cutsem et al., 2016). An estimated more than 780,000 people died from stomach cancer in 2018, accounting for 8% of total cancer-related deaths, according to the Global Cancer Observatory (Bray et al., 2018). Therefore, GC remains a significant public health issue. Approximately 90% of all GC correspond to adenocarcinomas, which in turn can be classified as either diffuse- of intestinal-type, following the Lauren classification (Lauren, 1965; reviewed in Correa et al., 2009). Molecular criteria can be employed for identifying different subgroups, and some genetic abnormalities have been associated to GC (reviewed in detail by Van Cutsem et al., 2016; Ajani et al., 2017). Overall, gastric adenocarcinoma is conceived as a multistep process, sometimes referred to as the "Correa cascade" (Correa, 1988), where intestinal-type gastric cancers are preceded by a series of precancerous lesions, starting from gastritis, leading to metaplasia and invasive carcinoma (reviewed in Correa et al., 2009). In this regard, *Helicobacter pylori* infection constitutes a risk factor, due to induction of inflammation in the gastric mucosa. At later stages, epithelial gastric adenocarcinomas evolve to invasive lesions, where cancerous cells invade through the basement membrane and penetrate the mucosa and submucosa. Diffuse-type GC is also characterized by the stiffening of the gastric wall, or "linitis plastica" (Carneiro and Lauwers, 2012). Of note, other classifications for gastric adenocarcinomas have been proposed (reviewed in Carneiro and Lauwers, 2012), and other non-epithelial gastric tumors can also be identified (Wall and Nickl, 2019).

Given the role of Wnt signaling in cancer, several studies have analyzed the expression of Wnt ligands in GC. *WNT5A* mRNA was first shown to be up-regulated in samples of primary GC, compared to normal samples (Saitoh et al., 2002), and subsequent reports confirmed this observation. Kurayoshi

and coworkers used GC tissue samples and matched non-neoplastic mucosa, reporting a 2.6-fold up-regulation of *WNT5A* expression by using semi-quantitative PCR (Kurayoshi et al., 2006). More recently, a bioinformatic meta-analysis of published transcriptomic data reported *WNT5A* expression in 617 out of 1,034 GC patients (Nam et al., 2014). At the protein level, Kurayoshi and coworkers reported Wnt5a expression in 30% of GC cases analyzed by immunohistochemical staining (Kurayoshi et al., 2006).

At the histological level, *WNT5A* is up-regulated in both intestinal-type (IGC) and diffuse-type (DGC) GC samples (Kurayoshi et al., 2006). Another study, performed with samples from Australian and Chinese patients, also showed significant up-regulation of *WNT5A* in both IGC and DGC (Boussioutas et al., 2003). More recently, Li and coworkers detected significant up-regulation of *WNT5A* in 21 out of 36 GC samples analyzed (Li et al., 2014). Of note, six out of the 36 samples showed down-regulation of *WNT5A* in this study. Therefore, it remains possible that GC might proceed following not only Wnt5a overexpression but also impaired or unbalanced Wnt ligand availability. Finally, high Wnt5a expression is correlated with poor prognosis (Kurayoshi et al., 2006), and there is a statistically significant correlation between Wnt5a expression and several clinical parameters, such as lymph node metastasis and tumor depth (Nam et al., 2017).

Collectively, these reports indicate that Wnt5a is highly abundant in GC, and likely plays a role in GC establishment and progression. However, the precise source of Wnt5a is unclear. While most reports cited previously employed GC samples for mRNA expression analysis or histological staining, the analysis of GC cell lines shows mixed results. Several GC cell lines have been used and characterized for *in vitro* studies. Although most of these cell lines share the same ethnicity, they differ in origin and histological type, in their expression profile for growth factors and cell cycle regulators, and their profile for common oncogenes (Yokozaki, 2000). Although genetic alterations for β-catenin and APC have not been reported in some of these cell lines, mutations in these genes have been described in AGS, MKN-28, and MKN-74 cells (Ikenoue et al., 2002; Ebert et al., 2003).

The expression of Wnt5a in GC cell lines is variable. For instance, Saitoh et al. (2002) reported undetectable levels of *WNT5A* in MNK-7 cells and low levels in MKN-45 cells; in contrast, Kurayoshi et al. (2006) reported an opposite expression profile. Both studies report undetectable levels of *WNT5A* in several GC cell lines, such as TMK-1, MKN-28, MKN-74, and KATO-III. On the other hand, Kanzawa and coworkers also observed Wnt5a protein expression in several GC cell lines, including MKN-7 cells (Kanzawa et al., 2013), while Zhao and coworkers analyzed Wnt5a expression in five GC cell lines, detecting it only in the MKN-45 cell line (Zhao et al., 2013). Miwa and coworkers also reported variable expression levels of *WNT5A* across a panel of GC cell lines (Miwa et al., 2017). Finally, Nam and coworkers observed variable Wnt5a protein expression in several GC cell lines, including the commonly used MKN-1, MKN-45, AGS, and NCI-N87 (Nam et al., 2014). Of note, the same report shows that Wnt3a, a prototypical canonical ligand, only has limited expression in a few GC cell lines.

Therefore, the evidence suggests that *WNT5A* might be poorly expressed in GC cell lines, thus raising the question about the source of this ligand in GC. One possibility is that Wnt5a might be expressed by cells residing in the tumor stroma. For instance, cancer-associated myofibroblasts (CAMs, also known as cancer-associated fibroblasts, or CAFs) from GC consistently displayed increased expression of Wnt5a, compared to adjacent tissue myofibroblasts (ATMs) (Wang et al., 2016). More recently, a study comparing the methylation and trimethylation (H3K23me3) patterns between CAFs and non-CAFs also identified *WNT5A* as a target for H3K23me3 predominantly in CAFs and corroborated that CAFs secreted more *WNT5A* than GC cell lines (Maeda et al., 2019). More importantly, this report showed that, in histological samples, *WNT5A* had higher expression in fibroblasts (which were identified by α-SMA staining), compared to cancer cells (Maeda et al., 2019).

Wnt5a might also be secreted by tumor-associated macrophages (TAMs), which are observed in GC and correlate with poor prognosis (Räihä and Puolakkainen, 2018). Macrophages secrete Wnt5a in response to LPS treatment and *H. pylori* infection (Zhao et al., 2013). In turn, Wnt5a might induce the recruitment of immune cells, sustaining an environment favorable for non-canonical Wnt signaling. One report showed that Wnt5a induces the expression of MCP-1 (monocyte chemotactic protein 1, also known as C-C Motif Chemokine Ligand 2, CCL2), a protein involved in macrophage recruitment (reviewed by Yoshimura, 2017), in two GC cell lines (BGC-803 and HGC-27) (Li et al., 2014). This report also showed that conditioned medium from Wnt5a-treated GC cells induced macrophage migration in Transwell assays, and this effect was lost after a neutralizing MCP-1 antibody was added to the medium, providing further support to a functional relationship between Wnt5a and MCP-1 in GC. In addition, *WNT5A* is correlated with *IL1B* and *CCL2* expression in GC tissues (Li et al., 2014). In this same line, it has been reported that Wnt5a is expressed by $Cxcr4^+$ intraepithelial gastric innate lymphoid cells (ILCs) located in the isthmus, where the authors describe the existence of $Mist1^+$ stem cells (Hayakawa et al., 2015). Wnt5a enhances the colony formation ability of these $Mist1^+$ cells and, more importantly, cancer progression is impaired when Wnt5a expression is eliminated in the ILCs in a transgenic mouse model that develops diffuse-type GC following E-Cadherin depletion (Hayakawa et al., 2015).

Alternatively, Wnt5a might be specifically expressed in response to certain signals, such as environmental conditions or the interaction with stromal cells. In the first case, *H. pylori* infection has been linked to Wnt5a expression since *H. pylori* eradication leads to lower Wnt5a levels (Matsuo et al., 2012). Li et al. (2014) also reported significant upregulation of *WNT5A* in samples from *H. pylori*-positive patients compared to *H. pylori*-negative cases. On the other hand, MKN-7 cells (which, as mentioned above, exhibit low to moderate expression of Wnt5a) co-cultured with bone marrow mesenchymal stem cells show increased levels of *WNT5A* (Nishimura et al., 2012).

In conclusion, the discrepancy between high Wnt5a expression in GC biopsies or tissue arrays and modest or

low expression observed in some GC cell lines can be explained by the presence of stromal cells or other inflammatory and environmental signals. Moreover, the evidence analyzed above suggests that GC cells have diverse sources of Wnt5a in the tumor microenvironment. In consequence, Wnt5a might be a suitable clinical target, at least in a subset of GC cases, fostering interest for studies addressing the molecular roles of Wnt5a in GC, which remain to be fully understood, as discussed below.

WNT5A IN GASTRIC CANCER: MOLECULAR MECHANISMS

The role of Wnt5a has been studied in several cancer types, providing valuable insights into the possible mechanisms by which Wnt5a might influence cancer cell behavior. Wnt5a can function either as a regulator of cell migration and invasion or as a tumor suppressor (for two extensive reviews, see Kikuchi et al., 2012; Endo et al., 2015), leading to the notion of complex and opposing roles of this ligand in cancer (Pukrop and Binder, 2008; McDonald and Silver, 2009). Regarding the role of Wnt5a specifically in GC, it must be noted that overexpression of Wnt5a during adulthood failed to induce tumor initiation (Bakker et al., 2012), thus suggesting that Wnt5a alone is not sufficient for gastric cancer establishment. In addition, induction of Wnt5a overexpression from E13.5 during mouse development affected the intestinal tract; however, the stomach was not reported to be altered (van Amerongen et al., 2012). On the other hand, the tumor suppressor role of Wnt5a is commonly associated with low expression of this ligand (McDonald and Silver, 2009). The high expression of Wnt5a in GC, the lack of tumor initiation after overexpression in mice, and the evidence that will be reviewed in this section, collectively suggest that the predominant function of Wnt5a in GC is the regulation of cell migration and invasion.

Cell adhesion to the extracellular matrix (ECM) depends on integrin receptors and a complex set of intracellular proteins, which collectively form integrin-adhesion complexes (IACs) (Horton et al., 2016). In turn, cell migration and mechanotransduction depend on proper modulation of integrins and IAC proteins; therefore, signals able to modulate IAC dynamics are likely to be involved in cell migration and invasion, particularly in the context of cancer (Hamidi and Ivaska, 2018). Wnt5a stimulates cell migration in GC cell lines, whereas Wnt5a knockdown suppresses cell migration and invasion in Matrigel (Kurayoshi et al., 2006). Importantly, the relative migration of GC cell lines correlated with their relative levels of *WNT5A*, while the effect of Wnt5a was reduced by the negative Wnt regulator sFRP2 and by an anti-Wnt5a antibody, thus confirming the specificity of Wnt5a. This report also showed that Wnt5a increased MKN-45 cell adhesion, suggesting the involvement of IACs. In agreement with this observation, the abrogation of Wnt5a expression decreased the rate of assembly and disassembly of GFP-paxillin positive adhesions in MKN-1 cells. Of note, Wnt5a induced FAK Tyr397 phosphorylation and Rac activation in an Src- and PKC-dependent manner (Kurayoshi et al., 2006).

By promoting IAC dynamics, Wnt5a might lead to enhanced cell invasion. Supporting this idea, the injection of GC cell lines (KKLS and TMK-1) with reduced Wnt5A expression has less metastatic activity *in vivo* (Yamamoto et al., 2009). Furthermore, the treatment of GC cells with a polyclonal Wnt5a antibody (pAb5a-5) decreased cell adhesion, migration, and invasion of GC cell lines *in vitro*, and reduced the metastatic activity of the GC cell line KKLS *in vivo* (Hanaki et al., 2012).

Mechanistically, the Wnt5a antibody blocked Wnt5a- and clathrin-dependent internalization of Frizzled-2 and Ror2 receptors (Hanaki et al., 2012). A subsequent report from this group corroborated these observations using a second antibody targeting Wnt5a (mAb5A16), which reduced endocytosis of Ror-2 and Frizzled-2 and decreased the metastatic activity of the GC cell line KKLS *in vivo* (Shojima et al., 2015). On the other hand, a recent report unveiled the involvement of Ryk, another non-canonical Wnt receptor, in GC (Fu et al., 2019). The authors showed that Ryk is expressed in GC cell lines and samples from GC patients, correlating with clinical parameters such as wall invasion and liver metastasis. In addition, Ryk was shown to be required for migration and invasion in scratch and transwell assays (Fu et al., 2019). Of note, Ryk interacts with Vangl2, another non-canonical Wnt receptor, and Ryk knockdown impaired cell attachment. Collectively, these results suggest that non-canonical Wnt receptors are required for Wnt5a to modulate GC cell migration and invasion.

In order to modulate cell adhesion, Wnt5a must be able to functionally interact with intracellular effectors. The scaffolding protein Disheveled (Dvl) is a crucial effector in signaling through both canonical and non-canonical Wnt pathways. Dvl is required for HeLa S3 cells to remodel their focal adhesions, while Dvl knockdown impaired FAK Tyr397 phosphorylation and adhesion to fibronectin and collagen (Matsumoto et al., 2010). Mechanistically, Dvl localized to the cell periphery upon stimulation with Wnt5a, forming a complex with Frizzled-2 and APC, and interacting with FAK (Matsumoto et al., 2010). More importantly, Wnt5a required the Dvl-APC interaction to promote adhesion dynamics. The authors proposed a model whereby Wnt5a, Frizzled-2, and Disheveled form a complex proximal to integrins, FAK, and Paxillin, promoting adhesion dynamics through microtubule stabilization (Matsumoto et al., 2010).

A crucial aspect of Wnt signaling is the ability of Dvl to interact with other proteins (Sharma et al., 2018). A Dvl-interacting protein that is involved in Wnt5a-mediated adhesion dynamics is Daple (*Dvl-associating protein with a high frequency of leucine residues*). Daple promotes the interaction between Dvl and the PKCλ isoform of aPKC (Ishida-Takagishi et al., 2012), thus linking Dvl with the induction of FAK Tyr397 phosphorylation by Wnt5a (Kurayoshi et al., 2006). Daple was required for Dvl and PKCλ localization at the leading edge in migrating cells, whereas the Dvl-Daple interaction was also shown to be required for Rac1 activation and modulation of cell migration by Wnt5a. However, the precise molecular mechanism was not completely elucidated in this report (Ishida-Takagishi et al., 2012). The authors proposed a model whereby Daple allows the formation of a Dvl-PKCλ complex at the leading edge of Wnt5a-induced migrating cells, thus promoting Rac activation and actin reorganization.

Although Ishida-Takagishi et al. (2012) mainly used Vero and HEK293T cells in their study, evidence from a subsequent report provided further support for a role of Daple in GC. Daple was shown to be highly expressed in GC tumors, correlating with pathological characteristics (depth of gastric wall invasion, frequency of lymph node metastasis, and clinical stage), Wnt5a/b expression, and metastasis in xenograft tumor assays (Ara et al., 2016). More importantly, Daple knockdown impaired Wnt5a-induced Rac1 and JNK activation, decreased laminin γ2 expression in MKN-45 cells and attenuated MKN-45 and KKLS cell invasion in Matrigel assays, as well as the metastatic potential of KKLS cells *in vivo* (Ara et al., 2016). In consequence, Daple is likely to play a significant role in Wnt5a signaling in GC.

Another example of a Dvl-interacting protein is given by the microtubule (MT)-associated proteins Map7/7D1. Map7/7D1 binds to Dvl and modulates MT remodeling in HeLa cells, whereas Map7/7D1 knockdown impaired MT plus-end cortical targeting and focal adhesion turnover. Furthermore, Map7/7D1 promotes the cortical targeting of Dvl in response to Wnt5a, providing further support to the role of Dvl in cell migration dynamics during Wnt5a signaling (Kikuchi et al., 2018). However, it must be stressed that the specific relevance of these findings for gastric cancer remains to be fully explored.

Two additional Dvl-interacting proteins that have been associated with GC are Dapper homologs 1 (DACT1) and 2 (DACT2). DACT1 interacts with Dvl and induces its degradation and antagonizes canonical Wnt signaling (Zhang et al., 2006). DACT1 is also required for non-canonical Wnt/PCP signaling (Wen et al., 2010). Of note, *DACT1* levels are abrogated in several GC cell lines by hypermethylation, whereas DACT1 protein abundance is reduced in GC tissues compared to adjacent non-tumor tissue (Wang et al., 2012). Relevantly, *DACT1* promoter methylation was correlated with tumor size and metastasis (Wang et al., 2012). On the other hand, *DACT2* is also methylated in several GC cell lines, while protein levels are lower in GC tissue relative to normal mucosa (Yu et al., 2014). Of note, restoring DACT2 expression abrogated migration and invasion of the GC cell line SGC-7901 and tumor growth in a xenograft assay (Yu et al., 2014). Although the precise relationship of DACT1/2 with Wnt5a signaling was not addressed in these reports, Wnt5a might also influence GC by modulating these proteins. It remains possible that fine-tuned levels of these proteins might be required for proper Wnt5a signaling, and either gain or loss of expression might lead to imbalances and abnormal signaling.

The involvement of Dvl in Wnt5a-mediated adhesion dynamics is highly significant since this protein is at the crossroads of the canonical and non-canonical Wnt signaling pathways. The proper role of Dvl likely differs across tissues, depending on the balance between canonical and non-canonical Wnt signals, the availability of specific receptors and co-receptors, and the expression of Dvl-interacting proteins. Nevertheless, lessons from studies about Disheveled and Wnt5a in GC might shed light on the mechanisms of Wnt signaling in other cancer types. On the other hand, considering the high number of Dvl-interacting proteins (reviewed in Sharma et al., 2018), there is still much to be learned from Dvl in GC.

In addition to Dvl-mediated mechanisms, Wnt5a might also promote other intracellular responses, such as the expression of secreted proteins. For instance, Wnt5a was shown to promote the expression of laminin γ2, a component of the basement membrane protein laminin-5 (Yamamoto et al., 2009). This effect of Wnt5a is exerted through an AP-1 responsive element found in the *LAMC2* promoter and requires JNK and PKC activation, as well as the Frizzled-2 receptor. Knockdown of *LAMC2* decreased the invasive activity of TMK-1 and MKN-1 cells (the two cell lines in the study where *WNT5A* abundance best correlated with that of *LAMC2*), whereas Wnt5a showed a tendency to correlate with laminin γ2 expression in scirrhous GC biopsies (Yamamoto et al., 2009). Further research showed that the treatment of GC cells with the pAb5a-5 antibody impaired laminin γ2 expression and confirmed that TMK-1 cells with reduced expression of laminin γ2 exhibited decreased metastatic potential (Hanaki et al., 2012). Hence, Wnt5a might modulate the deposition of basement membrane proteins and other components of the extracellular matrix, including laminin γ2, thus promoting tumorigenesis by providing a favorable environment for GC progression and responsiveness to other secreted ligands. Finally, Wnt5a might also activate other signaling effectors. For instance, Liu and coworkers have reported that Wnt5a activates PI3K/Akt signaling in the GC cell line SGC-7901, resulting in GSK-3β phosphorylation and RhoA activation, promoting cell migration (Liu et al., 2013).

Other studies report additional effects that Wnt5a might play during GC establishment. For instance, Hayakawa et al. (2015) showed that Wnt5a activates RhoA in AGS and KATO-III cells, and increased the survival of E-Cadherin-deficient $Mist1^{+}$ cells *in vitro*, in a mechanism involving RhoA. Wnt5a might also influence the interaction between GC cells and their tumor microenvironment (TME), contributing to a supportive environment for migration and invasion of transformed GC cells. In agreement with this idea, it has been reported that Wnt5a/Ror2 signaling in MSCs promotes the secretion of CXCL16, which requires the CXCR6 receptor on MKN-45 cells to induce proliferation (Takiguchi et al., 2016). Of note, MSCs express high levels of *ROR2* and *WNT5A* compared to MKN-45 cells, and abrogation of *ROR2* or *WNT5A* expression in MSCs impaired MSC-induced MKN-45 cell proliferation. Therefore, this report adds a new role for Wnt5a, namely the induction of cell proliferation *via* the CXCR6/CXCL16 axis. Considering the known role of CXCL16 in other cancers (Deng et al., 2010), the abovementioned data highlight the multiple functions that might be exerted by Wnt5a during GC.

Inflammation is another context where Wnt5a likely plays an important role. As mentioned above, *WNT5A* correlates with *IL1B* and *CCL2* (MCP-1) expression in GC tissues (Li et al., 2014). Mechanistically, Wnt5a promotes IL-1β and TNF-α expression in the GC cell line BGC-803, as well as *CCL2* expression in GC cell lines and increased macrophage migration in Transwell assays (Li et al., 2014). The link between Wnt5a and inflammation is well established (reviewed by Pashirzad et al., 2017). Therefore, a feedback mechanism might ensue in the event of inflammation, whereby early inflammatory cues induce Wnt5a expression, which in turn leads to the secretion of inflammatory chemokines,

sustaining continued expression of these signals and leading to increased tumorigenicity.

Collectively, these reports suggest a model for Wnt5a signaling in GC. Kikuchi and coworkers (Kikuchi et al., 2012) have proposed a model where initial epithelial cell transformation might be followed by the acquisition of mesenchymal traits due to epithelial-to-mesenchymal transition, likely due to pathways other than the non-canonical Wnt branch. In turn, transformed cells gain the ability to invade the underlying stroma. In this scenario, Wnt5a likely plays a role in promoting IAC turnover and the invasive capacity of GC cells. It is possible to expand this model to include other roles of Wnt5a, such as those related to gene expression and inflammation. An expanded overview for Wnt5a signaling, including possible roles described in this review, is depicted in **Figure 1**.

This model strongly supports the notion of Wnt5a expression as a negative prognosis factor in GC. However, limited evidence also suggests the opposite role for Wnt5a. Zhang et al. (2015) reported that the downregulation of Wnt5a is required for EGF-induced EMT in the GC cell line SGC-7901. In this report, the knockdown of Wnt5a increased cell migration, while the overexpression of Wnt5a impaired EGF-induced N-Cadherin and Vimentin expression. Mechanistically, Arf6 was required for EGF-induced EMT and downregulation of Wnt5a expression. In turn, the downregulation of Wnt5a expression required nuclear translocation of phosphorylated ERK and its binding to the *WNT5A* promoter (Zhang et al., 2015). In a subsequent report, it was shown that knockdown of Arf6 abrogated cell migration and invasion in the SGC-7901 cell line *in vitro*, strengthening a negative role of Wnt5a in this cell line (Qiu et al., 2018). On the contrary, Wnt5a induces EMT in the MKN-7 GC cell line (Kanzawa et al., 2013).

How can these contradictory findings be reconciled? Several explanations might be proposed. Interestingly, when Zhang et al. (2015) analyzed the effect of Wnt5a on EMT marker expression, the overexpression of Wnt5a seemed to have little or no effect. Of note, the report shows that the SGC-7901 cell line already express high levels of Wnt5a. On the other hand, Kanzawa and coworkers used MKN-7 cells, which showed the lowest expression of Wnt5a among a panel of five GC cell lines (Kanzawa et al., 2013). Therefore, the observed discrepancy might be explained by the relative expression of Wnt5a among GC cell lines. The SGC-7901 cell line also differs from other GC cell lines in terms of the expression of Wnt-related proteins, such as soluble Frizzled receptor protein 1 (SFRP1; Zhao et al., 2007) and Wls (Zhang et al., 2017). Therefore, different GC cell lines may exhibit different responses to Wnt proteins, depending on specific Wnt signaling contexts.

Finally, it remains possible that the role of Wnt5a in restricting EMT might be a specific feature of the SGC-7901 cell line. Zheng and colleagues did not corroborate their findings in other GC cell lines; meanwhile, several reports have shown the promotion of cell invasion by Wnt5a in many GC cell lines, as described in this review. Furthermore, Zheng and colleagues failed to assess the effects of EGF treatments on cell invasion in the context of Wnt5a, and most experiments were limited to morphological changes and EMT marker expression. Another interesting possibility is that Wnt5a expression must be abolished in earlier phases of EMT, but its expression might be required in later stages to promote cell migration and invasion. Notwithstanding, these findings posit a caution note when selecting cell lines for studies addressing the role of Wnt ligands in GC.

In summary, it is possible to distinguish between Dvl-mediated mechanisms, leading to IAC turnover, and other mechanisms that might be less dependent on Dvl, which might lead to modulation of the GC environment. The former likely requires the known receptor machinery for Wnt5a, including Frizzled-2 and Ror2; however, the latter might require alternative or additional receptors and intracellular effectors. Wnt5a signaling mechanisms might be also classified as those modulating the cytoskeleton (**Figure 1**, left half) or those modulating other cellular processes (**Figure 1**, right half). In addition, these roles for Wnt5a might either overlap or represent a multi-step process, with Wnt5a playing different roles during EMT (**Figure 2**).

FUTURE DIRECTIONS AND CONCLUSION

Although the evidence discussed above strongly supports a role for Wnt5a in gastric cancer development, further research is still needed to fully understand the proper function of this Wnt ligand in the context of GC *in vivo*. Current evidence suggests that the mechanical properties of the extracellular matrix can play a significant role in cancer establishment and progression (reviewed by Pickup et al., 2014). Increased stiffness of the extracellular matrix (ECM) surrounding the tumor (usually referred to as the tumor microenvironment, or TME) can influence critical aspects of cancer cell biology, such as gene expression, invasion, and chemoresistance (Northey et al., 2017). Therefore, it would be interesting to study the mechanical changes in gastric tissues in GC and to elucidate the precise role of Wnt5a in conditions mimicking the elasticity of gastric tissue *in vivo*.

In this regard, gastric adenocarcinomas are usually preceded by mucosal atrophy and dysplasia (Lauwers and Srivastava, 2007). In addition, peritoneal dissemination (PD) is a common manifestation of GC and is associated with poor prognosis (Kanda and Kodera, 2016). PD is usually described as a multi-step process, where GC cells must invade the gastric wall and reach the peritoneal cavity (Kanda and Kodera, 2016). Carneiro and Lauwers have noted that stiffening of the gastric wall is observed during invasive adenocarcinoma, due to the desmoplasia following tumor cell invasion (Carneiro and Lauwers, 2012).

Stiffening of the ECM is partly explained by collagen cross-linking due to the action of lysyl oxidase (LOX) enzymes (Barker et al., 2012), and existing evidence suggests that LOX proteins might also play a role in GC progression (reviewed by Añazco et al., 2016). In line with these observations, Yashiro and coworkers reported that conditioned medium from the GC cell line OCUM-2MD3 induced peritoneal fibrosis in mice (Yashiro et al., 1996). Moreover, OCUM-2MD3 cells showed enhanced tumorigenicity in mice with peritoneal fibrosis induced

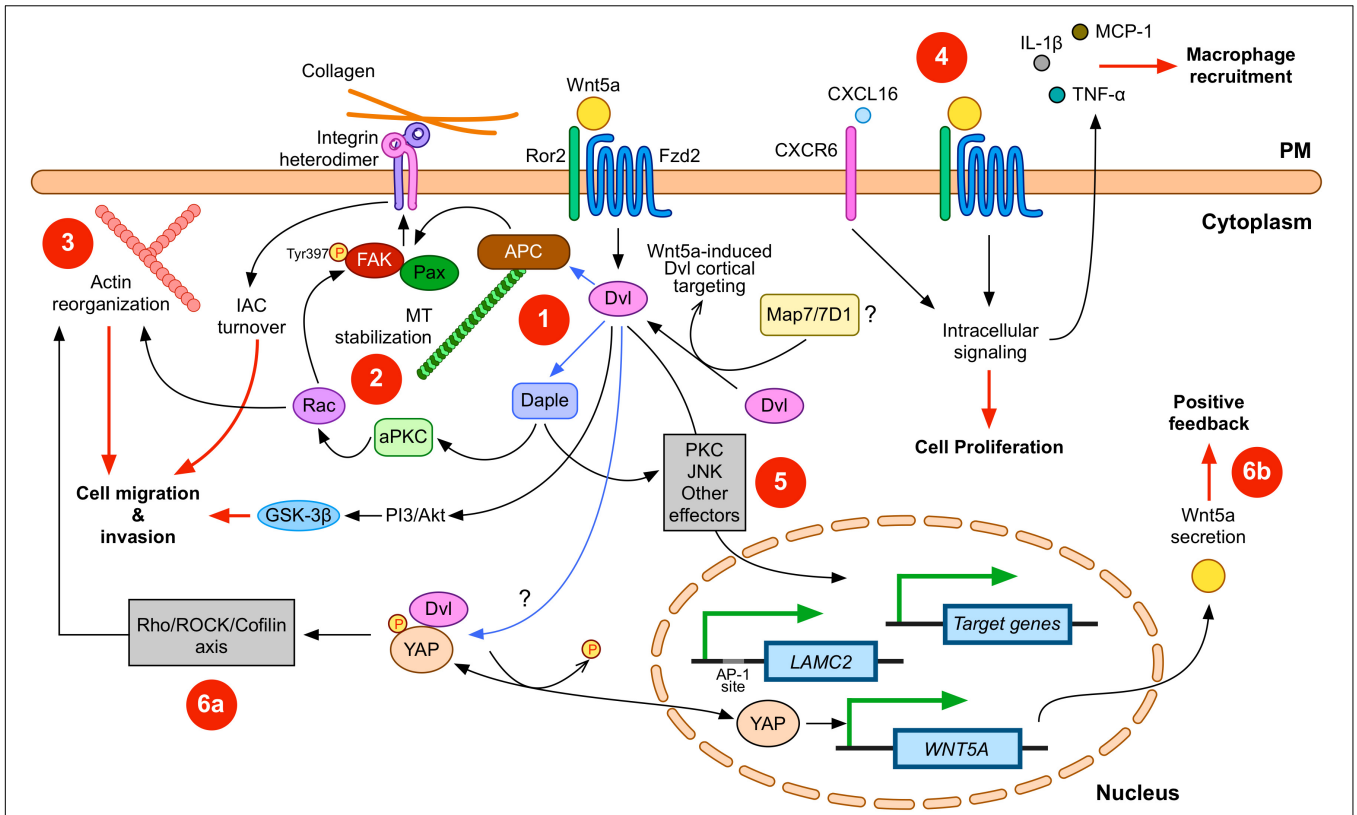

FIGURE 1 | Wnt5a signaling in gastric cancer (GC). Wnt5a interacts with APC and Daple to modulate integrin adhesion complex (IAC) turnover **(1)**; this effect involves microtubule (MT) stabilization **(2)** and actin reorganization **(3)**. Disheveled (Dvl) plays a central role in this signaling axis. In addition, other signals, such as CXCL16, can cooperate with Wnt5a. Wnt5a also correlates with increased expression of pro-inflammatory cytokines **(4)**. Wnt5a might also induce changes in gene expression **(5)**. For instance, *LAMC2* is induced by Wnt5a, but other target genes might be also modulated. Finally, other signaling pathways might cooperate with Wnt5a signaling. Considering the evidence summarized here, YAP/TAZ signaling likely interacts with Wnt5a. This interaction might include direct modulation of actin remodeling **(6a)**, as well as direct induction of *WNT5A* expression after YAP dephosphorylation **(6b)**. Please note that Wnt5a might activate only some of these routes during specific stages along GC cell transformation. In addition, Dvl might be involved in all the signaling routes induced by Wnt5a. Physical interactions between Dvl and other proteins are indicated with blue arrows; biological effects are indicated by red lines. PM, plasma membrane. Frizzled-2 (Fzd2) and Ror2 are shown; however, other co-receptors and Frizzled members are likely involved. Some players and interactions are omitted for simplicity. See the main text for more details.

by conditioned medium, illustrating the relevance of fibrosis for GC dissemination.

Therefore, mechanical cues from a more rigid TME might influence early steps of GC initiation, as well as later stages during PD and metastasis. The response of cancer cell lines from several tissues to mechanical cues has been characterized. However, GC cell lines have been somewhat less studied in this context, and most reports addressing the role of Wnt5a at the cellular level have been performed using GC cell lines cultured in a rigid context. Nevertheless, some limited evidence is available for GC cells. For instance, Jabbari et al. (2015) studied the behavior of AGS cells encapsulated in PEG diacrylate (PEGDA) gels, reporting that these cells are indeed sensitive to the stiffness of the PEGDA. Moreover, Branco da Cunha et al. (2016) reported a sensitivity of GC cell lines to RGD-coupled alginate hydrogels with varying stiffness. Consequently, GC cells might be responsive to mechanical cues from the TME, thus suggesting the need to evaluate such responses.

On the other hand, proteomic studies have addressed the composition of IACs in response to mechanical tension, highlighting changes in the variety and abundance of adhesome components (Humphries et al., 2009; Kuo et al., 2011; Schiller et al., 2011; Horton et al., 2015). In this regard, and given the role of Wnt5a in the turnover of focal adhesions in GC cells, it will be of interest to analyze the composition of IACs in GC cells cultured on substrates with elasticities like those found *in vivo* in gastric cancer, and to confirm if Wnt5a does modulate IAC turnover in these mechanical contexts. Tunable three-dimensional cultures of stomach organoids (McCracken et al., 2014) might be greatly useful to confirm this point.

In addition, recent evidence highlights the role of specific signaling pathways and proteins, such as YAP/TAZ (Dupont et al., 2011), in mediating cellular responses to mechanical cues. YAP and TAZ are especially interesting in this context since both proteins have been related to Wnt signaling. Initial studies focused on the role of YAP/TAZ in the context of β-catenin and Disheveled (Varelas et al., 2010; Azzolin et al., 2012, 2014; Imajo et al., 2012; Park et al., 2015). Studies have also related YAP and TAZ to cancer (reviewed by Moroishi et al., 2015; Zanconato et al., 2016), including in the gastrointestinal tract (for

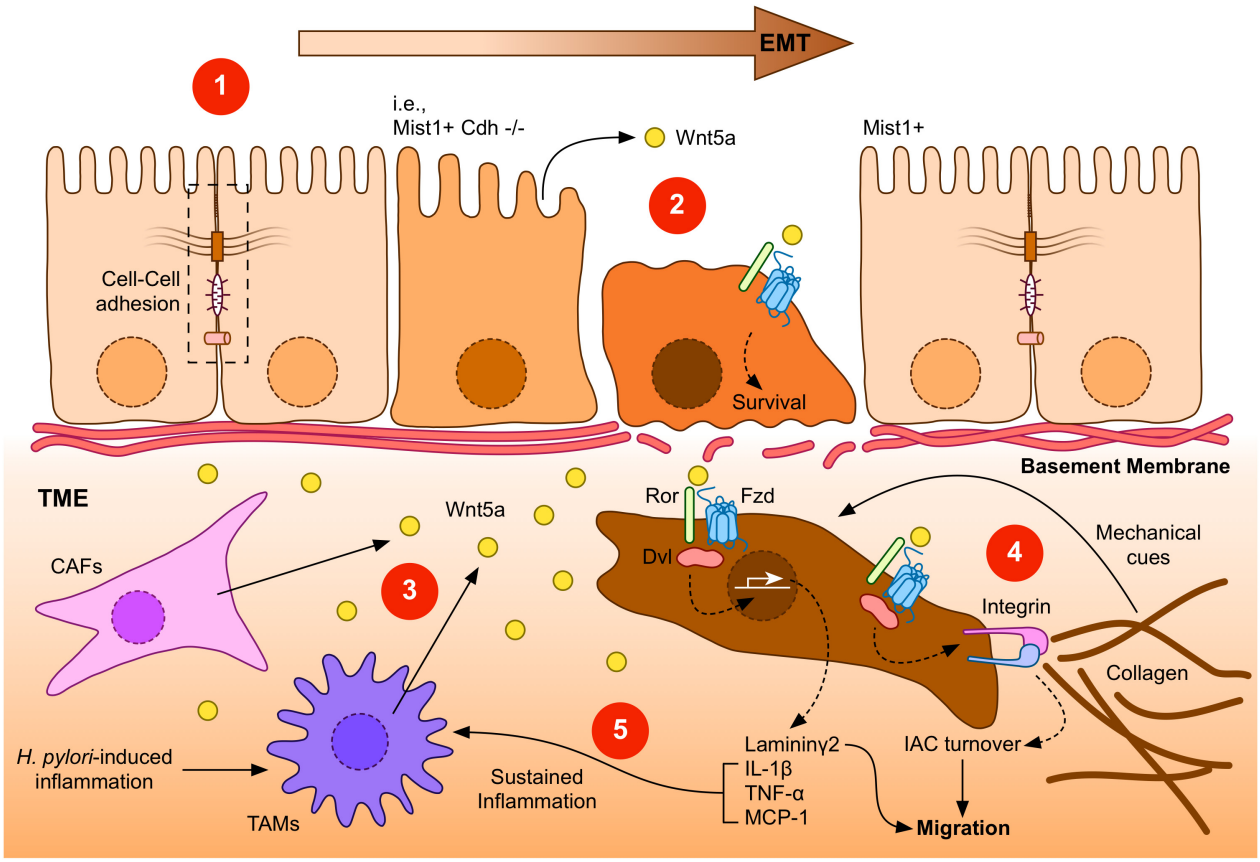

FIGURE 2 | A general overview of Wnt5a signaling during GC. **(1)** Gastric epithelial cells might undergo epithelial-to-mesenchymal transition (EMT) in response to specific signals, such as loss of E-Cadherin expression (indicated as Mist1+ Cdh–/–). Transformed cells lose their epithelial characteristics, such as cell-cell interactions (dashed box). **(2)** Low levels of Wnt5a might be expressed by gastric epithelial cells. This source of Wnt5a might induce cell survival. **(3)** After the breakage of the basement membrane, transformed gastric cancer cells might find additional sources of Wnt5a, particularly from cancer-associated fibroblasts (CAFs) or tumor-associated macrophages (TAMs). In turn, increased levels of Wnt5a might signal through Frizzled (Fzd) receptors and co-receptors, such as Ror1/2 (Ror), to induce gene expression, integrin adhesion turnover, and other biological effects. **(4)** Integrins bind collagen in the tumor microenvironment (TME), forming integrin adhesion complexes (IACs). Increased turnover of IACs induced by Dvl-dependent Wnt5a signaling might promote migration and invasion of GC cells. In addition, the tumor microenvironment might provide mechanical cues, such as extracellular matrix stiffening. **(5)** Laminin γ2, which is expressed after Wnt5a stimulation, might also cooperate to promote enhanced invasiveness. Wnt5a can also induce the expression of pro-inflammatory molecules, leading to a sustained inflammatory environment, further stimulating Wnt5a secretion. *Helicobacter pylori* infection can also contribute to this environment, by promoting Wnt5a secretion.

an updated review, see Li et al., 2019), although most articles focus on intestinal cancer (for instance, see Llado et al., 2015; Oudhoff et al., 2016; Diamantopoulou et al., 2017). However, a growing body of evidence indicates that YAP and TAZ also play a role in gastric cancer. YAP expression is commonly observed in GC samples and GC cell lines, and its expression and nuclear localization correlate with poor prognosis (Kang et al., 2011; Song et al., 2012; Zhang et al., 2012). Relevantly, YAP expression in the GC cell line MKN-28 modulates actin remodeling and promotes cell migration, while the loss of YAP induces cell stiffening and impaired migration (Qiao et al., 2017). Mechanistically, YAP directly modulates the expression of ARHGAP29, a Rho-GAP that suppresses the RhoA/LIMK/Cofilin axis. Therefore, YAP signaling via this axis results in the destabilization of actin, leading to increased cell migration (**Figure 1**). On the other hand, high expression of TAZ has also been detected in GC (Yue et al., 2014; Melucci et al., 2018; Wei et al., 2019). Interestingly, Melucci and coworkers evaluated the association between YAP/TAZ expression and localization, and the presence of mutations in three Wnt pathway genes (*CTNNB1*, *APC*, and *FBXW7*) in 86 patients with advanced GC. The authors reported a significant association between nuclear TAZ and mutations in the studied Wnt genes, a signature that the authors linked to increased risk of progression and reduced overall survival (Melucci et al., 2018).

Considering the role of Dvl in the context of adhesion dynamics in GC, it is of great interest to study a possible link between Wnt5a, Dvl, and YAP/TAZ in GC. Some evidence suggests potential cooperativity between these proteins in the context of tumorigenesis. Dvl physically interacts with phosphorylated YAP, promoting YAP nuclear export, and suppressing its transcriptional activity, while treatment with Wnt1 or Wnt3a induces YAP dephosphorylation, reducing its binding to Dvl and thus promoting its nuclear translocation

(Lee et al., 2018). Given that Wnt5a also induces YAP dephosphorylation (Park et al., 2015), Wnt5a might also activate YAP by abrogating its binding to Dvl, thus promoting YAP nuclear translocation. In addition, TAZ also interacts with Dvl (Varelas et al., 2010). Since *WNT5A* is also a YAP/TAZ-TEAD target gene (Park et al., 2015), YAP/TAZ activation might induce Wnt5a expression, leading to positive feedback (**Figure 1**, bottom right). Therefore, YAP and Wnt5a might promote cell migration by two parallel mechanisms: by activating the RhoA/ROCK/LIMK/Cofilin axis to promote stress fiber dynamics, and by promoting IAC turnover, respectively. Collectively, these data suggest that YAP/TAZ and Wnt signaling components can cooperate in the establishment of GC, thus highlighting the need for further studies focused on YAP/TAZ/Wnt5a signaling in GC.

Finally, the findings reviewed in this article raise interest in possible pharmacological approaches. Several drugs have been tested in clinical trials to modulate the Wnt pathway, but most abrogate either general Wnt ligand secretion or β-catenin activity (Harb et al., 2019). Therefore, molecules specifically targeting Wnt5a signaling are needed. However, and given the multiple roles of Wnt5a, clinical approaches must be carefully designed. In this regard, a better understanding of the mechanisms of Wnt5a signaling in GC might allow the development of drugs targeting specific biological interactions triggered by this ligand, and which might also be employed in other cancers where the non-canonical pathway plays a relevant role in tumor progression and metastasis (Kikuchi et al., 2012; Endo et al., 2015; Asem et al., 2016).

In summary, the evidence analyzed in this review suggests that Wnt5a plays a significant role in gastric cancer. However, whether this role is centered on transformed cells or in cells from the TME, or whether this role is predominantly focused on IAC turnover, gene expression or inflammation, are outstanding questions. Therefore, future studies should be aimed to understand these processes in the context of mechanically pertinent environments.

AUTHOR CONTRIBUTIONS

PA performed the literature analysis, prepared the figures, and drafted the manuscript.

FUNDING

This work was supported by the following grant: "CONICYT PAI Convocatoria Nacional Subvención a la Instalación en la Academia, Convocatoria Año 2017, No. 77170063."

REFERENCES

Ajani, J. A., Lee, J., Sano, T., Janjigian, Y. Y., Fan, D., and Song, S. (2017). Gastric adenocarcinoma. *Nat. Rev. Dis. Primers* 3:17036. doi: 10.1038/nrdp.2017.36

Anastas, J. N., and Moon, R. T. (2013). WNT signalling pathways as therapeutic targets in cancer. *Nat. Rev. Cancer* 13, 11–26. doi: 10.1038/nrc3419

Añazco, C., Delgado-López, F., Araya, P., González, I., Morales, E., Pérez-Castro, R., et al. (2016). Lysyl oxidase isoforms in gastric cancer. *Biomark. Med.* 10, 987–998. doi: 10.2217/bmm-2016-0075

Ara, H., Takagishi, M., Enomoto, A., Asai, M., Ushida, K., Asai, N., et al. (2016). Role for Daple in non-canonical Wnt signaling during gastric cancer invasion and metastasis. *Cancer Sci.* 107, 133–139. doi: 10.1111/cas.12848

Asem, M. S., Buechler, S., Wates, R. B., Miller, D. L., and Stack, M. S. (2016). Wnt5a signaling in Cancer. *Cancers (Basel)* 8:79. doi: 10.3390/cancers8090079

Azzolin, L., Panciera, T., Soligo, S., Enzo, E., Bicciato, S., Dupont, S., et al. (2014). YAP/TAZ incorporation in the β-catenin destruction complex orchestrates the Wnt response. *Cell* 158, 157–170. doi: 10.1016/j.cell.2014.06.013

Azzolin, L., Zanconato, F., Bresolin, S., Forcato, M., Basso, G., Bicciato, S., et al. (2012). Role of TAZ as mediator of Wnt signaling. *Cell* 151, 1443–1456. doi: 10.1016/j.cell.2012.11.027

Bakker, E. R. M., Raghoebir, L., Franken, P. F., Helvensteijn, W., van Gurp, L., Meijlink, F., et al. (2012). Induced Wnt5a expression perturbs embryonic outgrowth and intestinal elongation, but is well-tolerated in adult mice. *Dev. Biol.* 369, 91–100. doi: 10.1016/j.ydbio.2012.06.007

Barker, H. E., Cox, T. R., and Erler, J. T. (2012). The rationale for targeting the LOX family in cancer. *Nat. Rev. Cancer* 12, 540–552. doi: 10.1038/nrc3319

Binnerts, M. E., Kim, K.-A., Bright, J. M., Patel, S. M., Tran, K., Zhou, M., et al. (2007). R-Spondin1 regulates Wnt signaling by inhibiting internalization of LRP6. *Proc. Natl. Acad. Sci. U.S.A.* 104, 14700–14705. doi: 10.1073/pnas.0702305104

Boussioutas, A., Li, H., Liu, J., Waring, P., Lade, S., Holloway, A. J., et al. (2003). Distinctive patterns of gene expression in premalignant gastric mucosa and gastric cancer. *Cancer Res.* 63, 2569–2577.

Branco da Cunha, C., Klumpers, D. D., Koshy, S. T., Weaver, J. C., Chaudhuri, O., Seruca, R., et al. (2016). CD44 alternative splicing in gastric cancer cells is regulated by culture dimensionality and matrix stiffness. *Biomaterials* 98, 152–162. doi: 10.1016/j.biomaterials.2016.04.016

Bray, F., Ferlay, J., Soerjomataram, I., Siegel, R. L., Torre, L. A., and Jemal, A. (2018). Global cancer statistics 2018: GLOBOCAN estimates of incidence and mortality worldwide for 36 cancers in 185 countries. *CA Cancer J. Clin.* 68, 394–424. doi: 10.3322/caac.21492

Carneiro, F., and Lauwers, G. Y. (2012). "Epithelial tumours of the stomach," in *Morson and Dawson's Gastrointestinal Pathology*, eds N. A. Shepherd, B. F. Warren, G. T. Williams, J. K. Greenson, G. Y. Lauwers, and M. R. Novelli (Oxford: Wiley-Blackwell), 180–222. doi: 10.1002/9781118399668.ch13

Chien, A. J., Conrad, W. H., and Moon, R. T. (2009). A Wnt survival guide: from flies to human disease. *J. Invest. Dermatol.* 129, 1614–1627. doi: 10.1038/jid.2008.445

Correa, P. (1988). A human model of gastric carcinogenesis. *Cancer Res.* 48, 3554–3560.

Correa, P., Camargo, M. C., and Piazuelo, M. B. (2009). "Overview and pathology of gastric cancer," in *The Biology of Gastric Cancers*, eds T. C. Wang, J. G. Fox, and A. S. Giraud (New York, NY: Springer), 1–24. doi: 10.1007/978-0-387-69182-4_1

Davidson, G., Wu, W., Shen, J., Bilic, J., Fenger, U., Stannek, P., et al. (2005). Casein kinase 1 gamma couples Wnt receptor activation to cytoplasmic signal transduction. *Nature* 438, 867–872. doi: 10.1038/nature04170

de Lau, W., Barker, N., Low, T. Y., Koo, B.-K., Li, V. S. W., Teunissen, H., et al. (2011). Lgr5 homologues associate with Wnt receptors and mediate R-spondin signalling. *Nature* 476, 293–297. doi: 10.1038/nature10337

Deng, L., Chen, N., Li, Y., Zheng, H., and Lei, Q. (2010). CXCR6/CXCL16 functions as a regulator in metastasis and progression of cancer. *Biochim. Biophys. Acta* 1806, 42–49. doi: 10.1016/j.bbcan.2010.01.004

Diamantopoulou, Z., White, G., Fadlullah, M. Z. H., Dreger, M., Pickering, K., Maltas, J., et al. (2017). TIAM1 antagonizes TAZ/YAP both in the destruction complex in the cytoplasm and in the nucleus to inhibit invasion of intestinal epithelial cells. *Cancer Cell* 31, 621–634.e6. doi: 10.1016/j.ccell.2017.03.007

Dupont, S., Morsut, L., Aragona, M., Enzo, E., Giulitti, S., Cordenonsi, M., et al. (2011). Role of YAP/TAZ in mechanotransduction. *Nature* 474, 179–183. doi: 10.1038/nature10137

Ebert, M. P. A., Yu, J., Hoffmann, J., Rocco, A., Röcken, C., Kahmann, S., et al. (2003). Loss of beta-catenin expression in metastatic gastric cancer. *J. Clin. Oncol.* 21, 1708–1714. doi: 10.1200/JCO.2003.10.017

Endo, M., Nishita, M., Fujii, M., and Minami, Y. (2015). Insight into the role of Wnt5a-induced signaling in normal and cancer cells. *Int. Rev. Cell Mol. Biol.* 314, 117–148. doi: 10.1016/bs.ircmb.2014.10.003

Filipovich, A., Gehrke, I., Poll-Wolbeck, S. J., and Kreuzer, K.-A. (2011). Physiological inhibitors of Wnt signaling. *Eur. J. Haematol.* 86, 453–465. doi: 10.1111/j.1600-0609.2011.01592.x

Fu, Y., Chen, Y., Huang, J., Cai, Z., and Wang, Y. (2019). RYK, a receptor of non-canonical Wnt ligand Wnt5a, is positively correlated with gastric cancer tumorigenesis and potential of liver metastasis. *Am. J. Physiol. Gastrointest. Liver Physiol.* 318, G352–G360. doi: 10.1152/ajpgi.00228.2019

Gammons, M., and Bienz, M. (2018). Multiprotein complexes governing Wnt signal transduction. *Curr. Opin. Cell Biol.* 51, 42–49. doi: 10.1016/j.ceb.2017.10.008

Glinka, A., Dolde, C., Kirsch, N., Huang, Y.-L., Kazanskaya, O., Ingelfinger, D., et al. (2011). LGR4 and LGR5 are R-spondin receptors mediating Wnt/β-catenin and Wnt/PCP signalling. *EMBO Rep.* 12, 1055–1061. doi: 10.1038/embor.2011.175

Hamidi, H., and Ivaska, J. (2018). Every step of the way: integrins in cancer progression and metastasis. *Nat. Rev. Cancer* 18, 533–548. doi: 10.1038/s41568-018-0038-z

Hanaki, H., Yamamoto, H., Sakane, H., Matsumoto, S., Ohdan, H., Sato, A., et al. (2012). An anti-Wnt5a antibody suppresses metastasis of gastric cancer cells *in vivo* by inhibiting receptor-mediated endocytosis. *Mol. Cancer Ther.* 11, 298–307. doi: 10.1158/1535-7163.MCT-11-0682

Hao, H.-X., Xie, Y., Zhang, Y., Charlat, O., Oster, E., Avello, M., et al. (2012). ZNRF3 promotes Wnt receptor turnover in an R-spondin-sensitive manner. *Nature* 485, 195–200. doi: 10.1038/nature11019

Harb, J., Lin, P.-J., and Hao, J. (2019). Recent development of Wnt signaling pathway inhibitors for cancer therapeutics. *Curr. Oncol. Rep.* 21:12. doi: 10.1007/s11912-019-0763-9

Hayakawa, Y., Ariyama, H., Stancikova, J., Sakitani, K., Asfaha, S., Renz, B. W., et al. (2015). Mist1 expressing gastric stem cells maintain the normal and neoplastic gastric epithelium and are supported by a perivascular stem cell niche. *Cancer Cell* 28, 800–814. doi: 10.1016/j.ccell.2015.10.003

Horton, E. R., Byron, A., Askari, J. A., Ng, D. H. J., Millon-Frémillon, A., Robertson, J., et al. (2015). Definition of a consensus integrin adhesome and its dynamics during adhesion complex assembly and disassembly. *Nat. Cell Biol.* 17, 1577–1587. doi: 10.1038/ncb3257

Horton, E. R., Humphries, J. D., James, J., Jones, M. C., Askari, J. A., and Humphries, M. J. (2016). The integrin adhesome network at a glance. *J. Cell Sci.* 129, 4159–4163. doi: 10.1242/jcs.192054

Humphries, J. D., Byron, A., Bass, M. D., Craig, S. E., Pinney, J. W., Knight, D., et al. (2009). Proteomic analysis of integrin-associated complexes identifies RCC2 as a dual regulator of Rac1 and Arf6. *Sci. Signal.* 2:ra51. doi: 10.1126/scisignal.2000396

Ikenoue, T., Ijichi, H., Kato, N., Kanai, F., Masaki, T., Rengifo, W., et al. (2002). Analysis of the β-catenin/T cell factor signaling pathway in 36 gastrointestinal and liver cancer cells. *Jpn. J. Cancer Res.* 93, 1213–1220. doi: 10.1111/j.1349-7006.2002.tb01226.x

Imajo, M., Miyatake, K., Iimura, A., Miyamoto, A., and Nishida, E. (2012). A molecular mechanism that links Hippo signalling to the inhibition of Wnt/β-catenin signalling. *EMBO J.* 31, 1109–1122. doi: 10.1038/emboj.2011.487

Ishida-Takagishi, M., Enomoto, A., Asai, N., Ushida, K., Watanabe, T., Hashimoto, T., et al. (2012). The Dishevelled-associating protein Daple controls the non-canonical Wnt/Rac pathway and cell motility. *Nat. Commun.* 3:859. doi: 10.1038/ncomms1861

Jabbari, E., Sarvestani, S. K., Daneshian, L., and Moeinzadeh, S. (2015). Optimum 3D matrix stiffness for maintenance of cancer stem cells is dependent on tissue origin of cancer cells. *PLoS One* 10:e0132377. doi: 10.1371/journal.pone.0132377

Kanda, M., and Kodera, Y. (2016). Molecular mechanisms of peritoneal dissemination in gastric cancer. *World J. Gastroenterol.* 22, 6829–6840. doi: 10.3748/wjg.v22.i30.6829

Kang, W., Tong, J. H. M., Chan, A. W. H., Lee, T.-L., Lung, R. W. M., Leung, P. P. S., et al. (2011). Yes-associated protein 1 exhibits oncogenic property in gastric cancer and its nuclear accumulation associates with poor prognosis. *Clin. Cancer Res.* 17, 2130–2139. doi: 10.1158/1078-0432.CCR-10-2467

Kanzawa, M., Semba, S., Hara, S., Itoh, T., and Yokozaki, H. (2013). WNT5A is a key regulator of the epithelial-mesenchymal transition and cancer stem cell properties in human gastric carcinoma cells. *Pathobiology* 80, 235–244. doi: 10.1159/000346843

Kikuchi, A., Yamamoto, H., Sato, A., and Matsumoto, S. (2012). Wnt5a: its signalling, functions and implication in diseases. *Acta Physiol. (Oxf.)* 204, 17–33. doi: 10.1111/j.1748-1716.2011.02294.x

Kikuchi, K., Nakamura, A., Arata, M., Shi, D., Nakagawa, M., Tanaka, T., et al. (2018). Map7/7D1 and Dvl form a feedback loop that facilitates microtubule remodeling and Wnt5a signaling. *EMBO Rep.* 19:e45471. doi: 10.15252/embr.201745471

Kim, K.-A., Wagle, M., Tran, K., Zhan, X., Dixon, M. A., Liu, S., et al. (2008). R-Spondin family members regulate the Wnt pathway by a common mechanism. *Mol. Biol. Cell* 19, 2588–2596. doi: 10.1091/mbc.e08-02-0187

Koo, B.-K., Spit, M., Jordens, I., Low, T. Y., Stange, D. E., van de Wetering, M., et al. (2012). Tumour suppressor RNF43 is a stem-cell E3 ligase that induces endocytosis of Wnt receptors. *Nature* 488, 665–669. doi: 10.1038/nature11308

Kuo, J.-C., Han, X., Hsiao, C.-T., Yates, J. R., and Waterman, C. M. (2011). Analysis of the myosin-II-responsive focal adhesion proteome reveals a role for β-Pix in negative regulation of focal adhesion maturation. *Nat. Cell Biol.* 13, 383–393. doi: 10.1038/ncb2216

Kurayoshi, M., Oue, N., Yamamoto, H., Kishida, M., Inoue, A., Asahara, T., et al. (2006). Expression of Wnt-5a is correlated with aggressiveness of gastric cancer by stimulating cell migration and invasion. *Cancer Res.* 66, 10439–10448. doi: 10.1158/0008-5472.CAN-06-2359

Lauren, P. (1965). The two histological main types of gastric carcinoma: diffuse and so-called intestinal-type carcinoma. An attempt at a histo-clinical classification. *Acta Pathol. Microbiol. Scand.* 64, 31–49. doi: 10.1111/apm.1965.64.1.31

Lauwers, G. Y., and Srivastava, A. (2007). Gastric preneoplastic lesions and epithelial dysplasia. *Gastroenterol. Clin. North Am.* 36, 813–829. doi: 10.1016/j.gtc.2007.08.008

Lee, Y., Kim, N. H., Cho, E. S., Yang, J. H., Cha, Y. H., Kang, H. E., et al. (2018). Dishevelled has a YAP nuclear export function in a tumor suppressor context-dependent manner. *Nat. Commun.* 9:2301. doi: 10.1038/s41467-018-04757-w

Li, N., Lu, N., and Xie, C. (2019). The Hippo and Wnt signalling pathways: crosstalk during neoplastic progression in gastrointestinal tissue. *FEBS J.* 286, 3745–3756. doi: 10.1111/febs.15017

Li, S., Wang, W., Zhang, N., Ma, T., and Zhao, C. (2014). IL-1β mediates MCP-1 induction by Wnt5a in gastric cancer cells. *BMC Cancer* 14:480. doi: 10.1186/1471-2407-14-480

Li, V. S. W., Ng, S. S., Boersema, P. J., Low, T. Y., Karthaus, W. R., Gerlach, J. P., et al. (2012). Wnt signaling through inhibition of β-catenin degradation in an intact Axin1 complex. *Cell* 149, 1245–1256. doi: 10.1016/j.cell.2012.05.002

Liu, J., Zhang, Y., Xu, R., Du, J., Hu, Z., Yang, L., et al. (2013). PI3K/Akt-dependent phosphorylation of GSK3β and activation of RhoA regulate Wnt5a-induced gastric cancer cell migration. *Cell. Signal.* 25, 447–456. doi: 10.1016/j.cellsig.2012.10.012

Llado, V., Nakanishi, Y., Duran, A., Reina-Campos, M., Shelton, P. M., Linares, J. F., et al. (2015). Repression of intestinal stem cell function and tumorigenesis through direct phosphorylation of β-catenin and Yap by PKCζ. *Cell Rep.* 10, 740–754. doi: 10.1016/j.celrep.2015.01.007

Logan, C. Y., and Nusse, R. (2004). The Wnt signaling pathway in development and disease. *Annu. Rev. Cell Dev. Biol.* 20, 781–810. doi: 10.1146/annurev.cellbio.20.010403.113126

Maeda, M., Takeshima, H., Iida, N., Hattori, N., Yamashita, S., Moro, H., et al. (2019). Cancer cell niche factors secreted from cancer-associated fibroblast by loss of H3K27me3. *Gut* 69, 243–251. doi: 10.1136/gutjnl-2018-317645

Matsumoto, S., Fumoto, K., Okamoto, T., Kaibuchi, K., and Kikuchi, A. (2010). Binding of APC and dishevelled mediates Wnt5a-regulated focal adhesion dynamics in migrating cells. *EMBO J.* 29, 1192–1204. doi: 10.1038/emboj.2010.26

Matsuo, T., Ito, M., Tatsugami, M., Boda, T., Takata, S., Tanaka, S., et al. (2012). Gastric cancer development after *Helicobacter pylori* eradication therapy: a new form of gastric neoplasia. *Digestion* 85, 61–67. doi: 10.1159/000335260

McCracken, K. W., Catá, E. M., Crawford, C. M., Sinagoga, K. L., Schumacher, M., Rockich, B. E., et al. (2014). Modelling human development and disease in pluripotent stem-cell-derived gastric organoids. *Nature* 516, 400–404. doi: 10.1038/nature13863

McDonald, S. L., and Silver, A. (2009). The opposing roles of Wnt-5a in cancer. *Br. J. Cancer* 101, 209–214. doi: 10.1038/sj.bjc.6605174

Melucci, E., Casini, B., Ronchetti, L., Pizzuti, L., Sperati, F., Pallocca, M., et al. (2018). Expression of the Hippo transducer TAZ in association with Wnt pathway mutations impacts survival outcomes in advanced gastric cancer patients treated with first-line chemotherapy. *J. Transl. Med.* 16:22. doi: 10.1186/s12967-018-1385-y

Mikels, A. J., and Nusse, R. (2006). Purified Wnt5a protein activates or inhibits beta-catenin-TCF signaling depending on receptor context. *PLoS Biol.* 4:e115. doi: 10.1371/journal.pbio.0040115

Miwa, T., Kanda, M., Tanaka, H., Tanaka, C., Kobayashi, D., Umeda, S., et al. (2017). FBXO50 enhances the malignant behavior of gastric cancer cells. *Ann. Surg. Oncol.* 24, 3771–3779. doi: 10.1245/s10434-017-5882-7

Moroishi, T., Hansen, C. G., and Guan, K.-L. (2015). The emerging roles of YAP and TAZ in cancer. *Nat. Rev. Cancer* 15, 73–79. doi: 10.1038/nrc3876

Nam, S., Chang, H. R., Kim, K.-T., Kook, M.-C., Hong, D., Kwon, C. H., et al. (2014). PATHOME: an algorithm for accurately detecting differentially expressed subpathways. *Oncogene* 33, 4941–4951. doi: 10.1038/onc.2014.80

Nam, S., Chung, J.-W., and Yang, J.-Y. (2017). WNT5A correlates with clinicopathological characteristics in gastric cancer: a meta-analysis. *Cell. Physiol. Biochem.* 41, 33–40. doi: 10.1159/000455934

Niehrs, C. (2012). The complex world of WNT receptor signalling. *Nat. Rev. Mol. Cell Biol.* 13, 767–779. doi: 10.1038/nrm3470

Nishimura, K., Semba, S., Aoyagi, K., Sasaki, H., and Yokozaki, H. (2012). Mesenchymal stem cells provide an advantageous tumor microenvironment for the restoration of cancer stem cells. *Pathobiology* 79, 290–306. doi: 10.1159/000337296

Northey, J. J., Przybyla, L., and Weaver, V. M. (2017). Tissue force programs cell fate and tumor aggression. *Cancer Discov.* 7, 1224–1237. doi: 10.1158/2159-8290.CD-16-0733

Oudhoff, M. J., Braam, M. J. S., Freeman, S. A., Wong, D., Rattray, D. G., Wang, J., et al. (2016). SETD7 controls intestinal regeneration and tumorigenesis by regulating Wnt/β-catenin and Hippo/YAP signaling. *Dev. Cell* 37, 47–57. doi: 10.1016/j.devcel.2016.03.002

Park, H. W., Kim, Y. C., Yu, B., Moroishi, T., Mo, J.-S., Plouffe, S. W., et al. (2015). Alternative Wnt signaling activates YAP/TAZ. *Cell* 162, 780–794. doi: 10.1016/j.cell.2015.07.013

Pashirzad, M., Shafiee, M., Rahmani, F., Behnam-Rassouli, R., Hoseinkhani, F., Ryzhikov, M., et al. (2017). Role of Wnt5a in the pathogenesis of inflammatory diseases. *J. Cell. Physiol.* 232, 1611–1616. doi: 10.1002/jcp.25687

Pickup, M. W., Mouw, J. K., and Weaver, V. M. (2014). The extracellular matrix modulates the hallmarks of cancer. *EMBO Rep.* 15, 1243–1253. doi: 10.15252/embr.201439246

Pukrop, T., and Binder, C. (2008). The complex pathways of Wnt 5a in cancer progression. *J. Mol. Med.* 86, 259–266. doi: 10.1007/s00109-007-0266-2

Qiao, Y., Chen, J., Lim, Y. B., Finch-Edmondson, M. L., Seshachalam, V. P., Qin, L., et al. (2017). YAP regulates actin dynamics through ARHGAP29 and promotes metastasis. *Cell Rep.* 19, 1495–1502. doi: 10.1016/j.celrep.2017.04.075

Qiu, J., Tao, L., Wei, Q., and Zhang, P. (2018). Knockdown of Arf6 increases drug sensitivity and inhibits proliferation, migration and invasion in gastric cancer SGC-7901 cells. *Oncol. Lett.* 15, 2147–2152. doi: 10.3892/ol.2017.7558

Räihä, M. R., and Puolakkainen, P. A. (2018). Tumor-associated macrophages (TAMs) as biomarkers for gastric cancer: a review. *Chronic Dis. Transl. Med.* 4, 156–163. doi: 10.1016/j.cdtm.2018.07.001

Saitoh, T., Mine, T., and Katoh, M. (2002). Frequent up-regulation of WNT5A mRNA in primary gastric cancer. *Int. J. Mol. Med.* 9, 515–519.

Schiller, H. B., Friedel, C. C., Boulegue, C., and Fässler, R. (2011). Quantitative proteomics of the integrin adhesome show a myosin II-dependent recruitment of LIM domain proteins. *EMBO Rep.* 12, 259–266. doi: 10.1038/embor.2011.5

Schlessinger, K., Hall, A., and Tolwinski, N. (2009). Wnt signaling pathways meet Rho GTPases. *Genes Dev.* 23, 265–277. doi: 10.1101/gad.1760809

Semenov, M. V., Habas, R., Macdonald, B. T., and He, X. (2007). SnapShot: noncanonical Wnt signaling pathways. *Cell* 131:1378. doi: 10.1016/j.cell.2007.12.011

Sharma, M., Castro-Piedras, I., Simmons, G. E., and Pruitt, K. (2018). Dishevelled: a masterful conductor of complex Wnt signals. *Cell. Signal.* 47, 52–64. doi: 10.1016/j.cellsig.2018.03.004

Shimizu, H., Julius, M. A., Giarré, M., Zheng, Z., Brown, A. M., and Kitajewski, J. (1997). Transformation by Wnt family proteins correlates with regulation of beta-catenin. *Cell Growth Differ.* 8, 1349–1358.

Shojima, K., Sato, A., Hanaki, H., Tsujimoto, I., Nakamura, M., Hattori, K., et al. (2015). Wnt5a promotes cancer cell invasion and proliferation by receptor-mediated endocytosis-dependent and -independent mechanisms, respectively. *Sci. Rep.* 5:8042. doi: 10.1038/srep08042

Song, M., Cheong, J.-H., Kim, H., Noh, S. H., and Kim, H. (2012). Nuclear expression of Yes-associated protein 1 correlates with poor prognosis in intestinal type gastric cancer. *Anticancer Res.* 32, 3827–3834.

Taelman, V. F., Dobrowolski, R., Plouhinec, J.-L., Fuentealba, L. C., Vorwald, P. P., Gumper, I., et al. (2010). Wnt signaling requires sequestration of glycogen synthase kinase 3 inside multivesicular endosomes. *Cell* 143, 1136–1148. doi: 10.1016/j.cell.2010.11.034

Takiguchi, G., Nishita, M., Kurita, K., Kakeji, Y., and Minami, Y. (2016). Wnt5a-Ror2 signaling in mesenchymal stem cells promotes proliferation of gastric cancer cells by activating CXCL16-CXCR6 axis. *Cancer Sci.* 107, 290–297. doi: 10.1111/cas.12871

Torres, M. A., Yang-Snyder, J. A., Purcell, S. M., DeMarais, A. A., McGrew, L. L., and Moon, R. T. (1996). Activities of the Wnt-1 class of secreted signaling factors are antagonized by the Wnt-5A class and by a dominant negative cadherin in early *Xenopus* development. *J. Cell Biol.* 133, 1123–1137. doi: 10.1083/jcb.133.5.1123

Valenta, T., Hausmann, G., and Basler, K. (2012). The many faces and functions of β-catenin. *EMBO J.* 31, 2714–2736. doi: 10.1038/emboj.2012.150

van Amerongen, R., Fuerer, C., Mizutani, M., and Nusse, R. (2012). Wnt5a can both activate and repress Wnt/β-catenin signaling during mouse embryonic development. *Dev. Biol.* 369, 101–114. doi: 10.1016/j.ydbio.2012.06.020

Van Cutsem, E., Sagaert, X., Topal, B., Haustermans, K., and Prenen, H. (2016). Gastric cancer. *Lancet* 388, 2654–2664. doi: 10.1016/S0140-6736(16)30354-3

Varelas, X., Miller, B. W., Sopko, R., Song, S., Gregorieff, A., Fellouse, F. A., et al. (2010). The Hippo pathway regulates Wnt/beta-catenin signaling. *Dev. Cell* 18, 579–591. doi: 10.1016/j.devcel.2010.03.007

Veeman, M. T., Axelrod, J. D., and Moon, R. T. (2003). A second canon. Functions and mechanisms of beta-catenin-independent Wnt signaling. *Dev. Cell* 5, 367–377. doi: 10.1016/s1534-5807(03)00266-1

Wall, K., and Nickl, N. (2019). "Subepithelial tumors of the esophagus and stomach," in *Clinical Gastrointestinal Endoscopy*, eds V. Chandrasekhara, B. J. Elmunzer, M. Khashab, and V. R. Muthusamy (Philadelphia, PA: Elsevier), 337–348.e3.

Wang, L., Steele, I., Kumar, J. D., Dimaline, R., Jithesh, P. V., Tiszlavicz, L., et al. (2016). Distinct miRNA profiles in normal and gastric cancer myofibroblasts and significance in Wnt signaling. *Am. J. Physiol. Gastrointest. Liver Physiol.* 310, G696–G704. doi: 10.1152/ajpgi.00443.2015

Wang, S., Kang, W., Go, M. Y. Y., Tong, J. H. M., Li, L., Zhang, N., et al. (2012). Dapper homolog 1 is a novel tumor suppressor in gastric cancer through inhibiting the nuclear factor-κB signaling pathway. *Mol. Med.* 18, 1402–1411. doi: 10.2119/molmed.2012.00243

Wei, J., Wang, L., Zhu, J., Sun, A., Yu, G., Chen, M., et al. (2019). The Hippo signaling effector WWTR1 is a metastatic biomarker of gastric cardia adenocarcinoma. *Cancer Cell Int.* 19:74. doi: 10.1186/s12935-019-0796-z

Wei, Q., Yokota, C., Semenov, M. V., Doble, B., Woodgett, J., and He, X. (2007). R-spondin1 is a high affinity ligand for LRP6 and induces LRP6 phosphorylation and beta-catenin signaling. *J. Biol. Chem.* 282, 15903–15911. doi: 10.1074/jbc.M701927200

Wen, J., Chiang, Y. J., Gao, C., Xue, H., Xu, J., Ning, Y., et al. (2010). Loss of Dact1 disrupts planar cell polarity signaling by altering dishevelled activity and leads to posterior malformation in mice. *J. Biol. Chem.* 285, 11023–11030. doi: 10.1074/jbc.M109.085381

Yamamoto, H., Kitadai, Y., Yamamoto, H., Oue, N., Ohdan, H., Yasui, W., et al. (2009). Laminin γ2 mediates Wnt5a-induced invasion of gastric cancer cells. *Gastroenterology* 137, 242–252.e6. doi: 10.1053/j.gastro.2009.02.003

Yashiro, M., Chung, Y. S., Nishimura, S., Inoue, T., and Sowa, M. (1996). Fibrosis in the peritoneum induced by scirrhous gastric cancer cells may act as "soil" for peritoneal dissemination. *Cancer* 77, 1668–1675. doi: 10.1002/(SICI)1097-0142(19960415)77:8<1668::AID-CNCR37>3.0.CO;2-W

Yokozaki, H. (2000). Molecular characteristics of eight gastric cancer cell lines established in Japan. *Pathol. Int.* 50, 767–777. doi: 10.1046/j.1440-1827.2000.01117.x

Yoshimura, T. (2017). The production of monocyte chemoattractant protein-1 (MCP-1)/CCL2 in tumor microenvironments. *Cytokine* 98, 71–78. doi: 10.1016/j.cyto.2017.02.001

Yu, Y., Yan, W., Liu, X., Jia, Y., Cao, B., Yu, Y., et al. (2014). DACT2 is frequently methylated in human gastric cancer and methylation of DACT2 activated Wnt signaling. *Am. J. Cancer Res.* 4, 710–724.

Yue, G., Sun, X., Gimenez-Capitan, A., Shen, J., Yu, L., Teixido, C., et al. (2014). TAZ is highly expressed in gastric signet ring cell carcinoma. *Biomed Res. Int.* 2014:393064. doi: 10.1155/2014/393064

Zanconato, F., Cordenonsi, M., and Piccolo, S. (2016). YAP/TAZ at the roots of cancer. *Cancer Cell* 29, 783–803. doi: 10.1016/j.ccell.2016.05.005

Zeng, X., Tamai, K., Doble, B., Li, S., Huang, H., Habas, R., et al. (2005). A dual-kinase mechanism for Wnt co-receptor phosphorylation and activation. *Nature* 438, 873–877. doi: 10.1038/nature04185

Zhan, T., Rindtorff, N., and Boutros, M. (2017). Wnt signaling in cancer. *Oncogene* 36, 1461–1473. doi: 10.1038/onc.2016.304

Zhang, J., Xu, Z.-P., Yang, Y.-C., Zhu, J.-S., Zhou, Z., and Chen, W.-X. (2012). Expression of Yes-associated protein in gastric adenocarcinoma and inhibitory effects of its knockdown on gastric cancer cell proliferation and metastasis. *Int. J. Immunopathol. Pharmacol.* 25, 583–590. doi: 10.1177/039463201202500304

Zhang, L., Gao, X., Wen, J., Ning, Y., and Chen, Y.-G. (2006). Dapper 1 antagonizes Wnt signaling by promoting dishevelled degradation. *J. Biol. Chem.* 281, 8607–8612. doi: 10.1074/jbc.M600274200

Zhang, W., Tao, H., Chen, X., Sugimura, H., Wang, J., and Zhou, P. (2017). High expression of Wls is associated with lymph node metastasis and advanced TNM stage in gastric carcinomas. *Pathol. Int.* 67, 141–146. doi: 10.1111/pin.12508

Zhang, Y., Du, J., Zheng, J., Liu, J., Xu, R., Shen, T., et al. (2015). EGF-reduced Wnt5a transcription induces epithelial-mesenchymal transition via Arf6-ERK signaling in gastric cancer cells. *Oncotarget* 6, 7244–7261. doi: 10.18632/oncotarget.3133

Zhao, C., Ma, H., Bu, X., Wang, W., and Zhang, N. (2013). SFRP5 inhibits gastric epithelial cell migration induced by macrophage-derived Wnt5a. *Carcinogenesis* 34, 146–152. doi: 10.1093/carcin/bgs309

Zhao, C.-H., Bu, X.-M., and Zhang, N. (2007). Hypermethylation and aberrant expression of Wnt antagonist secreted frizzled-related protein 1 in gastric cancer. *World J. Gastroenterol.* 13, 2214–2217. doi: 10.3748/wjg.v13.i15.2214

Conflict of Interest: The author declares that the research was conducted in the absence of any commercial or financial relationships that could be construed as a potential conflict of interest.

frontiers in Cell and Developmental Biology

ORIGINAL RESEARCH
published: 02 April 2020
doi: 10.3389/fcell.2020.00215

GJB2 Mutations Linked to Hearing Loss Exhibit Differential Trafficking and Functional Defects as Revealed in Cochlear-Relevant Cells

*Rianne Beach[1], Julia M. Abitbol[1], Brian L. Allman[1], Jessica L. Esseltine[2], Qing Shao[1] and Dale W. Laird[1]**

[1] Department of Anatomy and Cell Biology, Schulich School of Medicine & Dentistry, University of Western Ontario, London, ON, Canada, [2] Division of BioMedical Sciences, Faculty of Medicine, Memorial University of Newfoundland, St. John's, NL, Canada

OPEN ACCESS

Edited by:
José Lozano,
University of Málaga, Spain

Reviewed by:
Sally Ann Moody,
The George Washington University, United States
Pedro A. Lazo,
University of Salamanca, Spain

***Correspondence:**
Dale W. Laird
Dale.Laird@schulich.uwo.ca

Specialty section:
This article was submitted to Signaling, a section of the journal Frontiers in Cell and Developmental Biology

Received: 19 December 2019
Accepted: 12 March 2020
Published: 02 April 2020

Citation:
Beach R, Abitbol JM, Allman BL, Esseltine JL, Shao Q and Laird DW (2020) GJB2 Mutations Linked to Hearing Loss Exhibit Differential Trafficking and Functional Defects as Revealed in Cochlear-Relevant Cells. Front. Cell Dev. Biol. 8:215. doi: 10.3389/fcell.2020.00215

GJB2 gene (that encodes Cx26) mutations are causal of hearing loss highlighting the importance of Cx26-based channel signaling amongst the supporting cells in the organ of Corti. While the majority of these *GJB2* mutations are inherited in an autosomal recessive manner, others are inherited in an autosomal dominant manner and lead to syndromic hearing loss as well as skin diseases. To assess if common or divergent mechanisms are at the root of *GJB2*-linked hearing loss, we expressed several mutants in cochlear-relevant HEI-OC1 cells derived from the developing organ of Corti. Since supporting cells of the mature mammalian organ of Corti have negligible Cx43, but HEI-OC1 cells are rich in Cx43, we first used CRISPR-Cas9 to ablate endogenous Cx43, thus establishing a connexin-deficient platform for controlled reintroduction of hearing-relevant connexins and Cx26 mutants. We found three distinct outcomes and cellular phenotypes when hearing loss-linked Cx26 mutants were expressed in cochlear-relevant cells. The dominant syndromic Cx26 mutant N54K had trafficking defects and did not fully prevent wild-type Cx26 gap junction plaque formation but surprisingly formed gap junctions when co-expressed with Cx30. In contrast, the dominant syndromic S183F mutant formed gap junctions incapable of transferring dye and, as expected, co-localized in the same gap junctions as wild-type Cx26 and Cx30, but also gained the capacity to intermix with Cx43 within gap junctions. Both recessive non-syndromic Cx26 mutants (R32H and R184P) were retained in intracellular vesicles including early endosomes and did not co-localize with Cx30. As might be predicted, none of the Cx26 mutants prevented Cx43 gap junction plaque formation in Cx43-rich HEI-OC1 cells while Cx43-ablation had little effect on the expression of reference genes linked to auditory cell differentiation. We conclude from our studies in cochlear-relevant cells that the selected Cx26 mutants likely evoke hearing loss via three unique connexin defects that are independent of Cx43 status.

Keywords: GJB2, hearing loss, Cx26, cochlear cells, mutants, disease

INTRODUCTION

Nearly half of all inherited sensorineural hearing loss is attributed to mutations in one of four members of the 21 connexin gene family (Chan and Chang, 2014), although *GJB2* gene (encoding Cx26) mutations linked to hereditary deafness are by far the most common (Duman and Tekin, 2012; Mammano, 2019). Connexins (Cxs) oligomerize into hexameric arrangements called connexons or hemichannels. At the cell surface, hemichannels may function as highly regulated communication conduits to the extracellular milieu but more often proceed to dock with hemichannels from a contacting cell to form gap junction channels (Laird, 2006). These channels facilitate the direct intercellular exchange of metabolites, ions, and small molecules (<1 kDa) in a process known as gap junctional intercellular communication (GJIC) (Alexander and Goldberg, 2003). The principal connexin isoforms implicated in hearing loss are Cx26 and Cx30, which are abundantly expressed in two independent gap junction networks in the cochlea: the epithelial and connective tissue networks (Kikuchi et al., 2000b; Ahmad et al., 2003; Forge et al., 2003; Liu et al., 2009). The connective tissue network exists amongst the cells of the cochlear lateral wall while the epithelial gap junction network is found amongst supporting cells that are precisely configured around the mechanosensory hair cells in the organ of Corti (Jagger and Forge, 2015). Cx26 and Cx30 also have the capacity to co-oligomerize and form heteromeric and/or heterotypic (mixed) channels within these networks enhancing the scope of GJIC and possibly hemichannel function (Yum et al., 2007; Martinez et al., 2009). Hair cells are completely devoid of connexins even though hair cell loss is a consequential outcome of connexin-based sensorineural hearing loss (Jagger and Forge, 2006; Forge et al., 2013). The exact role of connexins in supporting cell signal propagation has been extensively debated (Zhao, 2017). Hearing initiates through an influx of potassium ions into hair cells that drives their depolarization and subsequent propagation of electrical signals along the auditory nerve, ultimately relaying sensory information into the central auditory system (Wangemann, 2006). After hair cell stimulation, gap junction networks have been proposed to be important in buffering and recycling potassium ions back into the potassium-rich endolymph fluid that bathes the hair cells, and is crucial for hair cell depolarization (Kikuchi et al., 2000a; Jagger and Forge, 2015). Furthermore, gap junction networks have been demonstrated to be vital in cochlear development, homeostasis, and nutrient transfer (Zhao et al., 2006; Chang et al., 2008; Liang et al., 2012).

Approximately 135 different hearing loss mutations in the *GJB2* gene have been identified (Laird, 2008; Laird et al., 2017) that span the entire amino acid polypeptide sequence of Cx26 (Martinez et al., 2009). In an attempt to correlate genotype changes to phenotype outcomes, some of these mutants have been expressed and examined in tumor cells and other cells unrelated to hearing. Based on these studies, connexin mutants can be categorized as exhibiting either loss-of-function or gain-of-function properties (Kelly et al., 2014; Verselis, 2019). Loss-of-function mutants can result in defective trafficking of the Cx26 mutant through the endoplasmic reticulum (ER) and Golgi apparatus, misfolding and aberrant oligomerization, and non-functional hemichannels and/or gap junction formation (Laird, 2008; Kelly et al., 2015). In contrast, abnormal oligomerization of a Cx26 mutant with other connexin isoforms, formation of leaky hemichannels, formation of hyperactive hemichannels and/or gap junctions are all characteristics of gain-of-function mutants (Press et al., 2017; Srinivas et al., 2018). Loss-of-function Cx26 mutants typically produce hearing loss as the pathological outcome and are characterized as non-syndromic mutations, where hearing loss is the only phenotype (Kenneson et al., 2002). Gain-of-function Cx26 mutants frequently result in syndromic disease, where hearing loss is also accompanied with other co-morbidities, as these mutants often induce a skin disorder (Srinivas et al., 2018). Evidence suggests that gain-of-function Cx26 mutants induce skin disorders because of their inhibitory trans-dominant effects on other connexin isoforms expressed in the epidermis (Press et al., 2017). In all cases, Cx26 mutants drive moderate to profound hearing loss raising questions as to whether this is rooted in how the Cx26 mutants are trafficked, assembled, and functionally dysregulated (D'Andrea et al., 2002; Snoeckx et al., 2005; Xiao et al., 2011). Because of the diversity and extent of hearing loss that occurs when Cx26 mutants are expressed in the organ of Corti, the mechanisms of hearing loss need to be investigated in a tissue-relevant setting.

Hair cells and supporting cells develop from common progenitor cells within the prosensory domain of the developing cochlea. At an early stage of development, specification of cell fate depends on the crucial coordination and timing of gene expression (Basch et al., 2016). The expression of Cx26 within the epithelial gap junction network begins to occur around embryonic day 16 in mice (Frenz and Van De Water, 2000) and continues for approximately two weeks after birth as mouse hearing matures. As revealed in mouse studies, improper cochlear development is a pathological outcome of Cx26 mutant expression or Cx26 ablation as noted by the deformation of hair cells and disrupted formation of the tunnel of Corti, which is formed by supporting cells (Wang et al., 2009; Mese et al., 2011; Schutz et al., 2011; Inoshita et al., 2014; Anzai et al., 2015; Lee et al., 2015; Zhu et al., 2015; Chen et al., 2018b). A few rare mutations in *GJC3* (Cx30.2/Cx29) and *GJB3* (Cx31) have also been linked to hearing loss but it is unclear what role these connexins play and even where these connexins are localized in the auditory tract (Wingard and Zhao, 2015). Cx43 is expressed early on in cochlear development, however Cx43 expression is negligible in the mature organ of Corti (Cohen-Salmon et al., 2004) although mice expressing a loss-of-function G60S Cx43 mutant were found to have severe hearing loss (Abitbol et al., 2018).

Since *GJB2* is the primary connexin gene linked to sensorineural hearing loss (Johnson et al., 2017) and its mechanism of action in the cochlea remains uncertain, it is the connexin of focus in the present study. Cx26 has been shown to facilitate the passage of miRNAs necessary for coordinated development and differentiation of the organ of Corti (Zhao, 2017). Thus, Cx26 status may impact the expression of key factors necessary for proper organ of Corti formation. These factors include the Sox2 transcription factor, which is necessary for

the designation of the prosensory domain containing progenitor cells (Atkinson et al., 2018). Increased expression of the transcription factor Atoh1 is essential for the initiation of hair cell differentiation (Chonko et al., 2013). Many other proteins are exclusively expressed in mature hair cells such as the motor protein prestin, unconventional myosin proteins, and calcium binding proteins (Hasson et al., 1995; Zheng et al., 2000; Keller et al., 2014). Nevertheless, the mechanisms underpinning how Cx26 mutations and aberrant Cx26 channel function influences gene expression as well as differentiation and maintenance of hair cells within the organ of Corti remains unclear.

In order to examine Cx26 mutants in a more hearing-relevant cellular context, we employed HEI-OC1 cells derived from the progenitor region of P7 mouse cochlear explants, associated with the epithelium of the organ of Corti. These cochlear-relevant cells have been shown to differentiate into both supporting cells and hair cell-like cells that express hair cell specific genes (Kalinec et al., 2003; Kalinec G. M. et al., 2016; So et al., 2005; Park et al., 2016). HEI-OC1 cells have been utilized as a model to study cell fate and differentiation, and the onset of hearing loss that occurs after therapeutic drug usage (Youn et al., 2015; Kalinec G. M. et al., 2016; Kim et al., 2016; Pang et al., 2018; Choi et al., 2019; Lim et al., 2019). Surprisingly, HEI-OC1 cells lack the protein expression of Cx26 and Cx30 found in the organ of Corti, but abundantly express Cx43. In the current study, we selected four different missense *GJB2* mutations, which result in either syndromic or non-syndromic hearing loss, in order to compare and contrast their cellular localization and function in auditory cells before and after Cx43 ablation. Collectively, we identified that the selected Cx26 mutants acquired three cellular phenotypes that underpin how they cause either syndromic or non-syndromic hearing loss.

MATERIALS AND METHODS

Cell Culture and Reagents

House Ear Institute-Organ of Corti 1 (HEI-OC1) cells were generously provided by Dr. Kalinec (House Ear Institute, Los Angeles, CA) (Kalinec et al., 2003; Kalinec G. et al., 2016; Kalinec G. M. et al., 2016; Kelly et al., 2019). HEI-OC1 cells were grown as we recently described (Abitbol et al., 2020). To induce hair cell-like cell differentiation, HEI-OC1 cells that were ∼80% confluent were transferred into non-permissive conditions (39°C and 5% CO_2) for ten days and regular media was replenished every other day to remove dead cells.

Cell Engineering

The *Gja1* gene encoding Cx43 was ablated from mouse HEI-OC1 cells using a CRISPR-Cas9 strategy as we described (Abitbol et al., 2020). These Cx43-null cells are referred to as Cx43 knockout (KO) cells. Constructs encoding wild type (WT) Cx26, Cx30, and Cx26 mutants (N54K, S183F, R32H, and R184P) were sub-cloned into moxGFP vectors (Addgene). Sequences were verified by NorClone Biotech Laboratories. Cx26-RFP and Cx30-RFP were generated as previously described (Berger et al., 2014). HEI-OC1 cells at ∼60% confluency in six well dishes were transiently transfected with 1 μg of the desired cDNA construct using Mirus TransIT-LT1 Transfection Reagent (Cat# MIR2304, Mirus Bio). Co-transfection of Cx26-RFP and Cx30-RFP with Cx26 mutant constructs were done at a 1:1 ratio consisting of 0.75 μg of each cDNA vector to approximate equal protein expression. Cells were then fixed ∼30 h after a successful transfection. In some cases where cells were prepared for imaging, HEI-OC1 cells that lacked Cx43, were grown on 35 mm glass bottom dishes coated with sterile filtered type I rat tail collagen (Cat# 354236, Corning Life Sciences) diluted in 0.02 M acetic acid for one hour. Once cells were ∼60% confluent they were transfected with 1 μg of either Cx26-GFP or S183F-GFP cDNA constructs using Mirus TransIT-LT1 Transfection Reagent. For all experiments involving Cx43 KO cells, two independent CRISPR clones were used and pooled together for analysis.

Western Blotting and Immunofluorescence

Western blotting for Cx43, Cx30, Cx26, and GAPDH was performed on HEI-OC1 cell lysates using immunoblotting procedures as we described (Abitbol et al., 2020). Primary antibodies included: mouse anti-GAPDH (1:5000, Cat# MAB374, EMD Millipore), rabbit anti-GAPDH (1:5000, Cat# G9545, Sigma), rabbit anti-Cx43 (1:5000, Cat# C6219, Sigma), mouse anti-Cx26 (1:1000, Cat# 138100, Life Technologies), and rabbit anti-Cx30 (1:1000, Cat# 712200, Life Technologies). For immunofluorescence, HEI-OC1 cells grown on glass coverslips were fixed with 4% paraformaldehyde for 10 minutes prior to being washed with phosphate-buffered saline (PBS). HEI-OC1 cells treated with 0.1% Triton X-100 + 3% bovine serum albumin (BSA) for one hour were incubated with primary antibodies diluted in 0.1% Triton X-100 + 3% BSA overnight at 4°C. Primary antibodies included: rabbit anti-Cx43 (1:750, Cat# C6219, Sigma), mouse anti-Cx26 (1:200, Cat# 138100, Life Technologies), rabbit anti-Cx30 (1:200, Cat# 712200, Life Technologies), mouse anti-GM130 (1:500, Cat# 610822, BD Biosciences), rabbit anti-EEA1 (1:500, Cat# ab2900, Abcam), rabbit anti-prestin (1:200, Cat# AV447176, Sigma), and mouse anti-Sox2 (1:50, Cat# sc-365823, Santa Cruz). Coverslips were washed with PBS and incubated with secondary antibodies diluted in 0.1% Triton X-100 + 3% BSA for one hour at room temperature. Secondary antibodies included: goat anti-mouse 633 (Cat# A21052, Invitrogen), goat anti-rabbit 568 (Cat# A11036, Invitrogen), and goat anti-mouse 555 (Cat# A21422, Invitrogen). Cells were stained with Hoechst (1:1000 diluted in distilled H_2O, Cat# H3570, Molecular Probes) for 10 minutes to visualize the nuclei and coverslips were mounted using Airvol. C57BL/6 mouse cochleae were dissected and used in a cell lysate or cryosectioned, and immunolabeled as previously described (Kelly et al., 2019). Mouse usage for this purpose was approved by the Animal Care Committee at the University of Western Ontario. Cell images were captured using a Zeiss LSM800 confocal microscope equipped with airyscan and a 63x oil immersion objective. Representative images of wild-type connexins and Cx26 mutants were selected from a minimum of three independent transfections involving four coverslips

per treatment and after interrogation of dozens of transfected cells per coverslip.

Scrape Loading Dye Transfer

Wild type and Cx43-ablated HEI-OC1 cells were seeded onto culture dishes coated with sterile filtered type I rat tail collagen diluted in 0.02 M acetic acid. Once cells were ∼80% confluent they were washed twice with Hank's balanced salt solution (HBSS) and a scrape line was made in the presence of the gap junction permeable molecule, neurobiotin (2 mg/ml, Cat# SP-1120, Vector), and the gap junction impermeable molecule, dextran rhodamine (0.5 mg/ml, Cat# D1824, Invitrogen). After five minutes at 33°C and 10% CO_2, the cells were washed with HBSS and fixed for 10 min in 4% paraformaldehyde. Cells were permeabilized in 0.1% Triton X-100 for 30 min, before incubating for one hour in the presence of Alexa Fluor 488-conjugated streptavidin (1:1000, Cat# S11223, Invitrogen) to label the trapped neurobiotin. Samples were imaged using a Zeiss LSM 800 confocal microscope equipped with a 10x objective. In three independent experiments, a minimum of six images were taken per experiment and four measurements per image were collected for a total of at least 72 individual measurements. ImageJ was used to measure the distance of neurobiotin spread (μm) beyond the first row of damaged cells along the scrape line and an unpaired *t*-test was performed.

Fluorescence Recovery After Photobleaching (FRAP)

Cell cultures expressing Cx26-GFP or S183F-GFP were incubated in HBSS containing 2 mM calcein-AM for five minutes at room temperature. Cell cultures were washed with HBSS and replenished with warm media at 33°C prior to imaging selected regions where adjacent cells expressed fluorescent protein-tagged Cx26 or S183F. A region of interest (ROI) was photobleached to ∼30% of initial fluorescence intensity. FRAP images were captured every 10 seconds for five minutes and dye recovery within the ROI was determined using the Time Series Analyzer V3 plugin on ImageJ. For each ROI, fluorescence recovery was measured using Recovery (%) = $(F_t - F_0/F_b) \times 100$ (F_t fluorescence at each time point after photobleaching, F_0: fluorescence at 0 s after photobleaching, F_b: fluorescence before photobleaching) (Simek et al., 2009). Fluorescence recovery was plotted as an average of three replicates each consisting of a minimum of four pairs of connexin or mutant expressing cells. The mean area under the curve was then calculated and compared using an unpaired *t*-test. Negative controls consisted of FRAP imaging of Cx43-ablated HEI-OC1 cells.

Quantitative Real Time Polymerase Chain Reaction

Total RNA was collected from permissive and non-permissive HEI-OC1 cells after differentiation using RNeasy Mini Protocol for Isolation of Total RNA from Animal Cells (Cat# 74106, Qiagen) and was converted to cDNA using the High Capacity cDNA Reverse Transcription Kit (Cat# 4368814, Applied Biosystems). qRT-PCR was conducted using PowerUp SYBR Green Master Mix (Cat# A25742, Life Technologies) and the cycle conditions for each primer consisted of: 50°C for 2 min, 95°C for 2 min, 95°C for 5 s, and 60°C for 15 s for 40 cycles, followed by a melt curve. The following primers were used: 18s rRNA, the house keeping gene (forward, 5′-GTAACCCGTTGAACCCCATT; reverse, 5′-CCATCCAATCGGTAGTAGCG), Atoh1 (forward, 5′- GAGTG GGCTGAGGTAAAAGAGT; reverse, 5′- GGTCGGTGCTA TCCAGGAG), calsequestrin (forward, 5′- CGAGACTTGGG AGGATGACC; reverse, 5′- TCGGGGTTCTCAGTGTTGTC), myosin VIIa (forward, 5′- TGGTACACTTGACACTGAAG; reverse, 5′- CCATCGTTCAGCCTCTTGGT), and nestin (forward, 5′- GCTGGAACAGAGATTGGAAGG; reverse, 5′- CCAGGATCTGAGCGATCTGAC). mRNA levels were normalized to 18S rRNA levels and measured using the $2^{-\Delta\Delta CT}$ method.

Statistical Analysis

A two-way ANOVA and a Tukey's *post hoc* test was used to determine statistical significance between mRNA expression of permissive and non-permissive WT and Cx43-ablated cells. An unpaired *t*-test was used to compare mRNA expression before and after differentiation.

All statistical analysis was conducted using Graph Pad Prism 6 and results were indicated as statistically significant when $P < 0.05$. Outliers were removed using the ROUT method with Q set to 1%. Results are presented as mean ± SEM unless stated otherwise.

RESULTS

HEI-OC1 Cells Express Cx43 but Become GJIC-Deficient Upon Its Ablation

Previous studies have used cells unrelated to the organ of Corti to characterize the etiology of several hearing loss-linked Cx26 mutants. Here we employed HEI-OC1 cells (Kalinec et al., 2003; Kalinec G. M. et al., 2016) that were derived from the progenitor epithelium of the organ of Corti from P7 mice as a tissue-relevant cell model to assess several Cx26 mutants that have been associated with non-syndromic and syndromic hearing loss. Since western blotting and immunofluorescence revealed that these cells were rich in Cx43 (**Figure 1A**), we used CRISPR-Cas9 to genetically ablate the *Gja1* gene and all subsequent Cx43 expression from these cells (**Figures 1A, B**). Cx43 is not an endogenous connexin typically expressed in the mature organ of Corti (Forge et al., 2003), but is often upregulated in cultured cells. Not surprisingly since the expression of most connexin gene isoforms are silenced in cultured cells, neither Cx26 or Cx30 were expressed in WT cells or found in cells lacking Cx43 (**Figures 1A,B**).

To investigate the consequence of Cx43 ablation on GJIC, confluent cultures of WT HEI-OC1 cells and cells lacking Cx43 were scraped and incubated with a gap junction permeable positively charged small molecule, neurobiotin (287 Da). Neurobiotin was found to spread beyond the first row of damaged cells to an average distance of 122.3 μm in WT cells, but in

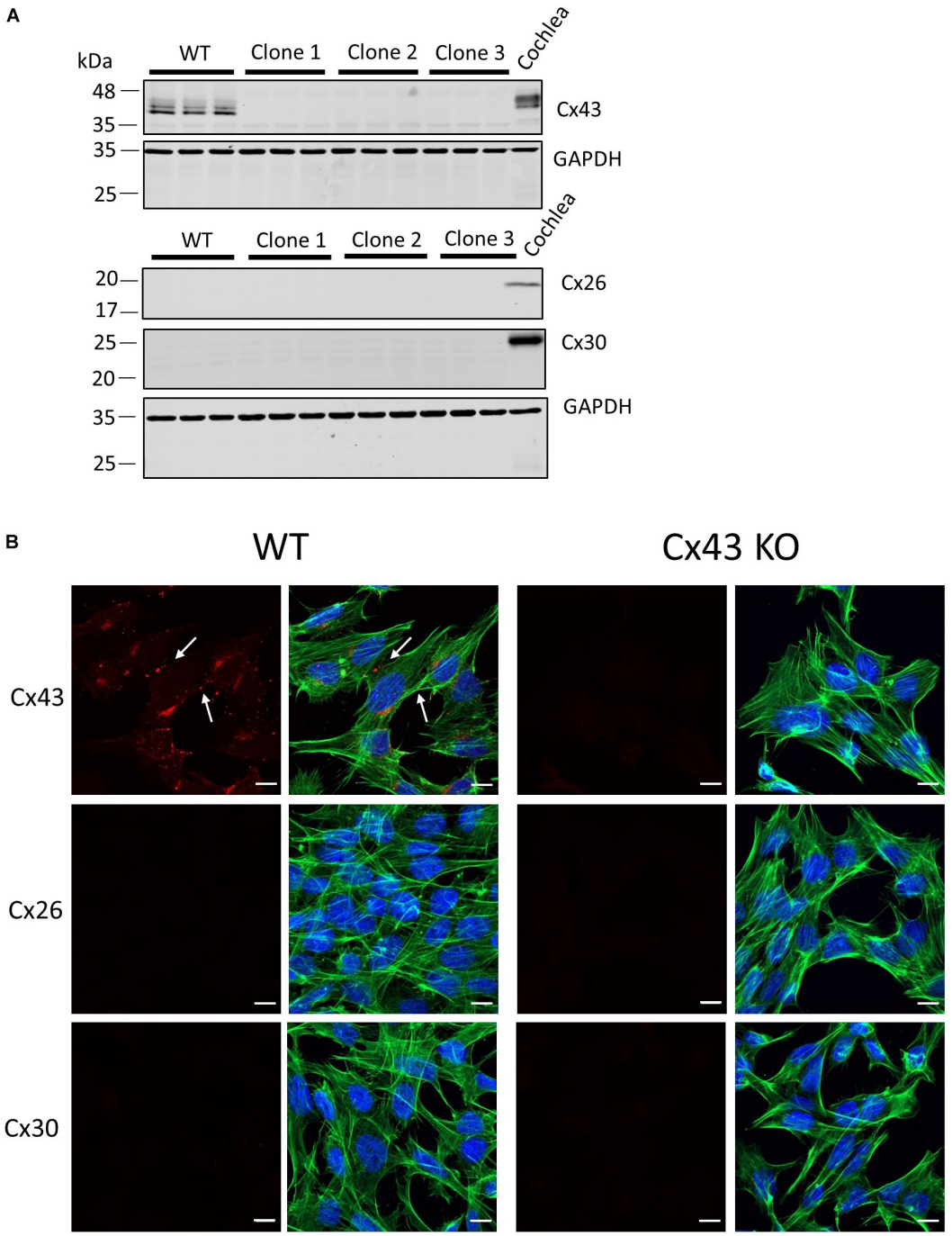

FIGURE 1 | Characterization of connexin expression and Cx43 ablation in HEI-OC1 cells. **(A)** Western blots for Cx43, Cx26, and Cx30 protein in wild type (WT) and three independent clones of CRISPR-Cas9 Cx43-knockout (Cx43-KO) HEI-OC1 cells where adult mouse cochlear lysate was used as a positive control. Molecular weight standards are denoted in kDa. **(B)** Immunolabeling revealed Cx43 gap junctions only in WT cells denoted by white arrows. Note Cx26 and Cx30 were not detected in WT or Cx43 KO cells **(A,B)**. Red = Cx43, Cx26, and Cx30, green = phalloidin staining of actin filaments, blue = Hoechst stained nuclei. Bars = 10 μm.

Cx43 KO cells neurobiotin travelled only an average distance of 13.4 μm (**Figure 2A**). FRAP was also completed to further determine the level of GJIC in HEI-OC1 cells using a negatively charged gap junction permeable dye calcein-AM (623 Da). FRAP revealed that the Cx43-rich WT cells were significantly more capable of passing calcein through gap junctions than Cx43 KO cells (**Figure 2B**). These findings demonstrate that WT HEI-OC1 cells have abundant gap junction function, while the lack of Cx43 greatly reduced GJIC. Thus, Cx43 KO cells were utilized as GJIC-deficient in subsequent experiments, where Cx26

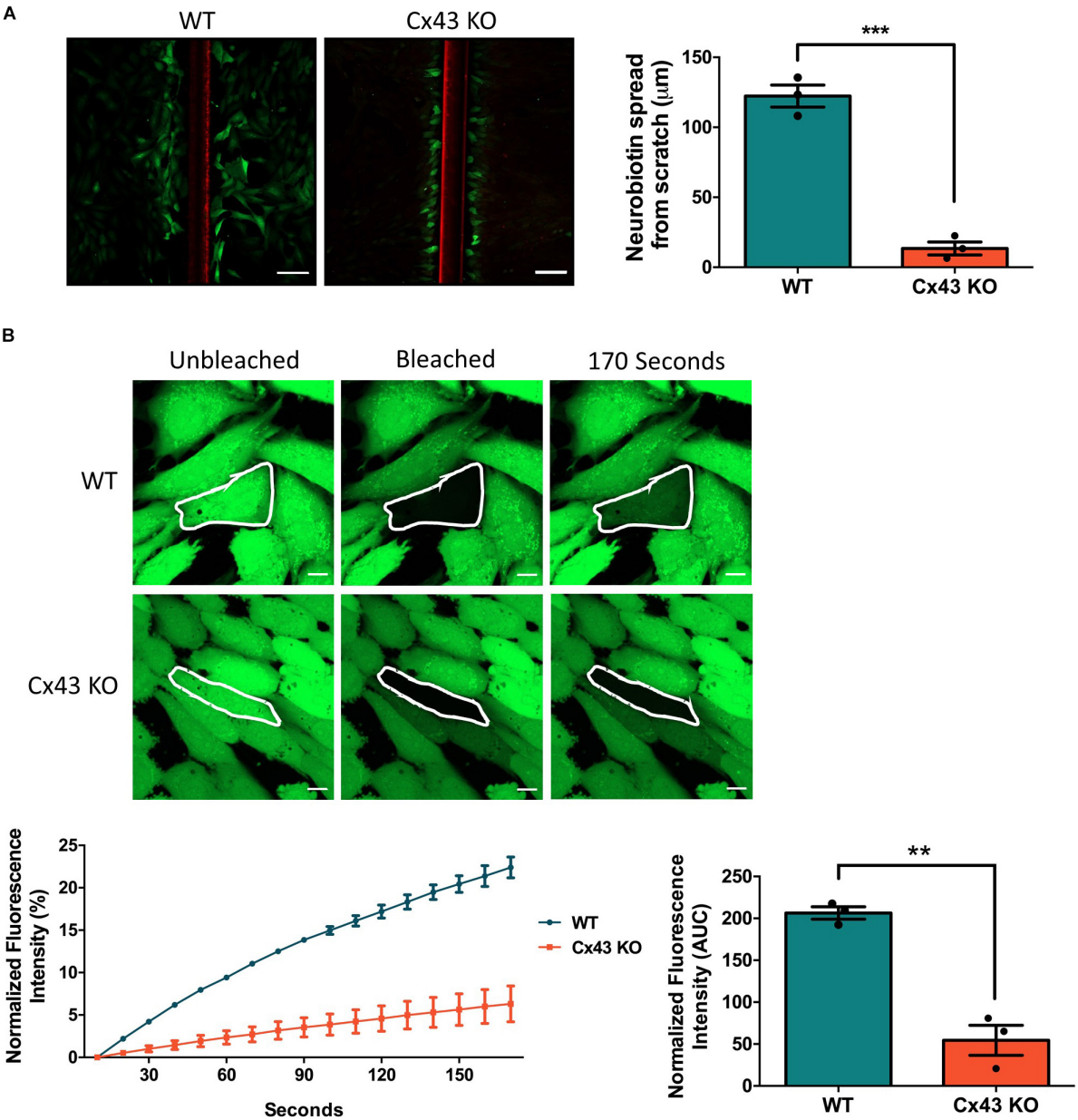

FIGURE 2 | Ablation of Cx43 greatly reduces dye transfer. **(A)** Representative micrographs of a scrape loading dye transfer assay performed on WT and Cx43 KO HEI-OC1 cells. Cells were scraped and incubated with the gap junction permeable tracer neurobiotin (green) and impermeable dextran rhodamine dye (red) that typically gets washed out during the sample preparation. Cx43 KO cells exhibited significantly less neurobiotin transfer from the first row of damaged cells than WT cells. **(B)** Representative micrographs of WT and Cx43 KO cells loaded with calcein-AM and subjected to fluorescence recovery after photobleaching of a selected cell (outlined in white). Dye recovery and area under the curve (AUC) was measured over 170 s. Cx43 KO cells had significantly less dye recovery after photobleaching compared to WT cells. Data represent mean ± SEM from three independent experiments and were analyzed using an unpaired *t*-test. ***$p < 0.001$, **$p < 0.01$. Bars in **(A)** = 100 μm and **(B)** = 10 μm.

mutants could be expressed in a connexin-deficient cochlear-relevant cell system.

Differential Distribution of Cx26 Mutants in Cx43 KO Cells

To assess the localization of various hearing loss-linked Cx26 mutants, WT Cx26 and N54K, S183F, R32H, and R184P Cx26 mutants were expressed in Cx43 KO cells. Cx26 successfully trafficked to the plasma membrane and gap junction plaques were readily found (**Figure 3A**). In comparison to WT Cx26, the syndromic N54K mutant was retained within an intracellular compartment, but did not colocalize well with the GM130 resident protein of the Golgi apparatus (**Figure 3A**). In contrast, the syndromic S183F mutant was able to traffic

to the plasma membrane and form gap junction plaques (**Figure 3A**), although some intracellular reservoirs of the mutant were found. Both recessive non-syndromic R32H and R184P mutants did not form clearly identifiable gap junction plaques but appeared to be partially localized within intracellular vesicles (**Figure 3A**). Some of these intracellular vesicles containing R32H and R184P immunolabeled for EEA1, an early endosomal marker (**Figure 3B**). Overall, the S183F mutation found within the 2nd extracellular loop (**Figure 3C**), was the mutant most capable of forming gap junction plaques in Cx43 KO cells.

The S183F Mutant Forms Gap Junction Channels Incapable of Dye Transfer

FRAP was conducted using calcein-AM dye to analyze whether the S183F mutant formed gap junction channels capable of dye transfer. Cx43 KO cell pairs or cell clusters expressing Cx26 or the S183F mutant were subjected to FRAP as a surrogate to measure GJIC. S183F-GFP expressing cells, similar to Cx43 KO cells, exhibited essentially no fluorescence dye recovery after photobleaching compared to Cx26-GFP expressing cells, quantified by measuring the area under the curve (**Figures 4A–C**).

Cx30, but Not Cx26, Can Rescue the Assembly of the N54K Mutant Into Gap Junctions

Since autosomal dominant inherited Cx26 mutants are co-expressed with WT Cx26, we examined whether GFP-tagged N54K and S183F mutants might alter the intracellular localization of RFP-tagged WT Cx26. While both the S183F mutant and WT Cx26 could be found within the same gap junctions at the cell surface and within intracellular structures, the N54K mutant colocalized with WT Cx26 within intracellular stores but not typically with Cx26-RFP gap junction plaques (**Figure 5**). This suggests that WT Cx26 could not intermix with the N54K mutant and rescue its assembly into gap junction plaques but rather the N54K mutant impeded the trafficking of Cx26.

Cx30 is also highly expressed in the organ of Corti and co-oligomerizes with Cx26 to form mixed gap junction plaques *in vivo* (Ahmad et al., 2003). As might be expected, we found that Cx30-RFP could form gap junctions in Cx43 KO cells (**Figure 6A**). We next tested if this Cx30 tissue-relevant connexin could interact with the Cx26 N54K mutant and potentially rescue its assembly into cell surface gap junctions. As also observed for the S183F mutant, the N54K mutant extensively co-localized with Cx30-RFP including within many gap junctions at sites of cell-cell apposition. However, the autosomal recessive inherited R32H and R184P mutants showed very little co-localization with Cx30 (**Figure 6B**). These results suggest that both the syndromic mutants (N54K and S183F) have transdominant properties and intermix with Cx30 while the non-syndromic mutants (R32H and R184P) do not.

The S183F Mutant Intermixes With Endogenous Cx43 Gap Junctions

The expression of Cx43 in the mature organ of Corti appears negligible, however Cx43 is temporally expressed during development of the human and mouse inner ear (Cohen-Salmon et al., 2004; Locher et al., 2015). Hearing loss-linked Cx26 mutants may therefore be co-expressed with Cx43 during the development of the inner ear. To assess whether Cx26 mutants have gain-of-function properties and intermix with Cx43 within the same gap junctions, the Cx26 mutants were expressed in WT HEI-OC1 cells that contain endogenous Cx43. Previous studies have shown that Cx26 and Cx43 do not intermix to form heteromeric gap junctions under physiological conditions, but are able to partition to separate domains within the same gap junction plaques (Falk, 2000; Gemel et al., 2004). Both Cx26 and Cx43 formed gap junction plaques in HEI-OC1 cells, however, they appeared to segregate within different regions of the gap junction plaques (**Figures 7A, B**). Similarly, the N54K, R32H, and R184P mutants all localized to distinct locations from Cx43 (**Figure 7A**). However, the S183F mutant not only colocalized with Cx43 into the same gap junctions, but high magnification enface images revealed that the Cx26 S183F mutant and Cx43 were evenly distributed throughout the gap junction plaque suggesting that they intermixed indicative of a gain-of-function channel characteristic (**Figure 7B**).

Cx43 and GJIC Are Not Necessary for the Partial Differentiation of HEI-OC1 Cells

HEI-OC1 cells have previously been shown to differentiate into hair cell-like cells under non-permissive conditions by upregulating hair cell specific molecular markers (Kalinec G. M. et al., 2016). Here we show that after ten days in non-permissive conditions designed to promote cell differentiation, both WT and Cx43 KO cell cultures contained heterogeneous clusters of cells that increased in size (arrows) while others continued to proliferate or undergo apoptosis (**Figure 8A**). Immunolabeling for the hair cell marker protein, prestin, revealed its detection in outer hair cells of the mouse cochlea, but no prestin was detected in HEI-OC1 cells grown in permissive or non-permissive temperatures (**Figure 8B**). Consistently, we did not observe the expected decrease in Sox2 labeling, a progenitor cochlear cell marker, in Cx43-negative or WT HEI-OC1 cells which would be expected if these progenitor cells had successfully differentiated into hair cell-like cells. This premise was supported by the fact that the mRNA expression of Atoh1, a transcription factor expressed during the initiation of hair cell development, was not altered under non-permissive conditions in either WT or Cx43 KO cells (**Figure 9A**). However, we suspected that the HEI-OC1 cells may have partially differentiated but failed to progress to a mature hair cell-like state. In support of this notion, qPCR results provided evidence that mature hair cell markers calsequestrin and myosin VIIa both significantly increased in Cx43 KO cells in non-permissive conditions, whereas calsequestrin also increased in WT cells (**Figures 9B, C**), suggesting that both the Cx43-rich and null HEI-OC1 cells exhibit some capacity to reprogram genes necessary for cell differentiation. Yet, the mRNA expression

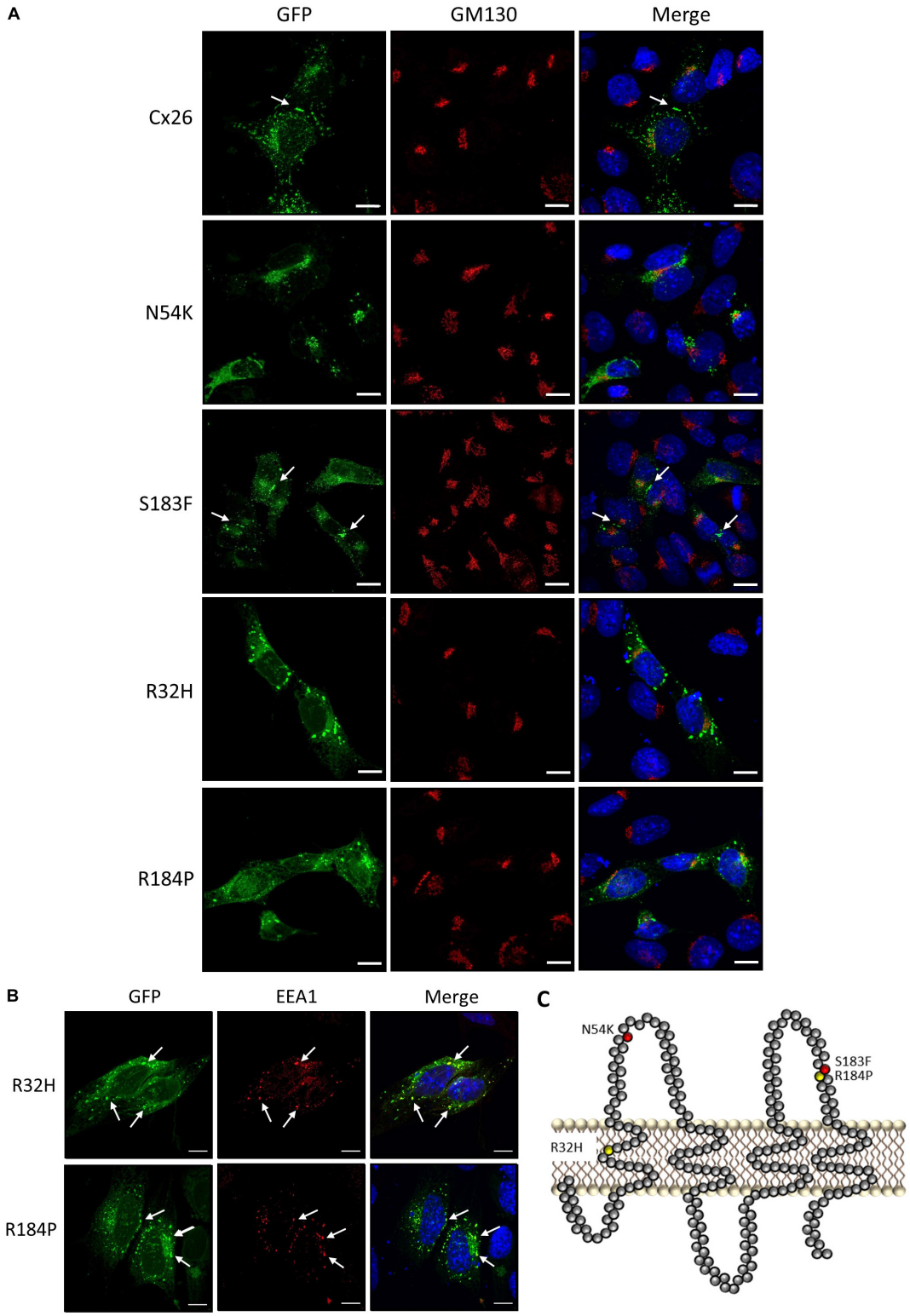

FIGURE 3 | Intracellular localization of syndromic and non-syndromic hearing loss-linked Cx26 mutants **(A)** Representative micrographs of Cx26-GFP and various GFP-tagged hearing loss-linked Cx26 mutants transiently expressed in Cx43 KO cells. Cells were co-immunolabeled with GM130 (red) to visualize the location of the Golgi apparatus and Hoechst (blue) to visualize the nuclei. The N54K, R32H, and R184P mutants failed to form gap junctions. Arrows denote gap junction plaques. **(B)** A sub-population of the R32H and R184P mutants co-localized with EEA1, an early endosomal marker, denoted by arrows. **(C)** Topological model of Cx26 depicting the approximate locations of the syndromic (red) and non-syndromic (yellow) mutations. Bars = 10 μm.

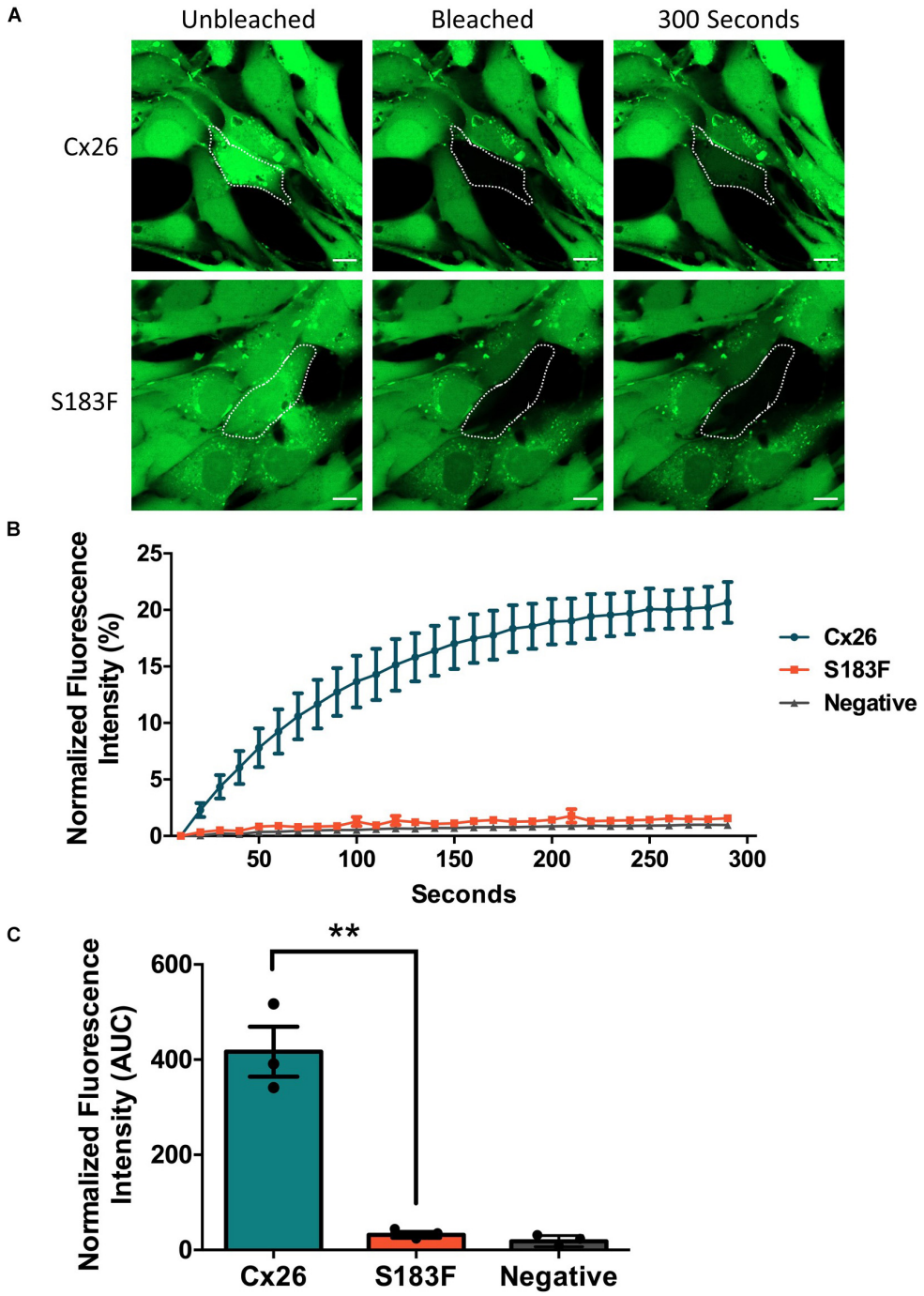

FIGURE 4 | The S183F mutant does not form dye-permeable gap junction channels. **(A)** Negative (Cx43 KO cells) or Cx43 KO cells expressing Cx26-GFP or S183F-GFP were loaded with gap junction permeable dye calcein-AM (green) and subjected to FRAP. **(B)** A selected cell within a pair or cluster of Cx26 or S183F mutant expressing cells was photobleached and dye recovery over 300 s was measured. **(C)** Area under the curve (AUC) of fluorescence recovery was measured. Cx43 KO cells and cells expressing the S183F mutant had negligible dye recovery while WT Cx26 expressing cells exhibited significant dye recovery. Data represents mean ± SEM of three independent experiments and were analyzed using an unpaired *t*-test, $^{**}p < 0.01$. Bars = 10 μm.

of the intermediate filament protein nestin, a stem-cell like marker found in cochlear progenitor cells and downregulated as cochlear development proceeds, was not altered in non-permissive conditions (**Figure 9D**). Overall, both WT and Cx43 KO cells may have initiated some gene regulation to promote cell differentiation but this was insufficient to drive major cellular changes in the majority of the cells and appeared independent of the presence of Cx43 and overall GJIC.

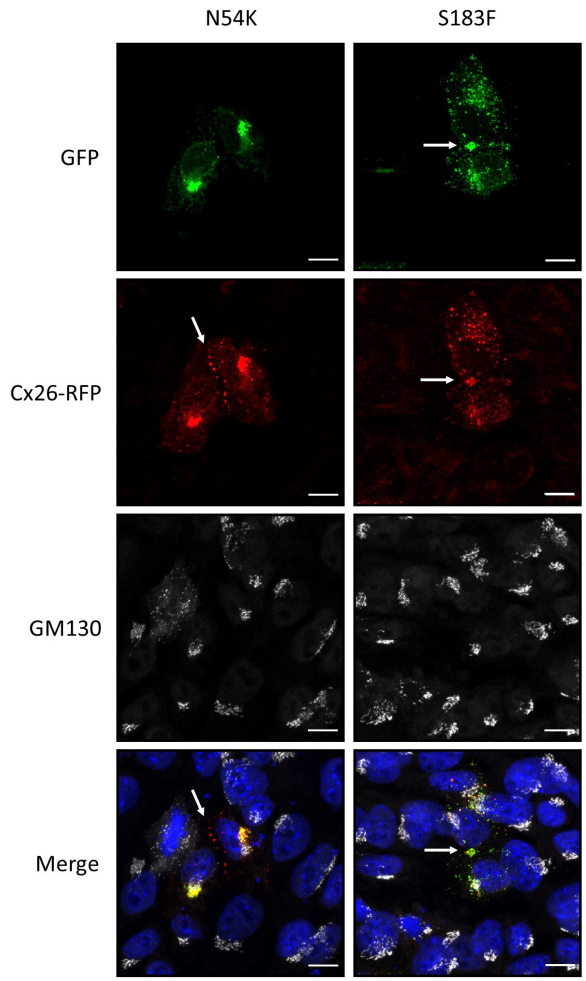

FIGURE 5 | The expression of Cx26-RFP did not alter the distribution of the N54K or S183F mutant. Representative micrographs of Cx43 KO HEI-OC1 cells co-expressing Cx26-RFP and N54K-GFP or S183F-GFP. Cells were immunolabeled with GM130 (white) to visualize the location of the Golgi apparatus and counterstained with Hoechst (blue) to demarcate the nuclei. Bars = 10 μm.

DISCUSSION

Understanding the etiology of connexin gene mutations linked to hearing loss remains an essential step for connexin therapeutics and in the emerging therapeutic era of strategic gene editing (Laird and Lampe, 2018). In the past, many non-tissue relevant and often cancerous cell lines have been used to express Cx26 mutants to uncover that *GJB2* gene mutations linked to hearing loss fall into either loss-of-function or gain-of-function mutations (White, 2000; Zhao et al., 2006; Sanchez and Verselis, 2014). However, conclusions from these less than ideal cell culture models must be extrapolated to a cochlear-relevant context and further translated to the *in vivo* setting with the ultimate hope that they inform on the human condition. In the current study we move one step closer to understanding how various *GJB2* gene mutations cause hearing loss by exploring their characteristics in cochlear-relevant cells obtained from the developing organ of Corti. Using this novel strategy we uncovered that autosomal recessive non-syndromic mutants (R32H and R184P) largely traffic and assemble into gap junctions independent of co-expressed cochlear connexins while autosomal dominant syndromic mutants (N54K and S183F) selectively intermixed with Cx26, Cx30, and Cx43. Our findings in HEI-OC1 cells inform on how strategies to up-regulate compensatory connexins may potentially rescue autosomal recessive hearing loss while such strategies may have limited benefit in autosomal dominant disease due to potential connexin isoform intermixing and inactivation.

HEI-OC1 cells that resemble a common progenitor to supporting cells and hair cells were derived from the epithelial region of the organ of Corti in mouse cochlear explants (Kalinec et al., 2003; Kalinec G. et al., 2016; Kalinec G. M. et al., 2016; Kelly et al., 2019). In keeping with most cell lines grown in culture, we observed that Cx43 was abundantly expressed in HEI-OC1 cells. To circumvent the fact that Cx43 is not the predominant connexin isoform found in the mature organ of Corti, we used CRISPR-Cas9 to ablate Cx43 from HEI-OC1 cells and established a Cx43 KO cell platform for the controlled reintroduction of cochlear-relevant connexins and hearing loss-linked mutants. In excess of 135 mutations in the *GJB2* gene encoding Cx26 have been linked to inherited sensorineural hearing loss ranging from moderate to profound severities (Laird et al., 2017) but none of these Cx26 mutants have been investigated in a cochlear-relevant cell line that has retained some capacity for differentiation.

Hearing loss-linked single amino acid substitutions have been identified in each of the five major Cx26 polypeptide domains signifying the importance of each domain (Martinez et al., 2009; Xu and Nicholson, 2013). Here, we chose to examine two mutations linked to syndromic hearing loss (N54K and S183F) (Richard et al., 2004; de Zwart-Storm et al., 2008; Shuja et al., 2016; Press et al., 2017) and two mutations linked to non-syndromic hearing loss (R32H and R184P) (Rabionet et al., 2000; Santos et al., 2005; Mani et al., 2009; Xiao et al., 2011). Our strategy was to use two mutations found within or near each of the 1st and 2nd extracellular loop regions of Cx26. Interestingly, only one of the mutants in each domain caused syndromic disease suggesting that the defect caused by each amino acid substitution can have profoundly different functional outcomes and disease burden.

Both dominant syndromic mutations (N54K and S183F) are found in extracellular loop domains of Cx26 thought to be critical in hydrogen bond-mediated hemichannel docking to form a fully functional gap junction channel (Bruzzone et al., 1996; Maeda et al., 2009). The substitution of asparagine to a lysine (the N54K mutant) results in Cx26 being retained in an intracellular compartment manifesting as the skin pathology Bart-Pumphrey syndrome with accompanying hearing loss (Richard et al., 2004). The intracellular retention of the N54K mutant and its inability to form gap junctions was further supported by our previous studies in HeLa cells and rat epidermal keratinocytes (Press et al., 2017). In the current study, we show that the N54K mutant is indeed retained in an intracellular compartment when expressed alone in GJIC-deficient cochlear-relevant cells. However, when this

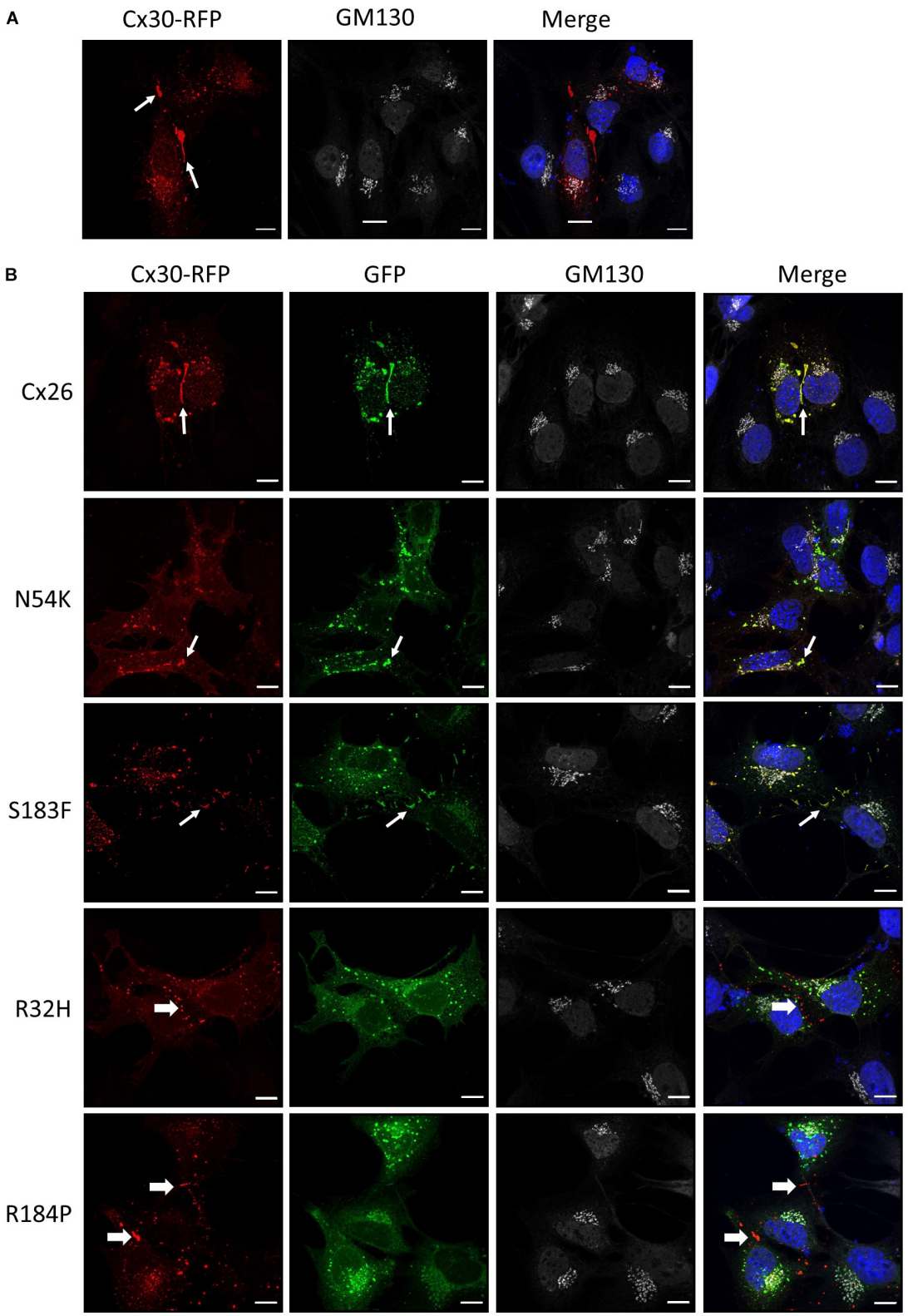

FIGURE 6 | Cx30 expression partially rescued the aberrant localization of the N54K mutant. **(A)** Cx30-RFP assembled into gap junctions (arrows) when expressed in Cx43 KO cells that were immunostained for GM130 (white) and counterstained with Hoechst (blue) to demarcate the nuclei. **(B)** Cx30 and co-expressed Cx26 or the S183F and N54K mutants localized within the same gap junction plaques, denoted by the thin white arrows. Both recessive mutants, R32H and R184P, remained intracellularly and failed to co-localize with Cx30 (thick arrows). Bars = 10 μm.

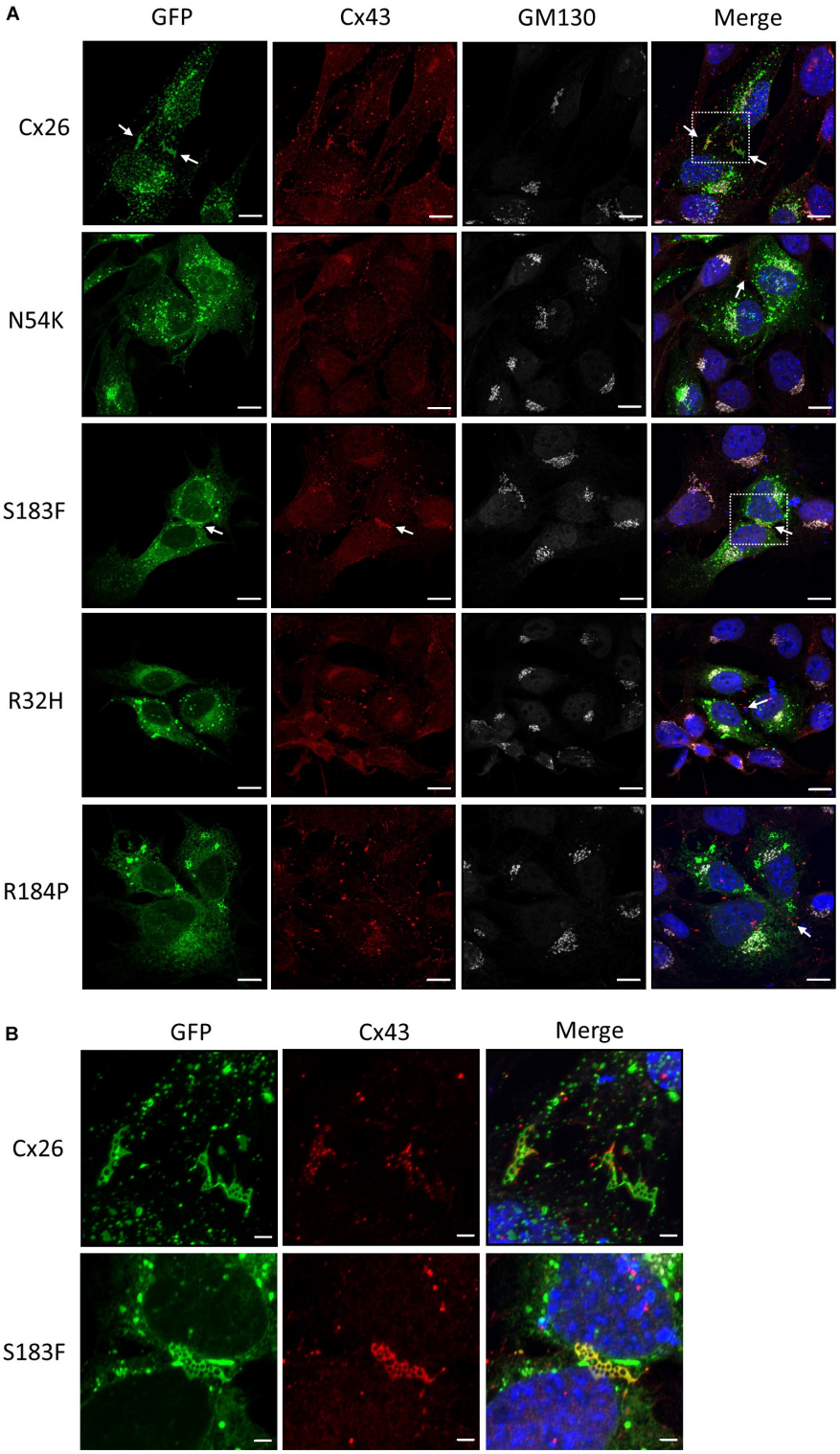

FIGURE 7 | The S183F mutant intermixes with endogenous Cx43 within the same gap junctions. **(A)** Representative micrographs of wild type HEI-OC1 cells expressing Cx26-GFP or Cx26 mutants, and co-immunolabeled for Cx43 (red) and GM130 (white) prior to counterstaining with Hoechst (blue). The N54K, R32H, and R184P mutants typically localize to sites that do not contain Cx43 while WT Cx26 and the S183F mutant appear to closely associate with the position of Cx43 (arrows). **(B)** High magnification of dashed boxed image areas in **(A)** revealed that WT Cx26 segregates to gap junction domains that are part of a Cx43 gap junction (note the separation of red and green signals). However, *en face* imaging of S183F expressing cells revealed that Cx43 and the S183F mutant fully intermixed as revealed by the yellow color. Bars = 10 μm.

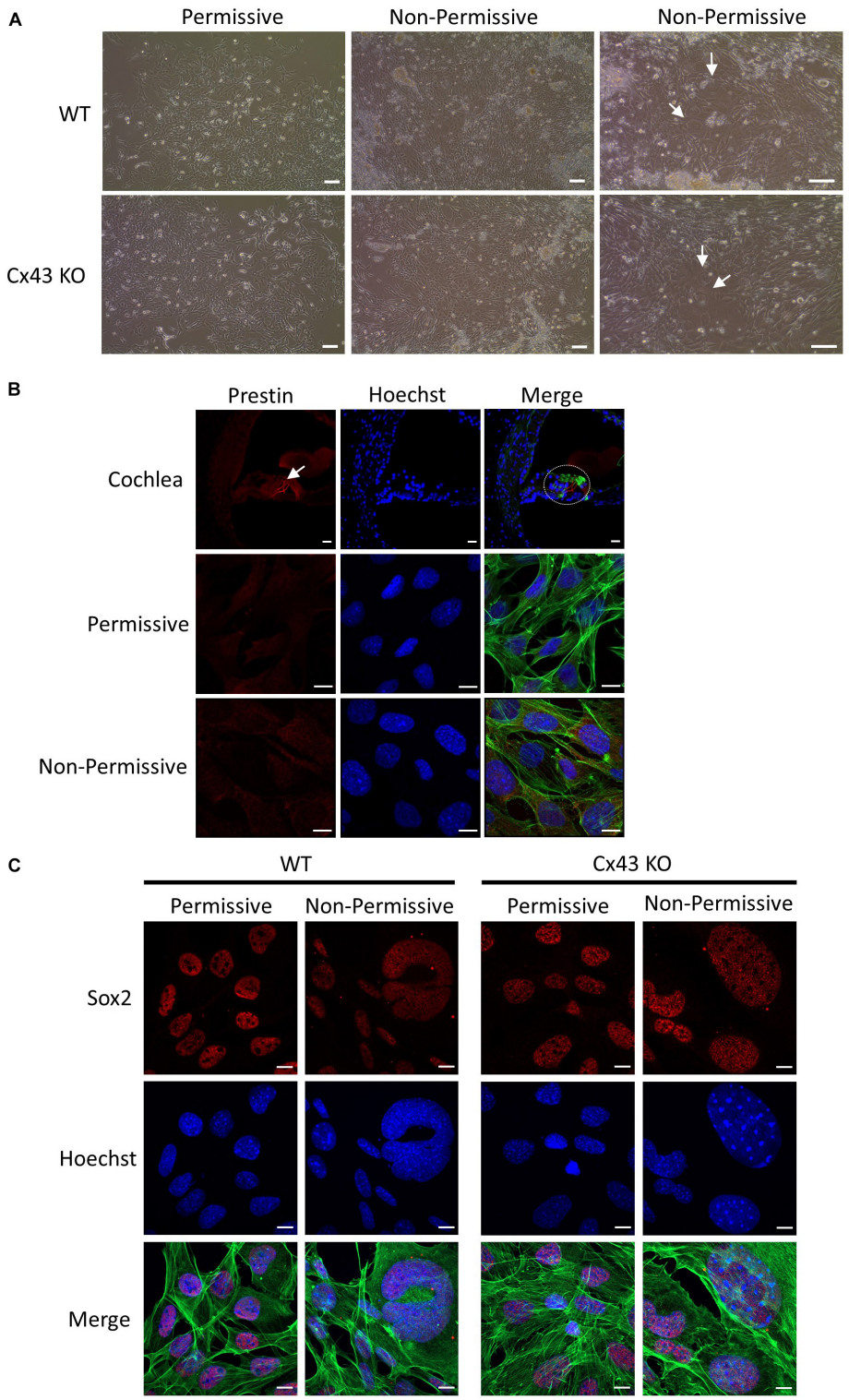

FIGURE 8 | HEI-OC1 cells enlarged but failed to exhibit characteristics of hair cell-like cells when induced to differentiate. **(A)** Light microscope images of WT and Cx43 KO HEI-OC1 cells grown in permissive and non-permissive conditions for 10 days. Arrows denote large cells that appear to have undergone some level of differentiation. **(B)** The motor protein prestin (red) was successfully detected in outer hair cells of a postnatal mouse cochlea cross section (dashed oval) but was not detected in WT HEI-OC1 cells grown in permissive or non-permissive conditions. **(C)** The progenitor cell marker Sox2 (red) expression was detected in HEI-OC1 cells cultured under all conditions. Green = xphalloidin staining, blue = Hoechst stained nuclei. Bars = (A) HEI-OC1 cells = 100 μm, **(B,C)** HEI-OC1 cells = 10 μm, **(B)** cochlea = 20 μm.

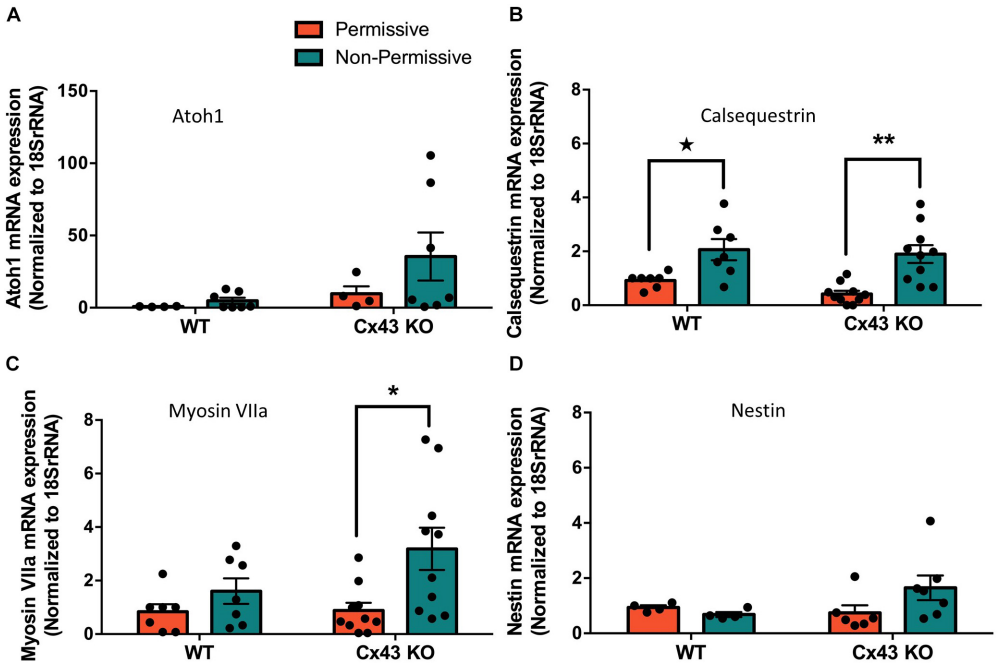

FIGURE 9 | Partial differentiation of HEI-OC1 cells in non-permissive cultures was independent of Cx43 status. **(A)** Real-time qPCR normalized to 18SrRNA revealed that Atoh1 mRNA levels were unchanged when wild type (WT) or Cx43 KO cells were grown for 10 days in non-permissive conditions. **(B)** WT and Cx43 KO cells exhibited increased calsequestrin mRNA levels when cultured in non-permissive conditions, and **(C)** Cx43 KO cells had higher myosin VIIa mRNA levels. **(D)** The progenitor cell marker nestin mRNA expression was unaltered under any conditions tested. Data represent mean ± SEM of four independent experiments comprised of two independent Cx43 KO clones. (*$p < 0.05$, **$p < 0.01$ two-way ANOVA and Tukey's *post hoc*, ⋆$p < 0.05$ unpaired *t*-test).

mutant was co-expressed with Cx30, but not typically with Cx26 or Cx43, it was abundantly found in gap junctions suggesting that Cx30 not only intermixed with the N54K mutant but rescued its delivery to the cell surface and assembly into gap junctions. It is notable that the original patients identified to harbor the N54K mutant exhibited a compensatory upregulation of Cx30 (Richard et al., 2004). Collectively, all lines of evidence point to N54K being a loss-of-function trafficking defective mutant that can be rescued by the co-expression of Cx30, which is typically co-expressed with Cx26 in the organ of Corti and may serve to reduce the severity of hearing loss that might otherwise occur.

The second syndromic mutant (S183F) investigated in HEI-OC1 cells exhibited characteristics of being able to form gap junctions. This serine to phenylalanine substitution linked to palmoplantar keratoderma and hearing loss (de Zwart-Storm et al., 2008) was previously shown to form non-functional gap junctions in HeLa cells (Shuja et al., 2016; Press et al., 2017) suggesting that the hydrogen bonding generated by the 2nd extracellular loop is sufficiently retained to ensure hemichannel docking in the assembly of functionally dead gap junctions. In keeping with Shuja et al. (2016) who provided evidence that the S183F mutant may have exhibited the gain-of-function characteristic of being able to intermix with Cx43 into heteromeric and heterotypic channels (Shuja et al., 2016), we also found that the S183F mutant fully intermixed with Cx43 within gap junctions formed in cochlear-relevant cells. These findings are unexpected as normally Cx26 and Cx43 are unable to co-oligomerize and remained segregated to different subdomains of the gap junctions (Falk, 2000), although other Cx26 mutants linked to skin diseases have been shown to intermix with Cx43 (Garcia et al., 2015). Furthermore, the connexin motifs that have been reported to govern oligomerization are believed to be localized between the amino terminal and 3rd transmembrane domain (Martinez et al., 2011) which are distant sites from the location of the S183F mutation. Collectively, these studies point to a new role for the 2nd extracellular loop in governing connexin oligomerization properties. Interestingly, the S183F mutant also retained the properties of being able to reside in both Cx26 and Cx30 gap junctions suggesting that its gain-of-function characteristics of being able to intermix with Cx43 did not come with a concomitant loss of the ability to intermix with these critical cochlear connexins.

Intriguingly, even though Arg184 resides next to Ser183 within the second extracellular loop, homozygous *GJB2* allelic mutations resulting in an arginine to proline (R184P) change only causes hearing loss while heterozygous carriers of this mutation are unaffected (Mani et al., 2009). This arginine residue is thought to be important for inter-protomer interactions between the second extracellular loop and the adjacent connexon (Maeda et al., 2009). The R184P mutant has been reported in reference cells to exhibit some trafficking deficits with an inability to form gap junctions (Bruzzone et al., 2003; Mani et al., 2009; Xiao et al., 2011) and may be prematurely degraded (Thonnissen et al., 2002; Mani et al., 2009). When expressed in cochlear-relevant cells, we found that gap junctions were rarely assembled and this mutant frequently localized to early endosomes suggesting it may

have reached the cell surface before being retrieved for imminent degradation in lysosomes.

The R32H mutation resides within the 1st transmembrane domain near the 1st extracellular domain; a polypeptide motif that likely has multiple roles in the formation of intra-protomer interactions, connexin folding, oligomerization, and channel pore formation (Maeda et al., 2009). Little is known about the fate of the autosomal recessive mutation that encodes the R32H mutant (Mustapha et al., 2001), although one study showed that it localized to the endoplasmic reticulum when expressed in HeLa cells (Xiao et al., 2011). This did not seem to be the case when this R32H mutant was expressed in HEI-OC1 cells as it partially localized to early endosomes with no clear evidence that it was trapped in the endoplasmic reticulum. Thus, this mutant appears to be following a similar fate as the R184P mutant and maybe destined for premature degradation. This finding highlights the importance of examining hearing loss linked mutants in a cochlear-relevant system as their expression within different tissue types may lead to distinctly different outcomes. Our results support the notion that non-syndromic mutants do not acquire gain-of-function properties but cause hearing loss via their loss-of-function and premature targeting to the degradation pathway.

Finally, we wanted to determine if the state of GJIC altered the ability of HEI-OC1 cells to differentiate toward supporting cell and/or hair cell fates. Since Cx43 is endogenously expressed in these cochlear-relevant cells and Cx43 channels typically allows for permissive small molecule exchanges that exceeds the scope of gap junction exchange that can occur through Cx26 channels (Harris, 2008; Lopez et al., 2014), we used these cells as a surrogate for GJIC that occurs *in vivo* and assessed cell differentiation before and after Cx43 ablation. We also knew that GJIC is critically important in the organ of Corti as hair cells are deformed and the tunnel of Corti formed by supporting cells is absent in conditional Cx26 null mouse models (Inoshita et al., 2008; Chang et al., 2015; Zhu et al., 2015; Chen et al., 2018a). Further, transgenic mice expressing the dominant Cx26 mutant R75W displayed delayed apoptosis during cochlear development and the organ of Corti was malformed (Inoshita et al., 2014). In our studies, we found HEI-OC1 cells were not able to fully differentiate into hair cell-like cells expressing protein markers and genes of *in vivo* hair cells, including prestin, even though prestin has previously been reported to be expressed in differentiated HEI-OC1 cells (Kalinec G. M. et al., 2016; Park et al., 2016). We suspect that the HEI-OC1 cells we used are somewhat heterogeneous and may have lost their full potential to differentiate into hair cell-like cells in non-permissive conditions since their original isolation nearly 20 years ago (Kalinec et al., 2003). Nevertheless, we found that there were pockets of cells within the cultures that appeared to differentiate amongst unchanged cells supporting the notion that the cultures had mixed cell phenotypes. Others have noted this heterogeneity amongst different batches of HEI-OC1 cells (Cederroth, 2012). In our studies, we did find that the ablation of Cx43 drove a higher expression of myosin V11a and calsequestrin suggesting that Cx43 mediated GJIC may be acting as a negative regulator of some genes important in cell differentiation. Calsequestrin was also elevated in wild type cells and Sox2 was abundantly found in both Cx43 positive and negative cultures. These findings are all consistent with a small subpopulation of HEI-OC1 cells retaining the capacity to differentiate with the majority of the cells remaining in a progenitor state. Nevertheless, these cells remain the best cochlear-relevant cell line to interrogate the functional status of hearing loss-linked Cx26 mutants.

In summary, sensorineural hearing loss linked to *GJB2* gene mutations is one of the most common inherited conditions found worldwide affecting as many as 1/2000 live births (Chan and Chang, 2014). Our understanding of how these mutations induce hearing loss is still emerging and must be fully understood to establish a platform for tactical drug design and rational treatment strategies. Here, we used a cochlear-relevant cell line to further investigate two syndromic and two non-syndromic Cx26 mutants that are found within or near the extracellular loop regions of the connexin polypeptide. Collectively, we found that each of the syndromic mutations exhibited unique gain-of-function properties while the two non-syndromic mutants exhibited common loss-of-function characteristics.

DATA AVAILABILITY STATEMENT

All datasets generated for this study are included in the article/supplementary material.

ETHICS STATEMENT

The animal study was reviewed and approved by the Animal Care Committee at the University of Western Ontario.

AUTHOR CONTRIBUTIONS

RB performed the bulk of the experiments, prepared the figures and drafted the manuscript. JA trained RB, cultured cells, prepared the mouse material and proof-read the manuscript. BA obtained the cells used, provided advice and proof-read the manuscript. JE assisted in engineering the Cx43-ablated cells and proof-read the manuscript. QS oversaw the generation of the Cx26 mutants and proof-read the manuscript. DL supervised the project, obtained funding and refined the manuscript for submission.

FUNDING

This research was funded by a Canadian Institutes of Health Research grant (148584) to DL and NSERC CGSM scholarship to RB.

ACKNOWLEDGMENTS

We would like to thank Dr. Federico Kalinec for supplying the HEI-OC1 cells.

REFERENCES

Abitbol, J. M., Beach, R., Barr, K., Esseltine, J. L., Allman, B. L., and Laird, D. W. (2020). Cisplatininduced ototoxicity in organotypic cochlear cultures occurs independent of Gap junctional intercellular communication. *Cell Death Dis.* (in press).

Abitbol, J. M., Kelly, J. J., Barr, K. J., Allman, B. L., and Laird, D. W. (2018). Mice harbouring an oculodentodigital dysplasia-linked Cx43 G60S mutation have severe hearing loss. *J. Cell Sci.* 131:jcs214635.

Ahmad, S., Chen, S., Sun, J., and Lin, X. (2003). Connexins 26 and 30 are co-assembled to form gap junctions in the cochlea of mice. *Biochem. Biophys. Res. Commun.* 307, 362–368.

Alexander, D. B., and Goldberg, G. S. (2003). Transfer of biologically important molecules between cells through gap junction channels. *Curr. Med. Chem.* 10, 2045–2058.

Anzai, T., Fukunaga, I., Hatakeyama, K., Fujimoto, A., Kobayashi, K., Nishikawa, A., et al. (2015). Deformation of the outer hair cells and the accumulation of caveolin-2 in Connexin 26 deficient mice. *PLoS One* 10:e0141258. doi: 10.1371/journal.pone.0141258

Atkinson, P. J., Dong, Y., Gu, S., Liu, W., Najarro, E. H., Udagawa, T., et al. (2018). Sox2 haploinsufficiency primes regeneration and Wnt responsiveness in the mouse cochlea. *J. Clin. Invest.* 128, 1641–1656. doi: 10.1172/JCI97248

Basch, M. L., Brown, R. M. II, Jen, H. I., and Groves, A. K. (2016). Where hearing starts: the development of the mammalian cochlea. *J. Anat.* 228, 233–254. doi: 10.1111/joa.12314

Berger, A. C., Kelly, J. J., Lajoie, P., Shao, Q., and Laird, D. W. (2014). Mutations in Cx30 that are linked to skin disease and non-syndromic hearing loss exhibit several distinct cellular pathologies. *J. Cell Sci.* 127(Pt 8), 1751–1764. doi: 10.1242/jcs.138230

Bruzzone, R., Veronesi, V., Gomes, D., Bicego, M., Duval, N., Marlin, S., et al. (2003). Loss-of-function and residual channel activity of connexin26 mutations associated with non-syndromic deafness. *FEBS Lett.* 533, 79–88.

Bruzzone, R., White, T. W., and Paul, D. L. (1996). Connections with connexins: the molecular basis of direct intercellular signaling. *Eur. J. Biochem.* 238, 1–27.

Cederroth, C. R. (2012). Loss of aminoglycoside sensitivity in HEI-OC1 cells? *Hear. Res.* 292, 83–85. doi: 10.1016/j.heares.2012.08.011

Chan, D. K., and Chang, K. W. (2014). GJB2-associated hearing loss: systematic review of worldwide prevalence, genotype, and auditory phenotype. *Laryngoscope* 124, E34–E53. doi: 10.1002/lary.24332

Chang, Q., Tang, W., Ahmad, S., Zhou, B., and Lin, X. (2008). Gap junction mediated intercellular metabolite transfer in the cochlea is compromised in connexin30 null mice. *PLoS One* 3:e4088. doi: 10.1371/journal.pone.0004088

Chang, Q., Tang, W., Kim, Y., and Lin, X. (2015). Timed conditional null of connexin26 in mice reveals temporary requirements of connexin26 in key cochlear developmental events before the onset of hearing. *Neurobiol. Dis.* 73, 418–427. doi: 10.1016/j.nbd.2014.09.005

Chen, S., Xie, L., Xu, K., Cao, H. Y., Wu, X., Xu, X. X., et al. (2018a). Developmental abnormalities in supporting cell phalangeal processes and cytoskeleton in the Gjb2 knockdown mouse model. *Dis. Model. Mech.* 11:dmm033019.

Chen, S., Xu, K., Xie, L., Cao, H. Y., Wu, X., Du, A. N., et al. (2018b). The spatial distribution pattern of Connexin26 expression in supporting cells and its role in outer hair cell survival. *Cell Death Dis.* 9:1180. doi: 10.1038/s41419-018-1238-x

Choi, M. J., Kang, H., Lee, Y. Y., Choo, O. S., Jang, J. H., Park, S. H., et al. (2019). Cisplatin-induced ototoxicity in rats is driven by RIP3-dependent necroptosis. *Cells* 8:E409.

Chonko, K. T., Jahan, I., Stone, J., Wright, M. C., Fujiyama, T., Hoshino, M., et al. (2013). Atoh1 directs hair cell differentiation and survival in the late embryonic mouse inner ear. *Dev. Biol.* 381, 401–410. doi: 10.1016/j.ydbio.2013.06.022

Cohen-Salmon, M., Maxeiner, S., Kruger, O., Theis, M., Willecke, K., and Petit, C. (2004). Expression of the connexin43- and connexin45-encoding genes in the developing and mature mouse inner ear. *Cell Tissue Res.* 316, 15–22.

D'Andrea, P., Veronesi, V., Bicego, M., Melchionda, S., Zelante, L., Di Iorio, E., et al. (2002). Hearing loss: frequency and functional studies of the most common connexin26 alleles. *Biochem. Biophys. Res. Commun.* 296, 685–691.

de Zwart-Storm, E. A., van Geel, M., van Neer, P. A., Steijlen, P. M., Martin, P. E., and van Steensel, M. A. (2008). A novel missense mutation in the second extracellular domain of GJB2, p.Ser183Phe, causes a syndrome of focal palmoplantar keratoderma with deafness. *Am. J. Pathol.* 173, 1113–1119.

Duman, D., and Tekin, M. (2012). Autosomal recessive nonsyndromic deafness genes: a review. *Front. Biosci.* 17, 2213–2236. doi: 10.2741/4046

Falk, M. M. (2000). Connexin-specific distribution within gap junctions revealed in living cells. *J. Cell Sci.* 113(Pt 22), 4109–4120.

Forge, A., Jagger, D. J., Kelly, J. J., and Taylor, R. R. (2013). Connexin30-mediated intercellular communication plays an essential role in epithelial repair in the cochlea. *J. Cell Sci.* 126(Pt 7), 1703–1712. doi: 10.1242/jcs.125476

Forge, A., Marziano, N. K., Casalotti, S. O., Becker, D. L., and Jagger, D. (2003). The inner ear contains heteromeric channels composed of cx26 and cx30 and deafness-related mutations in cx26 have a dominant negative effect on cx30. *Cell Commun. Adhes.* 10, 341–346.

Frenz, C. M., and Van De Water, T. R. (2000). Immunolocalization of connexin 26 in the developing mouse cochlea. *Brain Res. Brain Res. Rev.* 32, 172–180.

Garcia, I. E., Maripillan, J., Jara, O., Ceriani, R., Palacios-Munoz, A., Ramachandran, J., et al. (2015). Keratitis-ichthyosis-deafness syndrome-associated Cx26 mutants produce nonfunctional gap junctions but hyperactive hemichannels when co-expressed with wild type Cx43. *J. Invest. Dermatol.* 135, 1338–1347. doi: 10.1038/jid.2015.20

Gemel, J., Valiunas, V., Brink, P. R., and Beyer, E. C. (2004). Connexin43 and connexin26 form gap junctions, but not heteromeric channels in co-expressing cells. *J .Cell Sci.* 117(Pt 12), 2469–2480. doi: 10.1242/jcs.01084

Harris, A. L. (2008). Connexin specificity of second messenger permeation: real numbers at last. *J. Gen. Physiol.* 131, 287–292.

Hasson, T., Heintzelman, M. B., Santos-Sacchi, J., Corey, D. P., and Mooseker, M. S. (1995). Expression in cochlea and retina of myosin VIIa, the gene product defective in Usher syndrome type 1B. *Proc. Natl. Acad. Sci. U.S.A.* 92, 9815–9819. doi: 10.1073/pnas.92.21.9815

Inoshita, A., Iizuka, T., Okamura, H. O., Minekawa, A., Kojima, K., Furukawa, M., et al. (2008). Postnatal development of the organ of Corti in dominant-negative Gjb2 transgenic mice. *Neuroscience* 156, 1039–1047.

Inoshita, A., Karasawa, K., Funakubo, M., Miwa, A., Ikeda, K., and Kamiya, K. (2014). Dominant negative connexin26 mutation R75W causing severe hearing loss influences normal programmed cell death in postnatal organ of Corti. *BMC Genet.* 15:1. doi: 10.1186/1471-2156-15-1

Jagger, D. J., and Forge, A. (2006). Compartmentalized and signal-selective gap junctional coupling in the hearing cochlea. *J. Neurosci.* 26, 1260–1268.

Jagger, D. J., and Forge, A. (2015). Connexins and gap junctions in the inner ear–it's not just about K(+) recycling. *Cell Tissue Res.* 360, 633–644. doi: 10.1007/s00441-014-2029-z

Johnson, S. L., Ceriani, F., Houston, O., Polishchuk, R., Polishchuk, E., Crispino, G., et al. (2017). Connexin-mediated signaling in nonsensory cells is crucial for the development of sensory inner hair cells in the mouse cochlea. *J. Neurosci.* 37, 258–268. doi: 10.1523/JNEUROSCI.2251-16.2016

Kalinec, G., Thein, P., Park, C., and Kalinec, F. (2016). HEI-OC1 cells as a model for investigating drug cytotoxicity. *Hear. Res.* 335, 105–117.

Kalinec, G. M., Park, C., Thein, P., and Kalinec, F. (2016). Working with auditory HEI-OC1 cells. *J. Vis. Exp.* 115, 1–10. doi: 10.3791/54425

Kalinec, G. M., Webster, P., Lim, D. J., and Kalinec, F. (2003). A cochlear cell line as an in vitro system for drug ototoxicity screening. *Audiol. Neurootol.* 8, 177–189. doi: 10.1159/000071059

Keller, J. P., Homma, K., Duan, C., Zheng, J., Cheatham, M. A., and Dallos, P. (2014). Functional regulation of the SLC26-family protein prestin by calcium/calmodulin. *J. Neurosci.* 34, 1325–1332. doi: 10.1523/JNEUROSCI.4020-13.2014

Kelly, J. J., Abitbol, J. M., Hulme, S., Press, E. R., Laird, D. W., and Allman, B. L. (2019). The connexin 30 A88V mutant reduces cochlear gap junction expression and confers long-term protection against hearing loss. *J. Cell Sci.* 132, 1–12.

Kelly, J. J., Simek, J., and Laird, D. W. (2014). Mechanisms linking connexin mutations to human diseases. *Cell Tissue Res.* 360, 701–721. doi: 10.1007/s00441-014-2024-4

Kelly, J. J., Simek, J., and Laird, D. W. (2015). Mechanisms linking connexin mutations to human diseases. *Cell Tissue Res.* 360, 701–721.

Kenneson, A., Van Naarden Braun, K., and Boyle, C. (2002). GJB2 (connexin 26) variants and nonsyndromic sensorineural hearing loss: a HuGE review. *Genet. Med.* 4, 258–274.

Kikuchi, T., Adams, J. C., Miyabe, Y., So, E., and Kobayashi, T. (2000a). Potassium ion recycling pathway via gap junction systems in the mammalian cochlea and its interruption in hereditary nonsyndromic deafness. *Med. Electron. Microsc.* 33, 51–56. doi: 10.1007/s007950070001

Kikuchi, T., Kimura, R. S., Paul, D. L., Takasaka, T., and Adams, J. C. (2000b). Gap junction systems in the mammalian cochlea. *Brain Res. Brain Res. Rev.* 32, 163–166.

Kim, S. H., Choi, J., and Park, M. K. (2016). Letter to the editor regarding effects of caffeic acid on cisplatin-induced hair cell damage in HEI-OC1 auditory cells. *Int. J. Pediatr. Otorhinolaryngol.* 81:105. doi: 10.1016/j.ijporl.2015.12.010

Laird, D. W. (2006). Life cycle of connexins in health and disease. *Biochem. J.* 394(Pt 3), 527–543.

Laird, D. W. (2008). Closing the gap on autosomal dominant connexin-26 and connexin-43 mutants linked to human disease. *J. Biol. Chem.* 283, 2997–3001.

Laird, D. W., and Lampe, P. D. (2018). Therapeutic strategies targeting connexins. *Nat. Rev. Drug Discov.* 17, 905–921. doi: 10.1038/nrd.2018.138

Laird, D. W., Naus, C. C., and Lampe, P. D. (2017). SnapShot: connexins and disease. *Cell* 170:1260.

Lee, M. Y., Takada, T., Takada, Y., Kappy, M. D., Beyer, L. A., Swiderski, D. L., et al. (2015). Mice with conditional deletion of Cx26 exhibit no vestibular phenotype despite secondary loss of Cx30 in the vestibular end organs. *Hear. Res.* 328, 102–112. doi: 10.1016/j.heares.2015.07.018

Liang, C., Zhu, Y., Zong, L., Lu, G. J., and Zhao, H. B. (2012). Cell degeneration is not a primary causer for connexin26 (GJB2) deficiency associated hearing loss. *Neurosci. Lett.* 528, 36–41. doi: 10.1016/j.neulet.2012.08.085

Lim, J. O., Ko, J. W., Shin, N. R., Jung, T. Y., Moon, C., Kim, H. C., et al. (2019). Cisplatin-induced ototoxicity involves interaction of PRMT3 and cannabinoid system. *Arch. Toxicol.* 93, 2335–2346. doi:10.1007/s00204-019-02507-5

Liu, W., Bostrom, M., Kinnefors, A., and Rask-Andersen, H. (2009). Unique expression of connexins in the human cochlea. *Hear. Res.* 250, 55–62.

Locher, H., de Groot, J.C., van Iperen, L., Huisman, M.A., Frijns, J.H., and Chuva de Sousa Lopes SM. (2015). Development of the stria vascularis and potassium regulation in the human fetal cochlea: insights into hereditary sensorineural hearing loss. *Dev. Neurobiol.* 75, 1219–1240. doi: 10.1002/dneu.22279

Lopez, W., Liu, Y., Harris, A. L., and Contreras, J. E. (2014). Divalent regulation and intersubunit interactions of human connexin26 (Cx26) hemichannels. *Channels* 8, 1–4. doi: 10.4161/chan.26789

Maeda, S., Nakagawa, S., Suga, M., Yamashita, E., Oshima, A., Fujiyoshi, Y., et al. (2009). Structure of the connexin 26 gap junction channel at 3.5 A resolution. *Nature* 458, 597–602.

Mammano, F. (2019). Inner ear connexin channels: roles in development and maintenance of cochlear function. *Cold Spring Harb. Perspect. Med.* 9:a033233.

Mani, R. S., Ganapathy, A., Jalvi, R., Srikumari Srisailapathy, C. R., Malhotra, V., Chadha, S., et al. (2009). Functional consequences of novel connexin 26 mutations associated with hereditary hearing loss. *Eur. J. Hum. Genet.* 17, 502–509.

Martinez, A. D., Acuna, R., Figueroa, V., Maripillan, J., and Nicholson, B. (2009). Gap-junction channels dysfunction in deafness and hearing loss. *Antioxid. Redox Signal.* 11, 309–322. doi: 10.1089/ars.2008.2138

Martinez, A. D., Maripillan, J., Acuna, R., Minogue, P. J., Berthoud, V. M., and Beyer, E. C. (2011). Different domains are critical for oligomerization compatibility of different connexins. *Biochem. J.* 436, 35–43. doi: 10.1042/BJ20110008

Mese, G., Sellitto, C., Li, L., Wang, H. Z., Valiunas, V., Richard, G., et al. (2011). The Cx26-G45E mutation displays increased hemichannel activity in a mouse model of the lethal form of keratitis-ichthyosis-deafness syndrome. *Mol. Biol. Cell* 22, 4776–4786. doi: 10.1091/mbc.E11-09-0778

Mustapha, M., Salem, N., Delague, V., Chouery, E., Ghassibeh, M., Rai, M., et al. (2001). Autosomal recessive non-syndromic hearing loss in the Lebanese population: prevalence of the 30delG mutation and report of two novel mutations in the connexin 26 (GJB2) gene. *J. Med. Genet.* 38:E36.

Pang, J., Xiong, H., Zhan, T., Cheng, G., Jia, H., Ye, Y., et al. (2018). Sirtuin 1 and autophagy attenuate cisplatin-induced hair cell death in the mouse cochlea and zebrafish lateral line. *Front. Cell Neurosci.* 12:515. doi:10.3389/fncel.2018.00515

Park, C., Thein, P., Kalinec, G., and Kalinec, F. (2016). HEI-OC1 cells as a model for investigating prestin function. *Hear. Res.* 335, 9–17.

Press, E. R., Shao, Q., Kelly, J. J., Chin, K., Alaga, A., and Laird, D. W. (2017). Induction of cell death and gain-of-function properties of connexin26 mutants predict severity of skin disorders and hearing loss. *J. Biol. Chem.* 292, 9721–9732. doi: 10.1074/jbc.M116.770917

Rabionet, R., Zelante, L., Lopez-Bigas, N., D'Agruma, L., Melchionda, S., Restagno, G., et al. (2000). Molecular basis of childhood deafness resulting from mutations in the GJB2 (connexin 26) gene. *Hum. Genet.* 106, 40–44.

Richard, G., Brown, N., Ishida-Yamamoto, A., and Krol, A. (2004). Expanding the phenotypic spectrum of Cx26 disorders: bart-pumphrey syndrome is caused by a novel missense mutation in GJB2. *J. Invest. Dermatol.* 123, 856–863.

Sanchez, H. A., and Verselis, V. K. (2014). Aberrant Cx26 hemichannels and keratitis-ichthyosis-deafness syndrome: insights into syndromic hearing loss. *Front. Cell Neurosci.* 8:354. doi: 10.3389/fncel.2014.00354

Santos, R. L., Wajid, M., Pham, T. L., Hussan, J., Ali, G., Ahmad, W., et al. (2005). Low prevalence of Connexin 26 (GJB2) variants in Pakistani families with autosomal recessive non-syndromic hearing impairment. *Clin. Genet.* 67, 61–68.

Schutz, M., Auth, T., Gehrt, A., Bosen, F., Korber, I., Strenzke, N., et al. (2011). The connexin26 S17F mouse mutant represents a model for the human hereditary keratitis-ichthyosis-deafness syndrome. *Hum. Mol. Genet.* 20, 28–39. doi: 10.1093/hmg/ddq429

Shuja, Z., Li, L., Gupta, S., Mese, G., and White, T. W. (2016). Connexin26 mutations causing palmoplantar keratoderma and deafness interact with connexin43, modifying gap junction and hemichannel properties. *J. Invest. Dermatol.* 136, 225–235. doi: 10.1038/JID.2015.389

Simek, J., Churko, J., Shao, Q., and Laird, D. W. (2009). Cx43 has distinct mobility within plasma-membrane domains, indicative of progressive formation of gap-junction plaques. *J. Cell Sci.* 122(Pt 4), 554–562.

Snoeckx, R. L., Huygen, P. L., Feldmann, D., Marlin, S., Denoyelle, F., Waligora, J., et al. (2005). GJB2 mutations and degree of hearing loss: a multicenter study. *Am. J. Hum. Genet.* 77, 945–957.

So, H. S., Park, C., Kim, H. J., Lee, J. H., Park, S. Y., Lee, Z. W., et al. (2005). Protective effect of T-type calcium channel blocker flunarizine on cisplatin-induced death of auditory cells. *Hear. Res.* 204, 127–139.

Srinivas, M., Verselis, V. K., and White, T. W. (2018). Human diseases associated with connexin mutations. *Biochim. Biophys. Acta* 1860, 192–201.

Thonnissen, E., Rabionet, R., Arbones, M. L., Estivill, X., Willecke, K., and Ott, T. (2002). Human connexin26 (GJB2) deafness mutations affect the function of gap junction channels at different levels of protein expression. *Hum. Genet.* 111, 190–197.

Verselis, V. K. (2019). Connexin hemichannels and cochlear function. *Neurosci. Lett.* 695, 40–45.

Wang, Y., Chang, Q., Tang, W., Sun, Y., Zhou, B., Li, H., et al. (2009). Targeted connexin26 ablation arrests postnatal development of the organ of Corti. *Biochem. Biophys. Res. Commun.* 385, 33–37.

Wangemann, P. (2006). Supporting sensory transduction: cochlear fluid homeostasis and the endocochlear potential. *J. Physiol.* 576(Pt 1), 11–21.

White, T. W. (2000). Functional analysis of human Cx26 mutations associated with deafness. *Brain Res. Brain Res. Rev.* 32, 181–183.

Wingard, J. C., and Zhao, H. B. (2015). Cellular and deafness mechanisms underlying connexin mutation-induced hearing loss — a common hereditary deafness. *Front. Cell Neurosci.* 9:202. doi: 10.3389/fncel.2015.00202

Xiao, Z., Yang, Z., Liu, X., and Xie, D. (2011). Impaired membrane targeting and aberrant cellular localization of human Cx26 mutants associated with inherited recessive hearing loss. *Acta Otolaryngol.* 131, 59–66. doi: 10.3109/00016489.2010.506885

Xu, J., and Nicholson, B. J. (2013). The role of connexins in ear and skin physiology - functional insights from disease-associated mutations. *Biochim. Biophys. Acta* 1828, 167–178. doi: 10.1016/j.bbamem.2012.06.024

Youn, C. K., Kim, J., Park, J. H., Do, N. Y., and Cho, S. I. (2015). Role of autophagy in cisplatin-induced ototoxicity. *Int. J. Pediatr. Otorhinolaryngol.* 79, 1814–1819. doi: 10.1016/j.ijporl.2015.08.012

Yum, S. W., Zhang, J., Valiunas, V., Kanaporis, G., Brink, P. R., White, T. W., et al. (2007). Human connexin26 and connexin30 form functional heteromeric and heterotypic channels. *Am. J. Physiol. Cell Physiol.* 293, C1032–C1048.

Zhao, H. B. (2017). Hypothesis of K(+)-recycling defect is not a primary deafness mechanism for Cx26 (GJB2) deficiency. *Front. Mol. Neurosci.* 10:162. doi: 10.3389/fnmol.2017.00162

Zhao, H. B., Kikuchi, T., Ngezahayo, A., and White, T. W. (2006). Gap junctions and cochlear homeostasis. *J. Membr. Biol.* 209, 177–186. doi: 10.1007/s00232-005-0832-x

Zheng, J., Shen, W., He, D. Z., Long, K. B., Madison, L. D., and Dallos, P. (2000). Prestin is the motor protein of cochlear outer hair cells. *Nature* 405, 149–155. doi: 10.1038/3501 2009

Zhu, Y., Chen, J., Liang, C., Zong, L., Jones, R. O., and Zhao, H. B. (2015). Connexin26 (GJB2) deficiency reduces active cochlear amplification leading to late-onset hearing loss. *Neuroscience* 284, 719–729. doi: 10.1016/j.neuroscience.2014.10.061

Conflict of Interest: The authors declare that the research was conducted in the absence of any commercial or financial relationships that could be construed as a potential conflict of interest.

frontiers in Cell and Developmental Biology

REVIEW
published: 19 August 2020
doi: 10.3389/fcell.2020.00780

Role of Hippo-YAP Signaling in Osseointegration by Regulating Osteogenesis, Angiogenesis, and Osteoimmunology

Anqi Zhou[1†], Hui Yu[1,2†], Jiayi Liu[1], Jianan Zheng[1], Yinan Jia[1], Bingfeng Wu[1] and Lin Xiang[1,2]*

[1] State Key Laboratory of Oral Diseases & National Clinical Research Center for Oral Diseases, West China Hospital of Stomatology, Sichuan University, Chengdu, China, [2] Department of Oral Implantology, West China Hospital of Stomatology, Sichuan University, Chengdu, China

OPEN ACCESS

Edited by:
Bin Ren,
University of Alabama at Birmingham, United States

Reviewed by:
Qiulun Lu,
Nanjing Medical University, China
Li Ma,
Shandong University, China

***Correspondence:**
Lin Xiang
dentistxiang@126.com

[†] *These authors have contributed equally to this work*

Specialty section:
This article was submitted to Signaling, a section of the journal Frontiers in Cell and Developmental Biology

Received: *29 May 2020*
Accepted: *24 July 2020*
Published: *19 August 2020*

Citation:
Zhou A, Yu H, Liu J, Zheng J, Jia Y, Wu B and Xiang L (2020) Role of Hippo-YAP Signaling in Osseointegration by Regulating Osteogenesis, Angiogenesis, and Osteoimmunology. Front. Cell Dev. Biol. 8:780. doi: 10.3389/fcell.2020.00780

The social demand for dental implantation is growing at a rapid rate, while dentists are faced with the dilemma of implantation failures associated with unfavorable osseointegration. Clinical-friendly osteogenesis, angiogenesis and osteoimmunology around dental implants play a pivotal role in a desirable osseointegration and it's increasingly appreciated that Hippo-YAP signaling pathway is implicated in those biological processes both *in vitro* and *in vivo* in a variety of study. In this article we review the multiple effects of Hippo-YAP signaling in osseointegration of dental implants by regulating osteogenesis, angiogenesis and osteoimmunology in peri-implant tissue, as well as highlight prospective future directions of relevant investigation.

Keywords: osseointegration, Hippo-YAP, osteogenesis, angiogenesis, osteoimmunology, bone remodeling, implants

INTRODUCTION

With the increasing social burden of growing elderly population, some age-implicated diseases are changing people's demand for medical services including tooth loss. American Association of Oral and Maxillofacial Surgeons illustrates that 70% adults between 35 and 44 years old have at least one permanent tooth lost and 26% adults lose all by 74 years old, which has significant impacts on general health physically and mentally through direct and indirect mechanisms (Barboza-Solís et al., 2019; Bollman et al., 2020). Therefore, high-quality and efficient treatment to restore the function and esthetics for the cases of tooth loss is in increasing demand right now and facing great challenges. In the past, removable dentures and bridges were used in patients to replace missing teeth. However, over the last few decades dental implant has become very popular and a mainstream treatment for the advantages of high predictability and success rate as well as fewer complications during and after implantation (Shemtov-Yona and Rittel, 2015; Zohrabian et al., 2015). In addition, Howe et al. conducted a meta-analysis of 10-year dental implant survival and it turned out that the survival rate was 96.4% (Howe et al., 2019). However, while the demand for dental implants is growing at a very rapid rate, dentists are faced with the dilemma of dental implant failure associated with peri-implant mucositis, peri-implantitis, esthetic failures, and complete loss of osseointegration in clinical cases (Hickin et al., 2017).

Brånemark originally proposed the concept of osseointegration to describe the direct and stable connection between bone tissue and titanium implants. Zarb proposed a clinical description that it was a clinically asymptomatic fixation of functional-loaded implants (Zarb and Albrektsson, 1991). A desirable osseointegration is the key to a success implantation, which has been an ultimate goal for dentists to achieve. Bai et al. (2018a) attributed most implant failures to insufficient osseointegration between host bone and the surface of implants. In recent years, research on improving osseointegration to gain a higher survival rate of dental implant has become a hot topic in dentistry.

A favorable osseointegration of bone-implant interface is attributed to peri-implant osteogenesis, angiogenesis and osteoimmunology properties. On the one hand, these three factors play their respective important roles in regulating the process of osseointegration. Peri-implant bone osteogenesis is indispensable for stability and function of dental implants, which is regulated by the dynamic balance of osteoblasts, osteoclasts, osteocytes, etc. (Insua et al., 2017; Bai et al., 2018a). Angiogenesis is also an important component of accelerating bone repair since newborn blood vessels provide oxygen and nutrients for bone tissue and create routines for cell migration (Hankenson et al., 2011). As foreign bodies in bone tissue, successful dental implant is strongly dependent on a promising local immune microenvironment and proper osteoimmunomodulation to reach a favorable osseointegration which is dominated by the variety of peri-implant immune cells (Bai et al., 2018b; Wang J. et al., 2018.) On the other hand, the three factors are highly related and interact on each other. Numerous compelling evidences have showed that osteogenesis and angiogenesis are coupled to promote bone regeneration by wild cross-talk via various mediators and signals and both accelerated by favorable osteoimmunology properties to reach a clinical-friendly osseointegration, therefore the concept of osteoimmunology and osteo/angio-genesis overlap to a certain degree (Dohle et al., 2014; Shi et al., 2016, 2017; Okamoto et al., 2017; Bai et al., 2018a; Ma et al., 2018; Trindade et al., 2018; Tsukasaki and Takayanagi, 2019; Brunetti et al., 2020; Gao et al., 2020; Guder et al., 2020). Nevertheless, the specific regulation mechanisms on these three independent but wildly interrelated biological processes remain to be further clarified.

Hippo-YAP, a highly implicated pathway, is known to be involved in regulating organ size, tissue regeneration and cancer development. Hippo signaling senses and responds to upstream cell biomechanical cues including cell contacts, cell polarity and other biomechanical signals. MST1/2 and SAV1 are phosphorylated and activate the complex of LATS1/2 and MOB1A/B, thus activating downstream reaction (Xiang et al., 2018). Negatively modulated by Hippo signaling, Yes-associated protein (YAP) is a key downstream effector and regulates various cell properties such as controlling cell proliferation and fate by influencing gene expression with transcriptional enhancer associated domain transcription factors (TEADs), the main transcriptional factors interact with YAP.

OSTEOGENESIS, ANGIOGENESIS AND OSTEOIMMUNOLOGY AND THEIR EFFECTS ON OSSEOINTEGRATION (FIGURE 1)

Osteoimmunology

The concept of osteoimmunology was first established by Arror et al., emphasizing the interaction between skeletal and immune system (Arron and Choi, 2000; Tsukasaki and Takayanagi, 2019). On the one hand, cells of skeletal system are involved in immune regulation by secreting key cytokines in bone marrow microenvironment, where immune cells and their progenitors are harbored and nourished initially (Walsh et al., 2018; Tsukasaki and Takayanagi, 2019). On the other hand, the abnormal activation of immune cells may affect osteogenesis and angiogenesis, contributing to the development of pathological bone damage diseases, such as periodontitis and rheumatoid arthritis, as well as slow bone repair. As the bridge between skeletal and immune system, osteoimmunology plays a significant regulatory role in a variety of essential biological processes, including the osseointegration procedure of implants.

Inflammatory response around dental implants is usually considered a pathological process. In fact, as a process of direct connection between foreign body and bone tissue, osseointegration would initially raise the foreign-body reaction to implants. The foreign-body reaction starts with layer of proteins that come from blood and interstitium immediately forming on the surface of biomaterial after implantation, which activates inflammatory reaction of related cells as a result (Wilson et al., 2005; Singhatanadgit et al., 2019). Researches on enhancing the biocompatibility of implant material have been a hot topic in dentistry, for instance, surface modification (Hamlet and Ivanovski, 2011; Hamlet et al., 2012; Palmquist et al., 2013; Fukuda et al., 2019). as well as changing the design and composition of implants (Cooper et al., 2016; Wang Y. et al., 2019) are generally proposed as available strategies. Additionally, biofilm consisted of various subgingival bacteria may form upon the material at once after implantation, which stimulates excessive inflammatory response provided that microbiome dysbiosis occurs, leading peri-implant mucositis or even peri-implantitis that threatens the stability and survival of dental implants (Wisdom et al., 2019).

But our current knowledge of the effects of inflammatory response is that osseointegration is a complicated process relying on a dynamically balanced early inflammatory response of immune cells to implant, especially the response performed by macrophages, the main participants in reacting to biomaterials (Brown et al., 2017; Gibon et al., 2017; Lee and Bance, 2019). According to the activation pathway, secretion and function, macrophages are classified into classically activated macrophages (M1) and alternatively activated macrophages (M2). M1/M2 macrophages lead to opposite reacting process in response to different microenvironment. M1 is described as pro-inflammatory cell type that induces osseointegration failure with a layer of fibrous tissue surrounding the implants. While M2 is the anti-inflammatory/regulatory one (Brown et al., 2017) that

FIGURE 1 | Procedure of osseointegration. The histological change of dental implants in bone can be divided into three phases in general. In phase one, as soon as the implantation, the implant surface is surrounded by blood and immediately biomolecules including proteins, lipids and glycoproteins are absorbed to the surface, forming a temporary bioactive layer, with bone marrow cells scattering around. In phase two, about 1 month after the operation, some parts of bone tissue become absorbed due to the excessive pressure exerted on them, which is driven by osteoclasts. Simultaneously, the temporary bioactive layer is absorbed by macrophages and osteogenic cells such as mesenchymal stem cells (MSCs) and osteoblasts are stimulated to migrate to osteogenic area on the surface of implants and start to proliferate and differentiate thus mineralization procedure is initiated. In phase three, about 3 months after the implantation, the implant surface is surrounded by osteoblasts and osteocytes which get mature gradually, thus osseointegration is done progressively over time.

attracts cells, proteins and other bioactive substances around implants and hence plays a dominant role in osseointegration. However, *in vivo* the two extreme polarization states hardly exist since in most cases macrophages display both M1 and M2 characteristics phenotypes and exist as an intermediate state along the polarization spectrum (Brown et al., 2017). Although there are more subtypes and advanced classification pattern discussed nowadays, Wang et al. propose that regulating macrophage polarizing along M1 and M2 direction leads to influencing microenvironment of inflammation and regeneration thus coordinating osseointegration (Wang J. et al., 2018). The classic M1/M2 dichotomy is still popular in the latest study (Gao et al., 2020; **Figure 2**). Moreover, besides macrophages, there are other immune cells being discussed to play their respective promising roles in osteoimmunology-mediated osseointegration as well, such as T lymphocytes (Singhatanadgit et al., 2019) and mast cells (Zizzi et al., 2011; Marcatti Amarú Maximiano et al., 2017).

Osteogenesis

Dental implant is most widely contacted with bone tissue. Osseointegration, the fundamental theory of modern oral implantology, is the process of establishing a direct connection between ordered bone tissue and surface of a loaded-implant without soft tissue involvement. Osseointegration starts with inserting implant into the drilled hole and obtains passive and mechanical primary stability between interfacial bone and biomaterial surface (Lee and Bance, 2019). The biological responses are activated afterward. As soon as the dental implant is implanted into bone tissue, the peri-implant area becomes congested and immediately some biomolecules from surrounding blood and interstitial fluid are absorbed to the implant surface to form a temporary bioactive layer for preparation of cell reaction, with bone marrow cells scattering around. MSCs and osteoblasts are stimulated and facilitated to migrate to osteogenic area on the surface of dental implants and start to proliferate and differentiate thus mineralization procedure is initiated. Simultaneously, osteoclasts are activated to drive bone resorption process after the formation of woven bone to replace it by lamellar bone with a higher degree of mineralization and load intensity (Lee and Bance, 2019). During the terminal stage of osteogenesis process, osteocytes and the surface of implant are directly contiguous with or without the dendritic structures of osteocytes, building a bioactive network in bone-implant area, which probably suggest the structural basis of osseoperception (Du et al., 2016). To harmonize the whole dynamic process of bone formation as well as bone resorption, bone remodeling cell populations including bone marrow mesenchymal stem cells (BMSCs), osteoblasts, osteoclasts and osteocytes etc. detect

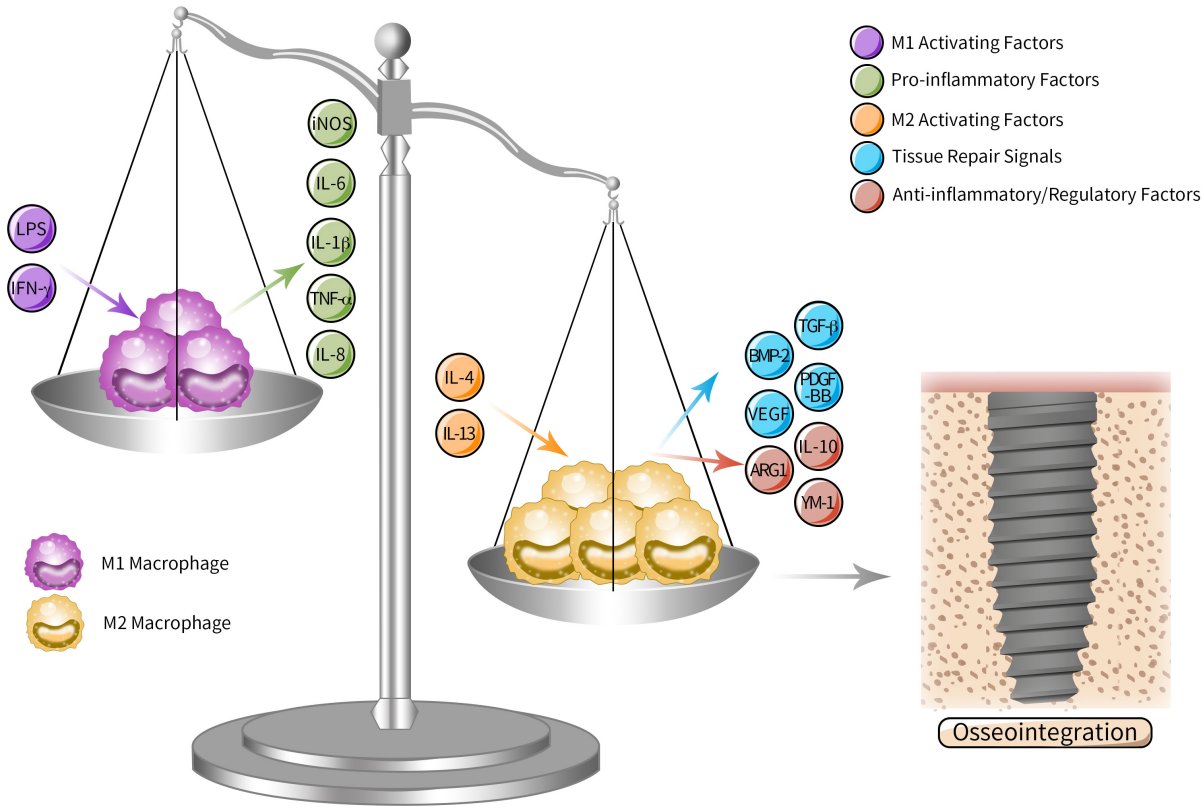

FIGURE 2 | M1/M2 polarization spectrum in osteoimmunology mediated osseointegration. As the key participants in peri-implant osteoimmunology, macrophages can be subdivided into M1 and M2 according to the activation pathway, secretion and function. M1 is the pro-inflammatory type activated by M1 activating factors such as LPS and IFN-γ, inducing excessive fibrosis and osseointegration failure by secreting pro-inflammatory cytokines, while M2 is activated by M2 activating factors such as IL-4 and IL-13, which promote osseointegration through anti-inflammatory and regulatory cytokines. Although *in vivo* macrophages actually display an intermediate state along the polarization spectrum, tipping the polarizing "scale" of macrophage from M1 to M2 leads to influencing microenvironment of inflammation and regeneration around implants and promoting osseointegration.

and translate biological signals in microenvironment then react to the given cues. The tight communication and multiple crosstalk among different cell populations are involved as well (Lotz et al., 2018; Shen et al., 2019; Sims and Martin, 2020; Tilkin et al., 2020; Wang H. et al., 2020). Therefore, it is of great significance to study the biochemistry and physiology phenomenon and, more importantly, the regulation mechanism on bone-implant interface to reach a clinical-friendly osseointegration.

Angiogenesis

Bone tissue is well known as a high vascularization tissue. A normal vascular structure and a favorable microcirculation contribute to the health of peri-implant bone tissue and a clinical-friendly osseointegration, since the microvasculature transports nutrients and metabolites and provides a pivotal microenvironment for migration, proliferation and differentiation of osteogenesis-related cells. Saghiri et al. (2016) reviewed researches on effects of titanium alloys and surface characteristics and treatments of dental implants on angiogenesis process and highlighted that pro-angiogenic surface played a pivotal role in facilitating osseointegration.

A healthy and functional microvascular network attributes to promising vessel sprouting and vascular tube extension, respectively, under specification of tip cells and stalk cells, the two main populations of vascular endothelial cells (ECs), which are equally necessary in angiogenesis and vessel remodeling. Moreover, the process of angiogenesis involves several signals and pathways, mainly including growth factors (VEGF, FGF, PDGF, TGF-β, et al.), Notch signaling, MMPs and so on (Potente et al., 2011).

ROLE OF HIPPO-YAP SIGNALING IN OSTEOGENESIS, ANGIOGENESIS AND OSTEOIMMUNOLOGY

Hippo-YAP Upstream Signals and Downstream Responses

Hippo-YAP responds to a variety of upstream signals in both intracellular and extracellular microenvironment. Hippo-YAP takes part in cell biomechanical respond mechanism to ECM, specifically, low ECM resistance leads to inhibiting activation

of YAP/TAZ while high ECM resistance stimulates YAP/TAZ nuclear translocation (Totaro et al., 2017, 2018b; Moya and Halder, 2019). What's more, some extracellular lipids or hormone signals can bond to G-protein-coupled receptors (GPCRs) and regulates Hippo-YAP signaling mediated by F-actin signaling (Moya and Halder, 2019). Based on a series of researches on the crosstalk between lysophosphatidic acid (LPA) and Hippo-YAP signaling, it is suggested that LPA is an upstream signal of Hippo pathway, binding to GPCRs and regulating the activity of the downstream effector YAP, which further mediates gene expression and cell behaviors (Yu et al., 2012; Moroishi et al., 2015; Park et al., 2016; Wang X. et al., 2018). In addition, Wnt signaling, cell polarity and metabolic property also enrich the transduction mechanism of Hippo-YAP signaling pathway (Totaro et al., 2018b; Xiang et al., 2018; Moya and Halder, 2019).

After dephosphorylation and nucleus translocation, YAP bonds on the enhancer of the target gene with TEAD1-4 to regulate gene transcription. It has been revealed by ChIP-seq data that AP-1 is also widely recruited to transcription regulatory sequences with YAP/TAZ-TEAD complex (Totaro et al., 2018b). By regulating expression of key genes, Hippo-YAP signaling pathway plays a versatile and significant regulatory role in organ development and regeneration in mammal, indicating their potential impacts on osseointegration induced by osteogenesis, angiogenesis and osteoimmunology.

The Influence of Hippo-YAP Signaling on Osteogenesis

There is strong evidence indicates that BMSCs are regulated by some biological signals on differentiation into bone tissue via Hippo-YAP pathway. The knockout of GNAS activates Hippo signaling pathway and eventually suppresses osteogenic differentiation of BMSCs (An et al., 2019), consistently, through the regulation of Hippo-YAP signaling pathway RAMP1 can promote the osteogenesis process of BMSCs that induced by CGRP (Zhang et al., 2019). Tang and Weiss (2017) revealed an interaction of Snail/Slug and YAP/TAZ, which regulates the differentiation ability of BMSCs in a cooperative way, suggesting a potential impact on the properties of osteogenesis. In addition, it is lately identified that Hippo pathway plays an important role in the competing adipo-osteogenic differentiation of MSCs and it turns out that YAP promotes osteogenic differentiation and in contrast it antagonizes adipogenic differentiation (Lorthongpanich et al., 2019). However, Seo et al. (2013) reported that SOX2-YAP1 axis significantly contributed to maintained stemness and inhibited osteoblastic differentiation of BMSCs, which may be attributed to Dkk1-mediated repression of Wnt signaling induced by YAP1/β-catenin.

Hippo-YAP signaling pathway is also involved in osteoblast differentiation through multiple biological mechanisms. The suppression of YAP may induce lowering ligand bmp2a in MSCs, leading to a severe damage of Bmp signals in osteoblasts nearby, which downregulates osteoblast differentiation through a cell non-autonomous way (Brandão et al., 2019). In a recent vivo study it is demonstrated that suppression of OLFML1, a missense mutant gene in patients with congenital scoliosis, leads to the nuclear translocation of YAP thus promoting expression of target genes and results in an accelerated mineralization process of osteoblasts, suggesting OLFML1 inhibits bone development through a biomechanical mechanism dependent on Hippo-YAP signaling pathway in osteoblasts (Murakami et al., 2018). Despite a certain amount of evidence has been shown to support its pivotal functions in bone metabolism and osteogenesis process, the multiple effects of Hippo-YAP signaling pathway in osteoblast differentiation are still controversial and ambiguous and need to be further clarified. It is lately indicated that Ti ions toxicity impair surrounding bone tissue by inducing dephosphorylation of YAP and its expression in nuclear to suppress osteogenic differentiation of osteoblasts, likewise knockdown of YAP expression leads to rescuing the harm of toxic Ti ions from implants, though Hippo-YAP is definitely not the only underlying biological cue responded by osteoblasts (Zhu et al., 2018).

The dynamic balance between bone formation and resorption plays a pivotal role in a favorable osteogenesis and mounting evidence has indicated regulatory effects of Hippo-YAP on osteoclastogenesis and resorption activity to influence bone homeostasis. Deficiency of MST2 in bone marrow-derived macrophages (BMMs) exhibits increased osteoclast differentiation and conversely MST2 overexpression inhibits it (Lee et al., 2015). Zhao et al. confirm that inhibition of YAP1 and its association with the main transcriptional factor TEADs weakens formation and osteoclastic resorption of osteoclasts, as well as NF-κB signaling induced by RANKL, a mainly investigated signaling pathway that regulates osteoclast differentiation in previous study (Yang et al., 2018; Zhao et al., 2018). Moreover, Limd1 is considered as an important negative regulator of Hippo pathway (Thakur et al., 2010; Jagannathan et al., 2016). It has been concluded recently *in vitro* that *Polygonatum sibiricum* polysaccharide (PSP) suppresses Hippo-YAP pathway to inhibit differentiation of osteoclasts from BMMs through downregulating expression of miRNA-1224, of which the target gene is Limd1 (Li B. et al., 2019). Additionally, the further mechanism of Hippo-YAP signaling regulating osteoclastogenesis is probably implicated to the transcriptional regulation by TEAD1 that binds to an upstream enhancer element of osteoprotegerin (OPG) and promotes its expression, which was revealed in human periodontal ligament cells (PDLCs) (Li Q. et al., 2019). Although PDLCs are supposed to be the absent cell population in bone-implant interface tissue, however, there's an increasing number of researches that uncover the significance of retaining PDL in the socket after tooth extraction and the promising contribution of PDLCs to implant osseointegration and bone repair (Pei et al., 2017; Washio et al., 2018; Karimi Dastgerdi et al., 2020). Osteoclastogenesis may also be partially dependent on potential YAP-GDF15 mechanism since in a recent study GDF-15 has been demonstrated to induce NF-κB activation in monocytic macrophages which contributes to further formation of osteoclasts and YAP has been indicated as an upstream signal of GDF15 in human PDLCs (Li et al., 2020).

Crosstalk between osteoblasts and osteoclasts can influence bone remodeling in a cell non-autonomous way. It is uncovered in a recent study that mechanical sensing protein PIEZO1 in osteoblastic cells promotes nuclear translocation of YAP and

increases type II and IX collagens expression through PIEZO1-YAP axis mechanistically, causing inhibition of osteoclast resorption activity (Wang L. et al., 2020).

Hippo-YAP signaling in osteocytes seems to be poorly understood in relevant fields. While osteocytes interconnect and communicate with each other on the basis of lacunar/canalicular system, playing a pivotal role in bone metabolism and remodeling. Besides, during the terminal stage of osteogenesis process in osseointegration, osteocytes contribute to compensating the microenvironment of periodontal ligament around nature teeth, at least partially, providing a cushion for masticatory forces and inducing osseoperception (Du et al., 2016). Therefore, it is of great value to uncover the molecular mechanisms that control osteocytes-induced osseointegration thus improving the survival rate and long-term stability of implants. Kegelman et al. clarified that deficiency of YAP/TAZ in osteocytes impaired bone accrual, matrix collagen and mechanical intensity *in vivo*, which was mediated by perilacunar/canalicular weakened remodeling, indicating a perspective target for future study (Kegelman et al., 2020). However, the specific role that Hippo-YAP signaling plays and other involved signals and pathways remain to be further clarified.

Hippo-YAP Impacts on Angiogenesis

Vessel Sprouting

YAP/TAZ promote sprouting angiogenesis by contributing to activity and function of vascular tip cells. Mechanistically, YAP/TAZ promotes migration of tip cells by activating CDC42 and facilitates the formation and junction of filopodia, an essential dynamic structure of tip cell that dominates its sprouting function, by promoting the remodeling of actin cytoskeleton (Kim et al., 2017; Sakabe et al., 2017). Likewise, the identity of tip cells are induced by CCN1, through interaction with integrin αvβ3/VEGFR and activation of downstream Hippo pathway thus promoting nucleus translocation of YAP/TAZ, which coordinates CCN1 in turn as a positive feedback (Park et al., 2019). While overactivating YAP/TAZ leads to pathologic sprouting pattern (Astone et al., 2018). Therefore, a proper regulatory effect of Hippo-YAP signaling plays a significant role in sprouting angiogenesis.

It's also worth noticing the crosstalk between Hippo-YAP pathway and Notch signaling in regulating angiogenesis. Notch signaling plays a significant role in vessel sprouting (Pitulescu et al., 2017; Fournier et al., 2020). There are two interaction patterns that are mainly investigated between YAP/TAZ and Notch pathways: first, YAP/TAZ regulate Notch pathways by controlling gene expression level of Notch receptors and/or ligands through nuclear translocation of YAP/TAZ, inducing Notch signaling turning on in surrounding cells; second, YAP/TAZ and Notch intracellular domain (NICD) are co-activated to translocate to nuclear and co-regulate their common targets genes (Totaro et al., 2018a). Notch signaling has also been reported to interact with LPA, an upstream signaling of Hippo pathway, which is suggested to play a role in a series of cell functions including angiogenesis through Hippo-YAP signaling. Yasuda et al. figured out that endothelial LPA4 and LPA6, receptors that coupled with Gα12/Gα13, regulate expression of Notch ligand Dll4 via YAP/TAZ and play a crucial role in sprouting angiogenesis (Yasuda et al., 2019). In addition, Ren et al. (2019) identified that Notch1, one of the single-stranded transmembrane receptors of Notch pathway, may interact with LPA2 and mediate cell biological performances.

Extension of the Vascular Tube

The favorable proliferation capability of EC promotes extension of vascular tubes, mostly dependent on the proliferation of stalk cells (Potente et al., 2011). Hippo-YAP has also been discovered to regulate metabolism and proliferation activity in ECs.

As a major growth factor of vascular development, interaction mechanism of VEGF with Hippo-YAP pathway has been investigated in recent years. Mechanistically, the pro-angiogenic effect of VEGF is mediated by actin cytoskeleton activity, which triggers Hippo-YAP axis and transcriptional regulatory activity of YAP, targeting cell viability-related genes (Wang et al., 2017). Also, VEGF may activate Hippo-YAP pathway mediated by PI3K/MAPK signaling (Azad et al., 2018). Moreover, YAP/TAZ regulates metabolism and proliferation activity of ECs by promoting MYC signaling (Kim et al., 2017). However, Hippo-YAP shows opposing regulatory manner in hypoxic microenvironment. The viability and migration ability of ECs are promoted in myocardial infarction by miR-93, through suppressing LATS2 to inhibit Hippo-YAP pathway (Ma et al., 2020), which may be attributed to YAP/TAZ inactivating hypoxia-inducible factor 1α (HIF1α) signaling in ECs (Sivaraj et al., 2020). Therefore, more attention should be paid to the different regulatory roles of Hippo-YAP in different organs, especially the property in angiogenic osseointegration.

Hippo-YAP Pathway Regulates Osteoimmunology

As major participants in osteoimmunology response, macrophages react to diverse biological signalings to adapt to different microenvironment, including Hippo-YAP signaling. Based on recent publications, it remains controversial on what kind of character YAP plays in macrophage polarization to M1/M2 phenotypes. It was reported that TGFβ1-mediated M2 polarization was facilitated by Wnt5a via stimulating YAP/TAZ (Feng et al., 2018). Consistently, Li C. et al. (2019) demonstrated *in vivo* that the expression profile of M1 phenotypic proinflammatory factors TNF-α and IL-1β were augmented while M2 characteristic anti-inflammatory factors IL-10 and TGF-β were weakened in myeloid-specific YAP knockout mice. Similar results can be found in tumor-associated macrophages (TAMs) as well (Huang et al., 2017; Jia et al., 2020; Zhao et al., 2020). However, some contrary results with regard to the regulatory effect of YAP in macrophages have been described. Zhou et al. pointed out that YAP promoted M1 but decreased M2 polarization based on the experimental results that specific knockout of myeloid YAP activated M2 polarization with IL-10 increase and IL-1β decrease but without any effect on production of TNF-α1, which is in conflict with the precious studies (Zhou et al., 2019). Additionally, Song et al. (2020) revealed the

mechanism of YAP aggravating M1 phenotype in Kupffer cells that LPS-stimulated YAP upregulated expression of the classic proinflammatory cytokines including IL-6, TNF-α, and MCP-1 by binding to their promoter regions through association with its transcriptional factor TEADs.

Besides macrophages, there are other immune cells should be involved in this discussion, since they dominate early inflammatory response in the primary stage of osseointegration. While mostly relevant investigations rarely involve osseointegration procedure of foreign implants. Further study may uncover the role of Hippo-YAP in early peri-implant inflammatory response.

DISCUSSION AND FUTURE OUTLOOK

Potential Roles of LPA

LPA is a bioactive small ubiquitous lipid which naturally exists in the body and it contributes to a various of biological effects in nervous system, cardiovascular, cancer, immune system etc. (Choi et al., 2010; Yung et al., 2014). LPA's unique physiological and pathological roles are revealed to be driven by extracellular signals through particular GPCRs which are called LPA1-6 (Choi et al., 2010). Specifically, the regulation effects of LPA on bone metabolism are mainly mediated by LPA1, LPA3, and LPA4 (Liu et al., 2010; Chen et al., 2019; Wu et al., 2019; Alioli et al., 2020); LPA4 and LPA6 play a facilitating role in developmental angiogenesis and LPA1 and LPA3 are found to mediate LPA/PKD-1-CD36 axis regulating proangiogenic and proarteriogenic reprogramming and *de novo* arteriogenesis (Ren et al., 2016; Dong et al., 2017; Yasuda et al., 2019); it is also worth noticing that LPA contributes to the formation of macrophages from monocytes in both mice and humans (Ray and Rai, 2017) and promotes LPA1 and LPA3 mediated conversion to foam cells (Chen et al., 2017). Numerous LPA-induced biological effects have been described and those cooperative and antagonistic signaling regulates cell activity in a highly complex manner. The investigations around LPA also suggest the potential role of LPA on osteogenesis, angiogenesis and osteoimmunology which may facilitate osseointegration procedure of implants, while its specific mechanism remains to be further clarified.

The previous study has showed the evidence on the downstream signaling pathway and cellular functions of LPA, whereby we further suppose that LPA may act as an upstream signal of Hippo pathway and promote LPA-Hippo axis mediated osteogenesis, angiogenesis and osteoimmunology, thus facilitating osseointegration process of implants or bone defect repair effectively (**Figure 3**). The potential mechanism around the series of molecular events remains controversial, which may suggest a prospective future research direction in involved fields.

Friend or Foe? The Discrepancy Around Hippo-YAP Regulatory Effects on Osteogenesis-Related Cells

As mentioned above, the existing researches have revealed some inconsistent results on role of YAP that it represses osteogenic behaviors of MSCs and osteoblasts according to some reports. Friend or foe? The osteogenic potential of Hippo-YAP signaling still remains as a highly controversial and ambiguous issue. Here, we analyze the possible influencing factors that raise the discrepancy and suppose the potential regulatory pattern of Hippo-YAP in osteogenesis-related cells.

First of all, Hippo-YAP pathway may play an inconsistent role in osteogenic cells of different maturity stage and the osteogenic impact of YAP is maturity-dependent, which kind of explain the negative results in osteogenic cells of early maturity stages. Xiong et al. (2018) observed that in mesenchymal progenitors and osteoblasts of early stage YAP/TAZ suppressed their differentiation to mature osteoblasts and led to decreased bone mass, whereas, osteoblast popularity and bone formation were promoted by YAP/TAZ expression in mature osteoblasts and osteocytes. Seo et al. (2013) and Xiong et al. (2018) suggested that the negative osteogenic effects were attributed to the impaired Wnt signaling by YAP.

What's more, the discrepancy around Hippo-YAP regulatory impacts may be caused by different properties of microenvironment. Yang et al. mimicked inflammatory microenvironment *in vitro* with TNF-α, the classic pro-inflammatory cytokine, then discovered an upregulated expression of pro-inflammatory IL-6 and RANKL and a reduced expression of anti-inflammatory OPG after knockdown of YAP1 in MC3T3-E1 cells (Yang et al., 2020). However, during the natural development procedure of mice, YAP knockdown in mature osteoblasts and osteocytes did not lead to changes on the expression of OPG or RANKL (Xiong et al., 2018). In a word, these discoveries suggest that the opposing regulatory role of YAP may due to the discrepancy between healthy and inflammatory local bone microenvironment, while further evidences should be shown to prove this inference.

In addition, Hippo-YAP is definitely not the only signaling pathway that plays pivotal roles in bone metabolism and regeneration (Ramasamy et al., 2016; Chen et al., 2018; Aslani et al., 2019; Luo et al., 2019; Maeda et al., 2019; Wang P. et al., 2019). In fact, osteogenesis is a complex and but orderly procedure induced and regulated by multiple synergistic and antagonistic effects.

Last but not least, it's worth noticing that Hippo-YAP regulates cellular osteogenic function in not only cell autonomous mode but also non-autonomous mode (Brandão et al., 2019; Wang L. et al., 2020), which further contributes to the complexity of the working manner of Hippo-YAP pathway.

Taking all these factors into consideration, it's hard to reach a consensus on the main reasons that cause the discrepancy around Hippo-YAP regulatory effect on osteogenesis-related cells. A compelling explanation will provide a deeper understanding of Hippo-YAP and indicate promising future research directions. We also suggest that researchers focus more on the conditions of Hippo-YAP promoting osteogenesis in future study, which is of great significance for further clarifying the multiple effects of Hippo-YAP pathway as well as exploring the potential clinical value.

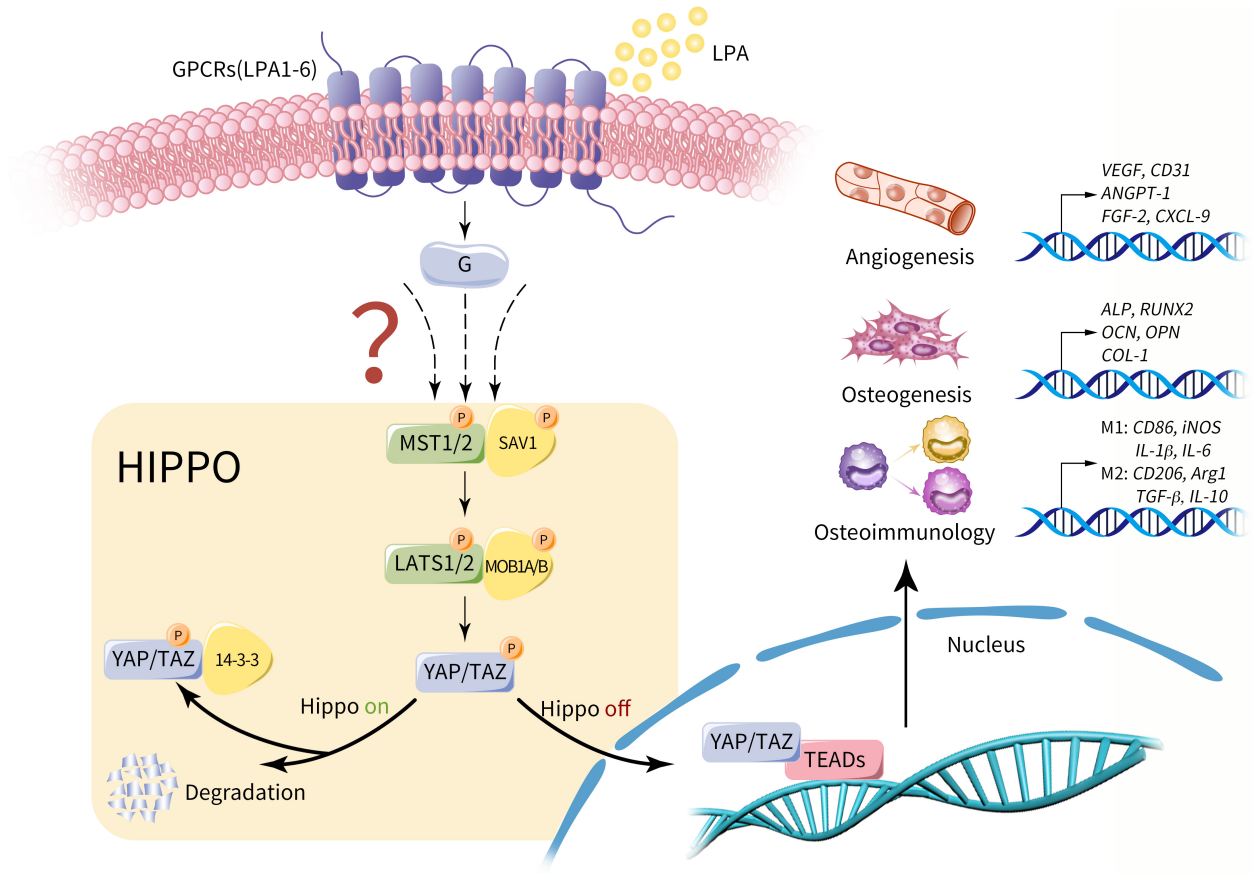

FIGURE 3 | Potential role of LPA on Hippo-YAP mediated osteogenesis, angiogenesis and osteoimmunology. LPA may act as an upstream extracellular signal of Hippo pathway via GPCRs (LPA1-6). Provided that Hippo pathway is activated, MST1/2 and SAV1 are phosphorylated and activate the complex of LATS1/2 and MOB1A/B. As a result, the phosphorylated YAP/TAZ is sequestrated in the cytoplasm by interacting with 14-3-3 proteins or degraded. Conversely, in the context of Hippo off, YAP/TAZ is dephosphorylated and translocate into nucleus, regulating a variety of cell properties by influencing gene expression with its main transcriptional factor TEAD, including genes that dominate osteogenesis, angiogenesis and osteoimmunology. Therefore, we propose that LPA-Hippo axis may perform regulatory effects on osseointegration procedure by influencing osteogenesis, angiogenesis and osteoimmunology.

The Controversial Issues on Roles of YAP in Macrophages Polarization

YAP was proved to play controversial roles in macrophages polarization in mainstream studies as mentioned before and these inconsistent and ambiguous results raise our great interests in the dynamic regularity of macrophages YAP expression in inflammatory tissues as well as its deeper and further significances. Here, we analyze possible influencing factors and highlight potential future study directions.

Firstly, there is high heterogeneity among macrophages from distinct origins including M1 and M2 characteristics, indicating potential effects on the accuracy of experimental results. Macrophages widely exist in organs and tissues of the body, with high heterogeneity among specific subpopulations. Bone marrow derived macrophages (BMMs) are differentiated from monocytes with hematopoietic system origin, while as tissue−resident macrophages, peritoneal macrophages (PEMs) are indicated to be independent of hematopoietic progenitors and originated from yolk sac in recent works (Cain et al., 2013; Davies and Taylor, 2015). However, we notice that BMMs and PEMs were used asynchronously to conclude the deficiency of YAP in macrophages induced macrophage polarization to M2 while the activation of M1 macrophages was suppressed, whereby suggesting therapeutic impact on inflammatory microenvironment (Zhou et al., 2019). In fact, the sources macrophages derived from may have an impact on polarizing signatures, since the different expression levels of M1/M2-related genes in BMMs and PEMs have been proved, including both surface markers and soluble mediators, which, respectively, indicate discrepancies in phenotype and cellular function (Bisgaard et al., 2016). Besides, properties of aging-related phagocytosis and immigration in 3D microenvironment were compared between BMMs and PEMs and the two subpopulations presented inconsistent results (Cougoule et al., 2012; Linehan et al., 2014). Therefore, it is of value to reevaluate the inherent differences between distinct original macrophages to promote convincingness and applicability of involved researches, especially the ones with regard to polarization tendency into

M1 or M2. Nevertheless, the proper cell model to simulate macrophage polarization and figure out its role in implicated diseases still needs to be further clarified.

Additionally, the classic M1/M2 dichotomy has been enriched in study on macrophage. As major participants in inflammatory response, macrophages show diverse phenotypic and functional differences reacting to different microenvironment. Based on the stimuli, macrophages are divided into classically activated macrophages (M1) and alternatively activated macrophages (M2) according to the existing classification model, with specific cytokine profile and biologic functions, respectively. In fact, as two extreme activated states, M1 and M2 rarely exist in microenvironment since macrophages are actually polarizing along the polarization spectrum and present some transitional state signatures with both M1 and M2 hallmarks (Davies and Taylor, 2015; Brown et al., 2017). In recent years, based on M1/M2 dichotomy, researchers have identified more subtypes of macrophages and expanded the definition of macrophage category, since as two extremes of a continuum and there are strong biochemistry and physiology differences between M1 and M2. For instance, M2 macrophages are further categorized into M2a, M2b, and M2c, the subtypes, respectively, activated by IL-4 and IL-13, immune complexes and LPS, and IL-10, presenting different biologic characteristics and effects, respectively (Mantovani et al., 2004). Additionally, there are more classifying patterns to describe a specific macrophage population that have been proposed to obtain more precise descriptions, such as $CD169^+$ and TCR^+ macrophages (Chávez-Galán et al., 2015). In conclusion, the previous studies have showed an enrichment of the classic M1/M2 dichotomy and choosing a suitable classifying pattern can be taken in to consideration in future researches.

CONCLUSION

In this review we suggest that a clinical-friendly osseointegration is essentially determined by favorable osteogenesis, angiogenesis and osteoimmunology, with a complex series of peri-implant cellular and molecular events happening during those procedures. Moreover, Hippo-YAP signaling pathway plays pivotal multiple regulatory roles in osteogenesis, angiogenesis and osteoimmunology. In short, the potential effects of Hippo-YAP on promoting osseointegration will contribute to the discovery of prospective clinical therapy.

AUTHOR CONTRIBUTIONS

AZ and HY designed the outline and drafted and critically revised the manuscript. JL designed the figures. JZ, YJ, and BW contributed to drafting the manuscript. LX contributed to designing and critically revising the manuscript. All authors contributed to the article and approved the submitted version.

FUNDING

This work was supported by grants from the National Natural Science Foundation of China (No. 81701007), Sichuan Science and Technology Program (No. 2018RZ0087), the Fundamental Research Funds for the Central Universities (No. 2018SCUH0006), the Research Funding for Talents Developing, West China Hospital of Stomatology Sichuan University (No. RCDWJS2020-6), and the Basic and Applied Basic Research Projects of West China Hospital of Stomatology of Sichuan University (No. RD-02-201902).

REFERENCES

Alioli, C. A., Demesmay, L., Laurencin-Dalacieux, S., Beton, N., Farlay, D., Follet, H., et al. (2020). Expression of the type 1 lysophosphatidic acid receptor in osteoblastic cell lineage controls both bone mineralization and osteocyte specification. *Biochim. Biophys. Acta* 1865:158715. doi: 10.1016/j.bbalip.2020.158715

An, J., Li, G., Zhang, J., Zhou, H., Jiang, J., Wang, X., et al. (2019). GNAS knockdown suppresses osteogenic differentiation of mesenchymal stem cells via activation of Hippo signaling pathway. *J. Cell. Physiol.* 234, 22299–22310. doi: 10.1002/jcp.28796

Arron, J. R., and Choi, Y. (2000). Bone versus immune system. *Nature* 408, 535–536. doi: 10.1038/35046196

Aslani, S., Abhari, A., Sakhinia, E., Sanajou, D., Rajabi, H., and Rahimzadeh, S. (2019). Interplay between microRNAs and Wnt, transforming growth factor-β, and bone morphogenic protein signaling pathways promote osteoblastic differentiation of mesenchymal stem cells. *J. Cell. Physiol.* 234, 8082–8093. doi: 10.1002/jcp.27582

Astone, M., Lai, J. K. H., Dupont, S., Stainier, D. Y. R., Argenton, F., and Vettori, A. (2018). Zebrafish mutants and TEAD reporters reveal essential functions for Yap and Taz in posterior cardinal vein development. *Sci. Rep.* 8:10189. doi: 10.1038/s41598-018-27657-x

Azad, T., Janse van Rensburg, H. J., Lightbody, E. D., Neveu, B., Champagne, A., Ghaffari, A., et al. (2018). A LATS biosensor screen identifies VEGFR as a regulator of the Hippo pathway in angiogenesis. *Nat. Commun.* 9:1061. doi: 10.1038/s41467-018-03278-w

Bai, L., Du, Z., Du, J., Yao, W., Zhang, J., Weng, Z., et al. (2018a). A multifaceted coating on titanium dictates osteoimmunomodulation and osteo/angio-genesis towards ameliorative osseointegration. *Biomaterials* 162, 154–169. doi: 10.1016/j.biomaterials.2018.02.010

Bai, L., Liu, Y., Du, Z., Weng, Z., Yao, W., Zhang, X., et al. (2018b). Differential effect of hydroxyapatite nano-particle versus nano-rod decorated titanium micro-surface on osseointegration. *Acta Biomater.* 76, 344–358. doi: 10.1016/j.actbio.2018.06.023

Barboza-Solís, C., Porras-Chaverri, M., and Fantin, R. (2019). Is tooth loss important when evaluating perceived general health? Findings from a nationally representative study of Costa Rican adults. *Community Dent. Oral Epidemiol.* 47, 358–365. doi: 10.1111/cdoe.12466

Bisgaard, L. S., Mogensen, C. K., Rosendahl, A., Cucak, H., Nielsen, L. B., Rasmussen, S. E., et al. (2016). Bone marrow-derived and peritoneal macrophages have different inflammatory response to oxLDL and M1/M2 marker expression – implications for atherosclerosis research. *Sci. Rep.* 6:35234. doi: 10.1038/srep35234

Bollman, M., Malbrue, R., Li, C., Yao, H., Guo, S., and Yao, S. (2020). Improvement of osseointegration by recruiting stem cells to titanium implants fabricated with 3D printing. *Ann. N. Y. Acad. Sci.* 1463, 37–44. doi: 10.1111/nyas.14251

Brandão, A. S., Bensimon-Brito, A., Lourenço, R., Borbinha, J., Soares, A. R., Mateus, R., et al. (2019). Yap induces osteoblast differentiation by modulating Bmp signalling during zebrafish caudal fin regeneration. *J. Cell Sci.* 132:jcs231993. doi: 10.1242/jcs.231993

Brown, B. N., Haschak, M. J., Lopresti, S. T., and Stahl, E. C. (2017). Effects of age-related shifts in cellular function and local microenvironment upon the innate

immune response to implants. *Semin. Immunol.* 29, 24–32. doi: 10.1016/j.smim.2017.05.001

Brunetti, G., D'Amelio, P., Mori, G., and Faienza, M. F. (2020). Editorial: updates on osteoimmunology: what's new on the crosstalk between bone and immune cells. *Front. Endocrinol.* 11:74. doi: 10.3389/fendo.2020.00074

Cain, D. W., O'Koren, E. G., Kan, M. J., Womble, M., Sempowski, G. D., Hopper, K., et al. (2013). Identification of a tissue-specific, C/EBPβ-dependent pathway of differentiation for murine peritoneal macrophages. *J. Immunol.* 191, 4665–4675. doi: 10.4049/jimmunol.1300581

Chávez-Galán, L., Olleros, M. L., Vesin, D., and Garcia, I. (2015). Much More than M1 and M2 Macrophages, There are also CD169+ and TCR+ Macrophages. *Front. Immunol.* 6:263. doi: 10.3389/fimmu.2015.00263

Chen, L., Zhang, J., Deng, X., Liu, Y., Yang, X., Wu, Q., et al. (2017). Lysophosphatidic acid directly induces macrophage-derived foam cell formation by blocking the expression of SRBI. *Biochem. Biophys. Res. Commun.* 491, 587–594. doi: 10.1016/j.bbrc.2017.07.159

Chen, S., Guo, Y., Liu, R., Wu, S., Fang, J., Huang, B., et al. (2018). Tuning surface properties of bone biomaterials to manipulate osteoblastic cell adhesion and the signaling pathways for the enhancement of early osseointegration. *Colloids Surf. B Biointerfaces* 164, 58–69. doi: 10.1016/j.colsurfb.2018.01.022

Chen, X., Song, Z., Chen, R., Tan, S., Huang, C., Liu, Y., et al. (2019). Lysophosphatidic acid enhanced the osteogenic and angiogenic capability of osteoblasts via LPA1/3 receptor. *Connect. Tissue Res.* 60, 85–94. doi: 10.1080/03008207.2018.1439485

Choi, J. W., Herr, D. R., Noguchi, K., Yung, Y. C., Lee, C.-W., Mutoh, T., et al. (2010). LPA receptors: subtypes and biological actions. *Annu. Rev. Pharmacol. Toxicol.* 50, 157–186. doi: 10.1146/annurev.pharmtox.010909.105753

Cooper, L., Tarnow, D., Froum, S., Moriarty, J., and De Kok, I. (2016). Comparison of marginal bone changes with internal conus and external hexagon design implant systems: a prospective, randomized study. *Int. J. Periodontics Restorative Dent.* 36, 631–642. doi: 10.11607/prd.2433

Cougoule, C., Van Goethem, E., Le Cabec, V., Lafouresse, F., Dupré, L., Mehraj, V., et al. (2012). Blood leukocytes and macrophages of various phenotypes have distinct abilities to form podosomes and to migrate in 3D environments. *Eur. J. Cell Biol.* 91, 938–949. doi: 10.1016/j.ejcb.2012.07.002

Davies, L. C., and Taylor, P. R. (2015). Tissue-resident macrophages: then and now. *Immunology* 144, 541–548. doi: 10.1111/imm.12451

Dohle, E., Bischoff, I., Böse, T., Marsano, A., Banfi, A., Unger, R. E., et al. (2014). Macrophage-mediated angiogenic activation of outgrowth endothelial cells in co-culture with primary osteoblasts. *Eur. Cell. Mater.* 27, 149–165. doi: 10.22203/eCM.v027a12

Dong, L., Yuan, Y., Opansky, C., Chen, Y., Aguilera-Barrantes, I., Wu, S., et al. (2017). Diet-induced obesity links to ER positive breast cancer progression via LPA/PKD-1-CD36 signaling-mediated microvascular remodeling. *Oncotarget* 8, 22550–22562. doi: 10.18632/oncotarget.15123

Du, Z., Ivanovski, S., Hamlet, S. M., Feng, J. Q., and Xiao, Y. (2016). The ultrastructural relationship between osteocytes and dental implants following osseointegration: osteocytes and dental implants. *Clin. Implant Dent. Relat. Res.* 18, 270–280. doi: 10.1111/cid.12257

Feng, Y., Liang, Y., Zhu, X., Wang, M., Gui, Y., Lu, Q., et al. (2018). The signaling protein Wnt5a promotes TGFβ1-mediated macrophage polarization and kidney fibrosis by inducing the transcriptional regulators Yap/Taz. *J. Biol. Chem.* 293, 19290–19302. doi: 10.1074/jbc.RA118.005457

Fournier, P., Viallard, C., Dejda, A., Sapieha, P., Larrivée, B., and Royal, I. (2020). The protein tyrosine phosphatase PTPRJ/DEP-1 contributes to the regulation of the Notch-signaling pathway and sprouting angiogenesis. *Angiogenesis* 23, 145–157. doi: 10.1007/s10456-019-09683-z

Fukuda, N., Tsuchiya, A., Sunarso, Toita, R., Tsuru, K., Mori, Y., et al. (2019). Surface plasma treatment and phosphorylation enhance the biological performance of poly(ether ether ketone). *Colloids Surf. B Biointerfaces* 173, 36–42. doi: 10.1016/j.colsurfb.2018.09.032

Gao, A., Liao, Q., Xie, L., Wang, G., Zhang, W., Wu, Y., et al. (2020). Tuning the surface immunomodulatory functions of polyetheretherketone for enhanced osseointegration. *Biomaterials* 230:119642. doi: 10.1016/j.biomaterials.2019.119642

Gibon, E., Lu, L. Y., Nathan, K., and Goodman, S. B. (2017). Inflammation, ageing, and bone regeneration. *J. Orthop. Transl.* 10, 28–35. doi: 10.1016/j.jot.2017.04.002

Guder, C., Gravius, S., Burger, C., Wirtz, D. C., and Schildberg, F. A. (2020). Osteoimmunology: a current update of the interplay between bone and the immune system. *Front. Immunol.* 11:58. doi: 10.3389/fimmu.2020.00058

Hamlet, S., Alfarsi, M., George, R., and Ivanovski, S. (2012). The effect of hydrophilic titanium surface modification on macrophage inflammatory cytokine gene expression. *Clin. Oral Implants Res.* 23, 584–590. doi: 10.1111/j.1600-0501.2011.02325.x

Hamlet, S., and Ivanovski, S. (2011). Inflammatory cytokine response to titanium chemical composition and nanoscale calcium phosphate surface modification. *Acta Biomater.* 7, 2345–2353. doi: 10.1016/j.actbio.2011.01.032

Hankenson, K. D., Dishowitz, M., Gray, C., and Schenker, M. (2011). Angiogenesis in bone regeneration. *Injury* 42, 556–561. doi: 10.1016/j.injury.2011.03.035

Hickin, M. P., Shariff, J. A., Jennette, P. J., Finkelstein, J., and Papapanou, P. N. (2017). Incidence and determinants of dental implant failure: a review of electronic health records in a U.S. dental school. *J. Dent. Educ.* 81, 1233–1242. doi: 10.21815/jde.017.080

Howe, M.-S., Keys, W., and Richards, D. (2019). Long-term (10-year) dental implant survival: a systematic review and sensitivity meta-analysis. *J. Dent.* 84, 9–21. doi: 10.1016/j.jdent.2019.03.008

Huang, Y.-J., Yang, C.-K., Wei, P.-L., Huynh, T.-T., Whang-Peng, J., Meng, T.-C., et al. (2017). Ovatodiolide suppresses colon tumorigenesis and prevents polarization of M2 tumor-associated macrophages through YAP oncogenic pathways. *J. Hematol. Oncol.* 10:60.

Insua, A., Monje, A., Wang, H.-L., and Miron, R. J. (2017). Basis of bone metabolism around dental implants during osseointegration and peri-implant bone loss. *J. Biomed. Mater. Res. A* 105, 2075–2089. doi: 10.1002/jbm.a.36060

Jagannathan, R., Schimizzi, G. V., Zhang, K., Loza, A. J., Yabuta, N., Nojima, H., et al. (2016). AJUBA LIM proteins limit Hippo activity in proliferating cells by sequestering the Hippo core kinase complex in the cytosol. *Mol. Cell Biol.* 36, 2526–2542. doi: 10.1128/mcb.00136-16

Jia, J., Zhang, H., He, L., Zhang, H., and Shu, M. (2020). Cutaneous neurofibroma cells with active YAP promotes proliferation of macrophages resulting in increased accumulation of macrophages by modulating CCL5 and TGF-β1. *Oncol. Rep.* 43, 1319–1330. doi: 10.3892/or.2020.7513

Karimi Dastgerdi, A., Rouhi, G., Dehghan, M. M., Farzad-Mohajeri, S., and Barikani, H. R. (2020). Linear momenta transferred to the dental implant-bone and natural tooth—PDL-bone constructs under impact loading: a comparative *in-vitro* and *in-silico* Study. *Front. Bioeng. Biotechnol.* 8:544. doi: 10.3389/fbioe.2020.00544

Kegelman, C. D., Coulombe, J. C., Jordan, K. M., Horan, D. J., Qin, L., Robling, A. G., et al. (2020). YAP and TAZ mediate osteocyte perilacunar/canalicular remodeling. *J. Bone Miner. Res.* 35, 196–210. doi: 10.1002/jbmr.3876

Kim, J., Kim, Y. H., Kim, J., Park, D. Y., Bae, H., Lee, D.-H., et al. (2017). YAP/TAZ regulates sprouting angiogenesis and vascular barrier maturation. *J. Clin. Invest.* 127, 3441–3461. doi: 10.1172/JCI93825

Lee, J., Youn, B. U., Kim, K., Kim, J. H., Lee, D., Seong, S., et al. (2015). Mst2 controls bone homeostasis by regulating osteoclast and osteoblast differentiation. *J. Bone Miner. Res.* 30, 1597–1607. doi: 10.1002/jbmr.2503

Lee, J. W. Y., and Bance, M. L. (2019). Physiology of osseointegration. *Otolaryngol. Clin. North Am.* 52, 231–242. doi: 10.1016/j.otc.2018.11.004

Li, B., Wu, P., Fu, W., Xiong, Y., Zhang, L., Gao, Y., et al. (2019). The role and mechanism of miRNA-1224 in the *Polygonatum sibiricum* polysaccharide regulation of bone marrow-derived macrophages to osteoclast differentiation. *Rejuvenation Res.* 22, 420–430. doi: 10.1089/rej.2018.2126

Li, C., Jin, Y., Wei, S., Sun, Y., Jiang, L., Zhu, Q., et al. (2019). Hippo signaling controls NLR family pyrin domain containing 3 activation and governs immunoregulation of mesenchymal stem cells in mouse liver injury. *Hepatology* 70, 1714–1731. doi: 10.1002/hep.30700

Li, Q., Han, G., Liu, D., and Zhou, Y. (2019). Force-induced decline of TEA domain family member 1 contributes to osteoclastogenesis via regulation of Osteoprotegerin. *Arch. Oral Biol.* 100, 23–32. doi: 10.1016/j.archoralbio.2019.01.020

Li, S., Li, Q., Zhu, Y., and Hu, W. (2020). GDF15 induced by compressive force contributes to osteoclast differentiation in human periodontal ligament cells. *Exp. Cell Res.* 387:111745. doi: 10.1016/j.yexcr.2019.111745

Linehan, E., Dombrowski, Y., Snoddy, R., Fallon, P. G., Kissenpfennig, A., and Fitzgerald, D. C. (2014). Aging impairs peritoneal but not bone marrow-derived macrophage phagocytosis. *Aging Cell* 13, 699–708. doi: 10.1111/acel.12223

Liu, Y.-B., Kharode, Y., Bodine, P. V. N., Yaworsky, P. J., Robinson, J. A., and Billiard, J. (2010). LPA induces osteoblast differentiation through interplay of two receptors: LPA1 and LPA4. *J. Cell. Biochem.* 109, 794–800. doi: 10.1002/jcb.22471

Lorthongpanich, C., Thumanu, K., Tangkiettrakul, K., Jiamvoraphong, N., Laowtammathron, C., Damkham, N., et al. (2019). YAP as a key regulator of adipo-osteogenic differentiation in human MSCs. *Stem Cell Res. Ther.* 10:402. doi: 10.1186/s13287-019-1494-4

Lotz, E. M., Berger, M. B., Schwartz, Z., and Boyan, B. D. (2018). Regulation of osteoclasts by osteoblast lineage cells depends on titanium implant surface properties. *Acta Biomater.* 68, 296–307. doi: 10.1016/j.actbio.2017.12.039

Luo, Z., Shang, X., Zhang, H., Wang, G., Massey, P. A., Barton, S. R., et al. (2019). Notch signaling in osteogenesis, osteoclastogenesis, and angiogenesis. *Am. J. Pathol.* 189, 1495–1500. doi: 10.1016/j.ajpath.2019.05.005

Ma, C., Peng, P., Zhou, Y., Liu, T., Wang, L., and Lu, C. (2020). MicroRNA-93 promotes angiogenesis and attenuates remodeling via inactivation of the Hippo/Yap pathway by targeting Lats2 after myocardial infarctionω. *Mol. Med. Rep.* 22, 483–493. doi: 10.3892/mmr.2020.11085

Ma, Q., Fang, L., Jiang, N., Zhang, L., Wang, Y., Zhang, Y., et al. (2018). Bone mesenchymal stem cell secretion of sRANKL/OPG/M-CSF in response to macrophage-mediated inflammatory response influences osteogenesis on nanostructured Ti surfaces. *Biomaterials* 154, 234–247. doi: 10.1016/j.biomaterials.2017.11.003

Maeda, K., Kobayashi, Y., Koide, M., Uehara, S., Okamoto, M., Ishihara, A., et al. (2019). The regulation of bone metabolism and disorders by Wnt signaling. *Int. J. Mol. Sci.* 20:5525. doi: 10.3390/ijms20225525

Mantovani, A., Sica, A., Sozzani, S., Allavena, P., Vecchi, A., and Locati, M. (2004). The chemokine system in diverse forms of macrophage activation and polarization. *Trends Immunol.* 25, 677–686. doi: 10.1016/j.it.2004.09.015

Marcatti Amarú Maximiano, W., Marino Mazucato, V., Tambasco de Oliveira, P., Célia Jamur, M., and Oliver, C. (2017). Nanotextured titanium surfaces stimulate spreading, migration, and growth of rat mast cells: nanotextured titanium surfaces stimulate mast cells. *J. Biomed. Mater. Res. A* 105, 2150–2161. doi: 10.1002/jbm.a.36076

Moroishi, T., Park, H. W., Qin, B., Chen, Q., Meng, Z., Plouffe, S. W., et al. (2015). A YAP/TAZ-induced feedback mechanism regulates Hippo pathway homeostasis. *Genes Dev.* 29, 1271–1284. doi: 10.1101/gad.262816.115

Moya, I. M., and Halder, G. (2019). Hippo-YAP/TAZ signalling in organ regeneration and regenerative medicine. *Nat. Rev. Mol. Cell Biol.* 20, 211–226. doi: 10.1038/s41580-018-0086-y

Murakami, K., Kikugawa, S., Kobayashi, Y., Uehara, S., Suzuki, T., Kato, H., et al. (2018). Olfactomedin-like protein OLFML1 inhibits Hippo signaling and mineralization in osteoblasts. *Biochem. Biophys. Res. Commun.* 505, 419–425. doi: 10.1016/j.bbrc.2018.09.112

Okamoto, K., Nakashima, T., Shinohara, M., Negishi-Koga, T., Komatsu, N., Terashima, A., et al. (2017). Osteoimmunology: the conceptual framework unifying the immune and skeletal systems. *Physiol. Rev.* 97, 1295–1349. doi: 10.1152/physrev.00036.2016

Palmquist, A., Johansson, A., Suska, F., Brånemark, R., and Thomsen, P. (2013). Acute inflammatory response to laser-induced micro- and nano-sized titanium surface features: inflammatory response to laser-modified titanium. *Clin. Implant Dent. Relat. Res.* 15, 96–104. doi: 10.1111/j.1708-8208.2011.00361.x

Park, M.-H., Kim, A. K., Manandhar, S., Oh, S.-Y., Jang, G.-H., Li, K., et al. (2019). CCN1 interlinks integrin and hippo pathway to autoregulate tip cell activity. *eLife* 8:e46012. doi: 10.7554/eLife.46012

Park, R., Moon, U. Y., Park, J. Y., Hughes, L. J., Johnson, R. L., Cho, S.-H., et al. (2016). Yap is required for ependymal integrity and is suppressed in LPA-induced hydrocephalus. *Nat. Commun.* 7:10329. doi: 10.1038/ncomms10329

Pei, X., Wang, L., Chen, C., Yuan, X., Wan, Q., and Helms, J. A. (2017). Contribution of the PDL to osteotomy repair and implant osseointegration. *J. Dent. Res.* 96, 909–916. doi: 10.1177/0022034517707513

Pitulescu, M. E., Schmidt, I., Giaimo, B. D., Antoine, T., Berkenfeld, F., Ferrante, F., et al. (2017). Dll4 and Notch signalling couples sprouting angiogenesis and artery formation. *Nat. Cell Biol.* 19, 915–927. doi: 10.1038/ncb3555

Potente, M., Gerhardt, H., and Carmeliet, P. (2011). Basic and therapeutic aspects of angiogenesis. *Cell* 146, 873–887. doi: 10.1016/j.cell.2011.08.039

Ramasamy, S. K., Kusumbe, A. P., Itkin, T., Gur-Cohen, S., Lapidot, T., and Adams, R. H. (2016). Regulation of hematopoiesis and osteogenesis by blood vessel–derived signals. *Annu. Rev. Cell Dev. Biol.* 32, 649–675. doi: 10.1146/annurev-cellbio-111315-124936

Ray, R., and Rai, V. (2017). Lysophosphatidic acid converts monocytes into macrophages in both mice and humans. *Blood* 129, 1177–1183. doi: 10.1182/blood-2016-10-743757

Ren, B., Best, B., Ramakrishnan, D. P., Walcott, B. P., Storz, P., and Silverstein, R. L. (2016). LPA/PKD-1-FoxO1 signaling axis mediates endothelial cell CD36 transcriptional repression and proangiogenic and proarteriogenic reprogramming. *Arterioscler. Thromb. Vasc. Biol.* 36, 1197–1208. doi: 10.1161/ATVBAHA.116.307421

Ren, Z., Zhang, C., Ma, L., Zhang, X., Shi, S., Tang, D., et al. (2019). Lysophosphatidic acid induces the migration and invasion of SGC-7901 gastric cancer cells through the LPA2 and Notch signaling pathways. *Int. J. Mol. Med.* 44, 67–78. doi: 10.3892/ijmm.2019.4186

Saghiri, M.-A., Asatourian, A., Garcia-Godoy, F., and Sheibani, N. (2016). The role of angiogenesis in implant dentistry part I: review of titanium alloys, surface characteristics and treatments. *Med. Oral Patol. Oral Cirugia Bucal* 21, e514–e525.

Sakabe, M., Fan, J., Odaka, Y., Liu, N., Hassan, A., Duan, X., et al. (2017). YAP/TAZ-CDC42 signaling regulates vascular tip cell migration. *Proc. Natl. Acad. Sci. U.S.A.* 114, 10918–10923. doi: 10.1073/pnas.1704030114

Seo, E., Basu-Roy, U., Gunaratne, P. H., Coarfa, C., Lim, D.-S., Basilico, C., et al. (2013). SOX2 regulates YAP1 to maintain stemness and determine cell fate in the osteo-adipo lineage. *Cell Rep.* 3, 2075–2087. doi: 10.1016/j.celrep.2013.05.029

Shemtov-Yona, K., and Rittel, D. (2015). An overview of the mechanical integrity of dental implants. *Biomed Res. Int.* 2015:547384. doi: 10.1155/2015/547384

Shen, X., Yu, Y., Ma, P., Luo, Z., Hu, Y., Li, M., et al. (2019). Titania nanotubes promote osteogenesis via mediating crosstalk between macrophages and MSCs under oxidative stress. *Colloids Surf. B Biointerfaces* 180, 39–48. doi: 10.1016/j.colsurfb.2019.04.033

Shi, M., Chen, Z., Farnaghi, S., Friis, T., Mao, X., Xiao, Y., et al. (2016). Copper-doped mesoporous silica nanospheres, a promising immunomodulatory agent for inducing osteogenesis. *Acta Biomater.* 30, 334–344. doi: 10.1016/j.actbio.2015.11.033

Shi, M., Xia, L., Chen, Z., Lv, F., Zhu, H., Wei, F., et al. (2017). Europium-doped mesoporous silica nanosphere as an immune-modulating osteogenesis/angiogenesis agent. *Biomaterials* 144, 176–187. doi: 10.1016/j.biomaterials.2017.08.027

Sims, N. A., and Martin, T. J. (2020). Osteoclasts provide coupling signals to osteoblast lineage cells through multiple mechanisms. *Annu. Rev. Physiol.* 82, 507–529. doi: 10.1146/annurev-physiol-021119-034425

Singhatanadgit, W., Toso, M., Pratheepsawangwong, B., Pimpin, A., and Srituravanich, W. (2019). Titanium dioxide nanotubes of defined diameter enhance mesenchymal stem cell proliferation via JNK- and ERK-dependent up-regulation of fibroblast growth factor-2 by T lymphocytes. *J. Biomater. Appl.* 33, 997–1010. doi: 10.1177/0885328218816565

Sivaraj, K. K., Dharmalingam, B., Mohanakrishnan, V., Jeong, H.-W., Kato, K., Schröder, S., et al. (2020). YAP1 and TAZ negatively control bone angiogenesis by limiting hypoxia-inducible factor signaling in endothelial cells. *eLife* 9:e50770. doi: 10.7554/eLife.50770

Song, K., Kwon, H., Han, C., Chen, W., Zhang, J., Ma, W., et al. (2020). Yes-associated protein in Kupffer cells enhances the production of pro-inflammatory cytokines and promotes the development of non-alcoholic steatohepatitis. *Hepatology* 72, 72–87. doi: 10.1002/hep.30990

Tang, Y., and Weiss, S. J. (2017). Snail/Slug-YAP/TAZ complexes cooperatively regulate mesenchymal stem cell function and bone formation. *Cell Cycle* 16, 399–405. doi: 10.1080/15384101.2017.1280643

Thakur, M. D., Feng, Y., Jagannathan, R., Seppa, M. J., Skeath, J. B., and Longmore, G. D. (2010). Ajuba LIM proteins are negative regulators of the Hippo signaling pathway. *Curr. Biol.* 20, 657–662. doi: 10.1016/j.cub.2010.02.035

Tilkin, R. G., Régibeau, N., Lambert, S. D., and Grandfils, C. (2020). Correlation between surface properties of polystyrene and polylactide materials and fibroblast and osteoblast cell line behavior: a critical overview of the literature. *Biomacromolecules* 21, 1995–2013. doi: 10.1021/acs.biomac.0c00214

Totaro, A., Castellan, M., Battilana, G., Zanconato, F., Azzolin, L., Giulitti, S., et al. (2017). YAP/TAZ link cell mechanics to Notch signalling to control epidermal stem cell fate. *Nat. Commun.* 8:15206. doi: 10.1038/ncomms15206

Totaro, A., Castellan, M., Di Biagio, D., and Piccolo, S. (2018a). Crosstalk between YAP/TAZ and Notch signaling. *Trends Cell Biol.* 28, 560–573. doi: 10.1016/j.tcb.2018.03.001

Totaro, A., Panciera, T., and Piccolo, S. (2018b). YAP/TAZ upstream signals and downstream responses. *Nat. Cell Biol.* 20, 888–899. doi: 10.1038/s41556-018-0142-z

Trindade, R., Albrektsson, T., Galli, S., Prgomet, Z., Tengvall, P., and Wennerberg, A. (2018). Osseointegration and foreign body reaction: titanium implants activate the immune system and suppress bone resorption during the first 4 weeks after implantation. *Clin. Implant Dent. Relat. Res.* 20, 82–91. doi: 10.1111/cid.12578

Tsukasaki, M., and Takayanagi, H. (2019). Osteoimmunology: evolving concepts in bone-immune interactions in health and disease. *Nat. Rev. Immunol.* 19, 626–642. doi: 10.1038/s41577-019-0178-8

Walsh, M. C., Takegahara, N., Kim, H., and Choi, Y. (2018). Updating osteoimmunology: regulation of bone cells by innate and adaptive immunity. *Nat. Rev. Rheumatol.* 14, 146–156. doi: 10.1038/nrrheum.2017.213

Wang, H., Yang, G., Xiao, Y., Luo, G., Li, G., and Li, Z. (2020). Friend or foe? Essential roles of osteoclast in maintaining skeletal health. *Biomed Res. Int.* 2020:4791786. doi: 10.1155/2020/4791786

Wang, J., Meng, F., Song, W., Jin, J., Ma, Q., Fei, D., et al. (2018). Nanostructured titanium regulates osseointegration via influencing macrophage polarization in the osteogenic environment. *Int. J. Nanomed.* 13, 4029–4043. doi: 10.2147/IJN.S163956

Wang, L., You, X., Lotinun, S., Zhang, L., Wu, N., and Zou, W. (2020). Mechanical sensing protein PIEZO1 regulates bone homeostasis via osteoblast-osteoclast crosstalk. *Nat. Commun.* 11:282. doi: 10.1038/s41467-019-14146-6

Wang, P., Perche, F., Logeart-Avramoglou, D., and Pichon, C. (2019). RNA-based therapy for osteogenesis. *Int. J. Pharm.* 569:118594. doi: 10.1016/j.ijpharm.2019.118594

Wang, X., Hou, H., Song, K., Zhang, Z., Zhang, S., Cao, Y., et al. (2018). Lpar2b controls lateral line tissue size by regulating Yap1 activity in zebrafish. *Front. Mol. Neurosci.* 11:34. doi: 10.3389/fnmol.2018.00034

Wang, Y., Zhang, Y., Sculean, A., Bosshardt, D. D., and Miron, R. J. (2019). Macrophage behavior and interplay with gingival fibroblasts cultured on six commercially available titanium, zirconium, and titanium-zirconium dental implants. *Clin. Oral Investig.* 23, 3219–3227. doi: 10.1007/s00784-018-2736-z

Wang, X., Freire Valls, A., Schermann, G., Shen, Y., Moya, I. M., Castro, L., et al. (2017). YAP/TAZ orchestrate VEGF signaling during developmental angiogenesis. *Dev. Cell* 42, 462–478.e7. doi: 10.1016/j.devcel.2017.08.002

Washio, K., Tsutsumi, Y., Tsumanuma, Y., Yano, K., Srithanyarat, S. S., Takagi, R., et al. (2018). *In vivo* periodontium formation around titanium implants using periodontal ligament cell sheet. *Tissue Eng. Part A* 24, 1273–1282. doi: 10.1089/ten.tea.2017.0405

Wilson, C. J., Clegg, R. E., Leavesley, D. I., and Pearcy, M. J. (2005). Mediation of biomaterial-cell interactions by adsorbed proteins: a review. *Tissue Eng.* 11, 1–18. doi: 10.1089/ten.2005.11.1

Wisdom, C., Chen, C., Yuca, E., Zhou, Y., Tamerler, C., and Snead, M. L. (2019). Repeatedly applied peptide film kills bacteria on dental implants. *JOM* 71, 1271–1280. doi: 10.1007/s11837-019-03334-w

Wu, X., Ma, Y., Su, N., Shen, J., Zhang, H., and Wang, H. (2019). Lysophosphatidic acid: its role in bone cell biology and potential for use in bone regeneration. *Prostaglandins Other Lipid Mediat.* 143:106335. doi: 10.1016/j.prostaglandins.2019.106335

Xiang, L., Yu, H., Zhang, X., Wang, B., Yuan, Y., Zhang, Q., et al. (2018). The versatile hippo pathway in oral-maxillofacial development and bone remodeling. *Dev. Biol.* 440, 53–63. doi: 10.1016/j.ydbio.2018.05.017

Xiong, J., Almeida, M., and O'Brien, C. A. (2018). The YAP/TAZ transcriptional co-activators have opposing effects at different stages of osteoblast differentiation. *Bone* 112, 1–9. doi: 10.1016/j.bone.2018.04.001

Yang, B., Sun, H., Xu, X., Zhong, H., Wu, Y., and Wang, J. (2020). YAP1 inhibits the induction of TNF-α-stimulated bone-resorbing mediators by suppressing the NF-κB signaling pathway in MC3T3-E1 cells. *J. Cell. Physiol.* 235, 4698–4708. doi: 10.1002/jcp.29348

Yang, W., Han, W., Qin, A., Wang, Z., Xu, J., and Qian, Y. (2018). The emerging role of Hippo signaling pathway in regulating osteoclast formation. *J. Cell. Physiol.* 233, 4606–4617. doi: 10.1002/jcp.26372

Yasuda, D., Kobayashi, D., Akahoshi, N., Ohto-Nakanishi, T., Yoshioka, K., Takuwa, Y., et al. (2019). Lysophosphatidic acid-induced YAP/TAZ activation promotes developmental angiogenesis by repressing Notch ligand Dll4. *J. Clin. Invest.* 129, 4332–4349. doi: 10.1172/JCI121955

Yu, F.-X., Zhao, B., Panupinthu, N., Jewell, J. L., Lian, I., Wang, L. H., et al. (2012). Regulation of the Hippo-YAP pathway by G-protein-coupled receptor signaling. *Cell* 150, 780–791. doi: 10.1016/j.cell.2012.06.037

Yung, Y. C., Stoddard, N. C., and Chun, J. (2014). LPA receptor signaling: pharmacology, physiology, and pathophysiology. *J. Lipid Res.* 55, 1192–1214. doi: 10.1194/jlr.R046458

Zarb, G., and Albrektsson, T. (1991). Osseointegration: a requiem for the periodontal ligament? *Int. J. Periodontics Restorative Dent.* 11, 81–91.

Zhang, Q., Guo, Y., Yu, H., Tang, Y., Yuan, Y., Jiang, Y., et al. (2019). Receptor activity-modifying protein 1 regulates the phenotypic expression of BMSCs via the Hippo/Yap pathway. *J. Cell. Physiol.* 234, 13969–13976. doi: 10.1002/jcp.28082

Zhao, L., Guan, H., Song, C., Wang, Y., Liu, C., Cai, C., et al. (2018). YAP1 is essential for osteoclastogenesis through a TEADs-dependent mechanism. *Bone* 110, 177–186. doi: 10.1016/j.bone.2018.01.035

Zhao, X., Wang, X., You, Y., Wen, D., Feng, Z., Zhou, Y., et al. (2020). Nogo-B fosters HCC progression by enhancing Yap/Taz-mediated tumor-associated macrophages M2 polarization. *Exp. Cell Res.* 391:111979. doi: 10.1016/j.yexcr.2020.111979

Zhou, X., Li, W., Wang, S., Zhang, P., Wang, Q., Xiao, J., et al. (2019). YAP aggravates inflammatory bowel disease by regulating M1/M2 macrophage polarization and gut microbial homeostasis. *Cell Rep.* 27, 1176–1189.e5. doi: 10.1016/j.celrep.2019.03.028

Zhu, W., Ming, P., Qiu, J., Shao, S., Yu, Y., Chen, J., et al. (2018). Effect of titanium ions on the Hippo/YAP signaling pathway in regulating biological behaviors of MC3T3-E1 osteoblasts: regulation of osteoblasts by Ti ions via Hippo/YAP. *J. Appl. Toxicol.* 38, 824–833. doi: 10.1002/jat.3590

Zizzi, A., Aspriello, S. D., Rubini, C., and Goteri, G. (2011). Peri-implant diseases and host inflammatory response involving mast cells: a review. *Int. J. Immunopathol. Pharmacol.* 24, 557–566. doi: 10.1177/039463201102400302

Zohrabian, V. M., Sonick, M., Hwang, D., and Abrahams, J. J. (2015). Dental implants. *Semin. Ultrasound CT MRI* 36, 415–426. doi: 10.1053/j.sult.2015.09.002

Conflict of Interest: The authors declare that the research was conducted in the absence of any commercial or financial relationships that could be construed as a potential conflict of interest.

frontiers in Cell and Developmental Biology

BRIEF RESEARCH REPORT
published: 15 October 2020
doi: 10.3389/fcell.2020.576396

α_2-Adrenergic Disruption of β Cell BDNF-TrkB Receptor Tyrosine Kinase Signaling

Michael A. Kalwat, Zhimin Huang†, Derk D. Binns, Kathleen McGlynn and Melanie H. Cobb*

Department of Pharmacology, UT Southwestern Medical Center, Dallas, TX, United States

Adrenergic signaling is a well-known input into pancreatic islet function. Specifically, the insulin-secreting islet β cell expresses the $G_{i/o}$-linked α_2-adrenergic receptor, which upon activation suppresses insulin secretion. The use of the adrenergic agonist epinephrine at micromolar doses may have supraphysiological effects. We found that pretreating β cells with micromolar concentrations of epinephrine differentially inhibited activation of receptor tyrosine kinases. We chose TrkB as an example because of its relative sensitivity to the effects of epinephrine and due to its potential regulatory role in the β cell. Our characterization of brain-derived neurotrophic factor (BDNF)-TrkB signaling in MIN6 β cells showed that TrkB is activated by BDNF as expected, leading to canonical TrkB autophosphorylation and subsequent downstream signaling, as well as chronic effects on β cell growth. Micromolar, but not nanomolar, concentrations of epinephrine blocked BDNF-induced TrkB autophosphorylation and downstream mitogen-activated protein kinase pathway activation, suggesting an inhibitory phenomenon at the receptor level. We determined epinephrine-mediated inhibition of TrkB activation to be $G_{i/o}$-dependent using pertussis toxin, arguing against an off-target effect of high-dose epinephrine. Published data suggested that inhibition of potassium channels or phosphoinositide-3-kinase signaling may abrogate the negative effects of epinephrine; however, these did not rescue TrkB signaling in our experiments. Taken together, these results show that (1) TrkB kinase signaling occurs in β cells and (2) use of epinephrine in studies of insulin secretion requires careful consideration of concentration-dependent effects. BDNF-TrkB signaling in β cells may underlie pro-survival or growth signaling and warrants further study.

Keywords: cell signaling, pancreatic islet, extracellular-signal-regulated kinase, brain-derived neurotrophic factor, BDNF/NT-3 growth factors receptor, epinephrine, adrenergic receptor, diabetes

OPEN ACCESS

Edited by:
José Lozano, University of Malaga, Spain

Reviewed by:
Michelle L. Halls, Monash University, Australia
Piero Crespo, Consejo Superior de Investigaciones Científicas, Spain

****Correspondence:***
Michael A. Kalwat
Michael.Kalwat@utsouthwestern.edu

†Present address:
Zhimin Huang, Department of Endocrinology and Diabetes Center, First Affiliated Hospital of Sun Yat-sen University, Guangzhou, China

Specialty section:
This article was submitted to Signaling, a section of the journal Frontiers in Cell and Developmental Biology

Received: *26 June 2020*
Accepted: *14 September 2020*
Published: *15 October 2020*

Citation:
Kalwat MA, Huang Z, Binns DD, McGlynn K and Cobb MH (2020) α_2-Adrenergic Disruption of β Cell BDNF-TrkB Receptor Tyrosine Kinase Signaling. Front. Cell Dev. Biol. 8:576396. doi: 10.3389/fcell.2020.576396

INTRODUCTION

Glucose homeostasis is largely controlled by the metered secretion of insulin from pancreatic islet β cells. β cells respond to elevated circulating glucose via coupling its metabolism to membrane depolarization, calcium (Ca^{2+}) influx, and insulin exocytosis (Kalwat and Cobb, 2017). Secreted insulin suppresses liver gluconeogenesis and stimulates peripheral glucose uptake. Diabetes is a disease of hyperglycemia caused by deficient insulin production and action. In diabetes, β cells are

either destroyed by the immune system (type 1 diabetes) or unable to secrete sufficient insulin in response to stimulation (type 2 diabetes). In order to function properly, pancreatic β cells integrate a diverse array of inputs, including nutrients and hormones. To accomplish this, β cells utilize a variety of signaling mechanisms such as G-protein-coupled receptors (GPCRs) (Holst, 2007; Straub and Sharp, 2012) and receptor tyrosine kinases (RTKs) (Kulkarni et al., 1999, 2002; Song et al., 2016). Reported cross talk between GLP1R and EGFR in islet β cells lends support to the idea of more general GPCR-RTK signaling interactions in β cells (Fusco et al., 2017).

Extracellular regulated kinase 1/2 (ERK1/2) is activated by insulin secretagogues (e.g., glucose, amino acids) and blunted by inhibitors of secretion (e.g., epinephrine) and is therefore frequently used as a proxy for β cell responsiveness (Longuet et al., 2005; Jaques et al., 2008; Goehring et al., 2011). ERK1/2 activation has long been recognized for its role in β cell growth and insulin gene expression (Hugl et al., 1998; Briaud et al., 2003; Khoo et al., 2003; Lawrence et al., 2008). Recently, acute ERK2 activity was demonstrated to be critical for the first phase of insulin secretion (Leduc et al., 2017). Our interest in the pathways leading to ERK1/2 activation and the inhibitory functions of epinephrine in β cells led us to test the impact of epinephrine on RTK signaling to ERK1/2. Epinephrine has different effects on the ERK1/2 pathway depending on cell type and receptors expressed. In β cells, epinephrine activates α_2-adrenergic receptors and inhibits insulin secretion as well as glucose-stimulated ERK1/2 activation (Peterhoff et al., 2003; Gibson et al., 2006).

We discovered that epinephrine suppressed RTK signaling in a concentration-dependent manner and with varying potency depending on the RTK. Activation of α_2-adrenergic receptors in pancreatic islet β cells has been extensively studied and is well-known to suppress or completely inhibit insulin secretion through $G\alpha_{i/o}$-dependent signaling (Sharp, 1996; Straub and Sharp, 2012). While physiological circulating concentrations of catechols (epinephrine, norepinephrine) range from picomolar to low nanomolar (Clutter et al., 1980; Dodt et al., 1997; Kienbaum et al., 1998), often micromolar concentrations are used to investigate pancreatic islet function (Sieg et al., 2004; Gibson et al., 2006; Iwanir and Reuveny, 2008; Zhao et al., 2008; Zhang et al., 2009; Slucca et al., 2010; Tian et al., 2011). Among the RTKs we tested in β cells, we chose TrkB for its sensitivity to stimulation with ligand, inhibition by epinephrine, and relative lack of knowledge of its role in β cells. Our characterization and analysis of BDNF-TrkB signaling to ERK1/2 in MIN6 β cells revealed effects on growth and interactions with insulin secretagogues and that epinephrine blocks TrkB signaling at the receptor level in a G_i-dependent manner. We conclude from our findings that the doses of epinephrine used in β cell experiments should be carefully considered.

MATERIALS AND METHODS

Antibodies, Plasmids, and Reagents

All chemicals were purchased through Fisher Scientific unless otherwise indicated and listed in **Supplementary Table 1**. All relevant reagents used in this study are listed in **Supplementary Table 1**. Concentrations of compounds and ligands were chosen based either on the literature or on empirical testing in MIN6 cells with dose–response curves. For BDNF, the 10-ng/mL dose was chosen based on dose–response curve stimulations of ERK1/2 activation in MIN6 cells. Above that dose, no substantial increase in pERK1/2 was observed. As the dose of epinephrine is a major point of this work, we used commonly used micromolar doses found in the literature, as well as less frequently used nanomolar doses in our experiments.

Immunoblotting

Cleared cell lysates (40–50 μg) were separated on 10% gels by SDS-PAGE and transferred to nitrocellulose for immunoblotting. All membranes were blocked in Odyssey blocking buffer (Licor) for 1 h before overnight incubation with primary antibodies diluted in blocking buffer. After three 10-min washes in 20 mM Tris–HCl pH 7.6, 150 mM NaCl, 0.1% Tween-20 (TBS-T), membranes were incubated with fluorescent secondary antibodies for 1 h at room temperature. After three 10-min washes in TBS-T, membranes were imaged on a Licor Odyssey scanner.

MIN6 Cell Culture and Transfections

MIN6 β cells were cultured in Dulbecco's modified Eagle's medium (D6429), supplemented with 15% fetal bovine serum, 100 units/ml penicillin, 100 μg/ml streptomycin, 292 μg/ml L-glutamine, and 50 μM β-mercaptoethanol (Kalwat et al., 2016). MIN6 cells in 12-well dishes were untreated or transfected with Lipofectamine 2000 according to the manufacturer's instructions and cultured 48 h before use in experiments. For chronic BDNF treatment, cells were incubated with 100 ng/ml BDNF in complete culture media. Prior to stimulation, MIN6 cells were washed twice with and incubated for 2 h in freshly prepared glucose-free modified Krebs–Ringer bicarbonate buffer (MKRBB: 5 mM KCl, 120 mM NaCl, 15 mM HEPES, pH 7.4, 24 mM $NaHCO_3$, 1 mM $MgCl_2$, 2 mM $CaCl_2$, and 1 mg/ml radioimmunoassay-grade BSA). Cells were lysed in 25 mM HEPES, pH 7.4, 1% Non-idet P-40, 10% glycerol, 50 mM sodium fluoride, 10 mM sodium pyrophosphate, 137 mM NaCl, 1 mM sodium vanadate, 1 mM phenylmethylsulfonyl fluoride, 10 μg/ml aprotinin, 1 μg/ml pepstatin, and 5 μg/ml leupeptin and cleared of insoluble material by centrifugation at 10,000 × *g* for 10 min at 4°C for subsequent use.

Human Pancreatic Tissue Microscopy

Paraffin-embedded formalin-fixed 5-μm sections of de-identified human pancreas tissue on glass slides were obtained through the Simmons Comprehensive Cancer Center at UT Southwestern Medical. Slides were deparaffinized with the assistance of the UTSW Molecular Pathology Core using an automated system for xylene and ethanol washes. Antigen retrieval was performed by heating in citrate buffer[1]. After three 10-min washes in PBS-T (137 mM NaCl, 2.7 mM KCl, 10 mM Na_2HPO_4, 1.8 mM KH_2PO_4, pH 7.4, 0.05% Tween-20), slides were blocked for

[1]http://www.ihcworld.com/_protocols/epitope_retrieval/citrate_buffer.htm

1 h at room temperature in normal donkey serum (NDS) block solution (2% donkey serum, 1% bovine serum albumin, 0.1% cold fish skin gelatin, 0.1% Triton X-100, 0.05% sodium azide, PBS-T). Sections were outlined with a barrier pen and incubated overnight at 4°C with primary antibodies. Primary antibodies were diluted in NDS blocking solution at the indicated dilutions (**Supplementary Table 1**). After three 10-min washes in PBS-T, slides were incubated in secondary antibodies in NDS block for 1 h at room temperature. The washed slides were mounted with Dapi Fluoromount-G (SouthernBiotech #0100-20) and imaged on either an LSM700 Zeiss AxioObserver confocal microscope equipped with a Plan-Apochromat 20x/0.8 M27 objective and a MBS 405/488/555/639 beam splitter. Laser lines were 639 nm (for TrkB), 555 nm (for Insulin), 488 nm (for Glucagon), and 405 nm (for DAPI) each at 2% power. Images were processed in Zeiss' Zen software to add scale bars, set coloration for channels, and generate merged images. Scale bars indicate 50 μm.

Statistical Analysis

Quantitated data are expressed as mean ± SD. Data were evaluated using Student's t test or ANOVA with multiple comparisons test as appropriate and considered significant if $P < 0.05$. Graphs were made in GraphPad Prism 8.

RESULTS

Epinephrine Differentially Blocks Activation of RTK Signaling in MIN6 β Cells

In our studies of β cell ERK1/2 activation, we noted an interaction between signaling downstream of RTKs and α_2-adrenergic receptor stimulation. To expand upon these observations, we stimulated MIN6 β cells with different RTK ligands to examine the effects of epinephrine. EGF, BDNF, and FGF1 stimulated ERK1/2 phosphorylation within 5 min (**Figure 1A**). Pretreatment with epinephrine for 15 min blocked downstream phosphorylation of ERK1/2 to varying degrees depending on the RTK in question (**Figure 1A**). We found that EGF signaling to ERK1/2 was partially inhibited by epinephrine (**Figure 1A**); however, BDNF- and FGF1-induced signaling appeared more sensitive. We chose BDNF-TrkB for our experiments because of its sensitivity to epinephrine and because it is relatively underexplored compared to other RTK signaling pathways in β cells.

To confirm the involvement of that α_2-adrenergic receptor activation, we tested the isoform-selective adrenergic agonist UK14304, which also suppressed BDNF-TrkB signaling to ERK1/2 in MIN6 cells (**Figure 1B**). We also found that epinephrine's effects on BDNF-TrkB signaling were prevented by the α_2-adrenergic receptor antagonist yohimbine (**Figure 1C**).

TrkB Is Expressed in Human Islets and Promotes Cell Growth in MIN6 β Cells

TrkB was reported to be expressed only in α cells (Shibayama and Koizumi, 1996; Hanyu et al., 2003); however, given our

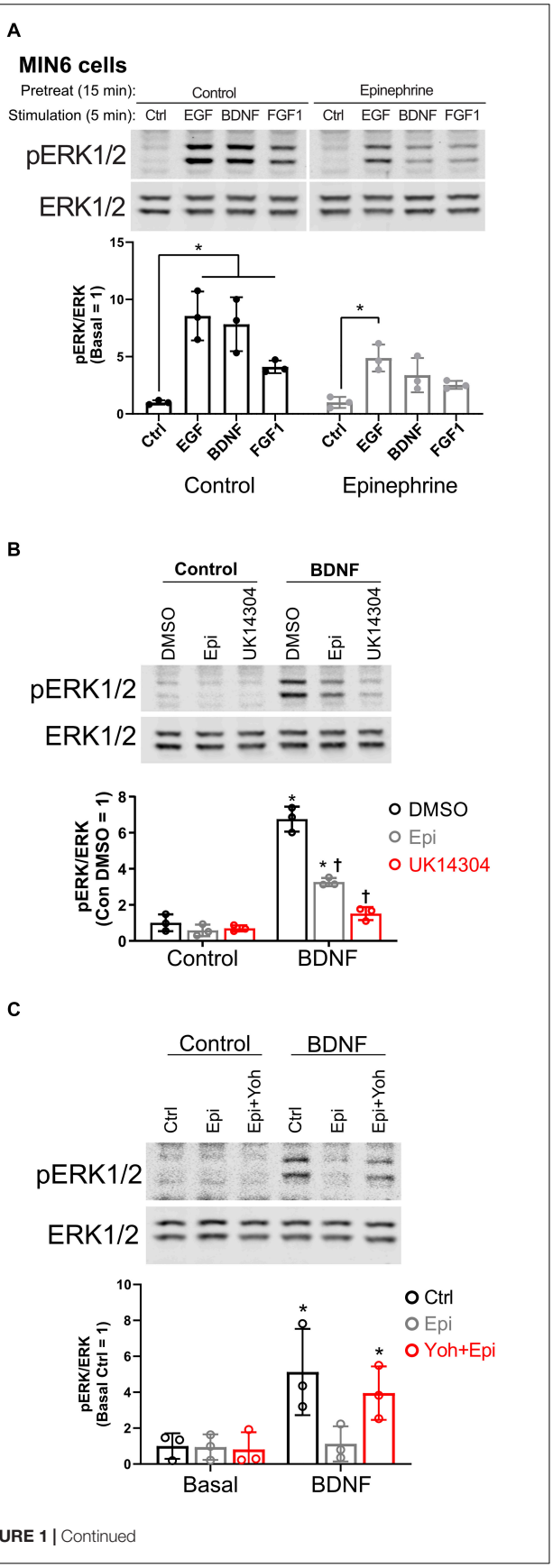

FIGURE 1 | Continued

FIGURE 1 | α_2-adrenergic stimulation suppresses receptor tyrosine kinase signaling in MIN6 β cells. **(A)** To determine the effects of epinephrine pretreatment on receptor tyrosine kinase signaling in β cells, MIN6 cells were preincubated in KRBH with 2 mM glucose for 1 h 45 min before addition of epinephrine (10 μM) for 15 min. Cells were stimulated with the indicated ligand for 5 min (EGF 10 ng/ml; BDNF 10 ng/ml; FGF1 10 ng/ml). Immunoblots are shown for phospho-ERK1/2 (pERK1/2) and total ERK1/2, and data are the mean ± SD for three independent experiments. $^*P < 0.05$ vs Ctrl by two-way ANOVA with Dunnett's multiple-comparison test. **(B)** To confirm that α_2-adrenergic stimulation prevents BDNF-stimulated signaling, MIN6 cells were preincubated in KRBH for 1 h 45 min before treatment with 0.1% DMSO, 10 μM epinephrine (Epi), or 10 μM UK14304 for 15 min. Cells were then stimulated with BDNF (10 ng/ml) for 5 min. Immunoblots are shown for phospho-ERK1/2 (pERK1/2) and total ERK1/2, and data are the mean ± SD of three independent experiments. $^*P < 0.05$ for Control vs BDNF and $^\dagger P < 0.05$ for DMSO vs drug by 2-way ANOVA with Tukey's multiple-comparison test. **(C)** To determine if epinephrine-mediated inhibition of BDNF-TrkB signaling is due to its action on the α_2-adrenergic receptor, MIN6 cells were preincubated in glucose-free KRBH for 1 h and 40 min and then treated with or without the α_2-adrenergic receptor antagonist yohimbine (10 μM). After 5 min, epinephrine (5 μM) was added as indicated. After 15 min, cells were stimulated with BDNF (10 ng/ml) for 5 min. Immunoblots for pERK1/2 and total ERK1/2 are shown with bar graph quantitation being the mean ± SD of three independent experiments.

β cell line data, we sought to confirm expression in human islets with multiple antibodies. TrkB was detected in both β and α cells in human (**Figure 2A**) and mouse (**Supplementary Figure 1A**) pancreatic islets by immunocytochemistry with independently validated anti-TrkB antibodies (**Supplementary Figure 1B**). The NTRK2 gene encodes multiple isoforms of TrkB. The major forms are full-length kinase domain-containing TrkB (TrkB.FL) and a truncated form, TrkB.T1, which is missing in the kinase domain (Fenner, 2012). A TrkB antibody against a C-terminal epitope only found in TrkB.FL showed primarily α cell labeling (**Figure 2A**; SCBT), in agreement with previous work (Shibayama and Koizumi, 1996; Hanyu et al., 2003). However, antibodies with extracellular N-terminal epitopes labeled both α and β cells (**Figure 2A**; Millipore, Abcam). We found that clonal rodent β cell lines responded to as little as 2.5 ng/ml BDNF, leading to activation of ERK1/2 within 5 min of stimulation (**Supplementary Figures 1C–E**). BDNF had a negligible effect on the phosphorylation of Akt but increased S6 phosphorylation at 30 min (**Supplementary Figure 1F**).

BDNF-stimulated activation of ERK1/2 was blocked by small-molecule TrkB inhibitors (GNF-5837 and lestaurtinib) (**Supplementary Figures 1G,H**) as well as by CRISPR/Cas9-mediated knockout of TrkB (TrkB-KO) (**Figure 2B**). Multiple clonal lines of TrkB knockout MIN6 cells were confirmed to lack TrkB by immunoblotting and verified to retain glucose-induced ERK1/2 activation (**Supplementary Figure 1I**). BDNF-stimulated ERK1/2 signaling was rescued upon transient re-expression of TrkB.FL but not TrkB.T1 (**Figure 2B**). Additionally, we observed that 48 h of BDNF treatment increased viability (**Figure 2C**). We did not observe any effects of chronic BDNF treatment on glucose-stimulated insulin secretion under similar conditions (**Supplementary Figure 1J**).

Epinephrine Inhibits TrkB Signaling at the Receptor Level and Only at Micromolar Concentrations

To determine how α_2-adrenergic stimulation could prevent BDNF-TrkB signaling to ERK1/2, we probed the upstream phosphorylation state of TrkB itself. Typically, BDNF stimulates autophosphorylation of the TrkB receptor at several tyrosine residues (Huang and Reichardt, 2003). We found that BDNF-induced tyrosine autophosphorylation of TrkB was blocked by epinephrine in MIN6 β cells (**Figure 3A**), raising the possibility of direct effects on the TrkB receptor tyrosine kinase. Because nanomolar concentrations of epinephrine are sufficient to inhibit glucose-stimulated insulin secretion in our InsGLuc-MIN6 reporter cells (**Figure 3B**), we tested the ability of both 5 nM and 5 μM epinephrine to affect MIN6 responses to BDNF or EGF. 5 nM epinephrine suppressed neither BDNF or EGF signaling to ERK nor TrkB tyrosine phosphorylation, while 5 μM epinephrine blocked BDNF signaling, yet EGF retained its significant ability to activate ERK1/2 (**Figure 3C**).

Epinephrine-Mediated Inhibition of BDNF-TrkB Signaling Depends on G_i but Does Not Involve Calcium Influx or cAMP Generation

Epinephrine inhibits insulin secretion in β cells through α_2-adrenergic receptors linked to $G\alpha_i$ (Straub and Sharp, 2012). To delve further into the mechanism of epinephrine-mediated blockade of BDNF-TrkB signaling, we treated cells with pertussis toxin (PTX) which inactivates $G\alpha_i$. INS1 β cells were used because in our experience they exhibited a more robust response to PTX than MIN6 cells, and INS1 cells responded well to BDNF (**Supplementary Figure 1C**). PTX prevented the effects of epinephrine on BDNF- and glucose-mediated activation of ERK1/2 (**Figure 4A**), indicating a requirement for $G\alpha_{i/o}$ signaling.

Cross talk between receptor tyrosine kinases and GPCRs has been found (Marty and Ye, 2010), although little is known about these pathway interactions in β cells. One mechanism $G\alpha_{i/o}$ uses to suppress β cell function is through inhibition of adenylyl cyclase (Straub and Sharp, 2012). Therefore, we performed a series of experiments to determine the cross talk between BDNF-TrkB and pathways that generate cAMP. We tested whether BDNF exhibited cross talk with epinephrine, glucagon-like peptide 1 receptor (GLP-1R) agonism, cAMP analogs, and glucose. Pretreatment with GLP-1R agonists GLP-1 or exendin-4, or with the cAMP analog Sp-8Br-cAMPS, enhanced ERK1/2 phosphorylation in response to BDNF in the presence of glucose (**Supplementary Figures 2A,B**), suggesting interactions among TrkB, the GLP-1 receptor/cAMP, and glucose metabolic pathways. Epinephrine pretreatment dramatically inhibited ERK1/2 activation in response to either glucose, BDNF or their combination.

We also tested whether BDNF on its own can induce cAMP generation in MIN6 cells expressing a bioluminescence-resonance energy transfer-based cAMP reporter (cAMP sensor

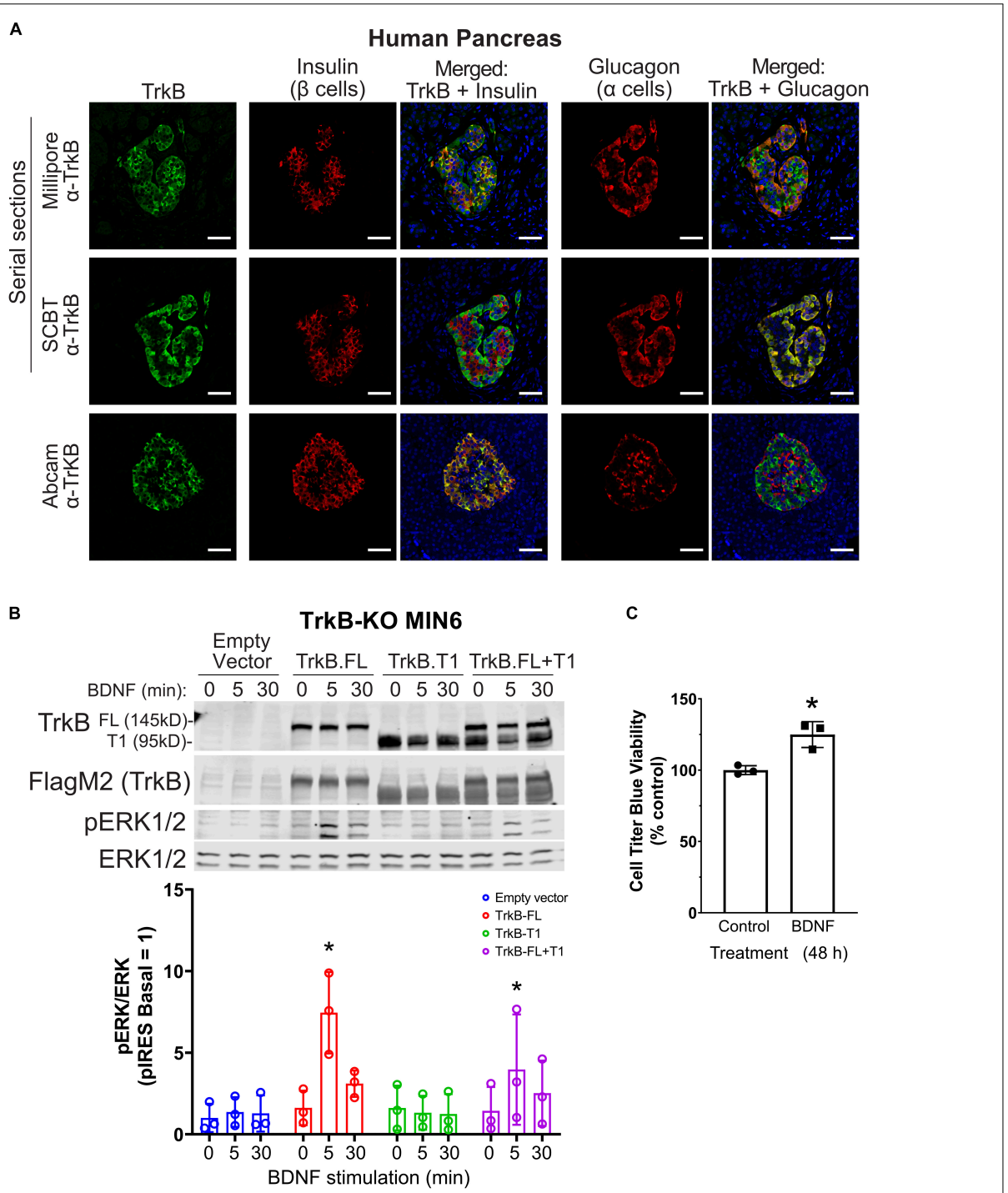

FIGURE 2 | TrkB is expressed in pancreatic islets and chronic BDNF signaling promotes insulin secretion and β cell growth. **(A)** Human pancreas tissue sections were immunostained with antibodies against TrkB (shown in green), insulin to stain β cells (shown in red), glucagon to stain α cells (shown in red), and DAPI to stain nuclei (shown in blue). For the example shown of Millipore and Santa Cruz anti-TrkB antibody staining, serial sections from the same tissue block were stained with different TrkB antibodies and the same islet was located for imaging. Separate panels are shown to illustrate the overlap of TrkB with β cells (insulin) and TrkB with α cells (glucagon). Overlapping regions of green TrkB staining and red insulin/glucagon staining show up yellow. Data are representative of imaging from 2 human pancreas tissue donors. Scale bar, 50 μm. **(B)** To confirm that TrkB-FL is indeed the BDNF receptor signaling to ERK1/2 in β cells, TrkB KO MIN6 cells were transfected with plasmids expressing full-length TrkB (TrkB-FL), TrkB-T1, both, or empty vector (pIRES-3xFlag-dsRed). After 48 h cells were preincubated in KRBH with 4.5 mM glucose for 2 h and stimulated with 10 ng/ml BDNF for 5 and 30 min. Data are the mean ± SD of three independent experiments. *$P < 0.05$ for 0 vs 5 min of BDNF stimulation by two-way ANOVA using Dunnett's multiple-comparison test. **(C)** To assess pro-growth effects of chronic BDNF stimulation, MIN6 cells plated in 96-well dishes were incubated for 48 h with BDNF (100 ng/ml) followed by Cell Titer Blue assay for viability. Bar graph is the mean ± SD from three independent passages of cells. *$P < 0.05$ Control vs. BDNF by Student's *t*-test.

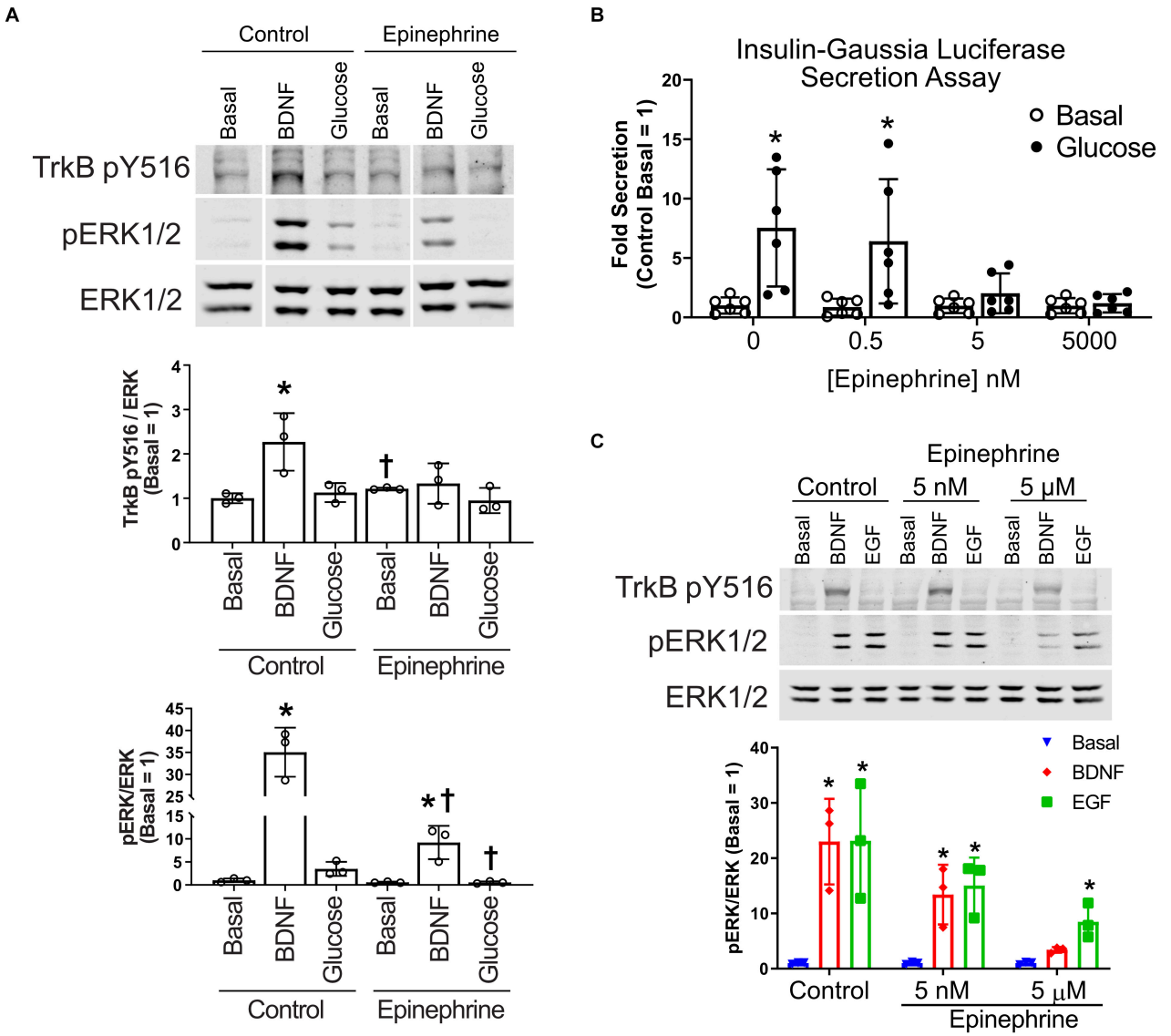

FIGURE 3 | Epinephrine suppresses BDNF signaling to ERK by blocking TrkB activation. **(A)** To determine if epinephrine affected the upstream activation of TrkB itself, MIN6 cells were preincubated in KRBH containing 2 mM glucose for 1 h 45 min before addition of epinephrine (10 μM) for 15 min. Cells were then stimulated with BDNF (10 ng/ml) or glucose (20 mM) for 5 min. Western blot analysis shows phosphorylated TrkB (pY516) and ERK1/2 (pERK1/2) normalized to total ERK1/2 ($N = 3$). Vertical white lines indicate that intervening lanes have been spliced out. *$P < 0.05$ vs. respective basal. †$P < 0.05$ Control vs. Epinephrine by Student's *t*-test. **(B)** InsGLuc-MIN6 cells were preincubated in glucose-free KRBH for 1 h followed by stimulation with glucose (20 mM) in the presence or absence of epinephrine (0.5 nM, 5 nM, or 5 μM) for 1 h. Supernatant was collected for Gaussia luciferase assays and the data are reported as the fold change with respect to basal unstimulated cells ($N = 6$). All graphs are the mean ± SD. *$P < 0.05$ Basal vs. Glucose by two-way ANOVA using Dunnett's multiple-comparison test. **(C)** MIN6 cells were treated as in panel **(A)**; however, the cells were pretreated with either 5 nM or 5 μM epinephrine prior to stimulation with EGF or BDNF for 5 min. Western blot analysis shows only 5 μM epinephrine suppressed pTrkB ($N = 2$) and pERK1/2 ($N = 3$) signaling by BDNF. Bar graph is the mean ± SD. *$P < 0.05$ vs. respective Basal by two-way ANOVA using Dunnett's multiple-comparison test.

using YFP-Epac-RLuc or CAMYEL) (Jiang et al., 2007; Guerra et al., 2017). While the known G_s activator GLP-1 increased cAMP (Holst, 2007), BDNF had no effect, either alone or in combination with glucose or GLP-1 (**Supplementary Figure 2C**). However, through inhibition of adenylyl cyclase, $G\alpha_{i/o}$ suppresses cAMP generation, and basal levels of cAMP may play a role in supporting BDNF-TrkB signaling (Ji et al., 2005). Therefore, we tested whether adenylyl cyclase inhibitors dideoxyadenosine (ddAd) and SQ22536 had the same effect as epinephrine. These compounds did not impact BDNF-stimulated ERK1/2 activation (**Supplementary Figure 2D**). Therefore, while BDNF-TrkB signaling can synergize with cAMP to enhance ERK1/2 activation, these data suggest against a requirement for cAMP production for BDNF-TrkB signaling in MIN6 β cells.

We also examined the involvement of calcium influx, which regulates ERK1/2 activation in β cells and is inhibited by

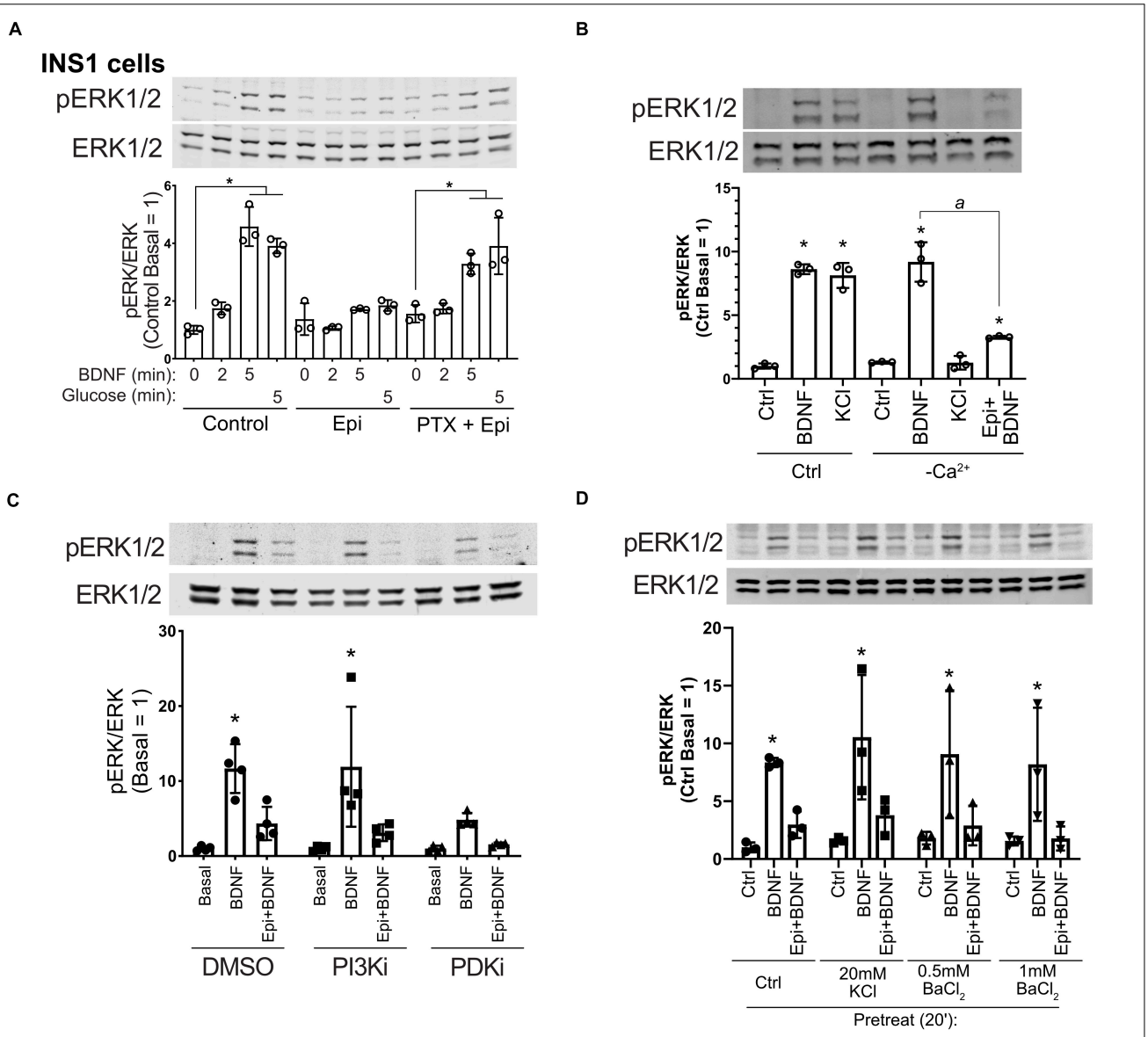

FIGURE 4 | Epinephrine blockade of BDNF signaling depends on $G\alpha_{i/o}$ but is unaffected by Ca^{2+} influx, PI3K/PDK1 inhibition, or treatment with KCl or $BaCl_2$. **(A)** To determine the dependence of epinephrine on $G_{i/o}$ activation, INS1 β cells were treated with 200 ng/ml pertussis toxin (PTX) for 18 h in the culture medium. Cells were then incubated in KRBH with 2 mM glucose in the continued presence or absence of PTX for 2 h. Prior to stimulation, cells were treated with or without 10 μM epinephrine for 15 min. Cells were stimulated with or without 10 ng/ml BDNF or 20 mM glucose for the indicated time. Data are the mean ± SD of three independent experiments. *$P < 0.05$ vs respective basal by two-way ANOVA using Dunnett's multiple-comparison test. **(B)** To determine the requirement of Ca^{2+} influx for BDNF-TrkB signaling, MIN6 cells were preincubated in normal (Ca^{2+}-containing) or Ca^{2+}-free KRBH (compensated with additional 2 mM $MgCl_2$) without glucose for 2 h. 15 min prior to stimulation, 10 μM epinephrine was added where indicated. Cells were stimulated with 10 ng/ml BDNF or 50 mM KCl for 5 min. Data are the mean ± SD. *$P < 0.05$ compared to respective basal; a, $P < 0.05$ by one-way ANOVA using Tukey's multiple-comparison test. **(C)** To determine if PI3K/PDK1 inhibition prevents the effects of epinephrine on BDNF signaling, MIN6 cells were preincubated for 1.5 h in glucose-free KRBH and then treated with DMSO (0.1%), GDC-0941 (250 nM), or GSK2334470 (250 nM) for 15 min. Cells were then treated or not with 5 μM epinephrine for 15 min before stimulation with BDNF (10 ng/ml) for 5 min. Bar graph represents the mean ± SE for four independent experiments. *$P < 0.05$ vs. Basal by two-way ANOVA with Dunnett's multiple-comparison test. **(D)** To block potassium channels potentially involved in membrane hyperpolarization, MIN6 cells were preincubated in glucose-free KRBH for 1 h and 40 min at which point KCl or $BaCl_2$ were added. At 1 h and 45 min, epinephrine (5 μM) was added. At 2 h cells were stimulated with BDNF for 5 min and then harvested for Western blot analysis. All data are the mean ± SD of $N = 3$ experiments. *$P < 0.05$ by two-way ANOVA using Dunnett's multiple comparisons test.

epinephrine (Straub and Sharp, 2012). Eliminating calcium influx by removal of calcium from the incubation buffer had no impact on BDNF signaling to ERK1/2, nor did it prevent the inhibiting effect of epinephrine on BDNF-induced ERK1/2 activation. KCl-mediated depolarization no longer activated ERK1/2 in the absence of calcium (**Figure 4B**), demonstrating the mechanistic dichotomy between growth factor and depolarization-stimulated ERK1/2 activation.

Epinephrine Inhibition of RTKs Is Not Prevented by PI3K/PDK1 Inhibition or by Blockade of Potassium Channels With KCl or $BaCl_2$

Inhibition of the phosphoinositide-3-kinase signaling pathway is reported to abrogate the hyperpolarizing effects of micromolar epinephrine (Zhang et al., 2009). We pretreated MIN6 β cells with well-characterized inhibitors for PI3K (GDC-0941) and PDK1 (GSK2334470) followed by epinephrine and analyzed the response to BDNF. These inhibitors did not rescue BDNF-induced ERK1/2 activation (**Figure 4C**), suggesting that the PI3K/PDK1 pathway is not required for the G_i-dependent blockade of TrkB activation.

Sieg et al. (2004) found that epinephrine hyperpolarizes cells in a PTX-sensitive manner through unidentified K^+ channels that can be blocked by low-dose (20 mM) KCl or 0.5–1 mM $BaCl_2$. We tested these conditions and found that treating with KCl or $BaCl_2$ prior to addition of micromolar epinephrine did not rescue BDNF-TrkB signaling to ERK1/2 (**Figure 4D**). Another possible explanation is that epinephrine induces TrkB receptor internalization. However, surface biotinylation experiments did not show a significant effect of epinephrine on the amount of surface TrkB (**Supplementary Figure 3**), suggesting alternative mechanisms.

DISCUSSION

How Does α_2-Adrenergic Stimulation Block Activation of RTKs Like TrkB?

In addition to the events that distinguish signaling by BDNF and glucose, the unexpected sensitivity of BDNF to inhibition by α_2-adrenergic agonism suggests a connection between signaling by BDNF and insulin secretagogues. RTKs share certain signaling pathways; the Ras-ERK1/2, PI3K-Akt and PLCγ pathways are the most recognized (Minichiello, 2009). Depending on the context, different ligand–receptor family members may signal independently within the same cell to different pathways or exhibit inter-pathway cross talk (Coster et al., 2017), but the exact molecular mechanisms are not always clear. Other inputs such as glucose-stimulated metabolic pathways can act on some of the same signaling pathways seemingly by independent mechanisms (Khoo and Cobb, 1997; Khoo et al., 2004; Kalwat et al., 2013). α_2-Adrenergic signaling is well-known to antagonize insulin secretion in β cells, largely through heterotrimeric $G_{i/o}$ proteins (Gibson et al., 2006; Zhao et al., 2010; Straub and Sharp, 2012; Ito et al., 2017). In tandem with this effect, α_2-adrenergic signaling blocks glucose-stimulated ERK1/2 phosphorylation (Gibson et al., 2006), by mechanisms including inhibition of adenylyl cyclase and blockade of calcium influx. We found that BDNF signaling through the ERK1/2 pathway is also blocked in β cells by epinephrine through a G_i-dependent mechanism at the level of TrkB activation, indicating that essential β cell regulatory inputs are shared between RTKs and glucose-stimulated signaling pathways.

G_i-dependent cross talk between α_2-adrenergic receptors and RTKs is a relatively unexplored aspect of β cell signaling. GPCR-RTK cross talk has been observed to activate RTK pathways, but reports of G protein inhibition of RTKs are uncommon (Marty and Ye, 2010). Endogenous plasma epinephrine concentrations in humans normally range from 10 to 100 pg/ml (54.5–545 pM) (Dodt et al., 1997; Kienbaum et al., 1998) but can increase to 1,000 pg/ml (5.4 nM) (Clutter et al., 1980) during infusions of drugs or epinephrine itself. Micromolar and nanomolar concentrations of epinephrine have been proposed to inhibit insulin secretion through different mechanisms (Ito et al., 2017). In the case of nanomolar concentrations of epinephrine, cAMP-TRPM2 channel activity is suppressed, blunting glucose-induced insulin secretion, although sulfonylurea-induced secretion is unaffected (Ito et al., 2017). At ≥1 μM epinephrine, secretion under nearly all conditions is inhibited and the plasma membrane is hyperpolarized. In work from Peterhoff et al., 1 μM epinephrine was shown to inhibit adenylyl cyclase and hyperpolarize the plasma membrane in wild-type but not in $\alpha_{2A/C}$-adrenergic receptor knockout β cells, suggesting that the actions of micromolar concentrations of epinephrine occur specifically through its receptor (Peterhoff et al., 2003). It is worth noting recent findings showing that even relatively low concentrations of ligand in the aqueous phase above cells can become concentrated at the cell membrane due to interactions with the phospholipid bilayer or receptors (Gherbi et al., 2018), and GPCRs may also be activated by ultralow ligand concentrations (Civciristov et al., 2018).

Because activation of RTK signaling by BDNF in MIN6 β cells appears unaffected by changes in intracellular calcium and did not induce cAMP on its own, suppression of these mechanisms is unlikely to account for the effect of epinephrine on BDNF-TrkB signaling. However, we found that micromolar concentrations of epinephrine were required for its inhibitory activity on TrkB. Why nanomolar epinephrine fails to block BDNF-TrkB signaling when it is also known to activate $G_{i/o}$ under those conditions is an open question. Possible mechanisms may include membrane hyperpolarization or activation of G protein-gated inward rectifier potassium channels (Iwanir and Reuveny, 2008), although it is unclear how membrane hyperpolarization could affect TrkB. One possibility is that $G_{i/o}$ binds directly to TrkB to inhibit its activation, as was shown for $G_{i/o}$ binding to insulin receptor in β cells (Kim et al., 2012); however, mechanisms for the concentration-dependent effects of epinephrine in such a process are unclear.

What Is the Role for BDNF-TrkB Signaling in β Cells?

BDNF and its receptor TrkB mediate aspects of neuronal development and differentiation and are involved in whole-body energy homeostasis (Hutchison, 2012, 2013) and diabetes (Verge et al., 2014). BDNF can indirectly regulate islet hormones, like glucagon, through actions in the hypothalamus and innervation of the islet (Gotoh et al., 2013) and was suggested to have direct effects on α cells (Hanyu et al., 2003). However, TrkB is expressed in both rodent and human β and α cells, as supported by our data

and others (Shibayama and Koizumi, 1996; Hanyu et al., 2003; Uhlen et al., 2015; DiGruccio et al., 2016; Segerstolpe et al., 2016; Fulgenzi et al., 2020). TrkB is expressed as two splice isoforms, full-length TrkB (TrkB.FL) and TrkB.T1 which is missing the cytosolic kinase domain, instead containing a short distinct cytosolic tail (Fenner, 2012). Recent work from Fulgenzi et al. (2020) has demonstrated that the TrkB splice isoform, TrkB.T1, is involved in BDNF-induced insulin secretion and that BDNF can induce insulin secretion from human islets at low glucose concentrations. The relative amounts of TrkB.FL and TrkB.T1 in islet β and α cells has not been defined and could potentially explain the different staining patterns we observe with antibodies to different epitopes. While TrkB.T1 mRNA expression is much greater than full-length TrkB in β cells, TrkB.FL is indeed expressed and even a relatively low amount of RTK at the protein level is sufficient for signaling. We have observed that even >90% knockdown of TrkB protein by siRNA was insufficient to blunt BDNF-stimulated ERK1/2 activation. Not until TrkB protein was eliminated completely by CRISPR/Cas9 did we prevent BDNF-ERK1/2 signaling (**Figure 2B**).

There are multiple studies linking circulating BDNF concentration to type 2 diabetes in humans and mice (Krabbe et al., 2007; Sha et al., 2007; Li et al., 2016; Murillo Ortiz et al., 2016) as well as in type 1 diabetic patients (Tonoli et al., 2015). Treating db/db mice with BDNF lowered blood glucose, and increased pancreatic insulin content (Tonra et al., 1999) and β cell area and staining intensity were increased (Yamanaka et al., 2006). BDNF may also have a cytoprotective role in the islet because treatment with BDNF prevented RIN5F β cell death in response to alloxan, streptozotocin, doxorubicin, and benzo(a)pyrene (Bathina et al., 2016). Additionally, we observed that the stimulatory concentration of BDNF is well within the range of the circulating hormone (Krabbe et al., 2007; Dell'Osso et al., 2009; Matthews et al., 2009; Karczewska-Kupczewska et al., 2012; Kurita et al., 2012; Pillai et al., 2012). These studies indicate the need for further analysis of the effects and mechanisms of action of BDNF-TrkB signaling in pancreatic islets.

TrkB is known to exhibit cross talk with other kinases, including Src-family kinases (Huang and McNamara, 2010), Ret (Esposito et al., 2008), and the EGF receptor (Puehringer et al., 2013). Oligomerization between receptor kinases TrkA and TrkB could potentially be a contributor to the actions of NGF and may also contribute to BDNF-TrkB signaling not reflected by ERK1/2 activity. Another factor that may complicate interpretation of BDNF function is the expression of isoforms lacking the kinase domain. In our knockout-rescue experiments, TrkB.T1 seemed to suppress the activity of the full-length receptor, as has been suggested in other systems (Eide et al., 1996; Fryer et al., 1997; De Wit et al., 2006). In the future, specific deletion of TrkB.FL from different islet cell types in mice from early in development or in the adult phase may deconvolute roles for TrkB.FL and TrkB.T1 in islet development and function.

Future Directions

Whether epinephrine or $G_{i/o}$ activation impacts RTK signaling in other cell types is an open question. Adrenergic stimulation of β cells has been suggested to impair β cell growth at near micromolar concentrations (Zhao et al., 2014), and while cAMP is potentially involved, other mechanisms including suppression of RTK signaling may be at work in such conditions.

Future studies are required to place these actions of BDNF in an *in vivo* context to assess their metabolic impact, as well as to elucidate the mechanism underlying the unanticipated finding that epinephrine prevents activation of TrkB itself by BDNF. If any components of that mechanism are pharmacologically targetable, it may be possible to modulate TrkB or other RTK signaling in islets *in vivo* for therapeutic benefit. Notably, single-nucleotide polymorphisms in and near the ADRA2A gene (encoding α_{2A}-adrenergic receptor) have been correlated with increased fasting glycemia and type 2 diabetes risk (Liggett, 2009; Dupuis et al., 2010; Talmud et al., 2011; Langberg et al., 2013); impaired glucose-stimulated insulin secretion is a factor in this increased risk. Our findings suggest there is potential for contribution of altered adrenergic cross talk with RTK signaling in disease. In addition, these results have implications for other systems in which adrenergic and receptor tyrosine kinase signaling may converge, such as cancer (Hui et al., 2008; Powe et al., 2011; Stock et al., 2013).

DATA AVAILABILITY STATEMENT

The raw data supporting the conclusions of this article will be made available by the authors, without undue reservation.

AUTHOR CONTRIBUTIONS

MK: conceptualization and formal analysis. MK, ZH, DB, and KM: investigation. MK and MC: writing—original draft, supervision, and funding acquisition. All authors contributed to the article and approved the submitted version.

FUNDING

NIH F32 DK100113 and JDRF 2-SRA-2019-702-Q-R to MK. NIH R01 DK55310, NIH R37 DK34128, and Welch I1243 to MC. UTSW Simmons Comprehensive Cancer Center, NCI P30 CA142543, supports multiple core services.

ACKNOWLEDGMENTS

Thanks are given to members of the Cobb and Albanesi labs for advice and specifically to Magdalena Grzemska and Ji-ung Jung for the critical reading of this manuscript and to Dionne Ware for administrative assistance. We thank the lab of James Collins for use of microscopes. We thank the UTSW Simmons Comprehensive Cancer Center (NCI P30 CA142543) cores for Live Cell Imaging, Tissue Management Shared Resource, and the UTSW histopathology core. Thanks are due to the UTSW Flow Cytometry facility. Thanks are also due to the lab of Louis Parada for the 3T3-TrkB cell line. During the course of this work, MK was supported by an NIH NRSA DK100113 and

a JDRF 2-SRA-2019-702-Q-R. ZH was supported by the UT Southwestern-Sun Yat-sen exchange program. Also supporting this work were R01 DK55310, R37 DK34128, and grant I1243 from the Welch Foundation to MC. This manuscript has been released as a preprint on the BioRxiv server (Kalwat et al., 2020).

SUPPLEMENTARY MATERIAL

The Supplementary Material for this article can be found online at: https://www.frontiersin.org/articles/10.3389/fcell.2020.576396/full#supplementary-material

REFERENCES

Bathina, S., Srinivas, N., and Das, U. N. (2016). BDNF protects pancreatic beta cells (RIN5F) against cytotoxic action of alloxan, streptozotocin, doxorubicin and benzo(a)pyrene in vitro. *Metabolism* 65, 667–684. doi: 10.1016/j.metabol.2016.01.016

Briaud, I., Lingohr, M. K., Dickson, L. M., Wrede, C. E., and Rhodes, C. J. (2003). Differential activation mechanisms of Erk-1/2 and p70S6K by glucose in pancreatic -cells. *Diabetes* 52, 974–983. doi: 10.2337/diabetes.52.4.974

Civciristov, S., Ellisdon, A. M., Suderman, R., Pon, C. K., Evans, B. A., Kleifeld, O., et al. (2018). Preassembled GPCR signaling complexes mediate distinct cellular responses to ultralow ligand concentrations. *Sci. Signal.* 11:eaan1188. doi: 10.1126/scisignal.aan1188

Clutter, W. E., Bier, D. M., Shah, S. D., and Cryer, P. E. (1980). Epinephrine plasma metabolic clearance rates and physiologic thresholds for metabolic and hemodynamic actions in man. *J. Clin. Invest.* 66, 94–101. doi: 10.1172/jci109840

Coster, A. D., Thorne, C. A., Wu, L. F., and Altschuler, S. J. (2017). Examining crosstalk among transforming growth factor beta, bone morphogenetic protein, and Wnt Pathways. *J. Biol. Chem.* 292, 244–250. doi: 10.1074/jbc.m116.759654

De Wit, J., Eggers, R., Evers, R., Castren, E., and Verhaagen, J. (2006). Long-term adeno-associated viral vector-mediated expression of truncated TrkB in the adult rat facial nucleus results in motor neuron degeneration. *J. Neurosci.* 26, 1516–1530. doi: 10.1523/jneurosci.4543-05.2006

Dell'Osso, L., Carmassi, C., Del Debbio, A., Catena Dell'Osso, M., Bianchi, C., da Pozzo, E., et al. (2009). Brain-derived neurotrophic factor plasma levels in patients suffering from post-traumatic stress disorder. *Prog. Neuropsychopharmacol. Biol. Psychiatry* 33, 899–902. doi: 10.1016/j.pnpbp.2009.04.018

DiGruccio, M. R., Mawla, A. M., Donaldson, C. J., Noguchi, G. M., Vaughan, J., Cowing-Zitron, C., et al. (2016). Comprehensive alpha, beta and delta cell transcriptomes reveal that ghrelin selectively activates delta cells and promotes somatostatin release from pancreatic islets. *Mol. Metab.* 5, 449–458. doi: 10.1016/j.molmet.2016.04.007

Dodt, C., Breckling, U., Derad, I., Fehm, H. L., and Born, J. (1997). Plasma epinephrine and norepinephrine concentrations of healthy humans associated with nighttime sleep and morning arousal. *Hypertension* 30(1 Pt 1), 71–76. doi: 10.1161/01.hyp.30.1.71

Dupuis, J., Langenberg, C., Prokopenko, I., Saxena, R., Soranzo, N., Jackson, A. U., et al. (2010). New genetic loci implicated in fasting glucose homeostasis and their impact on type 2 diabetes risk. *Nat. Genet.* 42, 105–116.

Eide, F. F., Vining, E. R., Eide, B. L., Zang, K., Wang, X. Y., and Reichardt, L. F. (1996). Naturally occurring truncated trkB receptors have dominant inhibitory effects on brain-derived neurotrophic factor signaling. *J. Neurosci.* 16, 3123–3129. doi: 10.1523/jneurosci.16-10-03123.1996

Esposito, C. L., D'Alessio, A., de Franciscis, V., and Cerchia, L. (2008). A cross-talk between TrkB and Ret tyrosine kinases receptors mediates neuroblastoma cells differentiation. *PLoS One* 3:e1643. doi: 10.1371/journal.pone.0001643

Fenner, B. M. (2012). Truncated TrkB: beyond a dominant negative receptor. *Cytokine Growth Factor Rev.* 23, 15–24. doi: 10.1016/j.cytogfr.2012.01.002

Fryer, R. H., Kaplan, D. R., and Kromer, L. F. (1997). Truncated trkB receptors on nonneuronal cells inhibit BDNF-induced neurite outgrowth in vitro. *Exp. Neurol.* 148, 616–627. doi: 10.1006/exnr.1997.6699

Fulgenzi, G., Hong, Z., Tomassoni-Ardori, F., Barella, L. F., Becker, J., Barrick, C., et al. (2020). Novel metabolic role for BDNF in pancreatic beta-cell insulin secretion. *Nat. Commun.* 11:1950.

Fusco, J., Xiao, X., Prasadan, K., Sheng, Q., Chen, C., Ming, Y. C., et al. (2017). GLP-1/Exendin-4 induces beta-cell proliferation via the epidermal growth factor receptor. *Sci. Rep.* 7:9100.

Gherbi, K., Briddon, S. J., and Charlton, S. J. (2018). Micro-pharmacokinetics: quantifying local drug concentration at live cell membranes. *Sci. Rep.* 8:3479.

Gibson, T. B., Lawrence, M. C., Gibson, C. J., Vanderbilt, C. A., McGlynn, K., Arnette, D., et al. (2006). Inhibition of glucose-stimulated activation of extracellular signal-regulated protein kinases 1 and 2 by epinephrine in pancreatic beta-cells. *Diabetes* 55, 1066–1073. doi: 10.2337/diabetes.55.04.06.db05-1266

Goehring, I., Sauter, N. S., Catchpole, G., Assmann, A., Shu, L., Zien, K. S., et al. (2011). Identification of an intracellular metabolic signature impairing beta cell function in the rat beta cell line INS-1E and human islets. *Diabetologia* 54, 2584–2594.

Gotoh, K., Masaki, T., Chiba, S., Ando, H., Fujiwara, K., Shimasaki, T., et al. (2013). Hypothalamic brain-derived neurotrophic factor regulates glucagon secretion mediated by pancreatic efferent nerves. *J. Neuroendocrinol.* 25, 302–311. doi: 10.1111/jne.12003

Guerra, M. L., Kalwat, M. A., McGlynn, K., and Cobb, M. H. (2017). Sucralose activates an ERK1/2-ribosomal protein S6 signaling axis. *FEBS Open Bio* 7, 174–186. doi: 10.1002/2211-5463.12172

Hanyu, O., Yamatani, K., Ikarashi, T., Soda, S., Maruyama, S., Kamimura, T., et al. (2003). Brain-derived neurotrophic factor modulates glucagon secretion from pancreatic alpha cells: its contribution to glucose metabolism. *Diabetes Obesity Metab.* 5, 27–37. doi: 10.1046/j.1463-1326.2003.00238.x

Holst, J. J. (2007). The physiology of glucagon-like peptide 1. *Physiol. Rev.* 87, 1409–1439.

Huang, E. J., and Reichardt, L. F. (2003). Trk receptors: roles in neuronal signal transduction. *Annu. Rev. Biochem.* 72, 609–642. doi: 10.1146/annurev.biochem.72.121801.161629

Huang, Y. Z., and McNamara, J. O. (2010). Mutual regulation of Src family kinases and the neurotrophin receptor TrkB. *J. Biol. Chem.* 285, 8207–8217. doi: 10.1074/jbc.m109.091041

Hugl, S. R., White, M. F., and Rhodes, C. J. (1998). Insulin-like growth factor I (IGF-I)-stimulated pancreatic -cell growth is glucose-dependent: synergistic activation of insulin receptor substrate-mediated signal transduction pathways by glucose and Igf-I In Ins-1 Cells. *J. Biol. Chem.* 273, 17771–17779. doi: 10.1074/jbc.273.28.17771

Hui, H., Fernando, M. A., and Heaney, A. P. (2008). The alpha1-adrenergic receptor antagonist doxazosin inhibits EGFR and NF-kappaB signalling to induce breast cancer cell apoptosis. *Eur. J. Cancer* 44, 160–166. doi: 10.1016/j.ejca.2007.10.002

Hutchison, M. R. (2012). BDNF alters ERK/p38 MAPK activity ratios to promote differentiation in growth plate chondrocytes. *Mol. Endocrinol.* 26, 1406–1416. doi: 10.1210/me.2012-1063

Hutchison, M. R. (2013). Mice with a conditional deletion of the neurotrophin receptor TrkB are dwarfed, and are similar to mice with a MAPK14 deletion. *PLoS One* 8:e66206. doi: 10.1371/journal.pone.0066206

Ito, K., Dezaki, K., Yoshida, M., Yamada, H., Miura, R., Rita, R. S., et al. (2017). Endogenous alpha2A-adrenoceptor-operated sympathoadrenergic tones attenuate insulin secretion via cAMP/TRPM2 Signaling. *Diabetes* 66, 699–709. doi: 10.2337/db16-1166

Iwanir, S., and Reuveny, E. (2008). Adrenaline-induced hyperpolarization of mouse pancreatic islet cells is mediated by G protein-gated inwardly rectifying potassium (GIRK) channels. *Pflugers Arch.* 456, 1097–1108. doi: 10.1007/s00424-008-0479-4

Jaques, F., Jousset, H., Tomas, A., Prost, A. L., Wollheim, C. B., Irminger, J. C., et al. (2008). Dual effect of cell-cell contact disruption on cytosolic calcium and insulin secretion. *Endocrinology* 149, 2494–2505. doi: 10.1210/en.2007-0974

Ji, Y., Pang, P. T., Feng, L., and Lu, B. (2005). Cyclic AMP controls BDNF-induced TrkB phosphorylation and dendritic spine formation in mature hippocampal neurons. *Nat. Neurosci.* 8, 164–172. doi: 10.1038/nn1381

Jiang, L. I., Collins, J., Davis, R., Lin, K. M., DeCamp, D., Roach, T., et al. (2007). Use of a cAMP BRET sensor to characterize a novel regulation of cAMP by

the sphingosine 1-phosphate/G13 pathway. *J. Biol. Chem.* 282, 10576–10584. doi: 10.1074/jbc.m609695200

Kalwat, M. A., and Cobb, M. H. (2017). Mechanisms of the amplifying pathway of insulin secretion in the beta cell. *Pharmacol. Ther.* 179, 17–30. doi: 10.1016/j.pharmthera.2017.05.003

Kalwat, M. A., Huang, Z., Binns, D. D., McGlynn, K., and Cobb, M. (2020). α2-adrenergic signaling disrupts β cell BDNF-TrkB receptor tyrosine kinase signaling. *BioRxiv* [Preprint]. doi: 10.1101/400010

Kalwat, M. A., Huang, Z., Wichaidit, C., McGlynn, K., Earnest, S., Savoia, C., et al. (2016). Isoxazole alters metabolites and gene expression, decreasing proliferation and promoting a neuroendocrine phenotype in beta-cells. *ACS Chem. Biol.* 11, 1128–1136. doi: 10.1021/acschembio.5b00993

Kalwat, M. A., Yoder, S. M., Wang, Z., and Thurmond, D. C. (2013). A p21-activated kinase (PAK1) signaling cascade coordinately regulates F-actin remodeling and insulin granule exocytosis in pancreatic beta cells. *Biochem. Pharmacol.* 85, 808–816. doi: 10.1016/j.bcp.2012.12.003

Karczewska-Kupczewska, M., Kowalska, I., Nikolajuk, A., Adamska, A., Zielinska, M., Kaminska, N., et al. (2012). Circulating brain-derived neurotrophic factor concentration is downregulated by intralipid/heparin infusion or high-fat meal in young healthy male subjects. *Diabetes Care* 35, 358–362. doi: 10.2337/dc11-1295

Khoo, S., and Cobb, M. H. (1997). Activation of mitogen-activating protein kinase by glucose is not required for insulin secretion. *Proc. Natl. Acad. Sci. U.S.A.* 94, 5599–5604. doi: 10.1073/pnas.94.11.5599

Khoo, S., Gibson, T. B., Arnette, D., Lawrence, M., January, B., McGlynn, K., et al. (2004). MAP kinases and their roles in pancreatic beta-cells. *Cell Biochem. Biophys.* 40(Supp l), 191–200. doi: 10.1007/bf02739023

Khoo, S., Griffen, S. C., Xia, Y., Baer, R. J., German, M. S., and Cobb, M. H. (2003). Regulation of insulin gene transcription by ERK1 and ERK2 in pancreatic beta cells. *J. Biol. Chem.* 278, 32969–32977. doi: 10.1074/jbc.m301198200

Kienbaum, P., Thurauf, N., Michel, M. C., Scherbaum, N., Gastpar, M., and Peters, J. (1998). Profound increase in epinephrine concentration in plasma and cardiovascular stimulation after mu-opioid receptor blockade in opioid-addicted patients during barbiturate-induced anesthesia for acute detoxification. *Anesthesiology* 88, 1154–1161. doi: 10.1097/00000542-199805000-00004

Kim, W., Lao, Q., Shin, Y. K., Carlson, O. D., Lee, E. K., Gorospe, M., et al. (2012). Cannabinoids induce pancreatic beta-cell death by directly inhibiting insulin receptor activation. *Sci. Signal.* 5:ra23. doi: 10.1126/scisignal.2002519

Krabbe, K. S., Nielsen, A. R., Krogh-Madsen, R., Plomgaard, P., Rasmussen, P., Erikstrup, C., et al. (2007). Brain-derived neurotrophic factor (BDNF) and type 2 diabetes. *Diabetologia* 50, 431–438.

Kulkarni, R. N., Brüning, J. C., Winnay, J. N., Postic, C., Magnuson, M. A., and Kahn, C. R. (1999). Tissue-specific knockout of the insulin receptor in pancreatic β cells creates an insulin secretory defect similar to that in Type 2 Diabetes. *Cell* 96, 329–339. doi: 10.1016/s0092-8674(00)80546-2

Kulkarni, R. N., Holzenberger, M., Shih, D. Q., Ozcan, U., Stoffel, M., Magnuson, M. A., et al. (2002). beta-cell-specific deletion of the Igf1 receptor leads to hyperinsulinemia and glucose intolerance but does not alter beta-cell mass. *Nat. Genet.* 31, 111–115. doi: 10.1038/ng872

Kurita, M., Nishino, S., Kato, M., Numata, Y., and Sato, T. (2012). Plasma brain-derived neurotrophic factor levels predict the clinical outcome of depression treatment in a naturalistic study. *PLoS One* 7:e39212. doi: 10.1371/journal.pone.0039212

Langberg, E. C., Seed Ahmed, M., Efendic, S., Gu, H. F., and Ostenson, C. G. (2013). Genetic association of adrenergic receptor alpha 2A with obesity and type 2 diabetes. *Obesity* 21, 1720–1725. doi: 10.1002/oby.20162

Lawrence, M., Shao, C., Duan, L., McGlynn, K., and Cobb, M. H. (2008). The protein kinases ERK1/2 and their roles in pancreatic beta cells. *Acta Physiol.* 192, 11–17. doi: 10.1111/j.1748-1716.2007.01785.x

Leduc, M., Richard, J., Costes, S., Muller, D., Varrault, A., Compan, V., et al. (2017). ERK1 is dispensable for mouse pancreatic beta cell function but is necessary for glucose-induced full activation of MSK1 and CREB. *Diabetologia* 60, 1999–2010. doi: 10.1007/s00125-017-4356-6

Li, B., Lang, N., and Cheng, Z. F. (2016). Serum levels of brain-derived neurotrophic factor are associated with diabetes risk, complications, and obesity: a cohort study from chinese patients with Type 2 Diabetes. *Mol. Neurobiol.* 53, 5492–5499. doi: 10.1007/s12035-015-9461-2

Liggett, S. B. (2009). alpha2A-adrenergic receptors in the genetics, pathogenesis, and treatment of type 2 diabetes. *Sci. Transl. Med.* 1:12s15.

Longuet, C., Broca, C., Costes, S., Hani, E. H., Bataille, D., and Dalle, S. (2005). Extracellularly regulated kinases 1/2 (p44/42 mitogen-activated protein kinases) phosphorylate synapsin I and regulate insulin secretion in the MIN6 beta-cell line and islets of Langerhans. *Endocrinology* 146, 643–654. doi: 10.1210/en.2004-0841

Marty, C., and Ye, R. D. (2010). Heterotrimeric G protein signaling outside the realm of seven transmembrane domain receptors. *Mol. Pharmacol.* 78, 12–18. doi: 10.1124/mol.110.063453

Matthews, V. B., Astrom, M. B., Chan, M. H., Bruce, C. R., Krabbe, K. S., Prelovsek, O., et al. (2009). Brain-derived neurotrophic factor is produced by skeletal muscle cells in response to contraction and enhances fat oxidation via activation of AMP-activated protein kinase. *Diabetologia* 52, 1409–1418. doi: 10.1007/s00125-009-1364-1

Minichiello, L. (2009). TrkB signalling pathways in LTP and learning. *Nat. Rev. Neurosci.* 10, 850–860. doi: 10.1038/nrn2738

Murillo Ortiz, B., Ramirez Emiliano, J., Ramos-Rodriguez, E., Martinez-Garza, S., Macias-Cervantes, H., Solorio-Meza, S., et al. (2016). Brain-derived neurotrophic factor plasma levels and premature cognitive impairment/dementia in type 2 diabetes. *World J. Diabetes* 7, 615–620. doi: 10.4239/wjd.v7.i20.615

Peterhoff, M., Sieg, A., Brede, M., Chao, C., Hein, L., and Ullrich, S. (2003). Inhibition of insulin secretion via distinct signaling pathways in alpha2-adrenoceptor knockout mice. *Eur. J. Endocrinol.* 149, 343–350. doi: 10.1530/eje.0.1490343

Pillai, A., Bruno, D., Sarreal, A. S., Hernando, R. T., Saint-Louis, L. A., Nierenberg, J., et al. (2012). Plasma BDNF levels vary in relation to body weight in females. *PLoS One* 7:e39358. doi: 10.1371/journal.pone.0039358

Powe, D. G., Voss, M. J., Habashy, H. O., Zanker, K. S., Green, A. R., Ellis, I. O., et al. (2011). Alpha- and beta-adrenergic receptor (AR) protein expression is associated with poor clinical outcome in breast cancer: an immunohistochemical study. *Breast Cancer Res. Treat.* 130, 457–463. doi: 10.1007/s10549-011-1371-z

Puehringer, D., Orel, N., Luningschror, P., Subramanian, N., Herrmann, T., Chao, M. V., et al. (2013). EGF transactivation of Trk receptors regulates the migration of newborn cortical neurons. *Nat. Neurosci.* 16, 407–415. doi: 10.1038/nn.3333

Segerstolpe, A., Palasantza, A., Eliasson, P., Andersson, E. M., Andreasson, A. C., Sun, X., et al. (2016). Single-cell transcriptome profiling of human pancreatic islets in health and Type 2 Diabetes. *Cell Metab.* 24, 593–607. doi: 10.1016/j.cmet.2016.08.020

Sha, H., Xu, J., Tang, J., Ding, J., Gong, J., Ge, X., et al. (2007). Disruption of a novel regulatory locus results in decreased Bdnf expression, obesity, and type 2 diabetes in mice. *Physiol. Genomics* 31, 252–263. doi: 10.1152/physiolgenomics.00093.2007

Sharp, G. W. (1996). Mechanisms of inhibition of insulin release. *Am. J. Physiol.* 271(6 Pt 1), C1781–C1799.

Shibayama, E., and Koizumi, H. (1996). Cellular localization of the Trk neurotrophin receptor family in human non-neuronal tissues. *Am. J. Pathol.* 148, 1807–1818.

Sieg, A., Su, J., Munoz, A., Buchenau, M., Nakazaki, M., Aguilar-Bryan, L., et al. (2004). Epinephrine-induced hyperpolarization of islet cells without KATP channels. *Am. J. Physiol. Endocrinol. Metab.* 286, E463–E471.

Slucca, M., Harmon, J. S., Oseid, E. A., Bryan, J., and Robertson, R. P. (2010). ATP-sensitive K+ channel mediates the zinc switch-off signal for glucagon response during glucose deprivation. *Diabetes* 59, 128–134. doi: 10.2337/db09-1098

Song, Z., Fusco, J., Zimmerman, R., Fischbach, S., Chen, C., Ricks, D. M., et al. (2016). EGFR signaling regulates beta cell proliferation in adult mice. *J. Biol. Chem.* 291, 22630–22637.

Stock, A. M., Powe, D. G., Hahn, S. A., Troost, G., Niggemann, B., Zanker, K. S., et al. (2013). Norepinephrine inhibits the migratory activity of pancreatic cancer cells. *Exp. Cell Res.* 319, 1744–1758. doi: 10.1016/j.yexcr.2013.04.015

Straub, S. G., and Sharp, G. W. (2012). Evolving insights regarding mechanisms for the inhibition of insulin release by norepinephrine and heterotrimeric G proteins. *Am. J. Physiol. Cell Physiol.* 302, C1687–C1698.

Talmud, P. J., Cooper, J. A., Gaunt, T., Holmes, M. V., Shah, S., Palmen, J., et al. (2011). Variants of ADRA2A are associated with fasting glucose, blood pressure,

body mass index and type 2 diabetes risk: meta-analysis of four prospective studies. *Diabetologia* 54, 1710–1719. doi: 10.1007/s00125-011-2108-6

Tian, G., Sandler, S., Gylfe, E., and Tengholm, A. (2011). Glucose- and hormone-induced cAMP oscillations in alpha- and beta-cells within intact pancreatic islets. *Diabetes* 60, 1535–1543. doi: 10.2337/db10-1087

Tonoli, C., Heyman, E., Roelands, B., Buyse, L., Piacentini, F., Berthoin, S., et al. (2015). BDNF, IGF-I, glucose and insulin during continuous and interval exercise in Type 1 Diabetes. *Int. J. Sports Med.* 36, 955–959. doi: 10.1055/s-0035-1548886

Tonra, J. R., Ono, M., Liu, X., Garcia, K., Jackson, C., Yancopoulos, G. D., et al. (1999). Brain-derived neurotrophic factor improves blood glucose control and alleviates fasting hyperglycemia in C57BLKS-Lepr(db)/lepr(db) mice. *Diabetes* 48, 588–594. doi: 10.2337/diabetes.48.3.588

Uhlen, M., Fagerberg, L., Hallstrom, B. M., Lindskog, C., Oksvold, P., Mardinoglu, A., et al. (2015). Proteomics. Tissue-based map of the human proteome. *Science* 347:1260419.

Verge, V. M., Andreassen, C. S., Arnason, T. G., and Andersen, H. (2014). Mechanisms of disease: role of neurotrophins in diabetes and diabetic neuropathy. *Handb. Clin. Neurol.* 126, 443–460.

Yamanaka, M., Itakura, Y., Inoue, T., Tsuchida, A., Nakagawa, T., Noguchi, H., et al. (2006). Protective effect of brain-derived neurotrophic factor on pancreatic islets in obese diabetic mice. *Metabolism* 55, 1286–1292. doi: 10.1016/j.metabol.2006.04.017

Zhang, Y., Shumilina, E., Haring, H. U., Lang, F., and Ullrich, S. (2009). Epinephrine-induced hyperpolarization of pancreatic islet cells is sensitive to PI3K-PDK1 signaling. *FEBS Lett.* 583, 3101–3106. doi: 10.1016/j.febslet.2009.08.027

Zhao, Y., Fang, Q., Straub, S. G., Lindau, M., and Sharp, G. W. (2010). Noradrenaline inhibits exocytosis via the G protein betagamma subunit and refilling of the readily releasable granule pool via the alpha(i1/2) subunit. *J. Physiol.* 588(Pt 18), 3485–3498. doi: 10.1113/jphysiol.2010.190090

Zhao, Y., Fang, Q., Straub, S. G., and Sharp, G. W. (2008). Both G i and G o heterotrimeric G proteins are required to exert the full effect of norepinephrine on the beta-cell K ATP channel. *J. Biol. Chem.* 283, 5306–5316. doi: 10.1074/jbc.m707695200

Zhao, Z., Low, Y. S., Armstrong, N. A., Ryu, J. H., Sun, S. A., Arvanites, A. C., et al. (2014). Repurposing cAMP-modulating medications to promote beta-cell replication. *Mol. Endocrinol.* 28, 1682–1697. doi: 10.1210/me.2014-1120

Conflict of Interest: The authors declare that the research was conducted in the absence of any commercial or financial relationships that could be construed as a potential conflict of interest.

frontiers in Cell and Developmental Biology

ORIGINAL RESEARCH
published: 22 October 2020
doi: 10.3389/fcell.2020.585640

Incoherent Feedforward Regulation via Sox9 and ERK Underpins Mouse Tracheal Cartilage Development

Takuya Yoshida[1], *Michiyuki Matsuda*[1,2] *and Tsuyoshi Hirashima*[2,3]*

[1] *Laboratory of Bioimaging and Cell Signaling, Graduate School of Biostudies, Kyoto University, Kyoto, Japan,* [2] *Department of Pathology and Biology of Diseases, Graduate School of Medicine, Kyoto University, Kyoto, Japan,* [3] *Japan Science and Technology Agency, PRESTO, Tokyo, Japan*

Tracheal cartilage provides architectural integrity to the respiratory airway, and defects in this structure during embryonic development cause severe congenital anomalies. Previous genetic studies have revealed genes that are critical for the development of tracheal cartilage. However, it is still unclear how crosstalk between these proteins regulates tracheal cartilage formation. Here we show a core regulatory network underlying murine tracheal chondrogenesis from embryonic day (E) 12.5 to E15.5, by combining volumetric imaging of fluorescence reporters, inhibitor assays, and mathematical modeling. We focused on SRY-box transcription factor 9 (Sox9) and extracellular signal-regulated kinase (ERK) in the tracheal mesenchyme, and observed a synchronous, inverted U-shaped temporal change in both Sox9 expression and ERK activity with a peak at E14.5, whereas the expression level of downstream cartilage matrix genes, such as collagen II alpha 1 (*Col2a1*) and aggrecan (*Agc1*), monotonically increased. Inhibitor assays revealed that the ERK signaling pathway functions as an inhibitory regulator of tracheal cartilage differentiation during this period. These results suggest that expression of the cartilage matrix genes is controlled by an incoherent feedforward loop via Sox9 and ERK, which is supported by a mathematical model. Furthermore, the modeling analysis suggests that a Sox9-ERK incoherent feedforward regulation augments the robustness against the variation of upstream factors. The present study provides a better understanding of the regulatory network underlying the tracheal development and will be helpful for efficient induction of tracheal organoids.

Keywords: chondrogenesis, FRET imaging, incoherent feedforward loop, mathematical model, MAP kinase/ERK, SOX9, trachea

OPEN ACCESS

Edited by:
Jose Maria Carvajal-Gonzalez, University of Extremadura, Spain

Reviewed by:
Frank Zaucke, Orthopaedic University Hospital Friedrichsheim, Germany
Debora Sinner, Cincinnati Children's Hospital Medical Center, United States
Tamas Juhasz, University of Debrecen, Hungary

***Correspondence:**
Tsuyoshi Hirashima
hirashima.tsuyoshi.2m@kyoto-u.ac.jp

Specialty section:
This article was submitted to Signaling, a section of the journal Frontiers in Cell and Developmental Biology

Received: *21 July 2020*
Accepted: *15 September 2020*
Published: *22 October 2020*

Citation:
Yoshida T, Matsuda M and Hirashima T (2020) Incoherent Feedforward Regulation via Sox9 and ERK Underpins Mouse Tracheal Cartilage Development. Front. Cell Dev. Biol. 8:585640. doi: 10.3389/fcell.2020.585640

INTRODUCTION

The mammalian trachea is a tubular organ of the respiratory system and is composed of several tissues from different origins, such as endoderm-derived epithelium and mesoderm-derived cartilage (Cardoso and Lü, 2006). The tracheal cartilage, also known as the tracheal ring, exhibits a C-shaped semi-ring architecture that surrounds the epithelial airway on the ventral side and provides structural support. Abnormal formation of the tracheal rings can collapse the airways and obstruct breathing, which leads to congenital defects, including tracheomalacia and tracheal stenosis (Arooj Sher and Liu, 2016). Thus, a fundamental understanding of the processes underpinning tracheal ring development is essential, yet it is still incomplete.

The development of tracheal rings has been investigated using mouse genetics, which has revealed the importance of multiple transcription factors and signaling pathways. Among these, SRY-box transcription factor 9 (Sox9) is known to be a master regulator that plays a critical role in cartilage differentiation by inducing gene expression of key cartilage matrix molecules, such as collagen II alpha 1 (Col2a1), and aggrecan (Agc1) (Bi et al., 1999; Han and Lefebvre, 2008). It has been demonstrated that SOX9 functions in each successive step of the cartilage differentiation processes, including mesenchymal condensation, commitment to the chondroprogenitor, and maintenance of proliferating chondrocytes (Bi et al., 1999; Akiyama et al., 2002). The importance of *Sox9* in tracheal development was revealed by reports which described a complete absence of the tracheal rings in mesenchymal *Sox9* knockout mice (Hines et al., 2013; Turcatel et al., 2013). In addition, the haploinsufficiency of *Sox9* caused hypoplastic cartilage formation, indicating that SOX9 dosage is critical to tracheal ring formation (Bi et al., 2001). In sonic hedgehog (Shh) knockout mice, *Sox9* mRNA expression was lost in the developing tracheae at a later stage of tracheal ring development, leading to the failure of tracheal ring formation, suggesting that Shh plays an important role in controlling Sox9 expression (Park et al., 2010).

Another important signaling pathway is the fibroblast growth factor (Fgf)—extracellular signal-regulated kinase (ERK) signaling axis. Previous studies showed that severe malformations of the tracheal rings were observed when *Fgf10* or its main receptor *Fgfr2b* were either ubiquitously knocked out or overexpressed in the tracheal mesenchyme (Tiozzo et al., 2009; Sala et al., 2011). Abnormal tracheal cartilage formation was also reported in the FGF18 overexpressing mice (Elluru et al., 2009). These results suggest that FGF signaling level must be within a specific range to ensure correct formation of the tracheal rings. The most downstream kinase of the signaling cascade, ERK, is considered to be essential for tracheal development because the genetic deletion of both *Mek1* and *Mek2* (upstream kinase of ERK) in the mesenchyme resulted in defective tracheal rings (Boucherat et al., 2014). These studies make a strong case for the necessity of Fgf-ERK signaling in the normal development of the tracheal rings; however, the mechanisms through which ERK activation regulates cartilage differentiation are still unknown. It is noteworthy that there are several studies which have presented conflicting results; on one hand, the ERK signaling enhances the expression of cartilage matrix molecules, shown using mouse primary chondrocytes (Murakami et al., 2000), while on the other, the ERK signaling suppresses it, demonstrated using chicken embryonic limb buds (Oh et al., 2000; Bobick and Kulyk, 2004; Zákány et al., 2005).

In this study, we explore the crosstalk between the Shh-Sox9 and Fgf-ERK signaling pathways and the regulatory network that contributes to tracheal ring development. We first show a synchronized temporal profile of Sox9 expression and ERK activity using volumetric imaging of fluorescence reporters. Combined with inhibitor assays, we then show that cartilage matrix genes are positively regulated by Sox9, and in parallel, negatively regulated by ERK activity, in an incoherent feedforward manner. Finally, a mathematical model demonstrates that an incoherent feedforward loop via Sox9 and ERK can explain the dynamics of cartilage matrix gene expression during tracheal cartilage formation.

RESULTS

Mesenchymal Condensation Begins Between E12.5 and E13.5

To morphologically characterize the developing murine trachea, we dissected tracheae from the embryos and processed the tissues using whole mount immunohistochemistry to examine the staining of the nuclei and cell membrane of the tracheal epithelium. We focused on the ventral region of the tracheal mesenchyme, where the tracheal cartilage rings are formed, and we show the frontal and sagittal planes of the ventral region (**Figure 1A**). We also show the flattening of nuclei, which were used to evaluate how flat the best fitting ellipse should be in comparison to a circle for nuclei evaluations (**Figure 1B**).

At E12.5, the mesenchymal nuclei were almost round and homogeneously distributed, in both the frontal and the sagittal planes (**Figure 1A**). At E13.5, some mesenchymal nuclei were more elongated and surrounded the cells close to the epithelium, forming a template of the chondrogenic nodule (**Figures 1A,C**). This process is known as mesenchymal condensation, the initial step of chondrogenesis in general (Goldring et al., 2006). These condensations were observed between the ridges of wavy tracheal epithelium (**Figure 1A'**). At E14.5, the peripheral nuclei of the mesenchymal condensations were further elongated and the azimuthal polarization pattern was observed (**Figure 1A–C**). This phenomenon is consistent with the formation of the perichondrium, the next step of mesenchymal condensation during chondrogenesis (Goldring et al., 2006). These observations indicate that mesenchymal cell differentiation into chondrocytes of the tracheal cartilage begins between E12.5 and E13.5.

Sox9 Expression Increases up to E14.5, and Decreases Thereafter

We next examined the expression of Sox9, the early differentiation marker of chondrocytes, in the developing murine tracheae from E12.5 to E15.5. For this purpose, we employed Sox9-EGFP knock-in mice, in which the expression level of EGFP has been shown to correlate with the endogenous expression of Sox9 (Nel-Themaat et al., 2009; Nakamura et al., 2011). EGFP fluorescence in the ventral side of the epithelium was observed using two-photon microscopy.

Observation by 3D imaging showed the appearance of distinct cell clusters, defined by EGFP intensity, from E13.5 onward (**Figure 2A**). These high-EGFP clusters are located between epithelial ridges, corresponding to the mesenchymal condensations (**Figure 1A** and **Supplementary Figure 1A**). The condensed mesenchymal cells with high EGFP intensity also exhibited a C-shaped semi-ring structure, indicating formation of the chondrogenic nodule (**Supplementary Figure 1B**). We then quantified the EGFP intensity in each mesenchymal cell.

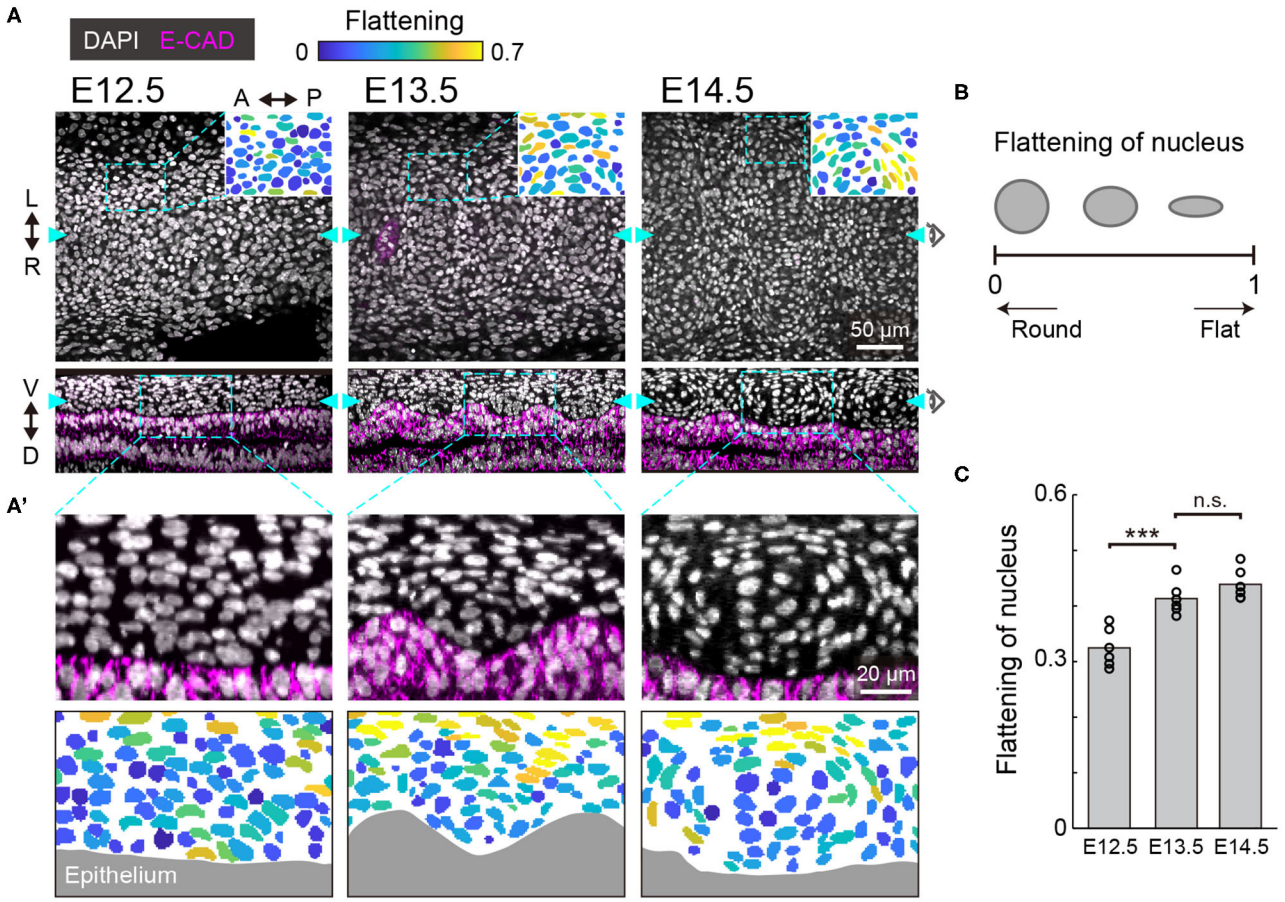

FIGURE 1 | Nuclear distribution in the developing trachea. **(A)** Immunofluorescence section images of anti-E-cadherin (magenta) with DAPI nuclear counterstaining (white) in developing murine tracheae from E12.5 to E14.5 (upper: frontal plane, lower: sagittal plane). The data for E15.5 are not included since there is no significant qualitative change of the nuclear configuration from E14.5. In the pictographic transcriptions in the top right corner, color denotes the flattening of nuclei seen in the dotted windows. Cyan arrowheads indicate the point visualized in the orthogonal views. Scale bar, 50 μm. **(A')** Magnified images corresponding to the dotted windows in the lower row of **(A)** (upper) and the flattening of nuclei. Gray indicates epithelium. Scale bar, 20 μm. L, left; R, right; A, anterior; P, posterior; V, ventral; D, dorsal. **(B)** Schematics of the flattened nuclei. **(C)** Flattening of nucleus from E12.5 to E14.5 in the sagittal plane. Each point represents the mean value within the sample. Welch's two-sample *t*-test, E12.5–E13.5: $p < 0.001$. E13.5–E14.5: $p = 0.152$. $n = 6$ from different trachea.

Although EGFP expression was uniform along the antero-posterior axis in the median line at E12.5, the periodic pattern of EGFP intensity was confirmed at E13.5 and the amplitude of this periodic intensity became larger at E14.5 (**Figure 2B**). The median EGFP intensity in the mesenchymal condensations increased 1.18-fold from E12.5 to E13.5, and 1.65-fold from E13.5 to E14.5 (**Figure 2C**), which linearly correlates with Sox9 protein levels (**Supplementary Figures 1C,D**). However, the EGFP intensity in the mesenchymal condensations decreased 0.56-fold from E14.5 to E15.5 (**Figures 2A–C**), indicating that Sox9 expression is suppressed at E14.5.

We also quantified the expression levels of various cartilage matrix genes (the major determinants of chondrogenesis), including *Col2a1* and *Agc1*, as well as *Sox9*, by RT-qPCR analysis. *Sox9* expression in the whole trachea showed an increasing profile from E12.5 to E14.5 and a slight decreasing profile from E14.5 to E15.5 (**Figure 2D**). Note that the RT-qPCR measures cell-ensemble of gene expressions in the whole trachea. Because the growth of the chondrogenic nodule was evident from E14.5 to E15.5 (**Figures 2A,B**), the value obtained by RT-qPCR at E15.5 was most likely to be larger than the net expression level in the chondrogenic nodule. Thus, *Sox9* expression would exhibit a non-monotonic profile with a peak at E14.5, similar to that obtained from our imaging analyses of Sox9-EGFP (**Figure 2D**). However, *Col2a1* and *Agc1* exhibited monotonic increases during progression through the developmental stages (**Figure 2D**). These results suggest that other signaling inputs, together with Sox9, primarily regulate the expression of the cartilage matrix genes.

ERK Activity Increases up to E14.5 and Decreases Thereafter, Alongside Sox9 Expression

Next, to examine the contribution of the Fgf-ERK axis, we quantified the spatiotemporal ERK activity in the developing

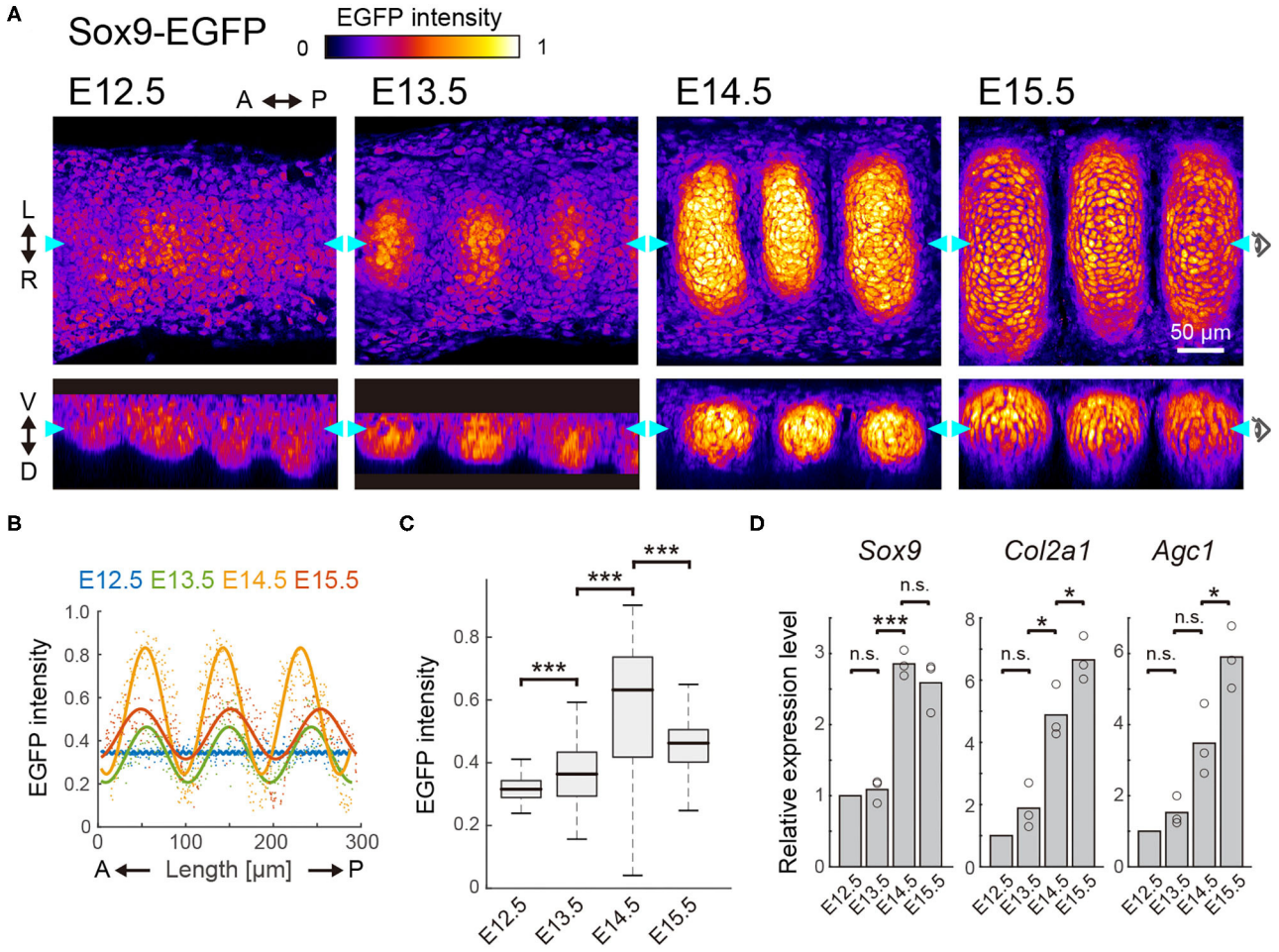

FIGURE 2 | Sox9 expression profile in the developing trachea. **(A)** Section view of EGFP in the frontal (upper) and sagittal (bottom) planes from E12.5 to E15.5. Color denotes the normalized EGFP intensity. Cyan arrowheads in each plane represent the position of orthogonal sections. Scale bar, 50 μm. L, left; R, right; A, anterior; P, posterior; V, ventral; D, dorsal. **(B)** EGFP intensity in each mesenchymal cell along the antero-posterior axis. Dots represent mean intensity in each cell and solid lines represent fitted line with a one-term Fourier function. $n > 200$ from 3 different tracheae in each stage. **(C)** EGFP intensity in the entire mesenchyme for E12.5 and within the cluster from E13.5 onward. Welch's two-sample *t*-test, E12.5–E13.5: $p < 0.001$, E13.5–E14.5: $p < 0.001$, E14.5–E15.5: $p < 0.001$. $n > 100$ from 3 different tracheae in each stage. **(D)** Relative expression level of *Sox9*, *Col2a1*, and *Agc1* from E12.5 to E15.5. One-sample *t*-test, Sox9, E13.5: $p = 0.464$, Col2a1, E13.5: $p = 0.171$, Agc1, E13.5: $p = 0.158$. Welch's two-sample *t*-test, Sox9, E13.5–E14.5: $p < 0.001$, E14.5–15.5: $p = 0.344$. Col2a1, E13.5–E14.5: $p = 0.011$, E14.5–15.5: $p = 0.048$. Agc1, E13.5–E14.5: $p = 0.063$, E14–E15: $p = 0.035$. $n = 3$ from independent experiments.

trachea. For this purpose, we used a reporter mouse line that expresses a Förster resonance energy transfer (FRET)-based biosensor for ERK activity, which is localized in the nucleus (Harvey et al., 2008; Komatsu et al., 2011, 2018). Despite being designed for ubiquitous expression, the fluorescence signal of non-chondrogenic nodules was so dim that ERK activity could be quantified only in the chondrogenic nodules.

FRET imaging by two-photon microscopy revealed that ERK activity in the mesenchymal condensations increased 1.05-fold from E12.5 to E13.5, and 1.26-fold from E13.5 to E14.5, but decreased 0.89-fold from E14.5 to E15.5, (**Figures 3A,B**). It is worth noting that this activity profile is similar to the expression profile of Sox9 (**Figure 2D**). Treatment with PD0325901, an inhibitor for MEK (the kinase upstream of ERK), led to a significant decrease in ERK activity at all stages (**Figure 3B**), meaning that the ERK is activated. This suggests that the level of ERK activity would have a potential role in the developmental process.

We also performed time-lapse imaging of the dissected tracheae using the FRET biosensor-expressing mice to continuously monitor the dynamics of the mesenchymal cells and the changes in ERK activity. In tracheae cultured from E12.5 embryos, the mesenchymal cells in the ventral epithelium formed some condensations and ERK activity gradually increased during this process (**Figures 3C,C'**). Single cell quantification indicated that averaged ERK activity

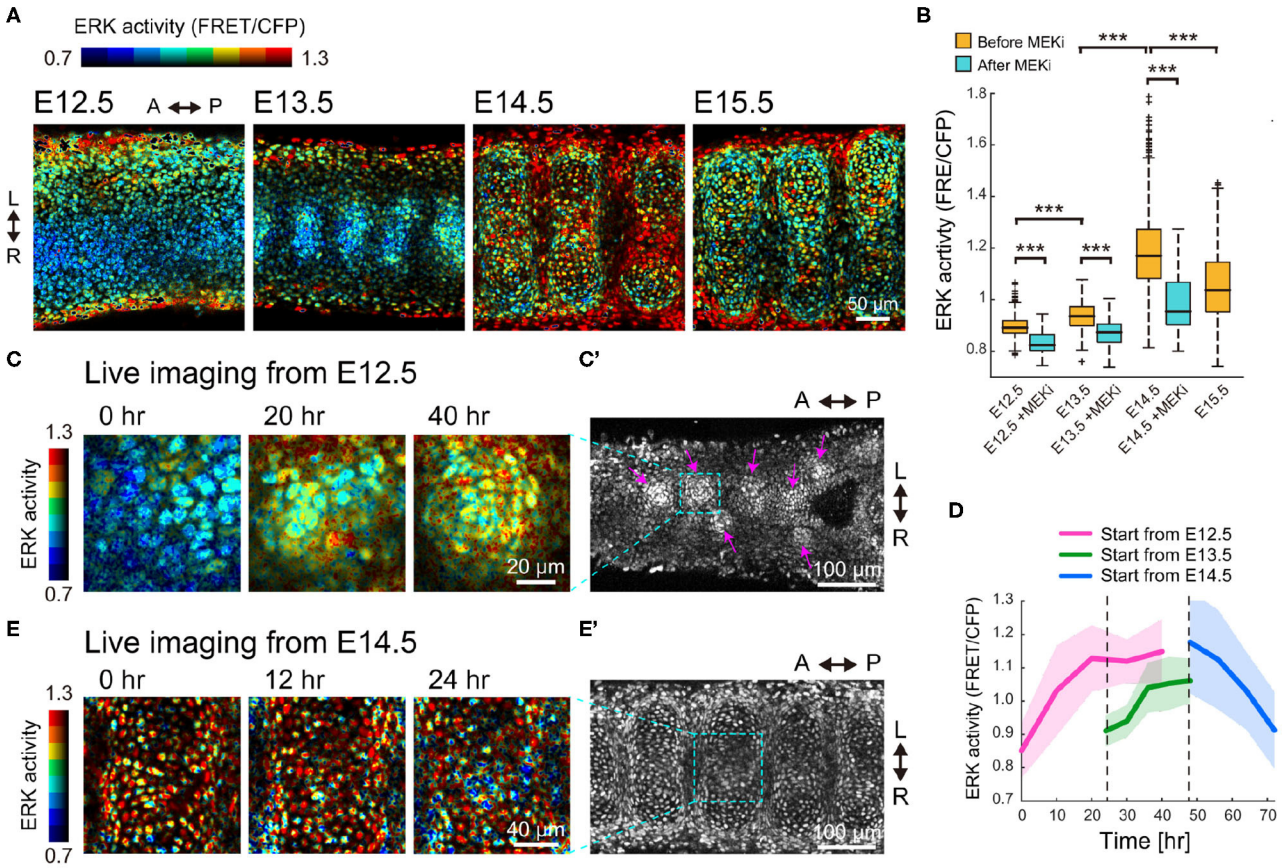

FIGURE 3 | ERK activity profile in the developing trachea. **(A)** ERK activity map in the trachea on the frontal plane of the ventral side of the epithelium. Color denotes levels of ERK activity. Scale bar, 50 μm. L, left; R, right; A, anterior; P, posterior. **(B)** ERK activity in the condensed region before and after 120 min of treatment with the MEK inhibitor (500 nM). Welch's two-sample *t*-test, $p < 0.001$ in all groups. $n > 480$ for each category from 3 independent experiments. **(C,C')** Time-lapse snapshots of ERK activity in the mesenchyme of an explant trachea cultured from E12.5. The far right panel in **(C)** corresponds to the dotted window in **(C')**. Magenta arrows indicate the mesenchymal condensations. Scale bars, 20 μm for **(C)** and 100 μm for **(C')**. **(D)** Time-series of ERK activity in nodule mesenchyme. Color denotes the different starting stages of the explant cultures. Explant tracheae were cultured from E12.5. Mean and s.d. $n > 70$ from 2 independent experiments. **(E,E')** Time-lapse snapshots of ERK activity in the mesenchyme of an explant trachea cultured from E14.5. The far right panel in **(E)** corresponds to the dotted window in **(E')**. Scale bars, 40 μm for **(E)** and 100 μm for **(E')**.

increased to a maximum of 1.31-fold when cultured from E12.5 for 40 h (**Figure 3D**). The increase in averaged ERK activity was also observed when E13.5 tracheae were cultured for 24 h (1.17-fold, **Figure 3D**). In contrast, ERK activity in the chondrogenic nodules decreased 0.78-fold when cultured from E14.5 (**Figures 3D,E,E'**). These observations confirmed that the gradual activation of ERK switches at E14.5 to inactivation.

ERK Activation Is Dispensable for Mesenchymal Condensation

We then explored the role of ERK activation in the development of tracheal cartilage. For these experiments, we treated tracheae dissected from E12.5 embryos with a MEK inhibitor under *ex vivo* culture conditions for 1 day. Since how the nuclei change shape in a way that is characteristic of mesenchymal condensation in the initial differentiation step occurring between E12.5 and E13.5 (**Figures 1A–C**), we focused on assessing the shape and distribution of the mesenchymal nuclei, as well as Sox9 levels in the condensations. We observed elongated mesenchymal nuclei, that were distributed concentrically in tracheae treated with the MEK inhibitor, similar to the control samples (**Figures 4A,B,D**) and to the E13.5 samples (**Figure 1A,A′**). Furthermore, the increase in Sox9 levels during mesenchymal condensation was confirmed in PD0325901-treated tracheae as well as in the control explants (**Figures 4A,B**). These results indicate that the activation of ERK between E12.5 and E13.5 is dispensable for mesenchymal condensation, which is consistent with a previous report (Oh et al., 2000).

We also examined the effect of mesenchymal condensation on the suppression of cell-generated contractile forces, since it has been shown that cell contraction drives mesenchymal condensation in the development of other organs (Mammoto et al., 2011; Shyer et al., 2017). Tracheae dissected at E12.5 were treated with blebbistatin, an inhibitor of non-muscle myosin II, and cultured for 1 day. Most mesenchymal nuclei remained

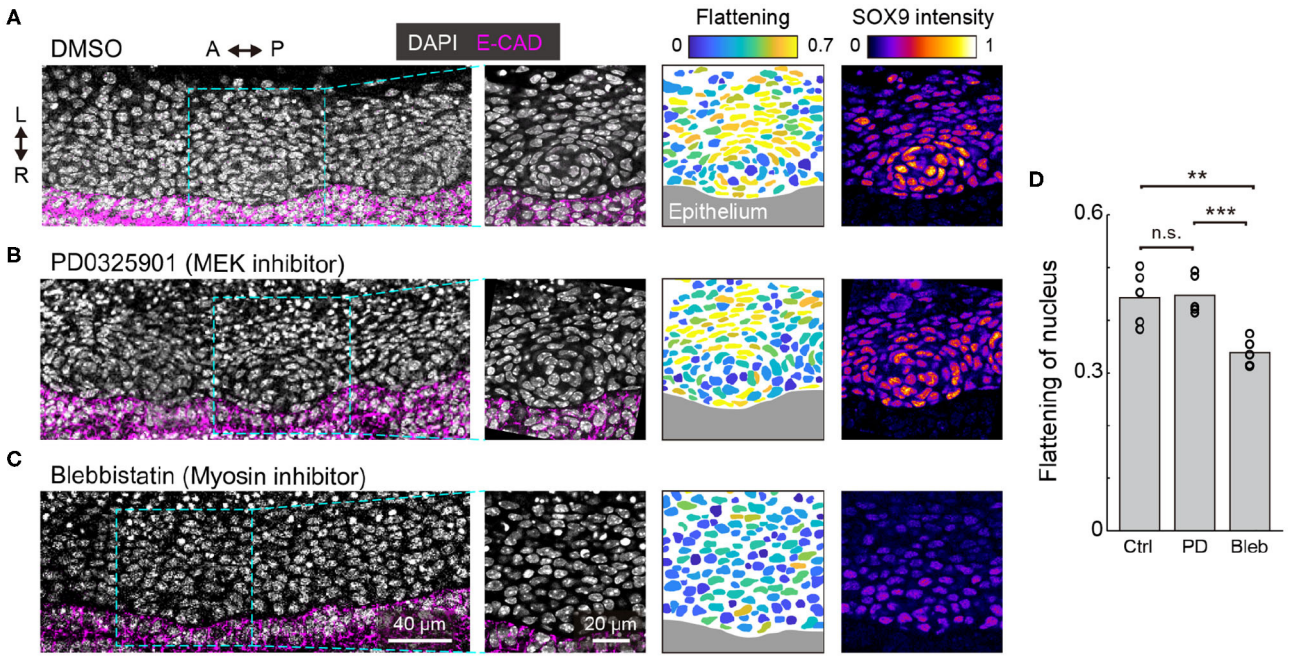

FIGURE 4 | ERK activation in mesenchymal condensation. **(A–C)** Immunohistochemistry images of anti-E-cadherin (magenta) and anti-SOX9 ("fire" pseudocolor) with DAPI nuclear counterstaining (white) at the frontal section of the trachea, cultured *ex vivo* from E12.5 for 1 day with drug treatment [**(A)**: DMSO, **(B)**: PD0325901 at 500 nM, **(C)**: Blebbistatin at 30 μM). (1st and 2nd columns) Magnified images from the dotted windows in the 1st column show concentric mesenchymal condensation in the DMSO control and PD0325901-treated **(A,B)** but not in the blebbistatin-treated **(C)** tracheae. (3rd and 4th columns) Color denotes the flattening of nuclei and Sox9 intensity, respectively, corresponding to the images from the 2nd column. Marked increases in Sox9 levels were observed in the DMSO control and PD0325901-treated **(A,B)** but not in the blebbistatin-treated **(C)** tracheae. Scale bars, 40 μm (1st column) and 20 μm (2nd-4th columns). L, left; R, right; A, anterior; P, posterior. **(D)** Flattening of nuclei in response to different treatments. Each point represents the mean value within a sample. Welch's two-sample *t*-test, Ctrl-PD: $p = 0.885$. Ctrl-Bleb: $p = 0.007$, PD-Bleb: $p = 0.001$. $n = 5$ from different tracheae.

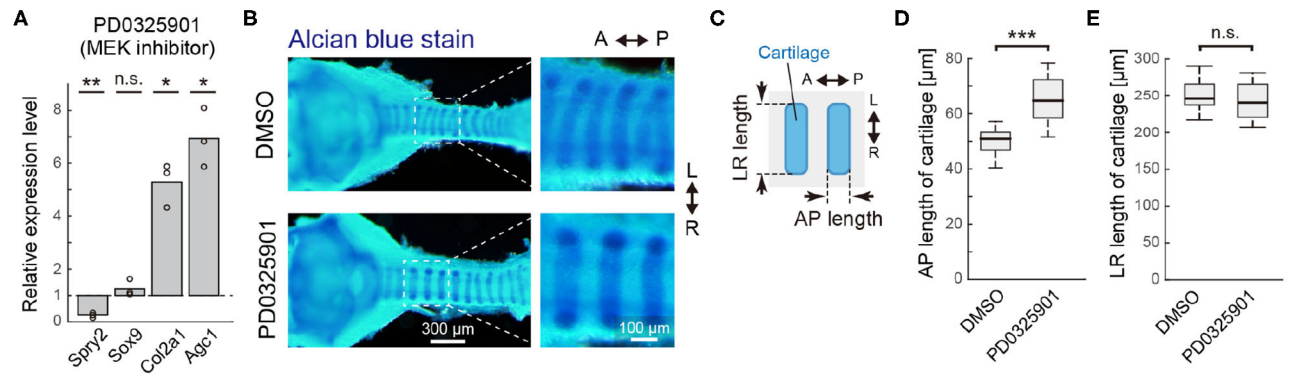

FIGURE 5 | ERK inactivation in cartilage matrix gene expression. **(A)** Relative gene expression in tracheae cultured *ex vivo* for 2 days from E13.5 with the PD0325901, compared to DMSO control, obtained by qPCR. Welch's one-sample *t*-test. *Spry2*: $p = 0.006$, *Sox9*: $p = 0.255$, *Col2a1*: $p = 0.013$, *Agc1*: $p = 0.012$. $n = 3$ from independent experiments. **(B)** Morphological change in tracheal cartilage treated with PD0325901. Cartilage rings were stained with Alcian blue and photographed on a dissecting microscope. Scale bars, 200 μm (left) and 100 μm (right). **(C)** Schematics showing the antero-posterior (AP) length and left-right (LR) length of the tracheal cartilage rings. The 3rd to 6th tracheal rings below the cricoid ring were measured. **(D)** AP length of cartilage rings exposed to the DMSO control or PD0325901 in the anterior region of trachea. Welch's two-sample *t*-test. $p < 0.001$. $n = 18$ different tracheae from 3 independent experiments. **(E)** LR length of cartilage rings exposed to the DMSO control or PD0325901 in the anterior region of trachea. Welch's two-sample *t*-test. $p = 0.281$. $n = 18$ different tracheae from 3 independent experiments. L, left; R, right; A, anterior; P, posterior.

round, and the tissue did not exhibit clear condensations or increased Sox9 expression near the epithelium (**Figures 4C,D**), suggesting that cell-generated contractile forces are required for mesenchymal condensations in tracheal development, but that ERK activation is dispensable for the regulation of contractile forces in this process.

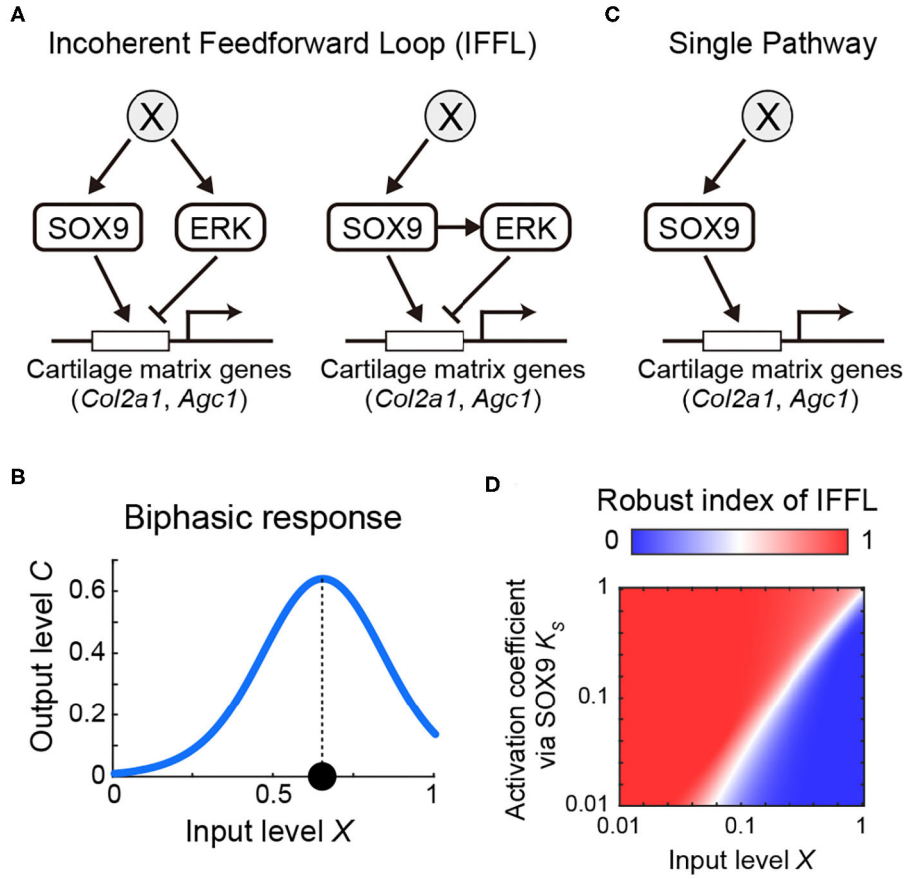

FIGURE 6 | Model of incoherent feedforward loop exploring the regulation of cartilage matrix genes by Sox9/ERK. **(A)** Possible network for cartilage matrix gene expression. **(B)** Input-output response of IFFL showing biphasic response. **(C)** Hypothetical single pathway. **(D)** Robust index of IFFL with regards to *X* and K'_S.

ERK Inactivation Promotes Expression of Cartilage Matrix Genes

To investigate the role of ERK activation in tracheal cartilage formation from E13.5 onwards, we measured the expression levels of *Sox9* and several cartilage matrix genes, which show a marked elevation in expression at this stage, in response to treatment with the MEK inhibitor (**Figure 2D**). The tracheae were dissected at E13.5 and cultured for 2 days in the presence of PD0325901 under *ex vivo* conditions. The expression of *Spry2*, an indicator of Ras–ERK cascade activity (Mason et al., 2006), was decreased by PD0325901 treatment, confirming the inhibition of ERK activation in this assay (**Figure 5A**). The expression of *Sox9* was unaffected, as anticipated from the data shown in **Figure 4**. We also confirmed that ERK inactivation did not affect *Sox9* expression using imaging measurements of Sox9-EGFP tracheae (**Supplementary Figure 2**). These data regarding ERK signaling are similar to those from a previous study which reported that inactivation of *Fgf10* did not affect *Sox9* expression (Sala et al., 2011). Interestingly, ERK inhibition significantly upregulated the expression of *Col2a1* and *Agc1* (**Figure 5A**). These findings suggest that ERK inactivation promotes gene expression of these cartilage matrix proteins in a manner independent of *Sox9* expression.

We next examined the impact of ERK inactivation on the tracheal cartilage phenotype. To this end, PD0325901 was administered to pregnant mice from E13.5 periodically for 2 days by oral gavage. The morphology of tracheal cartilage rings from dissected embryos was assessed by Alcian blue staining (**Figure 5B**), and the tracheae were evaluated in terms of antero-posterior (AP) and left-right (LR) lengths (**Figure 5C**). In the anterior region of trachea, close to larynx, ERK inactivation significantly increased the AP length (1.33-fold in median, **Figure 5D**), while it did not affect the LR length (0.98-fold in median, **Figure 5E**), indicating that cartilage matrix accumulation was enhanced due to ERK inactivation. Relative variance in each sample was <5% in either treatment (averaged in-sample coefficient of variance: 0.023 in the DMSO and 0.042 in the PD0325901). In the posterior region of trachea, close to the carina, the AP length was slightly increased by the ERK inactivation (1.07-fold in median) with large variance (**Supplementary Figure 3**). Together, our results suggest that active ERK represses the transcriptional activity of the cartilage

matrix genes, thereby influencing the AP length of the cartilage rings, especially in the anterior region.

Incoherent Feedforward Loop Can Explain the Regulation of Sox9-ERK-Cartilage Matrix Genes

Our results so far present two pathways which have antagonistic effects on the transcriptional regulation of the cartilage matrix genes, namely activation via Sox9 and repression via ERK. Furthermore, since Sox9 expression and ERK activity exhibited similar non-monotonic temporal profiles (**Figures 2C**, **3B**), it suggests that there may be a common upstream regulator X (**Figure 6A**, left) or positive regulation of ERK by Sox9 (**Figure 6A**, right). These network topologies are examples of a so-called incoherent feedforward loop (IFFL), known as a network motif, which represent recurrent patterns in transcriptional regulations (Shen-Orr et al., 2002; Mangan and Alon, 2003). We therefore considered the question of how these regulatory networks might function in tracheal development.

We modeled the possible core regulatory networks (**Figure 6A**) with a linear relation between X, Sox9, and ERK (see Mathematical analysis in Materials and Methods) because of the similar temporal variations, and found that, in either case, the expression level of the cartilage matrix genes in the steady state $\hat{C}$ converged to the following form:

$$\hat{C} = \frac{X^{h_S}}{X^{h_S} + {K'_S}^{h_S}} \frac{{K'_E}^{h_E}}{{K'_E}^{h_E} + X^{h_E}}. \quad (1)$$

The first term represents the activation by Sox9 with the coefficient K'_S, and the second term represents the repression via ERK with the coefficient K'_E, each of which is modeled by the Hill function with coefficient h_S or h_E, respectively, with input level X as the simplest form. The function of Equation 1 shows a biphasic inverse U-shape response, in which the output level $\hat{C}$ increases to a high level, and then decreases, as input level X increases, meaning that the output level reaches at its maximum at an intermediate input level (**Figure 6B** and **Supplementary Figure 4**). From Equation 1, the biphasic response modeled by the IFFL can explain the mapping of the non-monotonic temporal profiles of both Sox9 and ERK to the monotonic increases of the cartilage matrix genes (**Figure 2E**).

We next considered the role of ERK as a negative regulator of the pathways involved in chondrogenesis and queried the benefit of an IFFL involving ERK as a core regulatory design, compared with a single pathway regulated only by Sox9. To answer these questions, we analyzed the robustness of the steady state level of cartilage matrix gene expression $\hat{C}$ with respect to the input level X in the IFFL compared to the hypothetical single pathway (**Figures 6A,C**). To do this, we calculated the parameter sensitivity coefficient (Goldbeter and Koshland, 1981) of $\hat{C}$ with respect to X in both the IFFL (S_1) and in the single pathway (S_0), and obtained a condition of parameters which satisfies $S_1 > S_0$. That is, IFFL is more robust than the single pathway for input variations in the following inequality:

$$2\frac{h_S {K'_S}^{h_S}}{{K'_S}^{h_S} + X^{h_S}} > \frac{h_E X^{h_E}}{{K'_E}^{h_E} + X^{h_E}}. \quad (2)$$

Here we introduced a fraction of parameter sets that satisfy Eq. 2, designated Robust index of IFFL. When this value is more than 0.5, the IFFL is a more robust design compared with the single pathway, and vice versa. We then numerically investigated the dependency of the parameters X and K'_S, both of which are common to the IFFL and the single pathway, without fixing other parameters, and found that the parameter space where the index is more than 0.5 was larger than the area representing an index below 0.5 (**Figure 6D**). Collectively, our model analyses show that adopting ERK as a negative regulator of the regulatory chondrogenic pathways makes the system more robust against variations of the upstream regulator of Sox9 during chondrogenesis.

DISCUSSION

In this study, we demonstrate that there is an inverted U-shaped temporal change in Sox9 expression and ERK activity, while the expression of target cartilage matrix genes monotonically increases, during murine tracheal development. Using assays with a MEK inhibitor, we found that inhibiting ERK activity significantly promotes the expression of cartilage matrix genes. The role played by ERK during cartilage differentiation has been controversial in several *in vitro* studies (Murakami et al., 2000; Oh et al., 2000; Bobick and Kulyk, 2004; Zákány et al., 2005). Our results show that the ERK signaling pathway functions as an inhibitory regulator of tracheal cartilage differentiation, which has also been demonstrated in embryonic chicken limb buds (Oh et al., 2000; Bobick and Kulyk, 2004; Zákány et al., 2005).

Our findings led us to propose a model in which cartilage differentiation is controlled by an IFFL via positive and negative contributions of Sox9 and ERK activity, respectively. To delineate the core regulatory pathways, we tested two networks, one of which included a common upstream regulator without interactions between Sox9 and ERK, while the other network included a positive regulation of ERK by Sox9 (**Figure 6A**), although both of them resulted in the same class of output in the steady state (Equation 1). It has previously been demonstrated that the expression level of *Fgf10* does not change significantly even in *Sox9* knockout mice (Turcatel et al., 2013). Furthermore, there is evidence to imply that SHH, an upstream regulator of *Sox9*, could be a potential activator of *Fgf10* in tracheal development (Sala et al., 2011), and it raises the possibility that SHH could also be the common upstream regulator of Sox9 and ERK. It is therefore likely that the former regulatory network is adopted during tracheal ring formation.

The proposed core regulatory networks would be controlled by different types of stimulus, such as mechanical loading (O'Conor et al., 2013), oxidative stress (Zuscik et al., 2008), and electrical signals (Atsuta et al., 2019), through complex signaling pathways (Kozhemyakina et al., 2015). In chondroprogenitor cells derived from chicken limb buds, uniaxial cyclic compression increased the expression level of the cartilage matrix genes and elevated the activity of cyclic AMP-dependent protein kinase A (PKA) (O'Conor et al., 2013; Juhász et al., 2014), known to phosphorylate SOX9 (Huang et al., 2000). In addition, the

mechanical loading stimuli activated the pituitary adenylate cyclase activating polypeptide (PACAP) pathway, of which the classical downstream targets include PKA and MAPK signaling cascades (Juhász et al., 2015a,b), suggesting the common input to the Sox9 and the ERK activity. PACAP activation also inhibited the hedgehog signaling activity in the chondroprogenitor cell cultures. Thus, there would be an another IFFL at the upstream of Sox9-ERK signaling layer. Speaking of oxidative stress, it was shown that the hydrogen peroxide (H2O2) inhibited the chondrogenesis using the chicken limb bud cell cultures; H2O2 led to a concentration-dependent decrease of *Sox9* expression and an increase of ERK activity in a calcineurin-dependent manner (Zákány et al., 2005). This result suggests that the H2O2 would be a common input regulator to the Sox9 and the ERK activity, which brings a complex signaling crosstalk in the system.

In this study, we primarily focused on the expression of the cartilage matrix genes as an output, but the spatiotemporal dynamics of *Sox9* expression and ERK activity are likely to play roles in other aspects of cartilage differentiation. From E14.5 to E15.5, we observed a decrease in *Sox9* expression (**Figure 2C**). This may reflect the fact that the downregulation of SOX9 has multiple roles in the progression of cartilage differentiation, such as the transition of proliferating chondrocytes to a hypertrophic state, and cartilage vascularization (Akiyama et al., 2002; Hattori et al., 2010; Lefebvre et al., 2019). We also observed that endogenous ERK activation was maintained at a relatively low level from E12.5 to E13.5 (**Figure 3B**) and did not affect mesenchymal condensation, an initial step in tracheal ring patterning (**Figure 4B**). Since *Fgf10* overexpression in the mesenchyme between E11.5 and E13.5 was shown to cause disruption of the tracheal ring patterns (Sala et al., 2011), it is possible that ERK activity at below-moderate levels may be a key factor in normal tracheal development. Future studies should clarify the physiological importance of temporal ERK activity dynamics in this process. In addition, further systematic investigations of other signaling pathways, such as Wnt and bone morphogenetic protein (Bmp) signaling (Snowball et al., 2015; Kishimoto et al., 2018), as well as physical interactions with epithelia and smooth muscles (Hines et al., 2013; Yin et al., 2018), would improve our understanding of tracheal development and *in vitro* organoid systems (Conway et al., 2020; Kishimoto et al., 2020).

MATERIALS AND METHODS

Experiments and Quantification

Animals

For FRET imaging, we used transgenic mice that ubiquitously express an ERK biosensor with a long flexible linker, which has been described elsewhere (Harvey et al., 2008; Komatsu et al., 2011, 2018). Sox9-EGFP mice were provided from RIKEN BRC through the National BioResource Project of the MEXT/AMED, Japan (RBRC05651). Otherwise, we used ICR mice purchased from Japan SLC, Inc. The midnight preceding observation of a plug was designated as embryonic day 0.0 (E0.0), and all mice were sacrificed by cervical dislocation to minimize suffering. All the animal experiments were approved by the local ethical committee for animal experimentation (MedKyo 19090 and 20081) and were performed in compliance with the guide for the care and use of laboratory animals at Kyoto University.

Antibodies

The following primary and secondary antibodies were used for immunofluorescence: anti-E-cadherin rat antibody (#13-1900, 1:50 dilution, Thermo Fischer Scientific), anti-SOX9 rabbit antibody (#AB5535-25UG, 1:200 dilution, Merck Millipore), Alexa Fluor 546-conjugated goat anti-rat IgG (H+L) antibody (#A11081, 1:1000 dilution), Alexa Fluor 647-conjugated goat anti-rat IgG (H+L) antibody (#A21247, 1:1000 dilution), Alexa Fluor 647-conjugated goat anti-rabbit IgG (H+L) antibody (#A32733, 1:1000 dilution)(all Thermo Fisher Scientific).

Whole-Tissue Fluorescence Staining and Imaging

Staining and optical clearing of dissected tracheae were performed as described in a previous study (Hirashima and Adachi, 2015). Briefly, the samples were fixed with 4% PFA in PBS overnight at 4°C. For anti-SOX9 staining, the samples were incubated in 25 mg/mL hyaluronidase (Nacalai Tesque, #18240-36) for 1 h at 37°C, to digest hyaluronic acid. The samples were then blocked in 10% normal goat serum (Abcam, #ab156046) diluted in 0.1% Triton X-100/PBS (PBT) for 3 h at 37°C. The samples were treated with primary antibodies overnight at 4°C, washed in 0.1% PBT, and subsequently incubated in secondary antibodies conjugated to either Alexa Fluor 546 or Alexa Fluor 647 overnight at 4°C. DAPI was used for nuclear counterstaining (Dojindo Molecular Technologies, #D523-10, 1:200 dilution). The samples were mounted with 10 μL of 1% agarose gel onto a glass dish (Greiner Bio-One, #627871) for stable imaging. Then, the samples were immersed in CUBIC-R+ (Tokyo Chemical Industry Co., # T3741) solution for optical clearing. Images were acquired using the confocal laser scanning platform Leica TCS SP8 equipped with the hybrid detector Leica HyD, using a ×40 objective lens (NA = 1.3, WD = 240 μm, HC PL APO CS2, Leica) and the Olympus FluoView FV1000 with a ×30 objective lens (NA = 1.05, WD = 0.8 mm, UPLSAPO30XS, Olympus).

Alcian Blue Staining

The dissected tracheae were fixed in 4% PFA in PBS overnight at 4°C, and stained in Alcian Blue Solution (FUJIFILM Wako Pure Chemical Corporation, # 013-13801) for 60 min at 23°C. The samples were then washed with 20% acetic acid in PBS overnight at 23°C, and finally clarified in 50% glycerol in PBS for 2 hours at 37°C. The samples were visualized by the stereo microscopy (SZX16, Olympus).

Explant Cultures

The dissected tracheae were mounted on a 35 mm glass dish (Greiner, #627871) with 30 μL of growth factor-reduced Matrigel (Corning, #356231), and filled with 500 μL of DMEM culture medium including FluoroBrite (Thermo Fischer Scientific, #A1896701) with 1% GlutaMAX (Thermo Fischer Scientific, #35050061). The samples were incubated at 37°C under 5% CO_2.

Drug Administration

For the drug administration under *ex vivo* culture conditions, (-)-Blebbistatin (FUJIFILM Wako Pure Chemical Corporation, #021-17041) and PD0325901 (FUJIFILM Wako Pure Chemical Corporation, #162-25291) were mixed in the culture medium. Equivalent amounts of DMSO were used as a vehicle control for each drug. For administration by oral gavage, PD0325901 (ChemieTek, #CT-PD03) in 30% PEG400, 0.5% Tween 80 in PBS was administered to pregnant mice at a dose of 25 mg/kg body weight twice a day (at 8:00 a.m and 6:00 p.m) for 2 days from E13.5, i.e., 4 times in total.

Live Imaging for Explants

The samples were prepared for explant culture as described above and placed into an incubator-integrated multiphoton fluorescence microscope system (LCV-MPE, Olympus) with a ×25 water-immersion lens (NA=1.05, WD=2 mm, XLPLN25XWMP2, Olympus) and an inverted microscope (FV1200MPE-IX83, Olympus) with a ×30 silicone-immersion lens (NA=1.05, WD=0.8 mm, UPLSAPO30XS, Olympus). The excitation wavelengths were set to 840 or 930 nm, for the CFP of the ERK FRET biosensor and EGFP, respectively (InSight DeepSee, Spectra-Physics). The filter sets used were as follows; IR cut filter: RDM690 (Olympus), dichroic mirrors: DM505 and DM570 (Olympus), and emission filters: BA460-500 for CFP, BA520-560 for FRET, and BA495-540 for EGFP detection (Olympus).

Quantitative RT-PCR

Total RNA was extracted using the RNeasy Mini Kit (Qiagen, #74104), and cDNA was reverse transcribed using the High-Capacity cDNA Reverse Transcription Kit (Thermo Fisher Scientific, #4368814), according to the manufacturer's instructions. qPCR was performed using the StepOne real-time PCR system (Applied Biosystems) with PowerUp SYBR Green Master Mix (Thermo Fisher Scientific, #A25742). Primer sequences were as follows: *Agc1* forward 5′-GGTCACTG TTACCGCCACTT-3′ and reverse 5′-CCCCTTCGATAGTCC TGTCA-3′; *Col2a1* forward 5′-CTACGGTGTCAGGGCCAG-3' and reverse GCAAGATGAGGGCTTCCATA-3′; *Hprt1* forward 5′-TCAGTCAACGGGGGACATAAA-3′ and reverse GGGGCT GTACTGCTTAACCAG-3′;

Sox9 forward 5′-AGGAAGCTGGCAGACCAGTA-3′ and reverse TCCACGAAGGGTCTCTTCTC-3′; *Spry2* forward 5′-AGAGGATTCAAGGGAGAGGG-3′ and reverse 5′-CATC AGGTCTTGGCAGTGTG-3′. Relative expression levels were calculated using the ΔΔCT method with *Hprt1* expression as the internal control.

Target Region for Analysis

As the mesenchymal condensation simultaneously occurs in the whole trachea, we especially focused on anterior-ventral region, where the future 3rd to 7th tracheal cartilages below the cricoid ring are formed, for analysis. These regions were also convenient for imaging because the frontal plane is parallel to the optical plane.

FRET Image Analysis

The median filter of a 3×3 window was processed to remove shot noises, and the background signal was subtracted each in FRET and CFP channel. Then, the ratio of FRET intensity to the CFP intensity was calculated using a custom-designed MATLAB (MathWorks) script.

Quantification of Nuclear Shape

Since the nuclear configuration exhibited no significant differences throughout the trachea, we randomly chose one representative mesenchymal condensation from the ventral region where the future 3rd to 7th tracheal cartilages below the cricoid ring are formed. The DAPI staining images were smoothened using the median and gaussian filters, and the nuclei were then manually extracted. Flattening or ellipticity is defined as $1\text{-}b/a$, where a and b are the major and the minor axis length of the best fitting ellipse, respectively. The value is 0 for a circle, and it approaches 1 as it is compressed. All processing was done using ImageJ.

Single Cell Measurement

For the EGFP and FRET measurement at single cell resolution, we first manually extracted each cell or nucleus and measured the average intensity within the extracted region. Then, the background signal was subtracted from averaged signal. For the EGFP signal, the obtained intensity was normalized by the maximum value of the bit depth. All image processing was done using ImageJ.

Statistical Hypothesis Testing

Statistical tests, sample sizes, test statistics, and P-values are described in the main text. $P < 0.05$ were considered to be statistically significant in two-tailed tests, and were classified into 4 categories; * ($P < 0.05$), ** ($P < 0.01$), *** ($P < 0.001$), and n.s. (not significant, i.e., $P \geq 0.05$).

Software

For digital image processing, MATLAB (MathWorks) and ImageJ (National Institute of Health) were used. For graphics, MATLAB (MathWorks), Imaris (Bitplane) and ImageJ (National Institute of Health) were used. MATLAB (MathWorks) was used for statistical analysis and Mathematica (Wolfram Research) for mathematical analysis.

Graph

For the boxplot, the central mark indicates the median, and the bottom and top edges of the box indicate the 25th and 75th percentiles, respectively. The whiskers extend to the most extreme data points not considered outliers, and the outliers are plotted individually using the "+" symbol. All of the graphs were prepared in MATLAB.

Mathematical Analysis

Modeling

For model construction, we let X, S, E, C be input level, Sox9 concentration, ERK activity, and the expression level of cartilage matrix genes, respectively. Since Sox9 expression and

ERK activity showed similar temporal profiles, they would be regulated linearly by input level X. Thus,

$$\dot{S} = \alpha_S X - \gamma_S S, \tag{S1}$$

and

$$\dot{E} = \alpha_E X - \gamma_E E, \tag{S2}$$

where α and γ denote production rate and decay rate, respectively. Regarding the alternative regulation, i.e., X indirectly, but not directly, regulates ERK activity through Sox9, the regulation of ERK activity can be represented, instead of Equation S2, as

$$\dot{E} = \alpha_E S - \gamma_E E. \tag{S3}$$

As Sox9 and active ERK antagonistically regulate the expression level of cartilage matrix genes, the dynamics of C can be represented in the simplest form as follows:

$$\dot{C} = \alpha_C \frac{S^{h_S}}{S^{h_S} + K_S^{h_S}} \frac{K_E^{h_E}}{K_E^{h_E} + E^{h_E}} - \gamma_C C, \tag{S4}$$

where K_S is the activation coefficient via Sox9, K_E is the repression coefficient via ERK, and h denotes the Hill coefficient. Both combinations of Equations S1, S2, and S4, and Equations S1, S3, and S4 led to the following function of C in the steady state:

$$\hat{C} = {\alpha'}_C \frac{X^{h_S}}{X^{h_S} + {K'}_S^{h_S}} \frac{{K'}_E^{h_E}}{{K'}_E^{h_E} + X^{h_E}}, \tag{S5}$$

where parameters with prime represent integrated parameters, and the case with ${\alpha'}_C = 1$ is shown as the Equation 1 in the main text.

Parameter Ranges in Numerical Investigation

Owing to the importance of relativity for X, ${K'}_S$, and ${K'}_E$, we set those ranges as 0.01 to 1.0. For h_S and h_E, we set the range from 1 to 5 to consider non-linearity of reactions. ${\alpha'}_C$ was arbitrarily set to 1.

Parameter Dependence in the Steady State

Assuming $h_S = h_E = 1$ for simplicity and feasibility of analysis, we found that the input value at the output peak X^* was determined by the two parameters ${K'}_S$ and ${K'}_E$ as follows

$$X^* = \left\{ X \middle| \frac{\partial \hat{C}}{\partial X} = 0 \right\} = \sqrt{{K'}_S {K'}_E}, \tag{S6}$$

which corresponded to the numerical results (**Supplementary Figure 4B'**). Also, the function of $\hat{C}$ was convex upward at the peak as

$$\left. \frac{\partial^2 \hat{C}}{\partial X^2} \right|_{X=X^*} = -\frac{2{\alpha'}_C \sqrt{{K'}_E}}{\sqrt{{K'}_S} \left(\sqrt{{K'}_S} + \sqrt{{K'}_E} \right)^4} < 0. \tag{S7}$$

Moreover, the maximum level of $\hat{C}$ is represented as

$$\hat{C}_{\max} = \frac{{\alpha'}_C \sqrt{{K'}_E}}{\left(\sqrt{{K'}_S} + \sqrt{{K'}_E} \right)^2}. \tag{S8}$$

This clearly indicates that the output peak level decreases with increases in ${K'}_S$ and it increases with increasing ${K'}_E$, corresponding to the numerical results (**Supplementary Figure S4B'**).

Sensitivity Analysis for Robustness

The parameter sensitivity coefficient with respect to the input value X, denoted $S(\hat{C}, X)$, is defined as the relative change in $\hat{C}$ for a given small relative change in X:

$$S\left(\hat{C}, X\right) = \left| \frac{\Delta \hat{C}}{\hat{C}} \Big/ \frac{\Delta X}{X} \right|. \tag{S9}$$

From Equations S5 and S9, we obtained the explicit form S in the IFFL regulation.

$$S\left(\hat{C}, X\right) = \left| \frac{h_S {K'}_S{}^{h_S}}{{K'}_S{}^{h_S} + X^{h_S}} - \frac{h_E X^{h_E}}{{K'}_E{}^{h_E} + X^{h_E}} \right|. \tag{S10}$$

As an alternative regulation, we assumed a hypothetical single pathway regulation, instead of Equation S4

$$\dot{C}_0 = \alpha_C \frac{S^{h_S}}{S^{h_S} + K_S^{h_S}} - \gamma_C C_0, \tag{S11}$$

and from Equations S9 and S11, we obtained the parameter sensitivity coefficient for a single pathway as follows:

$$S\left(\hat{C}_0, X\right) = \left| \frac{h_S {K'}_S{}^{h_S}}{{K'}_S{}^{h_S} + X^{h_S}} \right|. \tag{S12}$$

We then evaluated the robustness of the IFFL compared to the single pathway by the inequality of the sensitivity coefficients:

$$S\left(\hat{C}_0, X\right) > S\left(\hat{C}, X\right). \tag{S13}$$

With Equations S10 and S12, Equation S13 reached the inequality condition shown in Eq. 2 in the main text.

DATA AVAILABILITY STATEMENT

All datasets presented in this study are included in the article/**Supplementary Material**.

ETHICS STATEMENT

The animal study was reviewed and approved by all the animal experiments were approved by the local ethical committee for animal experimentation (MedKyo 19090 and 20081) and were performed in compliance with the guide for the care and use of laboratory animals at Kyoto University.

AUTHOR CONTRIBUTIONS

TY and TH: conceptualization, methodology, validation, formal analysis, investigation, data curation, and writing–original draft. TH: software, visualization, and project administration. MM and TH: resources, writing–review & editing, supervision, and funding acquisition. All authors contributed to the article and approved the submitted version.

FUNDING

This work was supported by the JSPS KAKENHI 17KT0107 and 19H00993, 16H06280, by the JST PRESTO JPMJPR1949, by the CREST JPMJCR1654, by the AMED 19gm5010003h0003, and by the Medical Research Support Center of Kyoto University.

ACKNOWLEDGMENTS

We would like to thank Yu Kurata and Akane Kusumi for technical assistances, and Keisho Hirota and Mitsuru Morimoto for fruitful discussion.

SUPPLEMENTARY MATERIAL

The Supplementary Material for this article can be found online at: https://www.frontiersin.org/articles/10.3389/fcell.2020.585640/full#supplementary-material

Supplementary Figure 1 | Sox9-EGFP profile in the developing murine trachea. **(A)** A 3D-rendered image of Sox9-EGFP at E14.5, showing the C-shaped tracheal rings on the ventral side. L, left; R, right; A, anterior; P, posterior; V, ventral; D, dorsal. **(B)** Simultaneous visualization of EGFP ("fire" pseudocolor) and anti-E-cadherin (white) at E14.0. High EGFP expression cell clusters located between the ridges of wavy tracheal epithelium. Scale bar, 50 μm. **(C)** Simultaneous visualization of EGFP (green) and anti-SOX9 (red) at E14.5. Scale bar, 50 μm. **(D)** Relationship between EGFP and anti-SOX9 intensity from E12.5 to E14.5. Pearson's linear correlation coefficient: $\rho = 0.81$.

Supplementary Figure 2 | Effect of ERK inactivation on Sox9 expression. **(A)** Tracheae dissected at E12.5 from Sox9-EGFP mice were cultured for 1 day, together with PD0325901 (500 nM). EGFP intensity was measured by two-photon microscopy. **(B)** EGFP intensity with DMSO and PD0325901. Welch's two-sample *t*-test, $p = 0.012$. $n = 60$ different cells from the single experiment.

Supplementary Figure 3 | Morphological change of cartilages to the ERK inactivation in the posterior region of trachea. **(A)** AP length of cartilage rings exposed to the DMSO control or PD0325901 in the lower region of trachea. Welch's two-sample *t*-test. $p = 0.326$. $n = 12$ different tracheae from 3 independent experiments. **(B)** LR length of cartilage rings exposed to the DMSO control or PD0325901 in the lower region of trachea. Welch's two-sample *t*-test. $p = 0.413$. $n = 12$ different trachea from 3 independent experiments.

Supplementary Figure 4 | Parameter dependence of the model. **(A)** Schematics showing the input-output relationship. **(B,B')** Parameter dependence of (1) the output peak level and (2) the input level at the output peak. Axes are shown in **(B)**.

REFERENCES

Akiyama, H., Chaboissier, M. C., Martin, J. F., Schedl, A., and De Crombrugghe, B. (2002). The transcription factor Sox9 has essential roles in successive steps of the chondrocyte differentiation pathway and is required for expression of Sox5 and Sox6. *Genes Dev.* 16, 2813–2828. doi: 10.1101/gad.1017802

Arooj Sher, Z., and Liu, K. J. (2016). Congenital tracheal defects: embryonic development and animal models. *AIMS Genet.* 3, 60–73. doi: 10.3934/genet.2016.1.60

Atsuta, Y., Tomizawa, R. R., Levin, M., and Tabin, C. J. (2019). L-type voltage-gated Ca 2+ channel Ca V 1.2 regulates chondrogenesis during limb development. *Proc. Natl. Acad. Sci. U.S.A.* 116, 21592–21601. doi: 10.1073/pnas.1908981116

Bi, W., Deng, J. M., Zhang, Z., Behringer, R. R., and de Crombrugghe, B. (1999). Sox9 is required for cartilage formation. *Nat. Genet.* 22, 85–89. doi: 10.1038/8792

Bi, W., Huang, W., Whitworth, D. J., Deng, J. M., Zhang, Z., Behringer, R. R., et al. (2001). Haploinsufficiency of Sox9 results in defective cartilage primordia and premature skeletal mineralization. *Proc. Natl. Acad. Sci. U.S.A.* 98, 6698–6703. doi: 10.1073/pnas.111092198

Bobick, B. E., and Kulyk, W. M. (2004). The MEK-ERK signaling pathway is a negative regulator of cartilage-specific gene expression in embryonic limb mesenchyme. *J. Biol. Chem.* 279, 4588–4595. doi: 10.1074/jbc.M309805200

Boucherat, O., Nadeau, V., Berube-Simard, F.-A., Charron, J., and Jeannotte, L. (2014). Crucial requirement of ERK/MAPK signaling in respiratory tract development. *Development* 141, 3197–3211. doi: 10.1242/dev.110254

Cardoso, W. V., and Lü, J. (2006). Regulation of early lung morphogenesis: questions, facts and controversies. *Development* 133, 1611–1624. doi: 10.1242/dev.02310

Conway, R. F., Frum, T., Conchola, A. S., and Spence, J. R. (2020). Understanding human lung development through *in vitro* model systems. *Bioessays* 42:2000006. doi: 10.1002/bies.202000006

Elluru, R. G., Thompson, F., and Reece, A. (2009). Fibroblast growth factor 18 gives growth and directional cues to airway cartilage. *Laryngoscope* 119, 1153–1165. doi: 10.1002/lary.20157

Goldbeter, A., and Koshland, D. E. (1981). An amplified sensitivity arising from covalent modification in biological systems. *Proc. Natl. Acad. Sci. U.S.A.* 78, 6840–6844. doi: 10.1073/pnas.78.11.6840

Goldring, M. B., Tsuchimochi, K., and Ijiri, K. (2006). The control of chondrogenesis. *J. Cell. Biochem.* 97, 33–44. doi: 10.1002/jcb.20652

Han, Y., and Lefebvre, V. (2008). L-Sox5 and Sox6 drive expression of the aggrecan gene in cartilage by securing binding of Sox9 to a far-upstream enhancer. *Mol. Cell. Biol.* 28, 4999–5013. doi: 10.1128/MCB.00695-08

Harvey, C. D., Ehrhardt, A. G., Cellurale, C., Zhong, H., Yasuda, R., Davis, R. J., et al. (2008). A genetically encoded fluorescent sensor of ERK activity. *Proc. Natl. Acad. Sci. U.S.A.* 105, 19264–19269. doi: 10.1073/pnas.0804598105

Hattori, T., Muller, C., Gebhard, S., Bauer, E., Pausch, F., Schlund, B., et al. (2010). SOX9 is a major negative regulator of cartilage vascularization, bone marrow formation and endochondral ossification. *Development* 137, 901–911. doi: 10.1242/dev.045203

Hines, E. A., Jones, M.-K. N., Verheyden, J. M., Harvey, J. F., and Sun, X. (2013). Establishment of smooth muscle and cartilage juxtaposition in the developing mouse upper airways. *Proc. Natl. Acad. Sci. U.S.A.* 110, 19444–19449. doi: 10.1073/pnas.1313223110

Hirashima, T., and Adachi, T. (2015). Procedures for the quantification of whole-tissue immunofluorescence images obtained at single-cell resolution during murine tubular organ development. *PLoS ONE* 10:e0135343. doi: 10.1371/journal.pone.0135343

Huang, W., Zhou, X., Lefebvre, V., and de Crombrugghe, B. (2000). Phosphorylation of SOX9 by cyclic AMP-dependent protein kinase a enhances SOX9's ability to transactivate aCol2a1 chondrocyte-specific enhancer. *Mol. Cell. Biol.* 20, 4149–4158. doi: 10.1128/MCB.20.11.4149-4158.2000

Juhász, T., Helgadottir, S. L., Tamás, A., Regldi, D., and Zákány, R. (2015a). PACAP and VIP signaling in chondrogenesis and osteogenesis. *Peptides* 66, 51–57. doi: 10.1016/j.peptides.2015.02.001

Juhász, T., Matta, C., Somogyi, C., Katona, É., Takács, R., Soha, R. F., et al. (2014). Mechanical loading stimulates chondrogenesis via the PKA/CREB-Sox9 and PP2A pathways in chicken micromass cultures. *Cell. Signal.* 26, 468–482. doi: 10.1016/j.cellsig.2013.12.001

Juhász, T., Szentléleky, E., Somogyi, C., Takács, R., Dobrosi, N., Engler, M., et al. (2015b). Pituitary adenylate cyclase activating polypeptide (PACAP) pathway is induced by mechanical load and reduces the activity of hedgehog signaling in chondrogenic micromass cell cultures. *Int. J. Mol. Sci.* 16, 17344–17367. doi: 10.3390/ijms160817344

Kishimoto, K., Furukawa, K. T., Luz-Madrigal, A., Yamaoka, A., Matsuoka, C., Habu, M., et al. (2020). Bidirectional Wnt signaling between endoderm and mesoderm confers tracheal identity in mouse and human cells. *Nat. Commun.* 11:4159. doi: 10.1038/s41467-020-17969-w

Kishimoto, K., Tamura, M., Nishita, M., Minami, Y., Yamaoka, A., Abe, T., et al. (2018). Synchronized mesenchymal cell polarization and differentiation shape

the formation of the murine trachea and esophagus. *Nat. Commun.* 9:2816. doi: 10.1038/s41467-018-05189-2

Komatsu, N., Aoki, K., Yamada, M., Yukinaga, H., Fujita, Y., Kamioka, Y., et al. (2011). Development of an optimized backbone of FRET biosensors for kinases and GTPases. *Mol. Biol. Cell* 22, 4647–4656. doi: 10.1091/mbc.e11-01-0072

Komatsu, N., Terai, K., Imanishi, A., Kamioka, Y., Sumiyama, K., Jin, T., et al. (2018). A platform of BRET-FRET hybrid biosensors for optogenetics, chemical screening, and *in vivo* imaging. *Sci. Rep.* 8:8984. doi: 10.1038/s41598-018-27174-x

Kozhemyakina, E., Lassar, A. B., and Zelzer, E. (2015). A pathway to bone: signaling molecules and transcription factors involved in chondrocyte development and maturation. *Development* 142, 817–831. doi: 10.1242/dev.105536

Lefebvre, V., Angelozzi, M., and Haseeb, A. (2019). SOX9 in cartilage development and disease. *Curr. Opin. Cell Biol.* 61, 39–47. doi: 10.1016/j.ceb.2019.07.008

Mammoto, T., Mammoto, A., Torisawa, Y., Tat, T., Gibbs, A., Derda, R., et al. (2011). Mechanochemical control of mesenchymal condensation and embryonic tooth organ formation. *Dev. Cell* 21, 758–769. doi: 10.1016/j.devcel.2011.07.006

Mangan, S., and Alon, U. (2003). Structure and function of the feed-forward loop network motif. *Proc. Natl. Acad. Sci. U.S.A.* 100, 11980–11985. doi: 10.1073/pnas.2133841100

Mason, J. M., Morrison, D. J., Albert Basson, M., and Licht, J. D. (2006). Sprouty proteins: multifaceted negative-feedback regulators of receptor tyrosine kinase signaling. *Trends Cell Biol.* 16, 45–54. doi: 10.1016/j.tcb.2005.11.004

Murakami, S., Kan, M., McKeehan, W. L., and de Crombrugghe, B. (2000). Up-regulation of the chondrogenic Sox9 gene by fibroblast growth factors is mediated by the mitogen-activated protein kinase pathway. *Proc. Natl. Acad. Sci. U.S.A.* 97, 1113–1118. doi: 10.1073/pnas.97.3.1113

Nakamura, Y., Yamamoto, K., He, X., Otsuki, B., Kim, Y., Murao, H., et al. (2011). Wwp2 is essential for palatogenesis mediated by the interaction between Sox9 and mediator subunit 25. *Nat. Commun.* 2:251. doi: 10.1038/ncomms1242

Nel-Themaat, L., Vadakkan, T. J., Wang, Y., Dickinson, M. E., Akiyama, H., and Behringer, R. R. (2009). Morphometric analysis of testis cord formation in Sox9-EGFP mice. *Dev. Dyn.* 238, 1100–1110. doi: 10.1002/dvdy.21954

O'Conor, C. J., Case, N., and Guilak, F. (2013). Mechanical regulation of chondrogenesis. *Stem Cell Res. Ther.* 4:61. doi: 10.1186/scrt211

Oh, C.-D., Chang, S.-H., Yoon, Y.-M., Lee, S.-J., Lee, Y.-S., Kang, S.-S., et al. (2000). Opposing role of mitogen-activated protein kinase subtypes, Erk-1/2 and p38, in the regulation of chondrogenesis of mesenchymes. *J. Biol. Chem.* 275, 5613–5619. doi: 10.1074/jbc.275.8.5613

Park, J., Zhang, J. J. R., Moro, A., Kushida, M., Wegner, M., and Kim, P. C. W. (2010). Regulation of Sox9 by sonic hedgehog (Shh) is essential for patterning and formation of tracheal cartilage. *Dev. Dyn.* 239, 514–526. doi: 10.1002/dvdy.22192

Sala, F. G., Del Moral, P.-M., Tiozzo, C., Alam, D. A., Warburton, D., Grikscheit, T., et al. (2011). FGF10 controls the patterning of the tracheal cartilage rings via Shh. *Development* 138, 273–282. doi: 10.1242/dev.051680

Shen-Orr, S. S., Milo, R., Mangan, S., and Alon, U. (2002). Network motifs in the transcriptional regulation network of *Escherichia coli*. *Nat. Genet.* 31, 64–68. doi: 10.1038/ng881

Shyer, A. E., Rodrigues, A. R., Schroeder, G. G., Kassianidou, E., Kumar, S., and Harland, R. M. (2017). Emergent cellular self-organization and mechanosensation initiate follicle pattern in the avian skin. *Science* 357, 811–815. doi: 10.1126/science.aai7868

Snowball, J., Ambalavanan, M., Whitsett, J., and Sinner, D. (2015). Endodermal wnt signaling is required for tracheal cartilage formation. *Dev. Biol.* 405, 56–70. doi: 10.1016/j.ydbio.2015.06.009

Tiozzo, C., Langhe, S., De Carraro, G., Alam, D., Al, Nagy, A., Wigfall, C., et al. (2009). Fibroblast growth factor 10 plays a causative role in the tracheal cartilage defects in a mouse model of apert syndrome. *Pediatr. Res.* 66, 386–390. doi: 10.1203/PDR.0b013e3181b45580

Turcatel, G., Rubin, N., Menke, D. B., Martin, G., Shi, W., and Warburton, D. (2013). Lung mesenchymal expression of Sox9 plays a critical role in tracheal development. *BMC Biol.* 11:117. doi: 10.1186/1741-7007-11-117

Yin, W., Kim, H.-T., Wang, S., Gunawan, F., Wang, L., Kishimoto, K., et al. (2018). The potassium channel KCNJ13 is essential for smooth muscle cytoskeletal organization during mouse tracheal tubulogenesis. *Nat. Commun.* 9:2815. doi: 10.1038/s41467-018-05043-5

Zákány, R., Szíjgyártó, Z., Matta, C., Juhász, T., Csortos, C., Szucs, K., et al. (2005). Hydrogen peroxide inhibits formation of cartilage in chicken micromass cultures and decreases the activity of calcineurin: implication of ERK1/2 and Sox9 pathways. *Exp. Cell Res.* 305, 190–199. doi: 10.1016/j.yexcr.2004.12.016

Zuscik, M. J., Hilton, M. J., Zhang, X., Chen, D., and O'Keefe, R. J. (2008). Regulation of chondrogenesis and chondrocyte differentiation by stress. *J. Clin. Invest.* 118, 429–438. doi: 10.1172/JCI34174

Conflict of Interest: The authors declare that the research was conducted in the absence of any commercial or financial relationships that could be construed as a potential conflict of interest.

frontiers in Cell and Developmental Biology

REVIEW
published: 14 December 2020
doi: 10.3389/fcell.2020.595849

Phosphoinositide Signaling and Mechanotransduction in Cardiovascular Biology and Disease

Amanda Krajnik[1†], Joseph A. Brazzo III[1†], Kalyanaraman Vaidyanathan[1], Tuhin Das[2], Javier Redondo-Muñoz[3,4] and Yongho Bae[1]*

[1] Department of Pathology and Anatomical Sciences, Jacobs School of Medicine and Biomedical Sciences, University at Buffalo, State University of New York, Buffalo, NY, United States, [2] Cell Biology Program, Memorial Sloan Kettering Cancer Center, New York, NY, United States, [3] Department of Molecular Biomedicine, Centro de Investigaciones Biológicas Margarita Salas, Madrid, Spain, [4] Lydia Becker Institute of Immunology and Inflammation, Faculty of Biology, Medicine and Health, School of Biological Sciences, University of Manchester, Manchester, United Kingdom

OPEN ACCESS

Edited by:
Isabel Merida,
Consejo Superior de Investigaciones Científicas (CSIC), Spain

Reviewed by:
Tibor Rohacs,
Rutgers New Jersey Medical School, United States
Emilio Hirsch,
University of Turin, Italy

***Correspondence:**
Yongho Bae
yonghoba@buffalo.edu

[†] These authors have contributed equally to this work

Specialty section:
This article was submitted to Signaling, a section of the journal Frontiers in Cell and Developmental Biology

Received: 17 August 2020
Accepted: 25 November 2020
Published: 14 December 2020

Citation:
Krajnik A, Brazzo JA III, Vaidyanathan K, Das T, Redondo-Muñoz J and Bae Y (2020) Phosphoinositide Signaling and Mechanotransduction in Cardiovascular Biology and Disease. Front. Cell Dev. Biol. 8:595849. doi: 10.3389/fcell.2020.595849

Phosphoinositides, which are membrane-bound phospholipids, are critical signaling molecules located at the interface between the extracellular matrix, cell membrane, and cytoskeleton. Phosphoinositides are essential regulators of many biological and cellular processes, including but not limited to cell migration, proliferation, survival, and differentiation, as well as cytoskeletal rearrangements and actin dynamics. Over the years, a multitude of studies have uniquely implicated phosphoinositide signaling as being crucial in cardiovascular biology and a dominant force in the development of cardiovascular disease and its progression. Independently, the cellular transduction of mechanical forces or mechanotransduction in cardiovascular cells is widely accepted to be critical to their homeostasis and can drive aberrant cellular phenotypes and resultant cardiovascular disease. Given the versatility and diversity of phosphoinositide signaling in the cardiovascular system and the dominant regulation of cardiovascular cell functions by mechanotransduction, the molecular mechanistic overlap and extent to which these two major signaling modalities converge in cardiovascular cells remain unclear. In this review, we discuss and synthesize recent findings that rightfully connect phosphoinositide signaling to cellular mechanotransduction in the context of cardiovascular biology and disease, and we specifically focus on phosphatidylinositol-4,5-phosphate, phosphatidylinositol-4-phosphate 5-kinase, phosphatidylinositol-3,4,5-phosphate, and phosphatidylinositol 3-kinase. Throughout the review, we discuss how specific phosphoinositide subspecies have been shown to mediate biomechanically sensitive cytoskeletal remodeling in cardiovascular cells. Additionally, we discuss the direct interaction of phosphoinositides with mechanically sensitive membrane-bound ion channels in response to mechanical stimuli. Furthermore, we explore the role of phosphoinositide subspecies in association with critical downstream effectors of mechanical signaling in cardiovascular biology and disease.

Keywords: phosphoinositides, cardiovascular mechanotransduction, actin cytoskeleton, ion channel, focal adhesion, PIP_2, PIP_3, PI3K

INTRODUCTION

Phosphoinositides (PPIs) constitute less than five percent of all cell membrane phospholipids (Hammond and Hong, 2018) but are essential to the integrity of all living cells (Dickson and Hille, 2019). Numerous studies have shown that PPIs are critical to cellular functions, including but not limited to cell proliferation, survival, motility, differentiation, and cytoskeletal dynamics (Di Paolo et al., 2004; Huang et al., 2004; Tsujita and Itoh, 2015; De Craene et al., 2017; Senju et al., 2017; Hao et al., 2018; Ramos et al., 2018; Bilanges et al., 2019; Li H. et al., 2019; Hirsch et al., 2020). The generation of PPIs is mediated by phosphorylation and dephosphorylation of phosphatidylinositol, the membrane lipid precursor (De Craene et al., 2017). More specifically, the inositol head of phosphatidylinositol can be phosphorylated at the 3-, 4-, and 5-hydroxyl positions of the inositol ring. The attachment of phosphate(s) can occur at any of these positions singularly or in combination to generate seven biologically active PPI subspecies: PI(3)P, PI(4)P, PI(5)P, PI(3,4)P_2, PI(4,5)P_2, PI(3,5)P_2, and PI(3,4,5)P_3 (Di Paolo and De Camilli, 2006; De Craene et al., 2017). All seven PPI subspecies naturally occur in the cell membrane of eukaryotes to varying degrees and are chemically interconverted by cell-specific kinases (purple-colored text in **Figure 1**) and phosphatases (red-colored text in **Figure 1**). PPI subspecies are shown as the black-colored text in **Figure 1**. Once biochemically active, PPIs modulate a tremendous breadth of horizontal and vertical cell signaling crosstalk spanning the cell membrane and cytoplasm, respectively, in which high-affinity interactions occur among various pleckstrin homology (PH) domain-containing membrane-based and cytosolic effector proteins, including protein kinase B (PKB)/Akt, protein kinase C (PKC), phosphoinositide phospholipase C (PLC), 3-phosphoinositide-dependent protein kinase-1 (PDK1), and small G proteins (Prestwich, 2004; Ghigo and Li, 2015; Manna and Jain, 2015; De Craene et al., 2017). In the cardiovascular system, activated PPI signaling mediates enzymatic organic modification of secondary messenger proteins because PPIs are crucial scaffolding proteins to complex signalosomes of cardiac and vascular cellular functions, and their aberration is a prominent driving force in cardiovascular pathology (Falkenburger et al., 2010; Ghigo and Li, 2015; Schink et al., 2016).

Mechanotransduction describes the physiological process by which cells perceive and respond to mechanical stimuli, including tensile stretch and compression, shear stress, and extracellular matrix (ECM) stiffness. Moreover, mechanical cues are converted into intracellular biochemical signals in which the resultant cytoskeletal and nuclear remodeling modulates cellular functions (Tschumperlin, 2011; Maurer and Lammerding, 2019). Mechanotransduction is vital to cardiovascular tissue development, growth, and homeostasis because cells are continuously under mechanical stress (Garoffolo and Pesce, 2019). Dysregulation of the mechanical harmony between the cell and ECM can drive the development and progression of pathology, including but not limited to cardiac ischemia and fibrosis, hypertension, and atherosclerosis (Gimbrone and Garcia-Cardena, 2013; Yue et al., 2015; Schafer et al., 2017; Ochoa et al., 2018; Russo et al., 2018). Only recently have we begun to understand the cellular mechanisms that mediate the signal transduction of mechanical stimuli, which greatly overlap with canonical biochemical cellular signaling pathways.

Today, cardiovascular disease (CVD) remains the leading cause of death and morbidity worldwide. A great majority of biomedical research in CVD centers around the known mechanisms of biochemical and molecular biology modalities. With the recent emergence of novel biomechanical and cell biological technologies and techniques, there has been a new integrative movement toward understanding the mechanical regulation of cellular biochemistry and molecular biology inside the cell. This review will span the most recent findings in phosphoinositide biology as it relates to mechanically sensitive cellular processes in cardiovascular cells in both homeostasis and disease. We will discuss how specific PPI subspecies mediate cytoskeletal remodeling processes known to be dominantly regulated by mechanotransduction and the direct interaction of PPIs with membrane-bound channels in response to mechanical stress in cardiovascular cells. Furthermore, we will explore the role of PPI subspecies in association with the essential effectors of mechanical signaling in cardiovascular biology and disease.

PHOSPHATIDYLINOSITOL-4,5-BISPHOSPHATE (PIP_2)

PIP_2 Association With Actin Cytoskeleton Dynamics

The actin cytoskeleton is a complex and dynamic intracellular structure that gives mechanical rigor to the cell while simultaneously mediating the transduction of mechanical stress into biochemical signals. Given the unique contractile properties of cardiac and vascular cells, the actin cytoskeleton is most essential to their integrity (Allahverdian et al., 2018; Zhang et al., 2018). Alteration of cytoskeletal organization, specifically actin filament dynamics, can result in gene expression and cell proliferation modification with the subsequent adaptation of and changes to intracellular biochemical responses and cellular functions, respectively. Thus, cytoskeletal remodeling can mediate mechanical stress-induced gene expression, cell proliferation, and pathological processes (Ohashi et al., 2017; Martino et al., 2018). Recent studies have shown that PIPs regulate cytoskeletal arrangement and signaling dynamics (Di Paolo and De Camilli, 2006; Saarikangas et al., 2010; Senju and Lappalainen, 2019). Specifically, PIP_2 is involved in cytoskeletal reorganizational events, including vesicle trafficking, cell migration, phagocytosis, and membrane cytoskeletal adhesion (Saarikangas et al., 2010; Shewan et al., 2011; Dickson and Hille, 2019; Phan et al., 2019). PIP_2 binds to and affects actin-binding proteins, such as myristoylated alanine-rich C kinase substrate (MARCKS), cofilin, gelsolin, α-actinin, Wiskott-Aldrich syndrome protein (WASP), and the Rho family of small GTPases (Janmey et al., 2018; **Figure 2**). MARCKS is an actin-binding protein found in mammalian tissues and, upon phosphorylation, it binds reversibly to

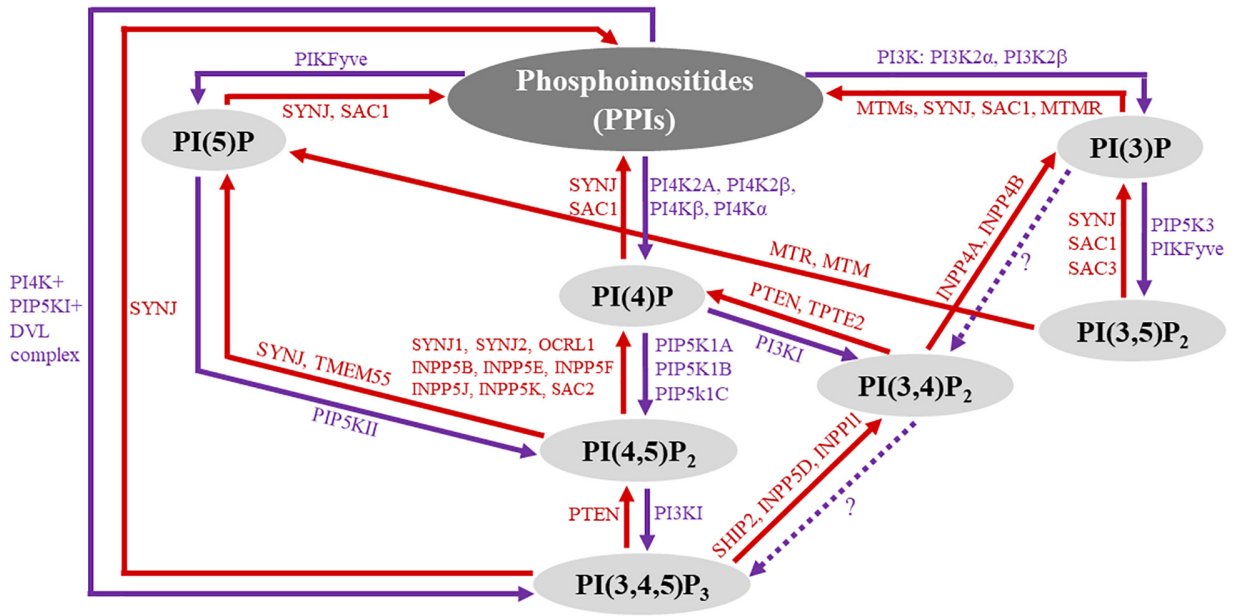

FIGURE 1 | Overview of phosphoinositide (PPI) signaling. The diagram represents an overview of PPI subspecies and their biochemical interconversion. The seven biologically active PPI subspecies are highlighted in gray circles. PPI phosphatases are labeled red, and their associated reactions are represented by red arrows, indicating the direction of the reaction. Similarly, kinase reactions are represented by purple arrows with kinase enzymes labeled purple. Question marks along the dotted arrows represent areas that have yet to be explored.

structural and regulatory molecules in the cell in which there is an associated decrease in PIP_2 binding (Nairn and Aderem, 1992; Sheetz et al., 2006). Additionally, in vascular endothelial cells (ECs), MARCKS directly modulates PIP_2-mediated insulin signaling. The treatment of vascular ECs with insulin increases the levels of PIP_2, which is also released into lipid rafts (caveolar and non-caveolar fractions) to bind to the cytoskeletal protein, N-WASP. Subsequently, N-WASP phosphorylation and interaction with actin-related proteins 2/3 (Arp2/3) cause cytoskeletal remodeling to induce cell migration (Kalwa and Michel, 2011). Furthermore, MARCKS mediates a PIP_2-dependent actin rearrangement process. In this process, when low levels of MARCKS are present, actin filaments form an actin gel. Conversely, actin filaments aggregate upon increased levels of MARCKS. In the plasma membrane, the overall PIP_2 levels are relatively constant; however, changes in PIP_2 levels can be observed locally in the membrane directly overlying actin protrusions and membrane ruffles (Sheetz et al., 2006).

Rac, a downstream small GTPase effector, is a regulator of membrane ruffles (Ridley, 1994). In addition, Rac is instrumental to the transduction of external mechanical stimuli (Labouesse, 2011; Lawson and Burridge, 2014; McGowan and McCoy, 2017), including the mechanotransduction of the FAK-Cas-Rac axis, which transmits ECM stiffness into intracellular stiffness and mechanosensitive cell cycling (Bae et al., 2014). Moreover, PIP_2 levels fluctuate in membrane ruffles in a Rac-dependent manner. Although the immediate relationship of PIP_2 and Rac has not been explored in the context of cardiovascular biology and disease specifically, acknowledging their possible connection could better aid the understanding of their effects in different cellular pathways and help implicate PIP_2 as a Rac-mediated effector in vascular pathology (Polacheck et al., 2017; Narumiya and Thumkeo, 2018).

PIP_2 Association With CapZ and Mechanical Stiffness

In striated muscle, capping protein Z (CapZ), an actin-capping protein, regulates cytoskeletal remodeling (Edwards et al., 2014). CapZ's relationship with PIP_2 (**Figure 3**) has been recently observed in relation to mechanical stiffness and cytoskeletal remodeling, and the PIP_2-mediated interaction with CapZ has been shown to regulate cardiac myocyte hypertrophy (Li et al., 2016) and actin dynamics (Li and Russell, 2013). More specifically, ECM stiffening induces cardiac myocyte hypertrophy by increased PIP_2 localization at the sarcomere Z-discs in cardiac myocytes (Li et al., 2016). The Z-disc is a critical site for mechanotransduction and the location of the β1-isoform of CapZ (CapZβ1) (Russell et al., 2010). Moreover, the localization of PIP_2 to the sarcomere Z-disc is crucial to ventricular cardiac myocyte mechanotransduction and associated with pathological hypertrophic remodeling. Dysregulation of PIP_2 signaling alters sarcomere integrity by modulating the function of CapZβ1 and actin dynamics. Taken together, PIP_2 is vital to cardiac cell physiology, where it regulates CapZβ1 and actin dynamics in response to mechanical stimuli. Additionally, mechanical stimulation causes the production of PIP_2, specifically through the RhoA/Rho-associated kinase (ROCK) pathway (Li and Russell, 2013). Solís et al. explored

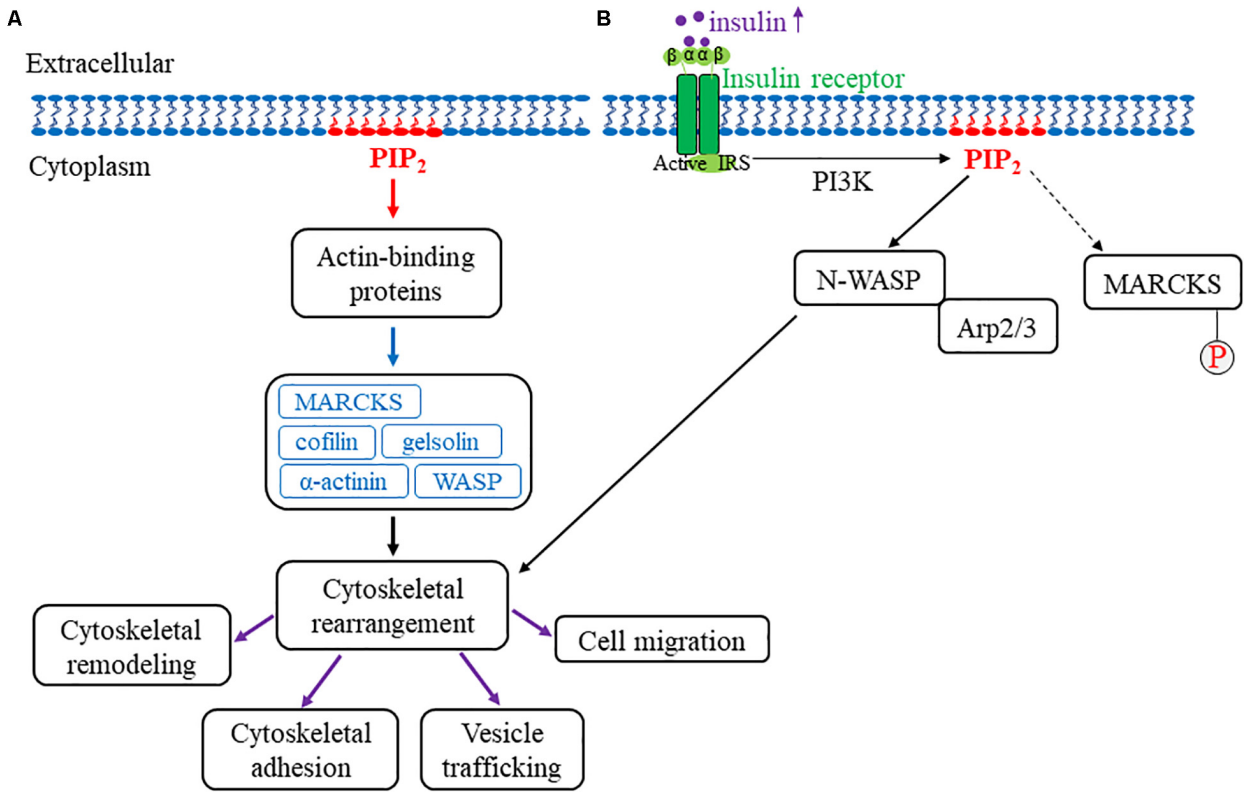

FIGURE 2 | Model for PIP_2 association with the actin cytoskeleton. **(A)** An overview of PIP_2's role in actin cytoskeletal remodeling. The red arrow represents PIP_2 intracellular association with actin-binding proteins. The blue arrow represents the various PIP_2-associated actin-binding proteins, including MARCKS, cofilin, WASP, gelsolin, and α-actinin. Upon interaction with PIP_2, these proteins collectively mediate cellular cytoskeletal rearrangement (indicated by the black arrow). More specifically, actin cytoskeletal remodeling, cytoskeletal adhesion, vesicle trafficking, and cell migration are associated with cytoskeletal rearrangements that are mediated by PIP_2 interaction with actin-binding proteins and are indicated by the purple arrows. **(B)** This figure depicts how PIP_2 regulates cytoskeletal rearrangement through N-WASP and Arp2/3 with MARCKS phosphorylation. Once the insulin receptor is activated, insulin increases intracellularly and subsequently mediates the dissociation of MARCKS from PIP_2 (as indicated by the dotted arrow) in which MARCKS is subsequently phosphorylated and activated. In addition, PIP_2 separately binds to and activates both N-WASP and Arp2/3, which drives actin cytoskeletal rearrangement. Together, these findings highlight the role of PIP_2 in mechanosensitive actin cytoskeletal rearrangement and remodeling.

PIP_2 signaling effects on CapZ through neomycin, a PIP_2 sequestering agent, in neonatal ventricular cardiomyocytes cultured on varying substrate stiffnesses. Further studies have assessed the molecular mechanisms by which different mechanotransduction signaling pathways mediate the capping and uncapping of CapZ from actin filaments via PIP_2. The results showed that interactions between PIP_2 and the β-tentacle of CapZ after molecular stimulation become considerably modified by phosphorylation. Moreover, CapZ is bound tightly to actin when inactive; however, upon phosphorylation and activation in growth states of hypertrophy, the binding is loosened. This is triggered by external stimuli, including mechanical flexing, loading, a stiffer substrate, angiotensin II, and phenylephrine. CapZ is modified by the stimuli's signaling pathways through phosphorylation, acetylation or PIP_2 binding. Thus, an actin assembly mechanism can be presented where phosphorylation, acetylation or PIP_2 anchorage causes CapZ to act as a nodal terminus for the integration of various signaling pathways (Solis and Russell, 2019). This mechanism implicates PIP_2 as a critical mediator of mechanotransduction in cardiac myocytes by directly affecting CapZ in response to mechanical stiffness.

PIP_2, PLC, and PKC Association With Store-Operated Channels TRPC1/3/6 and Orai 1

Phospholipase C (PLC) is a critical membrane-associated enzyme that, when stimulated by Gαq/11 subtype protein-coupled receptors (GαqPCRs), catalyzes the hydrolysis of PIP_2 phosphodiester bonds to generate inositol 1,4,5-triphosphate (IP_3) and diacylglycerol (DAG), which further activates PKC. These secondary messengers and downstream effector proteins are important for cardiovascular cell functions because they orchestrate the regulation of intracellular calcium mobilization, which is critical not only to the contractile apparatus but also to cell survival, proliferation, and differentiation. Plasma membrane store-operated channels (SOCs), particularly transient receptor potential canonical channels 1, 3, and 6 (TRPC1/3/6) and calcium release-activated calcium (CRAC), also called Orai 1, 2, and 3,

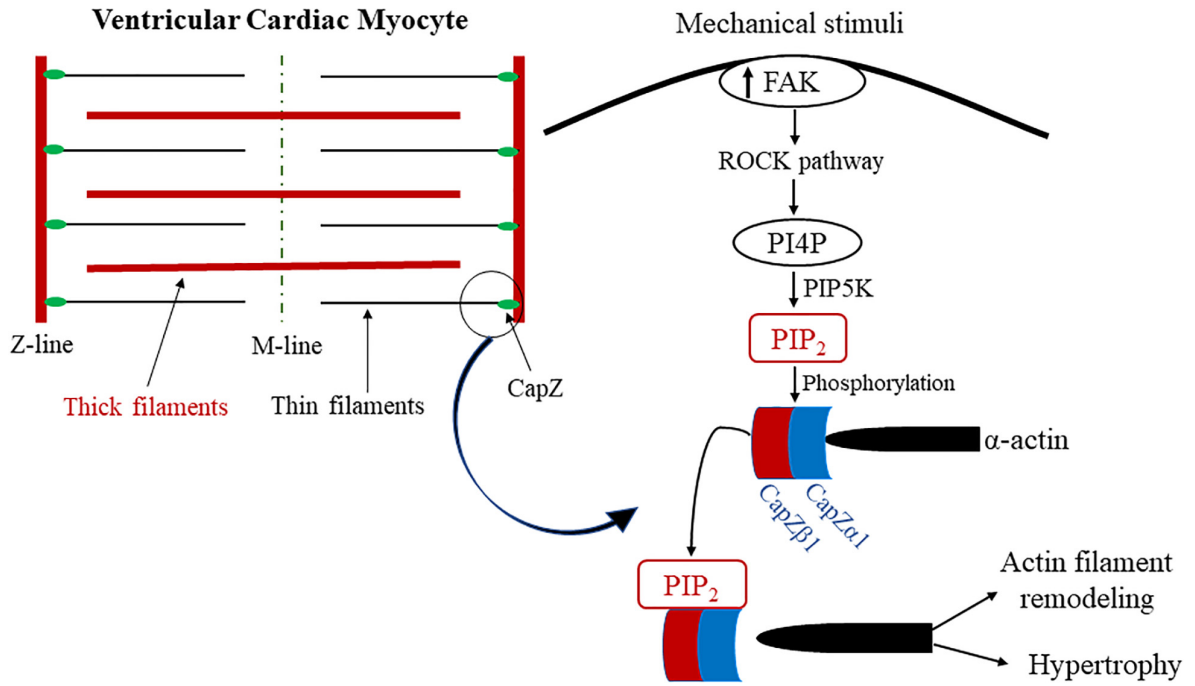

FIGURE 3 | Proposed model of PIP_2 and CapZ mechanotransduction in cardiac myocytes. Diagram of the proposed model for the mechanism of PIP_2 association with CapZ because of mechanical stimuli. Mechanical strain activates the ROCK pathway when there is an increase in mechanosensitive FAK activation, which results in PIP5K phosphorylating PI4P into PIP_2. PIP_2 phosphorylates CapZ, which mediates its uncapping from α-actin. This results in pathological actin filament remodeling and cardiac hypertrophy. PIP_2 is highlighted in and colored red. CapZα1 and CapZβ1 are colored blue to represent their association with PIP_2 as well as their intricacy with biomechanically sensitive actin filament remodeling and pathological cardiac hypertrophy.

are activated as a consequence of PLC activation (Abdullaev et al., 2008; Baudel et al., 2020; Wang et al., 2020). Vascular smooth muscle cell (VSMC) contraction, proliferation, and migration are regulated by the stimulation of SOCs at the plasma membrane and their associated Ca^{2+} influx pathways (Baudel et al., 2020). Moreover, these cellular behaviors are associated with the development of diseases of the vasculature, such as hypertension and atherosclerosis (Baudel et al., 2020). In VSMCs, PKC activity and PIP_2 are important in the activation pathway of SOCs, particularly transient receptor potential canonical channel 1 (TRPC1) (Saleh et al., 2009b; Shi et al., 2012; Baudel et al., 2020). Upon Ca^{2+} store depletion, TRPC1 is phosphorylated by PKC, which itself is stimulated by the PLC-PIP_2-DAG pathway (Saleh et al., 2009a), thus establishing a potentially direct link between TRPC1 and PIP_2. Additionally, TRPC1 is known to be an essential component of various mechanotransduction pathways, specifically in cells where TRPC1 is crucial for mechanosensitive cell migration (Formigli et al., 2009; Garrison et al., 2012; Canales et al., 2019; Li et al., 2019). Interestingly, TRPC1 is upregulated in pathological neointima remodeling in vessels induced by vascular injury, further suggesting that the induction of these channels is mechanosensitive (Kumar et al., 2006). Recent findings by Nikolaev et al. have suggested that the TRP ion channel superfamily is involved in a wide variety of mechanosensory processes, yet it has been shown that such channels are insensitive to tension induced by cell membrane stretching. Thus, although several TRP channels, including TRPC1, are essential components of mammalian stretch-activated mechanosensitive calcium-permeable cation channel heterologous systems, their true role in mechanotransduction remains unclear (Gottlieb et al., 2008). It is quite plausible that these ion channels are more likely to be activated by upstream components and consequently act as amplifiers of cellular mechanosensory signaling cascades, including PLC and PKC (Nikolaev et al., 2019). In addition to TRPC, the Orai channel, or CRAC, is another class of Ca^{2+}-selective SOC activated as a consequence of PLC activation and subsequent PIP_2 depletion (Abdullaev et al., 2008; Baudel et al., 2020; Wang et al., 2020). This channel is expressed in VSMCs and upregulated in such cells in vascular pathologies, including vascular injury and restenosis, which are known to be mechanically mediated (Wang et al., 2008; Spinelli and Trebak, 2016). Previous reports have shown that Orai interacts with TRPC channel subtypes, including TRPC3 and TRPC6 (Liao et al., 2007); however, TRPC 1 is independent of Orai function (DeHaven et al., 2009; Shi et al., 2017). Although these two proteins share great similarity in their functionality, it has yet to be explored how they may be coupled mechanically. Previous studies have assessed the mechanosensitivity of the Orai channel; however, it remains to be empirically determined (Dong et al., 2019). Furthermore, Piezo1 is a recently characterized putative mechanically activated calcium permeable cation channel that is ubiquitously expressed through the cardiovascular system (Beech and Kalli, 2019). It has been uniquely shown that Piezo1's mechanosensitivity to membrane tension is regulated by PIP_2

levels. Upon activation of TRPV1, PLC is activated and depletes the local levels of PIP_2, which subsequently inhibits Piezo1's mechanosensitive activity (Borbiro et al., 2015).

PIP_2 in Mechanotransduction of Capillary Signaling

The capillary endothelial cell (cEC) inward rectifier K^+ channel Kir2.1 is critical to sensing and translating neural activity and neurovascular coupling in brain cECs (Longden and Nelson, 2015). This process of capillary-to-arteriole signaling in cECs is regulated by PIP_2. Moreover, PIP_2 levels are required for sustained Kir2.1 activity, and such regulation of Kir2.1 channels mediates electrical signaling during neurovascular coupling (Harraz et al., 2018a). More specifically, GαqPCRs stimulate PLC to rapidly either deplete or decrease PIP_2 levels and subsequently suppresses Kir2.1 channel signaling (Harraz et al., 2018a). This depletion of PIP_2 also promotes the activation of transient receptor potential vanilloid 4 (TRPV4), a channel found in cECs that is inhibited by PIP_2 under basal conditions and because of GαqPCR activation (Harraz et al., 2018b). Furthermore, PIP_2 levels govern capillary-to-arteriole electrical signaling by modulating the activity of TRPV4 and Kir2.1, which regulate the cellular states of depolarization and hyperpolarization. Thus, the levels of PIP_2 considerably modulate the magnitude of electrical signaling across cerebral capillaries, which ultimately affects cerebral microcirculatory blood flow in cECs (Harraz et al., 2018a,b). The relationship of TRPV4 to PIP_2 is important given TRPV4's involvement in shear stress mechanotransduction in endothelial cells and mesenchymal cells and its ability to act mechanosensitively (Kohler and Hoyer, 2007; Yin and Kuebler, 2010; Corrigan et al., 2018). Therefore, the role of PIP_2 in this signaling pathway and its interaction with a known mechanotransducer, TRPV4, suggests that PIP_2 itself acts in the mechanotransduction of capillary electrical signaling.

PHOSPHATIDYLINOSITOL-4-PHOSPHATE 5-KINASE (PIP5K)

PIP5K Association in Focal Adhesion and the Cytoskeleton

Phosphatidylinositol-4-phosphate 5-kinase (PIP5K) phosphorylates the fifth position of the inositol head of phosphatidylinositol-4-phosphate. The type 1 PIP5K subfamily comprises three isoforms, Iα, Iβ, and Iγ, and is critical to many cytoskeletal processes. It has been reported that the overexpression of these isoforms induces the formation of stress fibers, membrane ruffles, and microvilli and regulates actin cytoskeletal dynamics, suggesting that this enzyme and its PIP_2 products are mechanosensitive (Chatah and Abrams, 2001). Weernink et al. reported that RhoA and its kinase, ROCK, which are both dominant effectors of mechanotransduction, are essential regulators of PIP5K in HEK-293 cells. The overexpression of ROCK enhances the PIP5K activity and subsequently elevates PIP_2 formation. Conversely, the chemical inhibition of ROCK decreases PIP5K activity and PIP_2 formation (Oude Weernink et al., 2000). Furthermore, Weernink et al. examined Type 1 PIP5K through other Rho family small GTPases, including Rac1 and Cdc42. Rho GTPases, RhoA, Rac1, and Cdc42 all mediate the PIP5K levels and lead to an increase in PIP_2 levels (Weernink et al., 2004). Therefore, PIP5K activity is RhoA-dependent in which signals from RhoA to the actin cytoskeleton are mediated, and synthesis of PIP_2 is enhanced (Oude Weernink et al., 2000).

The PIP_2 synthesis pathway in platelets through the isoform PIP5K Iα was more closely studied by Chatah and Abrams (2001) and Trepat et al. (2005). Thrombin, a known mediator of actin cytoskeleton remodeling (Chatah and Abrams, 2001; Trepat et al., 2005), promotes PIP_2 synthesis by PIP5K from PI4P in response to G protein-coupled receptor stimulation. PIP5K Iα localizes in the Golgi under basal conditions. Following stimulation of PAR1, a thrombin receptor, or overexpression of the active variant of $G\alpha_q$, PIP5K Iα relocates to the plasma membrane. This translocation of PIP5K Iα is dependent on Rac1 and RhoA. Rac1 has been suggested to affect PIP5K indirectly, and activation is required by Rho (Chatah and Abrams, 2001).

Although these studies independently identified Rho GTPases in mediating PIP5K activity, the mechanisms by which Rho GTPase is suggested to activate PIP5K are separate. Taken together, these findings indicate that members of the Rho GTPase family, RhoA, Rac, and Cdc42, are vital in mediating PIP5K activation and, consequently, PIP_2 synthesis, regardless of their interconversional crosstalk (Oude Weernink et al., 2000; Chatah and Abrams, 2001; Weernink et al., 2004). Furthermore, these GTPases act as a dynamic molecular switch between various cells, which play a key role in vascular pathology (Cai et al., 2015; Karoor et al., 2018; Barlow and Cleaver, 2019) and are involved in mechanosensing and mechanotransduction pathways (Verma et al., 2011; Chaterji et al., 2014; Zegers and Friedl, 2014; Ohashi et al., 2017). The relationship of PIP5K with small downstream GTPases in vascular pathology and mechanotransduction has not yet been explored. Due to the relevance of the small GTPases Rho, Rac, and Cdc42 for PIP5K activity and PIP_2 synthesis, this pathway may be vitally important for better understanding vascular disease and may be potentially significant in the overall study of mechanotransduction in the context of vascular pathology. Therefore, the relationship of these PIP5Ks and these downstream GTPases should be explored in relation to mechanotransduction and vascular disease.

PHOSPHOINOSITIDE 3-KINASE (PI3K) AND PHOSPHATIDYLINOSITOL-3,4,5-TRIPHOSPHATE (PIP_3)

Akt/PI3K Signaling in the Mechanotransduction of Ventricular Cardiomyocytes

Phosphoinositide 3-kinase (PI3K) is a family of evolutionarily conserved lipid kinases that mediate many cellular responses to physiological and pathophysiological stimuli. The PI3K family

is divided into three subgroups (classes I, II, and III), which together include eight isoforms. The class I isoforms, PI3Kα, PI3Kβ, PI3Kγ, and PI3Kδ, convert PIP_2 to phosphatidylinositol-3,4,5-triphosphate (PIP_3) (Vanhaesebroeck et al., 2010; Miller et al., 2019). Activated PI3K produces PIP_3, which further recruits 3-phosphoinositide-dependent kinase 1 (PDK1) to the plasma membrane (Hagiwara et al., 2012). PIP_3 activates PDK1 through its PH domain. PDK1 subsequently phosphorylates and activates Akt at threonine residue 308 (T308) (Ghigo and Li, 2015; Manning and Toker, 2017). More importantly, the phosphorylation of serine residue 473 (S473) by the mechanistic target of the mammalian target of rapamycin complex 2 (mTORC2) stabilizes not only T308 phosphorylation but also AKT in its active state (Manning and Toker, 2017). Together, Akt and PI3K create a unique signaling pathway (Akt/PI3K) that is instrumental in cardiomyocyte mechanotransduction (Li C.J. et al., 2019). Moreover, the Akt/PI3K signaling pathway regulates intracellular and extracellular activities in response to mechanical stress and molecular effectors, leading to a robust cellular mechanotransduction signaling cascade in cardiac myocytes. These cellular responses include modulation of cell metabolism, growth, proliferation, angiogenesis, and cardiac adaptation (Aoyagi and Matsui, 2011; Markowska et al., 2014; Yang et al., 2018). In a disease model, chronic activation of the Akt/PI3K pathway dysregulates cell contractility, which induces compensatory cardiac hypertrophy with preserved contractility and ultimately advances to chronic dilated cardiomyopathy (Shiojima et al., 2005; Li C.J. et al., 2019). Furthermore, alterations in the function and structure of titin, a giant sarcomeric filament protein, have been observed in similar cardiomyopathies, including cardiac remodeling, hypertrophy, and heart failure (Linke, 2008; Kruger and Linke, 2009; Lyon et al., 2015). In cardiac sarcomeres, titin isoforms exhibit varying properties of mechanical elasticity and are differentially expressed throughout cardiac development and during disease in which isoform switching is dynamically regulated by the Akt/PI3K signaling pathway (Kruger and Linke, 2009). Moreover, it is believed that these properties of titin are uniquely positioned to serve as a molecular sensor of mechanical stress in cardiac myocytes, including oscillatory changes in cell stretching known to induce PI3K activation through molecular mechanisms that remain unclear (Miller et al., 2004; Linke, 2008; Leychenko et al., 2011; Voelkel and Linke, 2011).

PIP_3, PI3Kα, and PI3Kγ Association With Mechanotransduction Through Gelsolin and Cyclic Adenosine Monophosphate (cAMP)

In cardiac myocytes, mechanotransduction critically mediates remodeling of the cytoskeleton, and dysregulation of this process can drive heart disease in response to aberrant biomechanical stress. Biomedical research on patients with hypertension has revealed how critical cardiac mechanotransduction plays in this response (Patel et al., 2013). One study by Patel et al. demonstrated that PI3Kα, a major PI3K isoform in the heart, negatively regulates gelsolin activity and suppresses pathological cytoskeletal remodeling in response to biomechanical stress-induced cardiac mechanotransduction and the resulting dilated cardiomyopathy (Guo et al., 2010). Similarly, a separate study showed that loss of PTEN in ventricular cardiac myocytes increases PI3Kα activity, which attenuates pressure overload-induced heart failure but loss of myocardial contractility (Oudit et al., 2008). Conversely, however, other studies have shown that constitutively activated PI3K drives the growth and hypertrophy of such cells, greatly increasing the heart size in mice, while knocking down PI3Kα results in mice with smaller hearts (Shioi et al., 2000). In response to mechanical stress, PI3Kα translocates to the plasma membrane to convert PIP_2 to PIP_3, which subsequently recruits gelsolin to the plasma membrane (Patel et al., 2018). A resulting spatial colocalization occurs between p110α, the catalytic subunit of PI3Kα, and gelsolin in which p110α-catalyzed PIP_3 negatively regulates gelsolin activity and thus diminishes unfavorable remodeling of the actin cytoskeleton while conserving the cytoskeletal integrity. Consequently, PI3Kα-generated PIP_3 plays a critical role in the mechanotransduction of cardiomyocytes by negatively regulating gelsolin, which subsequently inhibits actin remodeling (Patel et al., 2018).

In cardiac myocytes, GPCRs activate PI3Kγ in response to pressure overload or biomechanical stress, which mediates the adaptive role in cardiac mechanotransduction by negatively regulating cyclic adenosine monophosphate (cAMP) levels (Guo et al., 2010). It was first shown that complete deletion of PI3Kγ in cardiac myocytes alters heart function by inducing cell hypercontractility as a result of cAMP accumulation but does not alter the cell structure or growth (Crackower et al., 2002; Patrucco et al., 2004); however, a separate study has shown that deletion of PI3Kγ accelerates the development of pathological hypertrophy (Guo et al., 2010). Intriguingly, the regulation of cell contractility by PI3Kγ in response to mechanical stress is independent of its activity or functional kinase domain (Patrucco et al., 2004). More specifically, cardiac myocytes lacking PI3Kγ activity with preserved expression exhibit normal levels of cAMP that are believed to be the result of phosphodiesterase 3B positive regulation by a PI3Kγ-associated multifunctional protein complex (Patrucco et al., 2004). Critical to this complex is the anchoring of PKA to PI3Kγ and downstream activation of phosphodiesterases, type 3 and 4 (PDE3/4), and subsequently reducing the cAMP levels; upon its anchoring, PKA also phosphorylates and inhibits PI3Kγ lipid kinase activity, resulting in a reduction in PIP_3 (Perino et al., 2011; Ghigo et al., 2017). In pressure overload-mediated sympathetic overdrive of cardiac myocytes, the beta2 adrenergic receptor is desensitized and internalized as a result of PKA-escaped PI3Kγ kinase activity and ultimately induces hypokinetic dilated heart failure (Prasad et al., 2005; Perino et al., 2011; Ghigo and Li, 2015; Ghigo et al., 2017). Despite enhanced calcium dynamics and contractility upon the loss of PI3Kγ in cardiac myocytes, decompensation ensues because of dysregulated cellular-ECM interactions (Guo et al., 2010). Furthermore, a more direct relationship between PI3Kγ and cardiac mechanotransduction

TABLE 1 | Overview of phosphoinositide signaling and mechanotransduction in cardiovascular biology and pathology.

PPIs	Associated protein(s)	Cell type(s)	Known related function(s)	Proposed mediation in mechanotransduction
PIP_2	**MARCKS**	**vECs** (Kalwa and Michel, 2011)	Cytoskeletal rearrangement: - PIP_2 and MARCKS interaction observed in membrane ruffles of which Rac is a regulator. - PIP_2 levels fluctuate in membrane ruffles in a Rac-dependent manner-indicating a possible relationship between Rac and PIP_2 (Kalwa and Michel, 2011)	Rac involved in numerous mechanotransduction pathways (i.e., FAK-Cas-Rac axis) (Labouesse, 2011; Lawson and Burridge, 2014; McGowan and McCoy, 2017)
PIP_2	**CapZ**	**Ventricular CMs** (Solis and Russell, 2019)	PIP_2 acts as a mechanical sensor at sarcomere Z-disc in response to mechanical stimuli (Solis and Russell, 2019)	Sarcomere Z-disc located on CapZβ1 is a site for mechanotransduction (Russell et al., 2010)
PIP_2 and PKC	**TRPC1**	**VSMCs** (Saleh et al., 2009b; Shi et al., 2012; Baudel et al., 2020)	Functions are associated with the development of vascular diseases (Saleh et al., 2009b; Shi et al., 2012; Baudel et al., 2020)	TRPC1 is implicated in mechanotransduction (Formigli et al., 2009; Garrison et al., 2012; Canales et al., 2019; Li N. et al., 2019)
PIP_2	**Kir2.1 and TRPV4**	**Cerebral capillary ECs** (Harraz et al., 2018a,b)	PIP_2 controls the capillary-to-arteriole electrical signaling through depolarization or hyperpolarization of TRPV4 and Kir2.1 (Harraz et al., 2018a,b)	TRPV4 has been observed in shear stress-mediated mechanotransduction in ECs and mesenchymal cells (Kohler and Hoyer, 2007; Yin and Kuebler, 2010; Corrigan et al., 2018)
PI3K	**Akt**	**Ventricular CMs** (Aoyagi and Matsui, 2011; Markowska et al., 2014; Yang et al., 2018)	Akt/PI3K signaling pathway regulates cellular functions in response to mechanical stress, including cell metabolism, growth, proliferation, angiogenesis, and cardiac adaptation (Aoyagi and Matsui, 2011; Markowska et al., 2014; Yang et al., 2018)	The Akt/PI3K signaling is a known mediator of mechanotransduction in ventricular CMs (Li et al., 2019)
PI3Kα	**Gelsolin**	**Ventricular CMs** (Guo et al., 2010)	PI3Kα regulates gelsolin activity (Guo et al., 2010)	PI3Kα plays a role in biomechanical stress-induced ventricular CM mechanotransduction (Guo et al., 2010)
PI3Kγ	**cAMP**	**Ventricular CMs** (Guo et al., 2010)	In response to biomechanical stress, G protein-coupled receptors activate PI3Kγ, and thus negatively regulate cAMP (Guo et al., 2010)	PI3Kγ plays a role in ventricular CM mechanotransduction (Guo et al., 2010)
PI3K	**PTEN**	**Ventricular CMs** (Shioi et al., 2000; Luo et al., 2005)	Overexpression of PTEN reduces the levels of PI3K and influences the growth and the hypertrophy of ventricular cardiomyocytes (Shioi et al., 2000; Luo et al., 2005)	
PI3Kα	**Gelsolin and p110α**	**Ventricular CMs** (Patel et al., 2018)	PI3Kα translocates and induces the spatial colocalization between p110α and gelsolin, resulting in the attenuation of actin cytoskeleton remodeling (Patel et al., 2018)	PI3Kα-generated PIP_3 plays a critical role in the mechanotransduction through gelsolin (Patel et al., 2018)
PI3K	**Hippo pathway through YAP/TAZ**	**Epithelial cells** (Borreguero-Munoz et al., 2019)	Inhibition of the Hippo signaling pathway promotes tissue growth via PI3K-PDK1-Akt axis (Borreguero-Munoz et al., 2019)	YAP and TAZ are essential effectors of mechanotransduction and effectors of mechanical cues (Halder et al., 2012; Codelia et al., 2014; Meng et al., 2016)
PI3Kγ	**cAMP, N-cadherin and gelsolin**	**Ventricular CMs** (Guo et al., 2010)	- Reduction of N-cadherin and an increase in cAMP levels result in the loss of p110γ function, which can lead to heart failure. - Actin polymerization is promoted through gelsolin in response to biomechanical stress (Guo et al., 2010)	PI3Kγ plays a role in ventricular CM mechanotransduction (Chan et al., 2004)

(Continued)

TABLE 1 | Continued

PPIs	Associated protein(s)	Cell type(s)	Known related function(s)	Proposed mediation in mechanotransduction
PI3K	**Hippo pathway through YAP/TAZ**	**Human umbilical arterial SMCs** (Wang et al., 2018)	Mechanical cell stretching regulates YAP/TAZ activity *via* PI3K/PDK1-mediated pathway (Wang et al., 2018)	YAP and TAZ are essential effectors of mechanotransduction and effectors of mechanical cues (Halder et al., 2012; Codelia et al., 2014; Meng et al., 2016)
PI3Kβ	**RGS (Regulator of G protein signaling 5)**	**Pericytes** (Figueiredo et al., 2020)	Accurate PI3K signaling is necessary for pericyte maturation and correct vessel formation (Figueiredo et al., 2020)	Mechanotransduction induces physiological vascular remodeling (Qi et al., 2018)
PI3Kα	**Receptor tyrosine kinase**	**VSMCs** (Vantler et al., 2015)	Catalytic subunit of PI3Kα, p110α, is essential to pathological neointima formation (Vantler et al., 2015)	Mechanotransduction induces pathological vascular remodeling in atherosclerosis (Yu et al., 2018)
PI3Kγ	**Elastin-derived peptides and GPCR kinase-2**	**Leukocytes and CMs** (Fougerat et al., 2008)	- PI3Kγ is involved in Neu-1 signaling which governs atherosclerosis development (Gayral et al., 2014) - Genetic and chemical inhibition of PI3Kγ reduces atherosclerosis *in vivo* (Fougerat et al., 2008) - PI3Kγ directly interacts with GPCR kinase-2 which is observed in cardiac failure (Ghigo and Li, 2015)	Mechanotransduction induces pathological vascular remodeling in atherosclerosis (Yu et al., 2018)
PIP5K*	**RhoA and ROCK**	**HEK-293** (Weernink et al., 2004)	- RhoA, Rac1, and Cdc42 regulate cellular PIP5K levels. - PIP5K activity is RhoA-dependent in which signals from RhoA to the actin cytoskeletal mediate enhanced PIP_2 synthesis (Weernink et al., 2004)	RhoA, Rac, and Cdc42 are mediators of mechanotransduction (Verma et al., 2011; Chaterji et al., 2014; Zegers and Friedl, 2014; Ohashi et al., 2017)
PIP5K*	**Thrombin, Rac, and Rho**	**HEK 293 and Cos-7** (Chatah and Abrams, 2001; Trepat et al., 2005)	- Thrombin promotes PIP_2 synthesis and separately relocates PIP5K Iα to the plasma membrane. - Translocation of PIP5K Iα is dependent on Rac1 and RhoA; Rac1 is suggested to effect PIP5K indirectly and activation is required by RhoA (Chatah and Abrams, 2001; Trepat et al., 2005)	Rho GTPase family, RhoA, Rac, and Cdc42 are known mechanosensors (Verma et al., 2011; Chaterji et al., 2014; Zegers and Friedl, 2014; Ohashi et al., 2017)

*This table summarizes all the main phosphoinositide (PPI) subspecies, in the context of cardiovascular pathology and biology, which are assessed in our review with their main associations and the cellular target(s) of these interactions. The main function from these associations and how the PPIs are connected to mechanotransduction or as mechanosensors are further highlighted in this table. *These studies express interconversional crosstalk. Although regardless of their crosstalk these results indicate RhoA, Rac, and Cdc42 are essential in mediating PIP5K activation. vECs, Vascular endothelial cells; VSMCs, Vascular smooth muscle cells; CMs, Cardiomyocytes.*

is observed upon the loss of PI3Kγ, in which elevated cAMP levels mediate extracellular matrix remodeling and interactions (Guo et al., 2010). In this particular instance, inhibiting the beta2 adrenergic receptor protects N-cadherin adhesion complexes from degradation (Guo et al., 2010), whereas the loss of p110γ function, the catalytic subunit of PI3Kγ, leads to heart failure by the deterioration of N-cadherin and an increase in cAMP levels (Patel et al., 2018). Furthermore, N-cadherin complexes actively perceive biomechanical stress, and through the regulation of gelsolin, actin polymerization is promoted, therefore expressing a collaborative relationship between PI3Kγ and PI3Kα in cardiac mechanotransduction (Chan et al., 2004).

PI3K Mechanotransduction Association With the Hippo Pathway Through YAP/TAZ

The Hippo signaling pathway, which was originally observed in Drosophila, mediates the VSMC stretch response that inhibits cell proliferation and participates in mechanotransduction pathways (Huang et al., 2005; Ota and Sasaki, 2008; Yu et al., 2015; Chakraborty et al., 2017; Fletcher et al., 2018). Inhibition of the Hippo pathway promotes tissue growth in epithelial cells through the PI3K-PDK1-Akt axis upon mechanical stimulation and growth factor signaling (Borreguero-Munoz et al., 2019). Yes-associated protein 1 (YAP) and transcriptional coactivator with the PDZ-binding motif (TAZ) are downstream transcriptional activators of the Hippo pathway (Halder et al., 2012). These effectors are regulated by mechanical cues, specifically, matrix stiffness, stretch, and cell density, which influence cell proliferation and differentiation (Halder et al., 2012; Codelia et al., 2014; Meng et al., 2016). Thus, YAP and TAZ function as essential effectors of mechanotransduction (Meng et al., 2018). YAP/TAZ-dependent glutaminolysis and anaplerosis are mechanoactivated by vascular stiffness to drive cell proliferation in pulmonary hypertension (Bertero et al., 2016). Additionally, mechanical stretching regulates YAP/TAZ activity via the PI3K-PDK1-mediated pathway in human umbilical arterial VSMCs (Wang et al., 2018). Furthermore, the PDK1 interaction

with the Hippo complex is mediated through Sav1, where PDK1 directly controls the Hippo pathway (Wang et al., 2018). The consequential association of PI3K with the Hippo signaling pathway effectors YAP and TAZ in vascular cells further implicates PI3K in the mechanotransduction of the cardiovascular system.

PI3K Implication in Mechanotransduction of Vascular Remodeling

Mechanical forces of a hemodynamic nature are uniquely fundamental for vascular homeostasis as well as pathological vascular remodeling that are commonly observed in CVD (Cahill and Redmond, 2016; Russo et al., 2018). In cells of the vasculature, harmony in cell proliferation, apoptosis, migration, and differentiation is integral to vascular wall homeostasis. Mechanical forces perceived by ECs and VSMCs generate a biological response, i.e., mechanotransduction to induce physiological vascular remodeling (Qi et al., 2018). Consequently, vascular remodeling involves a variety of cellular components to mediate these biophysical and biochemical events, including PI3K, which has previously been connected to the vascular remodeling pathway. During angiogenesis, vessel remodeling can help with cell proliferation and maturation (Wang and Khalil, 2018). Vascular remodeling in pericytes is regulated by PI3Kβ. Mature pericytes, which are mostly found in vessels undergoing remodeling, are quiescent and express low activation of the PI3K signaling. Inactivation of PI3Kβ in these cells generates early pericyte maturation, with an increase in PI3K signaling that obstructs pericyte maturation. Thus, pericytes in a sustained immature state will result in vascular hyperplasia and block vascular remodeling, whereas accurate PI3K signaling is necessary for pericyte maturation and correct vessel formation (Figueiredo et al., 2020).

One of the most prevalent cardiovascular diseases involving vascular remodeling is atherosclerosis. During atherosclerosis, vascular injury occurs, causing abnormal proliferation of VSMCs, which leads to neointima formation and vessel lumen narrowing and ultimately limits blood flow and oxygen supply (Yu et al., 2018). PI3K has been directly associated with the molecular pathways that mediate vascular remodeling and atherosclerosis. The catalytic subunit of PI3Kα, p110α, is important for receptor tyrosine kinase (RTK) signaling, which is upstream of class 1A PI3K isoforms, in VSMCs. Furthermore, p110α is critical to neointima formation after balloon angioplasty by mediating VSMC proliferation and migration, while the PI3Kα isoforms p100β and p110δ do not play a significant role (Vantler et al., 2015).

PI3Kγ functions in both leukocytes and cardiomyocytes and plays a role in atherosclerosis and heart disease. PI3Kγ controls leukocyte infiltration in the myocardium and arteries. PI3Kγ is involved in neuraminidase-1 (Neu-1) signaling, which governs atherosclerosis development (Gayral et al., 2014). Genetic and pharmacological inhibitory targeting of PI3Kγ in leukocytes reduces atherosclerosis in mouse models (Fougerat et al., 2008). Ghigo et al. (2017) recently reviewed PI3K and calcium signaling in cardiovascular disease. The PI3K pathway has recently been interconnected with Ca^{2+} signaling. PI3Kγ appears to be preferentially linked to Ca^{2+} signaling in smooth muscle cells (Lupieri et al., 2020), where Class I PI3Ks are highly expressed. This interconnection between the PI3Kγ pathway and Ca^{2+} signaling has been involved in smooth muscle cell proliferation and migration, atherosclerosis and arterial injury. The development of arterial lesions through various immune functions requires PI3Kγ activity with PI3Kγ playing an important role in arterial injury in T cells. For example, it has been found that PI3Kγ regulates T-cell function, and it has been proposed that PI3Kγ interacts with Ca^{2+} signaling, leading to Ca^{2+} influx downstream of T-cell receptor activation; thus, PI3Kγ interconnects with Ca^{2+}, playing an important role in arterial injury (Smirnova et al., 2014; Lupieri et al., 2015; Ghigo et al., 2017). Taken together, PI3Kβ and PI3Kγ are paramount pathways that drive cardiovascular remodeling seen in heart failure as well as in atherosclerosis, and this strongly suggests that PI3K is critically involved in mechanotransduction-mediated cardiovascular disease.

CONCLUSION

This review summarizes the relationship between PPIs and mechanotransduction in regard to cardiovascular biology and disease (**Table 1**). PPIs are central mediators in multiple biological processes, although understanding the specific contribution of PPIs to cellular dynamics can be difficult, especially regarding mechanotransduction in cardiovascular disease. PIP_2, PIP_3, PI3K, and PIP5K all play important roles in different mechanotransduction pathways of the cardiovascular system. These PPI functions include cytoskeletal arrangements, association with actin-binding proteins and ion channels, and response to mechanical stimuli. Indeed, PPIs are critical modulators of mechanotransduction. Complete knowledge of these pathways is not yet fully known and should be further explored to address how these pathways influence cellular mechanotransduction in cardiovascular cells in both homeostasis and disease.

AUTHOR CONTRIBUTIONS

AK, JB, and YB conceptualized the review. AK, JB, KV, TD, and YB wrote the original draft. AK and JB prepared the figures and table. AK, JB, KV, TD, JR-M, and YB critically reviewed and edited the final manuscript version. All authors contributed to the article and approved the submitted version.

FUNDING

This work was supported by the American Heart Association Career Development Award (18CDA34080415) to YB.

REFERENCES

Abdullaev, I. F., Bisaillon, J. M., Potier, M., Gonzalez, J. C., Motiani, R. K., and Trebak, M. (2008). Stim1 and Orai1 mediate CRAC currents and store-operated calcium entry important for endothelial cell proliferation. *Circ. Res.* 103, 1289–1299.doi: 10.1161/01.RES.0000338496.95579.56

Allahverdian, S., Chaabane, C., Boukais, K., Francis, G. A., and Bochaton-Piallat, M. L. (2018). Smooth muscle cell fate and plasticity in atherosclerosis. *Cardiovasc. Res.* 114, 540–550.doi: 10.1093/cvr/cvy022

Aoyagi, T., and Matsui, T. (2011). Phosphoinositide-3 kinase signaling in cardiac hypertrophy and heart failure. *Curr. Pharm. Des.* 17, 1818–1824.doi: 10.2174/138161211796390976

Bae, Y. H., Mui, K. L., Hsu, B. Y., Liu, S. L., Cretu, A., Razinia, Z., et al. (2014). A FAK-Cas-Rac-lamellipodin signaling module transduces extracellular matrix stiffness into mechanosensitive cell cycling. *Sci. Signal.* 7:ra57.doi: 10.1126/scisignal.2004838

Barlow, H. R., and Cleaver, O. (2019). Building Blood Vessels-One Rho GTPase at a Time. *Cells* 8:545.doi: 10.3390/cells8060545

Baudel, M., Shi, J., Large, W. A., and Albert, A. P. (2020). Insights into activation mechanisms of store-operated TRPC1 channels in vascular smooth muscle. *Cells* 9:179.doi: 10.3390/cells9010179

Beech, D. J., and Kalli, A. C. (2019). Force sensing by Piezo channels in cardiovascular health and disease. *Arterioscler. Thromb. Vasc. Biol.* 39, 2228–2239.doi: 10.1161/ATVBAHA.119.313348

Bertero, T., Oldham, W. M., Cottrill, K. A., Pisano, S., Vanderpool, R. R., Yu, Q., et al. (2016). Vascular stiffness mechanoactivates YAP/TAZ-dependent glutaminolysis to drive pulmonary hypertension. *J. Clin. Invest.* 126, 3313–3335.doi: 10.1172/JCI86387

Bilanges, B., Posor, Y., and Vanhaesebroeck, B. (2019). PI3K isoforms in cell signalling and vesicle trafficking. *Nat. Rev. Mol. Cell Biol.* 20, 515–534.doi: 10.1038/s41580-019-0129-z

Borbiro, I., Badheka, D., and Rohacs, T. (2015). Activation of TRPV1 channels inhibits mechanosensitive Piezo channel activity by depleting membrane phosphoinositides. *Sci. Signal.* 8:ra15.doi: 10.1126/scisignal.2005667

Borreguero-Munoz, N., Fletcher, G. C., Aguilar-Aragon, M., Elbediwy, A., Vincent-Mistiaen, Z. I., and Thompson, B. J. (2019). The Hippo pathway integrates PI3K-Akt signals with mechanical and polarity cues to control tissue growth. *PLoS Biol.* 17:e3000509.doi: 10.1371/journal.pbio.3000509

Cahill, P. A., and Redmond, E. M. (2016). Vascular endothelium - Gatekeeper of vessel health. *Atherosclerosis* 248, 97–109. doi: 10.1016/j.atherosclerosis.2016.03.007

Cai, A., Zhou, Y., and Li, L. (2015). Rho-GTPase and atherosclerosis: pleiotropic effects of statins. *J. Am. Heart Assoc.* 4:e002113. doi: 10.1161/JAHA.115.002113

Canales, J., Morales, D., Blanco, C., Rivas, J., Diaz, N., Angelopoulos, I., et al. (2019). A TR(i)P to cell migration: new roles of TRP channels in mechanotransduction and cancer. *Front. Physiol.* 10:757. doi: 10.3389/fphys.2019.00757

Chakraborty, S., Njah, K., Pobbati, A. V., Lim, Y. B., Raju, A., Lakshmanan, M., et al. (2017). Agrin as a mechanotransduction signal regulating YAP through the hippo pathway. *Cell Rep.* 18, 2464–2479.doi: 10.1016/j.celrep.2017.02.041

Chan, M. W., El Sayegh, T. Y., Arora, P. D., Laschinger, C. A., Overall, C. M., Morrison, C., et al. (2004). Regulation of intercellular adhesion strength in fibroblasts. *J. Biol. Chem.* 279, 41047–41057.doi: 10.1074/jbc.M406631200

Chatah, N. E., and Abrams, C. S. (2001). G-protein-coupled receptor activation induces the membrane translocation and activation of phosphatidylinositol-4-phosphate 5-kinase I alpha by a Rac- and Rho-dependent pathway. *J. Biol. Chem.* 276, 34059–34065.doi: 10.1074/jbc.M104917200

Chaterji, S., Kim, P., Choe, S. H., Tsui, J. H., Lam, C. H., Ho, D. S., et al. (2014). Synergistic effects of matrix nanotopography and stiffness on vascular smooth muscle cell function. *Tissue Eng. Part A* 20, 2115–2126.doi: 10.1089/ten.tea.2013.0455

Codelia, V. A., Sun, G., and Irvine, K. D. (2014). Regulation of YAP by mechanical strain through Jnk and Hippo signaling. *Curr. Biol.* 24, 2012–2017.doi: 10.1016/j.cub.2014.07.034

Corrigan, M. A., Johnson, G. P., Stavenschi, E., Riffault, M., Labour, M. N., and Hoey, D. A. (2018). TRPV4-mediates oscillatory fluid shear mechanotransduction in mesenchymal stem cells in part via the primary cilium. *Sci. Rep.* 8:3824. doi: 10.1038/s41598-018-22174-3

Crackower, M. A., Oudit, G. Y., Kozieradzki, I., Sarao, R., Sun, H., Sasaki, T., et al. (2002). Regulation of myocardial contractility and cell size by distinct PI3K-PTEN signaling pathways. *Cell* 110, 737–749.doi: 10.1016/s0092-8674(02)00969-8

De Craene, J. O., Bertazzi, D. L., Bar, S., and Friant, S. (2017). Phosphoinositides, major actors in membrane trafficking and lipid signaling pathways. *Int. J. Mol. Sci.* 18:634.doi: 10.3390/ijms18030634

DeHaven, W. I., Jones, B. F., Petranka, J. G., Smyth, J. T., Tomita, T., Bird, G. S., et al. (2009). TRPC channels function independently of STIM1 and Orai1. *J. Physiol.* 587(Pt 10), 2275–2298.doi: 10.1113/jphysiol.2009.170431

Di Paolo, G., and De Camilli, P. (2006). Phosphoinositides in cell regulation and membrane dynamics. *Nature* 443, 651–657.doi: 10.1038/nature05185

Di Paolo, G., Moskowitz, H. S., Gipson, K., Wenk, M. R., Voronov, S., Obayashi, M., et al. (2004). Impaired PtdIns(4,5)P2 synthesis in nerve terminals produces defects in synaptic vesicle trafficking. *Nature* 431, 415–422.doi: 10.1038/nature02896

Dickson, E. J., and Hille, B. (2019). Understanding phosphoinositides: rare, dynamic, and essential membrane phospholipids. *Biochem. J.* 476, 1–23.doi: 10.1042/BCJ20180022

Dong, H., Zhang, Y., Song, R., Xu, J., Yuan, Y., Liu, J., et al. (2019). Toward a model for activation of Orai channel. *iScience* 16, 356–367. doi: 10.1016/j.isci.2019.05.041

Edwards, M., Zwolak, A., Schafer, D. A., Sept, D., Dominguez, R., and Cooper, J. A. (2014). Capping protein regulators fine-tune actin assembly dynamics. *Nat. Rev. Mol. Cell Biol.* 15, 677–689.doi: 10.1038/nrm3869

Falkenburger, B. H., Jensen, J. B., Dickson, E. J., Suh, B. C., and Hille, B. (2010). Phosphoinositides: lipid regulators of membrane proteins. *J. Physiol.* 588(Pt 17), 3179–3185.doi: 10.1113/jphysiol.2010.192153

Figueiredo, A. M., Villacampa, P., Dieguez-Hurtado, R., Lozano, J. J., Kobialka, P., Cortazar, A. R., et al. (2020). PI3Kbeta-regulated pericyte maturation governs vascular remodeling. *Circulation* 142, 688–704.doi: 10.1161/CIRCULATIONAHA.119.042354

Fletcher, G. C., Diaz-de-la-Loza, M. D., Borreguero-Munoz, N., Holder, M., Aguilar-Aragon, M., and Thompson, B. J. (2018). Mechanical strain regulates the Hippo pathway in *Drosophila*. *Development* 145:dev159467.doi: 10.1242/dev.159467

Formigli, L., Sassoli, C., Squecco, R., Bini, F., Martinesi, M., Chellini, F., et al. (2009). Regulation of transient receptor potential canonical channel 1 (TRPC1) by sphingosine 1-phosphate in C2C12 myoblasts and its relevance for a role of mechanotransduction in skeletal muscle differentiation. *J. Cell Sci.* 122(Pt 9), 1322–1333.doi: 10.1242/jcs.035402

Fougerat, A., Gayral, S., Gourdy, P., Schambourg, A., Ruckle, T., Schwarz, M. K., et al. (2008). Genetic and pharmacological targeting of phosphoinositide 3-kinase-gamma reduces atherosclerosis and favors plaque stability by modulating inflammatory processes. *Circulation* 117, 1310–1317.doi: 10.1161/circulationaha.107.720466

Garoffolo, G., and Pesce, M. (2019). Mechanotransduction in the cardiovascular system: from developmental origins to homeostasis and pathology. *Cells* 8:1607.doi: 10.3390/cells8121607

Garrison, S. R., Dietrich, A., and Stucky, C. L. (2012). TRPC1 contributes to light-touch sensation and mechanical responses in low-threshold cutaneous sensory neurons. *J. Neurophysiol.* 107, 913–922.doi: 10.1152/jn.00658.2011

Gayral, S., Garnotel, R., Castaing-Berthou, A., Blaise, S., Fougerat, A., Berge, E., et al. (2014). Elastin-derived peptides potentiate atherosclerosis through the immune Neu1-PI3Kgamma pathway. *Cardiovasc. Res.* 102, 118–127.doi: 10.1093/cvr/cvt336

Ghigo, A., Laffargue, M., Li, M., and Hirsch, E. (2017). PI3K and calcium signaling in cardiovascular disease. *Circ. Res.* 121, 282–292.doi: 10.1161/CIRCRESAHA.117.310183

Ghigo, A., and Li, M. (2015). Phosphoinositide 3-kinase: friend and foe in cardiovascular disease. *Front. Pharmacol.* 6:169. doi: 10.3389/fphar.2015.00169

Gimbrone, M. A. Jr., and Garcia-Cardena, G. (2013). Vascular endothelium, hemodynamics, and the pathobiology of atherosclerosis. *Cardiovasc. Pathol.* 22, 9–15.doi: 10.1016/j.carpath.2012.06.006

Gottlieb, P., Folgering, J., Maroto, R., Raso, A., Wood, T. G., Kurosky, A., et al. (2008). Revisiting TRPC1 and TRPC6 mechanosensitivity. *Pflugers Arch.* 455, 1097–1103.doi: 10.1007/s00424-007-0359-3

Guo, D., Kassiri, Z., Basu, R., Chow, F. L., Kandalam, V., Damilano, F., et al. (2010). Loss of PI3Kgamma enhances cAMP-dependent MMP remodeling of the myocardial N-cadherin adhesion complexes and extracellular matrix in response to early biomechanical stress. *Circ. Res.* 107, 1275–1289.doi: 10.1161/CIRCRESAHA.110.229054

Hagiwara, A., Cornu, M., Cybulski, N., Polak, P., Betz, C., Trapani, F., et al. (2012). Hepatic mTORC2 activates glycolysis and lipogenesis through Akt, glucokinase, and SREBP1c. *Cell Metab.* 15, 725–738.doi: 10.1016/j.cmet.2012.03.015

Halder, G., Dupont, S., and Piccolo, S. (2012). Transduction of mechanical and cytoskeletal cues by YAP and TAZ. *Nat. Rev. Mol. Cell Biol.* 13, 591–600.doi: 10.1038/nrm3416

Hammond, G. R., and Hong, Y. (2018). Phosphoinositides and membrane targeting in cell polarity. *Cold Spring Harb. Perspect. Biol.* 10:a027938.doi: 10.1101/cshperspect.a027938

Hao, X. J., Xu, C. Z., Wang, J. T., Li, X. J., Wang, M. M., Gu, Y. H., et al. (2018). miR-21 promotes proliferation and inhibits apoptosis of hepatic stellate cells through targeting PTEN/PI3K/AKT pathway. *J. Recept. Signal. Transduct. Res.* 38, 455–461.doi: 10.1080/10799893.2019.1585452

Harraz, O. F., Longden, T. A., Dabertrand, F., Hill-Eubanks, D., and Nelson, M. T. (2018a). Endothelial GqPCR activity controls capillary electrical signaling and brain blood flow through PIP2 depletion. *Proc. Natl. Acad. Sci. U.S.A.* 115, E3569–E3577. doi: 10.1073/pnas.1800201115

Harraz, O. F., Longden, T. A., Hill-Eubanks, D., and Nelson, M. T. (2018b). PIP2 depletion promotes TRPV4 channel activity in mouse brain capillary endothelial cells. *eLife* 7:e38689. doi: 10.7554/eLife.38689

Hirsch, E., Gulluni, F., and Martini, M. (2020). Phosphoinositides in cell proliferation and metabolism. *Adv. Biol. Regul.* 75:100693.doi: 10.1016/j.jbior.2020.100693

Huang, J., Wu, S., Barrera, J., Matthews, K., and Pan, D. (2005). The Hippo signaling pathway coordinately regulates cell proliferation and apoptosis by inactivating Yorkie, the *Drosophila* Homolog of YAP. *Cell* 122, 421–434.doi: 10.1016/j.cell.2005.06.007

Huang, S., Lifshitz, L., Patki-Kamath, V., Tuft, R., Fogarty, K., and Czech, M. P. (2004). Phosphatidylinositol-4,5-bisphosphate-rich plasma membrane patches organize active zones of endocytosis and ruffling in cultured adipocytes. *Mol. Cell. Biol.* 24, 9102–9123.doi: 10.1128/MCB.24.20.9102-9123.2004

Janmey, P. A., Bucki, R., and Radhakrishnan, R. (2018). Regulation of actin assembly by PI(4,5)P2 and other inositol phospholipids: an update on possible mechanisms. *Biochem. Biophys. Res. Commun.* 506, 307–314.doi: 10.1016/j.bbrc.2018.07.155

Kalwa, H., and Michel, T. (2011). The MARCKS protein plays a critical role in phosphatidylinositol 4,5-bisphosphate metabolism and directed cell movement in vascular endothelial cells. *J. Biol. Chem.* 286, 2320–2330.doi: 10.1074/jbc.M110.196022

Karoor, V., Fini, M. A., Loomis, Z., Sullivan, T., Hersh, L. B., Gerasimovskaya, E., et al. (2018). Sustained activation of Rho GTPases promotes a synthetic pulmonary artery smooth muscle cell phenotype in neprilysin null mice. *Arterioscler. Thromb. Vasc. Biol.* 38, 154–163.doi: 10.1161/ATVBAHA.117.310207

Kohler, R., and Hoyer, J. (2007). "Role of TRPV4 in the mechanotransduction of shear stress in endothelial cells," in *TRP Ion Channel Function in Sensory Transduction and Cellular Signaling Cascades*, eds W. B. Liedtke and S. Heller (Boca Raton, FL: CRC Press).

Kruger, M., and Linke, W. A. (2009). Titin-based mechanical signalling in normal and failing myocardium. *J. Mol. Cell. Cardiol.* 46, 490–498.doi: 10.1016/j.yjmcc.2009.01.004

Kumar, B., Dreja, K., Shah, S. S., Cheong, A., Xu, S. Z., Sukumar, P., et al. (2006). Upregulated TRPC1 channel in vascular injury in vivo and its role in human neointimal hyperplasia. *Circ. Res.* 98, 557–563.doi: 10.1161/01.RES.0000204724.29685.db

Labouesse, M. (2011). Rac GTPase signaling in mechanotransduction during embryonic morphogenesis. *Small GTPases* 2, 305–309.doi: 10.4161/sgtp.18035

Lawson, C. D., and Burridge, K. (2014). The on-off relationship of Rho and Rac during integrin-mediated adhesion and cell migration. *Small GTPases* 5:e27958.doi: 10.4161/sgtp.27958

Leychenko, A., Konorev, E., Jijiwa, M., and Matter, M. L. (2011). Stretch-induced hypertrophy activates NFkB-mediated VEGF secretion in adult cardiomyocytes. *PLoS One* 6:e29055.doi: 10.1371/journal.pone.0029055

Li, C. J., Chen, C. S., Yiang, G. T., Tsai, A. P., Liao, W. T., and Wu, M. Y. (2019). Advanced evolution of pathogenesis concepts in cardiomyopathies. *J. Clin. Med.* 8:520. doi: 10.3390/jcm8040520

Li, H., Mao, Y., Bouaziz, M., Yu, H., Qu, X., Wang, F., et al. (2019). Lens differentiation is controlled by the balance between PDGF and FGF signaling. *PLoS Biol.* 17:e3000133.doi: 10.1371/journal.pbio.3000133

Li, J., Mkrtschjan, M. A., Lin, Y. H., and Russell, B. (2016). Variation in stiffness regulates cardiac myocyte hypertrophy via signaling pathways. *Can. J. Physiol. Pharmacol.* 94, 1178–1186.doi: 10.1139/cjpp-2015-0578

Li, J., and Russell, B. (2013). Phosphatidylinositol 4,5-bisphosphate regulates CapZbeta1 and actin dynamics in response to mechanical strain. *Am. J. Physiol. Heart Circ. Physiol.* 305, H1614–H1623. doi: 10.1152/ajpheart.00477.2013

Li, N., He, Y., Yang, G., Yu, Q., and Li, M. (2019). Role of TRPC1 channels in pressure-mediated activation of airway remodeling. *Respir. Res.* 20:91. doi: 10.1186/s12931-019-1050-x

Li, N., He, Y., Yang, G., Yu, Q., and Li, M. (2019). Role of TRPC1 channels in pressure-mediated activation of airway remodeling. *Respir. Res.* 20:91. doi: 10.1186/s12931-019-1050-x

Liao, Y., Erxleben, C., Yildirim, E., Abramowitz, J., Armstrong, D. L., and Birnbaumer, L. (2007). Orai proteins interact with TRPC channels and confer responsiveness to store depletion. *Proc. Natl. Acad. Sci. U.S.A.* 104, 4682–4687.doi: 10.1073/pnas.0611692104

Linke, W. A. (2008). Sense and stretchability: the role of titin and titin-associated proteins in myocardial stress-sensing and mechanical dysfunction. *Cardiovasc. Res.* 77, 637–648. doi: 10.1016/j.cardiores.2007.03.029

Longden, T. A., and Nelson, M. T. (2015). Vascular inward rectifier K+ channels as external K+ sensors in the control of cerebral blood flow. *Microcirculation* 22, 183–196.doi: 10.1111/micc.12190

Luo, J., McMullen, J. R., Sobkiw, C. L., Zhang, L., Dorfman, A. L., Sherwood, M. C., et al. (2005). Class IA phosphoinositide 3-kinase regulates heart size and physiological cardiac hypertrophy. *Mol. Cell. Biol.* 25, 9491–9502.doi: 10.1128/MCB.25.21.9491-9502.2005

Lupieri, A., Smirnova, N., Malet, N., Gayral, S., and Laffargue, M. (2015). PI3K signaling in arterial diseases: non redundant functions of the PI3K isoforms. *Adv. Biol. Regul.* 59, 4–18.doi: 10.1016/j.jbior.2015.06.002

Lupieri, A., Smirnova, N. F., Solinhac, R., Malet, N., Benamar, M., Saoudi, A., et al. (2020). Smooth muscle cells-derived CXCL10 prevents endothelial healing through PI3Kgamma-dependent T cells response. *Cardiovasc. Res.* 116, 438–449. doi: 10.1093/cvr/cvz122

Lyon, R. C., Zanella, F., Omens, J. H., and Sheikh, F. (2015). Mechanotransduction in cardiac hypertrophy and failure. *Circ. Res.* 116, 1462–1476.doi: 10.1161/CIRCRESAHA.116.304937

Manna, P., and Jain, S. K. (2015). Phosphatidylinositol-3,4,5-triphosphate and cellular signaling: implications for obesity and diabetes. *Cell. Physiol. Biochem.* 35, 1253–1275.doi: 10.1159/000373949

Manning, B. D., and Toker, A. (2017). AKT/PKB signaling: navigating the network. *Cell* 169, 381–405.doi: 10.1016/j.cell.2017.04.001

Markowska, A., Pawalowska, M., Lubin, J., and Markowska, J. (2014). Signalling pathways in endometrial cancer. *Contemp. Oncol.* 18, 143–148.doi: 10.5114/wo.2014.43154

Martino, F., Perestrelo, A. R., Vinarsky, V., Pagliari, S., and Forte, G. (2018). Cellular mechanotransduction: from tension to function. *Front. Physiol.* 9:824. doi: 10.3389/fphys.2018.00824

Maurer, M., and Lammerding, J. (2019). The driving force: nuclear mechanotransduction in cellular function, fate, and disease. *Annu. Rev. Biomed. Eng.* 21, 443–468.doi: 10.1146/annurev-bioeng-060418-052139

McGowan, S. E., and McCoy, D. M. (2017). Platelet-derived growth factor receptor-alpha and Ras-related C3 botulinum toxin substrate-1 regulate mechano-responsiveness of lung fibroblasts. *Am. J. Physiol. Lung Cell. Mol. Physiol.* 313, L1174–L1187. doi: 10.1152/ajplung.00185.2017

Meng, Z., Moroishi, T., and Guan, K. L. (2016). Mechanisms of Hippo pathway regulation. *Genes Dev.* 30, 1–17.doi: 10.1101/gad.274027.115

Meng, Z., Qiu, Y., Lin, K. C., Kumar, A., Placone, J. K., Fang, C., et al. (2018). RAP2 mediates mechanoresponses of the Hippo pathway. *Nature* 560, 655–660.doi: 10.1038/s41586-018-0444-0

Miller, M. K., Granzier, H., Ehler, E., and Gregorio, C. C. (2004). The sensitive giant: the role of titin-based stretch sensing complexes in the heart. *Trends Cell Biol.* 14, 119–126.doi: 10.1016/j.tcb.2004.01.003

Miller, M. S., Thompson, P. E., and Gabelli, S. B. (2019). Structural determinants of isoform selectivity in PI3K inhibitors. *Biomolecules* 9:82.doi: 10.3390/biom9030082

Nairn, A. C., and Aderem, A. (1992). Calmodulin and protein kinase C cross-talk: the MARCKS protein is an actin filament and plasma membrane cross-linking protein regulated by protein kinase C phosphorylation and by calmodulin. *Ciba Found. Symp.* 164, 145–154.doi: 10.1002/9780470514207.ch10

Narumiya, S., and Thumkeo, D. (2018). Rho signaling research: history, current status and future directions. *FEBS Lett.* 592, 1763–1776.doi: 10.1002/1873-3468.13087

Nikolaev, Y. A., Cox, C. D., Ridone, P., Rohde, P. R., Cordero-Morales, J. F., Vasquez, V., et al. (2019). Mammalian TRP ion channels are insensitive to membrane stretch. *J. Cell Sci.* 132:jcs238360.doi: 10.1242/jcs.238360

Ochoa, C. D., Wu, R. F., and Terada, L. S. (2018). ROS signaling and ER stress in cardiovascular disease. *Mol. Aspects Med.* 63, 18–29.doi: 10.1016/j.mam.2018.03.002

Ohashi, K., Fujiwara, S., and Mizuno, K. (2017). Roles of the cytoskeleton, cell adhesion and rho signalling in mechanosensing and mechanotransduction. *J. Biochem.* 161, 245–254. doi: 10.1093/jb/mvw082

Ota, M., and Sasaki, H. (2008). Mammalian Tead proteins regulate cell proliferation and contact inhibition as transcriptional mediators of Hippo signaling. *Development* 135, 4059–4069.doi: 10.1242/dev.027151

Oude Weernink, P. A., Schulte, P., Guo, Y., Wetzel, J., Amano, M., Kaibuchi, K., et al. (2000). Stimulation of phosphatidylinositol-4-phosphate 5-kinase by Rho-kinase. *J. Biol. Chem.* 275, 10168–10174. doi: 10.1074/jbc.275.14.10168

Oudit, G. Y., Kassiri, Z., Zhou, J., Liu, Q. C., Liu, P. P., Backx, P. H., et al. (2008). Loss of PTEN attenuates the development of pathological hypertrophy and heart failure in response to biomechanical stress. *Cardiovasc. Res.* 78, 505–514.doi: 10.1093/cvr/cvn041

Patel, V. B., Wang, Z., Fan, D., Zhabyeyev, P., Basu, R., Das, S. K., et al. (2013). Loss of p47phox subunit enhances susceptibility to biomechanical stress and heart failure because of dysregulation of cortactin and actin filaments. *Circ. Res.* 112, 1542–1556.doi: 10.1161/CIRCRESAHA.111.300299

Patel, V. B., Zhabyeyev, P., Chen, X., Wang, F., Paul, M., Fan, D., et al. (2018). PI3Kalpha-regulated gelsolin activity is a critical determinant of cardiac cytoskeletal remodeling and heart disease. *Nat. Commun.* 9:5390. doi: 10.1038/s41467-018-07812-8

Patrucco, E., Notte, A., Barberis, L., Selvetella, G., Maffei, A., Brancaccio, M., et al. (2004). PI3Kgamma modulates the cardiac response to chronic pressure overload by distinct kinase-dependent and -independent effects. *Cell* 118, 375–387.doi: 10.1016/j.cell.2004.07.017

Perino, A., Ghigo, A., Ferrero, E., Morello, F., Santulli, G., Baillie, G. S., et al. (2011). Integrating cardiac PIP3 and cAMP signaling through a PKA anchoring function of p110gamma. *Mol. Cell* 42, 84–95. doi: 10.1016/j.molcel.2011.01.030

Phan, T. K., Williams, S. A., Bindra, G. K., Lay, F. T., Poon, I. K. H., and Hulett, M. D. (2019). Phosphoinositides: multipurpose cellular lipids with emerging roles in cell death. *Cell Death Differ.* 26, 781–793.doi: 10.1038/s41418-018-0269-2

Polacheck, W. J., Kutys, M. L., Yang, J., Eyckmans, J., Wu, Y., Vasavada, H., et al. (2017). A non-canonical Notch complex regulates adherens junctions and vascular barrier function. *Nature* 552, 258–262.doi: 10.1038/nature24998

Prasad, S. V., Jayatilleke, A., Madamanchi, A., and Rockman, H. A. (2005). Protein kinase activity of phosphoinositide 3-kinase regulates β-adrenergic receptor endocytosis. *Nat. Cell Biol.* 7, 785–796.doi: 10.1038/ncb1278

Prestwich, G. D. (2004). Phosphoinositide signaling; from affinity probes to pharmaceutical targets. *Chem. Biol.* 11, 619–637. doi: 10.1016/j.chembiol.2004.03.025

Qi, Y. X., Han, Y., and Jiang, Z. L. (2018). Mechanobiology and vascular remodeling: from membrane to nucleus. *Adv. Exp. Med. Biol.* 1097, 69–82.doi: 10.1007/978-3-319-96445-4_4

Ramos, A. R., Elong Edimo, W., and Erneux, C. (2018). Phosphoinositide 5-phosphatase activities control cell motility in glioblastoma: two phosphoinositides PI(4,5)P2 and PI(3,4)P2 are involved. *Adv. Biol. Regul.* 67, 40–48.doi: 10.1016/j.jbior.2017.09.001

Ridley, A. J. (1994). Membrane ruffling and signal transduction. *Bioessays* 16, 321–327.doi: 10.1002/bies.950160506

Russell, B., Curtis, M. W., Koshman, Y. E., and Samarel, A. M. (2010). Mechanical stress-induced sarcomere assembly for cardiac muscle growth in length and width. *J. Mol. Cell. Cardiol.* 48, 817–823.doi: 10.1016/j.yjmcc.2010.02.016

Russo, T. A., Stoll, D., Nader, H. B., and Dreyfuss, J. L. (2018). Mechanical stretch implications for vascular endothelial cells: altered extracellular matrix synthesis and remodeling in pathological conditions. *Life Sci.* 213, 214–225.doi: 10.1016/j.lfs.2018.10.030

Saarikangas, J., Zhao, H., and Lappalainen, P. (2010). Regulation of the actin cytoskeleton-plasma membrane interplay by phosphoinositides. *Physiol. Rev.* 90, 259–289.doi: 10.1152/physrev.00036.2009

Saleh, S. N., Albert, A. P., and Large, W. A. (2009a). Activation of native TRPC1/C5/C6 channels by endothelin-1 is mediated by both PIP3 and PIP2 in rabbit coronary artery myocytes. *J. Physiol.* 587(Pt 22), 5361–5375.doi: 10.1113/jphysiol.2009.180331

Saleh, S. N., Albert, A. P., and Large, W. A. (2009b). Obligatory role for phosphatidylinositol 4,5-bisphosphate in activation of native TRPC1 store-operated channels in vascular myocytes. *J. Physiol.* 587, 531–540.doi: 10.1113/jphysiol.2008.166678

Schafer, S., Viswanathan, S., Widjaja, A. A., Lim, W. W., Moreno-Moral, A., DeLaughter, D. M., et al. (2017). IL-11 is a crucial determinant of cardiovascular fibrosis. *Nature* 552, 110–115. doi: 10.1038/nature24676

Schink, K. O., Tan, K. W., and Stenmark, H. (2016). Phosphoinositides in control of membrane dynamics. *Annu. Rev. Cell Dev. Biol.* 32, 143–171.doi: 10.1146/annurev-cellbio-111315-125349

Senju, Y., Kalimeri, M., Koskela, E. V., Somerharju, P., Zhao, H., Vattulainen, I., et al. (2017). Mechanistic principles underlying regulation of the actin cytoskeleton by phosphoinositides. *Proc. Natl. Acad. Sci. U.S.A.* 114, E8977–E8986. doi: 10.1073/pnas.1705032114

Senju, Y., and Lappalainen, P. (2019). Regulation of actin dynamics by PI(4,5)P2 in cell migration and endocytosis. *Curr. Opin. Cell Biol.* 56, 7–13.doi: 10.1016/j.ceb.2018.08.003

Sheetz, M. P., Sable, J. E., and Dobereiner, H. G. (2006). Continuous membrane-cytoskeleton adhesion requires continuous accommodation to lipid and cytoskeleton dynamics. *Annu. Rev. Biophys. Biomol. Struct.* 35, 417–434.doi: 10.1146/annurev.biophys.35.040405.102017

Shewan, A., Eastburn, D. J., and Mostov, K. (2011). Phosphoinositides in cell architecture. *Cold Spring Harb. Perspect. Biol.* 3:a004796.doi: 10.1101/cshperspect.a004796

Shi, J., Ju, M., Abramowitz, J., Large, W. A., Birnbaumer, L., and Albert, A. P. (2012). TRPC1 proteins confer PKC and phosphoinositol activation on native heteromeric TRPC1/C5 channels in vascular smooth muscle: comparative study of wild-type and TRPC1-/- mice. *FASEB J.* 26, 409–419.doi: 10.1096/fj.11-185611

Shi, J., Miralles, F., Kinet, J. P., Birnbaumer, L., Large, W. A., and Albert, A. P. (2017). Evidence that Orai1 does not contribute to store-operated TRPC1 channels in vascular smooth muscle cells. *Channels* 11, 329–339.doi: 10.1080/19336950.2017.1303025

Shioi, T., Kang, P. M., Douglas, P. S., Hampe, J., Yballe, C. M., Lawitts, J., et al. (2000). The conserved phosphoinositide 3-kinase pathway determines heart size in mice. *EMBO J.* 19, 2537–2548. doi: 10.1093/emboj/19.11.2537

Shiojima, I., Sato, K., Izumiya, Y., Schiekofer, S., Ito, M., Liao, R., et al. (2005). Disruption of coordinated cardiac hypertrophy and angiogenesis contributes to the transition to heart failure. *J. Clin. Invest.* 115, 2108–2118.doi: 10.1172/JCI24682

Smirnova, N. F., Gayral, S., Pedros, C., Loirand, G., Vaillant, N., Malet, N., et al. (2014). Targeting PI3Kgamma activity decreases vascular trauma-induced intimal hyperplasia through modulation of the Th1 response. *J. Exp. Med.* 211, 1779–1792.doi: 10.1084/jem.20131276

Solis, C., and Russell, B. (2019). CapZ integrates several signaling pathways in response to mechanical stiffness. *J. Gen. Physiol.* 151, 660–669.doi: 10.1085/jgp.201812199

Spinelli, A. M., and Trebak, M. (2016). Orai channel-mediated Ca2+ signals in vascular and airway smooth muscle. *Am. J. Physiol. Cell Physiol.* 310, C402–C413. doi: 10.1152/ajpcell.00355.2015

Trepat, X., Grabulosa, M., Buscemi, L., Rico, F., Farre, R., and Navajas, D. (2005). Thrombin and histamine induce stiffening of alveolar epithelial cells. *J. Appl. Physiol.* 98, 1567–1574.doi: 10.1152/japplphysiol.00925.2004

Tschumperlin, D. J. (2011). Mechanotransduction. *Compr. Physiol.* 1, 1057–1073. doi: 10.1002/cphy.c100016

Tsujita, K., and Itoh, T. (2015). Phosphoinositides in the regulation of actin cortex and cell migration. *Biochim. Biophys. Acta* 1851, 824–831.doi: 10.1016/j.bbalip.2014.10.011

Vanhaesebroeck, B., Guillermet-Guibert, J., Graupera, M., and Bilanges, B. (2010). The emerging mechanisms of isoform-specific PI3K signalling. *Nat. Rev. Mol. Cell Biol.* 11, 329–341.doi: 10.1038/nrm2882

Vantler, M., Jesus, J., Leppanen, O., Scherner, M., Berghausen, E. M., Mustafov, L., et al. (2015). Class IA Phosphatidylinositol 3-Kinase isoform p110alpha mediates vascular remodeling. *Arterioscler. Thromb. Vasc. Biol.* 35, 1434–1444.doi: 10.1161/ATVBAHA.114.304887

Verma, S. K., Lal, H., Golden, H. B., Gerilechaogetu, F., Smith, M., Guleria, R. S., et al. (2011). Rac1 and RhoA differentially regulate angiotensinogen gene expression in stretched cardiac fibroblasts. *Cardiovasc. Res.* 90, 88–96.doi: 10.1093/cvr/cvq385

Voelkel, T., and Linke, W. A. (2011). Conformation-regulated mechanosensory control via titin domains in cardiac muscle. *Pflugers Arch.* 462, 143–154.doi: 10.1007/s00424-011-0938-1

Wang, H., Cheng, X., Tian, J., Xiao, Y., Tian, T., Xu, F., et al. (2020). TRPC channels: Structure, function, regulation and recent advances in small molecular probes. *Pharmacol. Ther.* 209, 107497.doi: 10.1016/j.pharmthera.2020.107497

Wang, X., and Khalil, R. A. (2018). Matrix metalloproteinases, vascular remodeling, and vascular disease. *Adv. Pharmacol.* 81, 241–330.doi: 10.1016/bs.apha.2017.08.002

Wang, Y., Cao, W., Cui, J., Yu, Y., Zhao, Y., Shi, J., et al. (2018). Arterial wall stress induces phenotypic switching of arterial smooth muscle cells in vascular remodeling by activating the YAP/TAZ signaling pathway. *Cell. Physiol. Biochem.* 51, 842–853.doi: 10.1159/000495376

Wang, Y., Deng, X., Hewavitharana, T., Soboloff, J., and Gill, D. L. (2008). Stim, ORAI and TRPC channels in the control of calcium entry signals in smooth muscle. *Clin. Exp. Pharmacol. Physiol.* 35, 1127–1133.doi: 10.1111/j.1440-1681.2008.05018.x

Weernink, P. A., Meletiadis, K., Hommeltenberg, S., Hinz, M., Ishihara, H., Schmidt, M., et al. (2004). Activation of type I phosphatidylinositol 4-phosphate 5-kinase isoforms by the Rho GTPases, RhoA, Rac1, and Cdc42. *J. Biol. Chem.* 279, 7840–7849. doi: 10.1074/jbc.M312737200

Yang, C. Y., Chen, C. S., Yiang, G. T., Cheng, Y. L., Yong, S. B., Wu, M. Y., et al. (2018). New insights into the immune molecular regulation of the pathogenesis of acute respiratory distress syndrome. *Int. J. Mol. Sci.* 19:588.doi: 10.3390/ijms19020588

Yin, J., and Kuebler, W. M. (2010). Mechanotransduction by TRP channels: general concepts and specific role in the vasculature. *Cell Biochem. Biophys.* 56, 1–18.doi: 10.1007/s12013-009-9067-2

Yu, B., Chen, Q., Le Bras, A., Zhang, L., and Xu, Q. (2018). Vascular stem/progenitor cell migration and differentiation in atherosclerosis. *Antioxid. Redox Signal.* 29, 219–235.doi: 10.1089/ars.2017.7171

Yu, F. X., Zhao, B., and Guan, K. L. (2015). Hippo pathway in organ size control, tissue homeostasis, and cancer. *Cell* 163, 811–828. doi: 10.1016/j.cell.2015.10.044

Yue, Z., Xie, J., Yu, A. S., Stock, J., Du, J., and Yue, L. (2015). Role of TRP channels in the cardiovascular system. *Am. J. Physiol. Heart Circ. Physiol.* 308, H157–H182. doi: 10.1152/ajpheart.00457.2014

Zegers, M. M., and Friedl, P. (2014). Rho GTPases in collective cell migration. *Small GTPases* 5:e28997. doi: 10.4161/sgtp.28997

Zhang, C., Wang, W., He, W., Xi, N., Wang, Y., and Liu, L. (2018). Dynamic model for characterizing contractile behaviors and mechanical properties of a cardiomyocyte. *Biophys. J.* 114, 188–200. doi: 10.1016/j.bpj.2017.11.002

Conflict of Interest: The authors declare that the research was conducted in the absence of any commercial or financial relationships that could be construed as a potential conflict of interest.

frontiers in Cell and Developmental Biology

ORIGINAL RESEARCH
published: 15 January 2021
doi: 10.3389/fcell.2020.591246

Epiregulin (EREG) and Myocardin Related Transcription Factor A (MRTF-A) Form a Feedforward Loop to Drive Hepatic Stellate Cell Activation

Xiaoyan Wu[1,4,5†], Wenhui Dong[4†], Tianyi Zhang[4†], Haozhen Ren[1,2], Jinglin Wang[1,2], Longcheng Shang[1], Zhengyi Zhu[1], Wei Zhu[3], Xiaolei Shi[1,2*] and Yong Xu[4,5]*

[1] Department of Hepatobiliary Surgery, The Affiliated Nanjing Drum Tower Hospital of Nanjing University Medical School, Nanjing, China, [2] Hepatobiliary Institute, Nanjing University, Nanjing, China, [3] Department of Anesthesiology, The Affiliated Drum Tower Hospital of Nanjing University Medical School, Nanjing, China, [4] Key Laboratory of Targeted Intervention of Cardiovascular Disease, Collaborative Innovation Center for Cardiovascular Translational Medicine, and Center for Experimental Medicine, Department of Pathophysiology, Nanjing Medical University, Nanjing, China, [5] Institute of Biomedical Research, Liaocheng University, Liaocheng, China

OPEN ACCESS

Edited by:
Pedro M. Fernández-Salguero, University of Extremadura, Spain

Reviewed by:
Manoj B. Menon, Indian Institute of Technology Delhi, India
Dae-Sik Lim, Korea Advanced Institute of Science and Technology, South Korea

***Correspondence:**
Xiaolei Shi
sxl@nju.edu.cn
Wei Zhu
chzhuwei118@qq.com

† These authors have contributed equally to this work

Specialty section:
This article was submitted to Signaling, a section of the journal Frontiers in Cell and Developmental Biology

Received: 05 August 2020
Accepted: 28 October 2020
Published: 15 January 2021

Citation:
Wu X, Dong W, Zhang T, Ren H, Wang J, Shang L, Zhu Z, Zhu W, Shi X and Xu Y (2021) Epiregulin (EREG) and Myocardin Related Transcription Factor A (MRTF-A) Form a Feedforward Loop to Drive Hepatic Stellate Cell Activation. Front. Cell Dev. Biol. 8:591246. doi: 10.3389/fcell.2020.591246

Trans-differentiation of quiescent hepatic stellate cells (HSC) into myofibroblast cells is considered the linchpin of liver fibrosis. A myriad of signaling pathways contribute to HSC activation and consequently liver fibrosis. Epidermal growth factor (EGF) family of cytokines signal through the cognate receptor EGFR to promote HSC activation. In the present study we investigated the transcription regulation of epiregulin (EREG), an EGFR ligand, during HSC activation. We report that EREG expression was significantly up-regulated in activated HSCs compared to quiescent HSCs isolated from mice. In addition, there was an elevation of EREG expression in HSCs undergoing activation *in vitro*. Of interest, deficiency of myocardin-related transcription factor A (MRTF-A), a well-documented regulator of HSC trans-differentiation, attenuated up-regulation of EREG expression both *in vivo* and *in vitro*. Further analysis revealed that MRTF-A interacted with serum response factor (SRF) to bind directly to the EREG promoter and activate EREG transcription. EREG treatment promoted HSC activation *in vitro*, which was blocked by MRTF-A depletion or inhibition. Mechanistically, EREG stimulated nuclear trans-location of MRTF-A in HSCs. Together, our data portray an EREG-MRTF-A feedforward loop that contributes to HSC activation and suggest that targeting the EREG-MRTF-A axis may yield therapeutic solutions against liver fibrosis.

Keywords: transcription regulation, hepatic stellate cell, liver fibrosis, epiregulin, MRTF-A, SRF

INTRODUCTION

Liver fibrosis is a key pathophysiological process taking place in response to various acute and chronic hepatic injuries (Lee et al., 2015). Whereas spatiotemporally controlled liver fibrosis is instrumental to the amelioration of liver injury and restoration of liver function, excessive and/or prolonged liver fibrosis leads to architectural and functional damages to the liver and

precipitates the development of such end-stage liver diseases as cirrhosis and hepatocellular carcinoma (Barry et al., 2020). Liver fibrosis can occur following the challenge of a myriad of injurious stimuli including pathogens, toxins, corrosive chemicals, and metabolites. Regardless of the specific triggering factor, myofibroblasts are considered the major effector cell type for liver fibrosis (Kisseleva, 2017). Myofibroblasts possess the characteristics of both muscle cells and fibroblast cells being able to contract and cover the wound and produce and lay down extracellular matrix proteins. The origins from which myofibroblasts arise during liver fibrosis have been a subject matter receiving extensive investigations. Recently lineage fate-mapping experiments have been determined that an overwhelming majority (>90%) of myofibroblasts in the liver are derived from hepatic stellate cells (HSC) that express lecithin retinol acyltransferase (Lrat), a supposedly HSC lineage-specific marker gene (Mederacke et al., 2013). Under physiological settings, quiescent HSCs primarily function as a deposit site for lipids and vitamin A; upon exposure to a pro-fibrogenic microenvironment, HSCs undergo trans-differentiation and become myofibroblasts. *In vitro* cultured HSCs can also be educated to switch to a myofibroblast-like phenotype by a host of growth factors including transforming growth factor (TGF-β) and platelet-derived growth factor (PDGF) (Hou and Syn, 2018).

Signaling through epidermal growth factor receptor (EGFR) has been shown to contribute to HSC activation and liver fibrosis. Scheving et al. have demonstrated that genetic deletion of EGFR attenuates CCl_4 induced liver fibrosis in mice (Scheving et al., 2016). Consistently, pharmaceutical inhibition of EGFR is associated with amelioration of liver fibrosis in different murine models (Fuchs et al., 2014; Liang et al., 2018). Previously, Perugorria et al. have shown the amphiregulin (AR), a ligand for EGFR, plays critical roles in HSC activation and liver fibrosis: AR treatment robustly promotes HSC activation *in vitro* whereas AR deletion protects the mice from CCl_4-induced liver fibrosis (Perugorria et al., 2008). Epiregulin, encoded by *EREG*, is an EGFR ligand that shares significant homology with amphiregulin (Riese and Cullum, 2014). Whether EREG can contribute to HSC activation remains undetermined.

Mounting evidence suggests that myocardin-related transcription factor A (MRTF-A) plays a pivotal role promoting the differentiation of myofibroblasts in multiple organs (Small, 2012). MRTF-A was initially characterized as a co-factor for serum response factor (SRF) to activate the transcription of muscle-lineage specific genes (Wang et al., 2002). MRTF-A can shuttle between the cytoplasm and the nucleus depending on cytoskeletal reshuffling (Olson and Nordheim, 2010). Previously we have reported that MRTF-A regulates liver fibrosis by transcriptionally programming HSC activation (Fan et al., 2015; Tian et al., 2015, 2016). Here we report that EREG expression is up-regulated during HSC activation both *in vivo* and *in vitro*. MRTF-A interacts with SRF to directly bind to the EREG promoter and activate EREG transcription. Reciprocally, EREG contributes to HSC activation by promoting nuclear translocation of MRTF-A. Therefore, targeting the EREG-MRTF-A axis may yield therapeutic solutions against liver fibrosis.

MATERIALS AND METHODS

Animals

All animal protocols were reviewed and approved the intramural Ethics Committee on Humane Treatment of Laboratory Animals of Nanjing Medical University. MRTF-A knockout (KO) mice were originally obtained from Steve Morris at St Jude Hospital (Sun et al., 2006). To induce liver fibrosis, MRTF-A KO mice and wild type (WT) littermates were injected with CCl_4 (1.0 mL/kg as 50% vol/vol), or injected with thioacetamide (TAA, 100 mg/kg), or subjected to bile duct ligation (BDL) as previously described (Li et al., 2019a,c; Lu et al., 2019).

Cell Culture, Plasmids, and Transient Transfection

Immortalized human HSC (LX-2) were maintained in DMEM supplemented with 10% FBS as previously described (Kong et al., 2019a,b). Primary HSC were isolated and maintained as previously described (Li et al., 2019b). Briefly, the animals were anesthetized by intraperitoneal injection with ketamine-xylazine. A laparotomy was performed and the portal vein was cut to allow retrograde perfusion with pronase (Sigma Aldrich, St. Louis, MO, United States) and collagenase (Roche, Germany) containing solutions. HSCs were isolated from the non-parenchymal fraction by 9.7% Nycodenz gradient centrifugation. Isolated HSCs were seeded in plastic culture dishes and allowed to undergo spontaneous activation. RNA targeting SRF (GAUGGAGUUCAUCGACAACAA) was purchased from Dharmacon. Recombinant TGF-β (100-21) was purchased from Peprotech. Recombinant EREG (1195-EP-025) was purchased from R&D. CCG-1423 (S7719) was purchased from Selleck. Full-length EREG promoter-luciferase construct (−1345/+118) and MRTF-A expression construct have been previously described (Kyotani et al., 2018; Mao et al., 2020b). Truncated and mutated EREG promoter-luciferase constructs were prepared with the QuikChange mutagenesis kit (Agilent). Conditioned media were harvested as previously described (Li et al., 2020a,b). Briefly, the cells were switched to and incubated with serum-free media overnight. The next day, the media were collected, centrifuged at 4,000 × *g* for 30 min at 4°C using 3-kDa MW cut-off filter units (Millipore) and sterilized through a 0.4-μm filter. Transient transfections were performed with Lipofectamine 2000. Luciferase activities were assayed 24–48 h after transfection using a luciferase reporter assay system (Promega) as previously described (Yang et al., 2019a,b).

Enzyme-Linked Immunosorbent Assay (ELISA)

Secreted epiregulin levels were measured using a commercially available ELISA (LS-F5753, Lifespan Biosciences) per vendor's recommendations.

Protein Extraction and Western Blot

Whole cell lysates were obtained by re-suspending cell pellets in RIPA buffer (50 mM Tris pH7.4, 150 mMNaCl, 1% Triton X-100) with freshly added protease inhibitor (Roche) as

previously described (Fan et al., 2020). Nuclear proteins were extracted using the NE-PER Kit (Pierce) following manufacturer's recommendation (Mao et al., 2020a). Western blot analyses were performed with anti-MRTF-A (Santa Cruz, sc-32909), anti-SRF (Cell Signaling Technology, 5147), anti-α-tubulin (Sigma, T6074), anti-Lamin A/C (Proteintech, 10298-1), anti-α-SMA (Abcam, ab5694), and anti-β-actin (Sigma, A1978). For densitometrical quantification, densities of target proteins were normalized to those of β-actin as previously described (Lv et al., 2020; Wu et al., 2020). Data are expressed as relative protein levels compared to the control group which is arbitrarily set as 1.

RNA Isolation and Real-Time PCR

RNA was extracted with the RNeasy RNA isolation kit (Qiagen). Reverse transcriptase reactions were performed using a SuperScript First-strand Synthesis System (Invitrogen) as previously described (Zhao et al., 2019; Dong et al., 2020). Real-time PCR reactions were performed on an ABI Prism 7,500 system with the following primers: human EREG, 5′-ACGTGTGGCTCAAGTGTCAA-3′ and 5′-CACTTCACACC TGCAGTAGTTT-3′; mouse Ereg, 5′-TGCTTTGTCTAGGTT CCCACC-3′ and 5′-GGCGGTACAGTTATCCTCGG-3′; human COL1A2, 5′-GTGGCAGTGATGGAAGTGTG-3′ and 5′-AGGA CCAGCGTTACCAACAG-3′; human ACTA2, 5′-CTATGCC TCTGGACGCACAACT-3′ and 5′-CAGATCCAGACGCAT GATGGCA-3′.Ct values of target genes were normalized to the Ct values of housekeekping control gene (18s, 5′-CGCGGTTCTATTTTGTTGGT-3′ and 5′-TCGTCTTCG AAACTCCGACT-3′ for both human and mouse genes) using the ΔΔCt method and expressed as relative mRNA expression levels compared to the control group which is arbitrarily set as 1.

Chromatin Immunoprecipitation

Chromatin Immunoprecipitation (ChIP) assays were performed essentially as described before (Sun et al., 2020). In brief, chromatin in control and treated cells were cross-linked with 1% formaldehyde. Cells were incubated in lysis buffer (150 mMNaCl, 25 mM Tris pH 7.5, 1% Triton X-100, 0.1% SDS, 0.5% deoxycholate) supplemented with protease inhibitor tablet and PMSF. DNA was fragmented into ∼200 bp pieces using a Branson 250 sonicator. Aliquots of lysates containing 200 μg of protein were used for each immunoprecipitation reaction with anti-MRTF-A (Santa Cruz, sc-32909), anti-SRF (Cell Signaling Technology, 5147), or pre-immune IgG. For re-ChIP, immune complexes were eluted with the elution buffer (1% SDS, 100 mM $NaCO_3$), diluted with the re-ChIP buffer (1% Triton X-100, 2 mM EDTA, 150 mMNaCl, 20 mM Tris pH 8.1), and subjected to immunoprecipitation with a second antibody of interest.

Immunofluorescence Microscopy

Immunofluorescence staining was performed as previously described. The cells were fixed with 4% formaldehyde, permeabilized with TBST (0.25% Triton X-100, 150 mM NaCl, 50 mM Tris pH7.4), blocked with 5% BSA, and incubated with indicated primary antibodies overnight. After several washes with PBS, cells were incubated with FITC-labeled secondary antibodies (Jackson) for 30 min. DAPI (Sigma) was added and incubated with cells for 5 min prior to observation. Immunofluorescence was visualized on a co-focal microscope (LSM 710, Zeiss). For each group, at least 10 fields were counted.

Statistical Analysis

One-way ANOVA with *post hoc* Scheff'e analyses were performed by SPSS software (IBM SPSS v18.0, Chicago, IL, United States). Unless otherwise specified, values of $p < 0.05$ were considered statistically significant.

RESULTS

EREG Expression Is Up-Regulated in Activated HSCs

Previously it has been shown that amphiregulin (AR), an EGFR ligand closely related to epiregulin (EREG), is activated during HSC trans-differentiation and contributes to liver fibrosis (Perugorria et al., 2008). We asked whether EREG expression levels might be altered during HSC activation. To this end, C57/BL6 mice were injected with CCl_4 to induce liver fibrosis (**Figure 1A**). Picrosirius red staining showed significant liver fibrosis in the CCl_4-injected mice compared to the vehicle-injected mice (**Figure 1B**). Primary HSCs were isolated from the mice with liver fibrosis and from the control mice receiving injection with corn oil. As shown in **Figure 1C**, expression of α-SMA (*Acta2*), a myofibroblast marker, was significantly up-regulated, as measured by qPCR, in the activated HSCs compared to the quiescent HSCs; a similar up-regulation of *Ereg* expression was detected in the HSCs isolated from the fibrotic livers compared to those isolated from the control livers. ELISA measurements confirmed that EREG protein levels were also up-regulated in the activated HSCs compared to the quiescent HSCs (**Figure 1D**). Next, liver fibrosis was induced in mice by injection with thioacetamide (TAA, **Figure 1E**). Picrosirius red staining showed significant liver fibrosis in the TAA-injected mice compared to the vehicle-injected mice (**Figure 1F**). Again, primary HSCs isolated from the fibrotic livers displayed higher levels of *Acta2* and *Ereg* than those isolated from the control livers (**Figure 1G**). A similar increase in EREG protein levels was detected by ELISA (**Figure 1H**). Finally, in a third model of liver fibrosis in which the mice were subjected to the BDL surgery (**Figure 1I**), picrosirius red staining showed significant liver fibrosis in the BDL mice compared to the sham-operated mice (**Figure 1J**). qPCR (**Figure 1K**) and ELISA (**Figure 1L**) assays showed that EREG expression levels were up-regulated during HSC activation *in vivo*.

We then evaluated the changes in epiregulin expression in cell models of liver fibrosis. In the first model, primary HSCs were isolated from C57/BL mice and allowed to undergo spontaneous activation *in vitro*. When the cells were harvested at different time points following their isolation, it was observed that *Ereg* expression was progressively up-regulated mirroring the changes in *Acta2* expression (**Figures 2A,B**). In the second model, LX-2 cells were treated with TGF-β, a well-documented pro-fibrogenic growth factor. Epiregulin expression was significantly

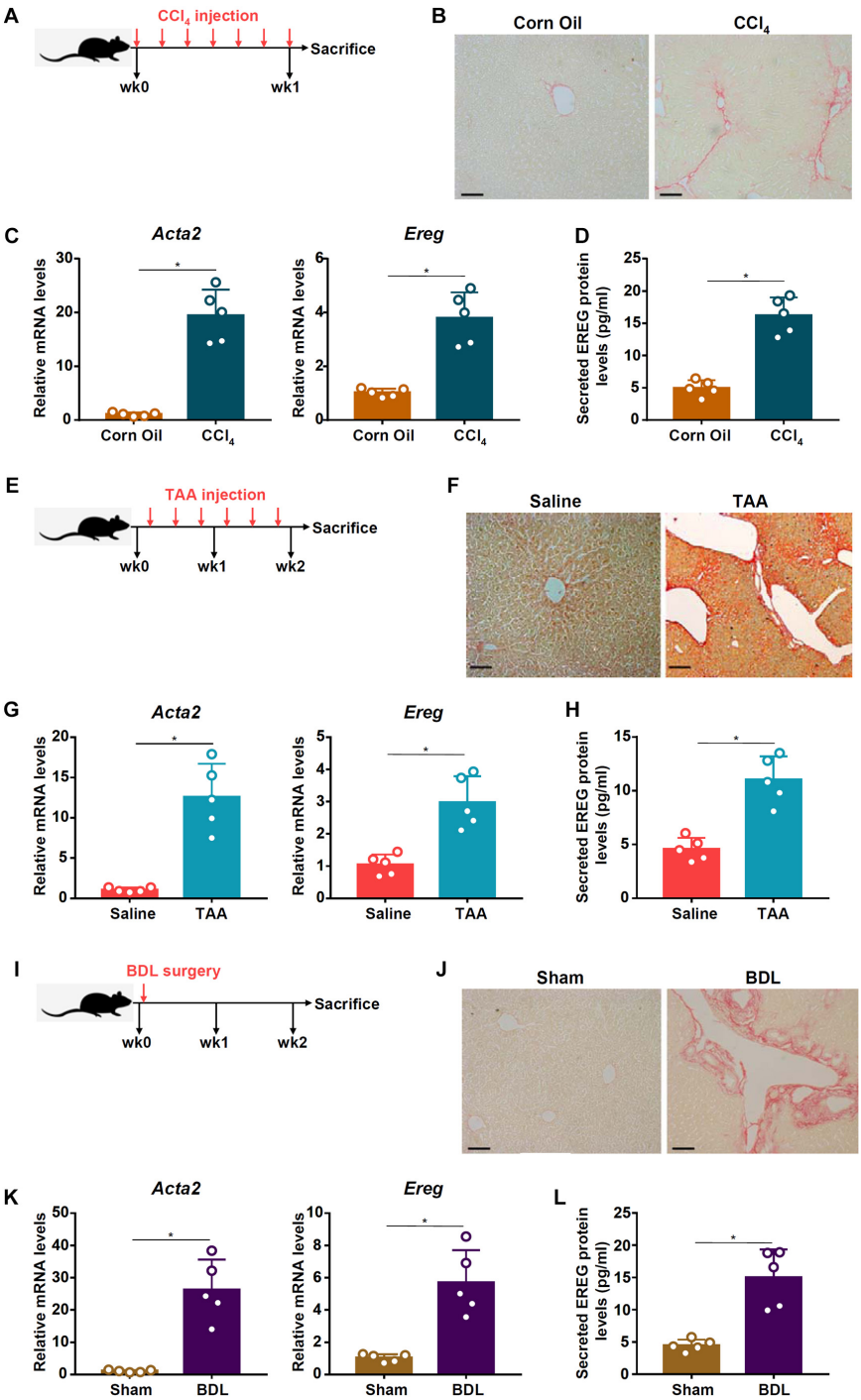

FIGURE 1 | EREG expression is up-regulated in activated HSCs in vivo. **(A–D)** C57/BL6 mice were injected with CCl_4 or corn oil for 7 days. Scheme of protocol **(A)**. Representative images of picrosirius red staining **(B)**. Primary HSCs were isolated from the mice and EREG expression levels were examined by qPCR **(C)** and ELISA **(D)**. *N* = 5 mice for each group. **(E–H)** C57/BL6 mice were injected with TAA or saline for 2 weeks. Scheme of protocol **(E)**. Representative images of picrosirius red staining **(F)**. Primary HSCs were isolated from the mice and EREG expression levels were examined by qPCR **(G)** and ELISA **(H)**. *N* = 5 mice for each group. **(I–L)** C57/BL6 mice were subjected to the BDL procedure or the sham surgery. The mice were sacrificed 2 weeks after the surgery and primary HSCs were isolated. Scheme of protocol **(I)**. Representative images of picrosirius red staining **(J)**. EREG expression levels were examined by qPCR **(K)** and ELISA **(L)**. *N* = 5 mice for each group.

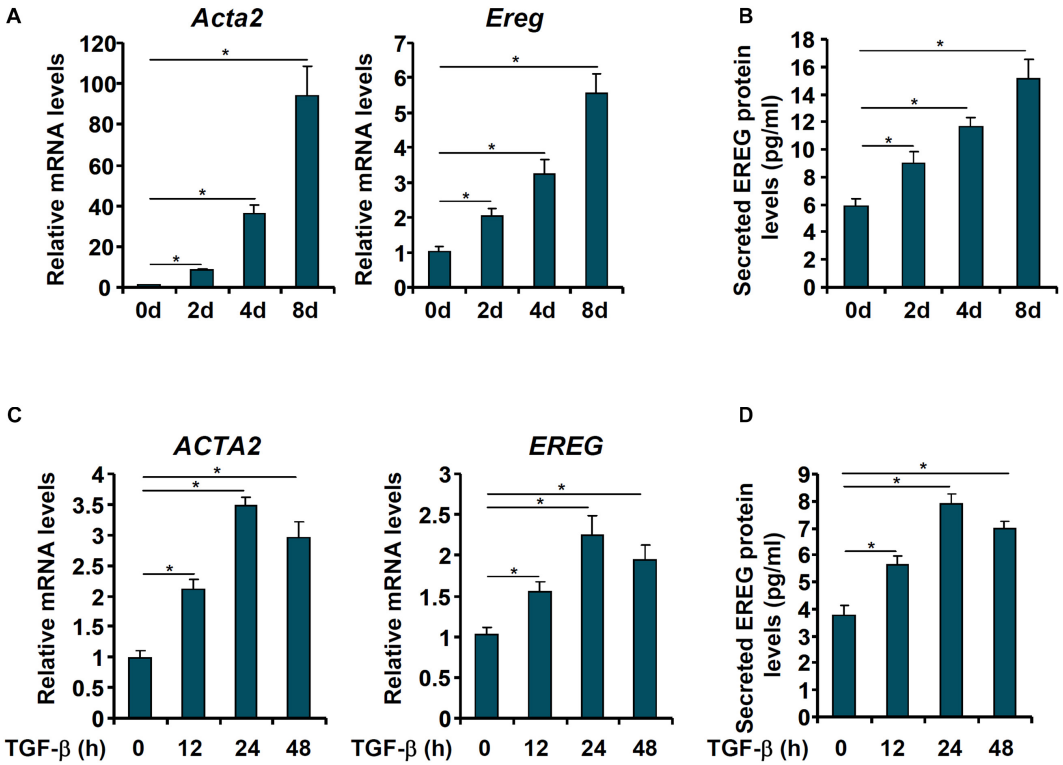

FIGURE 2 | EREG expression is up-regulated in activated HSCs in vitro. **(A,B)** Primary HSCs were isolated from C57/BL6 mice and underwent spontaneous activation by *in vitro* culture. The cells were harvested at indicated time points and EREG expression levels were examined by qPCR and ELISA. **(C,D)** LX-2 cells were treated with or without TGF-β (5 ng/ml) and harvested at indicated time points. EREG expression levels were examined by qPCR and ELISA.

up-regulated by TGF-β treatment mirroring the increase in α-SMA expression (**Figures 2C,D**). Taken together, these data suggest a positive correlation between epiregulin and hepatic stellate cell activation *in vivo* and *in vitro*.

EREG Stimulates Pro-fibrogenic Gene Expression in Hepatic Stellate Cells

Next, we evaluated the effect of epiregulin on pro-fibrogenic gene expression in hepatic stellatecells. Treatment with epiregulin led to a small but appreciable increase in pro-fibrogenic gene expression in LX-2 cells as early as 6 h after the treatment. Induction of pro-fibrogenic genes by epiregulin treatment were detected at 12 and 24 h by qPCR (**Figure 3A**) and Western blotting (**Figure 3B**). We also examined the effect of epiregulin treatment on pro-fibrogenic gene expression in spontaneously activated primary HSCs. As shown in **Figures 3C,D**, the addition of epiregulin augmented the up-regulation of pro-fibrogenic genes as primary HSCs transition from a quiescent state to an activated state. To make a broad point that HSCs can produce and release factors to promote/sustain activation in a feedforward fashion, conditioned media (CM) were harvested from spontaneously activated HSCs to treat quiescent HSCs. Indeed, quiescent HSCs treated with the CM transitioned into an activated state faster than the HSCs cultured in regular media (**Supplementary Figure 1**). Therefore, it appears that epiregulin may promote the activation of HSCs via an autocrine pathway *in vitro*.

MRTF-A Deficiency Results in Down-Regulation of EREG Expression in Hepatic Stellate Cells

MRTF-A is key determinant of myofibroblast maturation (Small, 2012). We have previously shown that MRTF-A deletion in mice attenuated liver fibrosis induced by TAA injection (Tian et al., 2016), by CCl_4 injection (Tian et al., 2015), or by the BDL procedure (Fan et al., 2015). Consistently, primary HSCs isolated from the MRTF-A KO mice exhibited reduced expression of *Acta2* compared to the WT mice following TAA injection (**Figure 4A**), CCl_4 injection (**Figure 4C**) or the BDL procedure (**Figure 4E**). Of interest, MRTF-A deficiency comparably decreased epiregulin expression in all three models as measured by qPCR (**Figures 4A,C,E**) and ELISA (**Figures 4B,D,F**). In keeping with these observations, induction of epiregulin expression was much more tepid during spontaneous activation of primary HSCs isolated from MRTF-A KO mice than from WT mice (**Figures 4G,H**). Finally, knockdown of MRTF-A by siRNAs repressed induction of epiregulin expression by TGF-β treatment in LX-2 cells (**Figures 4I,J**). In contrast, knockdown of MRTF-B, a closely related MRTF-A sibling, did not alter

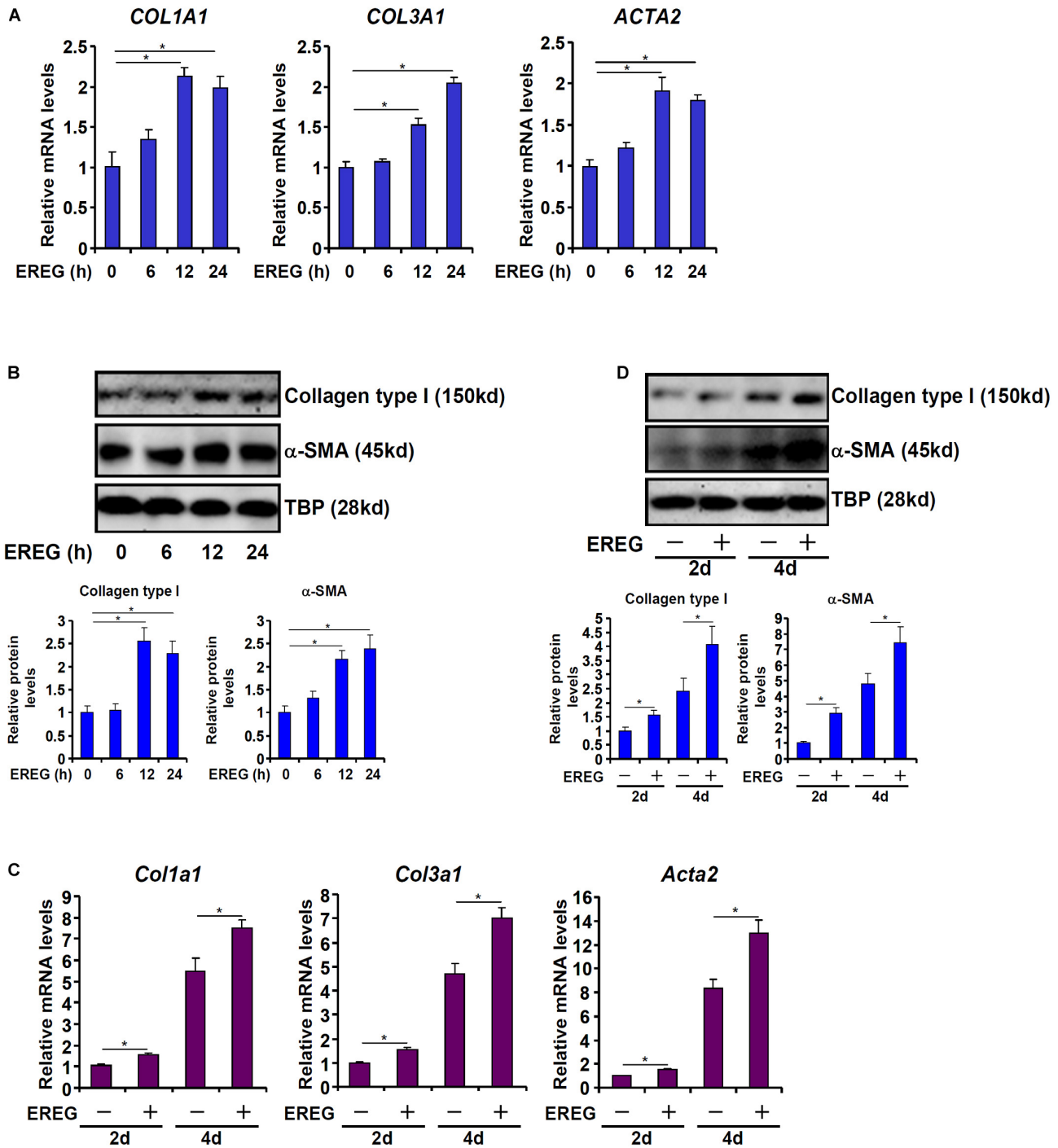

FIGURE 3 | EREG treatment stimulates the expression of fibrogenic genes in HSCs. **(A,B)** LX-2 cells were treated with or without EREG (5 ng/ml) and harvested at indicated time points. Gene expression levels were examined by qPCR and Western blotting. Quantification was performed with Image Pro based on three independent experiments. **(C,D)** Primary HSCs were isolated from C57/BL6 mice and underwent spontaneous activation by *in vitro* culture in the presence or absence of EREG. Gene expression levels were examined by qPCR and Western blotting. Quantification was performed with Image Pro based on three independent experiments.

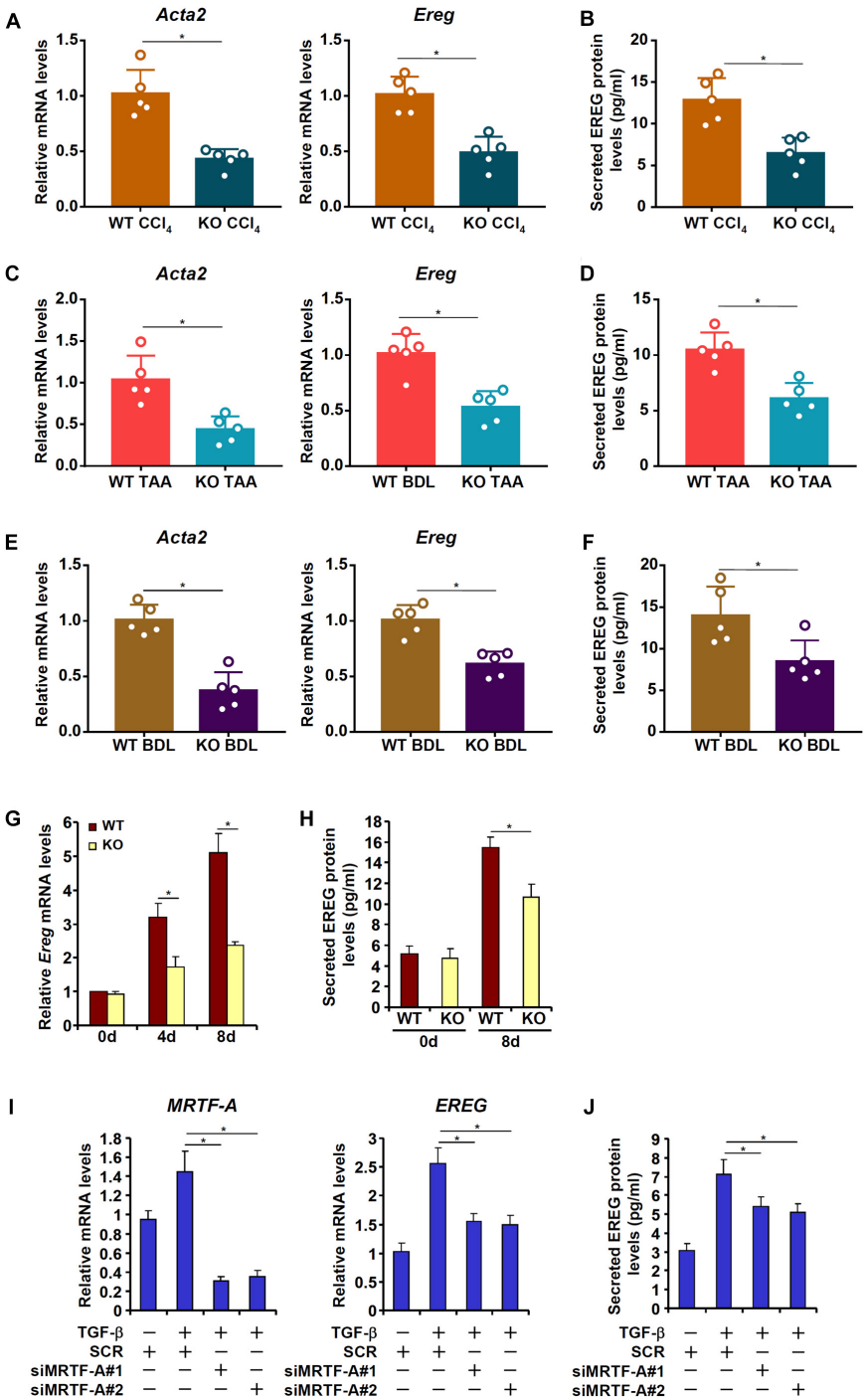

FIGURE 4 | MRTF-A deficiency attenuates EREG activation in HSCs. **(A,B)** WT and MRTF-A KO mice were injected with CCl_4 for 7 days. Primary HSCs were isolated from the mice and EREG expression levels were examined by qPCR and ELISA. *N* = 5 mice for each group. **(C,D)** WT and MRTF-A KO mice were injected with TAA for 2 weeks. Primary HSCs were isolated from the mice and EREG expression levels were examined by qPCR and ELISA. *N* = 5 mice for each group. **(E,F)** WT and MRTF-A KO mice were subjected to the BDL procedure. The mice were sacrificed 2 weeks after the surgery and primary HSCs were isolated. EREG expression levels were examined by qPCR and ELISA. *N* = 5 mice for each group. **(G,H)** Primary HSCs were isolated from WT and MRTF-A KO mice and underwent spontaneous activation for 7 days. EREG expression levels were examined by qPCR and ELISA. **(I,J)** LX-2 cells were transfected with siRNAs targeting MRTF-A or scrambled siRNAs (SCR) followed by treatment with TGF-β (5 ng/ml) for 24 h. EREG expression levels were examined by qPCR and ELISA.

epiregulin expression in either LX-2 cells or primary HSCs (**Supplementary Figure 2**).

MRTF-A Activates EREG Transcription by Interacting With SRF

We asked whether MRTF-A might regulate epiregulin expression at the transcriptional level. To test this hypothesis, an *EREG* promoter-luciferase fusion construct (−1345/ + 118) was transfected into LX-2 cells. Over-expression of MRTF-A dose-dependently up-regulated the *EREG* promoter activity (**Figure 5A**). A string of CArG box elements were identified within the *EREG* promoter (**Figure 5A**). Inward deletions introduced to the *EREG* promoter progressively removed the CArG box elements; the removal of the four more distal CArG boxes retained the responsiveness of the *EREG* promoter to MRTF-A over-expression whereas the removal of the most proximal CArG box rendered the *EREG* promoter inactive (**Figure 5B**). Several lines of additional evidence suggest that MRTF-A relies on the proximal CArG box to activate *EREG* transcription. ChIP assay showed that TGF-β treatment enhanced the association of MRTF-A with the proximal *EREG* promoter surrounding the innermost CArG box, but not with the intronic region, in LX-2 cells (**Figure 5C**). Similarly, association of MRTF-A with the *Ereg* promoter was stronger in activated primary HSCs compared to quiescent primary HSCs (**Supplementary Figure 3**). Re-ChIP assay confirmed that TGF-β treatment promoted the formation of an SRF-MRTF-A complex on the proximal *EREG* promoter (**Figure 5D**). Depletion of SRF with siRNA completely disrupted the binding of MRTF-A to the *EREG* promoter (**Figure 5E**). Finally, mutation of the most proximal CArG box abrogated the induction of the *EREG* promoter by MRTF-A (**Figure 5F**).

EREG Regulates HSC Activation by Promoting Nuclear Trans-Location of MRTF-A

Finally, we asked whether epiregulin could reciprocally influence MRTF-A activity. MRTF-A typically shuttles between the cytoplasm and the nucleus (Olson and Nordheim, 2010). Immunofluorescence staining showed that a large fraction of MRTF-A resides in the cytoplasm with only ∼10% located to the nucleus in LX-2 cells under normal conditions. When exposed to epiregulin treatment, MRTF-A started migrating into the nucleus: at 6 h following epiregulin treatment ∼35% of all MRTF-A proteins whereas at 24 h over 75% of all MRTF-A proteins were detected in the nucleus (**Figure 6A**). Similar discoveries were made by cell fractionation/Western blotting (**Figure 6B**). Conversely, induction of pro-fibrogenic genes by epiregulin treatment in LX-2 cells was markedly suppressed by MRTF-A knockdown at both mRNA (**Figure 6C**) and protein (**Figure 6D**) levels. Finally, inhibition of MRTF-A activity by CCG-1423 also dampened the up-regulation of pro-fibrogenic genes by epiregulin treatment (**Figures 6E,F**).

DISCUSSION

Activation of HSCs, a hallmark event in liver fibrosis, is programmed by a complex web of signaling cascades that relay the pro-fibrogenic cues to the nucleus, where profound changes in gene expression contribute to the transition of quiescent HSCs to mature myofibroblasts. In the present report, we provide data to show that epiregulin (EREG), belonging to the EGF family of growth factors, is a key regulator of HSC activation. Our data indicate that exposure of cultured HSCs to recombinant epiregulin accelerated the production of pro-fibrogenic genes (**Figure 3**). This is consistent with previously reported observations that other members of the EGF family including EGF (Lin and Chen, 2008), heparin-bound EGF (HB-EGF) (Takemura et al., 2013), FGF (Wang et al., 2020), and amphiregulin (Perugorria et al., 2008) all contribute to HSC trans-differentiation and liver fibrosis. Of note, all four EGF ligands signal through the same receptor (EGFR) (Riese and Cullum, 2014). Although existing evidence supports the argument that treatment with individual EGF growth factors is sufficient to promote HSC activation at least *in vitro*, the *in vivo* requirement/redundancy for each one of these proteins in the development of liver fibrosis is not clear. Deletion of either amphiregulin (AREG) or HB-EGF in mice leads to attenuation of liver fibrosis, suggesting that these growth factors may elicit different signaling cascades and downstream events to promote HSC maturation and fibrogenesis so that the loss of one EGF ligand cannot be fully compensated by other family members. Global EREG-null mice are viable and display no overt gross or liver abnormalities under physiological conditions (Lee et al., 2004). It remains to be ascertained whether these epiregulin deficient mice would phenocopy the $AREG^{-/-}$ mice and the $HB\text{-}EGF^{-/-}$ mice in models of liver fibrosis.

We show here that up-regulation of EREG expression during HSC activation *in vivo* and *in vitro* is mediated at the transcriptional level by MRTF-A, a well-established pro-fibrogenic molecule (Small, 2012). MRTF-A appears to activate EREG transcription by interacting with SRF and binding to one of the CArG boxes located on the proximal EREG promoter. Of interest, expression of other EGF family members has been shown to be regulated by SRF. For instance, differential regulation of neuregulin 1 (NRG1) in schizophrenia is controlled by several 5′ SNPs that create/abolish binding sites for a string of transcription factors including SRF (Law et al., 2006). On the other hand, SRF can be placed downstream of the EGFR signaling pathway. Augmented SRF activity by EGFR signaling is considered a paradigm in the pathogenesis of multiple cancers (Wee and Wang, 2017). More recently, Stern and colleagues have found that muscular conditional deletion of EGFR, which presumably blocks the signal transduction initiated by EGF, AREG, and EREG, protects the mice from diabetic complications, which is accompanied by changes in gene expression patterns reminiscent of suppressed SRF activity suggesting that EGFR likely regulates muscle cell behavior through stimulating SRF activity (Stern et al., 2020). It would be of great interest to delineate whether a reciprocal regulatory relationship exists between SRF and EREG in the process of HSC activation.

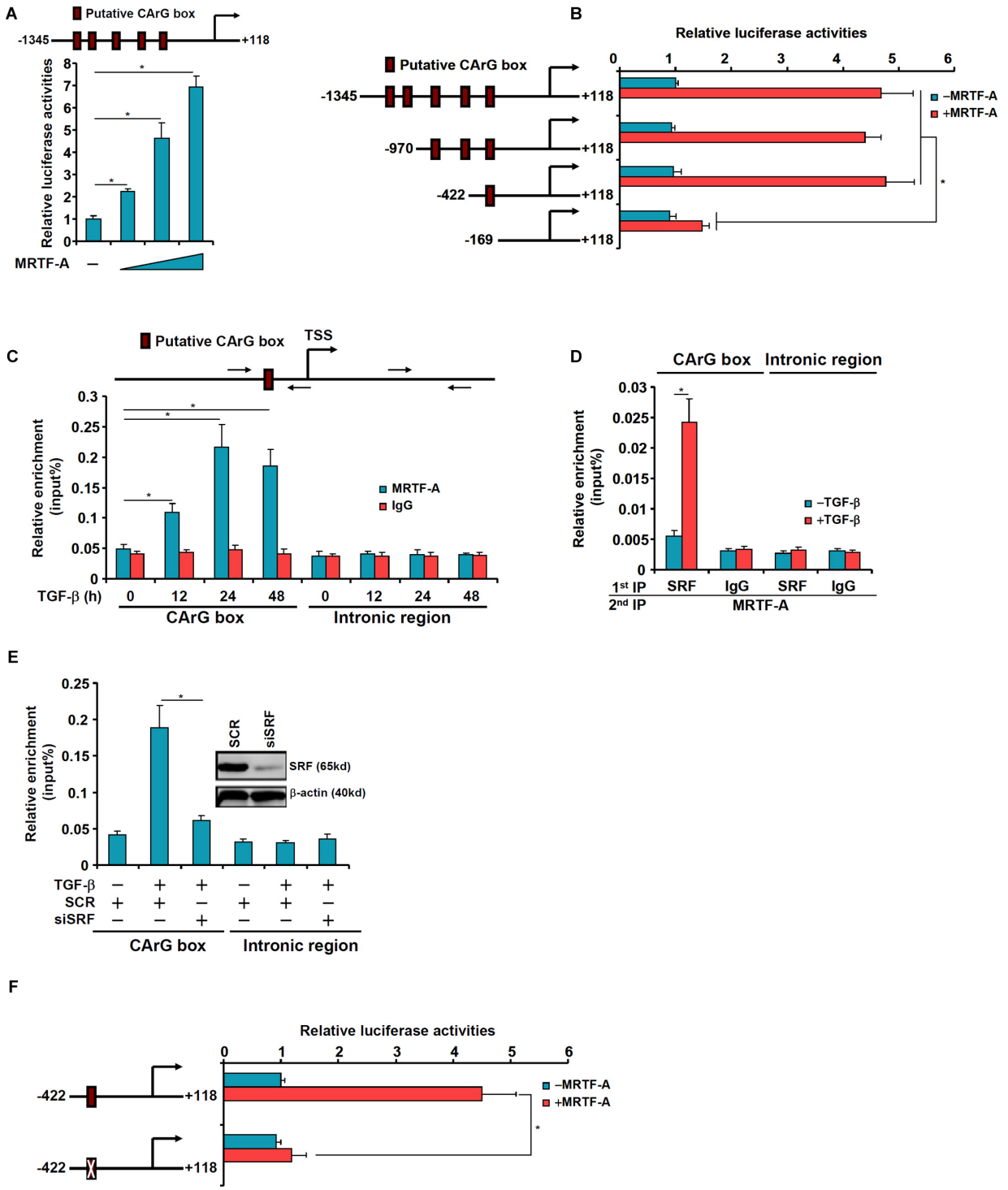

FIGURE 5 | MRTF-A directly activates EREG transcription. **(A)** A human EREG promoter-luciferase constructs (–1345/ + 118) were transfected into LX-2 cells with or without MRTF-A. Luciferase activities were normalized by protein concentration and GFP fluorescence. **(B)** Wild type or truncated EREG promoter-luciferase constructs were transfected transfected into LX-2 cells with or without MRTF-A. Luciferase activities were normalized by protein concentration and GFP fluorescence. **(C)** LX-2 cells were treated with or without TGF-β (5 ng/ml) and harvested at indicated time points. ChIP assays were performed with anti-MRTF-A or IgG. **(D)** LX-2 cells were treated with or without TGF-β (5 ng/ml) for 24 h. Re-ChIP assay was performed with indicated antibodies. **(E)** LX-2 cells were transfected with siRNA targeting SRF or scrambled siRNAs (SCR) followed by treatment with TGF-β (5 ng/ml) for 24 h. ChIP assays were performed with anti-MRTF-A. **(F)** Wild type or CArG mutated EREG promoter-luciferase construct were transfected into LX-2 cells with or without MRTF-A. Luciferase activities were normalized by protein concentration and GFP fluorescence.

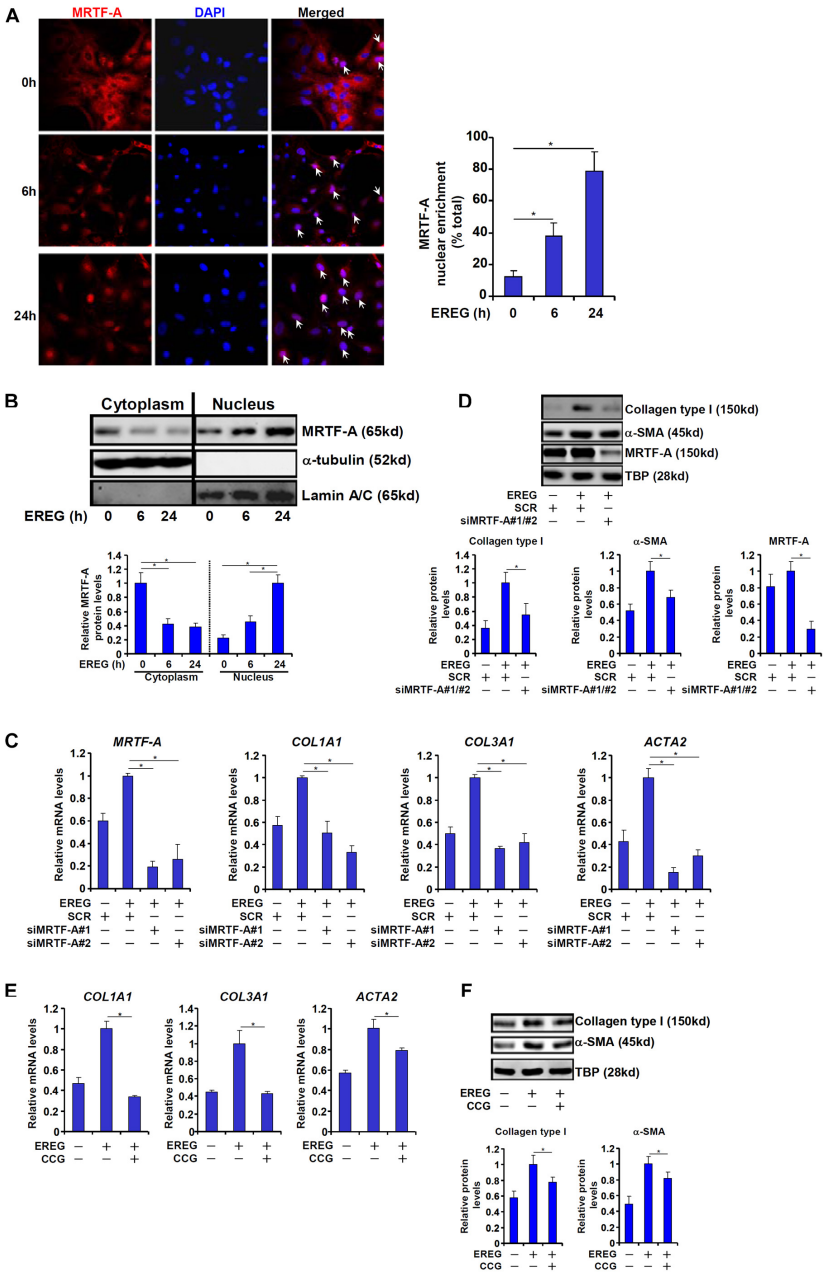

FIGURE 6 | EREG regulates HSC activation through MRTF-A. **(A)** LX-2 cells were treated with EREG (10 ng/ml) and harvested at indicated time points. MRTF-A localization was examined by immunofluorescence staining. **(B)** LX-2 cells were treated with EREG (10 ng/ml) and harvested at indicated time points. MRTF-A localization was examined by cell fractionation followed by Western blotting. Quantification was performed with Image Pro based on three independent experiments. **(C,D)** LX-2 cells were transfected with siRNAs targeting MRTF-A or scrambled siRNA (SCR) treated with recombinant EREG (10 ng/ml) for 24 h. Gene expression was examined by qPCR and Western. Quantification was performed with Image Pro based on three independent experiments. **(E,F)** LX-2 cells were treated with recombinant EREG (10 ng/ml) in the presence or absence of CCG for 24 h. Gene expression was examined by qPCR and Western. Quantification was performed with Image Pro based on three independent experiments.

Our data suggest that EREG promotes HSC activation at least in part by inducing MRTF-A nuclear translocation (**Figure 6**). Sub-cellular localization of MRTF-A is known to be regulated by its post-translational modifications. One of the best characterized modifications of MRTF-A is serine/threonine phosphorylation. The Treisman laboratory has systemically profiled the dynamic alteration of MRTF-A phosphorylation status in response to serum withdrawal/re-addition in fibroblasts uncovering a total of 26 putative S/T residues subjected to phosphorylation (Panayiotou et al., 2016). It is noteworthy that three out of the 26 sites, including S98, T545, and S549, are regulated by EGF stimulation in Hela cells (Olsen et al., 2006).

Whereas mutation of T545/S549 that renders the two sites unphosphorylatable did not impact the cytoplasm-nucleus shuttling of MRTF-A, S98 phosphorylation is critically required for its nuclear accumulation upon serum stimulation (Panayiotou et al., 2016). Thus, it is possible that EREG might promote MRTF-A nuclear translocation by inducing S98 phosphorylation. This hypothesis certainly deserves further investigation.

In summary, we report an epiregulin-MRTF-A feedforward loop that contributes to HSC activation. At least two issues need to be addressed in future studies. First, whether this feedforward loop is relevant *in vivo* needs to be verified in animal models of liver fibrosis. Second, the mechanism by which epiregulin regulates MRTF-A activity needs to explored in depth. The current data, however, do provide sufficient rationale for designing small-molecule compounds that can blockade this EREG-MRTF-A loop in the intervention of liver fibrosis.

DATA AVAILABILITY STATEMENT

The original contributions presented in the study are included in the article/**Supplementary Material**, further inquiries can be directed to the corresponding author/s.

ETHICS STATEMENT

The animal study was reviewed and approved by the Nanjing Medical University Ethics Committee on Humane Treatment of Experimental Animals.

AUTHOR CONTRIBUTIONS

XS and WZ conceived the project and secured funding and provided the supervision. XW, WD, and TZ designed the experiments. XW, WD, TZ, HR, JW, LS, and ZZ performed experiments and collected the data. YX wrote the manuscript. All authors contributed to the article and approved the submitted version.

FUNDING

This work was supported by the National Natural Science Foundation of China (81872359 and 81670566), Jiangsu Province's Key Provincial Talents Program (ZDRCA2016066), the Nanjing Medical Science and Technique Development Foundation (QRX17129), the Nanjing Health Science and Technology Development Project for Distinguished Young Scholars (JQX19002), the Nanjing Science and Technology Project (201911039), and Innovation and the Entrepreneurship Education Incubation Project of Nanjing University.

SUPPLEMENTARY MATERIAL

The Supplementary Material for this article can be found online at: https://www.frontiersin.org/articles/10.3389/fcell.2020.591246/full#supplementary-material

REFERENCES

Barry, A. E., Baldeosingh, R., Lamm, R., Patel, K., Zhang, K., Dominguez, D. A., et al. (2020). Hepatic Stellate Cells and Hepatocarcinogenesis. *Front. Cell. Dev. Biol.* 8:709. doi: 10.3389/fcell.2020.00709

Dong, W., Kong, M., Zhu, Y., Shao, Y., Wu, D., Lu, J., et al. (2020). Activation of TWIST Transcription by Chromatin Remodeling Protein BRG1 Contributes to Liver Fibrosis in Mice. *Front. Cell. Dev. Biol.* 8:340. doi: 10.3389/fcell.2020.00340

Fan, Z., Hao, C., Li, M., Dai, X., Qin, H., Li, J., et al. (2015). MKL1 is an epigenetic modulator of TGF-beta induced fibrogenesis. *Biochim. Biophys. Acta Gene. Regul. Mech.* 1849, 1219–1228. doi: 10.1016/j.bbagrm.2015.07.013

Fan, Z., Kong, M., Li, M., Hong, W., Fan, X., and Xu, Y. (2020). Brahma Related Gene 1 (Brg1) Regulates Cellular Cholesterol Synthesis by Acting as a Co-factor for SREBP2. *Front. Cell. Dev. Biol.* 8:259. doi: 10.3389/fcell.2020.00259

Fuchs, B. C., Hoshida, Y., Fujii, T., Wei, L., Yamada, S., Lauwers, G. Y., et al. (2014). Epidermal growth factor receptor inhibition attenuates liver fibrosis and development of hepatocellular carcinoma. *Hepatology* 59, 1577–1590. doi: 10.1002/hep.26898

Hou, W., and Syn, W. K. (2018). Role of Metabolism in Hepatic Stellate Cell Activation and Fibrogenesis. *Front. Cell. Dev. Biol.* 6:150. doi: 10.3389/fcell.2018.00150

Kisseleva, T. (2017). The origin of fibrogenic myofibroblasts in fibrotic liver. *Hepatology* 65, 1039–1043. doi: 10.1002/hep.28948

Kong, M., Chen, X., Lv, F., Ren, H., Fan, Z., Qin, H., et al. (2019a). Serum response factor (SRF) promotes ROS generation and hepatic stellate cell activation by epigenetically stimulating NCF1/2 transcription. *Redox Biol.* 26:101302. doi: 10.1016/j.redox.2019.101302

Kong, M., Hong, W., Shao, Y., Lv, F., Fan, Z., Li, P., et al. (2019b). Ablation of serum response factor in hepatic stellate cells attenuates liver fibrosis. *J. Mol. Med.* 97, 1521–1533. doi: 10.1007/s00109-019-01831-8

Kyotani, Y., Itaya-Hironaka, A., Yamauchi, A., Sakuramoto-Tsuchida, S., Makino, M., Takasawa, S., et al. (2018). Intermittent hypoxia-induced epiregulin expression by IL-6 production in human coronary artery smooth muscle cells. *FEBS Open Bio.* 8, 868–876. doi: 10.1002/2211-5463.12430

Law, A. J., Lipska, B. K., Weickert, C. S., Hyde, T. M., Straub, R. E., Hashimoto, R., et al. (2006). Neuregulin 1 transcripts are differentially expressed in schizophrenia and regulated by 5'. *SNPs associated with the disease. Proc. Natl. Acad. Sci. U S A.* 103, 6747–6752. doi: 10.1073/pnas.0602002103

Lee, D., Pearsall, R. S., Das, S., Dey, S. K., Godfrey, V. L., and Threadgill, D. W. (2004). Epiregulin is not essential for development of intestinal tumors but is required for protection from intestinal damage. *Mol. Cell. Biol.* 24, 8907–8916. doi: 10.1128/mcb.24.20.8907-8916.2004

Lee, Y. A., Wallace, M. C., and Friedman, S. L. (2015). Pathobiology of liver fibrosis: a translational success story. *Gut* 64, 830–841. doi: 10.1136/gutjnl-2014-306842

Li, N., Liu, S., Zhang, Y., Yu, L., Hu, Y., Wu, T., et al. (2020a). Transcriptional activation of matricellular protein Spondin2 (SPON2) by BRG1 in vascular endothelial cells promotes macrophage chemotaxis. *Front. Cell Dev. Biol.* 8:794. doi: 10.3389/fcell.2020.00794

Li, Z., Chen, B., Dong, W., Kong, M., Fan, Z., Yu, L., et al. (2019a). MKL1 promotes endothelial-to-mesenchymal transition and liver fibrosis by activating TWIST1 transcription. *Cell Death. Dis.* 10:899.

Li, Z., Li, P., Lu, Y., Sun, D., Zhang, X., and Xu, Y. (2019b). A non-autonomous role of MKL1 in the activation of hepatic stellate cells. *Biochim. Biophys. Acta Gene. Regul. Mech.* 1862, 609–618. doi: 10.1016/j.bbagrm.2019.03.001

Li, Z., Lv, F., Dai, C., Wang, Q., Jiang, C., Fang, M., et al. (2019c). Activation of galectin-3 (LGALS3) transcription by injurious stimuli in the liver is commonly

mediated by BRG1. *Front. Cell. Dev. Biol.* 7:310. doi: 10.3389/fcell.2019.00310

Li, Z., Zhang, Y., Yu, L., Xiao, B., Li, T., Kong, X., et al. (2020b). BRG1 Stimulates Endothelial Derived Alarmin MRP8 to Promote Macrophage Infiltration in an Animal Model of Cardiac Hypertrophy. *Front. Cell. Dev. Biol.* 8:569. doi: 10.3389/fcell.2020.00569

Liang, D., Chen, H., Zhao, L., Zhang, W., Hu, J., Liu, Z., et al. (2018). Inhibition of EGFR attenuates fibrosis and stellate cell activation in diet-induced model of nonalcoholic fatty liver disease. *Biochim. Biophys. Acta Mol. Basis Dis.* 1864, 133–142. doi: 10.1016/j.bbadis.2017.10.016

Lin, J., and Chen, A. (2008). Activation of peroxisome proliferator-activated receptor-gamma by curcumin blocks the signaling pathways for PDGF and EGF in hepatic stellate cells. *Lab. Invest.* 88, 529–540. doi: 10.1038/labinvest.2008.20

Lu, Y., Lv, F., Kong, M., Chen, X., Duan, Y., Sun, D., et al. (2019). A cAbl-MRTF-A Feedback Loop Contributes to Hepatic Stellate Cell Activation. *Front. Cell Dev. Biol.* 7:243. doi: 10.3389/fcell.2019.00243

Lv, F., Li, N., Kong, M., Wu, J., Miao, D., Ye, Q., et al. (2020). CDKN2a/p16 antagonizes hepatic stellate cell activation and liver fibrosis by modulating ROS levels. *Front. Cell. Dev. Biol.* 8:176. doi: 10.3389/fcell.2020.00176

Mao, L., Liu, L., Zhang, T., Qin, H., Wu, X., and Xu, Y. (2020a). Histone Deacetylase 11 Contributes to Renal Fibrosis by Repressing KLF15 Transcription. *Front. Cell. Dev. Biol.* 8:235. doi: 10.3389/fcell.2020.00235

Mao, L., Liu, L., Zhang, T., Wu, X., and Xu, Y. (2020b). MKL1 mediates TGF-beta-induced CTGF transcription to promote renal fibrosis. *J. Cell. Physiol.* 235, 4790–4803. doi: 10.1002/jcp.29356

Mederacke, I., Hsu, C. C., Troeger, J. S., Huebener, P., Mu, X., Dapito, D. H., et al. (2013). Fate tracing reveals hepatic stellate cells as dominant contributors to liver fibrosis independent of its aetiology. *Nat. Commun.* 4:2823.

Olsen, J. V., Blagoev, B., Gnad, F., Macek, B., Kumar, C., Mortensen, P., et al. (2006). Global, in vivo, and site-specific phosphorylation dynamics in signaling networks. *Cell* 127, 635–648. doi: 10.1016/j.cell.2006.09.026

Olson, E. N., and Nordheim, A. (2010). Linking actin dynamics and gene transcription to drive cellular motile functions. *Nat. Rev. Mol. Cell Biol.* 11, 353–365. doi: 10.1038/nrm2890

Panayiotou, R., Miralles, F., Pawlowski, R., Diring, J., Flynn, H. R., Skehel, M., et al. (2016). Phosphorylation acts positively and negatively to regulate MRTF-A subcellular localisation and activity. *Elife* 5:e15460.

Perugorria, M. J., Latasa, M. U., Nicou, A., Cartagena-Lirola, H., Castillo, J., Goni, S., et al. (2008). The epidermal growth factor receptor ligand amphiregulin participates in the development of mouse liver fibrosis. *Hepatology* 48, 1251–1261. doi: 10.1002/hep.22437

Riese, D. J. II, and Cullum, R. L. (2014). Epiregulin: roles in normal physiology and cancer. *Semin. Cell Dev. Biol.* 28, 49–56. doi: 10.1016/j.semcdb.2014.03.005

Scheving, L. A., Zhang, X., Threadgill, D. W., and Russell, W. E. (2016). Hepatocyte ERBB3 and EGFR are required for maximal CCl4-induced liver fibrosis. *Am. J. Physiol. Gastrointest Liver Physiol.* 311, G807–G816.

Small, E. M. (2012). The actin-MRTF-SRF gene regulatory axis and myofibroblast differentiation. *J. Cardiovasc. Transl. Res.* 5, 794–804. doi: 10.1007/s12265-012-9397-0

Stern, C., Schreier, B., Nolze, A., Rabe, S., Mildenberger, S., and Gekle, M. (2020). Knockout of vascular smooth muscle EGF receptor in a mouse model prevents obesity-induced vascular dysfunction and renal damage in vivo. *Diabetologia* 63, 2218–2234. doi: 10.1007/s00125-020-05187-4

Sun, L., Chen, B., Wu, J., Jiang, C., Fan, Z., Feng, Y., et al. (2020). Epigenetic regulation of a disintegrin and metalloproteinase (ADAM) promotes colorectal cancer cell migration and invasion. *Front. Cell Dev. Biol.* 8:581692. doi: 10.3389/fcell.2020.581692

Sun, Y., Boyd, K., Xu, W., Ma, J., Jackson, C. W., Fu, A., et al. (2006). Acute myeloid leukemia-associated Mkl1 (Mrtf-a) is a key regulator of mammary gland function. *Mol. Cell. Biol.* 26, 5809–5826. doi: 10.1128/mcb.00024-06

Takemura, T., Yoshida, Y., Kiso, S., Kizu, T., Furuta, K., Ezaki, H., et al. (2013). Conditional loss of heparin-binding EGF-like growth factor results in enhanced liver fibrosis after bile duct ligation in mice. *Biochem. Biophys. Res. Commun.* 437, 185–191. doi: 10.1016/j.bbrc.2013.05.097

Tian, W., Fan, Z., Li, J., Hao, C., Li, M., Xu, H., et al. (2016). Myocardin-related transcription factor A (MRTF-A) plays an essential role in hepatic stellate cell activation by epigenetically modulating TGF-beta signaling. *Int. J. Biochem. Cell Biol.* 71, 35–43. doi: 10.1016/j.biocel.2015.12.005

Tian, W., Hao, C., Fan, Z., Weng, X., Qin, H., Wu, X., et al. (2015). Myocardin related transcription factor A programs epigenetic activation of hepatic stellate cells. *J. Hepatol.* 62, 165–174. doi: 10.1016/j.jhep.2014.07.029

Wang, C., Li, Y., Li, H., Zhang, Y., Ying, Z., Wang, X., et al. (2020). Disruption of FGF Signaling Ameliorates Inflammatory Response in Hepatic Stellate Cells. *Front. Cell. Dev. Biol.* 8:601. doi: 10.3389/fcell.2020.00601

Wang, D. Z., Li, S., Hockemeyer, D., Sutherland, L., Wang, Z., Schratt, G., et al. (2002). Potentiation of serum response factor activity by a family of myocardin-related transcription factors. *Proc. Natl. Acad. Sci. U S A.* 99, 14855–14860. doi: 10.1073/pnas.222561499

Wee, P., and Wang, Z. (2017). Epidermal Growth Factor Receptor Cell Proliferation Signaling Pathways. *Cancers* 9:52. doi: 10.3390/cancers9050052

Wu, T., Wang, H., Xin, X., Yang, J., Hou, Y., Fang, M., et al. (2020). An MRTF-A-Sp1-PDE5 Axis Mediates Angiotensin-II-Induced Cardiomyocyte Hypertrophy. *Front. Cell Dev. Biol.* 8:839. doi: 10.3389/fcell.2020.00839

Yang, Y., Liu, L., Fang, M., Bai, H., and Xu, Y. (2019a). The chromatin remodeling protein BRM regulates the transcription of tight junction proteins: Implication in breast cancer metastasis. *Biochim. Biophys. Acta Gene. Regul. Mech.* 1862, 547–556. doi: 10.1016/j.bbagrm.2019.03.002

Yang, Y., Liu, L., Li, M., Cheng, X., Fang, M., Zeng, Q., et al. (2019b). The chromatin remodeling protein BRG1 links ELOVL3 trans-activation to prostate cancer metastasis. *Biochim. Biophys. Acta. Gene. Regul. Mech.* 1862, 834–845. doi: 10.1016/j.bbagrm.2019.05.005

Zhao, Q., Yang, J., Chen, H., Li, J., Que, L., Zhu, G., et al. (2019). Peli1 induction impairs cardiac microvascular endothelium through Hsp90 dissociation from IRE1alpha. *Biochim. Biophys. Acta Mol. Basis Dis.* 1865, 2606–2617. doi: 10.1016/j.bbadis.2019.06.017

Conflict of Interest: The authors declare that the research was conducted in the absence of any commercial or financial relationships that could be construed as a potential conflict of interest.

frontiers in Cell and Developmental Biology

MINI REVIEW
published: 11 March 2021
doi: 10.3389/fcell.2021.647311

Playing the Whack-A-Mole Game: ERK5 Activation Emerges Among the Resistance Mechanisms to RAF-MEK1/2-ERK1/2-Targeted Therapy

*Alessandro Tubita†, Ignazia Tusa† and Elisabetta Rovida**

Department of Experimental and Clinical Biomedical Sciences "Mario Serio", University of Florence, Florence, Italy

OPEN ACCESS

Edited by:
Matthias Gaestel,
Hannover Medical School, Germany

Reviewed by:
Patrick Thomas Flaherty,
Duquesne University, United States
Jurgen Muller,
University of Bradford,
United Kingdom
Jose M. Lizcano,
Universitat Autònoma de Barcelona,
Spain

***Correspondence:**
Elisabetta Rovida
elisabetta.rovida@unifi.it

† These authors have contributed equally to this work and share first authorship

Specialty section:
This article was submitted to Signaling, a section of the journal Frontiers in Cell and Developmental Biology

Received: *29 December 2020*
Accepted: *19 February 2021*
Published: *11 March 2021*

Citation:
Tubita A, Tusa I and Rovida E (2021) Playing the Whack-A-Mole Game: ERK5 Activation Emerges Among the Resistance Mechanisms to RAF-MEK1/2-ERK1/2-Targeted Therapy. Front. Cell Dev. Biol. 9:647311. doi: 10.3389/fcell.2021.647311

Molecularly tailored therapies have opened a new era, chronic myeloid leukemia being the ideal example, in the treatment of cancer. However, available therapeutic options are still unsatisfactory in many types of cancer, and often fail due to the occurrence of resistance mechanisms. With regard to small-molecule compounds targeting the components of the Mitogen-Activated Protein Kinase (MAPK) cascade RAF-MEK1/2-ERK1/2, these drugs may result ineffective as a consequence of the activation of compensatory pro-survival/proliferative signals, including receptor tyrosine kinases, PI3K, as well as other components of the MAPK family such as TPL2/COT. The MAPK ERK5 has been identified as a key signaling molecule in the biology of several types of cancer. In this review, we report pieces of evidence regarding the activation of the MEK5-ERK5 pathway as a resistance mechanism to RAF-MEK1/2-ERK1/2 inhibitors. We also highlight the known and possible mechanisms underlying the cross-talks between the ERK1/2 and the ERK5 pathways, the characterization of which is of great importance to maximize, in the future, the impact of RAF-MEK1/2-ERK1/2 targeting. Finally, we emphasize the need of developing additional therapeutically relevant MEK5-ERK5 inhibitors to be used for combined treatments, thus preventing the onset of resistance to cancer therapies relying on RAF-MEK1/2-ERK1/2 inhibitors.

Keywords: MAPK, ERK1/2/5, resistance mechanisms, combined therapy, targeted therapy, cancer

INTRODUCTION

The Mitogen-Activated Protein Kinase (MAPK) cascades are involved in a number of physiological processes and are activated by a large variety of stimuli. Conventional MAPKs include the four subfamilies of extracellular signal-regulated kinase 1 and 2 (ERK1/2), c-Jun N-terminal kinases 1–3, p38 α, β, γ, and δ, as well as ERK5. Atypical MAPKs have also been identified: ERK3, ERK4, ERK8 (also known as ERK7) and Nemo-like kinase (Cargnello and Roux, 2011).

Regarding the MAPK cascade culminating in ERK1/2 activation, a variety of mitogens activate receptor tyrosine kinases (RTKs) or G-protein-coupled receptors that, in turn, activate the small GTPase RAS proteins (K-RAS, H-RAS, or N-RAS) that are responsible for the recruitment of RAF kinases. Once activated, RAF-1 (also named c-RAF), ARAF or BRAF (Johnson and Lapadat, 2002;

Roux and Blenis, 2004; Kolch, 2005) phosphorylate at S/T residues and thus activate MEK1 and 2, that in turn, phosphorylate T and Y residues at the TEY sequence of ERK1/2, leading to its activation. Activated ERK1/2 phosphorylates many substrates, including transcription factors and protein kinases (Yoon and Seger, 2006). Subsequently, immediate early genes controlling cell proliferation are rapidly induced (Lewis et al., 1998). The RAS-RAF-MEK1/2-ERK1/2 pathway regulates multiple critical cellular functions including survival, proliferation and differentiation (Cargnello and Roux, 2011). The alteration of this pathway has been frequently reported in several types of cancer as a result of abnormal activation of RTKs or gain-of-function mutations mainly in the *RAS* or *RAF* genes. Accordingly, RAF-MEK1/2-ERK1/2 inhibitors are among the therapeutic options for the treatment of many types of cancers (Sebolt-Leopold and Herrera, 2004; Roberts and Der, 2007; Montagut and Settleman, 2009; Holderfield et al., 2014; Roskoski, 2018). Unfortunately, several resistance events have been reported, so that combined treatments are often needed and actively sought after (Little et al., 2013; Samatar and Poulikakos, 2014; Liu et al., 2018; Lee et al., 2020).

ERK5, the most recently identified MAPK, is the effector kinase of a typical three-tiered MAPK cascade (Lee et al., 1995; Zhou et al., 1995; Nithianandarajah-Jones et al., 2012). In response to several stimuli, the S/T kinases MEKK2 or MEKK3 activate MEK5, a dual specificity protein kinase active on ERK5. Once activated, MEK5 phosphorylates two residues at the TEY sequence of ERK5 and induces ERK5 nuclear translocation. Besides sharing high homology with ERK2 in the kinase domain and exhibiting in the activation loop a TEY motif identical to that of ERK1/2/8, ERK5 has a long C-terminal tail that is unique among all MAPK. The C-terminal tail includes a nuclear localization sequence (NLS) important for ERK5 nuclear targeting, two proline-rich (PR) domains (PR1 and PR2), which are considered potential binding sites for Src-homology 3 (SH3)-domain-containing proteins, a nuclear export sequence (NES) and a myocyte enhancer factor 2 (MEF2)-interacting region (Yan et al., 2001). The C-terminus of ERK5 also possesses a transcriptional activation domain (TAD) (Kasler et al., 2000) that undergoes autophosphorylation, thereby enabling ERK5 to directly regulate gene transcription (Morimoto et al., 2007). Known ERK5 substrates include the transcription factors Sap-1a, c-Fos, c-MYC, and MEF2 family members (A, C and D), as well as kinases such as the ribosomal s6 kinase and the serum/glucocorticoid-regulated kinase (Wang and Tournier, 2006; Nithianandarajah-Jones et al., 2012; Hoang et al., 2017). Despite mediating proliferation and differentiation signals similarly to ERK1/2, ERK5 emerged since its very discovery to have distinct roles with respect to ERK1/2, and to mediate signals which cannot be compensated for by other MAPKs (Cavanaugh et al., 2001; Nishimoto and Nishida, 2006). Accordingly, ERK5 null mice die early in their development (E9.5-10.5) because of severe defects in vasculature and cardiac development, pointing to a critical role of ERK5 in controlling angiogenesis, at least in mice (Hayashi and Lee, 2004). In normal cells, the MEK5-ERK5 pathway plays a central role in supporting cell survival, proliferation, differentiation, and motility, as well as in repressing apoptosis. Along this line, it is not surprising that there is increasing evidence regarding the involvement of this pathway in tumor development and progression (Stecca and Rovida, 2019). Based on that, targeting the MEK5-ERK5 pathway has clearly emerged among the possible strategies to reduce cancer growth (Simões et al., 2016; Hoang et al., 2017).

In this paper, we describe the accumulating lines of evidence pointing to ERK5 activation as a compensatory mechanism occurring upon RAF-MEK1/2-ERK1/2 inhibition, and determining *de facto* the resistance to therapeutic strategies based on this inhibition. ERK5 targeting should therefore be exploited to become part of new combination treatments capable of enhanced effectiveness against several types of cancer.

EVIDENCE FOR ERK5 ACTIVATION AS A RESISTANCE MECHANISM IN RAS-DRIVEN CANCERS

Because effective RAS-directed therapies are still lacking, targeting RAS-downstream signals such as MEK1/2 and/or ERK1/2 using small-molecule compounds is among the strategies used in RAS-driven cancer. However, MAPK inhibitors (MAPKi) are not very effective when used as single agents, due to intrinsic and/or acquired resistance toward ERK1/2i and/or MEK1/2i (Little et al., 2013; Samatar and Poulikakos, 2014; Dummer et al., 2017). In this respect, a number of papers have described the relevant role of MEK5-ERK5 pathway in the lack of effectiveness of MAPKi in RAS-driven cancer.

The first report shedding light on this important issue showed that the activation of the MEK5-ERK5 cascade conferred insensitivity to MEKi in intestinal epithelial cells (IEC) and in K-RAS-mutated colo-rectal carcinoma (CRC) cells (de Jong et al., 2016). ERK1/2 pathway appeared to be dispensable for IEC proliferation, and either ERK1/2 genetic deletion in primary IEC or treatment of human CRC cell lines with the MEK1/2 inhibitor PD0325901 led to compensatory activation of ERK5. The authors proposed a model in which, when the ERK1/2 module is intact, RAS-dependent signaling preferentially activates the RAF-MEK1/2-ERK1/2 cascade. In this context, ERK1/2-dependent negative feedback mechanisms stimulate dual specificity phosphatases (DUSPs) (Lake et al., 2016) that restrain the ERK5 pathway. On the other hand, upon MEK1/2 inhibition or genetic knockout of ERK1/2, this feedback is blocked, resulting in the upregulation of the RAS-RAF-MEK5-ERK5 module, which maintains IEC and CRC cell proliferation. Consistently, targeting both pathways caused a more effective suppression of cell proliferation in both murine intestinal organoids (genetic ERK1/2 inhibition plus ERK5 inhibitor XMD8-92) and human CRC cell lines (PD0325901 + XMD8-92) (de Jong et al., 2016).

Other evidences of the central role of MEK5-ERK5 in the resistance to MAPKi in RAS-driven cancers emerged in pancreatic ductal adenocarcinoma (PDAC), where K-RAS is mutated in 95% of cases (Waters and Der, 2018). Vaseva et al. (2018) found that the treatment of human PDAC cell

lines with the ERK1/2i SCH772984 led to compensatory phosphorylation/activation of the MEK5-ERK5 cascade. This activation promoted MYC protein stability as a consequence of phosphorylation at S62 by ERK5. Additionally, ERK1/2 inhibition caused a delayed increase in the phosphorylation of EGFR, HER2 and SRC, so that combined SCH772984/EGFRi (Poziotinib, Erlotinib) or SCH772984/SRCi (Saracatinib) prevented ERK5 phosphorylation. Based on all above, the authors proposed a model where ERK1/2 inhibition induces a EGFR/HER2/SRC-dependent feedforward activation of MEK5-ERK5, that prevents MYC degradation. Finally, concurrent inhibition of ERK5 (XMD8-92) and ERK1/2 (SCH772984) synergistically suppressed the growth of patient-derived PDAC xenografts. These results are of particular interest, as both RAS and MYC are very difficult to target directly (Dang et al., 2017).

K-RAS is the most commonly mutated member of the RAS family in non-small cell lung cancer (NSCLC) (Suzuki et al., 1990). MAPKi have proven ineffective in the treatment of NSCLC as much as in the other types of RAS-driven cancers (Carter et al., 2016; Jänne et al., 2017). Along this line, Dompe et al. (2018) found that the treatment of K-RAS-mutated NSCLC cell lines with the MEK1/2i Cobimetinib, that results in delayed activation of ERK1/2, increased ERK5 phosphorylation. Interestingly, ERK5 inhibition (XMD17-109) attenuated the re-activation of ERK1/2 signaling occurring upon MEK1/2 inhibition, pointing to a prominent role of ERK5 in mediating ERK1/2 reactivation upon MEK1/2 targeting. Finally, the combination of Cobimetinib (MEK1/2i) with the genetic knockdown of *MAPK7*, the gene encoding for ERK5, resulted more effective than single treatments in reducing the growth of K-RAS-mutated NSCLC xenografts (Dompe et al., 2018).

Advanced stage cutaneous melanoma is a highly malignant tumor characterized by somatic mutations of a number of oncogenes involved in the RAS-RAF-MEK1/2-ERK1/2 pathway, including N-RAS or BRAF, that lead to uncontrolled proliferation. MAPK pathway-targeting regimens are a valuable treatment option for BRAF-mutated melanoma (Luke et al., 2017; Ugurel et al., 2017). Unfortunately, patients with N-RAS mutation (around 20% of cases, e.g., N-RAS-Q61K/L) (Schadendorf et al., 2015) do not benefit from such therapies, owing to the lack of targetable BRAF mutations and a high degree of intrinsic and acquired resistance to MEK1/2 inhibition (Dummer et al., 2017). In keeping with a possible involvement of ERK5 in MAPKi resistance in N-RAS-mutated melanomas, a recent report showed that the treatment with MEK1/2i (Trametinib, Binimetinib, Selumetinib, or Cobimetinib) or ERK1/2i (GDC-0994; Robarge et al., 2014) determined a delayed activation of ERK5 through a PDGFRi-sensitive pathway (Adam et al., 2020). Combined MEK5-ERK5 co-targeting using Trametinib + XMD8-92 or Trametinib + ERK5 genetic inhibition (shRNA) prevented long-term growth *in vitro*, thus supporting the relevance of ERK5 in the proliferation and survival of N-RAS-mutated melanoma cells upon MEK1/2-ERK1/2 inhibition. More importantly, Trametinib + XMD8-92 effectively repressed the growth of N-RAS-mutated melanoma xenografts. Therefore, these data demonstrated that MEK1/2i + ERK5i co-treatment could improve the effectiveness of available MEK1/2i therapies in N-RAS-mutated melanoma patients (Adam et al., 2020).

EVIDENCE FOR ERK5 ACTIVATION AS A RESISTANCE MECHANISM IN BRAF-DRIVEN CANCERS

Mutated BRAF is responsible for ERK1/2 pathway activation in above 50% of patients with advanced melanoma (Davies et al., 2002; Flaherty et al., 2012). Unfortunately, BRAFi monotherapy (i.e., using the BRAFV600Ei Vemurafenib) frequently fails as a consequence of a resistance mechanism which leads to ERK1/2 pathway reactivation (Hauschild et al., 2012; Shi et al., 2014; Van Allen et al., 2014). To overcome this resistance, combined inhibition of BRAF and MEK1/2 (CIBM) is among the current approaches used in melanoma patients harboring BRAF-activating mutations (Larkin et al., 2014; Long et al., 2014). However, resistance to CIBM can be also developed, and represents a major obstacle to the long-term clinical benefit of therapy (Samatar and Poulikakos, 2014). A recent report showed that ERK5 phosphorylation is enhanced in BRAF-mutated melanoma cells resistant to CIBM (Song et al., 2017). The demonstration that ERK5 activation is associated with this resistance was achieved showing that either genetic (shRNA) or pharmacological (XMD8-92) ERK5 inhibition impaired the acquisition of resistance to CIBM and sensitized resistant cancer cells to Vemurafenib and/or Trametinib, restoring the anti-proliferative effect of the latter. The activating phosphorylation of ERK5 in response to CIBM therapy seemed to be sustained by a SRC/MEK5 cascade. Consistently, either CIBM + XMD8-92 or CIBM + SRCi (Dasatinib) were more effective than CIBM alone in reducing the growth of BRAF-mutated melanoma xenografts, and showed the same effects as CIBM + XMD8-92 + Dasatinib. In the same paper, the authors proposed that BRAF could be responsible for SRC activation, thus positioning BRAF upstream of ERK5 in CIBM-resistant cells (Song et al., 2017). A later work further supported the key role of ERK5 in MAPKi resistance in BRAF-mutated melanoma (Benito-Jardón et al., 2019). Indeed, besides confirming the activation of ERK5 upon CIBM, it was shown that melanoma cells double-resistant to either Vemurafenib and Trametinib or to Vemurafenib and SCH772984 (Morris et al., 2013) displayed enhanced IGF-1R expression and kinase activity, as well as increased IGF-1R-dependent MEK5-ERK5 activation. Consistently, inhibition of IGF-1R with Linsitinib reduced the proliferation of SCH772984-resistant cells, and prevented the activation of ERK5 in CIBM- or Vemurafenib/SCH772984-resistant cells. In the latter, Linsitinib decreased the growth of spheroids in 3D cultures as well as in xenografts in NOD/SCIDgamma mice (Benito-Jardón et al., 2019). Finally, a recent work identified an additional mechanism linking ERK5 to MAPKi resistance in BRAFV600E-mutated melanoma cells (Lee et al., 2020). In the study, the authors showed that the treatment of BRAFV600E-mutated melanoma cell lines with Cobimetinib or Vemurafenib resulted in the increase of ERK5 phosphorylation, and demonstrated that this effect was

mediated by Mir-211. In particular, the increased expression of Mir-211 upon Cobimetinib or Vemurafenib treatment was responsible for the inhibition of the expression of DUSP6, that resulted in ERK5 increased phosphorylation. Interestingly, DUSP6 overexpression prevented the increase in tumor growth occurring upon overexpression of Mir-211 in BRAFV600E-mutated melanoma xenografts. Consistent with a role for ERK5 in Mir-211 overexpressing cells, treatment with XMD8-92 or the MEK5 inhibitor BIX02189 reduced the proliferation of melanoma cells overexpressing Mir-211 (Lee et al., 2020). All above led to definitely include the ERK5 pathway among those involved in resistance to MAPKi in BRAFV600E-mutated melanoma cells.

EVIDENCE FOR ERK5 ACTIVATION AS A RESISTANCE MECHANISM IN ALK-DRIVEN CANCERS

The compensatory activation of ERK5 upon MEK1/2 targeting has also been reported in anaplastic lymphoma kinase (ALK)-addicted neuroblastoma cells (Umapathy et al., 2017). In this

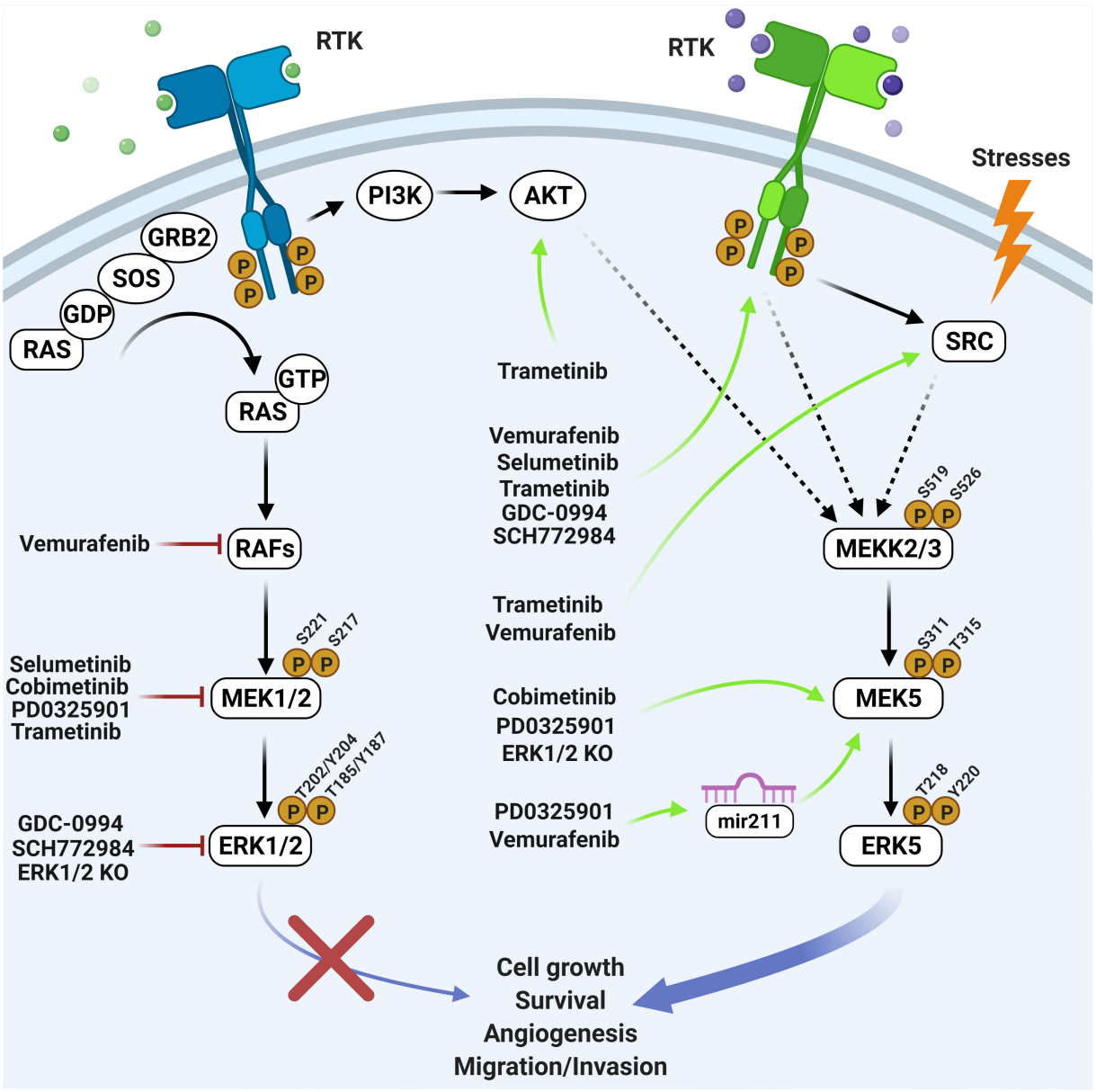

FIGURE 1 | Overview of the effects elicited by RAF-MEK1/2-ERK1/2 inhibitors on the MEK5-ERK5 pathway. Black arrows indicate direct activation mechanisms. Dashed arrows indicate demonstrated but not direct mechanisms. Red lines indicate inhibiting treatments. Green arrows indicate resistance mechanisms occurring upon genetic or pharmacological inhibition of the ERK1/2 pathway (created with Biorender.com).

study, the authors found that the growth of N-RAS-mutated neuroblastoma cell lines and xenografts is sensitive to MEK1/2-targeting therapy, while that of ALK-addicted neuroblastoma cells and xenografts is not. Interestingly, ALK-addicted neuroblastoma cells treated with the MEK1/2i Trametinib showed an increased phosphorylation/activation of the AKT and ERK5 kinases, that the authors proposed to be responsible for a compensatory mechanism supporting cell proliferation. On the basis of a previous report from the same group, the activation of ERK5 in ALK-addicted neuroblastoma cells was proposed to be due to the PI3K-AKT-MEKK3-MEK5 axis (Umapathy et al., 2014). Overall, these studies suggest that ERK5 pathway inhibition in combination with MEKi might be regarded as a potential therapeutic strategy in ALK-addicted neuroblastoma (Umapathy et al., 2017).

DEMONSTRATED AND POSSIBLE MECHANISMS OF ERK5 ACTIVATION UPON RAF-MEK1/2-ERK1/2 TARGETING

The above studies demonstrated the existence of a number of mechanisms responsible for MEK5-ERK5 activation following BRAF-MEK1/2-ERK1/2 inhibition (**Figure 1**). One of these mechanisms involved the increased expression of RTKs (Umapathy et al., 2017; Vaseva et al., 2018; Benito-Jardón et al., 2019; Adam et al., 2020). Additionally, as ERK1/2 activation may trigger a negative feedback directed to prevent an excessive level of activation of upstream activators, the pharmacological inhibition of ERK1/2 lead to loss of this feedback, resulting in a feedforward activation of RTKs (Lake et al., 2016) such as EGFR (Duncan et al., 2012; Lito et al., 2012). Both increased expression and activation of RTK resulted to be sufficient to activate MEK5-ERK5. Furthermore, the suppression of the above negative feedback elicited the activation of PI3K-AKT, leading to the subsequent increase of ERK5 signaling (Umapathy et al., 2014, 2017). Interestingly, even stronger evidence has been obtained that ERK5 activation itself leads to the activation of AKT (Lennartsson et al., 2010; Roberts et al., 2010; Bin et al., 2016), which in turn could strengthen the pro-survival role of ERK5 signaling in a context of resistance to treatment (Bera et al., 2014). Additional negative feedback mechanisms elicited by ERK1/2 involved DUSPs activation (Sarkozi et al., 2007). DUSPs prevented ERK5 phosphorylation, so that when MEK1/2-ERK1/2 is inhibited DUSPs inactivation resulted in enhanced

TABLE 1 | Cancer specific ERK5-activating resistance mechanisms following RAF-MEK1/2-ERK1/2 targeting.

Cancer type	Genomic alteration supporting ERK1/2 pathway activation	Ineffective targeting (pharmacological/ genetic inhibition)	ERK5-activating resistance mechanism	Effective combined targeting strategies	References
Colorectal cancer	K-RAS mutation	MEK1/2 (PD0325901) or ERK1/2 (KO)	Increased phosphorylation/activation of ERK5 likely due to DUSP deregulation	MEK1/2i + ERK5i (*in vitro*)	de Jong et al., 2016
Neuroblastoma	ALK mutation/amplification	MEK1/2 (Trametinib)	Increased activation of AKT-ERK5 signaling	MEK1/2i + ERK5i or AKTi (proposed)	Umapathy et al., 2017
Pancreatic ductal adenocarcinoma	K-RAS mutation	MEK1/2 (Selumetinib, Trametinib); ERK1/2 (SCH772984)	Upregulation of EGFR-SRC-ERK5 pathway	ERK1/2i + ERK5i (*in vivo*)	Vaseva et al., 2018
Non-small-cell lung carcinoma	K-RAS mutation	MEK1/2 (Cobimetinib)	Increased phosphorylation/activation of ERK5 likely dependent on RTKs	MEK1/2i + ERK5i or ERK5-KO (*in vitro*) or ERK5-KD (*in vitro* and *in vivo*)	Dompe et al., 2018
Melanoma	N-RAS mutation	MEK1/2 (Trametinib); ERK1/2 (GDC-0994)	Increased phosphorylation/activation of ERK5 likely dependent on PDGFRβ	ERK1/2i + ERK5i (*in vitro*); MEK1/2i + ERK5i (*in vitro* and *in vivo*)	Adam et al., 2020
Melanoma	BRAF mutation	BRAF + MEK1/2 (Vemurafenib + Trametinib)	Increased phosphorylation/activation of ERK5 mediated by SRC-MEK5 cascade	BRAFi/MEK1/2i + ERK5-KD (*in vitro*) or ERK5i (*in vitro* and *in vivo*)	Song et al., 2017
Melanoma	BRAF mutation	BRAF + MEK1/2 (Vemurafenib + Trametinib); BRAF + ERK1/2 (Vemurafenib + SCH772984)	Upregulation of IGF1R-MEK5-ERK5 pathway	ERK1/2i + IGF1Ri (*in vivo*)	Benito-Jardón et al., 2019
Melanoma	BRAF mutation	BRAF (Vemurafenib); MEK1/2 (PD0325901)	Increased phosphorylation/activation of ERK5 mediated by miR-211		Lee et al., 2020

KO, knock-out; KD, knock-down (shRNA).

ERK5 phosphorylation (de Jong et al., 2016). Along this line, DUSP6/MKP-3, initially reported to inactivate ERK1/2 but not ERK5 (Arkell et al., 2008), has been recently shown to participate in ERK5 activation following ERK1/2 pathway inhibition (Lee et al., 2020).

Besides the already elucidated mechanisms listed above, other compensatory processes underlying treatment resistance may occur upon RAF-MEK1/2-ERK1/2 targeting (Samatar and Poulikakos, 2014) and be mediated by upstream ERK5 activators (Stecca and Rovida, 2019). Among the latter, the MAP3K TPL2/COT (Chiariello et al., 2000) has been associated with *de novo* resistance to MEK1/2i or BRAFV600Ei in BRAF-mutated melanomas (Johannessen et al., 2010). Another possible mechanism may involve RAF-1, an additional possible ERK5 activator (English et al., 1999), the overexpression of which has been linked to acquired resistance to MAPKi (Samatar and Poulikakos, 2014). Additionally, BRAF, that may be amplified as a resistance mechanism to RAF-MEK1/2-ERK1/2 targeting (Samatar and Poulikakos, 2014), as well as BRAFV600E, has been recently demonstrated to activate ERK5 (Tusa et al., 2018). In support to the appropriateness of the dual targeting of the ERK5 and ERK1/2 pathways, in the same paper we showed that the combination Vemurafenib + XMD8-92 was more effective than either drug alone in reducing the growth of BRAF-mutated melanoma xenografts. Furthermore, Vemurafenib + XMD8-92 was necessary to reduce the amount of nuclear ERK5 (Tusa et al., 2018), which is critical for the support of cell proliferation (Raviv et al., 2004; Buschbeck and Ullrich, 2005; Iñesta-Vaquera et al., 2010; Gomez et al., 2016). Finally, CDK5, that plays a relevant role in tumorigenesis (Goodyear and Sharma, 2007; Eggers et al., 2011; Pozo et al., 2013), has been recently demonstrated to activate ERK5 (Zhuang et al., 2016). Because several reports have shown that CDK5 and ERK1/2 regulate each other, so that their activities may be inversely correlated (Sharma et al., 2002; Zheng et al., 2007; Banks et al., 2015), we may speculate that CDK5 may determine ERK5 activation upon ERK1/2 pathway inhibition.

CONCLUDING REMARKS

Members of conventional MAPK pathways are among the most sought-after oncogenic effectors for the development of novel strategies to treat cancer (Kim and Choi, 2010; Braicu et al., 2019). Despite the fact that the MEK5-ERK5 pathway has been the less-studied of MAPK cascades, several lines of evidence pinpointed its relevance in cancer biology (Simões et al., 2016; Stecca and Rovida, 2019; Tubita et al., 2020). Furthermore, the literature summarized in this paper highlights the involvement of MEK5-ERK5 activation as a compensatory/resistance mechanism to RAF-MEK1/2-ERK1/2 targeting (**Table 1**). However, the mechanisms underlying the cross-talk between the ERK1/2 and the ERK5 pathways have not been fully elucidated, so that they should be further explored in the future in order to reinforce the rationale for a combined targeting of ERK1/2 and ERK5 pathways in order to achieve a more effective response in RAS-RAF-MEK1/2-ERK1/2-addicted cancer.

Many small-molecule compounds targeting ERK5 (including XMD8-92, XMD17-109, JWG-071, AX15836, BAY-885) or MEK5 (BIX02188, BIX02189) have been developed (Tatake et al., 2008; Yang et al., 2010; Deng et al., 2013; Lin et al., 2016; Wang et al., 2018; Nguyen et al., 2019) and exhibited remarkable effects in reducing the growth of human tumor xenografts in mice. Recently, an orally bioactive ERK5 inhibitor (Compound 46) was developed (Myers et al., 2016). However, it is worth point out that the off-target effects of XMD8-92 and derivatives (Deng et al., 2013; Wang et al., 2018) on BRD4 (Lin et al., 2016; Williams et al., 2016) certainly hampered the interpretation of the results obtained with these compounds, unless a genetic approach was provided to support the data obtained via drug treatment. On the other hand, some ERK5i (i.e., XMD17-109 and AX15836) cause a conformational change in the ERK5 kinase domain which leads to the exposure of the C-terminal NLS and to a paradoxical activation of the ERK5 TAD (Lochhead et al., 2020), enabling ERK5 to regulate its downstream targets. None of these inhibitors, however, has been tested in humans so far. TG02, a dual ERK5/CDK inhibitor, has been tested in clinical trials for hematological malignancies following the promising results obtained in preclinical studies (Alvarez-Fernandez et al., 2013; Ortiz-Ruiz et al., 2014). Based on all above, concerted efforts should be pursued to develop therapeutically suitable MEK5-ERK5 inhibitors. Indeed, besides representing a promising strategy for cancer treatment *per se*, ERK5 pathway inhibition should be exploited to prevent acquired resistance in cancers where inhibition of the RAS-RAF-MEK1/2-ERK1/2 cascade represents a valuable therapeutic option.

AUTHOR CONTRIBUTIONS

ER conceptualized this review. AT, IT, and ER wrote and revised the manuscript. All authors approved the final version of the manuscript.

FUNDING

The work in ER's lab was supported by grants from the Associazione Italiana per la Ricerca sul Cancro, AIRC (IG-15282 and IG-21349), by the Ente Fondazione Cassa di Risparmio di Firenze (ECRF), and the Università degli Studi di Firenze (Fondo di Ateneo ex-60%). AT was supported by a "Carlo Zanotti" FIRC-AIRC fellowship (ID-23847).

ACKNOWLEDGMENTS

We are grateful to Persio Dello Sbarba for carefully discussing the content of the manuscript and for revising the English.

REFERENCES

Adam, C., Fusi, L., Weiss, N., Goller, S. G., Meder, K., Frings, V. G., et al. (2020). Efficient suppression of NRAS-driven melanoma by Co-inhibition of ERK1/2 and ERK5 MAPK pathways. *J. Invest. Dermatol.* 140, 2455–2465. doi: 10.1016/j.jid.2020.03.972

Alvarez-Fernandez, S., Ortiz-Ruiz, M. J., Parrott, T., Zaknoen, S., Ocio, E. M., San Miguel, J., et al. (2013). Potent antimyeloma activity of a novel ERK5/CDK inhibitor. *Clin. Cancer Res.* 19, 2677–2687. doi: 10.1158/1078-0432.CCR-12-2118

Arkell, R. S., Dickinson, R. J., Squires, M., Hayat, S., Keyse, S. M., Cook, S. J. (2008). DUSP6/MKP-3 inactivates ERK1/2 but fails to bind and inactivate ERK5. *Cell Signal.* 20, 836-843. doi: 10.1016/j.cellsig.2007.12.014

Banks, A. S., McAllister, F. E., Camporez, J. P., Zushin, P. J., Jurczak, M. J., Laznik-Bogoslavski, D., et al. (2015). An ERK/Cdk5 axis controls the diabetogenic actions of PPARgamma. *Nature* 517, 391–395. doi: 10.1038/nature13887

Benito-Jardón, L., Díaz-Martínez, M., Arellano-Sánchez, N., Vaquero-Morales, P., Esparís-Ogando, A., and Teixidó, J. (2019). Resistance to MAPK inhibitors in melanoma involves activation of the IGF-1R-MEK5-Erk5 pathway. *Cancer Res.* 79, 2244–2256. doi: 10.1158/0008-5472.CAN-18-2762

Bera, A., Das, F., Ghosh-Choudhury, N., Li, X., Pal, S., Gorin, Y., et al. (2014). A positive feedback loop involving Erk5 and Akt turns on mesangial cell proliferation in response to PDGF. *Am. J. Physiol. Cell Physiol*. 306, C1089–C1100. doi: 10.1152/ajpcell.00387.2013

Bin, G., Bo, Z., Jing, W., Jin, J., Xiaoyi, T., Cong, C., et al. (2016). Fluid shear stress suppresses TNF-α-induced apoptosis in MC3T3-E1 cells: involvement of ERK5-AKT-FoxO3a-Bim/FasL signaling pathways. *Exp. Cell Res.* 343, 208–217. doi: 10.1016/j.yexcr.2016.03.014

Braicu, C., Buse, M., Busuioc, C., Drula, R., Gulei, D., Raduly, L., et al. (2019). A comprehensive review on MAPK: a promising therapeutic target in cancer. *Cancers (Basel)* 11:1618. doi: 10.3390/cancers11101618

Buschbeck, M., and Ullrich, A. (2005). The unique C-terminal tail of the mitogen-activated protein kinase ERK5 regulates its activation and nuclear shuttling. *J. Biol. Chem*. 280, 2659–2667. doi: 10.1074/jbc.M412599200

Cargnello, M., and Roux, P. P. (2011). Activation and function of the MAPKs and their substrates, the MAPK-activated protein kinases. *Microbiol. Mol. Biol. Rev.* 75, 50–83. doi: 10.1128/MMBR.00031-10

Carter, C. A., Rajan, A., Keen, C., Szabo, E., Khozin, S., Thomas, A., et al. (2016). Selumetinib with and without erlotinib in KRAS mutant and KRAS wild-type advanced nonsmall-cell lung cancer. *Ann. Oncol.* 27, 693–699. doi: 10.1093/annonc/mdw008

Cavanaugh, J. E., Ham, J., Hetman, M., Poser, S., Yan, C., and Xia, Z. (2001). Differential regulation of mitogen-activated protein kinases ERK1/2 and ERK5 by neurotrophins, neuronal activity, and cAMP in neurons. *J. Neurosci.* 21, 434–443. doi: 10.1523/JNEUROSCI.21-02-00434.2001

Chiariello, M., Marinissen, M. J., and Gutkind, J. S. (2000). Multiple mitogen-activated protein kinase signaling pathways connect the cot oncoprotein to the c-jun promoter and to cellular transformation. *Mol. Cell. Biol.* 20, 1747–1758.

Dang, C. V., Reddy, E. P., Shokat, K. M., and Soucek, L. (2017). Drugging the 'undruggable' cancer targets. *Nat. Rev. Cancer* 17, 502–508. doi: 10.1038/nrc.2017.36Review

Davies, H., Bignell, G. R., Cox, C., Stephens, P., Edkins, S., Clegg, S., et al. (2002). Mutations of the BRAF gene in human cancer. *Nature* 417, 949–954. doi: 10.1038/nature00766

de Jong, P. R., Taniguchi, K., Harris, A. R., Bertin, S., Takahashi, N., Duong, J., et al. (2016). ERK5 signalling rescues intestinal epithelial turnover and tumour cell proliferation upon ERK1/2 abrogation. *Nat. Commun.* 7:11551. doi: 10.1038/ncomms11551

Deng, X., Elkins, J. M., Zhang, J., Yang, Q., Erazo, T., Gomez, N., et al. (2013). Structural determinants for ERK5 (MAPK7) and leucine rich repeat kinase 2 activities of benzo[e]pyrimido-[5,4-b]diazepine-6(11H)-ones. *Eur. J. Med. Chem.* 70, 758–767. doi: 10.1016/j.ejmech.2013.10.052

Dompe, N., Klijn, C., Watson, S. A., Leng, K., Port, J., Cuellar, T., et al. (2018). A CRISPR screen identifies MAPK7 as a target for combination with MEK inhibition in KRAS mutant NSCLC. *PLoS One* 13:e0199264. doi: 10.1371/journal.pone.0199264

Dummer, R., Schadendorf, D., Ascierto, P. A., Arance, A., Dutriaux, C., Di Giacomo, A. M., et al. (2017). Binimetinib versus dacarbazine in patients with advanced NRAS-mutant melanoma (NEMO): a multicentre, open-label, randomised, phase 3 trial. *Lancet Oncol.* 18, 435–445. doi: 10.1016/S1470-2045(17)30180-8

Duncan, J. S., Whittle, M. C., Nakamura, K., Abell, A. N., Midland, A. A., Zawistowski, J. S., et al. (2012). Dynamic reprogramming of the kinome in response to targeted MEK inhibition in triple-negative breast cancer. *Cell* 149, 307–321. doi: 10.1016/j.cell.2012.02.053

Eggers, J. P., Grandgenett, P. M., Collisson, E. C., Lewallen, M. E., Tremayne, J., Singh, P. K., et al. (2011). Cyclin-dependent kinase 5 is amplified and overexpressed inpancreatic cancer and activated by mutant K-Ras. *Clin. Cancer Res.* 17, 6140–6150. doi: 10.1158/1078-0432.CCR-10-2288

English, J. M., Pearson, G., Hockenberry, T., Shivakumar, L., White, M. A., and Cobb, M. H. (1999). Contribution of the ERK5/MEK5 pathway to Ras/Raf signaling and growth control. *J. Biol. Chem.* 274, 31588–31592. doi: 10.1074/jbc.274.44.31588

Flaherty, K. T., Hodi, F. S., and Fisher, D. E. (2012). From genes to drugs: targeted strategies for melanoma. *Nat. Rev.* 12, 349–361. doi: 10.1038/nrc3218

Gomez, N., Erazo, T., and Lizcano, J. M. (2016). ERK5 and cell proliferation: nuclear localization is what matters. *Front. Cell Dev. Biol.* 4:105. doi: 10.3389/fcell.2016.00105

Goodyear, S., and Sharma, M. C. (2007). Roscovitine regulates invasive breast cancer cell (MDA-MB231) proliferation and survival through cell cycle regulatory protein cdk5. *Exp. Mol. Pathol.* 82, 25–32. doi: 10.1016/j.yexmp.2006.09.002

Hauschild, A., Grob, J. J., Demidov, L. V., Jouary, T., Gutzmer, R., Millward, M., et al. (2012). Dabrafenib in BRAF-mutated metastatic melanoma: a multicentre, open label, phase 3 randomised controlled trial. *Lancet* 380, 358–365. doi: 10.1016/S0140-6736(12)60868-X

Hayashi, M., and Lee, J. D. (2004). Role of the BMK1/ERK5 signaling pathway: lessons from knockout mice. *J. Mol. Med.* 82, 800–808. doi: 10.1007/s00109-004-0602-8

Hoang, V. T., Yan, T. J., Cavanaugh, J. E., Flaherty, P. T., Beckman, B. S., and Burow, M. E. (2017). Oncogenic signaling of MEK5-ERK5. *Cancer Lett.* 392, 51–59. doi: 10.1016/j.canlet.2017.01.034

Holderfield, M., Deuker, M. M., McCormick, F., and McMahon, M. (2014). Targeting RAF kinases for cancer therapy: BRAF-mutated melanoma and beyond. *Nat. Rev. Cancer* 14, 455–467. doi: 10.1038/nrc3760

Iñesta-Vaquera, F. A., Campbell, D. G., Tournier, C., Gómez, N., Lizcano, J. M., and Cuenda, A. (2010). Alternative ERK5 regulation by phosphorylation during the cell cycle. *Cell Signal.* 22, 1829–1837. doi: 10.1016/j.cellsig.2010.07.010

Jänne, P. A., van den Heuvel, M. M., Barlesi, F., Cobo, M., Mazieres, J., Crinò, L., et al. (2017). Selumetinib plus docetaxel compared with docetaxel alone and progression-free survival in patients With KRAS-mutant advanced non-small cell lung cancer: the SELECT-1 randomized clinical trial. *JAMA* 317, 1844–1853. doi: 10.1001/jama.2017.3438

Johannessen, C. M., Boehm, J. S., Kim, S. Y., Thomas, S. R., Wardwell, L., Johnson, L. A., et al. (2010). COT drives resistance to RAF inhibition through MAP kinase pathway reactivation. *Nature* 468, 968–972. doi: 10.1038/nature09627

Johnson, G. L., and Lapadat, R. (2002). Mitogen-activated protein kinase pathways mediated by ERK, JNK, and p38 protein kinases. *Science* 298, 1911–1912. doi: 10.1126/science.1072682

Kasler, H. G., Victoria, J., Duramad, O., and Winoto, A. (2000). ERK5 is a novel type of mitogen-activated protein kinase containing a transcriptional activation domain. *Mol. Cell. Biol.* 20, 8382–8389.

Kim, E. K., and Choi, E. J. (2010). Pathological roles of MAPK signaling pathways in human diseases. *Biochim. Biophys. Acta* 1802, 396–405. doi: 10.1016/j.bbadis.2009.12.009

Kolch, W. (2005). Coordinating ERK/MAPK signalling through scaffolds and inhibitors. *Nat. Rev. Mol. Cell Biol.* 6, 827–837. doi: 10.1038/nrm1743

Lake, D., Corrêa, S. A., and Müller, J. (2016). Negative feedback regulation of the ERK1/2 MAPK pathway. *Cell. Mol. Life Sci.* 73, 4397–4413. doi: 10.1007/s00018-016-2297-8

Larkin, J., Ascierto, P. A., Dréno, B., Atkinson, V., Liszkay, G., Maio, M., et al. (2014). Combined vemurafenib and cobimetinib in BRAF-mutated melanoma. *N. Engl. J. Med.* 371, 1867–1876. doi: 10.1056/NEJMoa1408868

Lee, B., Sahoo, A., Sawada, J., Marchica, J., Sahoo, S., Layng, F. I. A. L., et al. (2020). MicroRNA-211 modulates the DUSP6-ERK5 signaling axis to promote

BRAFV600E-driven melanoma growth in vivo and BRAF/MEK inhibitor resistance. *J. Invest. Dermatol.* 141, 385–394. doi: 10.1016/j.jid.2020.06.038

Lee, J. D., Ulevitch, R. J., and Han, J. (1995). Primary structure of BMK1: a new mammalian map kinase. *Biochem. Biophys. Res. Commun.* 213, 715–724. doi: 10.1006/bbrc.1995.2189

Lennartsson, J., Burovic, F., Witek, B., Jurek, A., and Heldin, C. H. (2010). Erk 5 is necessary for sustained PDGF-induced Akt phosphorylation and inhibition of apoptosis. *Cell Signal.* 22, 955–960. doi: 10.1016/j.cellsig.2010.01.020

Lewis, T. S., Shapiro, P. S., and Ahn, N. G. (1998). Signal transduction through MAP kinase cascades. *Adv. Cancer Res.* 4, 49–139. doi: 10.1016/s0065-230x(08)60765-4

Lin, E. C., Amantea, C. M., Nomanbhoy, T. K., Weissig, H., Ishiyama, J., Hu, Y., et al. (2016). ERK5 kinase activity is dispensable for cellular immune response and proliferation. *Proc. Natl. Acad. Sci. U.S.A.* 113, 11865–11870. doi: 10.1073/pnas.1609019113

Lito, P., Pratilas, C. A., Joseph, E. W., Tadi, M., Halilovic, E., Zubrowski, M., et al. (2012). Relief of profound feedback inhibition of mitogenic signaling by RAF inhibitors attenuates their activity in BRAFV600E melanomas. *Cancer cell* 22, 668–682. doi: 10.1016/j.ccr.2012.10.009

Little, A., Smith, P., and Cook, S. (2013). Mechanisms of acquired resistance to ERK1/2 pathway inhibitors. *Oncogene* 32, 1207–1215. doi: 10.1038/onc.2012.160

Liu, F., Yang, X., Geng, M., and Huang, M. (2018). Targeting ERK, an Achilles' Heel of the MAPK pathway, in cancer therapy. *Acta Pharm. Sin. B* 8, 552–562. doi: 10.1016/j.apsb.2018.01.008

Lochhead, P. A., Tucker, J. A., Tatum, N. J., Wang, J., Oxley, D., Kidger, A. M., et al. (2020). Paradoxical activation of the protein kinase-transcription factor ERK5 by ERK5 kinase inhibitors. *Nat. Commun.* 11, 1383. doi: 10.1038/s41467-020-15031-3

Long, G. V., Stroyakovskiy, D., Gogas, H., Levchenko, E., de Braud, F., Larkin, J., et al. (2014). Combined BRAF and MEK inhibition versus BRAF inhibition alone in melanoma. *N. Engl. J. Med.* 371, 1877–1888. doi: 10.1056/NEJMoa1406037

Luke, J. J., Flaherty, K. T., Ribas, A., and Long, G. V. (2017). Targeted agents and immunotherapies: optimizing outcomes in melanoma. *Nat. Rev. Clin. Oncol.* 14, 463–482. doi: 10.1038/nrclinonc.2017.43

Montagut, C., and Settleman, J. (2009). Targeting the RAF–MEK–ERK pathway in cancer therapy. *Cancer Lett.* 283, 125–134. doi: 10.1016/j.canlet.2009.01.022

Morimoto, H., Kondoh, K., Nishimoto, S., Terasawa, K., and Nishida, E. (2007). Activation of a C-terminal transcriptional activation domain of ERK5 by autophosphorylation. *J. Biol. Chem.* 282, 35449–35456.

Morris, E. J., Jha, S., Restaino, C. R., Dayananth, P., Zhu, H., Cooper, A., et al. (2013). Discovery of a novel ERK inhibitor with activity in models of acquired resistance to BRAF and MEK inhibitors. *Cancer Discov.* 3, 742–750.

Myers, S. M., Bawn, R. H., Bisset, L. C., Blackburn, T. J., Cottyn, B., Molyneux, L., et al. (2016). High-throughput screening and hit validation of extracellular-related kinase 5 (ERK5) inhibitors. *ACS Comb. Sci.* 18, 444–455. doi: 10.1021/acscombsci.5b00155

Nguyen, D., Lemos, C., Wortmann, L., Eis, K., Holton, S. J., Boemer, U., et al. (2019). Discovery and characterization of the potent and highly selective (Piperidin-4-yl)pyrido[3,2- d]pyrimidine Based in Vitro Probe BAY-885 for the Kinase ERK5. *J. Med. Chem.* 62, 928–940. doi: 10.1021/acs.jmedchem.8b01606

Nishimoto, S., and Nishida, E. (2006). MAPK signalling: ERK5 versus ERK1/2. *EMBO Rep.* 7, 782–786. doi: 10.1038/sj.embor.7400755

Nithianandarajah-Jones, G. N., Wilm, B., Goldring, C. E., Müller, J., and Cross, M. J. (2012). ERK5:structure, regulation and function. *Cell Signal.* 24, 2187–2196. doi: 10.1016/j.cellsig.2012.07.007

Ortiz-Ruiz, M. J., Alvarez-Fernandez, S., Parrott, T., Zaknoen, S., Burrows, F. J., Ocana, A., et al. (2014). Therapeutic potential of ERK5 targeting in triple negative breast cancer. *Oncotarget* 5, 11308–11318. doi: 10.18632/oncotarget.2324

Pozo, K., Castro-Rivera, E., Tan, C., Plattner, F., Schwach, G., Siegl, V., et al. (2013). The role of Cdk5 in neuroendocrine thyroid cancer. *Cancer Cell* 24, 499–511. doi: 10.1016/j.ccr.2013.08.027

Raviv, Z., Kalie, E., and Seger, R. (2004). MEK5 and ERK5 are localized in the nuclei of resting as well as stimulated cells, while MEKK2 translocates from the cytosol to the nucleus upon stimulation. *J. Cell Sci.* 117, 1773–1784. doi: 10.1242/jcs.01040

Robarge, K., Schwarz, J., Blake, J., Burkard, M., Chan, J., Chen, H., et al. (2014). Abstract DDT02-03: discovery of GDC-0994, a potent and selective ERK1/2 inhibitor in early clinical development. *Cancer Res.* 74, DDT02–DDT03. doi: 10.1158/1538-7445.AM2014-DDT02-03

Roberts, O. L., Holmes, K., Müller, J., Cross, D. A., and Cross, M. J. (2010). ERK5 is required for VEGF-mediated survival and tubular morphogenesis of primary human microvascular endothelial cells. *J. Cell Sci.* 123(Pt 18), 3189–3200. doi: 10.1242/jcs.072801

Roberts, P. J., and Der, C. J. (2007). Targeting the Raf-MEK-ERK mitogen-activated protein kinase cascade for the treatment of cancer. *Oncogene* 26, 3291–3310. doi: 10.1038/sj.onc.1210422

Roskoski, R. Jr. (2018). Targeting oncogenic Raf protein-serine/threonine kinases in human cancers. *Pharmacol. Res.* 135, 239–258. doi: 10.1016/j.phrs.2018.08.013

Roux, P. P., and Blenis, J. (2004). ERK and p38 MAPK-activated protein kinases: a family of protein kinases with diverse biological functions. *Microbiol. Mol. Biol. Rev.* 68, 320–344. doi: 10.1128/MMBR.68.2.320-344.2004

Samatar, A. A., and Poulikakos, P. I. (2014). Targeting RAS-ERK signalling in cancer: promises and challenges. *Nat. Rev. Drug Discov.* 13, 928–942. doi: 10.1038/nrd4281

Sarkozi, R., Miller, B., Pollack, V., Feifel, E., Mayer, G., Sorokin, A., et al. (2007). ERK1/2-driven and MKP-mediated inhibition of EGF-induced ERK5 signaling in human proximal tubular cells. *J. Cell. Physiol.* 211, 88–100. doi: 10.1002/jcp.20909

Schadendorf, D., Fisher, D. E., Garbe, C., Gershenwald, J. E., Grob, J. J., Halpern, A., et al. (2015). Melanoma. *Nat. Rev. Dis. Primers* 23, 15003. doi: 10.1038/nrdp.2015.3

Sebolt-Leopold, J. S., and Herrera, R. (2004). Targeting the mitogen-activated protein kinase cascade to treat cancer. *Nat. Rev. Cancer* 4, 937–947. doi: 10.1038/nrc1503

Sharma, P., Veeranna, Sharma, M., Amin, N. D., Sihag, R. K., Grant, P., et al. (2002). Phosphorylation of MEK1 by cdk5/p35 down−regulates the mitogen−activated protein kinase pathway. *J. Biol. Chem.* 277, 528–534. doi: 10.1074/jbc.M109324200

Shi, H., Hugo, W., Kong, X., Hong, A., Koya, R. C., Moriceau, G., et al. (2014). Acquired resistance and clonal evolution in melanoma during BRAF inhibitor therapy. *Cancer Discov.* 4, 80–93. doi: 10.1158/2159-8290.CD-13-0642

Simões, A. E., Rodrigues, C. M., and Borralho, P. M. (2016). The MEK5/ERK5 signalling pathway in cancer: a promising novel therapeutic target. *Drug Discov. Today* 21, 1654–1663. doi: 10.1016/j.drudis.2016.06.010

Song, C., Wang, L., Xu, Q., Wang, K., Xie, D., Yu, Z., et al. (2017). Targeting BMK1 impairs the drug resistance to combined inhibition of BRAF and MEK1/2 in melanoma. *Sci. Rep.* 7:46244. doi: 10.1038/srep46244

Stecca, B., and Rovida, E. (2019). Impact of ERK5 on the Hallmarks of cancer. *Int. J. Mol. Sci.* 20:1426. doi: 10.3390/ijms20061426

Suzuki, Y., Orita, M., Shiraishi, M., Hayashi, K., and Sekiya, T. (1990). Detection of ras gene mutations in human lung cancers by single-strand conformation polymorphism analysis of polymerase chain reaction products. *Oncogene* 5, 1037–1043.

Tatake, R. J., O'Neill, M. M., Kennedy, C. A., Wayne, A. L., Jakes, S., Wu, D., et al. (2008). Identification of pharmacological inhibitors of the MEK5/ERK5 pathway. *Biochem. Biophys. Res. Commun.* 377, 120–125. doi: 10.1016/j.bbrc.2008.09.087

Tubita, A., Lombardi, Z., Tusa, I., Dello Sbarba, P., and Rovida, E. (2020). Beyond kinase activity: Erk5 nucleo-cytoplasmic shuttling as a novel target for anticancer therapy. *Int. J. Mol. Sci.* 21:938. doi: 10.3390/ijms21030938

Tusa, I., Gagliardi, S., Tubita, A., Pandolfi, S., Urso, C., Borgognoni, L., et al. (2018). ERK5 is activated by oncogenic BRAF and promotes melanoma growth. *Oncogene* 37, 2601–2614. doi: 10.1038/s41388-018-0164-9

Ugurel, S., Rohmel, J., Ascierto, P. A., Flaherty, K. T., Grob, J. J., Hauschild, A., et al. (2017). Survival of patients with advanced metastatic melanoma: the impact of novel therapies-update 2017. *Eur. J. Cancer* 83, 247–257. doi: 10.1016/j.ejca.2017.06.028

Umapathy, G., El Wakil, A., Witek, B., Chesler, L., Danielson, L., Deng, X., et al. (2014). The kinase ALK stimulates the kinase ERK5 to promote the expression of the oncogene MYCN in neuroblastoma. *Sci. Signal.* 7:349. doi: 10.1126/scisignal.2005470

Umapathy, G., Guan, J., Gustafsson, D. E., Javanmardi, N., Cervantes-Madrid, D., Djos, A., et al. (2017). MEK inhibitor trametinib does not prevent the growth of anaplastic lymphoma kinase (ALK)-addicted neuroblastomas. *Sci. Signal.* 10:507. doi: 10.1126/scisignal.aam7550

Van Allen, E. M., Wagle, N., Sucker, A., Treacy, D. J., Johannessen, C. M., Goetz, E. M., et al. (2014). The genetic landscape of clinical resistance to RAF inhibition in metastatic melanoma. *Cancer Discov.* 4, 94–109. doi: 10.1158/2159-8290.CD-13-0617

Vaseva, A. V., Blake, D. R., Gilbert, T. S. K., Ng, S., Hostetter, G., Azam, S. H., et al. (2018). KRAS suppression-induced degradation of MYC Is antagonized by a MEK5-ERK5 compensatory mechanism. *Cancer Cell* 34, 807–822. doi: 10.1016/j.ccell.2018.10.001

Wang, J., Erazo, T., Ferguson, F. M., Buckley, D. L., Gomez, N., Muñoz-Guardiola, P., et al. (2018). Structural and atropisomeric factors governing the selectivity of pyrimido-benzodiazipinones as inhibitors of kinases and bromodomains. *ACS Chem. Biol.* 13, 2438–2448. doi: 10.1021/acschembio.7b00638

Wang, X., and Tournier, C. (2006). Regulation of cellular functions by the ERK5 signalling pathway. *Cell Signal.* 18, 753–760. doi: 10.1016/j.cellsig.2005.11.003

Waters, A. M., and Der, C. J. (2018). KRAS: the critical driver and therapeutic target for pancreatic cancer. *Cold Spring Harb. Perspect. Med.* 4, 8–9. doi: 10.1101/cshperspect.a031435

Williams, C. A., Fernandez-Alonso, R., Wang, J., Toth, R., Gray, N. S., and Findlay, G. M. (2016). Erk5 is a key regulator of naive-primed transition and embryonic stem cell identity. *Cell Rep.* 16, 1820–1828. doi: 10.1016/j.celrep.2016.07.033

Yan, C., Luo, H., Lee, J. D., Abe, J., and Berk, B. C. (2001). Molecular cloning of mouse ERK5/BMK1 splice variants and characterization of ERK5 functional domains. *J. Biol. Chem.* 276, 10870–10878.

Yang, Q., Deng, X., Lu, B., Cameron, M., Fearns, C., Patricelli, M. P., et al. (2010). Pharmacological inhibition of BMK1 suppresses tumor growth through promyelocytic leukemia protein. *Cancer Cell* 18, 258–267. doi: 10.1016/j.ccr.2010.08.008

Yoon, S., and Seger, R. (2006). The extracellular signal-regulated kinase: multiple substrates regulate diverse cellular functions. *Growth Factors* 24, 21–44. doi: 10.1080/02699050500284218

Zheng, Y. L., Li, B. S., Kanungo, J., Kesavapany, S., Amin, N., Grant, P., et al. (2007). Cdk5 modulation of mitogen−activated protein kinase signaling regulates neuronal survival. *Mol. Biol. Cell* 18, 404–413. doi: 10.1091/mbc.e06-09-0851

Zhou, G., Bao, Z. Q., and Dixon, J. E. (1995). Components of a new human protein kinase signal transduction pathway. *J. Biol. Chem.* 270, 12665–12669.

Zhuang, K., Zhang, J., Xiong, M., Wang, X., Luo, X., Han, L., et al. (2016). CDK5 functions as a tumor promoter in human colorectal cancer via modulating the ERK5-AP-1 axis. *Cell Death Dis.* 7:e2415. doi: 10.1038/cddis.2016.333

Conflict of Interest: The authors declare that the research was conducted in the absence of any commercial or financial relationships that could be construed as a potential conflict of interest.

frontiers in Cell and Developmental Biology

REVIEW
published: 26 March 2021
doi: 10.3389/fcell.2021.652273

Biological Significance of NOTCH Signaling Strength

Wei Shen[1], Jiaxin Huang[2] and Yan Wang[1]**

[1] Xiamen Cardiovascular Hospital, Xiamen University, Xiamen, China, [2] Center for Structural Biology, School of Life Sciences and School of Medicine, Tsinghua University, Beijing, China

The evolutionarily conserved NOTCH signaling displays pleotropic functions in almost every organ system with a simple signaling axis. Different from many other signaling pathways that can be amplified via kinase cascades, NOTCH signaling does not contain any intermediate to amplify signal. Thus, NOTCH signaling can be activated at distinct signaling strength levels, disruption of which leads to various developmental disorders. Here, we reviewed mechanisms establishing different NOTCH signaling strengths, developmental processes sensitive to NOTCH signaling strength perturbation, and transcriptional regulations influenced by NOTCH signaling strength changes. We hope this could add a new layer of diversity to explain the pleotropic functions of NOTCH signaling pathway.

Keywords: Notch signaling, NICD, signaling strength, cell fate specification, development

OPEN ACCESS

Edited by:
Juan Jose Sanz-Ezquerro, Centro Nacional de Biotecnología, Consejo Superior de Investigaciones Científicas (CSIC), Spain

Reviewed by:
Ivan Maillard, University of Pennsylvania, United States
Luis Luna-Zurita, Spanish National Centre for Cardiovascular Research, Spain

****Correspondence:***
Wei Shen
shenwei@xmheart.com
Yan Wang
wy@medmail.com.cn

Specialty section:
This article was submitted to Signaling, a section of the journal Frontiers in Cell and Developmental Biology

Received: *12 January 2021*
Accepted: *23 February 2021*
Published: *26 March 2021*

Citation:
Shen W, Huang J and Wang Y (2021) Biological Significance of NOTCH Signaling Strength. Front. Cell Dev. Biol. 9:652273. doi: 10.3389/fcell.2021.652273

INTRODUCTION

Since the observation of notched wing in *Drosophila* and subsequent discovery of *notch* gene one century ago (Morgan, 1917), NOTCH signaling has been extensively studied. On/off switch of NOTCH signaling is found to play fundamental roles in cell differentiation, proliferation, and apoptosis across all species (Artavanis-Tsakonas et al., 1999; Harper et al., 2003; Lai, 2004; Lasky and Wu, 2005; Bolós et al., 2007; Penton et al., 2012). Surprisingly, the signaling axis of NOTCH is relatively simple despite its pleiotropic functions. Canonically, cell membrane-tethered NOTCH ligand binds to NOTCH receptor on the neighboring cell, which induces enzymatic cleavages of NOTCH receptor. The released notch intracellular domain (NICD) subsequently migrates into cell nucleus, where it binds with transcriptional factor CSL (CBF-1/RBP-J in mammal, Su(H) in *Drosophila*, and Lag-1 in *Caenorhabditis elegans*) together with other transcription co-factors to activate gene transcription (Kopan and Ilagan, 2009). Different from many other signaling pathways that contain kinase cascade-mediated signaling amplification processes, NOTCH signaling does not contain signaling intermediate to amplify the signal. In addition, NICD-CSL binding also triggers NICD ubiquitination that leads to its subsequent degradation (Fryer et al., 2004). Therefore, the scale and duration of gene transcription is sensitive to the dosage of NICD presented in cell nucleus.

Previous studies reviewed that protein level reduction caused by heterozygous mutation of NOTCH signaling components can lead to multiple developmental defects (Eldadah et al., 2001;

McCright et al., 2002; Saito et al., 2003; Gale et al., 2004; Hozumi et al., 2004; McDaniell et al., 2006; Warthen et al., 2006; McKellar et al., 2007; Wu et al., 2007; Rubio-Aliaga et al., 2009; Hassed et al., 2012; Sargin et al., 2013; Meester et al., 2015; Southgate et al., 2015; Fischer-Zirnsak et al., 2019; Blackwood et al., 2020), suggesting developmental processes are sensitive to NOTCH signaling dosage. In addition, certain binary cell fate specifications are dependent on high/low regulation of NOTCH signaling strength instead of on/off switch of NOTCH signaling (Van de Walle et al., 2009, 2013; Gama-Norton et al., 2015), further highlighting the importance of NOTCH signaling strength regulation during development. Here, we reviewed the mechanisms of NOTCH signaling strength regulation; NOTCH components exhibiting haploinsufficiency and cell differentiation processes rely on precise NOTCH signaling strength. We hope this can add an extra layer of diversity to NOTCH signaling that plays pleotropic functions in almost every organ system with a simple signaling axis.

NOTCH SIGNALING AND ITS STRENGTH REGULATION

NOTCH Signaling Can Be Activated at Different Strength Levels Resulting in Distinct Transcriptional Responses

The mechanism of NOTCH signaling activation is highly conserved during evolution except for slight difference in terms of the number of NOTCH ligands and receptors across different species. In mammals, there are five NOTCH ligands (Dll-1, Dll-4, Jag-1, and Jag-2 are activators, and Dll-3 is an inhibitor) and four NOTCH receptors (Notch-1, Notch-2, Notch-3, and Notch-4), all of which contain extracellular epidermal growth factor (EGF)-like domains executing ligand–receptor binding. Subsequently after binding, NOTCH receptor undergoes two successive enzymatic cleavages mediated by ADAM10 and γ-secretase, releasing the NICD into cell nucleus where it binds with NOTCH signaling transcription factor CSL together with other co-factors to activate gene transcription (**Figure 1**). The most conserved direct targets of NOTCH signaling are basic helix-loop-helix (bHLH) transcription factors of hairy/enhancer of split (Hes) family and hairy/enhancer of split related with YRPW motif (Hey) family (Iso et al., 2003; Borggrefe and Oswald, 2009).

Unlike many other signaling pathways, NOTCH signaling can be activated at distinct strength levels due to following three reasons: (1) one NOTCH receptor can only release one NICD after ligand–receptor binding, (2) no signal intermediate or kinase cascade is involved to amplify the initial signal, and (3) NICD is subjected to proteasome-mediated degradation after transcriptional activation (Fryer et al., 2004). Since CSL and other transcriptional co-factors are always readily present in cell nucleus, the level of NICD generated determines the strength and duration of NOTCH signaling. A recent study by Nandagopal et al. (2018) showed that ligand intracellular domain (ICD) determined distinct membrane distribution pattern of Dll-4 (which is dispersed over membrane) and Dll-1 (which is clustered in puncta), which triggered sustained and pulsatile release of NICD, respectively. Interestingly, the two patterns of NICD release resulted in distinct downstream gene expression and consequently a different cell fate choice during embryonic myogenesis (Nandagopal et al., 2018). This confirmed gene transcription and cell fate specification can be influenced by NOTCH signaling strength perturbations.

Mechanisms of NOTCH Signaling Strength Regulation

The frequency of NOTCH ligand and receptor binding determines the amount of NICD generated. In order to achieve a successful binding-induced NOTCH receptor cleavage, both ligand and receptor need to be presented on cell membrane in close proximity. Since all active NOTCH ligands and receptors are trans-membrane proteins that are subjected to consistent endocytosis, recycling, and degradation, the amount of NICD that could be potentially generated is affected by endocytic regulations of the ligands and receptors (Fortini and Bilder, 2009; Kandachar and Roegiers, 2012; Shen and Sun, 2020). Meanwhile, the four active NOTCH ligands (Jag-1, Jag-2, Dll-1, and Dll-4) in mammals exhibit different binding affinities (Benedito et al., 2009; Groot et al., 2014; Gama-Norton et al., 2015; Nandagopal et al., 2018), which further diversified the levels of NOTCH signaling strength in different cell contexts. The discovery of fringe glycosyltransferase also brought up the importance of EGF domain glycosylation, which can change ligand–receptor binding affinity and facilitate NOTCH receptor cleavage (Stanley and Okajima, 2010; Takeuchi and Haltiwanger, 2010; Kakuda and Haltiwanger, 2017). Thus, NOTCH signaling strength can be influenced by glycosylation of EGF domain in receptors. In addition to glycosylation, lipid composition of cell membrane can also influence NOTCH ligand–receptor binding via lipid–ligand interactions (Suckling et al., 2017). Underlying the binding affinity differences for different ligands, catch-bond that exhibited prolonged bond lifetimes upon tensile force application is shown to play important roles on modulating ligand–receptor binding (Luca et al., 2017). Collectively, the amount of ligand and receptor presented on cell membrane, the type of ligand binding to receptor, glycosylation of EGF domain, and lipid–ligand interaction all influence ligand–receptor binding and consequently the amount of NICD released.

The stability of NICD affects the duration of NOTCH signaling. NICD is generated following ligand–receptor binding and shuttles into cell nucleus, where it binds to transcription factor CSL together with co-factor of mastermind-like protein (MamL) and other chromatin modifiers to activate gene transcription. In addition to transcriptional regulations, CSL and MamL also recruit kinase CDK8 to phosphorylate NICD, which triggers protein ubiquitination on PEST (proline, glutamic acid, serine, and threonine-enriched) domain of NICD and proteasome-mediated NICD degradation (Fryer et al., 2004). Thus, NOTCH signaling is quickly turned down without re-supply of new NICD, which is a critical step to maintain proper levels of NOTCH signaling strength. Sustained NOTCH

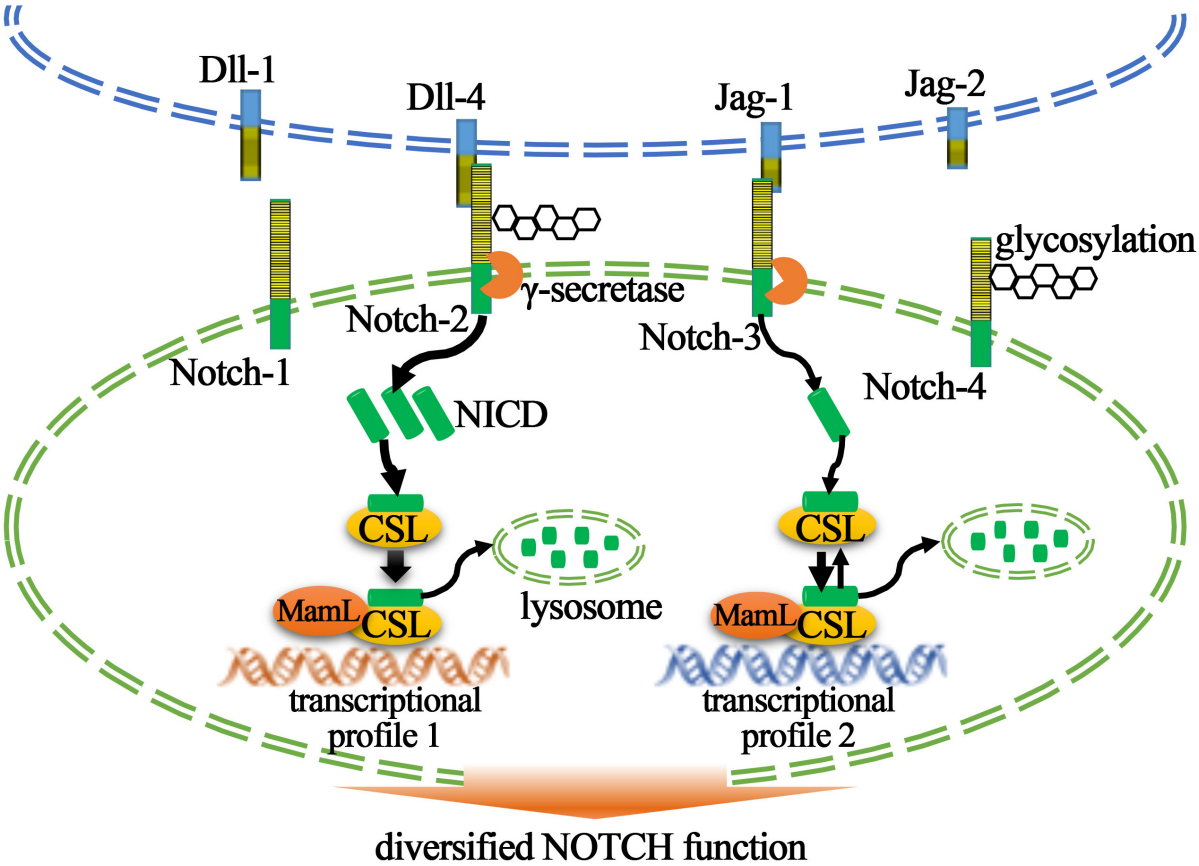

FIGURE 1 | Cartoon illustrating NOTCH signaling and its strength regulations. Binding of NOTCH ligand (Jag-1, Jag-2, Dll-1, and Dll-4) to NOTCH receptor (Notch1, Notch-2, Notch-3, and Notch-4), a process that can be influenced by glycosylation of epidermal growth factor (EGF) domain (yellow stripes), triggers γ-secretase-mediated NOTCH receptor cleavage. Notch intracellular domain (NICD) is then freed and migrates into cell nucleus where it binds with transcriptional factor CSL, increases CSL dwell time on DNA, and recruits co-factor MamL to initiate the gene transcription. The ultimate transcription profile is affected by the dosage of NICD, which is also regulated by lysosome-mediated NICD degradation.

activation due to mutations in PEST domain can disrupt cell homeostasis and lead to various diseases, such as chronic lymphocytic leukemia (CCL; Ianni et al., 2009; Puente et al., 2011), marginal zone lymphoma (Trøen et al., 2008; Kiel et al., 2012), and increased proliferation of B-cell lymphoma cell (Zhang et al., 2014). Therefore, maintaining a proper level of NOTCH signaling strength is important.

DEVELOPMENTAL PROCESSES SENSITIVE TO NOTCH SIGNALING STRENGTH PERTURBATION

Haploinsufficiency of NOTCH Signaling Leads to Various Developmental Disorders and Diseases

Haploinsufficiency of NOTCH signaling components, a condition caused by heterozygous mutation producing only half amount of proteins, is related to the development of Adams–Oliver syndrome (AOS) characterized by congenital defects of limbs and scalp. *Notch-1* haploinsufficiency has been discovered in AOS patients with variable levels of cardiovascular anomalies, such as ventricular septal defects, aortic stenosis, regurgitation, and coarctation (Southgate et al., 2015). In line with the *Notch-1* haploinsufficiency discovered in AOS patients, another NOTCH signaling component *RBP-J* (coding the mammalian form of CSL) is also found to be haploinsufficient in AOS patients (Hassed et al., 2012), implying a causative role of reduced NOTCH signaling strength during the development of AOS. In addition, Dll-4 is likely the NOTCH ligand responsible for generating the proper level of NOTCH signaling in this case, as AOS patients are also reported to carry *Dll-4* heterozygous mutation (Meester et al., 2015). Collectively, *Dll-4*, *Notch-1*, and *RBP-J* haploinsufficiencies are associated with AOS.

Haploinsufficiency of NOTCH signaling components also leads to the development of Alagille syndrome (AGS) that affects multiple organs including the liver, heart, eye, kidney, and bone. AGS patients are reported to carry heterozygous mutation of *Jag-1* (Warthen et al., 2006) or *Notch-2* (McDaniell et al., 2006) or both (Brennan and Kesavan, 2017). Mice models with heterozygous mutations of *Jag-1* and *Notch-2* also successfully

recapitulated certain symptoms of AGS (McCright et al., 2002), suggesting that reduction of NOTCH signaling leads to the development of AGS. Interestingly, some AGS-related defects can also be associated with NOTCH signaling components' haploinsufficiency independent of AGS. For example, tetralogy of Fallot, a congenital heart disease frequently observed in AGS patients, can be found patients carrying *Jag-1* heterozygous mutation without diagnosis of AGS (Eldadah et al., 2001; Bauer et al., 2010). Another congenital heart disease named bicuspid aortic valve, a condition lacking one valve between the left ventricle and main artery, is associated with *Notch-1* haploinsufficiency and also independent of AGS (McKellar et al., 2007). Therefore, NOTCH signaling haploinsufficiency can lead to the development of AGS and multiple cardiovascular defects.

Beyond above diseases, systematic examination of mice models also showed that NOTCH signaling haploinsufficiency can disrupt the development of many organs and tissues where NOTCH signaling plays essential functions. In addition to the reported AGS symptoms (Huppert, 2016), *Jag-1*$^{\pm}$ mice also showed degeneration of ganglionic eminence caused by suppressed neuronal progenitor cell proliferation (Blackwood et al., 2020) and spatial memory impairment (Sargin et al., 2013). *Dll-4*$^{\pm}$ mice displayed various artery defects including failed remodeling of yolk sac vasculature, artery regression, artery stenosis, atresia aorta, and defected arterial branching (Gale et al., 2004), consistent with the essential function of *Dll-4* during artery development (Shutter et al., 2000; Cristofaro et al., 2013). *Dll-1*$^{\pm}$ mice on the other hand displayed smaller bodies, reduced cholesterol and triglyceride levels, suppressed immune system, bradycardia (Rubio-Aliaga et al., 2009), and brain disorders (Fischer-Zirnsak et al., 2019). Collectively, haploinsufficiency of NOTCH signaling components can lead to various developmental disorders.

NOTCH Signaling Strength in Arterial Endothelial Cells

The change of NOTCH signaling strength influences artery endothelial cell fate (vs. hematopoietic stem cell fate) specification and artery branching (vs. elongation). During early embryonic development, progenitor cells resident in aorta-gonad-mesonephros (AGM) region can give rise to either arterial endothelial cell or hematopoietic stem cell (HSC) depending on NOTCH signaling strength. *In vivo* study found that Dll-4 activated high NOTCH signaling while Jag-1 activated low NOTCH signaling in AGM region, where high NOTCH signaling specifies endothelial cell fates while low NOTCH signaling specifies HSC fates. Neutralization of Dll-4 via antibody blockage lowered NOTCH activity and forced AGM cells to differentiate into HSCs, suggesting a NOTCH-strength-dependent cell fate specification (Gama-Norton et al., 2015). In addition, NOTCH signaling strength also influences branching of the artery during the generation of vascular network. New tip cell specification, a requirement for artery branching, is inhibited by Dll-4-activated high NOTCH signaling while requires Jag-1-activated low NOTCH signaling. *Jag-1* mutated mice, in which Dll-4 dominated in the artery and activated high NOTCH signaling, exhibited significantly reduced vascular branching. In contrast, overexpression of Jag-1 outcompeted Dll-4 and significantly promoted vascular branching. During the establishment of this signaling strength difference, fringe-mediated glycosylation of NOTCH played a critical role on potentiating Dll-4-activated high NOTCH signaling and suppressing Jag-1-mediated low NOTCH signaling. Removing fringe suppressed Dll-4-activated high NOTCH signaling and permitted Jag-1-activated low NOTCH signaling, resulting in enhanced vascular branching (Benedito et al., 2009).

Further study showed that the developmental difference resulting from Dll-4- and Jag-1-activated NOTCH signaling during vascular branching was purely due to the strength difference of NOTCH signaling. Administration of γ-secretase inhibitor (DAPT) into *Jag-1*-mutated mice lowered Dll-4-activated NOTCH signaling and rescued vascular branching defects (Benedito et al., 2009). Therefore, it is the strength of NOTCH signaling that determines the artery branching. Utilizing hybrid proteins created by swapping the ICD of Jag-1 and Dll-4 found that ICDs of NOTCH ligands determine the potential of NOTCH signaling strength that could be activated by Jag-1 or Dll-4. Cytoskeletal filament vimentin specifically binds to Jag-1 ICD and determines the pulling force critical for binding-induced NOTCH receptor cleavage. Hybrid protein fused by Jag1 ICD and Dll-4 extracellular domain (ECD) generated NOTCH signaling resembling ligand Jag-1 (Antfolk et al., 2017). Collectively, different NOTCH ligands hold distinct capacities to activate NOTCH signaling, and ligand ICDs play fundamental roles on influencing the activation potential.

NOTCH Signaling Strength in Vascular Smooth Muscle Cell

NOTCH signaling is required for vascular smooth muscle cell (VSMC) differentiation. VSMCs are recruited to vascular endothelial cells during vasculogenesis and play crucial roles on maintaining normal vascular tone in response to hemodynamic changes, especially in arteries where multiple layers of VSMCs are attached to endothelial cells (Zhuge et al., 2020). During vasculogenesis, VSMC progenitors are recruited to vascular bed where endothelial cell expresses Jag-1-activated NOTCH signaling in VSMC progenitor cells, resulting in expression of smooth cell markers of α-*SMA* and *SM-22*α and the final specification of VSMC fate (Noseda et al., 2006; High et al., 2008). Meanwhile, the activated NOTCH signaling in VSMCs also directly activated *Jag-1* expression in the newly formed VSMCs, allowing further propagation of NOTCH signaling in the outer layers of VSMCs (Hoglund and Majesky, 2012; Manderfield et al., 2012; van Engeland et al., 2019). Therefore, Jag-1-activated NOTCH signaling is essential to maintain VSMC fate and form a multiple-layer structure of VSMCs in the artery.

Elevated NOTCH signaling strength triggered the proliferation of VSMCs. Unlike skeletal muscle cells or cardiomyocytes, both of which are terminally differentiated and quiescent, VSMCs holds the ability to proliferate, dedifferentiate, and even transdifferentiate into macrophage-like cells in response to vascular injury or environmental stimulus

(Bennett et al., 2016; Basatemur et al., 2019; Zhuge et al., 2020). The elevated NOTCH signaling has been observed in arterial injury (Wang et al., 2002) and atherosclerotic lesions (Davis-Knowlton et al., 2019), both of which involve VSMC proliferation. An *in vitro* study also showed that over-expression of NICD in VSMCs can increase cell proliferation (Sweeney et al., 2004), which seems contradictory to the fact that NOTCH signaling promotes the quiescent status of VSMCs characterized by the expression of α-SMA. However, NICD over-expression generally resulted in sustained high NOTCH signaling, and detailed *in vitro* studies clarified that NOTCH downstream targets of Hey are promoted under this condition and are responsible for increased VSMC proliferation and suppressed α-SMA expression via negative feedback loops. Specifically, the increased Hey, a transcriptional repressor, can in term prevent the transcription of α-*SMA* through directly binding to α-*SMA* promoter (Tang et al., 2008). Meanwhile, Hey also inhibits the expression of cyclin-dependent kinase inhibitor $P27^{kip1}$, allowing re-entering into the cell cycle (Havrda et al., 2006). Conclusively, NOTCH signaling is required for expression of VSMC markers to maintain VSMC fate, while elevated NOTCH signaling can suppress VSMC marker expression and promote VSMC proliferation.

NOTCH Signaling Strength in T-Cell Lineage

NOTCH signaling strength determines αβ T-cell (vs. γδ T-cell) specification in T-cell lineage. Postnatal development of T immune cell in the thymus requires activation of NOTCH signaling in the hematopoietic progenitor cells (HPCs) that migrated from the bone marrow. NOTCH signaling activation inhibits non-T-cell cells including myeloid lineage during early stages and B-cell during late stages (Wilson et al., 2001). However, after T-cell fate is committed, the strength of NOTCH in T-cell lineage determines T-cell sub-lineage specifications between αβ T-cell and γδ T-cell. An *in vitro* study showed that human OP9-Dll1/4 that served as NOTCH signal-sending cell can stimulate the differentiation of human HPCs into T-cells populated with both αβ T-cell and γδ T-cell. Interestingly, lowering NOTCH signaling strength via adding a series of γ-secretase inhibitor (DAPT) with increasing concentrations gradually switched γδ T-cell into αβ T-cell (Van de Walle et al., 2009), documenting NOTCH-strength-dependent cell fate determination between the two T-cell subtypes.

The strength changes of NOTCH signaling in T-cell lineage is caused by binding with different NOTCH ligands that hold distinct receptor binding affinities. Still in human HPCs, Jag-2 exhibited strong NOTCH activation potential and directed HPCs predominantly into γδ T-cell (Van de Walle et al., 2011, 2013); Dll-4 instead induced a relatively weak NOTCH signaling and generated both γδ T-cell and αβ T-cell, while Jag-1 induced the weakest NOTCH signaling and generated mainly αβ T-cell (Van de Walle et al., 2013). Collectively, the diverted expression of NOTCH ligands maintained a diverse range of NOTCH signaling strength, which balanced the population of αβ T-cell and γδ T-cell. Surprisingly, mice HPCs also utilize the strength difference of NOTCH signaling to determine the αβ T-cell fate and γδ T-cell fate but in an opposite way that low NOTCH signaling favors γδ T-cell (Washburn et al., 1997). It is intriguing how this difference between human and mouse is generated, while the NOTCH-strength-dependent cell fate determination is indeed conserved during evolution.

NOTCH Signaling Strength in Marginal Zone B Cell

Differentiation of marginal zone B (MZB) cell, an immune cell developed in marginal zone of the spleen, relies on NOTCH signaling dosage. Notch-2 is preferentially expressed in B-cell and is prominent in splenic marginal zone, suggesting its potential function on MZB cell differentiation. Homozygous mutation of *Notch-2* completely eliminated MZB cells. Interestingly, heterozygous mutation of *Notch-2*, in which 50% of *Notch-2* mRNA still expressed, resulted in partial reduction of MZB cells (Saito et al., 2003). Consistent with *Notch-2* mutant, mutational study of *MamL-1* (transcriptional co-factor of CSL) showed a similar dose-dependent regulation of MZB cell differentiation. Wild-type, heterozygous mutation of *MamL-1* and homozygous mutation of *MamL-1* showed sequential reduction of MZB cell number (Wu et al., 2007), suggesting all these defects are due to reduction of NOTCH signaling strength.

Other studies on NOTCH ligands found that it is the ligand of Dll-1 that activates Notch-2 for MZB cell differentiation in the spleen. Mutational study of *Dll-1* similarly showed a sequential reduction of MZB cell among wild-type, heterozygous mutation of *Dll-1* and homozygous mutation of *Dll-1* (Hozumi et al., 2004). A later study in splenic stromal cells further confirmed that Dll-1 expressed by these cells are responsible for activating NOTCH signaling required for MZB cell differentiation (Fasnacht et al., 2014). Collectively, these comparison studies on heterozygous mutation of *Notch-2*, *MamL-1*, and *Dll-1* suggest that MZB cell differentiation is dependent on NOTCH dosage. MZB cell differentiation likely requires NOTCH signaling to be above certain threshold. Haploinsufficiency of these NOTCH signaling components made many cells fail to reach this threshold and resulted in big reduction of mature MZB cells.

NOTCH Signaling Strength in Pancreatic Progenitor Cells

Stepwise downregulation of NOTCH signaling strength in pancreatic endocrine progenitor cells drives the transition from quiescence to proliferation and from proliferation to differentiation. NOTCH signaling is well-known for its function on maintaining pancreatic progenitor cells, and suppressing NOTCH signaling triggered the progenitor cells to differentiate into pancreatic secreting cells (Apelqvist et al., 1999). Interestingly, lineage tracing observation of pancreas development in *zebrafish* discovered a stepwise downregulation of NOTCH signaling strength in quiescent endocrine progenitor cells, proliferating endocrine progenitor cells and differentiated mature endocrine cells. Lowering NOTCH signaling strength via applying low concentration of γ-secretase inhibitor (DAPT) to the developing pancreas promoted progenitor cell proliferation and consequently expanded pancreatic endocrine progenitor pool. However,

saturated DAPT led to differentiation of pancreatic secreting cells accompanied by drastically reduced progenitor pool (Ninov et al., 2012), confirming moderate NOTCH signaling strength is required for the proliferation of pancreatic endocrine progenitor cells.

Conclusively, high NOTCH signaling strength maintains quiescent state of pancreatic endocrine progenitor cell, moderate NOTCH signaling strength triggers its proliferation, and low NOTCH signaling strength leads to its final differentiation. Combining NOTCH haploinsufficiency-related disorders, precise strength requirements in artery endothelial cell, VSMC, T-cell, and MZB cell, developmental processes can be sensitive to NOTCH signaling strength perturbations (summarized in **Table 1**). Therefore, re-examining NOTCH-regulated processes with consideration of signaling strength would likely offer new insights to explain the pleotropic functions of NOTCH.

MECHANISMS UNDERLYING DISTINCT TRANSCRIPTIONAL ACTIVATION BY DIFFERENT STRENGTHS OF NOTCH SIGNALING

Different duration and dynamics of NOTCH signaling strengths yield distinct transcriptional responses, which resulted in distinct developmental consequences. A new study reported by Nandagopal et al. (2018) showed that the conserved NOTCH direct target genes of *Hes1* and *Hey1/L* responded differently to

TABLE 1 | Developmental processes sensitive to NOTCH signaling strength.

NOTCH changes	Phenotypic changes	Study species	Reference paper
Jag-1 haploinsufficiency	Alagille syndrome	Human	Warthen et al., 2006; Brennan and Kesavan, 2017
	Alagille syndrome	Mouse	McCright et al., 2002; Huppert, 2016
	Tetralogy of Fallot	Human	Eldadah et al., 2001; Bauer et al., 2010
	Brain malfunctions	Mouse	Sargin et al., 2013
	Neuron stem cell reduction	Mouse	Blackwood et al., 2020
Dll-1 haploinsufficiency	Brain malfunctions	Mouse	Fischer-Zirnsak et al., 2019
	Growth retardation and metabolic disorder	Mouse	Rubio-Aliaga et al., 2009
Dll-4 haploinsufficiency	Adams–Oliver syndrome	Human	Meester et al., 2015
	Broad artery defects	Mouse	Gale et al., 2004
Notch-1 haploinsufficiency	Adams–Oliver syndrome	Human	Southgate et al., 2015
	Bicuspid aortic valve	Human	McKellar et al., 2007
Notch-2 haploinsufficiency	Alagille syndrome	Human	McDaniell et al., 2006; Brennan and Kesavan, 2017
	Alagille syndrome	Mouse	McCright et al., 2002
RBP-J haploinsufficiency	Adams–Oliver syndrome	Human	Hassed et al., 2012
High NOTCH signal	AGM cell differentiates to endothelial cell	Mouse	Gama-Norton et al., 2015
Low NOTCH signal	AGM cell differentiates to hematopoietic stem cell		
High NOTCH signal	Inhibit artery tip cell specification and artery branching	Mouse	Benedito et al., 2009; Antfolk et al., 2017
Low NOTCH signal	Promote artery tip cell specification and artery branching		
High NOTCH signal	VSMC in proliferative state	Human, rat, mouse	Havrda et al., 2006; Tang et al., 2008
Moderate NOTCH signal	VSMC in contractile and quiescent state		Noseda et al., 2006; High et al., 2008
High NOTCH signal	Human HPC differentiates into γδ T-cell	Human	Van de Walle et al., 2013
Low NOTCH signal	Human HPC differentiates into αβ T-cell		
High NOTCH signal	Mouse HPC differentiates into αβ T-cell	Mouse	Washburn et al., 1997
Low NOTCH signal	Mouse HPC differentiates into γδ T-cell		
High NOTCH signal	Normal MZB cell differentiation	Mouse	Saito et al., 2003; Hozumi et al., 2004; Wu et al., 2007; Fasnacht et al., 2014
Moderate NOTCH signal	Reduced MZB cell differentiation		
No NOTCH signal	No MZB cell differentiation		
High NOTCH signal	Pancreatic progenitor in quiescent	Zebrafish	Ninov et al., 2012
Moderate NOTCH signal	Pancreatic progenitor in proliferation		
Low NOTCH signal	Pancreatic progenitor in differentiation		

the level changes of NICD, the active component of NOTCH signaling. Interestingly, *Hes1* and *Hey1/L* did not simply adjust their expression levels in proportion to the amount of NICD generated. High and sustained NOTCH activation induced by Dll-4 initiated *Hey1/L* transcription compared to pulsatile NOTCH activation induced by Dll-1, instead of proportionally increasing *Hes1* that was already transcribed under pulsatile NOTCH activation (Nandagopal et al., 2018). Considering NICD pattern change alone can initiate new gene expression, and it is likely that level changes of NICD would mediate chromatin modifications for gene transcription.

Dosage change of NICD can influence CSL-DNA binding kinetics, NICD dimerization, and chromatin opening. A recent study using live cell imaging changed the classical model that CSL stays on chromatin to repress gene transcription until the arrival of NICD that switches CSL into a transcriptional activator (Morel et al., 2001; Borggrefe and Oswald, 2009). Instead, CSL consistently binds to and detaches from DNA, and NICD along or together with co-factor of MamL can change the binding dynamics of CSL onto DNA by increasing its chromatin dwell time and potentially the binding loci (Gomez-Lamarca et al., 2018). NICD dimerization, utilizing two NICDs for gene transcription, is essential for certain NOTCH downstream gene expression. Suppressing of NICD dimerization leads to various developmental disorders including heart anomalies and defective MZB cell differentiation; therefore, shifted balance between dimerized NICD and monomer NICD that can be influenced by NICD dosage is going to affect transcriptional profile as well (Hass et al., 2015; Kobia et al., 2020). The changing of gene transcription under different NICD dosages can be further proven by the observation that NICD can change chromatin structure (Gomez-Lamarca et al., 2018), opening of which permits more gene transcription. Collectively, NICD not only switches CSL into transcription activator but also modulates the dynamics of CSL-DNA binding, NICD dimerization, and chromatin structure, thus affecting gene transcription both qualitatively and quantitatively.

CONCLUSION

The on/off switch of NOTCH signaling is well-recognized for its function on regulating cell differentiation, proliferation, and apoptosis. The pleotropic function of NOTCH signaling seems contradictory to the simple setting of NOTCH signaling axis. Genetic studies discovered heterozygous mutations of NOTCH signaling components in various developmental disorders and diseases, suggesting that organ development is also sensitive to NOTCH signaling dosage. More importantly, simple changes of NOTCH signaling strength influences the binary cell fate determinations and cell proliferation and differentiation during artery, postnatal T-cell, MZB cell, and pancreas development, suggesting that NOTCH signaling strength changes can be as important as on/off switch of the signaling. Underlying NOTCH signaling strength changes and NICD–CSL complex-mediated gene transcriptions are changed both quantitatively and qualitatively to direct distinct cellular responses. Therefore, NOTCH signaling strength can add a new layer of diversity to explain the pleotropic functions of NOTCH.

AUTHOR CONTRIBUTIONS

WS and YW conceived the study. All authors contributed their expertise in NOTCH signaling, epigenetic regulation, and cardiovascular development, respectively and contributed to the finalization of this manuscript significantly.

FUNDING

This work was supported by Xiamen Cardiovascular Hospital.

ACKNOWLEDGMENTS

We thank Dr. Jun Li from Shanghai Jiao Tong University for his discussions on this topic.

REFERENCES

Antfolk, D., Sjöqvist, M., Cheng, F., Isoniemi, K., Duran, C. L., Rivero-Muller, A., et al. (2017). Selective regulation of Notch ligands during angiogenesis is mediated by vimentin. *PNAS* 114, E4574–E4581. doi: 10.1073/pnas.1703057114

Apelqvist, A., Li, H., Sommer, L., Beatus, P., Anderson, D. J., Honjo, T., et al. (1999). Notch signalling controls pancreatic cell differentiation. *Nature* 400, 877–881. doi: 10.1038/23716

Artavanis-Tsakonas, S., Rand, M. D., and Lake, R. J. (1999). Notch signaling: cell fate control and signal integration in development. *Science* 284, 770–776.

Basatemur, G. L., Jørgensen, H. F., Clarke, M. C. H., Bennett, M. R., and Mallat, Z. (2019). Vascular smooth muscle cells in atherosclerosis. *Nat. Rev. Cardiol.* 16, 727–744. doi: 10.1038/s41569-019-0227-9

Bauer, R. C., Laney, A. O., Smith, R., Gerfen, J., Morrissette, J. J. D., Woyciechowski, S., et al. (2010). Jagged1 Mutations in Patients with Tetralogy of Fallot or Pulmonic Stenosis. *Hum. Mutat.* 31, 594–601. doi: 10.1002/humu.21231

Benedito, R., Roca, C., Sörensen, I., Adams, S., Gossler, A., Fruttiger, M., et al. (2009). The notch ligands Dll4 and Jagged1 have opposing effects on angiogenesis. *Cell* 137, 1124–1135. doi: 10.1016/j.cell.2009.03.025

Bennett, M. R., Sinha, S., and Owens, G. K. (2016). Vascular smooth muscle cells in atherosclerosis. *Circ. Res.* 118, 692–702. doi: 10.1161/CIRCRESAHA.115.306361

Blackwood, C. A., Bailetti, A., Nandi, S., Gridley, T., and Hébert, J. M. (2020). Notch Dosage: Jagged1 Haploinsufficiency Is Associated With Reduced Neuronal Division and Disruption of Periglomerular Interneurons in Mice. *Front. Cell Dev. Biol.* 8:00113. doi: 10.3389/fcell.2020.00113

Bolós, V., Grego-Bessa, J., and de la Pompa, J. L. (2007). Notch Signaling in Development and Cancer. *Endocr. Rev.* 28, 339–363. doi: 10.1210/er.2006-0046

Borggrefe, T., and Oswald, F. (2009). The Notch signaling pathway: transcriptional regulation at Notch target genes. *Cell Mol. Life Sci.* 66, 1631–1646. doi: 10.1007/s00018-009-8668-7

Brennan, A., and Kesavan, A. (2017). Novel Heterozygous Mutations in JAG1 and NOTCH2 Genes in a Neonatal Patient with Alagille Syndrome. *Case Rep. Pediatr.* 2017:1368189. doi: 10.1155/2017/1368189

Cristofaro, B., Shi, Y., Faria, M., Suchting, S., Leroyer, A. S., Trindade, A., et al. (2013). Dll4-Notch signaling determines the formation of native arterial collateral networks and arterial function in mouse ischemia models. *Development* 140, 1720–1729. doi: 10.1242/dev.092304

Davis-Knowlton, J., Turner, J. E., Turner, A., Damian-Loring, S., Hagler, N., Henderson, T., et al. (2019). Characterization of smooth muscle cells from human atherosclerotic lesions and their responses to Notch signaling. *Lab. Investig.* 99, 290–304. doi: 10.1038/s41374-018-0072-1

Eldadah, Z. A., Hamosh, A., Biery, N. J., Montgomery, R. A., Duke, M., Elkins, R., et al. (2001). Familial Tetralogy of Fallot caused by mutation in the jagged1 gene. *Hum. Mol. Genet.* 10, 163–169. doi: 10.1093/hmg/10.2.163

Fasnacht, N., Huang, H.-Y., Koch, U., Favre, S., Auderset, F., Chai, Q., et al. (2014). Specific fibroblastic niches in secondary lymphoid organs orchestrate distinct Notch-regulated immune responses. *J. Exp. Med.* 211, 2265–2279. doi: 10.1084/jem.20132528

Fischer-Zirnsak, B., Segebrecht, L., Schubach, M., Charles, P., Alderman, E., Brown, K., et al. (2019). Haploinsufficiency of the Notch Ligand DLL1 Causes Variable Neurodevelopmental Disorders. *Am. J. Hum. Genet.* 105, 631–639. doi: 10.1016/j.ajhg.2019.07.002

Fortini, M. E., and Bilder, D. (2009). Endocytic regulation of Notch signaling. *Curr. Opin. Genet. Dev.* 19, 323–328. doi: 10.1016/j.gde.2009.04.005

Fryer, C. J., White, J. B., and Jones, K. A. (2004). Mastermind recruits CycC:CDK8 to phosphorylate the Notch ICD and coordinate activation with turnover. *Mol. Cell* 16, 509–520. doi: 10.1016/j.molcel.2004.10.014

Gale, N. W., Dominguez, M. G., Noguera, I., Pan, L., Hughes, V., Valenzuela, D. M., et al. (2004). Haploinsufficiency of delta-like 4 ligand results in embryonic lethality due to major defects in arterial and vascular development. *PNAS* 101, 15949–15954. doi: 10.1073/pnas.0407290101

Gama-Norton, L., Ferrando, E., Ruiz-Herguido, C., Liu, Z., Liu, Z., Guiu, J., et al. (2015). Notch signal strength controls cell fate in the haemogenic endothelium. *Nat. Commun.* 6:8510. doi: 10.1038/ncomms9510

Gomez-Lamarca, M. J., Falo-Sanjuan, J., Stojnic, R., Abdul Rehman, S., Muresan, L., Jones, M. L., et al. (2018). Activation of the Notch Signaling Pathway In Vivo Elicits Changes in CSL Nuclear Dynamics. *Dev. Cell* 44, 611.e–623.e. doi: 10.1016/j.devcel.2018.01.020

Groot, A. J., Habets, R., Yahyanejad, S., Hodin, C. M., Reiss, K., Saftig, P., et al. (2014). Regulated Proteolysis of NOTCH2 and NOTCH3 Receptors by ADAM10 and Presenilins. *Mole. Cell. Biol.* 34, 2822–2832. doi: 10.1128/MCB.00206-14

Harper, J. A., Yuan, J. S., Tan, J. B., Visan, I., and Guidos, C. J. (2003). Notch signaling in development and disease. *Clin. Genet.* 64, 461–472.

Hass, M. R., Liow, H., Chen, X., Sharma, A., Inoue, Y. U., Inoue, T., et al. (2015). SpDamID: Marking DNA Bound by Protein Complexes Identifies Notch-Dimer Responsive Enhancers. *Mol. Cell* 59, 685–697. doi: 10.1016/j.molcel.2015.07.008

Hassed, S. J., Wiley, G. B., Wang, S., Lee, J.-Y., Li, S., Xu, W., et al. (2012). RBPJ Mutations Identified in Two Families Affected by Adams-Oliver Syndrome. *Am. J. Hum. Genet.* 91, 391–395. doi: 10.1016/j.ajhg.2012.07.005

Havrda, M. C., Johnson, M. J., O'Neill, C. F., and Liaw, L. (2006). A novel mechanism of transcriptional repression of p27kip1 through Notch/HRT2 signaling in vascular smooth muscle cells. *Thromb. Haemost.* 96, 361–370. doi: 10.1160/TH06-04-0224

High, F. A., Lu, M. M., Pear, W. S., Loomes, K. M., Kaestner, K. H., and Epstein, J. A. (2008). Endothelial expression of the Notch ligand Jagged1 is required for vascular smooth muscle development. *Proc. Natl. Acad. Sci. U S A* 105, 1955–1959. doi: 10.1073/pnas.0709663105

Hoglund, V. J., and Majesky, M. W. (2012). Patterning the artery wall by lateral induction of Notch signaling. *Circulation* 125, 212–215. doi: 10.1161/CIRCULATIONAHA.111.075937

Hozumi, K., Negishi, N., Suzuki, D., Abe, N., Sotomaru, Y., Tamaoki, N., et al. (2004). Delta-like 1 is necessary for the generation of marginal zone B cells but not T cells in vivo. *Nat. Immunol.* 5, 638–644. doi: 10.1038/ni1075

Huppert, S. S. (2016). A faithful JAGGED1 haploinsufficiency mouse model of arteriohepatic dysplasia (Alagille syndrome) after all. *Hepatology* 63, 365–367. doi: 10.1002/hep.28338

Ianni, M. D., Baldoni, S., Rosati, E., Ciurnelli, R., Cavalli, L., Martelli, M. F., et al. (2009). A new genetic lesion in B-CLL: a NOTCH1 PEST domain mutation. *Br. J. Haematol.* 146, 689–691. doi: 10.1111/j.1365-2141.2009.07816.x

Iso, T., Kedes, L., and Hamamori, Y. (2003). HES and HERP families: Multiple effectors of the notch signaling pathway. *J. Cell. Physiol.* 194, 237–255. doi: 10.1002/jcp.10208

Kakuda, S., and Haltiwanger, R. S. (2017). Deciphering the Fringe-Mediated Notch Code: Identification of Activating and Inhibiting Sites Allowing Discrimination between Ligands. *Dev. Cell* 40, 193–201. doi: 10.1016/j.devcel.2016.12.013

Kandachar, V., and Roegiers, F. (2012). Endocytosis and control of Notch signaling. *Curr. Opin. Cell Biol.* 24, 534–540. doi: 10.1016/j.ceb.2012.06.006

Kiel, M. J., Velusamy, T., Betz, B. L., Zhao, L., Weigelin, H. G., Chiang, M. Y., et al. (2012). Whole-genome sequencing identifies recurrent somatic NOTCH2 mutations in splenic marginal zone lymphoma. *J. Exp. Med.* 209, 1553–1565. doi: 10.1084/jem.20120910

Kobia, F. M., Preusse, K., Dai, Q., Weaver, N., Hass, M. R., Chaturvedi, P., et al. (2020). Notch dimerization and gene dosage are important for normal heart development, intestinal stem cell maintenance, and splenic marginal zone B-cell homeostasis during mite infestation. *PLoS Biol.* 18:e3000850. doi: 10.1371/journal.pbio.3000850

Kopan, R., and Ilagan, M. A. (2009). The Canonical Notch Signaling Pathway: Unfolding the Activation Mechanism. *Cell* 137, 216–233. doi: 10.1016/j.cell.2009.03.045

Lai, E. C. (2004). Notch signaling: control of cell communication and cell fate. *Development* 131, 965–973. doi: 10.1242/dev.01074

Lasky, J. L., and Wu, H. (2005). Notch Signaling, Brain Development, and Human Disease. *Pediatr. Res.* 57, 104R–109R. doi: 10.1203/01.PDR.0000159632.70510.3D

Luca, V. C., Kim, B. C., Ge, C., Kakuda, S., Wu, D., Roein-Peikar, M., et al. (2017). Notch-Jagged complex structure implicates a catch bond in tuning ligand sensitivity. *Science* 355, 1320–1324. doi: 10.1126/science.aaf9739

Manderfield, L. J., High, F. A., Engleka, K. A., Liu, F., Li, L., Rentschler, S., et al. (2012). Notch activation of Jagged1 contributes to the assembly of the arterial wall. *Circulation* 125, 314–323. doi: 10.1161/CIRCULATIONAHA.111.047159

McCright, B., Lozier, J., and Gridley, T. (2002). A mouse model of Alagille syndrome: Notch2 as a genetic modifier of Jag1 haploinsufficiency. *Dev.* 129, 1075–1082.

McDaniell, R., Warthen, D. M., Sanchez-Lara, P. A., Pai, A., Krantz, I. D., Piccoli, D. A., et al. (2006). NOTCH2 mutations cause Alagille syndrome, a heterogeneous disorder of the notch signaling pathway. *Am. J. Hum. Genet.* 79, 169–173. doi: 10.1086/505332

McKellar, S. H., Tester, D. J., Yagubyan, M., Majumdar, R., Ackerman, M. J., and Sundt, T. M. (2007). Novel NOTCH1 mutations in patients with bicuspid aortic valve disease and thoracic aortic aneurysms. *J. Thorac. Cardiovasc. Surg.* 134, 290–296. doi: 10.1016/j.jtcvs.2007.02.041

Meester, J. A. N., Southgate, L., Stittrich, A.-B., Venselaar, H., Beekmans, S. J. A., den Hollander, N., et al. (2015). Heterozygous Loss-of-Function Mutations in DLL4 Cause Adams-Oliver Syndrome. *Am. J. Hum. Genet.* 97, 475–482. doi: 10.1016/j.ajhg.2015.07.015

Morel, V., Lecourtois, M., Massiani, O., Maier, D., Preiss, A., and Schweisguth, F. (2001). Transcriptional repression by suppressor of hairless involves the binding of a hairless-dCtBP complex in Drosophila. *Curr. Biol.* 11, 789–792. doi: 10.1016/s0960-9822(01)00224-x

Morgan, T. H. (1917). The Theory of the Gene. *Am. Natural.* 51, 513–544. doi: 10.1086/279629

Nandagopal, N., Santat, L. A., LeBon, L., Sprinzak, D., Bronner, M. E., and Elowitz, M. B. (2018). Dynamic Ligand Discrimination in the Notch Signaling Pathway. *Cell* 172, 869.e–880.e. doi: 10.1016/j.cell.2018.01.002

Ninov, N., Borius, M., and Stainier, D. Y. R. (2012). Different levels of Notch signaling regulate quiescence, renewal and differentiation in pancreatic endocrine progenitors. *Development* 139, 1557–1567. doi: 10.1242/dev.076000

Noseda, M., Fu, Y., Niessen, K., Wong, F., Chang, L., McLean, G., et al. (2006). Smooth Muscle alpha-actin is a direct target of Notch/CSL. *Circ. Res.* 98, 1468–1470. doi: 10.1161/01.RES.0000229683.81357.26

Penton, A. L., Leonard, L. D., and Spinner, N. B. (2012). Notch signaling in human development and disease. *Semin. Cell Dev. Biol.* 23, 450–457. doi: 10.1016/j.semcdb.2012.01.010

Puente, X. S., Pinyol, M., Quesada, V., Conde, L., Ordóñez, G. R., Villamor, N., et al. (2011). Whole-genome sequencing identifies recurrent mutations in chronic lymphocytic leukaemia. *Nature* 475, 101–105. doi: 10.1038/nature10113

Rubio-Aliaga, I., Przemeck, G. K. H., Fuchs, H., Gailus-Durner, V., Adler, T., Hans, W., et al. (2009). Dll1 Haploinsufficiency in Adult Mice Leads to a Complex Phenotype Affecting Metabolic and Immunological Processes. *PLoS One* 4:e6054. doi: 10.1371/journal.pone.0006054

Saito, T., Chiba, S., Ichikawa, M., Kunisato, A., Asai, T., Shimizu, K., et al. (2003). Notch2 Is Preferentially Expressed in Mature B Cells and Indispensable for Marginal Zone B Lineage Development. *Immunity* 18, 675–685. doi: 10.1016/S1074-7613(03)00111-0

Sargin, D., Botly, L. C. P., Higgs, G., Marsolais, A., Frankland, P. W., Egan, S. E., et al. (2013). Disrupting Jagged1-Notch signaling impairs spatial memory formation in adult mice. *Neurobiol. Learn. Mem.* 103, 39–49. doi: 10.1016/j.nlm.2013.03.001

Shen, W., and Sun, J. (2020). Different modes of Notch activation and strength regulation in the spermathecal secretory lineage. *Development* 2020:184390. doi: 10.1242/dev.184390

Shutter, J. R., Scully, S., Fan, W., Richards, W. G., Kitajewski, J., Deblandre, G. A., et al. (2000). Dll4, a novel Notch ligand expressed in arterial endothelium. *Genes Dev.* 14, 1313–1318. doi: 10.1101/gad.14.11.1313

Southgate, L., Sukalo, M., Karountzos, A. S. V., Taylor, E. J., Collinson, C. S., Ruddy, D. et al. (2015). Haploinsufficiency of the NOTCH1 Receptor as a Cause of Adams–Oliver Syndrome With Variable Cardiac Anomalies. *Circulation* 8, 572–581. doi: 10.1161/CIRCGENETICS.115.001086

Stanley, P., and Okajima, T. (2010). Roles of glycosylation in Notch signaling. *Curr. Top Dev. Biol.* 92, 131–164. doi: 10.1016/S0070-2153(10)92004-8

Suckling, R. J., Korona, B., Whiteman, P., Chillakuri, C., Holt, L., Handford, P. A., et al. (2017). Structural and functional dissection of the interplay between lipid and Notch binding by human Notch ligands. *EMBO J.* 36, 2204–2215. doi: 10.15252/embj.201796632

Sweeney, C., Morrow, D., Birney, Y. A., Coyle, S., Hennessy, C., Scheller, A., et al. (2004). Notch 1 and 3 receptors modulate vascular smooth muscle cell growth, apoptosis and migration via a CBF-1/RBP-Jk dependent pathway. *FASEB J.* 18, 1421–1423. doi: 10.1096/fj.04-1700fje

Takeuchi, H., and Haltiwanger, R. S. (2010). Role of Glycosylation of Notch in Development. *Semin. Cell Dev. Biol.* 21:638. doi: 10.1016/j.semcdb.2010.03.003

Tang, Y., Urs, S., and Liaw, L. (2008). Hairy-Related Transcription Factors Inhibit Notch-Induced Smooth Muscle α-Actin Expression by Interfering With Notch Intracellular Domain/CBF-1 Complex Interaction With the CBF-1–Binding Site. *Circulat. Res.* 102, 661–668. doi: 10.1161/CIRCRESAHA.107.165134

Trøen, G., Wlodarska, I., Warsame, A., Llodrà, S. H., Wolf-Peeters, C. D., and Delabie, J. (2008). NOTCH2 mutations in marginal zone lymphoma. *Haematologica* 93, 1107–1109. doi: 10.3324/haematol.11635

Van de Walle, I., De Smet, G., De Smedt, M., Vandekerckhove, B., Leclercq, G., Plum, J., et al. (2009). An early decrease in Notch activation is required for human TCR-αβ lineage differentiation at the expense of TCR-γδ T cells. *Blood* 113, 2988–2998. doi: 10.1182/blood-2008-06-164871

Van de Walle, I., De Smet, G., Gärtner, M., De Smedt, M., Waegemans, E., Vandekerckhove, B., et al. (2011). Jagged2 acts as a Delta-like Notch ligand during early hematopoietic cell fate decisions. *Blood* 117, 4449–4459. doi: 10.1182/blood-2010-06-290049

Van de Walle, I., Waegemans, E., De Medts, J., De Smet, G., De Smedt, M., Snauwaert, S., et al. (2013). Specific Notch receptor-ligand interactions control human TCR-αβ/γδ development by inducing differential Notch signal strength. *J. Exp. Med.* 210, 683–697. doi: 10.1084/jem.20121798

van Engeland, N. C. A., Suarez Rodriguez, F., Rivero-Müller, A., Ristori, T., Duran, C. L., Stassen, O. M. J. A., et al. (2019). Vimentin regulates Notch signaling strength and arterial remodeling in response to hemodynamic stress. *Sci. Rep.* 9:12415. doi: 10.1038/s41598-019-48218-w

Wang, W., Campos, A. H., Prince, C. Z., Mou, Y., and Pollman, M. J. (2002). Coordinate Notch3-hairy-related transcription factor pathway regulation in response to arterial injury. Mediator role of platelet-derived growth factor and ERK. *J. Biol. Chem.* 277, 23165–23171. doi: 10.1074/jbc.M201409200

Warthen, D. M., Moore, E. C., Kamath, B. M., Morrissette, J. J. D., Sanchez-Lara, P. A., Sanchez, P., et al. (2006). Jagged1 (JAG1) mutations in Alagille syndrome: increasing the mutation detection rate. *Hum. Mutat.* 27, 436–443. doi: 10.1002/humu.20310

Washburn, T., Schweighoffer, E., Gridley, T., Chang, D., Fowlkes, B. J., Cado, D., et al. (1997). Notch activity influences the alphabeta versus gammadelta T cell lineage decision. *Cell* 88, 833–843. doi: 10.1016/s0092-8674(00)81929-7

Wilson, A., MacDonald, H. R., and Radtke, F. (2001). Notch 1-deficient common lymphoid precursors adopt a B cell fate in the thymus. *J. Exp. Med.* 194, 1003–1012. doi: 10.1084/jem.194.7.1003

Wu, L., Maillard, I., Nakamura, M., Pear, W. S., and Griffin, J. D. (2007). The transcriptional coactivator Maml1 is required for Notch2-mediated marginal zone B-cell development. *Blood* 110, 3618–3623. doi: 10.1182/blood-2007-06-097030

Zhang, X., Shi, Y., Weng, Y., Lai, Q., Luo, T., Zhao, J., et al. (2014). The Truncate Mutation of Notch2 Enhances Cell Proliferation through Activating the NF-κB Signal Pathway in the Diffuse Large B-Cell Lymphomas. *PLoS One* 9:e108747. doi: 10.1371/journal.pone.0108747

Zhuge, Y., Zhang, J., Qian, F., Wen, Z., Niu, C., Xu, K., et al. (2020). Role of smooth muscle cells in Cardiovascular Disease. *Int. J. Biol. Sci.* 16, 2741–2751. doi: 10.7150/ijbs.49871

Conflict of Interest: The authors declare that the research was conducted in the absence of any commercial or financial relationships that could be construed as a potential conflict of interest.

frontiers in Cell and Developmental Biology

ORIGINAL RESEARCH
published: 15 April 2021
doi: 10.3389/fcell.2021.631163

Taurine Attenuates the Hypotaurine-Induced Progression of CRC *via* ERK/RSK Signaling

Xiaodan Hou[1,2†], Junwei Hu[3†], Xinyu Zhao[1†], Qing Wei[1], Rongping Zhao[1], Min Li[1] and Qiong Li[1*]*

[1] Department of Laboratory Medicine, Renji Hospital, School of Medicine, Shanghai Jiaotong University, Shanghai, China, [2] Suzhou Institute of Systems Medicine, Center of Systems Medicine, Chinese Academy of Medical Sciences, Suzhou, China, [3] Department of Gastroenterology, Shanghai University of Medicine and Health Sciences Affiliated Zhoupu Hospital, Shanghai, China

Colorectal cancer (CRC) is one of the most common malignant tumors, and previous metabolomics work has demonstrated great promise in identifying specific small molecules of tumor phenotype. In the present study, we analyzed the metabolites of resected tissues through gas chromatography-mass spectrometry (GC-MS), and found that the concentration of taurine in CRC tissues diminished whereas the concentration of hypotaurine increased. The results *in vitro* demonstrated that taurine significantly suppressed cellular proliferation, metastasis, and colony formation whereas it induced apoptosis in CRC cells. Furthermore, taurine regulated the expression levels of epithelial mesenchymal transition (EMT)-associated genes in a dose-dependent manner. Taurine also alleviated hypotaurine-induced CRC progression, which was linked to the inhibition of the ERK/RSK-signaling pathway and diminution in intracellular hypotaurine. Taurine additionally attenuated hypotaurine-induced tumor growth and metastasis *in vivo.* Patients with CRC exhibited lower levels of serum taurine, suggesting that taurine might be a promising biomarker reflecting a poor prognosis in CRC. Collectively, our results demonstrated that taurine-attenuated, hypotaurine-induced CRC progression provides a potential target for CRC therapy.

Keywords: taurine, hypotaurine, tumor progression, ERK, colorectal cancer, prognosis

OPEN ACCESS

Edited by:
Narayanan Parameswaran, Michigan State University, United States

Reviewed by:
Rodrigo Franco, University of Nebraska-Lincoln, United States
Ankit Malik, University of Chicago, United States

****Correspondence:***
Min Li
ruth_limin@126.com
Qiong Li
qiongli@shsmu.edu.cn

† These authors have contributed equally to this work

Specialty section:
This article was submitted to Signaling, a section of the journal Frontiers in Cell and Developmental Biology

Received: *20 November 2020*
Accepted: *29 March 2021*
Published: *15 April 2021*

Citation:
Hou X, Hu J, Zhao X, Wei Q, Zhao R, Li M and Li Q (2021) Taurine Attenuates the Hypotaurine-Induced Progression of CRC via ERK/RSK Signaling. Front. Cell Dev. Biol. 9:631163. doi: 10.3389/fcell.2021.631163

INTRODUCTION

Colorectal cancer (CRC) is the third most common malignant disease worldwide, with an estimated 1.8 million new cases and 881,000 cancer deaths globally in 2018 (Bray et al., 2018; Siegel et al., 2019). The revised World Cancer Research Fund/American Institute for Cancer Research report points out that there is solid evidence that processed meat, alcohol, and obesity increase the risk of CRC. Although patients with early CRC can be cured by surgery (Shelton, 2002; Lieberman et al., 2012), patients with advanced CRC should not undergo surgery and chemotherapy (Imai et al., 2015). Therefore, more in-depth studies are needed regarding the underlying molecular mechanisms and drivers of CRC progression in order to find additional potential therapeutic targets and strategies.

Metabolomics can illuminate abnormal metabolic pathways associated with various tumor types. Taurine (2-aminoethanesulfonic acid) is a natural amino acid that is widely expressed in

mammalian tissues, and is critical for maintaining the functioning of the central nervous system, retinal neurons, cardiac, and skeletal muscle (Schaffer et al., 2010; Gaucher et al., 2012; Kilb and Fukuda, 2017; Khalil et al., 2018). As an antipyretic and anti-inflammatory drug, taurine has been used in the treatment of diabetes, cataracts, and cardiovascular disease (Song et al., 2003; Son et al., 2007; Megaraj et al., 2010; Das et al., 2012; El Zahraa et al., 2012; Yin et al., 2012). Recent evidence also shows that taurine possesses anti-tumor properties in cancer (Zhang et al., 2014, 2015). For example, previous studies have shown that taurine, with diethylnitrosamine as carcinogen and phenobarbital as cancer promoter, exerts a protective effect on chemically induced hepatomas in male F344 rats (Okamoto et al., 1996). After taurine treatment of S180 transplanted tumors in nude mice, apoptosis was significantly increased (Wang, 2008). Taurine can also upregulate the expression of *N*-acetyl galactosaminyl transferase 2 and downregulate the expression of matrix metalloproteinase-2, thus inhibiting potential invasion and metastasis by glioma cells (Neary et al., 2010). However, studies of the effects on CRC of taurine and its metabolic precursor hypotaurine remain limited.

In the present study, we first performed gas chromatography-mass spectrometry (GC-MS) to analyze the metabolites in CRC tissues. This investigation revealed that taurine was downregulated, whereas hypotaurine was upregulated in CRC. Next, we determined the functions of taurine in the regulation of hypotaurine-induced tumor progression. Finally, we explored the detailed molecular mechanisms responsible for taurine's function in CRC. Our data may provide new insights into the metabolic underpinnings of CRC progression, and offer key clues for developing new diagnostic and therapeutic targets for this devastating disease.

MATERIALS AND METHODS

Patients and Clinical Samples

Forty-two CRC patients underwent radical surgery without preoperative anti-cancer therapy at Renji Hospital, Shanghai Jiao Tong University School of Medicine, were enrolled in this study. Our study was authorized by the Renji Hospital Ethics Committee, and all patients were required to sign written informed consent. Serum samples were obtained prior to treatment, and fresh tissue specimens were collected after surgery. All clinical samples were stored immediately after collection at −80°C.

Cell Lines and Reagents

All human CRC cell lines were from the American Type Culture Collection (ATCC, Manassas, VA, United States) and authenticated by DNA profiling. All cells were cultured in DMEM supplemented with 10% FBS and 1% penicillin-streptomycin, in an incubator (Thermo Fisher Scientific, Waltham, MA, United States) at 37°C and 5% CO_2 in air. A MycoSEQ Detection kit was used to detect mycoplasma every 6 months (4460626; Thermo Fisher Scientific). Cell lines were utilized for less than 6 months after receipt or resuscitation from cryopreservation. We purchased taurine (HY-B0351) and hypotaurine (HY-100803) from MedChemExpress (Monmouth Junction, NJ, United States). SCH772984 (S7101), Ro 318220 (S7207), and Stattic (S7024) were used to inhibit different ERK-signaling pathways (Selleck Chemicals, Houston, TX, United States).

GC-MS and Liquid Chromatography-Tandem Mass Spectrometry (LC-MS/MS) in Metabolomics Analysis

Samples were prepared according to the manufacturer's protocols (Human Metabolome Technologies, HMT, Tokyo, Japan). GC-MS was conducted using an Agilent 7890A gas chromatography system combined with an Agilent 5975C inert MSD system (Agilent Technologies, Santa Clara, CA, United States). We performed LC-MS/MS using an Agilent 6460 Triple Quad LC/MS system (Agilent Technologies) with an electrospray ionization (ESI) source and using positive multiple reaction monitoring (MRM), and applied Agilent Mass Hunter Ver.B.04.00 software (Agilent Technologies) to collect the MS data. Peak picking and metabolite determination were conducted according to the manufacturer's protocol (HMT). Zero values were removed from the data based upon the 80%-rule as previously proposed (Bijlsma et al., 2006).

In vitro Cell Viability Assay

Prior to the application of different reagents at the indicated final concentrations, 5,000 cells/well were plated in triplicate in 96-well plates. We determined viability through Alamar Blue analysis as described after 5–7 days of culture (Zhang et al., 2017). All samples were tested in triplicate.

Soft-Agar Assay

Cells (5,000–10,000) were suspended in 0.3% agar containing DMEM and 10% FBS, and plated in triplicate in 24-well plates. After 3–4 weeks, the number of colonies per well was manually counted under an anatomical microscope (Olympus, Tokyo, Japan).

Caspase 3/7 Reporter Assay

All cells were seeded in triplicate in 96-well plates, and treated with different reagents for 24 h. The data were analyzed using a Synergy H4 Hybrid Multimode Microplate Reader (BioTek, Winooski, VT, United States). We purchased a caspase 3/7 reporter kit (G8091) from Promega (Madison, WI, United States).

Wound-Healing Assay

A total of approximately 2×10^5 cells were plated in 6-well plates. After starving overnight in the medium supplemented with 1% FBS, a confluent monolayer of >90% was scraped with a 200 μl pipette tip to form a linear wound. The plates were washed with PBS and incubated in complete medium with or without reagents for 24 h. A phase-contrast optical microscope (Olympus) was used to capture the wound images, and the horizontal distances

between the edges of the wounds were measured. All sampling was conducted in triplicate.

Transwell Invasion Assay

A total of approximately 5×10^4 cells were suspended in 200 μl of DMEM without serum and plated on the upper chamber of transwell filters in 24-well plates coated with Matrigel (354234; BD Biosciences, Franklin Lakes, NJ, United States), and filled with 500 μl of DMEM and 10% FBS with or without experimental agents. The lower chamber was fixed with 600 μl of DMEM. After 36 h of culture at 37°C, the non-invasive cells on the upper side of the membrane were removed, and the cells on the lower side of the membrane were fixed with 100% methanol for 20 min and stained with 1% crystal violet for 15 min at 37°C. The cell images were collected and five random fields were counted under an anatomical microscope. The sampling was conducted in triplicate.

Quantitative Real-Time Reverse Transcription Polymerase Chain Reaction Analysis

Trizol reagent (15596018; Thermo Fisher Scientific) was used to isolate total RNA from cells or tissues, and a One-Step RT-PCR kit (Qiagen, Dusseldorf, Germany) was used to synthesize cDNA. The ABI 7500 Real-time PCR system (Thermo Fisher Scientific) was used to evaluate the expression of CDH1, Snail, and FMO1. The primers were as follows: CDH1, 5′- AAGTGCTGCAGCCAAAGACAGA-3′ (forward) and 5′-AAATTGCCAGGCTCAATGACAAG-3′ (reverse); Snail, 5′-GGAAGCCTAACTACAGCGAGC-3′ (forward) and 5′-AGGACAGAGTCCCAGATGAGC-3′ (reverse); FMO1, 5′-GAGCGAAAGATAAACAACTGGCT-3′ (forward) and 5′-TGCTTGGCCTGATGAACACTT-3′ (reverse); GAPDH, 5′-GCACCGTCAAGGCTGAGAAC-3′ (forward); and 5′-ATGGTGGTGAAGACGCCAGT-3′ (reverse). GAPDH was used as a reference and the $2^{-\Delta\Delta Ct}$ methods were applied to quantify the relative expression levels.

Western Blotting Analysis

After treatment, RIPA lysis buffer [25 mmol/L Tris (pH7.4), 150 mmol/L NaCl, 5 mmol/L EDTA, and 1% Triton-X] plus phosphatase and protease inhibitors were used to harvest cells. A total of 30–50 μg of lysate was dissolved in the SDS-PAGE gels and then transferred to PVDF membranes (1620177; Bio-Rad, Hercules, CA, United States) that were blocked. The identification of target proteins was conducted with unique antibodies, followed by secondary antibodies. The commercial antibodies were purchased from Cell Signaling Technology (CST, Boston, MA, United States) as follows: rabbit monoclonal antibody to ERK1/2 (1:1000, 4695), rabbit monoclonal antibody to RSK (1:1000, 9355), phospho-ERK1/2 (T202/204) antibody (1:1000, 4370), phospho-RSK (S380) antibody (1:1000, 11989), and mouse monoclonal antibody to β-actin (1:1000, 3700). The secondary antibodies used in the experiments were IRDye 680RD donkey anti-mouse IgG (1:10000, 925-68072; LI-COR Biosciences, Lincoln, NE, United States) and IRDye 800CW goat anti-rabbit IgG (1:10000, 926-32211; LI-COR Biosciences). The blots were scanned using an Odyssey infrared imaging system (LI-COR Biosciences).

Xenograft Tumor Model

Our protocol was approved by the Ethics Committee of Renji Hospital. A total of 5×10^6 CRC cells were subcutaneously injected into the athymic flanks of 4-week-old BALB/c nude mice (Shanghai Laboratory Animal Center, Shanghai, China). Treatment was initiated when tumors approached a volume of approximately 100 mm^3, and tumor volume was calculated once per week using the formula $V = 1/2 (L \times W^2)$ (where L = length and W = width). The mice were then allocated to four groups according to the 4-week treatments as follows: (a) saline (vehicle), (b) taurine at 200 mg/kg/day, (c) hypotaurine at 200 mg/kg/day, and (d) taurine at 200 mg/kg/day plus hypotaurine at 200 mg/kg/day. At the end of the study, mice were euthanized, tumor weights were recorded, and the tumor tissues were collected for further analysis.

Orthotopic Model

Six-week-old NOD SCIDγ (NSG) mice were purchased from the Shanghai Laboratory Animal Center. The median incision in the abdominal wall was 1 cm, and the cecum was externalized. The mucous membrane was weakened in advance by mild rubbing against the wall to promote implantation, which was necessary to prevent tumor cells from infiltrating the cecal or peritoneal cavities. A 100 μl suspension containing 5×10^6 CT26 cells was then injected into the cecal wall. Mice were divided into four groups (six mice per group) seven days after implantation. We measured bioluminescence imaging (BLI) signals using the PhotonIMAGER Optima System (Biospace Lab, Nesles la Vallée, France), which can detect the presence of cecal, hepatic, and pulmonary tumors or micrometastases. Twenty-five days after implantation, the cecums, livers, and lungs were collected from treated mice and controls, and organs were fixed in 4% paraformaldehyde for 4 h for subsequent histologic and immunohistochemical analyses.

Histologic, Immunohistochemical, and Immunofluorescence Analyses

Tissues were stained with H&E after resection, fixed, and paraffin-embedded. Tumor nodules in livers and lungs were selected to evaluate the level of metastasis. For immunohistochemistry, 4 μm sections of tissue were incubated with cytokeratin 19 (1:200, 4,558; CST) antibody, and for immunofluorescence, fixed sections were incubated with primary antibodies to Ki67 (1:50, 9,449; CST), pan-keratin (1:50, 4,545; CST), or cleaved-caspase 3 (1:200, 9,664; CST). We quantified the number of Ki67-positive cells and apoptotic areas from two independent tumors of each group; this entailed 10 sections/tumor and 1 field/section, using a 20× objective, NIS-Elements software (Nikon, Tokyo, Japan), and a C2 + fluorescence confocal microscope.

Statistical Analysis

The data are presented as means ± standard error of the mean (SEM). We used an unpaired Student's *t* test to compare two groups, and one-way ANOVA followed by Tukey's *post hoc* test for multiple comparisons. The Prism 6 software program was used to analyze the data. All tests were two-tailed, and $P < 0.05$ was considered significant.

RESULTS

GC-MS of Metabolic Changes in CRC Tissues

We used GC-MS to examine the alterations of metabolites in CRC. We included World Health Organization (WHO) grade IV ($n = 3$) CRC specimens, and the normal colonic tissue around the tumor obtained during the operation was used as the control sample ($n = 3$). The analysis of raw GC-MS data has been described in previous protocols (Gao et al., 2010). The peak table file was imported into SIMCA (Version 11.0, Umetrics, Umea, Sweden), including principal component analysis (PCA), partial least squares-discriminant analysis (PLS-DA), and orthogonal partial least squares-discriminant analysis (OPLS-DA). Two PCs were each measured for tissue extracts explained by t1 and t2. The score curve showed that each group was scattered in different areas that represented a significant separation of cancer and non-cancer samples, indicating that colon cancer tissue had a specific metabolic spectrum that was different from that of the controls (**Figure 1**).

Taurine and Hypotaurine in CRC Tissues

In the OPLS-DA model, the variable importance in the project (VIP) was employed to express the importance of different features to sample discrimination. Characteristics with VIP values greater than one were chosen for further consideration, including the development of discriminatory models and the recognition of chemical structures. We analyzed and queried the parameters of each feature in the following databases: Kyoto Encyclopedia of Genes and Genomes (KEGG [1]), Human Metabolome Database (HMDB[2]), and Mass Bank[3]. The fold-change was measured as the binary logarithm of the mean normalized peak-intensity ratio between the cancer and normal groups, and a positive value indicated that the mean quality response of the cancer group was greater than that of the normal group. We ultimately identified the structures of 28 metabolites, and observed that the content of taurine in the cancer group was lower than that in the normal group, and that the content of hypotaurine in the cancer group was reciprocally higher than in the normal group (**Figure 2**).

[1]http://www.genome.jp/kegg/

[2]http://www.hmdb.ca/

[3]http://www.massbank.jp/

Taurine Attenuates Hypotaurine-Induced Tumor Progression in CRC Cells

We first examined the effect of taurine as a single agent in nine conventional monolayer-cultured CRC cell lines. After five days of culture in a 2D condition, the cell viability of all CRC cell lines was inhibited in a concentration-dependent manner. HT-29 and LoVo were two representative CRC cell lines that showed a significant difference in taurine sensitivity, and were therefore chosen for subsequent studies (**Figure 3A**). A variety of *in vitro* assays were employed to assess the effects of taurine on cellular functions, including proliferation, apoptosis, migration, and invasion, in order to identify whether taurine was functionally involved in CRC cells. **Figure 3B** illustrates that upregulation of taurine inhibited the proliferation of HT-29 and LoVo cells through Alamar Blue assays (**Figure 3B**), and colony formation assays verified that taurine exerted an inhibitory action on cellular proliferation (**Figure 3C**). Caspase-3/7 activity was measured to investigate the apoptotic action of taurine on both cell lines, and it significantly increased after treatment with taurine for 24 h (**Figure 3D**). In the wound-healing migration assay, taurine-treated cells displayed a suspension of wound healing (**Figures 3E,F**); and transwell assays showed that taurine significantly impaired cellular invasion in both cell lines (**Figures 3G,H**). To determine whether elevated taurine played an important role in hypotaurine induced-CRC progression, we treated CRC cells with a combination of taurine and hypotaurine, and the results revealed that taurine rescued the suppression of apoptosis, and enhanced proliferation, migration, and invasion of hypotaurine-treated CRC cells (**Figures 3A–H**).

Taurine Attenuates the Hypotaurine-Induced Epithelial Mesenchymal Transition in CRC Cells

The epithelial mesenchymal transition (EMT) is one of the critical factors in cellular proliferation, apoptosis, and metastasis. We determined the change in EMT markers in CRC cells with quantitative real-time reverse transcription polymerase chain reaction (qRT-PCR) analysis, and showed upregulation of CDH1 expression and downregulation of Snail in HT-29 and LoVo cells with taurine treatment. Compared with the control group, these effects persisted with increasing dose and duration of taurine treatment (**Figures 4A–D**), and thus taurine affected CDH1 and Snail expression levels in a dose- and time-dependent manner. Our data also showed that taurine reversed hypotaurine-mediated expression of EMT markers in CRC cells (**Figures 4E,F**).

Taurine Attenuates Hypotaurine-Induced Tumor Progression and the EMT *via* the Extracellular-Signal Regulated Kinase (ERK)/Ribosomal S6 Kinase (RSK) Pathway, and Decreases Hypotaurine Level in CRC Cells

To investigate the possible mechanism underlying taurine inhibition of hypotaurine-induced progression and EMT in CRC

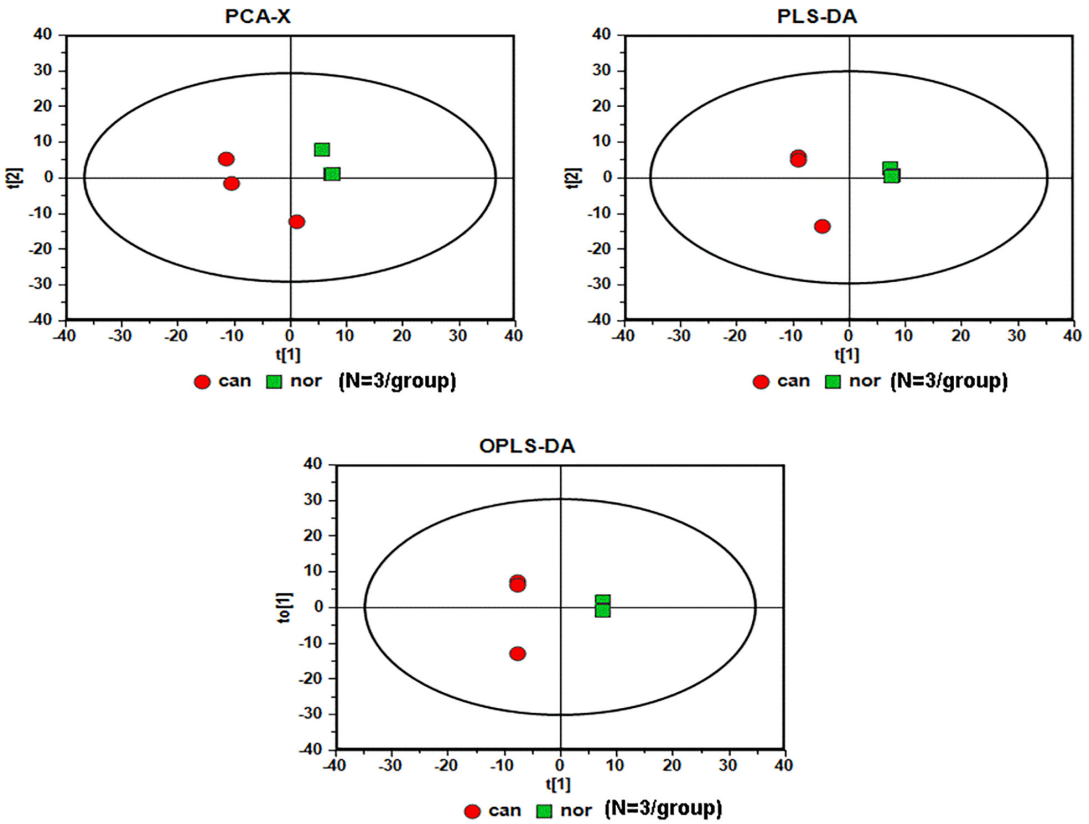

FIGURE 1 | Serummetabolic profiles derived from CRC tissues are different from those of healthy subjects (*N* = 3/group). Red circles, cancer samples; green squares, normal samples.

cells, we analyzed taurine and/or hypotaurine effects on the ERK pathway through western blotting analysis. Taurine significantly suppressed the levels of p-ERK and p-RSK in CRC cells, while hypotaurine induced ERK activation (**Figures 5A,B**). These data suggested that the ERK/RSK pathway may participate in taurine regulation of hypotaurine-induced progression and the EMT of CRC. Hypotaurine concentrations decreased significantly in a dose- dependent manner over a 24-h taurine exposure, while taurine levels did not increase during prolonged incubation of cells with these precursors (**Figures 5C,D**). This suggested that the enzymatic conversion of hypotaurine to taurine was either lacking or strictly regulated in these cell lines. The investigators recently demonstrated that the flavin-containing monooxygenase 1 (FMO1) oxygenated hypotaurine to produce taurine both *in vivo* and *in vitro* (Veeravalli et al., 2020). We thus executed qRT-PCR analysis using colonic tissues, and found the level of FMO1 mRNA to be significantly decreased in CRC compared to normal colonic tissues (**Figure 5E**). It has been reported that the phosphorylation-activated ERK1/2 translocates to the nucleus where it phosphorylates and activates mitogen- and stress-activated protein kinase (MSK), RSK, and signal transducer and activator of transcription 3 (STAT3) to stimulate cellular growth and proliferation (Zhang and Liu, 2002). To explore the possible downstream effectors of ERK1/2 signaling (besides RSK) in CRC cells, we analyzed the effects of three different ERK inhibitors on hypotaurine levels by LC-MS analysis. The results suggested that only the ERK/RSK inhibitor could regulate intracellular hypotaurine levels (**Figures 5F–H**). Collectively, our results strongly support our contention that the ERK/RSK pathway and decreased hypotaurine levels play important roles in taurine-mediated inhibition of tumor progression and the EMT.

The Inhibition of ERK/RSK Signaling Mimics the Counteracting Effects of Taurine on Hypotaurine

Previous research has established that RSKs are important regulators of migration and invasion in response to activation of the ERK/MAPK-signaling pathway (Sulzmaier and Ramos, 2013). To further verify whether ERK/RSK signaling contributed to hypotaurine-induced CRC progression and the EMT, we treated CRC cells with a combination of the ERK/RSK inhibitor and hypotaurine, and showed that SCH772984 rescued suppressed apoptosis and enhanced proliferation, migration, and invasion of hypotaurine-treated CRC cells (**Figures 6A–F** and **Supplementary Figures 7**, **8**). Furthermore, our data showed that SCH772984 reversed hypotaurine-mediated expression of EMT markers in CRC cells (**Figures 6G,H**). Taken together, our results strongly support our hypothesis that the

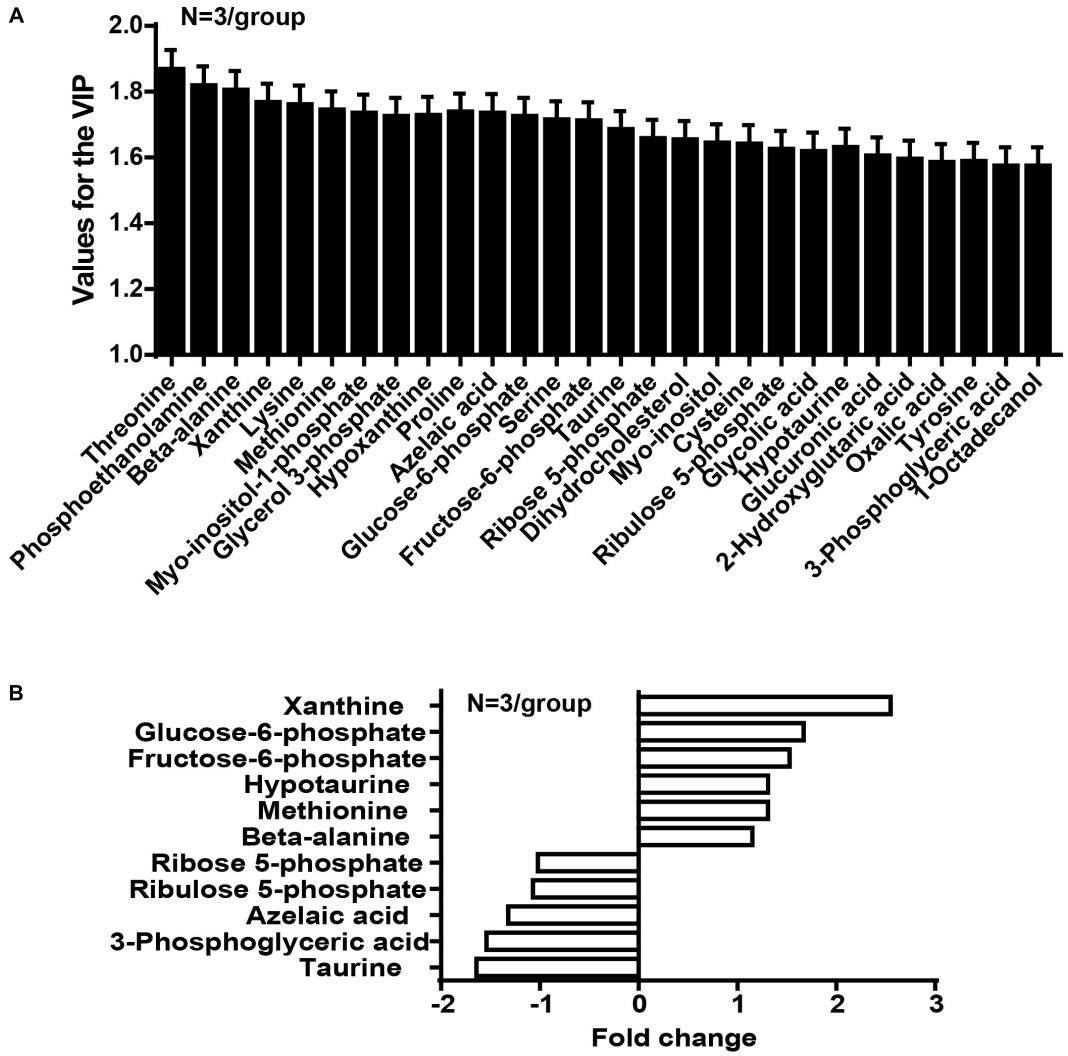

FIGURE 2 | The concentration of taurine is diminished whereas the concentration of hypotaurine is augmented in CRC tissues (N = 3/group). **(A)** Values for the VIP of 28 characteristics are depicted. Each column displays one feature of the PLS-DA model **(Figure 1)**. Error bars represent the SEM. **(B)** Different levels of compounds between cancer and normal groups (2-tailed t test, $P < 0.05$). The y-axis represents the various compounds, and the x-axis represents fold-change in metabolite levels.

inhibition of ERK/RSK signaling mimics the preventive effects of taurine on hypotaurine.

Taurine Attenuates Hypotaurine-Induced Tumor Growth *in vivo*

Our research has shown that taurine participates in hypotaurine-induced CRC growth *in vitro*, and that taurine reverses tumor growth in hypotaurine-treated xenograft mouse models. HT-29 and LoVo cells readily form tumors in immunocompromised mice, with a short latency period (∼14 days), and these were established in our nude mice (∼100 mm^3). Hypotaurine alone promoted tumor growth, but combination-treated tumors were lower in tumor volume and weight in both models (**Figures 7A,B,E,F**). Compared with hypotaurine treatment, the combination-treated tumors displayed increased apoptosis (as assessed by cleaved-caspase-3^+ area) and decreased proliferation (Ki-67^+) of neoplastic cells (dual pan-CK^+Ki-67^+cells) (**Figures 7C,D,G,H**). Our collective results strongly support taurine as reversing hypotaurine-induced tumor growth.

Taurine Attenuates Hypotaurine-Mediated Tumor Metastasis *in vivo*

As taurine was shown to attenuate the migration and invasion of hypotaurine-treated CRC cells, its effects *in vivo* were further examined. We thereby established an orthotopic colonic tumor model using spontaneous lung and liver metastasis xenografts in BALB/c mice. We initiated treatment once tumor establishment was confirmed by a positive bioluminescence

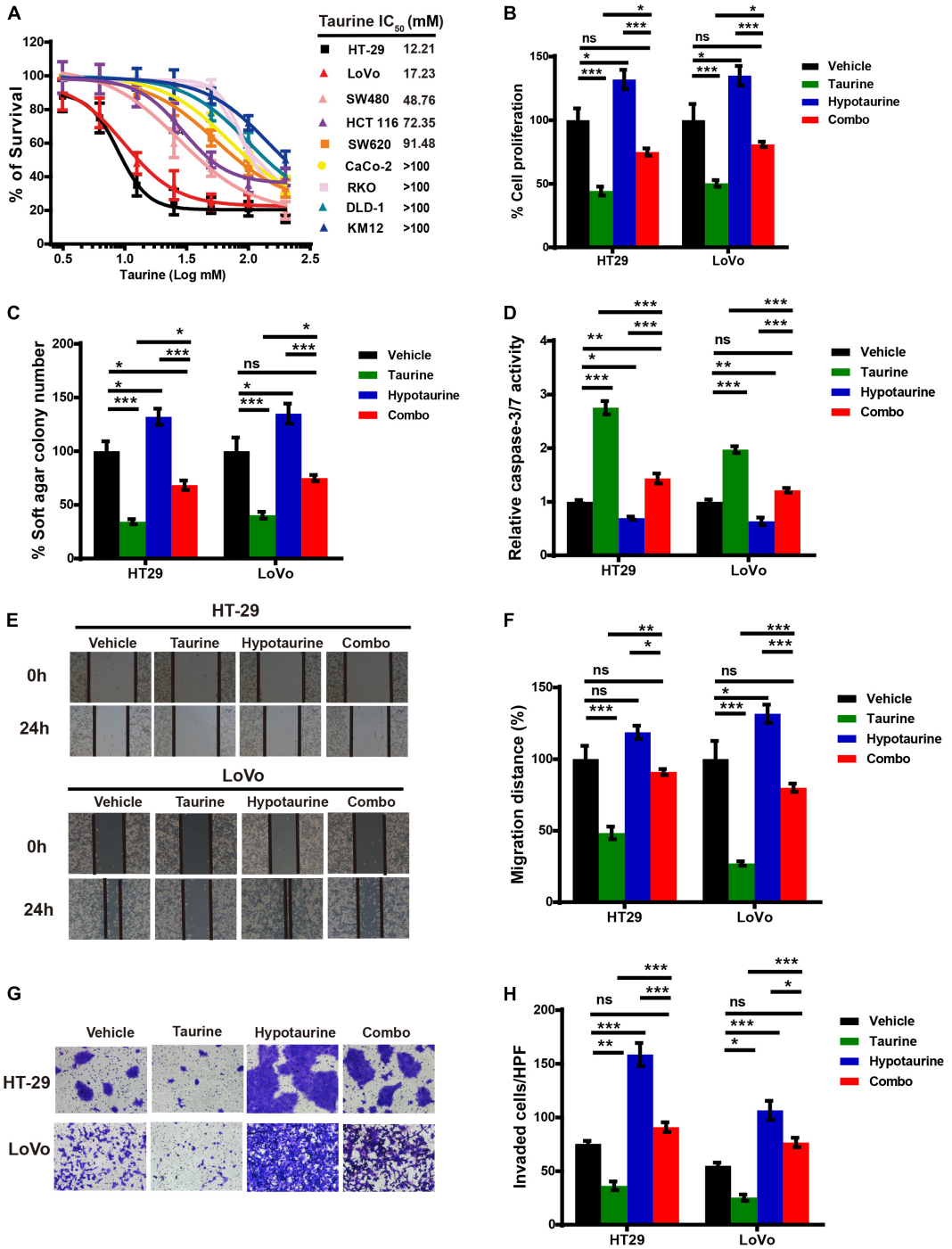

FIGURE 3 | Taurine reverses the promoting effects of hypotaurine on CRC progression. **(A)** The viability of CRC cell lines cultured for five days in serial concentrations of taurine, and each IC50 value were shown by Alamar Blue assay (means ± SEM). **(B)** The proliferative rate of CRC cell lines after treatment with taurine (10 mM) and/or hypotaurine (10 mM) (means ± SEM) (one-way ANOVA followed by Tukey's *post hoc* test, $^{*}P < 0.05$, $^{***}P < 0.001$). **(C)** Quantification of clones formed by the indicated CRC lines after treatment with taurine (5 mM) and/or hypotaurine (5 mM) for 3 weeks (means ± SEM) (one-way ANOVA followed by Tukey's *post hoc* test, $^{*}P < 0.05$, $^{***}P < 0.001$). **(D)** The proapoptotic effects of taurine (10 mM) and/or hypotaurine (10 mM) on CRC cells were detected by caspase 3/7 reporter assay (means ± SEM) (one-way ANOVA followed by Tukey's *post hoc* test, $^{*}P < 0.05$, $^{**}P < 0.01$, $^{***}P < 0.001$). **(E,F)** The cellular migratory effects of taurine (10 mM) and/or hypotaurine (10 mM) in CRC cells were evaluated by wound-healing assay and quantified. (means ± SEM) (one-way ANOVA followed by Tukey's post- hoc test, $^{*}P < 0.05$, $^{***}P < 0.001$). **(G,H)** The cellular invasive effects of taurine (10 mM) and/or hypotaurine (10 mM) in CRC cells were assessed using the transwell invasion assay and quantified (means ± SEM) (one-way ANOVA followed by Tukey's *post hoc* test, $^{*}P < 0.05$, $^{**}P < 0.01$, $^{***}P < 0.001$).

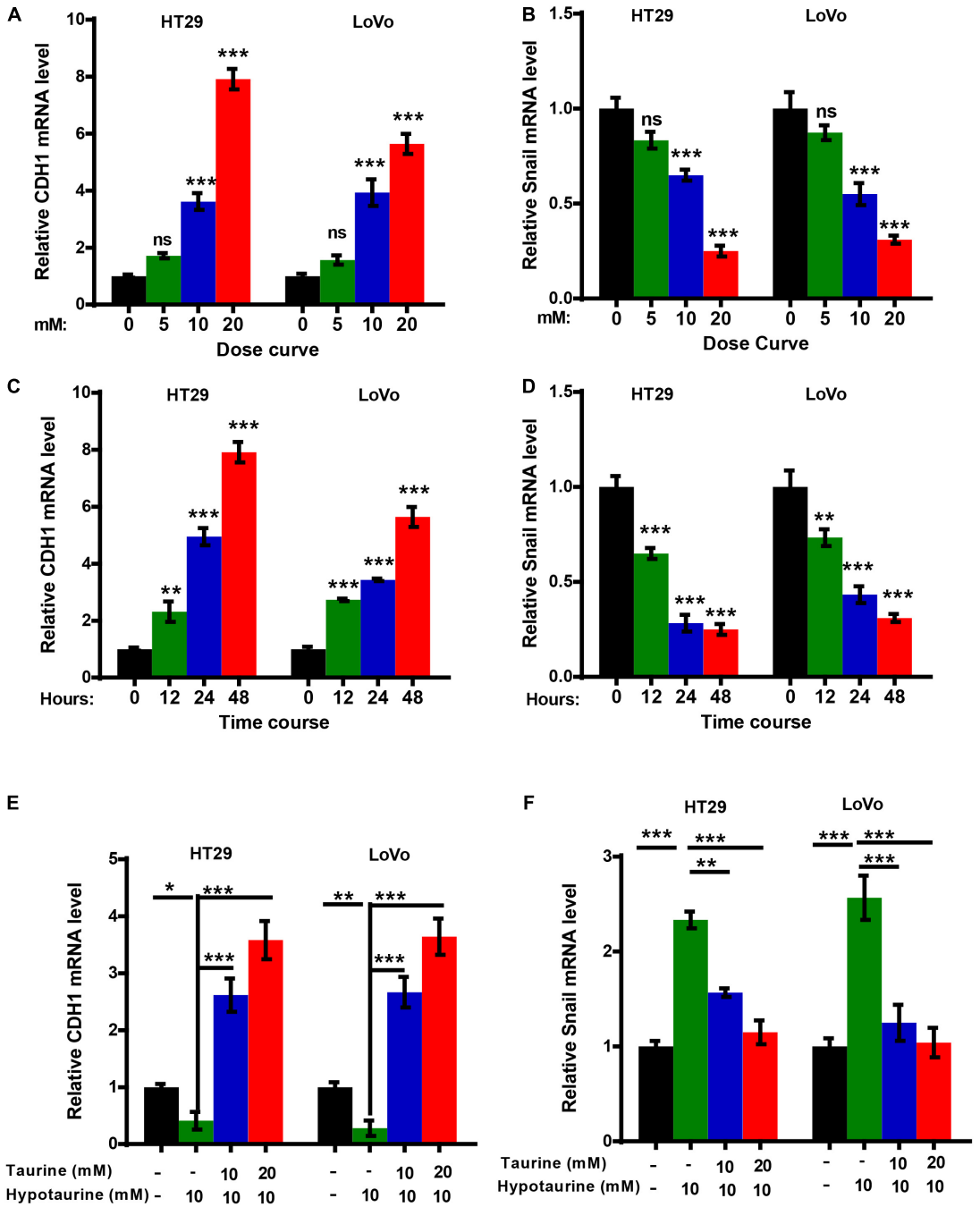

FIGURE 4 | Taurine reverses the promoting effect of hypotaurine on the EMT in CRC cells. **(A,B)** The dose-effect curve for taurine on EMT related-gene expression in CRC cells was determined by qRT-PCR (means ± SEM) (one-way ANOVA followed by Tukey's *post hoc* test, ***$P < 0.001$). **(C,D)** The time-effect curve for taurine on EMT related-gene expression in CRC cells was developed using qRT-PCR (means ± SEM) (one-way ANOVA followed by Tukey's *post hoc* test, **$P < 0.01$, ***$P < 0.001$). **(E,F)** The effects of taurine and/or hypotaurine on EMT markers in CRC cells were measured by qRT-PCR (means ± SEM) (one-way ANOVA followed by Tukey's *post hoc* test, *$P < 0.05$, **$P < 0.01$, ***$P < 0.001$).

signal. On day 25 (the day of sacrifice), macroscopic pulmonary and hepatic metastases were determined by bioluminescence signals and spots of tissue necrosis on the organs. H&E and cytokeratin 19 staining of lung and liver tissues were performed to assess tumor cell metastasis. Our representative photomicrographs depict the metastases of tumor cells to liver and lung, and the formation of tumor nodules (**Figures 8A,B**). Although the number of metastatic nodules in livers and lungs decreased with taurine treatment, hypotaurine promoted CRC cell metastasis (**Figures 8C,D**) indicating that taurine could

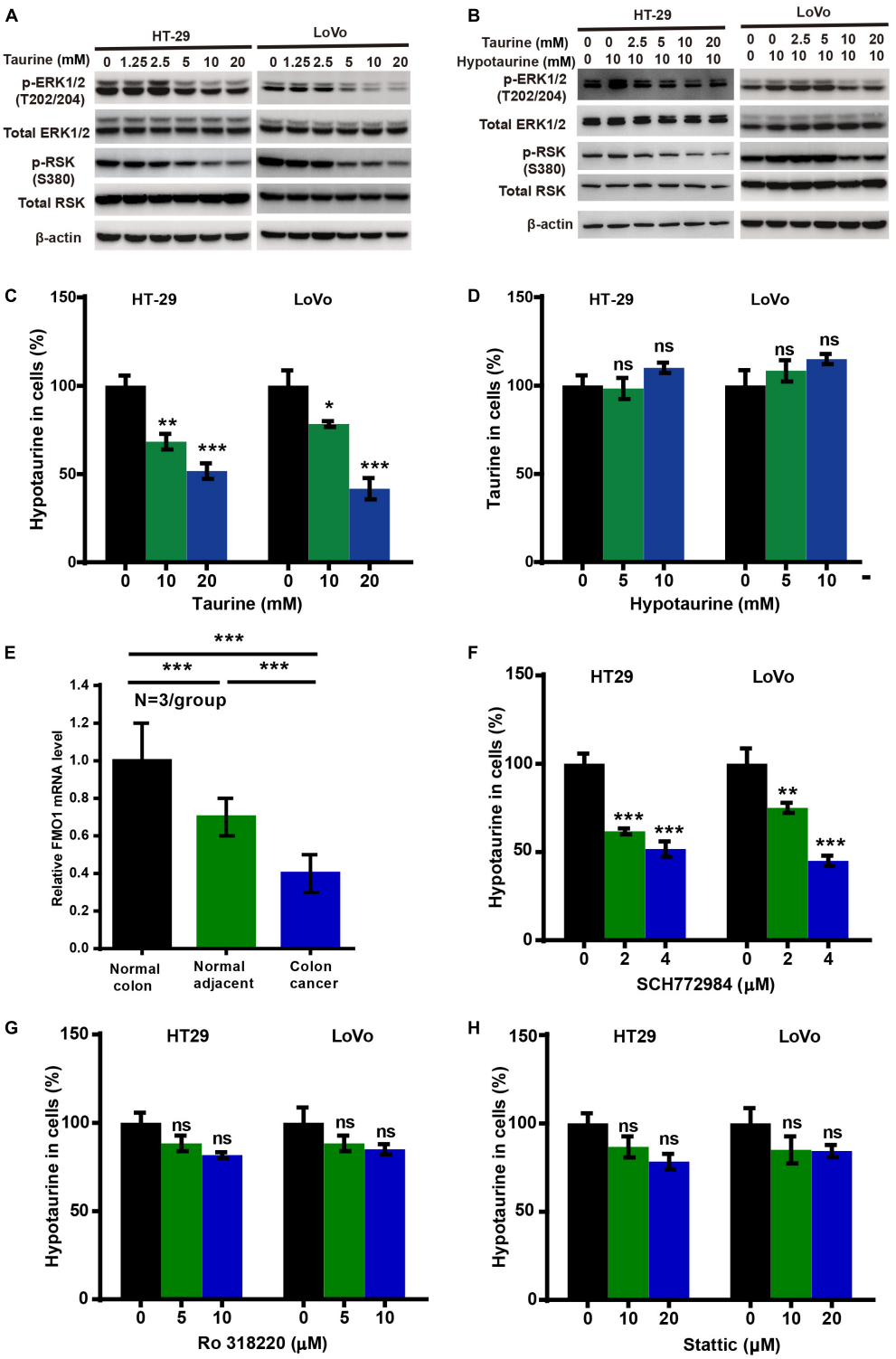

FIGURE 5 | Taurine reverses the promoting effects of hypotaurine on tumor progression and EMT through the ERK/RSK pathway, and decreases intracellular hypotaurine levels in CRC cells. **(A,B)** The effects of taurine and/or hypotaurine on the phosphorylation (denoted p-) status of ERK and RSK were assessed with western blotting analysis. **(C,D)** CRC cells were incubated for 24 h in medium with the indicated concentrations of taurine or hypotaurine, and intracellular hypotaurine or taurine concentrations were identified by LC-MS analysis (means ± SEM) (one-way ANOVA followed by Tukey's *post hoc* test, $^{*}P < 0.05$, $^{**}P < 0.01$, $^{***}P < 0.001$). **(E)** FMO1 mRNA expression in normal colon, normal colonic tissues adjacent to cancer, and colon cancer were determined by qRT-PCR (means ± SEM) (N = 3/group; one-way ANOVA followed by Tukey's post- hoc test, $^{***}P < 0.001$). **(F–H)** CRC cells were incubated for 24 h in medium with the indicated concentrations of different ERK inhibitors (SCH772984, Ro 318220, and Stattic), and intracellular hypotaurine concentrations were identified by LC-MS analysis (means ± SEM) (one-way ANOVA followed by Tukey's *post hoc* test, $^{**}P < 0.01$, $^{***}P < 0.001$).

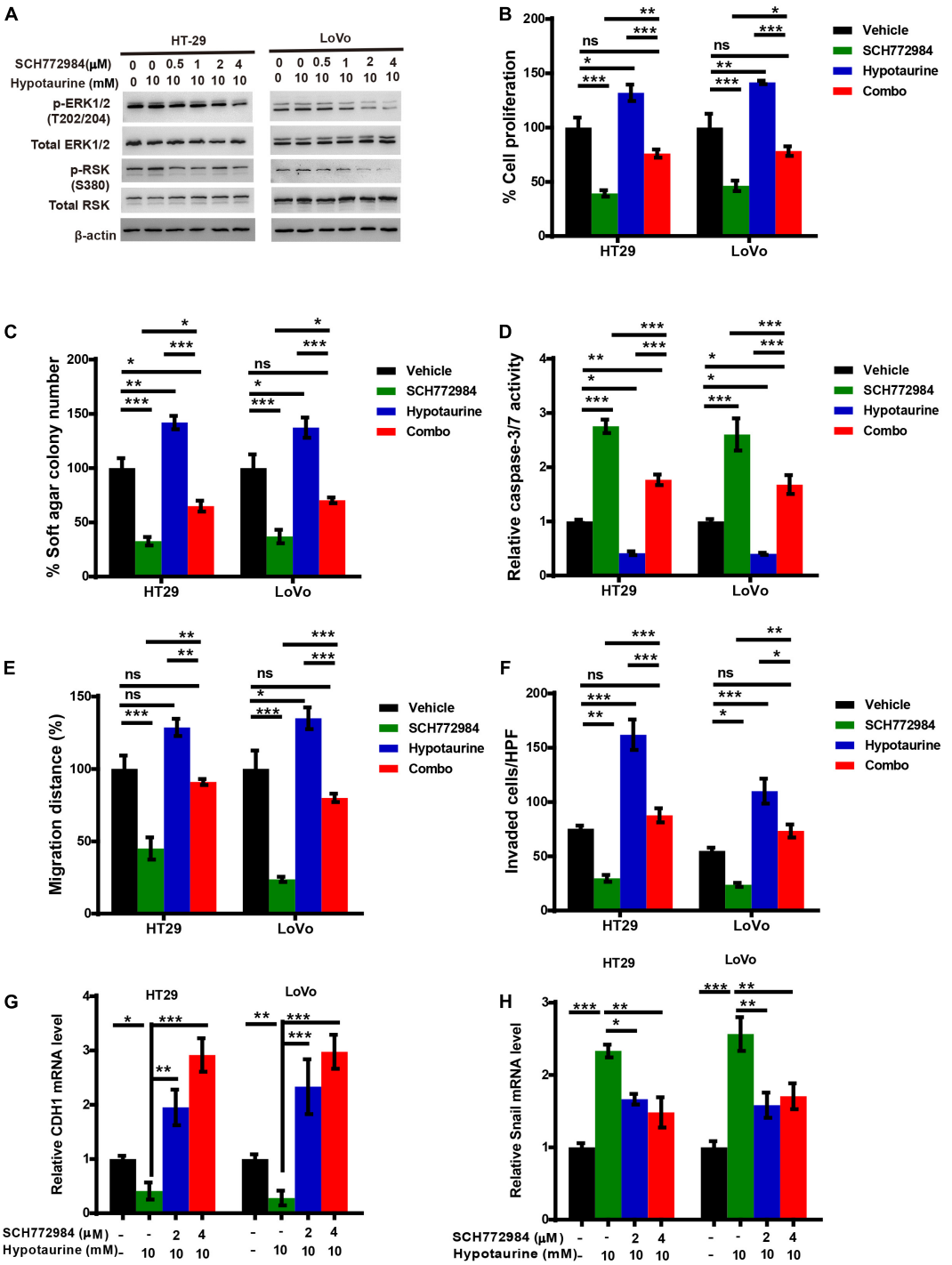

FIGURE 6 | An ERK/RSK inhibitor reverses the promoting effects of hypotaurine on tumor progression and EMT in CRC cells. **(A)** The effects of ERK/RSK inhibitor (SCH772984) on the phosphorylation (denoted p-) status of ERK and RSK were detected with western blotting analysis. **(B)** The proliferative rates of CRC cell lines after treatment with SCH772984 (2 μM) and/or hypotaurine (10 mM) (means ± SEM) (one-way ANOVA followed by Tukey's *post hoc* test, $^{*}P < 0.05$, $^{**}P < 0.01$, $^{***}P < 0.001$). **(C)** Quantification of clones formed by the indicated CRC lines after treatment with SCH772984 (1 μM) and/or hypotaurine (5 mM) for 3 weeks (means ± SEM) (one-way ANOVA followed by Tukey's *post hoc* test, $^{*}P < 0.05$, $^{**}P < 0.01$, $^{***}P < 0.001$). **(D)** The proapoptotic effects of SCH772984 (2 μM) and/or hypotaurine (10 mM) on CRC cells were observed with caspase 3/7 reporter assay (means ± SEM) (one-way ANOVA followed by Tukey's *post hoc* test, $^{*}P < 0.05$, $^{**}P < 0.01$, $^{***}P < 0.001$). **(E)** The cellular migratory effects of SCH772984 (2 μM) and/or hypotaurine (10 mM) on CRC cells were determined by wound-healing assay and quantified. (means ± SEM) (one-way ANOVA followed by Tukey's *post hoc* test, $^{*}P < 0.05$, $^{**}P < 0.01$, $^{***}P < 0.001$). **(F)** The cellular invasive effects of SCH772984 (2 μM) and/or hypotaurine (10 mM) on CRC cells were ascertained by transwell invasion assay and quantified (means ± SEM) (one-way ANOVA followed by Tukey's *post hoc* test, $^{*}P < 0.05$, $^{**}P < 0.01$, $^{***}P < 0.001$). **(G,H)** The effects of SCH772984 and/or hypotaurine on EMT markers in CRC cells were discerned using qRT-PCR (means ± SEM) (one-way ANOVA followed by Tukey's *post hoc* test, $^{*}P < 0.05$, $^{**}P < 0.01$, $^{***}P < 0.001$).

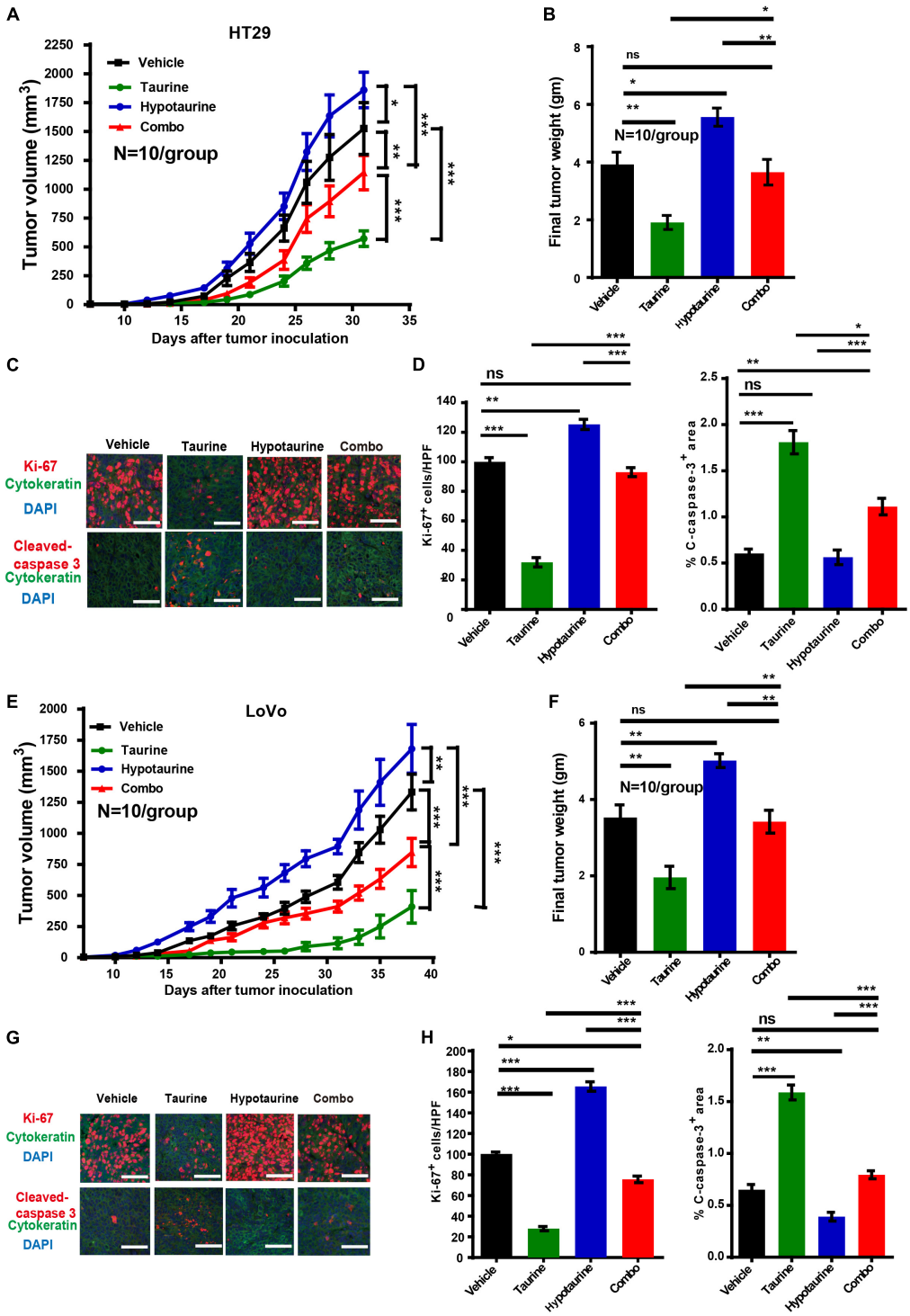

FIGURE 7 | Taurine reverses the promoting effects of hypotaurine on tumor growth *in vivo*. **(A,B)** Serial measurements of tumor volume and final weights of HT-29 tumors grown subcutaneously in nude mice treated as indicated (means ± SEM) (N = 10/group; one-way ANOVA followed by Tukey's *post hoc* test, $^{*}P < 0.05$, $^{**}P < 0.01$, $^{***}P < 0.001$). **(C,D)** Representative photomicrographs **(C)** and quantification of cleaved caspase-3^{+} area per × 200 field and dual CK^{+} and Ki-67^{+} cells per × 400 field **(D)** of HT-29 tumors treated as indicated using immunofluorescence. Ten random photographs were taken from each of 10 tumors per group (mean ± SEM) (one-way ANOVA followed by Tukey's *post hoc* test, $^{**}P < 0.01$, $^{***}P < 0.001$; scale bars, 50 μm). **(E,F)** Serial measurements of tumor volume and final weights of LoVo tumors grown subcutaneously in nude mice treated as indicated (means ± SEM) (N = 10/group; one-way ANOVA followed by Tukey's post-hoc test, $^{**}P < 0.01$, $^{***}P < 0.001$). **(G,H)** Representative photomicrographs **(G)** and quantification of cleaved caspase-3^{+} area/200 field, and dual CK^{+} and Ki-67^{+} cells/400 field **(H)** of LoVo tumors treated as indicated and determined by immunofluorescence. Ten photomicrographic images were captured randomly from each of 10 tumors per group (mean ± SEM) (one-way ANOVA followed by Tukey's *post hoc* test, $^{*}P < 0.05$, $^{**}P < 0.01$, $^{***}P < 0.001$; scale bars, 50 μm).

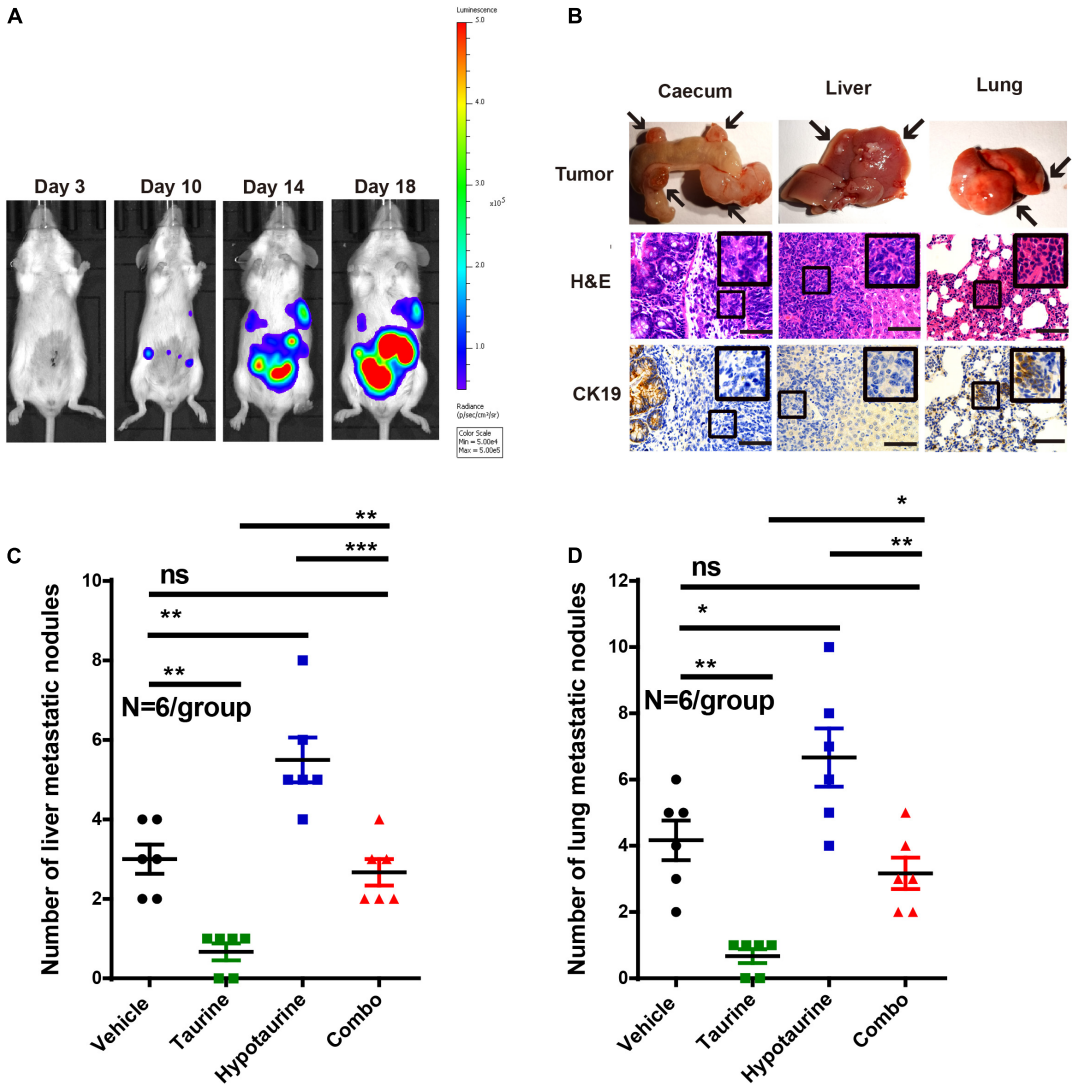

FIGURE 8 | Taurine reverses the promoting effects of hypotaurine on tumor metastasis *in vivo*. **(A)** Representative images of total mouse luciferase signal were shown, manifesting the presence of tumor formation, liver, and lung metastases. **(B)** The cecum, liver, and lung of mice were stained with H&E and cytokeratin 19. The arrows represented macroscopic cecal tumor and metastatic spots (magnification 200×; scale bars, 50 μm). **(C,D)** Quantitative results of metastatic area as liver/lung (mean ± SEM) (*N* = 6/group; one-way ANOVA followed by Tukey's *post hoc* test, $^{*}P < 0.05$, $^{**}P < 0.01$, $^{***}P < 0.001$).

suppress the metastasis of hypotaurine-induced colonic cancer to liver and lung.

Low Levels of Taurine in Serum Are Associated With a Poor Prognosis in CRC Patients

To investigate whether taurine might serve as a potential prognostic biomarker for CRC patients, we measured serum taurine levels in healthy donors and CRC patients by LC-MS. It is worth noting that when other clinicopathologic factors were controlled (**Supplementary Table 1**), we found that patients with metastatic CRC exhibited significantly lower serum concentrations of taurine relative to patients with primary CRC (**Figure 9**). These results thus showed that low serum taurine was correlated with poor prognosis in CRC patients.

DISCUSSION

The purpose of our study was to identify the abnormal metabolic pathways in CRC and their effects on tumor progression. Using GC-MS, we identified 28 metabolites, and also noted lower taurine and higher hypotaurine levels in the cancer group compared to the normal group. However, the biologic roles of taurine and hypotaurine remain elusive. The biosynthesis of taurine includes the oxidation of cysteine to cysteinesulfinic acid as catalyzed by cysteine dioxygenase, decarboxylation catalyzed by cysteine sulfite decarboxylase, and the oxidation of

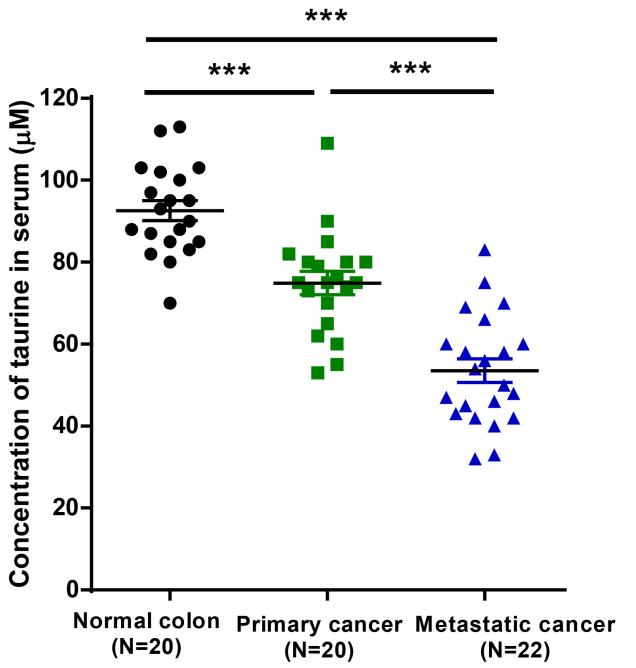

FIGURE 9 | Downregulated taurine levels in serum are correlated with a poor prognosis in CRC patients (mean ± SEM) (N = 20 normal and 42 patients; one-way ANOVA followed by Tukey's *post hoc* test, ***$P < 0.001$).

hypotaurine to taurine by hypotaurine dehydrogenase (Vitvitsky et al., 2011). In our study, taurine and hypotaurine might therefore play a critical role in the mechanisms underlying CRC. Although promising progress has been made in early diagnosis, surgical techniques, and chemotherapy, the prognosis of patients with CRC remains disappointing. Because abnormal metabolomic profiles have been reported to be linked to tumor progression (Chinnaiyan et al., 2012; Hadi et al., 2017), the elucidation of novel CRC-associated metabolomic biomarkers is critical for early diagnosis and to provide an effective strategy for advanced CRC.

A number of investigators have demonstrated that the antitumor effects of taurine contribute to its ability of promoting apoptosis and reducing proliferation (He et al., 2018; Tu et al., 2018). Gao et al. (2016) reported an enhancement of glioma cell proliferation and invasiveness by hypotaurine. In our study, taurine was examined as a single agent using a panel of CRC cell lines, and we observed a concentration-dependent inhibition of cellular viability in all the lines with a five day culture in 2D condition. HT-29 and LoVo were selected for subsequent investigation of the differences in their sensitivities to taurine, and a series of experiments was conducted to determine the effects of taurine on the development of CRC. Taurine induced apoptosis, inhibited cellular proliferation, migratory and invasive capabilities. We then evaluated CDH1 and Snail proteins as crucial markers of the EMT, as the EMT is principally involved in cellular proliferation, apoptosis, and metastasis. We found that taurine treatment promoted CDH1 levels while it inhibited Snail levels, indicating that taurine influences CRC cell metastasis, apoptosis, and proliferation involved in the EMT. We postulate that our results will engender a better understanding of the effects of taurine as a mediator of CRC pathophysiology, and the results indicate that taurine attenuates the malignant phenotype evoked by hypotaurine. The inhibitory effect of taurine on CRC thus suggests that taurine treatment may constitute a promising solution to halting the progression of CRC.

The mechanisms associated with taurine-mediated inhibition of the EMT in CRC are currently arcane. The proteins in the ERK-signaling pathway appear hyperactive and overexpressed in various forms of cancer, including CRC (Lok et al., 2011; Blaj et al., 2017), and the ERK pathway is known to regulate the EMT, tumor cell migration, invasion, and cell-cycle progression (Olea-Flores et al., 2019). Because of the specific structural properties of ERK, its mechanism of action, feedback mediation, and the various substrates catalyzed, ERK1/2 is a potential candidate for the development of strategies that could be used to inhibit tumor progression. However, the development of ERK-pathway molecules as therapeutic targets remains challenging because the potential for off-targeting and toxicity of these new compounds has also increased. It should be noted, however, that taurine as a natural amino acid can overcome these problems. Our *in vitro* results showed that phosphorylated ERK1/2 and RSK expression were reduced with taurine treatment in a dose-dependent manner, and with increasing hypotaurine concentration, ERK1/2 and RSK phosphorylation also increased commensurately. This dose-dependent activity may represent the primary mechanism by which taurine and hypotaurine exert opposing effects on CRC cells.

Additionally, our experiments showed an aberrant metabolic pathway involved in taurine-inhibited tumor progression in CRC cells. Taurine reduced intracellular hypotaurine levels, indicating that the availability of extracellular taurine may diminish synthesis of *de novo* hypotaurine. Previous evidence has shown decreased taurine levels in glioma tissue, and we found that alterations in taurine levels changed intracellular hypotaurine levels (Gao et al., 2016). In these cell lines, either the enzymatic conversion of subtaurine to taurine was lacking, or the transformation was strictly regulated; this inhibition might then be involved in the mechanism subserving reduced hypotaurine levels. We hypothesized that the changes in intracellular hypotaurine levels would be reflected in the effects on tumor metabolites, and this was supported by our results of hypotaurine's contribution to cellular invasion, proliferation, and apoptosis. We also conjecture that the inhibitory effects of taurine are mediated by the ERK/RSK cascade *via* the EMT and by taurine's competitive inhibition of hypotaurine.

Consistent with our *in vitro* results of taurine-attenuated, hypotaurine-induced tumor growth, taurine significantly decreased the growth of HT-29 and LoVo xenograft tumors, laying the foundation for further rational treatment of this kind in CRCs. In addition, the use of taurine can increase apoptosis and decrease proliferation *in vivo*. We herein also demonstrated that taurine inhibited cellular migration, invasion, and metastasis *in vitro* and *in vivo*. Orthotopic transplantation of CT26 cells into taurine-treated mice did not produce liver or lung metastasis, and this was supported by the number

of metastatic nodules and the expression of bioluminescent signals. Therefore, taurine treatment can prevent the EMT and inhibit CRC cell dissemination. Metabonomics has been widely used in uncovering biomarkers due to its close relationship with phenotype and sensitivity to many factors. As a "downstream" type of genomics, transcriptomics, and proteomics, metabonomics has been used to detect a variety of subtle modifications that reflect changes in biologic state, even if there are no measurable changes in corresponding genes and proteins. Therefore, candidates for potential biomarkers are more likely to be made available through metabonomics (Monteiro et al., 2013). By comparison, endogenous metabolites number fewer than genes, transcripts, and proteins, have the same basic chemical structures, and are extremely conserved, making it simpler to analyze metabolic results. Furthermore, metabonomics can be used for non-invasive assessments of biologic samples, and can be more easily translated into clinical practice. These metabolic abnormalities driven by cancer may represent the inherent characteristics of the tumor, and may even predict the pathogenesis of cancer, providing changes in serum metabolites related to systematic phenotypic biology (Tian et al., 2018). Therefore, changes in serum metabolites may reveal unique pathologic conditions, and provide early detection and prognosis. Our results showed that serum taurine could be used to differentiate CRC patients from healthy controls, and that the low taurine levels observed in CRC were correlated with metastases to lung and liver. Our multivariate analyses also indicated that a low level of taurine might be an independent risk factor in the progression of CRC.

In conclusion, we herein demonstrated that hypotaurine is involved in CRC progression, and that taurine attenuates this tendency. The inhibitory effects of taurine on CRC progression are likely mediated by the ERK/RSK cascade *via* the EMT, and by taurine's competitive inhibition of hypotaurine. Our results indicated that taurine may constitute a promising agent in the treatment of CRC. Our results also provided evidence of the interaction among metabolism, signal transduction, and tumor pathophysiology. Taurine attenuated hypotaurine-induced tumor invasion and proliferation, and this aspect provides a promising target for early diagnosis and therapy. It is, however, necessary to further study the role of taurine in order to provide a potential translational tool for CRC treatments.

DATA AVAILABILITY STATEMENT

The raw data supporting the conclusions of this article will be made available by the authors, without undue reservation.

ETHICS STATEMENT

The studies involving human participants were reviewed and approved by Shanghai Jiao Tong University School of Medicine, Renji Hospital Ethics Committee. The patients/participants provided their written informed consent to participate in this study. The animal study was reviewed and approved by Shanghai Jiao Tong University School of Medicine, Renji Hospital Ethics Committee.

AUTHOR CONTRIBUTIONS

XH, JH, and XZ designed the project and performed most of the experiments. QW and RZ contributed to acquisition of clinical data. QL and ML wrote the main manuscript text and supervised the entire project. All authors contributed to manuscript revision, read, and approved the submitted version.

FUNDING

This study was supported by grants from the Shanghai Municipal Health Commission: the Young Talent Plan of Medicine (No. 2020-087), South Campus of Renji Hospital: the Training Program of National Natural Science Foundation of China (No. 2019GZRPYMS02).

ACKNOWLEDGMENTS

We would like to thank ACCDON, LLC (www.letpub.com) for its linguistic assistance during the preparation of this manuscript.

SUPPLEMENTARY MATERIAL

The Supplementary Material for this article can be found online at: https://www.frontiersin.org/articles/10.3389/fcell.2021.631163/full#supplementary-material

REFERENCES

Bijlsma, S., Bobeldijk, I., Verheij, E. R., Ramaker, R., Kochhar, S., Macdonald, I. A., et al. (2006). Large-scale human metabolomics studies: a strategy for data (pre-) processing and validation. *Anal. Chem.* 78, 567–574. doi: 10.1021/ac051495j

Blaj, C., Schmidt, E. M., Lamprecht, S., Hermeking, H., Jung, A., Kirchner, T., et al. (2017). Oncogenic effects of high MAPK activity in colorectal cancer mark progenitor cells and persist irrespective of RAS mutations. *Cancer Res.* 77, 1763–1774. doi: 10.1158/0008-5472.CAN-16-2821

Bray, F., Ferlay, J., Soerjomataram, I., Siegel, R. L., Torre, L. A., and Jemal, A. (2018). Global cancer statistics 2018: GLOBOCAN estimates of incidence and mortality worldwide for 36 cancers in 185 countries. *CA Cancer J. Clin.* 68, 394–424. doi: 10.3322/caac.21492

Chinnaiyan, P., Kensicki, E., Bloom, G., Prabhu, A., Sarcar, B., Kahali, S., et al. (2012). The metabolomic signature of malignant glioma reflects accelerated anabolic metabolism. *Cancer Res.* 72, 5878–5888. doi: 10.1158/0008-5472.CAN-12-1572-T

Das, J., Vasan, V., and Sil, P. C. (2012). Taurine exerts hypoglycemic effect in alloxan-induced diabetic rats, improves insulin-mediated glucose transport signaling pathway in heart and ameliorates cardiac oxidative stress and apoptosis. *Toxicol. Appl. Pharmacol.* 258, 296–308. doi: 10.1016/j.taap.2011.11.009

El Zahraa, Z. E. A. F., Mahmoud, M. F., El Maraghy, N. N., and Ahmed, A. F. (2012). Effect of *Cordyceps sinensis* and taurine either alone or in combination on streptozotocin induced diabetes. *Food Chem. Toxicol.* 50, 1159–1165. doi: 10.1016/j.fct.2011.12.020

Gao, P., Yang, C., Nesvick, C. L., Feldman, M. J., Sizdahkhani, S., Liu, H., et al. (2016). Hypotaurine evokes a malignant phenotype in glioma through aberrant hypoxic signaling. *Oncotarget* 7, 15200–15214. doi: 10.18632/oncotarget.7710

Gao, X., Pujos-Guillot, E., and Sebedio, J. L. (2010). Development of a quantitative metabolomic approach to study clinical human fecal water metabolome based on trimethylsilylation derivatization and GC/MS analysis. *Anal. Chem.* 82, 6447–6456. doi: 10.1021/ac1006552

Gaucher, D., Arnault, E., Husson, Z., Froger, N., Dubus, E., Gondouin, P., et al. (2012). Taurine deficiency damages retinal neurones: cone photoreceptors and retinal ganglion cells. *Amino Acids* 43, 1979–1993. doi: 10.1007/s00726-012-1273-3

Hadi, N. I., Jamal, Q., Iqbal, A., Shaikh, F., Somroo, S., and Musharraf, S. G. (2017). Serum metabolomic profiles for breast cancer diagnosis, grading and staging by gas ghromatography-mass spectrometry. *Sci. Rep.* 7:1715. doi: 10.1038/s41598-017-01924-9

He, F., Ma, N., Midorikawa, K., Hiraku, Y., Oikawa, S., Zhang, Z., et al. (2018). Taurine exhibits an apoptosis-inducing effect on human nasopharyngeal carcinoma cells through PTEN/Akt pathways in vitro. *Amino Acids* 50, 1749–1758. doi: 10.1007/s00726-018-2651-2

Imai, H., Sawada, K., Sato, A., Nishi, K., Sasaki, T., Takahashi, T., et al. (2015). Complete resection of liver metastases of colorectal cancer after high efficacy bevacizumab, S-1, and CPT -11 combination chemotherapy. *Gan To Kagaku Ryoho* 42, 101–104.

Khalil, R. M., Abdo, W. S., Saad, A., and Khedr, E. G. (2018). Muscle proteolytic system modulation through the effect of taurine on mice bearing muscular atrophy. *Mol. Cell. Biochem.* 444, 161–168. doi: 10.1007/s11010-017-3240-5

Kilb, W., and Fukuda, A. (2017). Taurine as an essential neuromodulator during perinatal cortical development. *Front. Cell. Neurosci.* 11:328. doi: 10.3389/fncel.2017.00328

Lieberman, D. A., Rex, D. K., Winawer, S. J., Giardiello, F. M., Johnson, D. A., and Levin, T. R. (2012). Guidelines for colonoscopy surveillance after screening and polypectomy: a consensus update by the US multi-society task force on colorectal cancer. *Gastroenterology* 143, 844–857. doi: 10.1053/j.gastro.2012.06.001

Lok, G. T., Chan, D. W., Liu, V. W., Hui, W. W., Leung, T. H., Yao, K. M., et al. (2011). Aberrant activation of ERK/FOXM1 signaling cascade triggers the cell migration/invasion in ovarian cancer cells. *PLoS One* 6:e23790. doi: 10.1371/journal.pone.0023790

Megaraj, V., Iida, T., Jungsuwadee, P., Hofmann, A. F., and Vore, M. (2010). Hepatobiliary disposition of 3alpha, 6alpha, 7alpha, 12alpha-tetrahydroxy-cholanoyl taurine: a substrate for multiple canalicular transporters. *Drug Metab. Dispos.* 38, 1723–1730. doi: 10.1124/dmd.110.033480

Monteiro, M. S., Carvalho, M., Bastos, M. L., and Guedes de Pinho, P. (2013). Metabolomics analysis for biomarker discovery: advances and challenges. *Curr. Med. Chem.* 20, 257–271. doi: 10.2174/092986713804806621

Neary, P. M., Hallihan, P., Wang, J. H., Pfirrmann, R. W., Bouchier-Hayes, D. J., and Redmond, H. P. (2010). The evolving role of taurolidine in cancer therapy. *Ann. Surg. Oncol.* 17, 1135–1143. doi: 10.1245/s10434-009-0867-9

Okamoto, K., Sugie, S., Ohnishi, M., Makita, H., Kawamori, T., Watanabe, T., et al. (1996). Chemopreventive effects of taurine on diethylnitrosamine and phenobarbital-induced hepatocarcinogenesis in male F344 rats. *JPN. J. Cancer Res.* 87, 30–36. doi: 10.1111/j.1349-7006.1996.tb00196.x

Olea-Flores, M., Zuniga-Eulogio, M. D., Mendoza-Catalan, M. A., Rodriguez-Ruiz, H. A., Castaneda-Saucedo, E., Ortuno-Pineda, C., et al. (2019). Extracellular-signal regulated kinase: a central molecule driving epithelial-mesenchymal transition in cancer. *Int. J. Mol. Sci.* 20:2885. doi: 10.3390/ijms20122885

Schaffer, S. W., Jong, C. J., Ramila, K. C., and Azuma, J. (2010). Physiological roles of taurine in heart and muscle. *J. Biomed. Sci.* 17(Suppl. 1):S2. doi: 10.1186/1423-0127-17-S1-S2

Shelton, B. K. (2002). Introduction to colorectal cancer. *Semin. Oncol. Nurs.* 18, 2–12. doi: 10.1053/sonu.2002.33074

Siegel, R. L., Miller, K. D., and Jemal, A. (2019). Cancer statistics, 2019. *CA Cancer J. Clin.* 69, 7–34. doi: 10.3322/caac.21551

Son, H. Y., Kim, H., and Kwon, Y. H. (2007). Taurine prevents oxidative damage of high glucose-induced cataractogenesis in isolated rat lenses. *J. Nutr. Sci. Vitaminol.* 53, 324–330. doi: 10.3177/jnsv.53.324

Song, X. D., Chen, C. Z., Dong, B., Shi, Y. Y., Zhang, W., Yan, L. S., et al. (2003). Study on the intervening mechanism of taurine on streptozotocin-induced diabetic cataracts. *Zhonghua Yan Ke Za Zhi* 39, 605–609.

Sulzmaier, F. J., and Ramos, J. W. (2013). RSK isoforms in cancer cell invasion and metastasis. *Cancer Res.* 73, 6099–6105. doi: 10.1158/0008-5472.CAN-13-1087

Tian, Y., Wang, Z., Liu, X., Duan, J., Feng, G., Yin, Y., et al. (2018). Prediction of chemotherapeutic efficacy in non-small cell lung cancer by serum metabolomic profiling. *Clin. Cancer. Res.* 24, 2100–2109. doi: 10.1158/1078-0432.CCR-17-2855

Tu, S., Zhang, X. L., Wan, H. F., Xia, Y. Q., Liu, Z. Q., Yang, X. H., et al. (2018). Effect of taurine on cell proliferation and apoptosis human lung cancer A549 cells. *Oncol. Lett.* 15, 5473–5480. doi: 10.3892/ol.2018.8036

Veeravalli, S., Phillips, I. R., Freire, R. T., Varshavi, D., Everett, J. R., and Shephard, E. A. (2020). Flavin-containing monooxygenase 1 catalyzes the production of taurine from hypotaurine. *Drug Metab. Dispos.* 48, 378–385. doi: 10.1124/dmd.119.089995

Vitvitsky, V., Garg, S. K., and Banerjee, R. (2011). Taurine biosynthesis by neurons and astrocytes. *J. Biol. Chem.* 286, 32002–32010. doi: 10.1074/jbc.M111.253344

Wang, H. R. (2008). *Experimental Study of the Effect of Taurine on Sarcoma 180 (S180) in Mices*. Ph.D. dissertation. Qingdao: Qingdao University.

Yin, Y., Wen, K., Wu, Y., Kang, Y., and Lou, J. (2012). Inhibition of sodium current by taurine magnesium coordination compound prevents cesium chloride-induced arrhythmias. *Biol. Trace Elem. Res.* 146, 192–198. doi: 10.1007/s12011-011-9240-5

Zhang, D., Li, L., Jiang, H., Knolhoff, B. L., Lockhart, A. C., Wang-Gillam, A., et al. (2017). Constitutive IRAK4 activation underlies poor prognosis and chemoresistance in pancreatic ductal adenocarcinoma. *Clin. Cancer Res.* 23, 1748–1759. doi: 10.1158/1078-0432.CCR-16-1121

Zhang, W., and Liu, H. T. (2002). MAPK signal pathways in the regulation of cell proliferation in mammalian cells. *Cell Res.* 12, 9–18. doi: 10.1038/sj.cr.7290105

Zhang, X., Lu, H., Wang, Y., Liu, C., Zhu, W., Zheng, S., et al. (2015). Taurine induces the apoptosis of breast cancer cells by regulating apoptosis-related proteins of mitochondria. *Int. J. Mol. Med.* 35, 218–226. doi: 10.3892/ijmm.2014.2002

Zhang, X., Tu, S., Wang, Y., Xu, B., and Wan, F. (2014). Mechanism of taurine-induced apoptosis in human colon cancer cells. *Acta Biochim. Biophys. Sin. (Shanghai)* 46, 261–272. doi: 10.1093/abbs/gmu004

Conflict of Interest: The authors declare that the research was conducted in the absence of any commercial or financial relationships that could be construed as a potential conflict of interest.

frontiers in Cell and Developmental Biology

ORIGINAL RESEARCH
published: 29 April 2021
doi: 10.3389/fcell.2021.642625

ZNRF1 Mediates Epidermal Growth Factor Receptor Ubiquitination to Control Receptor Lysosomal Trafficking and Degradation

*Chia-Hsing Shen[1†], Chih-Chang Chou[1†], Ting-Yu Lai[1], Jer-En Hsu[1], You-Sheng Lin[1], Huai-Yu Liu[1], Yan-Kai Chen[1], I-Lin Ho[1], Pang-Hung Hsu[2], Tsung-Hsien Chuang[3], Chih-Yuan Lee[4] and Li-Chung Hsu[1,5]**

[1] Institute of Molecular Medicine, National Taiwan University, Taipei, Taiwan, [2] Department of Bioscience and Biotechnology, National Taiwan Ocean University, Keelung City, Taiwan, [3] Immunology Research Center, National Health Research Institutes, Zhunan, Taiwan, [4] Department of Surgery, National Taiwan University Hospital, Taipei, Taiwan, [5] Center of Precision Medicine, College of Medicine, National Taiwan University, Taipei, Taiwan

OPEN ACCESS

Edited by:
Arie Horowitz,
Université de Rouen, France

Reviewed by:
Brian Paul Ceresa,
University of Louisville, United States
Sara Sigismund,
Italian Foundation for Cancer Research (FIRC), Italy

***Correspondence:**
Li-Chung Hsu
lichunghsu@ntu.edu.tw

† These authors have contributed equally to this work and share first authorship

Specialty section:
This article was submitted to Signaling, a section of the journal Frontiers in Cell and Developmental Biology

Received: 15 January 2021
Accepted: 08 April 2021
Published: 29 April 2021

Citation:
Shen C-H, Chou C-C, Lai T-Y, Hsu J-E, Lin Y-S, Liu H-Y, Chen Y-K, Ho I-L, Hsu P-H, Chuang T-H, Lee C-Y and Hsu L-C (2021) ZNRF1 Mediates Epidermal Growth Factor Receptor Ubiquitination to Control Receptor Lysosomal Trafficking and Degradation. Front. Cell Dev. Biol. 9:642625. doi: 10.3389/fcell.2021.642625

Activation of the epidermal growth factor receptor (EGFR) is crucial for development, tissue homeostasis, and immunity. Dysregulation of EGFR signaling is associated with numerous diseases. EGFR ubiquitination and endosomal trafficking are key events that regulate the termination of EGFR signaling, but their underlying mechanisms remain obscure. Here, we reveal that ZNRF1, an E3 ubiquitin ligase, controls ligand-induced EGFR signaling via mediating receptor ubiquitination. Deletion of ZNRF1 inhibits endosome-to-lysosome sorting of EGFR, resulting in delayed receptor degradation and prolonged downstream signaling. We further demonstrate that ZNRF1 and Casitas B-lineage lymphoma (CBL), another E3 ubiquitin ligase responsible for EGFR ubiquitination, mediate ubiquitination at distinct lysine residues on EGFR. Furthermore, loss of ZNRF1 results in increased susceptibility to herpes simplex virus 1 (HSV-1) infection due to enhanced EGFR-dependent viral entry. Our findings identify ZNRF1 as a novel regulator of EGFR signaling, which together with CBL controls ligand-induced EGFR ubiquitination and lysosomal trafficking.

Keywords: ZNRF1, epidermal growth factor receptor (EGFR), ubiquitination, lysosomal trafficking, herpes simplex virus 1 (HSV-1)

INTRODUCTION

The epidermal growth factor receptor (EGFR) plays crucial roles in numerous cellular functions required for development and tissues homeostasis, including cell growth, proliferation, differentiation, and migration (Schlessinger, 2002). Binding of growth factors, such as epidermal growth factor (EGF), to the extracellular region of EGFR induces receptor dimerization and tyrosine kinase activation, resulting in its autophosphorylation. The phosphorylated tyrosine residues on the carboxy-terminus of EGFR serve as docking sites that recruit various adaptor proteins containing Src Homology 2 (SH2) or phosphotyrosine binding (PTB) domains, which further induces the activation of multiple downstream signaling pathways involved in distinct cellular functions (Lemmon et al., 2014). These signaling pathways include the phosphatidylinositol

3-kinase (PI3K)/AKT (Soltoff and Cantley, 1996), Ras/mitogen-activated kinase (MAPK) (Hallberg et al., 1994), mammalian target of rapamycin complex 1/p70 S6 kinase (mTORC1-S6K) (Fan et al., 2009), and phospholipase C-γ pathways (Wahl et al., 1990). EGFR signaling has recently been shown to participate in innate immune signaling including Toll-like receptors (TLRs) to promote host defense against pathogenic infection (Yamashita et al., 2012; Chattopadhyay et al., 2015). In contrast, viruses such as HSV-1 and vaccinia virus subvert EGFR signaling to facilitate their infection (Zheng et al., 2014; Beerli et al., 2019). Thus, EGFR expression and signaling must be tightly regulated. Aberrant EGFR activation often leads to the progression of various diseases and cancers (Du and Lovly, 2018).

Endocytic trafficking of EGFR is a key mechanism for regulating EGFR signaling (Madshus and Stang, 2009; Tomas et al., 2014). Upon EGF stimulation, activated EGFR is immediately internalized into the early endosomes, where it continues to transmit signals (Vieira et al., 1996; Brankatschk et al., 2012; Sousa et al., 2012). Endosomal EGFR is either recycled back to the cell surface (Sorkin et al., 1991), translocated to the nucleus (Demory et al., 2009; Wang et al., 2010), or trafficked to multivesicular bodies (MVBs)/lysosomes for degradation. Thereby, the sorting and lysosomal degradation of activated EGFR are important mechanisms for terminating EGFR signaling. EGFR mutants found in tumor patients are not internalized or transported to the MVBs/lysosomes, resulting in enhanced and prolonged activation of EGFR and its downstream MAPK signaling that is essential for tumor cell proliferation and invasion (Huang et al., 2006; Goh et al., 2010).

Accumulating evidence revealed that ubiquitination serves as a critical sorting signal for endocytic trafficking of EGFR (Clague et al., 2012). EGF engagement induces rapid ubiquitination of EGFR on lysine residues within its tyrosine kinase domain (TKD) (Stang et al., 2000; Huang et al., 2006). The endosomal complex required for transport (ESCRT) machinery then recognizes the ubiquitinated EGFR and sort the receptor into intraluminal vesicles of the MVBs for subsequent lysosomal degradation (Raiborg and Stenmark, 2009; Henne et al., 2011). Hepatocyte growth factor-regulated tyrosine kinase substrate (HRS), a component of the ESCRT-0 complex, first recognizes ubiquitinated EGFR via its ubiquitin-interacting motifs, and then recruits downstream ESCRT complexes (ESCRT-1, -II, and -III) to mediate EGFR intraluminal vesicle sorting (Raiborg et al., 2002). It was previously reported that the mutation of 15 lysine residues to arginine in the TKD (15KR mutant) diminished EGFR ubiquitination to a negligible level, and significantly blocked EGFR lysosomal sorting and degradation, suggesting that ubiquitination on some or all of these lysine residues is critical for EGFR lysosomal sorting and degradation (Huang et al., 2007). In addition, EGFR fused to associated molecule with the Src homology 3 domain of signal transducing adaptor molecule (AMSH), a deubiquitinating enzyme that specifically targets lysine 63-linked polyubiquitin chains, cannot be efficiently transported to the MVBs/lysosomes upon EGF engagement, resulting in prolonged EGFR signaling (Huang et al., 2013). Together, these findings demonstrate the essential role of EGFR ubiquitination in its lysosomal sorting and degradation. Casitas B-lineage lymphoma (CBL) is a well-known E3 ubiquitin ligase that mediates EGFR ubiquitination and trafficking (Levkowitz et al., 1998; Grovdal et al., 2004; Stang et al., 2004). Following EGF binding, CBL is recruited to the activated EGFR at the plasma membrane and remains associated with EGFR after receptor internalization to catalyze EGFR ubiquitination for subsequent lysosomal degradation (de Melker et al., 2001; Umebayashi et al., 2008). Despite the important role of CBL in regulating EGFR ubiquitination and lysosomal degradation, the specific CBL-mediated ubiquitin-conjugated lysine residues on EGFR remain unknown. Recently, two other E3 ubiquitin ligases, RNF126 and Rabring7, were shown to associate with EGFR and promote EGFR ubiquitination and degradation upon ligand engagement; but their functions require CBL activation (Smith et al., 2013). Nevertheless, the $EGFR^{Y1045F}$ mutant, which is unable to directly recruit CBL, is still modified by ubiquitination, but to a lesser extent, after EGF stimulation (Levkowitz et al., 1999), which means other E3 ubiquitin ligases also participate in the ubiquitination of EGFR. Therefore, we were interested in investigating if there were additional E3 ubiquitin ligases involved in EGFR ubiquitination and lysosomal degradation.

The zinc and ring finger 1 (ZNRF1) protein, a ring-type E3 ubiquitin ligase, was initially identified as a nerve injury-induced gene (Araki et al., 2001). We previously found that ZNRF1 regulates the Toll-like receptor 4 (TLR4) signaling pathway during inflammation and promotes caveolin-1 (CAV1) ubiquitination and degradation (Lee et al., 2017). CAV1 has been reported to play a role in regulating EGFR trafficking from early to late endosomes (Schmidt-Glenewinkel et al., 2012). Therefore, we hypothesized that ZNRF1 may modulate endosomal trafficking of EGFR and its downstream signaling.

In the present study, we surprisingly found that ZNRF1 regulates EGFR endocytic trafficking and promotes its degradation via receptor ubiquitination. We show that ZNRF1 associates with and ubiquitinates EGFR. Depletion of ZNRF1 in lung or cervical cancer cells results in decreased EGF-induced EGFR ubiquitination and increased accumulation of EGFR in the early endosomes, which eventually impedes EGFR degradation and leads to prolonged activation of AKT and extracellular signal-regulated kinase (ERK) signaling. Our results identify ZNRF1 as a novel regulator of EGFR signaling through regulation of EGFR ubiquitination, sorting, and degradation.

RESULTS

ZNRF1 Controls Ligand-Induced EGFR Degradation and Signaling

To investigate the role of ZNRF1 in EGFR signaling, we depleted expression of the *ZNRF1* gene in A549 non-small cell lung cancer cells by lentivirus-mediated small hairpin RNA (shRNA) transduction. Four shRNAs against different regions of the human *ZNRF1* gene reduced endogenous ZNRF1 protein expression by >70% as examined by immunoblot analysis (**Supplementary Figure 1A**). Silencing ZNRF1 in the A549 cells delayed EGFR degradation in response to

EGF stimulation, suggesting that ZNRF1 is involved in EGF-induced EGFR degradation (**Figure 1A**). Loss of ZNRF1 did not affect *EGFR* mRNA expression after EGF stimulation (**Supplementary Figure 1B**), confirming that its effect on EGFR is at the protein level. Our previous findings (Lee et al., 2017) had suggested that ZNRF1 may modulate EGFR endosomal trafficking through regulation of CAV1 stability. Surprisingly, exogenous overexpression of CAV1 to the level as that in ZNRF1-depeleted cells did not alter ligand-induced EGFR degradation (**Supplementary Figure 2**), indicating that overexpression of CAV1 is not sufficient to affect EGFR degradation triggered by its ligand. In addition to A549 cells that express endogenous wild type EGFR, similar results were observed in H3255 cells that express a constitutively active mutant $EGFR^{L858R}$ (Janne et al., 2005), indicating that ZNRF1-controlled EGFR degradation is independent of the EGFR mutation status (**Figure 1B**). Moreover, ZNRF1-mediated EGFR degradation was also observed in HeLa cervical cancer cells (**Figure 1C**), indicating that ZNRF1 involvement in EGFR degradation is not limited to lung cancer cells.

To exclude the possibility of an off-target effect by shRNAs, we generated *ZNRF1*$^{-/-}$ A549 cells by the CRISPR/Cas9 genomic editing technique. Two *ZNRF1*$^{-/-}$ A549 clones were generated using two different sgRNAs and indel mutations were confirmed by DNA sequencing (**Supplementary Figure 1C**). Consistent with the results in ZNRF1-silenced cells, EGF-triggered EGFR degradation was delayed in *ZNRF1*$^{-/-}$ A549 cells compared to wild type cells (**Figure 1D** and **Supplementary Figure 1D**). To examine whether the E3 ubiquitin ligase activity of ZNRF1 was required for the regulation of EGFR degradation, we examined EGF-induced EGFR degradation in *ZNRF1*$^{-/-}$ A549 cells reconstituted with wild type ZNRF1 or an E3 ligase activity inactive mutant of ZNRF1 (C184A) (Araki and Milbrandt, 2003; Lee et al., 2017). As shown in **Figure 1E**, EGF-induced EGFR degradation was promoted in *ZNRF1*$^{-/-}$ cells reconstituted with wild type ZNRF1 but not in cells reconstituted with the ZNRF1 C184A mutant, confirming that the E3 ligase activity of ZNRF1 is required for its modulation of EGFR degradation.

Both the ubiquitin/proteasomal and lysosomal pathways are known to participate in EGFR degradation in response to ligand stimulation (Alexander, 1998; Alwan et al., 2003). To determine the pathway involved in ZNRF1-regulated EGFR degradation, we treated cells with EGF in the presence or absence of the lysosome inhibitor chloroquine or the proteasome inhibitor MG132. Chloroquine treatment significantly attenuated EGFR degradation in control cells, but only had a minor inhibitory effect in ZNRF1-silenced cells (**Figure 1F**). Conversely, MG132 treatment did not inhibit EGF-induced EGFR degradation in either control or ZNRF1-deleted cells (**Figure 1G**). These results suggest that ZNRF1-mediated EGFR degradation is dependent on the lysosomal pathway. In line with this notion, deletion of ZNRF1 did not impact protein expression of transferrin receptor (TfR), which is not destined for lysosomal degradation (**Figure 1H**). We then investigated the impact of ZNRF1 depletion on EGFR signaling and found that loss of ZNRF1 resulted in enhanced and prolonged autophosphorylation of EGFR, and activation of the downstream kinases AKT and ERK in response to EGF stimulation (**Figure 2**). Taken together, these results indicate that ZNRF1 promotes ligand-triggered EGFR degradation and termination of EGFR signaling via the lysosomal pathway.

ZNRF1 Promotes EGFR Lysosomal Sorting

Endocytic trafficking is one of mechanisms that controls EGFR signaling and degradation (Kirisits et al., 2007; Tomas et al., 2014). To investigate whether ZNRF1 is involved in EGFR trafficking, we first assessed EGFR internalization by tracking the uptake of Alexa Fluor 488-labeled EGF. The amount of internalized EGF was observed to be comparable between control and ZNRF1-depleted cells (**Supplementary Figure 3A**), indicating that ZNRF1 does not participate in EGFR internalization. We next examined whether ZNRF1 controls EGFR endosomal trafficking, by co-staining EGFR with either the early endosome marker, early endosomal antigen 1 (EEA1), or the late endosome/lysosome marker, lysosomal-associated membrane protein 1 (LAMP1), under EGF stimulation. Co-localization of EGFR and EEA1 was observed in both control and ZNRF1-depleted cells 10 min after EGF stimulation, suggesting that ZNRF1 is not required for EGFR trafficking from the cell surface to the early endosome (**Figures 3A,B**). However, EGFR-EEA1 co-localization in ZNRF1-depleted cells was significantly higher than in control cells 60 min after EGF stimulation (**Figures 3A,B**), indicating that loss of ZNRF1 blocked EGFR transport beyond the early endosome. Furthermore, co-localization of EGFR and LAMP1 was significantly reduced in ZNRF1-depleted cells (**Figures 3C,D**). It was reported that internalized EGFR is recycled back to the cell surface after EGF stimulation (Sorkin et al., 1991). However, we observed no difference in EGFR recycling to the plasma membrane between control and ZNRF1 knockdown cells (**Supplementary Figures 3B–D**). These data indicate that ZNRF1 regulates EGFR trafficking from early endosomes to late endosomes/lysosomes.

ZNRF1 Associates With EGFR

It is well established that EGF stimulation induces EGFR ubiquitination, which is crucial for receptor sorting to the lysosome for degradation (Huang et al., 2006, 2013). ZNRF1 has been shown to mediate ubiquitination and degradation of AKT and CAV1 (Araki and Milbrandt, 2003; Wakatsuki et al., 2011; Lee et al., 2017), which prompted us to speculate that ZNRF1 might control EGFR trafficking by modulating EGFR ubiquitination. To address this possibility, we first examined whether ZNRF1 associates with EGFR. Reciprocal co-immunoprecipitations revealed an interaction between EGFR and ZNRF1 in A549 cells that transiently overexpressed ZNRF1 (**Figure 4A**). In addition, an association between endogenous EGFR and ZNRF1 was observed in A549 cells with and without EGF stimulation (**Figure 4B**). To identify the domains of ZNRF1 and EGFR required for their interaction, we constructed three ZNRF1 domain deletion mutants (**Figure 4C**)

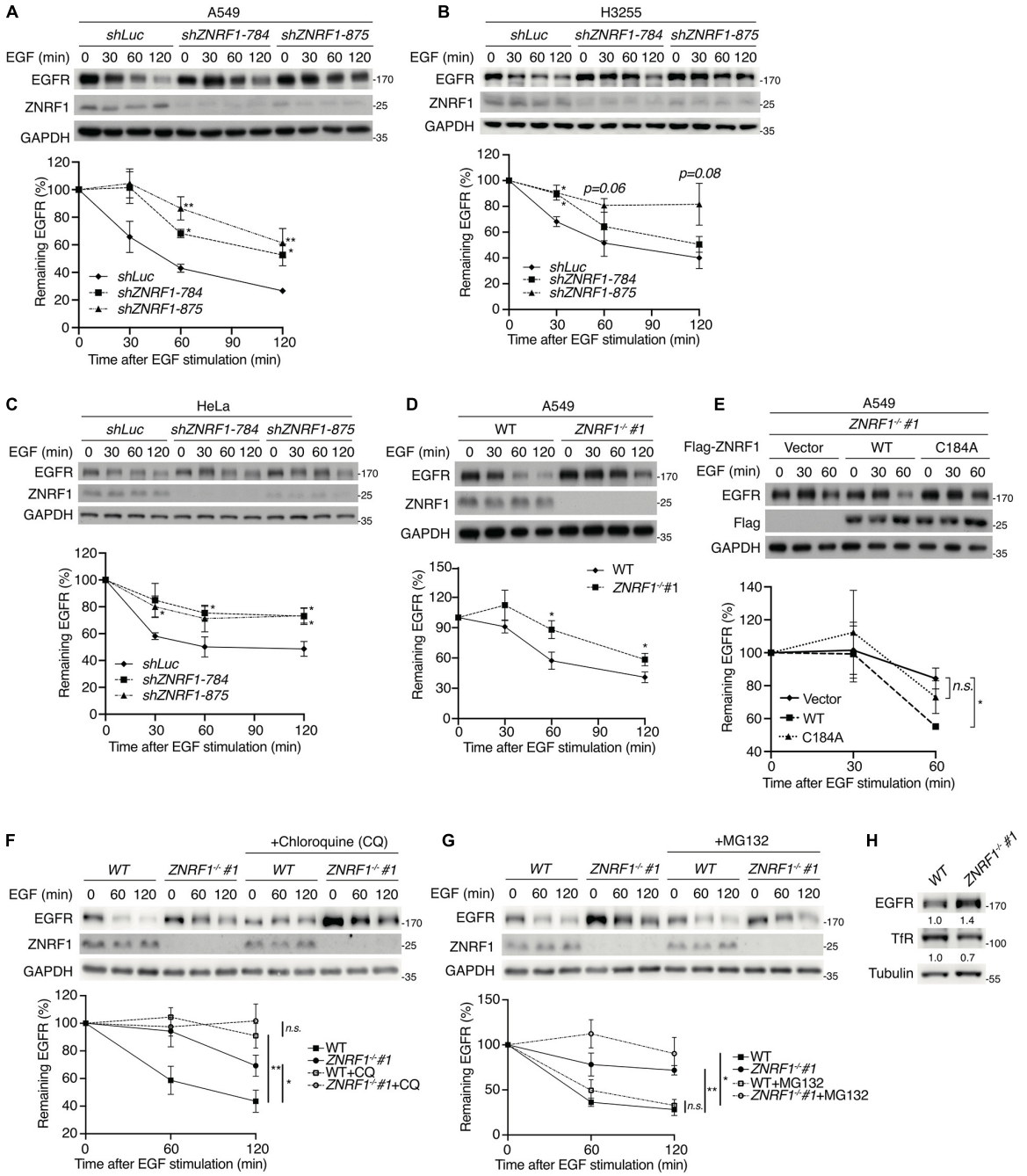

FIGURE 1 | ZNRF1 controls EGFR degradation. **(A–E)** A549 **(A)**, H3255 **(B)**, and HeLa **(C)** cells infected with lentivirus expressing shRNA against luciferase (*shLuc*) or ZNRF1 (*shZNRF1*), wild type or *ZNRF1*$^{-/-}$ A549 cells **(D)**, and *ZNRF1*$^{-/-}$ A549 cells transduced with lentiviruses encoding empty vector, Flag-ZNRF1 (WT), or Flag-ZNRF1 (C184A) **(E)** were serum-starved overnight and treated with 100 ng/mL EGF for the indicated times. **(F,G)** Wild type and *ZNRF1*$^{-/-}$ A549 cells were serum-starved overnight. Cells were then pre-treated with or without 100 μM Chloroquine **(F)** or 10 μM MG132 **(G)** for 1 h and stimulated with 100 ng/mL EGF for the indicated times. Cell lysates were prepared, and the levels of EGFR, ZNRF1 were analyzed by immunoblotting. Quantification of immunoblotting analysis data of three independent experiments are shown in the lower panels. **(H)** Cell lysates from wild type or *ZNRF1*$^{-/-}$ A549 cells were collected and the protein levels of EGFR and TfR were examined by immunoblotting. The intensities of the bands are expressed as fold increases compared to those of control cells (WT) after normalization to tubulin. Results are presented as averages ± SEM. n.s., no significant; *$P < 0.05$, **$P < 0.01$ (Student's *t*-test).

and four truncated forms of EGFR (**Figure 4D**) for co-immunoprecipitation experiments. In 293T cells, deletion of the ZNRF1 zinc finger domain strongly impeded ZNRF1 binding to EGFR (**Figure 4E**), indicating that the zinc finger domain mediates the ZNRF1-EGFR interaction. Two truncated forms of EGFR, TKD and TKD plus C-terminal domain, exhibited binding

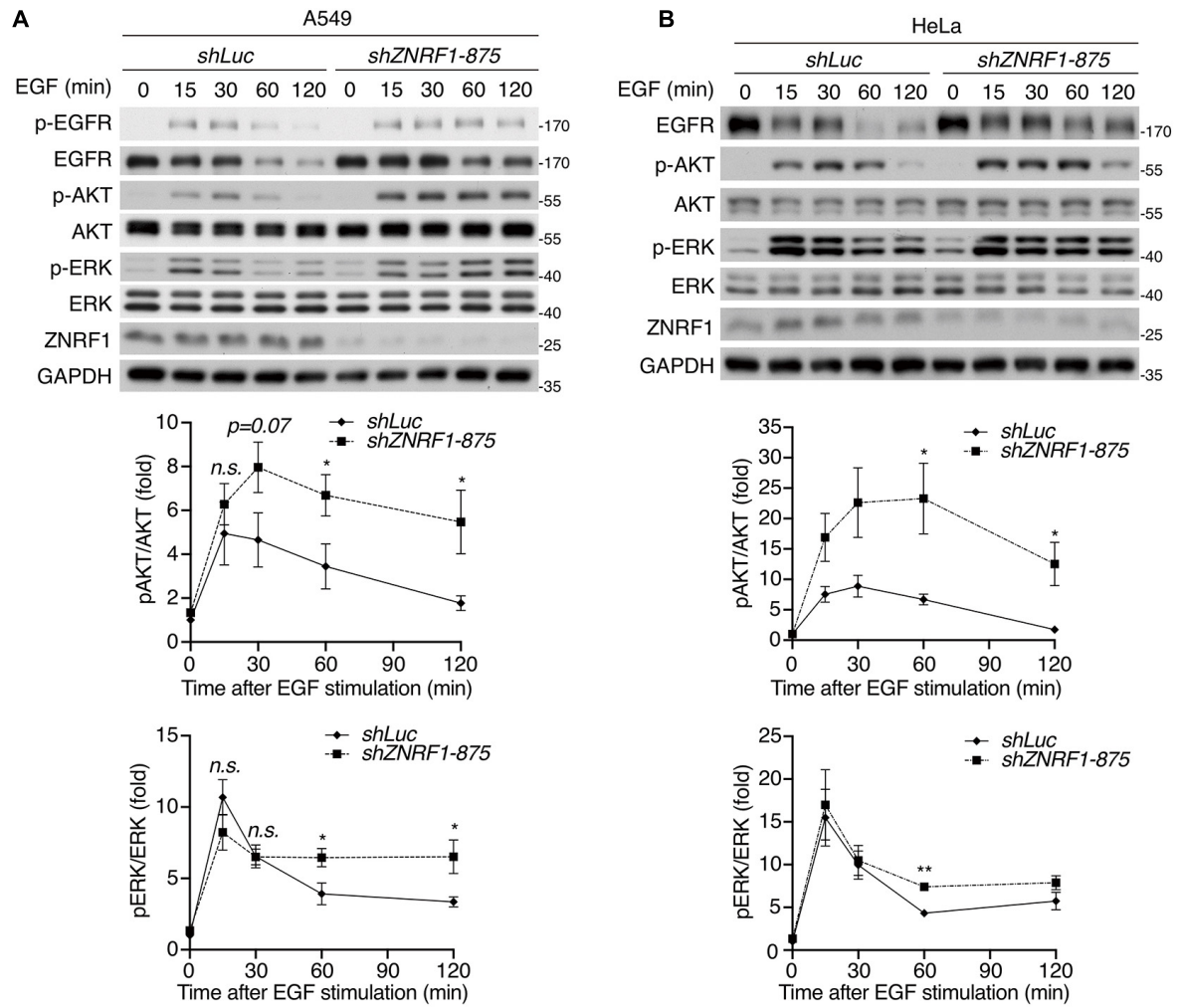

FIGURE 2 | ZNRF1 modulates EGFR signaling. A549 **(A)** and HeLa **(B)** cells infected with lentivirus expressing shRNA against luciferase (*shLuc*) or ZNRF1 (*shZNRF1*) were serum-starved overnight, and then stimulated with 100 ng/mL EGF for the indicated times. Cell lysates were prepared, and the levels of EGFR, ZNRF1, activation of EGFR, AKT, and ERK were analyzed by immunoblotting. Quantification of immunoblotting analysis data of three independent experiments are shown in the lower panels. Results are presented as averages ± SEM. n.s., no significant; $^{*}P < 0.05$, $^{**}P < 0.01$ (Student's *t*-test).

to ZNRF1 that was similar to full-length EGFR, whereas the N-terminal and C-terminal domains lost their association with ZNRF1 (**Figure 4F**), indicating that the TKD of EGFR is required for its interaction with ZNRF1. These results suggest that the zinc finger domain of ZNRF1 binds to the TKD of EGFR.

We further examined co-localization of ZNRF1 and EGFR in A549 cells by immunofluorescence staining. EGF stimulation rapidly induced EGFR internalization and accumulation in endosomes observed as large puncta in the cytosol. Co-immunofluorescence staining of ZNRF1 and EGFR revealed that ZNRF1 co-localized with these puncta (**Figure 4G**), consistent with their association revealed by co-immunoprecipitation. To confirm the interaction of ZNRF1 and EGFR *in situ*, we conducted a proximity ligation assay (PLA). Compared to the technical controls that lacked at least one essential component of the system, clear cytosolic fluorescence signals were detected in A549 cells (**Figure 4H**), demonstrating *in situ* interaction of ZNRF1 and EGFR. Taken together, these results confirm that ZNRF1 associates with EGFR.

ZNRF1 Mediates EGF-Induced EGFR Ubiquitination for Receptor Recruitment of the ESCRT Machinery

To determine if ZNRF1 modulates EGFR ubiquitination, we first examined endogenous EGFR ubiquitination following EGF stimulation. EGF induced EGFR ubiquitination within 5–10 min in wild type cells. However, EGF-induced EGFR ubiquitination was markedly diminished in *ZNRF1*$^{-/-}$ cells (**Figure 5A**) and *ZNRF1*-knockdown A549 cells (**Figure 5B**). We next performed an *in vitro* ubiquitination assay to investigate whether ZNRF1 directly catalyzes EGFR ubiquitination. A recombinant human EGFR peptide (a.a. 668–1210) containing the cytosolic region of EGFR was incubated with a recombinant ZNRF1 protein

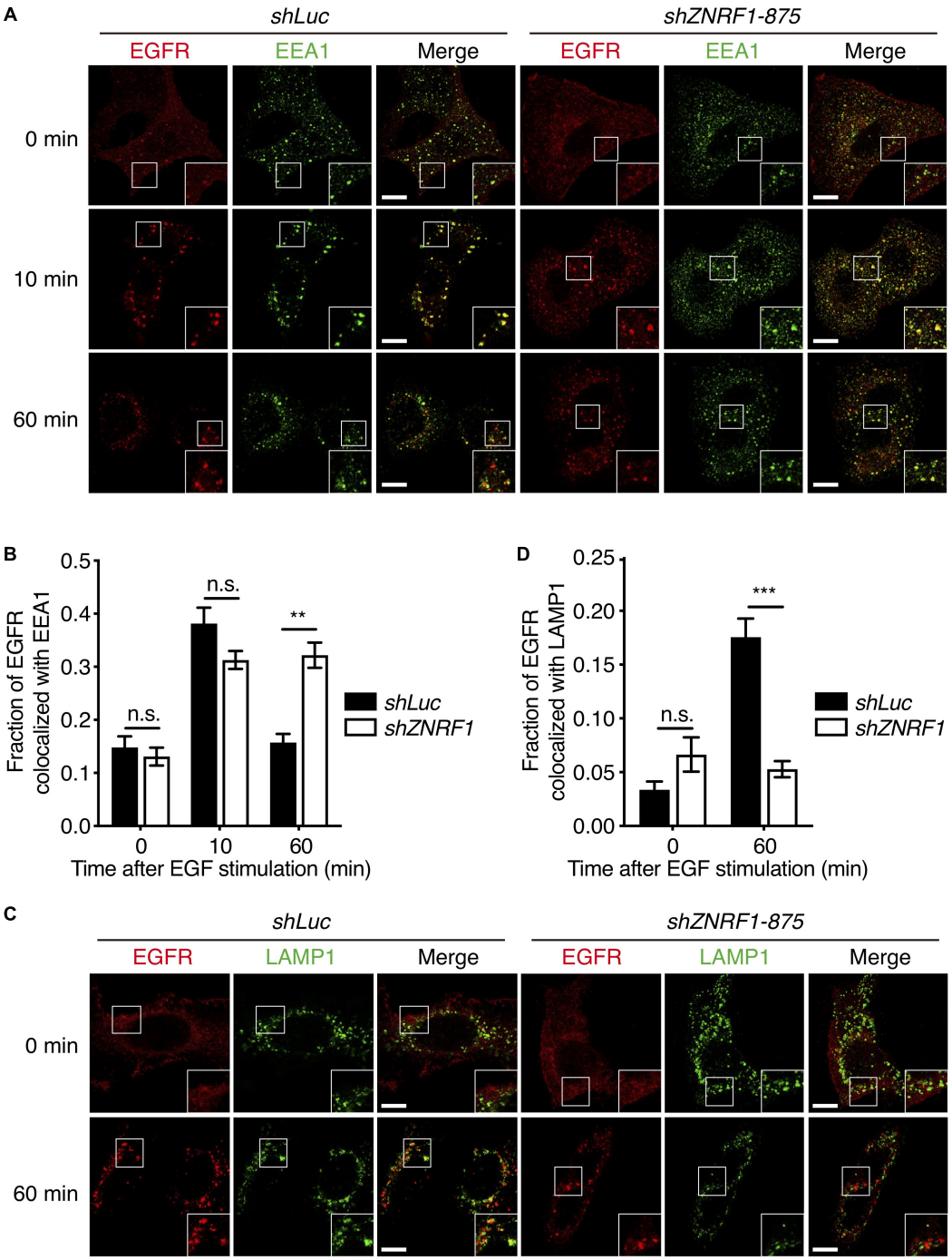

FIGURE 3 | ZNRF1 regulates EGFR trafficking. **(A)** A549 cells expressing *shLuc* or *shZNRF1* shRNA were serum-starved overnight and then stimulated with 100 ng/mL EGF for the indicated times. Cells were co-stained with antibodies against EGFR (red) and EEA1 (green). **(B)** Quantification of the fraction of EGFR co-localized with EEA1 at the indicated times. **(C)** Control and *shZNRF1*-expressing A549 cells pretreated with 100 μM Chloroquine for 1 h and stimulated with 100 ng/mL EGF for 60 min. Cells were stained with antibodies against EGFR (red) and LAMP1 (green). **(D)** Quantification of the fraction of EGFR co-localized with LAMP1 in **(C)**. Data are presented as mean ± SEM, $n > 500$ puncta from 20 cells for each group. Scale bar, 10 μm; n.s., no significant; $^{**}P < 0.01$, $^{***}P < 0.001$. All experiments were repeated two times with similar results.

and other essential components for ubiquitination. Our results show strong poly-ubiquitination of EGFR only in the presence of wild type ZNRF1, but not the ligase inactive C184A mutant (**Figure 5C**). These data indicate that ZNRF1 directly mediates EGFR ubiquitination in response to EGF stimulation. Given that CBL is a well-known E3 ubiquitin ligase involved in EGFR

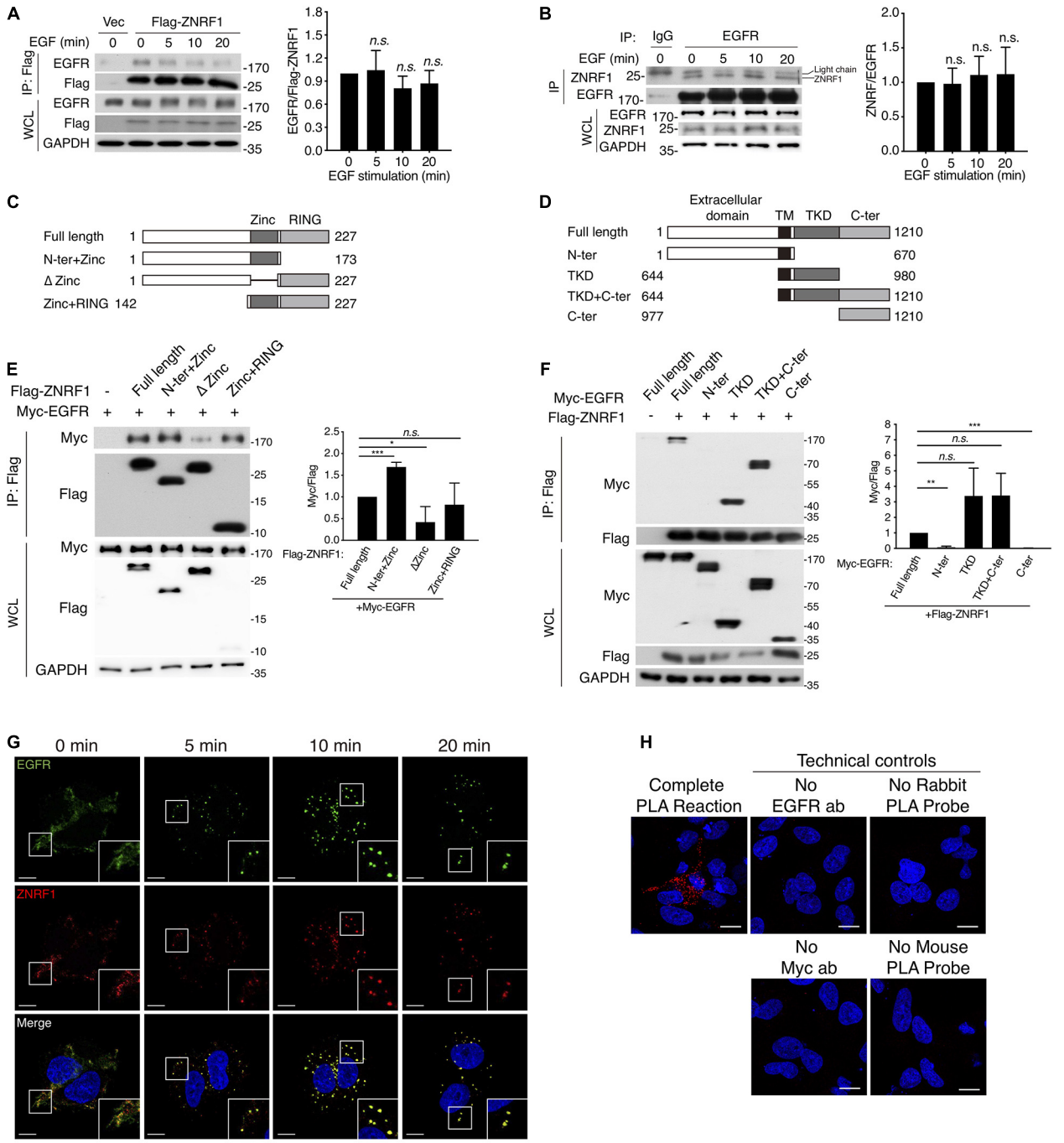

FIGURE 4 | ZNRF1 zinc domain interacts with EGFR TKD. **(A,B)** A549 cells expressing empty vector or Flag-ZNRF1 **(A)** and A549 cells **(B)** were serum-starved overnight and stimulated with 100 ng/mL EGF for the indicated times. EGFR was immunoprecipitated with the indicated antibodies. The immunocomplexes as well as whole cell lysates (WCL) were subjected to immunoblotting with the indicated antibodies. **(C)** Schematic diagram of full-length ZNRF1 and various deletion mutants of ZNRF1 with a C-terminal Flag tag. **(D)** Schematic diagram of full-length and truncated mutants of EGFR with a C-terminal Myc tag. TM, transmembrane domain; TKD, tyrosine kinase domain. **(E)** HEK293T cells were co-transfected with Myc-tagged EGFR and Flag-tagged full-length or truncated forms of ZNRF1 for 48 h, and interactions between EGFR and ZNRF1 were assessed by immunoprecipitation and immunoblotting with the indicated antibodies. **(F)** Flag-tagged ZNRF1 and Myc-tagged full-length or truncated mutants of EGFR were co-expressed in HEK293T cells, and the interactions between EGFR and ZNRF1 were determined by immunoprecipitation and immunoblotting with the indicated antibodies. Quantification of immunoblotting analysis data of three independent experiments are shown in the right panels. Results are presented as averages ± SEM. **(G)** A549 cells were serum-starved overnight and stimulated with 100 ng/mL EGF for the indicated times. Cells were fixed and co-stained with antibodies against ZNRF1 (red) and EGFR (green), and with DAPI (blue), followed by confocal microscopy. **(H)** A549 cells were transfected with Myc-tagged ZNRF1 for 48 h and then subjected to PLA using antibodies against EGFR and Myc. The detected interaction between ZNRF1 and EGFR is represented by red dots, and DAPI-stained cell nuclei are in blue. Scale bar, 10 μm. The experiment was repeated two times with similar results. n.s., no significant; $^{*}P < 0.05$, $^{**}P < 0.01$, $^{***}P < 0.001$ (Student's *t*-test).

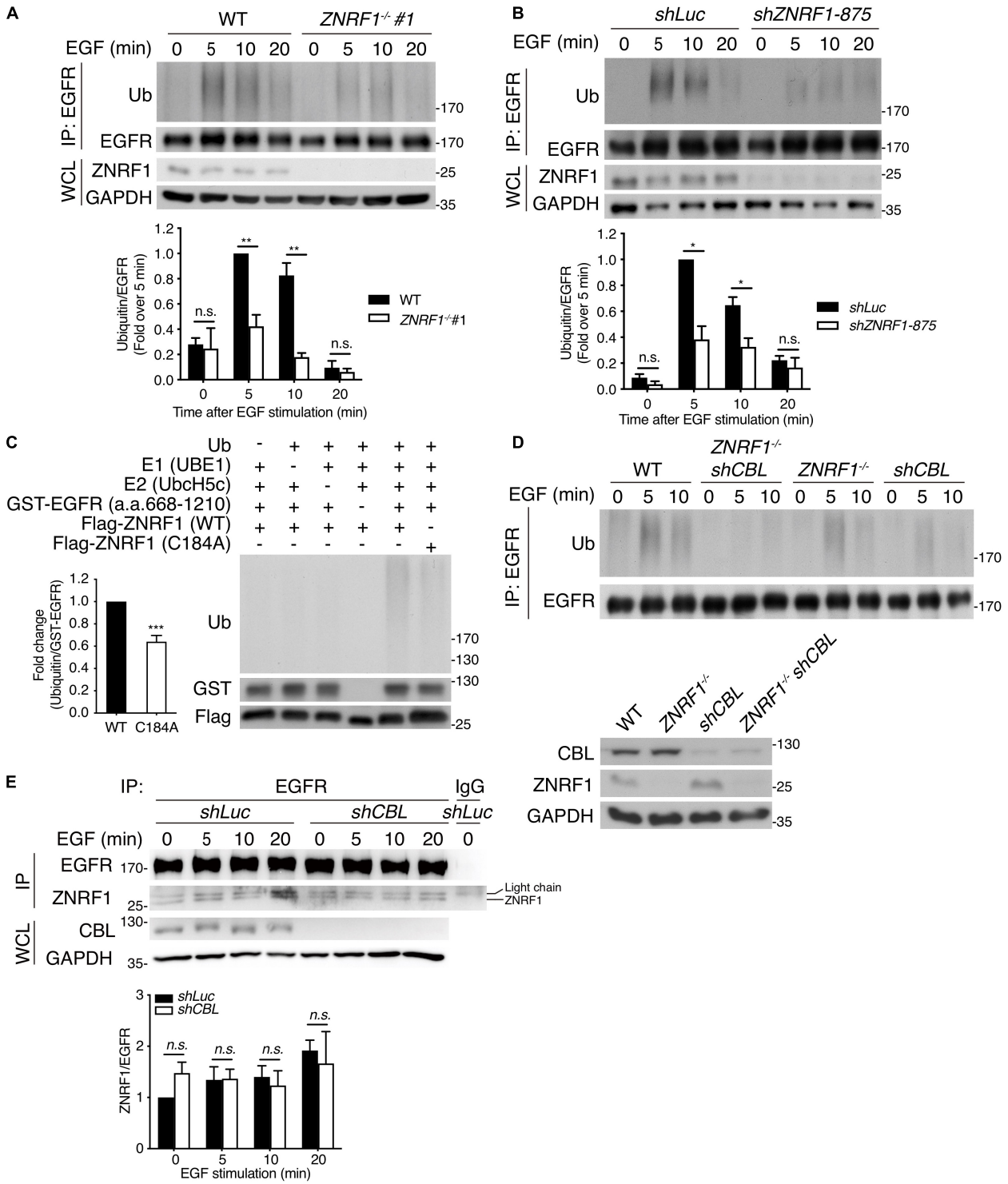

FIGURE 5 | ZNRF1 mediates EGF-induced EGFR ubiquitination. **(A)** Wild type (WT) and *ZNRF1*$^{-/-}$ **(B)** *shLuc* and *shZNRF1*-expressing A549 cells were serum-starved overnight and stimulated with 100 ng/mL EGF for the indicated times. EGFR was immunoprecipitated with anti-EGFR antibody, followed by immunoblotting with anti-ubiquitin and anti-EGFR antibodies. **(C)** *In vitro* ubiquitination assays were conducted with bacterially expressed Flag-tagged WT ZNRF1 or ZNRF1(C184A) mutant together with recombinant ubiquitin, E1, E2 (UbcH5c), and GST-tagged EGFR (a.a. 668–1210) as indicated. The reaction mixtures were subjected to immunoblotting using antibodies against ubiquitin, GST, and Flag antibodies. **(D,E)** Wild type, *ZNRF1*$^{-/-}$, *shCBL,* or *shCBL*-expressing *ZNRF1*$^{-/-}$ A549 cells **(D)**, or A549 cells expressing *shLuc* or *shCBL* shRNA **(E)** were serum-starved overnight and stimulated with 100 ng/mL EGF for the indicated times. EGFR was immunoprecipitated and the immunocomplexes as well as WCL were subjected to immunoblotting with the indicated antibodies. Quantification of immunoblotting analysis data of three independent experiments are shown in the lower panels. Results are presented as averages ± SEM. n.s., no significant; *$P < 0.05$, **$P < 0.01$, ***$P < 0.001$ (Student's *t*-test).

ubiquitination, endocytic trafficking, and degradation (Levkowitz et al., 1998; de Melker et al., 2001; Duan et al., 2003; Ravid et al., 2004; Umebayashi et al., 2008), we then investigated whether both ZNRF1 and CBL were required for EGFR ubiquitination. We knocked down *CBL* expression by shRNA in wild type or *ZNRF1*$^{-/-}$ A549 cells and examined EGFR ubiquitination after EGF stimulation. Loss of either *CBL* or *ZNRF1* reduced EGFR ubiquitination, however EGFR ubiquitination was further decreased to a negligible level in *ZNRF1/CBL* double deficient cells (**Figure 5D**). Notably, the interaction of EGFR and ZNRF1 was comparable between control and *CBL*-knockdown cells (**Figure 5E**). Similarly, depletion of ZNRF1 did not affect the association of EGFR and CBL (**Supplementary Figure 4**). These data indicate that ZNRF1 may function together with CBL to mediate EGFR ubiquitination and degradation.

Multiple studies show that during receptor endocytosis, ubiquitinated EGFR is recognized by ubiquitin binding domain-containing proteins including HRS and tumor susceptibility gene 101 (TSG101), which are essential components of the ESCRT machinery (Raiborg and Stenmark, 2009; Eden et al., 2012), eventually leading to receptor lysosomal targeting. Therefore, we speculated that reduced EGFR ubiquitination due to ZNRF1 deficiency may decrease its recognition by HRS resulting in decreased receptor lysosomal sorting. To test this hypothesis, we examined the co-localization of EGFR with HRS and TSG101. After ligand stimulation, EGFR showed significantly decreased co-localization with HRS (**Figures 6A,B**) and TSG101 (**Figures 6C,D**) in *ZNRF1*$^{-/-}$ cells in comparison with wild type cells. Loss of ZNRF1 did not reduce the protein levels of HRS and TSG101, indicating that the decreased EGFR-HRS and EGFR-TSG101 co-localizations in *ZNRF1*$^{-/-}$ cells was not the result of protein instability (**Figure 6E**). In addition, the size of the EGFR puncta was increased under ZNRF1 deficiency, reflecting the accumulation of internalized EGFR in early endosomes (**Figure 6F**). These results indicate that ZNRF1 modulates EGFR ubiquitination for recruitment of the ESCRT machinery, thereby contributing to receptor lysosomal sorting and degradation.

ZNRF1 and CBL Catalyze EGFR Ubiquitination on Distinct Lysine Residues Within the TKD of EGFR

Previously, analysis of EGF-induced EGFR ubiquitination by mass spectrometry revealed that ubiquitinated lysine residues were located in the TKD of EGFR (Huang et al., 2006). Interestingly, the specific lysine residues for the CBL-mediated polyubiquitination have not been identified. To investigate the differences in EGFR ubiquitination by ZNRF1 and CBL, we sought to identify the acceptor residues for polyubiquitin chains mediated by these two E3 ubiquitin ligases. We co-transfected HEK293T cells with EGFR and ZNRF1 or CBL, and immunoprecipitated EGFR for liquid chromatography-tandem mass spectrometry analysis. In two independent analyses, Lys^{716}, Lys^{757}, and Lys^{860} of EGFR were identified as acceptor sites for ZNRF1-mediated ubiquitination, whereas Lys^{737} was found to be an acceptor site for CBL-mediated ubiquitination (**Supplementary Figure 5** and **Table 1**). Due to the fact that the combined lysine residues of EGFR identified by mass spectrometry as targets of ZNRF1- and CBL-mediated ubiquitination are fewer than in previous reports (Huang et al., 2007; Tong et al., 2014), an alternative approach was used to systematically assess which EGFR lysine residues were acceptors for the polyubiquitination mediated by ZNRF1 and CBL, respectively. We first constructed an EGFR mutant (15KR), in which all 15 lysine residues in the TKD previously shown to be responsible for ligand-induced ubiquitination (Huang et al., 2007) were replaced by arginine (**Figure 7A**). We then generated a series of EGFR mutants by reintroducing individual lysine residues into the EGFR (15KR) mutant, and co-expressed these mutants with ZNRF1 or CBL in HeLa cells for immunoprecipitation and ubiquitination analyses. *In vivo* ubiquitination data revealed that ZNRF1 promoted polyubiquitination of wild type EGFR as well as the EGFR mutants K737, K860, K867, and K960 (**Figure 7B** and **Table 1**). CBL promoted polyubiquitination of wild type EGFR as well as the EGFR mutants K713, K716, K737, and K754 (**Figure 7C** and **Table 1**). To further confirm that these lysine residues were indeed acceptor sites for ZNRF1- and CBL-mediated ubiquitination, we generated two EGFR mutants, EGFR (K737R/K860R/K867R/K960R) and EGFR (K713R/K716R/K737R/K754R), by substituting the indicated lysine residues with arginine. ZNRF1 did not promote ubiquitination of EGFR (K737R/K860R/K867R/K960R), whereas CBL still facilitated its ubiquitination similar to wild type EGFR (**Figure 7D**). On the other hand, ubiquitination of EGFR (K713R/K716R/K737R/K754R) by CBL was attenuated, while its ubiquitination was still promoted by ZNRF1 as in wild type EGFR (**Figure 7E**). Together, these results demonstrate that ZNRF1 and CBL catalyze ubiquitination of EGFR at distinct lysine residues.

ZNRF1 Deficiency Increases Susceptibility to HSV-1 Infection

HSV-1, a highly prevalent pathogen in the human population, has developed numerous strategies to boost its capability to infect a broad range of host cells, including multiple entry modes and alternative receptors (Karasneh and Shukla, 2011). One of its entry strategies is to induce actin cytoskeleton remodeling via activation of EGFR signaling in host cells to facilitate viral entry (Zheng et al., 2014). We assessed whether dysregulated EGFR signaling caused by ZNRF1 deficiency enhances HSV-1 entry during early infection. HSV-1 infection induced a rapid activation of AKT and ERK in A549 cells, and the activity of both kinases was enhanced and prolonged in *ZNRF1*$^{-/-}$ cells compared to wild type cells (**Figure 8A**). Not surprisingly, EGFR degradation in response to HSV-1 infection was delayed in ZNRF1-deficient cells (**Figure 8B**). Next, we examined the expression of infected cell polypeptide 4 (ICP4), a viral immediate early gene required for transcription of early and late viral genes in HSV-1 infected cells (Smith et al., 1993; Lester and DeLuca, 2011). At 8 h post infection, ICP4 signals were significantly increased in *ZNRF1*$^{-/-}$ cells, indicating that loss of ZNRF1 increased HSV-1 infectivity (**Figures 9A,B**). Furthermore, a

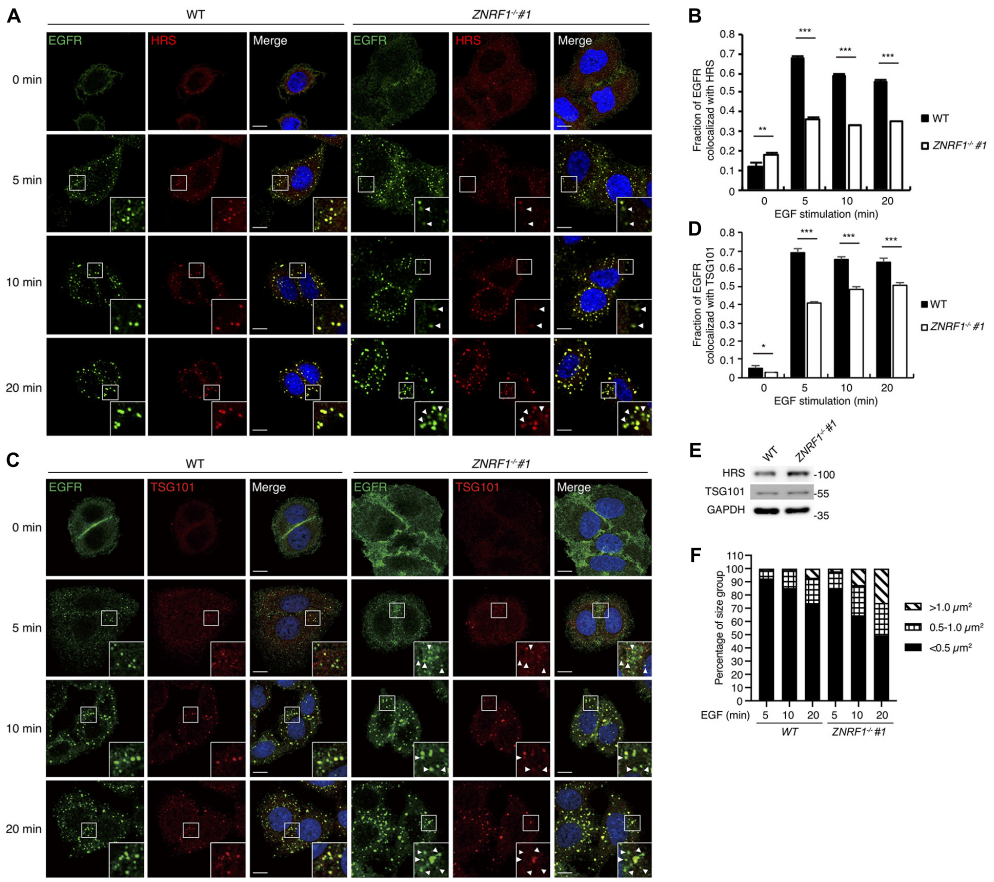

FIGURE 6 | ZNRF1 mediates the recruitment of ESCRT machinery to internalized EGFR. **(A–D)** Wild type or *ZNRF1*$^{-/-}$ A549 cells were serum-starved overnight and stimulated with 100 ng/mL EGF for 0, 5, 10, and 20 min. **(A)** Cells were co-stained with EGFR (Green) and HRS (Red) antibodies. **(B)** Quantification of the fraction of EGFR co-localized with HRS in **(A)**. **(C)** Cells were co-stained with EGFR (Green) and TSG101 (Red) antibodies. **(D)** Quantification of the fraction of EGFR co-localized with TSG101 in **(C)**. **(E)** Cell lysates from wild type and *ZNRF1*$^{-/-}$ A549 cells were prepared and the levels of HRS and TSG101 were analyzed by immunoblotting. **(F)** Quantification of the size distribution of EGFR puncta in **(A)**. White arrows indicate non-colocalized signals. Scale bar, 10 μm. Data are presented as mean ± SEM. $n > 1000$ puncta from at least 50 cells for each group; $^{*}P < 0.05$; $^{**}P < 0.01$; $^{***}P < 0.001$. All experiments were repeated two to three times with similar results.

higher viral load was detected in *ZNRF1*$^{-/-}$ cells infected with HSV-1 expressing GFP at 48 h post infection in comparison to wild type cells (**Figures 9C–E**). Consistent with prolonged EGFR activation, actin cytoskeleton rearrangement was promoted in HSV-1-infected *ZNRF1*$^{-/-}$ cells (**Figure 9F**). Inhibition of EGFR kinase activity by EGFR inhibitor Afatinib reduced HSV-1-GFP signals in *ZNRF1*$^{-/-}$ cells to the level that is similar to WT cells (**Figure 9G**), confirming that increased HSV-1 infectivity in *ZNRF1*$^{-/-}$ cells required EGFR activation. Taken together, these results suggest that ZNRF1 controls EGFR degradation and activation of its downstream signaling upon HSV-1 infection, which may contribute to host defense by constraining HSV-1 infection.

DISCUSSION

Epidermal growth factor receptor signaling is essential for numerous cellular functions, including cell proliferation, survival, differentiation, and the immune response (Schlessinger, 2002; Yamashita et al., 2012; Chattopadhyay et al., 2015). Although EGFR signaling is activated primarily at the plasma membrane, activated EGFR continues to deliver downstream signals from the early endosomes (Wang et al., 2002; Brankatschk et al., 2012; Sousa et al., 2012). Trafficking of EGFR to MVBs/lysosomes for the degradative pathway is critical for termination of EGFR signaling. Ubiquitination of EGFR is essential for EGFR sorting from the endosomes to MVBs/lysosomes. In this study, in addition to CBL, we identified an E3 ubiquitin ligase ZNRF1 that modulates EGFR ubiquitination, leading to EGFR trafficking to the MVBs/lysosomes for degradation. ZNRF1 deficiency resulted in decreased ligand-induced EGFR ubiquitination, thereby increasing endosomal accumulation of EGFR, leading to prolonged activation of the downstream pathways and enhanced HSV-1 infectivity. Our findings reveal ZNRF1 as a novel regulator of the EGFR signaling pathway that functions together with CBL

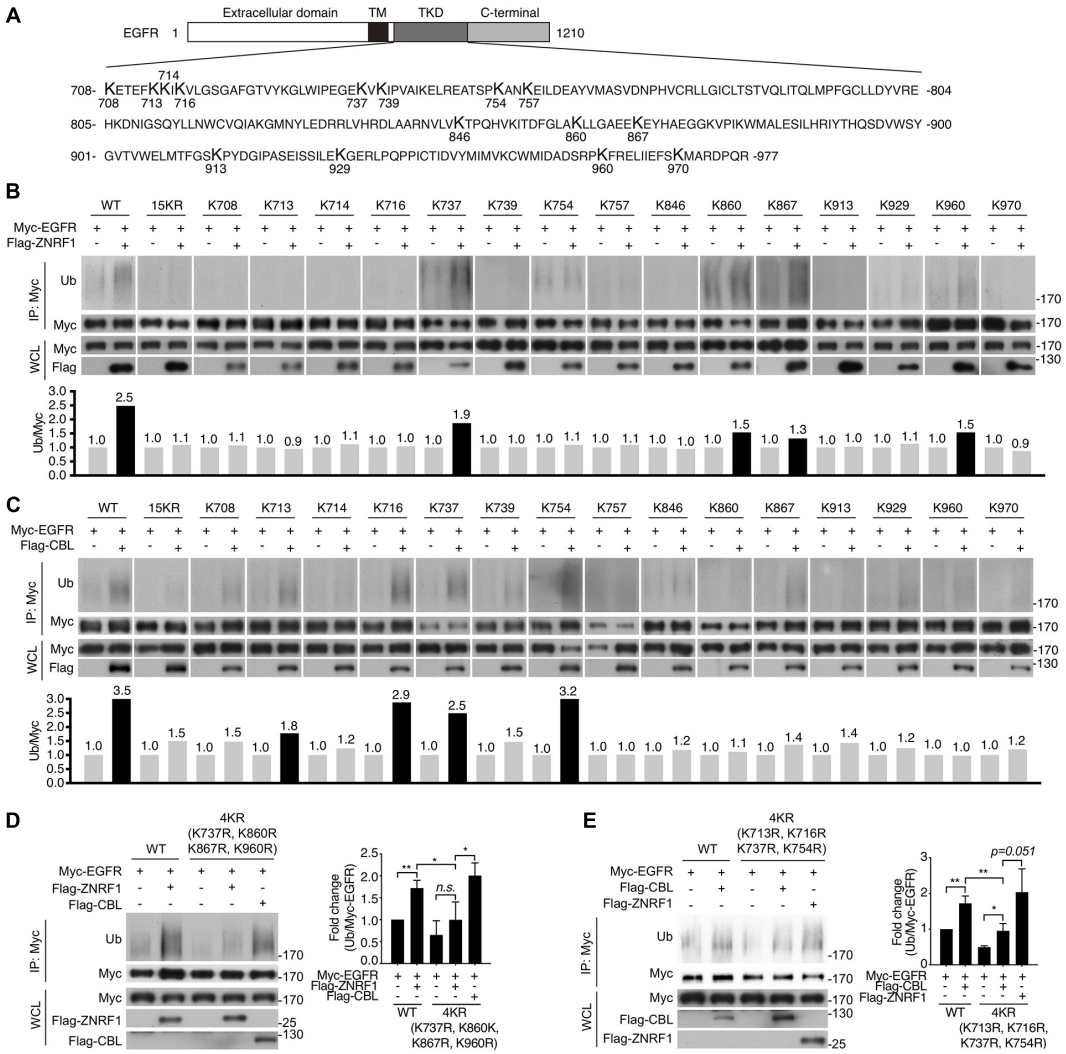

FIGURE 7 | Identification of ubiquitin-modified lysine residues on EGFR mediated by ZNRF1 and CBL in response to EGF. **(A)** Schematic diagram of EGFR TKD sequence and its 15 lysine residues. **(B–E)** HeLa cells were co-transfected with wild type or various EGFR mutants in combination with an empty vector or the E3 ubiquitin ligase ZNRF1 or CBL as indicated for 48 h. Cells were serum-starved and stimulated with 100 ng/mL EGF for 5 min. Ubiquitination of EGFR was examined by immunoprecipitation with Myc-conjugated agarose, followed by immunoblotting with anti-ubiquitin and anti-Myc antibodies. The experiments in **(B,C)** were repeated two times with similar results. Quantification of immunoblotting analysis data of three independent experiments are shown in the left panels of **(D,E)**. Results are presented as averages ± SEM. n.s., no significant; $^{*}P < 0.05$, $^{**}P < 0.01$ (Student's *t*-test).

by controlling EGFR ubiquitination, endosomal trafficking, and degradation.

ZNRF1 was originally identified in injured neurons (Araki et al., 2001) and later shown to exhibit E3 ubiquitin ligase activity (Araki and Milbrandt, 2003). Previous studies have demonstrated that ZNRF1 plays a critical role in Schwann cell differentiation and Wallerian degeneration by controlling the degradation of glutamine synthetase and AKT via the ubiquitin–proteasome pathway, respectively (Saitoh and Araki, 2010; Wakatsuki et al., 2011). Recently, we found that ZNRF1 modulates the Toll-like receptor 4-triggered immune response by targeting CAV1 ubiquitination and degradation (Lee et al., 2017). The expression of CAV1 protein was also elevated in ZNRF1-depleted A549 cells, but increased CAV1 was not sufficient to influence EGFR degradation triggered by its ligand. Nevertheless, we cannot rule out the possibility that defective CAV1 ubiquitination and degradation contributes to ligand-induced EGFR trafficking and degradation in ZNRF1 deficient cells. Our current findings unveil a novel function of ZNRF1 by modulating ligand-induced EGFR ubiquitination and degradation through the lysosomal degradation system.

Ubiquitination of EGFR is rapidly induced upon EGF stimulation. Accumulating data show that while EGFR ubiquitination is dispensable for its internalization, it is crucial for receptor sorting (Huang et al., 2007, 2013). Prior to this study, CBL was an key E3 ubiquitin ligase involved in mediating ligand-induced EGFR ubiquitination and lysosomal degradation, although two other E3 ubiquitin ligases were recently reported

TABLE 1 | Summary of ubiquitin-modified lysine residues on EGFR mediated by ZNRF1 and CBL in response to EGF.

Lysine no.	Residues identified by mass spectrometry	Residues identified by *In vivo* ubiquitination assay
708		
713		CBL
714		
716	ZNRF1	CBL
737	CBL	ZNRF1/CBL
739		
754		CBL
757	ZNRF1	
846		
860	ZNRF1	ZNRF1
867		ZNRF1
913		
929		
960		ZNRF1
970		

HEK293T cells were transfected with Myc-tagged EGFR with empty vector, ZNRF1, or CBL for 48 h. Cell lysates were prepared and subjected to immunoprecipitation with Myc-conjugated agarose, followed by mass spectrometry to identify the ubiquitinated residues on EGFR. The table summarizes the lysine residues identified by mass spectrometry and the in vivo ubiquitination assay described in ***Figure 7****. The original contributions presented in the study are publicly available. This data can be found here: [DOI: 10.6019/PXD024279/accession number: PXD024279].*

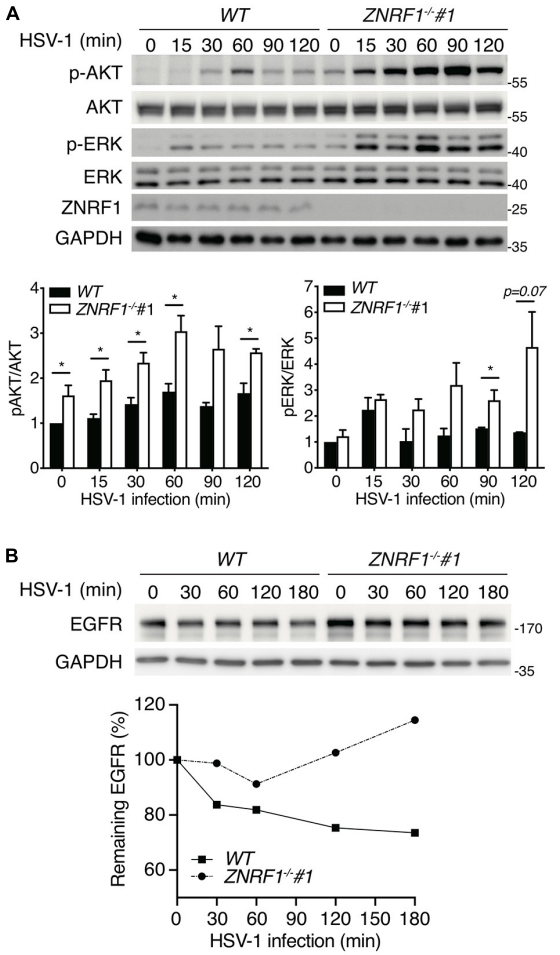

FIGURE 8 | ZNRF1 depletion enhances EGFR signaling after HSV-1 infection. **(A)** Wild type (WT) and *ZNRF1*$^{-/-}$ A549 cells were infected with HSV-1 (MOI = 10) for the indicated times. Activation of AKT and ERK was detected by immunoblotting. Quantification of immunoblotting analysis data of three independent experiments are shown in the lower panel. *$P < 0.05$ (Student's *t*-test). **(B)** Wild type and *ZNRF1*$^{-/-}$ A549 cells were serum-starved overnight and infected with HSV-1 (MOI = 15) for the indicated times. The protein levels of EGFR were detected by immunoblotting, quantified, and compared to untreated cells after normalization to GAPDH level. Quantification of EGFR level is shown in the lower panel. The data are representative of three independent experiments.

to participate in this events and act downstream of CBL (Smith et al., 2013). In addition, despite the discovery of CBL decades ago, its ubiquitin acceptor residues on EGFR have not been identified. Our findings indicate that ZNRF1 in combination with CBL regulate EGFR ubiquitination and lysosomal sorting. Deletion of both CBL and ZNRF1 diminished EGF-induced EGFR ubiquitination to a negligible level.

To identify the ubiquitination sites on EGFR mediated by ZNRF1 and CBL, we first immunoprecipitated receptors from HEK293T cells co-expressing EGFR and CBL or ZNRF1 for LC-MS analysis, which can assess EGFR ubiquitination on a proteome-wide level. We only mapped four ubiquitinated lysine residues on EGFR; Lys716, Lys757, and Lys 860 modulated by ZNRF1, and Lys737 modulated by CBL. This number is fewer than previous reported number of ubiquitinated lysine residues on EGFR (Huang et al., 2007; Tong et al., 2014). It is possible that low-abundance ubiquitinated EGFR peptides were missing during LC-MS analysis. We therefore performed an alternative approach, which was used systematic lysine-to-arginine mutagenesis in combination with *in vivo* ubiquitination assay. This approach allowed us to systematically assess which lysine residues in EGFR kinase domain were acceptors for the polyubiquitination mediated by ZNRF1 or CBL. By using this approach, we identified seven EGF-activated ubiquitin-conjugated lysine residues on EGFR: Lys737, Lys860, Lys867, and Lys960 mediated by ZNRF1, and Lys713, Lys716, Lys737, and Lys754 mediated by CBL. Our results indicate that ZNRF1 and CBL conjugate ubiquitin moieties to distinct lysine residues on EGFR. Interestingly, Lys716, Lys737, Lys754, and Lys867 were previously identified as ubiquitin acceptor sites on ligand-activated EGFR by mass spectrometry (Huang et al., 2006). Our findings are in agreement with the idea that the extent of ubiquitination in the EGFR kinase domain is correlated with the efficiency of EGFR lysosomal sorting and degradation (Huang et al., 2007). Nevertheless, based on a previous study (Huang et al., 2007), we only assessed the possible acceptor sites within the 15 lysine residues in the EGFR TKD for ZNRF1- and CBL-mediated ubiquitination in this study. Therefore, we cannot rule out the possibility that ZNRF1 and CBL may catalyze ubiquitination on additional lysine residues that are not located in TKD of EGFR. Moreover, it remains to be determined whether additional E3 ubiquitin ligases besides ZNRF1 and

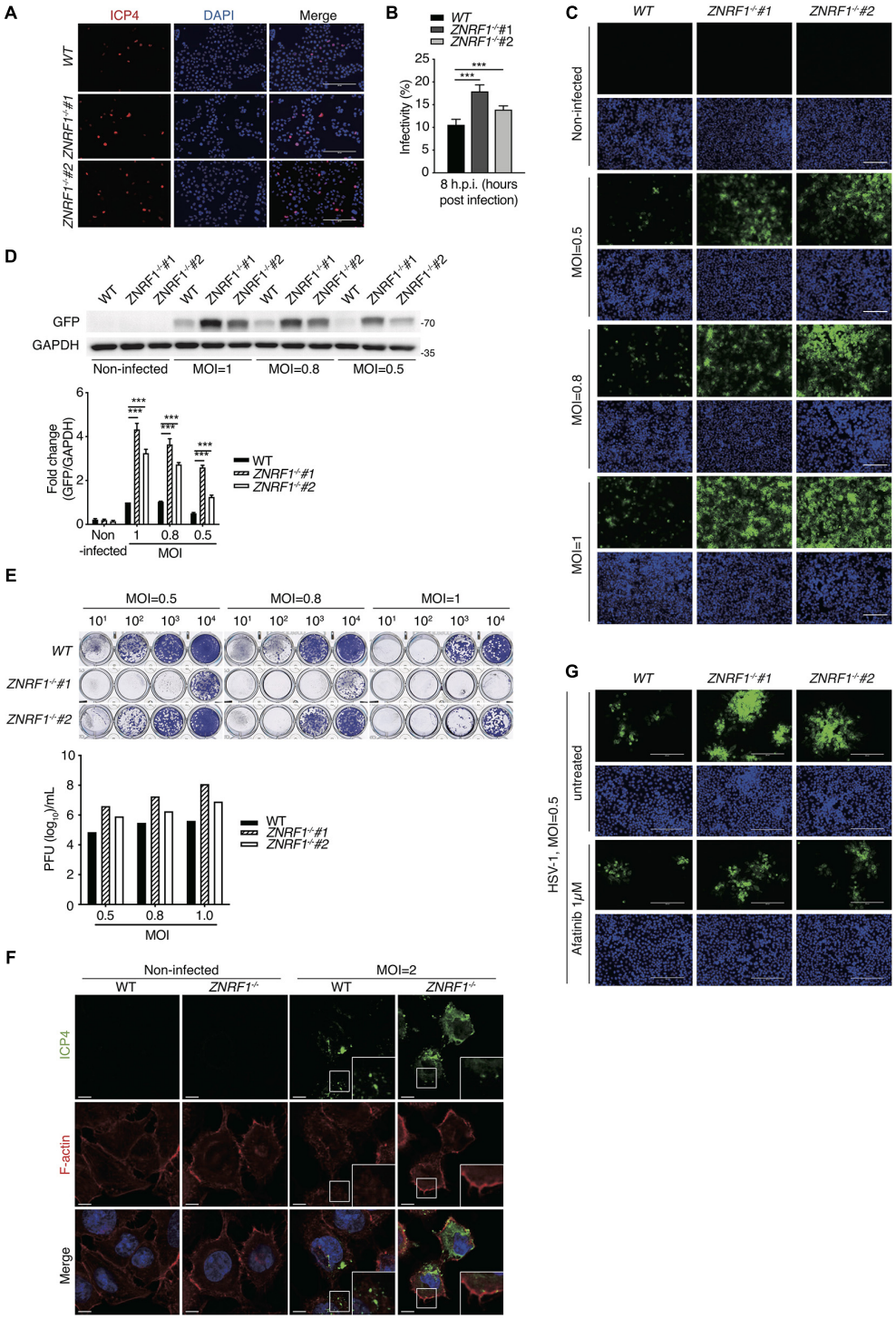

FIGURE 9 | ZNRF1 depletion enhances the entry of HSV-1 into A549 cells. **(A)** Wild type and *ZNRF1*$^{-/-}$ A549 cells were infected with HSV-1 (MOI = 8) for 8 h. Cells were fixed and stained with anti-ICP4 antibody (red) and DAPI (blue). **(B)** HSV-1 infectivity in **(A)** was quantified by the percentage of ICP4-positive cells in five random microscopic fields. Scale bar, 200 μm. ***$P < 0.001$. **(C–E)** Wild type and *ZNRF1*$^{-/-}$ A549 cells were infected with GFP-expressing HSV-1 (MOI = 0.5, 0.8, or 1.0) for 48 h. **(C)** Cells were collected and analyzed by fluorescence microscopy. **(D)** Cell lysates were collected and subjected to immunoblotting using anti-GFP antibody. Quantification of immunoblotting analysis data of three independent experiments are shown in the lower panel. **(E)** The titers of HSV-1 in culture medium from **(C)** were determined by a plaque assay using Vero cells. **(F)** Wild type and *ZNRF1*$^{-/-}$ A549 cells were infected with HSV-1 (MOI = 2) for 2 h. Cells were co-stained with ICP4 antibody (green) and filamentous actin (F-actin) (red). **(G)** WT and *ZNRF1*$^{-/-}$ A549 cells were pretreated with 1 μM Afatinib for 1 h and then infected with GFP-expressing HSV-1 (MOI = 0.5) for 48 h. Cells were collected and analyzed by fluorescence microscopy. Scale bar, 200 μm. Results are presented as averages ± SEM. ***$P < 0.001$ (Student's *t*-test). The data are representative of three independent experiments.

CBL participate in ligand-activated EGFR ubiquitination and subsequent lysosomal degradation.

Following receptor internalization into the early endosomes, the ubiquitinated receptor is recognized by the ESCRT machinery, allowing the cargo receptor to be destined for lysosomal degradation (Henne et al., 2011). The ESCRT-0 complex contains two ubiquitin-binding proteins, HRS and signal transducing adaptor molecule, which interact with the ubiquitinated receptor and initiate its intraluminal sorting. HRS is recruited to the endosome membrane through its binding to ubiquitinated proteins via its ubiquitin-interacting motif (Raiborg et al., 2002; Hirano et al., 2006). Our data show that a lack of ZNRF1-mediated EGFR ubiquitination decreased activated EGFR co-localization with HRS, suggesting reduced recruitment of HRS to ubiquitinated EGFR in the early endosomes. In addition, perturbations of the interaction between HRS and TSG101, a component of the ESCRT-I complex, block lysosomal trafficking of EGFR, leading to an accumulation of EGFR in the early endosomes (Lu et al., 2003). Moreover, our findings are consistent with the suggestion that multiple ubiquitin moieties on EGFR are required for efficient binding to the ESCRT machinery (Huang et al., 2006; Umebayashi et al., 2008; Raiborg and Stenmark, 2009). Many studies have demonstrated that when EGFR fails to bind to HRS, the receptor becomes trapped in the lining membrane of the endosomes, reflected by enlarged endosomes without intraluminal vesicles. In agreement with published data, we observed enlargement of EGFR-positive endosomes following ligand stimulation in ZNRF1-depleted cells. Taken together these results suggest that ZNRF1 mediates ligand-induced EGFR ubiquitination, which is required for a sufficient sorting signal for the recruitment of HRS.

Casitas B-lineage lymphoma is known to be recruited to activated EGFR at the plasma membrane upon ligand stimulation, and the carboxy-terminal domain of EGFR is critical for this interaction (Levkowitz et al., 1999; Waterman et al., 2002). We showed that ZNRF1 associates with the TKD of EGFR, indicating that ZNRF1 and CBL bind different regions of EGFR. Notably, when and how the ligase activity of ZNRF1 is induced upon EGF treatment remains unclear. A recent study in neuronal cells showed that under oxidative stress, ZNRF1 is phosphorylated at its Tyr^{103} residue by EGFR, which is critical for its E3 ligase activity (Wakatsuki et al., 2015). Hence, it is possible that ZNRF1 is phosphorylated by activated EGFR upon EGF stimulation, thereby allowing it to mediate EGFR ubiquitination, trafficking, and degradation. Further studies are required to verify this possibility.

Uncontrolled EGFR signaling is associated with numerous diseases, including cancer (Roepstorff et al., 2008; Tomas et al., 2014). In addition, EGFR activation is crucial for viral entry during HSV-1 infection, which causes a wide range of symptoms from skin lesions to deadly encephalitis. Considering the key role of EGFR ubiquitination and endosomal trafficking in terminating EGFR signaling, ZNRF1 likely acts in concert with CBL to regulate EGFR-mediated cellular functions. Further investigations of ZNRF1 function in the spatiotemporal regulation of EGFR trafficking and signaling may help in the design of novel therapeutic interventions for the treatment of diseases caused by uncontrolled EGFR signaling. Furthermore, HSV-1 has emerged as a promising oncolytic virus for the killing of cancer (Sokolowski et al., 2015), but infectivity efficiency of modified oncolytic HSV-1 is the major limiting factor in the application of oncolytic virus therapy for cancer treatment (Sanchala et al., 2017). In combination with ZNRF1 interference, which significant increases the infectivity of HSV-1, it may increase the efficacy of oncolytic virus therapy for the elimination of cancer.

MATERIALS AND METHODS

Generation of ZNRF1 Knockdown and Knockout Cells

ZNRF1 knockdown and knockout cells were generated using lentiviruses-mediated shRNAs transduction and CRISPR/Cas9/sgRNA system, respectively. Lentivirus production and transduction were performed following the instructions provided by the National RNAi Core Facility Platform at the Institute of Molecular Biology/Genomic Research Center, Academia Sinica, Taiwan.

Cell Culture and Plasmids

Non-small cell lung cancer A549 and H3255 cells were maintained in RPMI-1640 (Gibco, Carlsbad, CA, United States) supplemented with 10% (vol/vol) heat-inactivated fetal bovine serum (FBS) (Gibco) at 37°C with 5% CO_2. Human embryonic kidney 293T (HEK293T) and HeLa cells were cultured in high glucose DMEM (Gibco) containing 10% FBS. Chinese hamster ovary (CHO) cells were maintained in Ham's F-12K (Kaighn's Modification) (Gibco) containing 10% FBS. Plasmids encoding full-length ZNRF1 cDNA and deletion mutants were described previously (Lee et al., 2017). Flag-tagged ZNRF1 was cloned into the pcDNA3-myc vector (Addgene, Cambridge, MA, United States). The Myc-tagged EGFR expression construct was kindly provided by Dr. Ming-Shiue Lee (Institute of Biochemistry and Molecular Biology, National Taiwan University, Taiwan). The truncated forms of EGFR, including N-terminal, TKD, TKD plus C-terminal, and C-terminal, were generated by PCR using full-length EGFR cDNA as a template and cloned into the pcDNA3-myc vector (Addgene). The EGFR lysine-to-arginine substitution mutants were generated by PCR using the Q5® site-directed mutagenesis Kit (New England Biolabs, Ipswich, MA, United States) following the manufacturer's instructions.

Reagents and Antibodies

The recombinant human EGF protein and Alexa Fluor 488-conjugated EGF protein were purchased from Thermo Fisher Scientific (Boston, MA, United States). Antibodies against pEGFR Ser^{1068} (#3777), EGFR (#4267), pAKT Ser^{473} (#4060), AKT (#4691), pERK1/2$^{Thr202/Tyr204}$ (#9101), ERK1/2 (#9102), CBL (#8447), HRS (#15087), V5-tag (#13202), and Myc-tag (#2278) were obtained from Cell Signaling Technology (Danvers, MA, United States). GAPDH (GTX627408) and TSG101 (GTX70255) antibodies were purchased from GeneTex

(Irvine, CA, United States). Antibodies against Ubiquitin (P4D1) (sc-8017), GFP (sc-8334), and LAMP1 (sc-20011) were obtained from Santa Cruz Biotechnology (Santa Cruz, CA, United States). The anti-FLAG M2 affinity gel (A2220) and anti-c-Myc (A7470) agarose beads were purchased from Sigma-Aldrich (St Louis, MO, United States). EEA1 (#610456) and GST (#554805) antibodies was purchased from BD Bioscience (San Jose, CA, United States). ICP4 (ab6514) antibody was obtained from Abcam (Cambridge, United Kingdom). Rhodamine phalloidin (against F-actin) was purchased from Thermo Fisher Scientific (Boston, MA, United States). The anti-transferrin receptor monoclonal antibody (H68.4) was a kind gift from Dr. Ya-Wen Liu (Institute of Molecular Medicine, National Taiwan University, Taiwan). Antibodies against Flag were generated by Dr. Sheng-Chung Lee as described previously (Yang et al., 2013). The generation of the ZNRF1 antibody was described previously (Lee et al., 2017). EGFR kinase inhibitor Afatinib (ab142018) was purchased from Abcam (Cambridge, United Kingdom).

shRNA-Mediated Gene Silencing and Lentiviral Infection

Generation of replication-defective lentiviruses encoding shRNAs and lentiviral transduction were performed following the instructions provided by the National RNAi Core Facility Platform at the Institute of Molecular Biology/Genomic Research Center, Academia Sinica, Taiwan. In brief, pLKO-shRNA constructs and the packaging plasmids pMD.G and pCMVR8.91 were transfected into HEK293T cells using Turbofect (Fermentas, Schwerte, Germany) according to the manufacturer's instructions. The lentivirus-containing culture medium was collected 48 and 72 h after transfection. A549 or H3255 cells were infected with lentiviruses in the presence of 8 μg/mL polybrene (Sigma-Aldrich, St. Louis, MO, United States) for 24 h, and then selected in medium containing 2 μg/mL puromycin (Gold Biotechnology, St Louis, MO, United States) until uninfected cells were completely killed. The shRNA target sequences were 5′-CCTCCCTGAGGACACCAAATT-3′ for sh*ZNRF1*-298, 5′-TATGCCCATGGCAATGGTTAC-3′ for sh*ZNRF1*-362, 5′-CAGCTCGCATAGTGGTTTCAA-3′ for sh*ZNRF1*-784, 5′-ACAACGATGATGTGCTGACTA-3′ for sh*ZNRF1*-875, 5′-GCCGATGTGAAATTAAAGGTA-3′ for sh*CBL*-694, and 5′-CCAGTGAGTTGGGAGTTATTA-3′ for sh*CBL*-695.

Generation of ZNRF1 Knockout Cells Using the CRISPR/Cas9 System

HEK293T cells were transfected with lentiviral packaging plasmids pMD.G and pCMVR8.91, and CRISPR/sgRNA/puro expression plasmids encoding sgRNA sequence targeting exon 1 of human *ZNRF1*. Then the culture medium containing lentiviruses was collected and used to infect A549 cells for 24 h followed by puromycin selection. The sgRNA target sequences were 5′-GATTTCGGGCACTACCGGAC-3′ for sgRNA #1 and 5′-GCATTTCGGGCACTACCGGA-3′ for sgRNA #2. To verify gene editing in single cell clones, genomic DNA was purified and subjected to PCR and DNA sequencing. The primers used for PCR were: forward primer 5′-TTGACTCCCTCCCCCTTTATGCTCG-3′ and reverse primer 5′-ATAGGTGGAGTCGGACGCAGACCCT-3′ for clones from sgRNA #1, and forward primer 5′-TTGACTCCCTCCCCCTTTATGCTCG-3′ and reverse primer 5′-ATAGGTGGAGTCGGACGCAGACCCT-3′ for clones from sgRNA #2.

RNA Isolation and Quantitative RT-PCR (RT-qPCR)

Total cellular RNA was purified using TRIzol RNA Isolation Reagent (Thermo Fisher Scientific) according to the manufacturer's instructions. One μg of total RNA was then reverse transcribed to cDNA using the ReverAid H Minus First Strand cDNA Synthesis kit (Thermo Fisher Scientific) following the manufacturer's instructions. 1/20th volume of the cDNA was mixed with SYBR Green PCR Master Mix (Thermo Fisher Scientific) to analyze the amount of specific mRNA. The primer sequences used for RT-qPCR were: Cyclophilin A (forward 5′-AGGTCCCAAAGACAGCAGA-3′ and reverse 5′-TGTGAAGTCACCACCCTGA-3′), and EGFR (forward 5′-ACTCATGCTCTACAACCC-3′ and reverse 5′-CCAATACCTATTCCGTTACAC-3′). The relative EGFR mRNA expression was obtained by normalizing its qPCR value to the level of Cyclophilin A mRNA.

Immunoblotting

Cells were lysed in ice-cold lysis buffer containing 50 mM Tris-HCl pH 7.5, 150 mM NaCl, 2 mM EDTA, 1% Triton X-100, 0.5% NP-40, 10% Glycerol, protease inhibitors Aprotinin, Benzamidine, Pepstatin A, and Leupeptin (Sigma-Aldrich) and phosphatase inhibitors, sodium orthovanadate and *p*-nitrophenyl phosphate (pNPP) (Sigma-Aldrich). Cell extracts were collected and protein concentrations quantified using the Bio-Rad Protein Assay (Bio-Rad, Hercules, CA, United States). Cell lysates were resolved by SDS-PAGE and transferred to polyvinylidene fluoride (PVDF) membranes (Millipore, Billerica, MA, United States). The membranes were blocked with 10% non-fat milk in TBST (50 mM Tris-HCl pH 7.6, 150 mM NaCl, 0.05% Tween-20), Blocking One (Nacalai Trsque, Nakagyo-ku Kyoto, Japan), or 5% BSA (for phosphorylated protein) for 30 min at 25°C, and then incubated with the indicated primary antibody overnight at 4°C, followed by a horseradish peroxidase-conjugated secondary antibody (Jackson ImmunoResearch, West Grove, PA, United States) for 1 h at 25°C. Immunoreactive signals were detected using Luminata Western Chemiluminescent HRP substrates (Millipore) according to the manufacturer's instructions.

Immunoprecipitation

Cells were lysed in ice-cold lysis buffer containing 150 mM NaCl, 50 mM Tris-HCl pH 7.5, 2 mM EDTA, 1% Triton X-100, 0.5% NP-40, 10% Glycerol, protease inhibitors and phosphatase inhibitors. For immunoprecipitation of ubiquitin-modified proteins, 20 mM *N*-ethylmaleimide (Sigma-Aldrich) was added to the lysis buffer. Cell extracts were incubated

with anti-FLAG or c-Myc antibody-conjugated agarose beads at 4°C for 1.5 h or the indicated primary antibody overnight at 4°C followed by a 2 h incubation with Protein A Sepharose CL-4B (GE Healthcare, Piscataway, NJ, United States). The immunocomplexes were then subjected to SDS-PAGE followed by immunoblotting.

Immunofluorescence

Cells were seeded on coverslips and cultured overnight before treatment. Cells were then fixed with 4% paraformaldehyde (PFA) (Electron Microscopy Sciences, Hatfield, PA, United States) in phosphate-buffered saline (PBS) (Gibco) pH 7.4 at 37°C for 15 min and permeabilized with 0.25% Triton X-100 in PBS at room temperature for 15 min, followed by blocking with 1% BSA in PBST (0.25% Triton X-100 in PBS) at 25°C for 30 min. The coverslips were then incubated with primary antibody overnight at 4°C, washed with PBS, and stained with a fluorescent-conjugated secondary antibody (Jackson ImmunoResearch) at 25°C for 1 h. After extensive washings with PBS, the coverslips were mounted with DAPI Fluoromount-G (SouthernBiotech, Birmingham, AL, United States) to counterstain cell nuclei. Images were captured using a Zeiss LSM 700 Confocal microscope and the co-localization of EGFR with EEA1 and LAMP1 was analyzed using the ZEN imaging software (Zeiss, Oberkochen, Germany). The co-localization of EGFR with ESCRT complex protein (HRS and TSG101) was analyzed using Volocity 3D imaging software (PerkinElmer, Waltham, MA, United States). Briefly, the images were subtracted from background and then segmented using the minimal intensity of each individual organelle marker-labeled vesicles as the low threshold. The integrated voxel intensity of EGFR in the segmented image was considered as co-localization of EGFR with each individual organelle marker-labeled vesicles. The extent of co-localization was determined as the percentage of integrated EGFR fluorescence of the segmented image to the total fluorescence of the same fluorochromes. To quantify the size of EGFR puncta, the intensities and areas of EGFR signals were acquired and analyzed by Metamorph software (Molecular Devices, San Jose, CA, United States).

Proximity Ligation Assay (PLA)

Proximity ligation assays were performed by Duolink *In Situ*-Fluorescence Detection Reagent Red (Sigma-Aldrich) according to the manufacturer's instructions. In brief, cells were seeded on coverslips and cultured overnight followed by transfection of Myc-EGFR expression plasmid for 48 h. Cells were then fixed, permeabilized, and incubated with the primary antibody overnight at 4°C. On the following day, the cells were washed with PBS and incubated with PLA probes for 1 h at 37°C. The cells were then washed twice with buffer A (Sigma-Aldrich), incubated with ligation mixture for 1 h at 37°C, washed twice with buffer A, and incubated in amplification mixture (Sigma-Aldrich) for 100 min at 37°C. After three washes with buffer B (Sigma-Aldrich), the coverslips were mounted with DAPI Fluoromount-G (SouthernBiotech). Images were captured using a Zeiss LSM 700 Confocal microscope (Zeiss, Oberkochen, Germany).

EGFR Internalization and EGFR Recycling Assays

For the EGFR internalization assay, cells were serum starved overnight, stimulated with 2 μg/mL Alex Fluor 488-conjugated EGF (Thermo Fisher Scientific) for the indicated times at 37°C, and placed on ice to stop internalization. After three washings with ice-cold PBS, cells were subjected to an acid wash (0.2 M acetic and 0.5 M NaCl, pH 2.8) for 5 min at 4°C. Cells were then detached from the culture dishes, washed with PBS, and re-suspended in PBS containing 2% FBS and 0.01% sodium azide, followed by fixation with 4% PFA in PBS for 20 min. Fixed cells were analyzed by a BD LSR II flow cytometer (BD Biosciences, San Jose, CA, United States). For the EGFR recycling assay, cells were serum starved overnight, and pretreated with 10 μg/mL cycloheximide for 1 h. All the following steps were performed in the presence of cycloheximide to inhibit new synthesis of EGFR. To obtain the total amount of initial internalized EGFR, cells were stimulated with 2 μg/mL of AF488-conjugated EGF for 15 min at 37°C, and then washed and fixed with 4% PFA in PBS. To obtain the amount of recycled EGFR, cells were first stimulated with 1 ng/mL or 100 ng/mL of non-labeled EGF (Peprotech, Rocky Hill, NJ, United States) for 15 min at 37°C, rinsed three times with PBS, and chased for 1 or 2 h to allow EGFR recycling. Cells were then treated with AF488-conjugated EGF for 15 min, washed, fixed, and analyzed by flow cytometry to quantify the internalized EGF uptake by recycled EGFR. The ratio of recycled EGFR was determined by the total amount of recycled EGFR relative to the total amount of initial internalized EGFR.

Identification of Ubiquitination Sites by Liquid Chromatography (Nanoflow-LC-MS/MS)

To identify the ubiquitination sites of EGFR mediated by ZNRF1 and CBL, EGFR was isolated by SDS-PAGE followed by in-gel enzymatic digestion with a mixture of trypsin and chymotrypsin. The digested peptides were analyzed by nanoflow LC-MS/MS on an LTQ-FT hybrid mass spectrometer (Thermo Fisher Scientific) equipped with a nano-electrospray ion source (New Objective, Inc., Woburn, MA, United States) in positive ion mode. The liquid chromatography system used was the Agilent 1100 HPLC with the Famos Autosampler (LC Packings, Amsterdam, Netherlands). The digested peptide samples were subjected to nanoflow-LC-MS/MS as described previously (Chang et al., 2019). All experimental RAW files were converted to MGF format by MSConvert (ProteoWizard ver. 3.0.9134) (Chambers et al., 2012) and then submitted for MS/MS ion search on Mascot (ver. 2.3) (MatrixScience, Boston, MA, United States). The protein sequences of Homo sapiens from UniprotKB[1] were used for MS/MS data analysis. The search parameters of error tolerance of precursor ions and the MS/MS fragment ions in spectra were 10 ppm and 0.6 Da, respectively. The variable post-translational modifications of search parameters in Mascot include ubiquitination of lysine (GlyGly), carbamidomethylation

[1] https://www.uniprot.org

of cysteine, the oxidation of methionine, and phosphorylation of serine/threonine/tyrosine.

Quantification of HSV-1 Infectivity

For determination of HSV-1 entry, cells were seeded on coverslips and cultured in RPMI-1640 containing 10% FBS overnight. Cells were infected with HSV-1 at 4°C for 1 h, and then washed three times with PBS. After a 8-h incubation at 37°C, cells were fixed and subjected to immunofluorescence with the anti-ICP4 antibody. To detect HSV-1 infection, cells were incubated with GFP-expressing HSV-1 (Elliott and O'Hare, 1999) at 4°C for 1 h to allow adsorption, washed three times with PBS, and incubated at 37°C for 48 h. Infected cells were imaged by fluorescence microscopy, and viral titers in culture medium were determined by a plaque assay on Vero cells. Cell lysates were prepared and subjected to immunoblotting using anti-GFP antibody.

Statistical Analysis

Results were presented as mean ± SEM. Significant differences between two groups were assessed by the Student's *t*-test. *P*-values < 0.05 were considered statistically significant.

DATA AVAILABILITY STATEMENT

The datasets presented in this study can be found in online repositories. The names of the repository/repositories and accession number(s) can be found below: ProteomeXchange, PXD024279.

AUTHOR CONTRIBUTIONS

C-CC, C-HS, and L-CH designed the research. C-CC, C-HS, T-YL, J-EH, Y-SL, H-YL, Y-KC, and I-LH performed the experiments. P-HH performed the mass spectrometry analysis. T-HC generated the antibody. C-HS, C-CC, C-YL, and L-CH analyzed the data and wrote the manuscript. All authors contributed to the article and approved the submitted version.

FUNDING

This work was supported by the Center of Precision Medicine from The Featured Areas Research Center Program within the framework of the Higher Education Sprout Project by the Ministry of Education (MOE) in Taiwan, National Taiwan University (108L893604 to L-CH), the Ministry of Science and Technology (MOST) of Taiwan (105-2320-B-002-060-MY3 and 109-2320-B-002-018-MY3 to L-CH), National Health Research Institutes of Taiwan, (NHRI-EX108-10630SI to L-CH), and National Taiwan University Hospital (NTUH 106-07, NTUH 106-S3511, and UN106-055 to C-YL; NTUH 107-S3929 and NTUH 108-S4384 to Dr. Jin-Shing Chen).

ACKNOWLEDGMENTS

We thank Drs. Sheng-Chung Lee, Fang-Jen Lee, Ya-Wen Liu, Ming-Shyue Lee, Chia-Chi Ku, Pan-Chyr Yang, and Peter O'Hare for gifts of cell lines, GFP-expressing HSV-1, plasmids and antibodies; the Imaging Core at the First Core Labs, National Taiwan University College of Medicine; Dr. Jin-Shing Chen for advising this project, the Second and the Third Core Lab at the Department of Medical Research, National Taiwan University Hospital for providing technical service; and the National RNAi Core Facility at Academia Sinica in Taiwan for providing shRNA and CRISPR/Cas9 reagents.

SUPPLEMENTARY MATERIAL

The Supplementary Material for this article can be found online at: https://www.frontiersin.org/articles/10.3389/fcell.2021.642625/full#supplementary-material

REFERENCES

Alexander, A. (1998). Endocytosis and intracellular sorting of receptor tyrosine kinases. *Front. Biosci.* 3, d729–38. doi: 10.1101/cshperspect.a017459

Alwan, H. A., van Zoelen, E. J., and van Leeuwen, J. E. (2003). Ligand-induced lysosomal epidermal growth factor receptor (EGFR) degradation is preceded by proteasome-dependent EGFR de-ubiquitination. *J. Biol. Chem.* 278, 35781–35790. doi: 10.1074/jbc.m301326200

Araki, T., and Milbrandt, J. (2003). ZNRF proteins constitute a family of presynaptic E3 ubiquitin ligases. *J. Neurosci.* 23, 9385–9394. doi: 10.1523/jneurosci.23-28-09385.2003

Araki, T., Nagarajan, R., and Milbrandt, J. (2001). Identification of genes induced in peripheral nerve after injury. Expression profiling and novel gene discovery. *J. Biol. Chem.* 276, 34131–34141. doi: 10.1074/jbc.m104271200

Beerli, C., Yakimovich, A., Kilcher, S., Reynoso, G. V., Flaschner, G., Muller, D. J., et al. (2019). Vaccinia virus hijacks EGFR signalling to enhance virus spread through rapid and directed infected cell motility. *Nat. Microbiol.* 4, 216–225. doi: 10.1038/s41564-018-0288-2

Brankatschk, B., Wichert, S. P., Johnson, S. D., Schaad, O., Rossner, M. J., and Gruenberg, J. (2012). Regulation of the EGF transcriptional response by endocytic sorting. *Sci. Signal* 5:ra21. doi: 10.1126/scisignal.2002351

Chambers, M. C., Maclean, B., Burke, R., Amodei, D., Ruderman, D. L., Neumann, S., et al. (2012). A cross-platform toolkit for mass spectrometry and proteomics. *Nat. Biotechnol.* 30, 918–920.

Chang, S.-C., Lin, W.-L., Chang, Y. F., Lee, C.-T., Wu, J.-S., Hsu, P.-H., et al. (2019). Glycoproteomic identification of novel plasma biomarkers for oral cancer. *J. Food Drug Analy.* 27, 483–493. doi: 10.1016/j.jfda.2018.12.008

Chattopadhyay, S., Veleeparambil, M., Poddar, D., Abdulkhalek, S., Bandyopadhyay, S. K., Fensterl, V., et al. (2015). EGFR kinase activity is required for TLR4 signaling and the septic shock response. *EMBO Rep.* 16, 1535–1547. doi: 10.15252/embr.201540337

Clague, M. J., Liu, H., and Urbe, S. (2012). Governance of endocytic trafficking and signaling by reversible ubiquitylation. *Dev. Cell* 23, 457–467. doi: 10.1016/j.devcel.2012.08.011

de Melker, A. A., van der Horst, G., Calafat, J., Jansen, H., and Borst, J. (2001). c-Cbl ubiquitinates the EGF receptor at the plasma membrane and remains receptor associated throughout the endocytic route. *J. Cell. Sci.* 114, 2167–2178.

Demory, M. L., Boerner, J. L., Davidson, R., Faust, W., Miyake, T., Lee, I., et al. (2009). Epidermal growth factor receptor translocation to the mitochondria: regulation and effect. *J. Biol. Chem.* 284, 36592–36604.

Du, Z., and Lovly, C. M. (2018). Mechanisms of receptor tyrosine kinase activation in cancer. *Mol. Cancer* 17:58.

Duan, L., Miura, Y., Dimri, M., Majumder, B., Dodge, I. L., Reddi, A. L., et al. (2003). Cbl-mediated ubiquitinylation is required for lysosomal sorting of epidermal growth factor receptor but is dispensable for endocytosis. *J. Biol. Chem.* 278, 28950–28960. doi: 10.1074/jbc.m304474200

Eden, E. R., Huang, F., Sorkin, A., and Futter, C. E. (2012). The role of EGF receptor ubiquitination in regulating its intracellular traffic. *Traffic* 13, 329–337. doi: 10.1111/j.1600-0854.2011.01305.x

Elliott, G., and O'Hare, P. (1999). Live-cell analysis of a green fluorescent protein-tagged herpes simplex virus infection. *J. Virol.* 73, 4110–4119. doi: 10.1128/jvi.73.5.4110-4119.1999

Fan, Q. W., Cheng, C., Knight, Z. A., Haas-Kogan, D., Stokoe, D., James, C. D., et al. (2009). EGFR signals to mTOR through PKC and independently of Akt in glioma. *Sci. Signal* 2:ra4. doi: 10.1126/scisignal.2000014

Goh, L. K., Huang, F., Kim, W., Gygi, S., and Sorkin, A. (2010). Multiple mechanisms collectively regulate clathrin-mediated endocytosis of the epidermal growth factor receptor. *J. Cell. Biol.* 189, 871–883. doi: 10.1083/jcb.201001008

Grovdal, L. M., Stang, E., Sorkin, A., and Madshus, I. H. (2004). Direct interaction of Cbl with pTyr 1045 of the EGF receptor (EGFR) is required to sort the EGFR to lysosomes for degradation. *Exp. Cell. Res.* 300, 388–395. doi: 10.1016/j.yexcr.2004.07.003

Hallberg, B., Rayter, S. I., and Downward, J. (1994). Interaction of Ras and Raf in intact mammalian cells upon extracellular stimulation. *J. Biol. Chem.* 269, 3913–3916. doi: 10.1016/s0021-9258(17)41718-2

Henne, W. M., Buchkovich, N. J., and Emr, S. D. (2011). The ESCRT pathway. *Dev. Cell* 21, 77–91. doi: 10.1016/j.devcel.2011.05.015

Hirano, S., Kawasaki, M., Ura, H., Kato, R., Raiborg, C., Stenmark, H., et al. (2006). Double-sided ubiquitin binding of Hrs-UIM in endosomal protein sorting. *Nat. Struct. Mol. Biol.* 13, 272–277. doi: 10.1038/nsmb1051

Huang, F., Goh, L. K., and Sorkin, A. (2007). EGF receptor ubiquitination is not necessary for its internalization. *Proc. Natl. Acad. Sci. U. S. A.* 104, 16904–16909. doi: 10.1073/pnas.0707416104

Huang, F., Kirkpatrick, D., Jiang, X., Gygi, S., and Sorkin, A. (2006). Differential regulation of EGF receptor internalization and degradation by multiubiquitination within the kinase domain. *Mol. Cell* 21, 737–748. doi: 10.1016/j.molcel.2006.02.018

Huang, F., Zeng, X., Kim, W., Balasubramani, M., Fortian, A., Gygi, S. P., et al. (2013). Lysine 63-linked polyubiquitination is required for EGF receptor degradation. *Proc. Natl. Acad. Sci. U. S. A.* 110, 15722–15727. doi: 10.1073/pnas.1308014110

Janne, P. A., Engelman, J. A., and Johnson, B. E. (2005). Epidermal growth factor receptor mutations in non-small-cell lung cancer: implications for treatment and tumor biology. *J. Clin. Oncol.* 23, 3227–3234.

Karasneh, G. A., and Shukla, D. (2011). Herpes simplex virus infects most cell types in vitro: clues to its success. *Virol. J.* 8:481.

Kirisits, A., Pils, D., and Krainer, M. (2007). Epidermal growth factor receptor degradation: an alternative view of oncogenic pathways. *Int. J. Biochem. Cell. Biol.* 39, 2173–2182. doi: 10.1016/j.biocel.2007.07.012

Lee, C. Y., Lai, T. Y., Tsai, M. K., Chang, Y. C., Ho, Y. H., Yu, I. S., et al. (2017). The ubiquitin ligase ZNRF1 promotes caveolin-1 ubiquitination and degradation to modulate inflammation. *Nat. Commun.* 8:15502.

Lemmon, M. A., Schlessinger, J., and Ferguson, K. M. (2014). The EGFR family: not so prototypical receptor tyrosine kinases. *Cold Spring Harb. Perspect. Biol.* 6:a020768. doi: 10.1101/cshperspect.a020768

Lester, J. T., and DeLuca, N. A. (2011). Herpes simplex virus 1 ICP4 forms complexes with TFIID and mediator in virus-infected cells. *J. Virol.* 85, 5733–5744. doi: 10.1128/jvi.00385-11

Levkowitz, G., Waterman, H., Ettenberg, S. A., Katz, M., Tsygankov, A. Y., Alroy, I., et al. (1999). Ubiquitin ligase activity and tyrosine phosphorylation underlie suppression of growth factor signaling by c-Cbl/Sli-1. *Mol. Cell.* 4, 1029–1040. doi: 10.1016/s1097-2765(00)80231-2

Levkowitz, G., Waterman, H., Zamir, E., Kam, Z., Oved, S., Langdon, W. Y., et al. (1998). c-Cbl/Sli-1 regulates endocytic sorting and ubiquitination of the epidermal growth factor receptor. *Genes Dev.* 12, 3663–3674. doi: 10.1101/gad.12.23.3663

Lu, Q., Hope, L. W., Brasch, M., Reinhard, C., and Cohen, S. N. (2003). TSG101 interaction with HRS mediates endosomal trafficking and receptor down-regulation. *Proc. Natl. Acad. Sci. U. S. A.* 100, 7626–7631. doi: 10.1073/pnas.0932599100

Madshus, I. H., and Stang, E. (2009). Internalization and intracellular sorting of the EGF receptor: a model for understanding the mechanisms of receptor trafficking. *J. Cell. Sci.* 122, 3433–3439. doi: 10.1242/jcs.050260

Raiborg, C., Bache, K. G., Gillooly, D. J. I, Madshus, H., Stang, E., and Stenmark, H. (2002). Hrs sorts ubiquitinated proteins into clathrin-coated microdomains of early endosomes. *Nat. Cell. Biol.* 4, 394–398. doi: 10.1038/ncb791

Raiborg, C., and Stenmark, H. (2009). The ESCRT machinery in endosomal sorting of ubiquitylated membrane proteins. *Nature* 458, 445–452. doi: 10.1038/nature07961

Ravid, T., Heidinger, J. M., Gee, P., Khan, E. M., and Goldkorn, T. (2004). c-Cbl-mediated ubiquitinylation is required for epidermal growth factor receptor exit from the early endosomes. *J. Biol. Chem.* 279, 37153–37162. doi: 10.1074/jbc.m403210200

Roepstorff, K., Grovdal, L., Grandal, M., Lerdrup, M., and van Deurs, B. (2008). Endocytic downregulation of ErbB receptors: mechanisms and relevance in cancer. *Histochem. Cell. Biol.* 129, 563–578. doi: 10.1007/s00418-008-0401-3

Saitoh, F., and Araki, T. (2010). Proteasomal degradation of glutamine synthetase regulates schwann cell differentiation. *J. Neurosci.* 30, 1204–1212. doi: 10.1523/jneurosci.3591-09.2010

Sanchala, D. S., Bhatt, L. K., and Prabhavalkar, K. S. (2017). Oncolytic Herpes Simplex Viral Therapy: A Stride toward Selective Targeting of Cancer Cells. *Front. Pharmacol.* 8:270. doi: 10.3389/fphar.2017.00270

Schlessinger, J. (2002). Ligand-induced, receptor-mediated dimerization and activation of EGF receptor. *Cell* 110, 669–672. doi: 10.1016/s0092-8674(02)00966-2

Schmidt-Glenewinkel, H., Reinz, E., Bulashevska, S., Beaudouin, J., Legewie, S., Alonso, A., et al. (2012). Multiparametric image analysis reveals role of Caveolin1 in endosomal progression rather than internalization of EGFR. *FEBS Lett.* 586, 1179–1189. doi: 10.1016/j.febslet.2012.02.041

Smith, C. A., Bates, P., Rivera-Gonzalez, R., Gu, B., and DeLuca, N. A. (1993). ICP4, the major transcriptional regulatory protein of herpes simplex virus type 1, forms a tripartite complex with TATA-binding protein and TFIIB. *J. Virol.* 67, 4676–4687. doi: 10.1128/jvi.67.8.4676-4687.1993

Smith, C. J., Berry, D. M., and McGlade, C. J. (2013). The E3 ubiquitin ligases RNF126 and Rabring7 regulate endosomal sorting of the epidermal growth factor receptor. *J. Cell. Sci.* 126, 1366–1380. doi: 10.1242/jcs.116129

Sokolowski, N. A., Rizos, H., and Diefenbach, R. J. (2015). Oncolytic virotherapy using herpes simplex virus: how far have we come?. *Oncol. Vir.* 4, 207–219. doi: 10.2147/ov.s66086

Soltoff, S. P., and Cantley, L. C. (1996). p120cbl is a cytosolic adapter protein that associates with phosphoinositide 3-kinase in response to epidermal growth factor in PC12 and other cells. *J. Biol. Chem.* 271, 563–567. doi: 10.1074/jbc.271.1.563

Sorkin, A., Krolenko, S., Kudrjavtceva, N., Lazebnik, J., Teslenko, L., Soderquist, A. M., et al. (1991). Recycling of epidermal growth factor-receptor complexes in A431 cells: identification of dual pathways. *J. Cell Biol.* 112, 55–63. doi: 10.1083/jcb.112.1.55

Sousa, L. P., Lax, I., Shen, H., Ferguson, S. M., De Camilli, P., and Schlessinger, J. (2012). Suppression of EGFR endocytosis by dynamin depletion reveals that EGFR signaling occurs primarily at the plasma membrane. *Proc. Natl. Acad. Sci. U. S. A.* 109, 4419–4424. doi: 10.1073/pnas.1200164109

Stang, E., Blystad, F. D., Kazazic, M., Bertelsen, V., Brodahl, T., Raiborg, C., et al. (2004). Cbl-dependent ubiquitination is required for progression of EGF receptors into clathrin-coated pits. *Mol. Biol. Cell.* 15, 3591–3604. doi: 10.1091/mbc.e04-01-0041

Stang, E., Johannessen, L. E., Knardal, S. L., and Madshus, I. H. (2000). Polyubiquitination of the epidermal growth factor receptor occurs at the plasma membrane upon ligand-induced activation. *J. Biol. Chem.* 275, 13940–13947. doi: 10.1074/jbc.275.18.13940

Tomas, A., Futter, C. E., and Eden, E. R. (2014). EGF receptor trafficking: consequences for signaling and cancer. *Trends Cell. Biol.* 24, 26–34. doi: 10.1016/j.tcb.2013.11.002

Tong, J., Taylor, P., and Moran, M. F. (2014). Proteomic analysis of the epidermal growth factor receptor (EGFR) interactome and post-translational modifications associated with receptor endocytosis in response to EGF and stress. *Mol. Cell Proteom.* 13, 1644–1658. doi: 10.1074/mcp.m114.038596

Umebayashi, K., Stenmark, H., and Yoshimori, T. (2008). Ubc4/5 and c-Cbl continue to ubiquitinate EGF receptor after internalization to facilitate polyubiquitination and degradation. *Mol. Biol. Cell.* 19, 3454–3462. doi: 10.1091/mbc.e07-10-0988

Vieira, A. V., Lamaze, C., and Schmid, S. L. (1996). Control of EGF receptor signaling by clathrin-mediated endocytosis. *Science* 274, 2086–2089. doi: 10.1126/science.274.5295.2086

Wahl, M. I., Nishibe, S., Kim, J. W., Kim, H., Rhee, S. G., and Carpenter, G. (1990). Identification of two epidermal growth factor-sensitive tyrosine phosphorylation sites of phospholipase C-gamma in intact HSC-1 cells. *J. Biol. Chem.* 265, 3944–3948. doi: 10.1016/s0021-9258(19)39685-1

Wakatsuki, S., Furuno, A., Ohshima, M., and Araki, T. (2015). Oxidative stress-dependent phosphorylation activates ZNRF1 to induce neuronal/axonal degeneration. *J. Cell. Biol.* 211, 881–896. doi: 10.1083/jcb.201506102

Wakatsuki, S., Saitoh, F., and Araki, T. (2011). ZNRF1 promotes Wallerian degeneration by degrading AKT to induce GSK3B-dependent CRMP2 phosphorylation. *Nat. Cell. Biol.* 13, 1415–1423. doi: 10.1038/ncb2373

Wang, Y., Pennock, S., Chen, X., and Wang, Z. (2002). Endosomal signaling of epidermal growth factor receptor stimulates signal transduction pathways leading to cell survival. *Mol. Cell. Biol.* 22, 7279–7290. doi: 10.1128/mcb.22.20.7279-7290.2002

Wang, Y. N., Yamaguchi, H., Hsu, J. M., and Hung, M. C. (2010). Nuclear trafficking of the epidermal growth factor receptor family membrane proteins. *Oncogene* 29, 3997–4006. doi: 10.1038/onc.2010.157

Waterman, H., Katz, M., Rubin, C., Shtiegman, K., Lavi, S., Elson, A., et al. (2002). A mutant EGF-receptor defective in ubiquitylation and endocytosis unveils a role for Grb2 in negative signaling. *EMBO J.* 21, 303–313. doi: 10.1093/emboj/21.3.303

Yamashita, M., Chattopadhyay, S., Fensterl, V., Saikia, P., Wetzel, J. L., and Sen, G. C. (2012). Epidermal growth factor receptor is essential for Toll-like receptor 3 signaling. *Sci. Sign.* 5:ra50. doi: 10.1126/scisignal.2002581

Yang, F. C., Tan, B. C., Chen, W. H., Lin, Y. H., Huang, J. Y., Chang, H. Y., et al. (2013). Reversible acetylation regulates salt-inducible kinase (SIK2) and its function in autophagy. *J. Biol. Chem.* 288, 6227–6237. doi: 10.1074/jbc.m112.431239

Zheng, K., Xiang, Y., Wang, X., Wang, Q., Zhong, M., Wang, S., et al. (2014). Epidermal growth factor receptor-PI3K signaling controls cofilin activity to facilitate herpes simplex virus 1 entry into neuronal cells. *MBio* 5, :e00958–13.

Conflict of Interest: The authors declare that the research was conducted in the absence of any commercial or financial relationships that could be construed as a potential conflict of interest.

frontiers in Cell and Developmental Biology

REVIEW
published: 07 July 2021
doi: 10.3389/fcell.2021.673839

Novel Insights and Current Evidence for Mechanisms of Atherosclerosis: Mitochondrial Dynamics as a Potential Therapeutic Target

Dan Li[1], Shengjie Yang[1], Yanwei Xing[1], Limin Pan[1], Ran Zhao[1], Yixi Zhao[1], Longtao Liu[2†] and Min Wu[1*†]*

[1] Guang'an Men Hospital, China Academy of Chinese Medical Sciences, Beijing, China, [2] Xiyuan Hospital, China Academy of Chinese Medical Sciences, Beijing, China

OPEN ACCESS

Edited by:
Ana Cuenda,
Consejo Superior de Investigaciones Científicas (CSIC), Spain

Reviewed by:
Francisco Iñesta-Vaquera,
University of Dundee, United Kingdom
Muhammad Nawaz,
University of Gothenburg, Sweden

***Correspondence:**
Longtao Liu
liulongtao1976@126.com
Min Wu
wumin19762000@126.com

† These authors have contributed equally to this work

Specialty section:
This article was submitted to Signaling, a section of the journal Frontiers in Cell and Developmental Biology

Received: 01 March 2021
Accepted: 16 June 2021
Published: 07 July 2021

Citation:
Li D, Yang S, Xing Y, Pan L, Zhao R, Zhao Y, Liu L and Wu M (2021) Novel Insights and Current Evidence for Mechanisms of Atherosclerosis: Mitochondrial Dynamics as a Potential Therapeutic Target. Front. Cell Dev. Biol. 9:673839. doi: 10.3389/fcell.2021.673839

Cardiovascular disease (CVD) is the main cause of death worldwide. Atherosclerosis is the underlying pathological basis of CVD. Mitochondrial homeostasis is maintained through the dynamic processes of fusion and fission. Mitochondria are involved in many cellular processes, such as steroid biosynthesis, calcium homeostasis, immune cell activation, redox signaling, apoptosis, and inflammation, among others. Under stress conditions, mitochondrial dynamics, mitochondrial cristae remodeling, and mitochondrial ROS (mitoROS) production increase, mitochondrial membrane potential (MMP) decreases, calcium homeostasis is imbalanced, and mitochondrial permeability transition pore open (mPTP) and release of mitochondrial DNA (mtDNA) are activated. mtDNA recognized by TLR9 can lead to NF-κB pathway activation and pro-inflammatory factor expression. At the same time, TLR9 can also activate NLRP3 inflammasomes and release interleukin, an event that eventually leads to tissue damage and inflammatory responses. In addition, mitochondrial dysfunction may amplify the activation of NLRP3 through the production of mitochondrial ROS, which together aggravate accumulating mitochondrial damage. In addition, mtDNA defects or gene mutation can lead to mitochondrial oxidative stress. Finally, obesity, diabetes, hypertension and aging are risk factors for the progression of CVD, which are closely related to mitochondrial dynamics. Mitochondrial dynamics may represent a new target in the treatment of atherosclerosis. Antioxidants, mitochondrial inhibitors, and various new therapies to correct mitochondrial dysfunction represent a few directions for future research on therapeutic intervention and amelioration of atherosclerosis.

Keywords: mitochondria, morphology, fission, fusion, cytoskeleton, transport

INTRODUCTION

Atherosclerosis is a chronic inflammatory condition caused by abnormal lipid metabolism, oxidative stress, endothelial injury and other factors and can involve large and medium-sized arteries throughout the body (Gisterå and Ketelhuth, 2018). Atherosclerotic cardiovascular disease (ASCVD) is a major cause of mortality in many industrialized societies

(Commodore-Mensah et al., 2021). Lipid accumulation, local inflammatory responses, and endothelial injury are important factors in the development of atherosclerosis (Pham et al., 2021).

Over the past 20 years, studies have shown that mitochondrial dysfunction can lead to the occurrence and development of many diseases such as atherosclerosis (Sobenin et al., 2013a). Mitochondria are highly dynamic organelles that constantly produce adenosine triphosphate (ATP). Events, such as mitochondrial DNA (mtDNA) mutation, imbalance in calcium homeostasis, accumulation of oxidative stress products, and metabolic dysfunction are hallmarks of mitochondrial damage (Forte et al., 2019). When mitochondria are damaged or dysfunctional, energy production is limited and large quantities of reactive oxygen species (ROS) are produced. At the same time, mitochondria are vulnerable to damage from ROS. Cardiac cells, which are oxygen-hungry and mitochondria-rich, are also vulnerable to ROS damage. Studies have shown that ROS-mediated energy damage can induce systolic dysfunction of the heart (Luptak et al., 2019). In addition, ROS promote mutations and deletions in mtDNA (Li et al., 2021). Mitochondrial fusion can serve as a strategy to repair irreversibly damaged mitochondria, and at the same time, limit the accumulation of mtDNA mutations during aging. Irreversibly damaged mitochondria can also be repaired through fission (Yapa et al., 2021). Here we discuss the role of mitochondrial dynamics and its potential as a therapeutic target in this review.

MITOCHONDRIAL DYNAMICS AND DYSFUNCTION IN ATHEROSCLEROSIS

Mitochondria are organelles with a double-membrane structure and are the main components involved in aerobic respiration in most eukaryotic cells (Navaratnarajah et al., 2021). The mitochondrial membrane comprises three layers. The outer layer is known as the outer mitochondrial membrane (OMM). The mitochondrial intima contains enzymes responsible for oxidative phosphorylation (OXPHOS), which are components of a multi-protein complex of five large electron-transport (respiratory) chains (Song et al., 2019; **Figure 1A**). Increased ROS levels result in mitochondrial dysfunction in vascular cells, aggravated endothelial injury and smooth muscle cell proliferation, and are responsible for inducing vascular atherosclerosis development and other pathological changes (Hughes et al., 2020). Furthermore, in the mitochondria, the activity of ion channels—which modulate Ca^{2+} signal transduction—is regulated by the free radicals generated through the respiratory chain functions, and these phenomenon subsequently affect biosynthesis and degradation reactions in various organisms (Gherardi et al., 2020). In addition, mitochondria are directly and closely related to other organelles such as the endoplasmic reticulum (Lackner, 2019). For example, mitochondria-associated endoplasmic reticulum membranes (MAMs) play an important role in atherosclerosis development, heart failure, and other diseases by participating in lipid and calcium (Ca^{2+}) homeostasis, mitochondrial dynamics, inflammation, and apoptosis (Gao et al., 2020).

Studies have shown that the continuous fission and fusion of mitochondria are important for maintaining mitochondrial morphology and function (Kyriakoudi et al., 2021). Mammals contain two mitofusins, namely mitofusin (Mfn)-1 and Mfn2. These proteins contain two hydrophobic heptapeptide repeats, i.e., HR1 and HR2 at their N- and C-termini (located on both sides of the transmembrane domain) (Xin et al., 2021) (**Figure 1B**). In mammalian cells, mitochondrial fusion is mainly mediated by members of the of the GTPase protein family, i.e., Mfn1, Mfn2, and optic atropy-1 (OPA1) (Wolf et al., 2020). OPA1 and Mfn1 cooperate to enable organelle fusion. Transcript variants of *OPA1* encode two OPA1 protein isomers with different lengths, namely L-OPA1 and S-OPA1. As L-OPA1 has a better fusion efficiency than S-OPA1, its abnormal functioning can lead to reduced fusion activity, and thereby mitochondrial rupture and apoptosis (Wang et al., 2021a; **Figure 1C**). The collar structure comprising Drp1 polymer plays a central role in mitochondrial fission, and post-translational modification of Drp1 plays a major role in the formation of collar structures during mitochondrial fission (Breitzig et al., 2018; **Figure 1D**). Soluble substances can enter the mitochondria when the mPTP—located in the inner mitochondrial membrane—opens or closes, thereby affecting the MMP and inducing apoptosis (Du et al., 2021).

The expression of mitochondrial dynamin plays an important role in the development of atherosclerosis (Sharp and Archer, 2015). Chiong et al. (2014) found that the expression of Mfn2 is significantly reduced in the background of atherosclerosis in $ApoE^{-/-}$ mice and is also involved in the pathogenesis of atherosclerosis. Heterozygous deletion of *OPA1* in mice also results in abnormal mitochondrial morphology, such as cleavage of the mitochondrial cristae (Hu et al., 2020). In some cases, inhibition of Drp1 expression can increase the depolarization of mitochondria in heart cells (Ikeda et al., 2015). Drp1-induced disturbances in mitochondrial homeostasis can cause a variety of complex vascular diseases through mechanisms, such as myocardial ischemia-reperfusion (I/R) injury, heart failure, and endothelial dysfunction (Morales et al., 2020).

NOVEL MECHANISTIC INSIGHTS: FROM MITOCHONDRIAL DYNAMICS TO ATHEROSCLEROSIS

Mitochondrial ROS-Induced Oxidative Stress in Atherosclerosis

The fusion and fission of mitochondria are closely related to mitochondrial function. ROS are a byproduct produced during mitochondrial respiration; when mitochondrial ROS (mitoROS) levels are disturbed, interactions involving the structure and function of mitochondria may eventuate (Forrester et al., 2018) and play important roles in the development of inflammatory and metabolic disorders (such as atherosclerosis and diabetes) (Hu et al., 2020). Drp1 can affect mitochondrial fission by regulating the levels of mitoROS and subsequent oxidative stress (Cid-Castro and Morán, 2021). In addition, ROS also

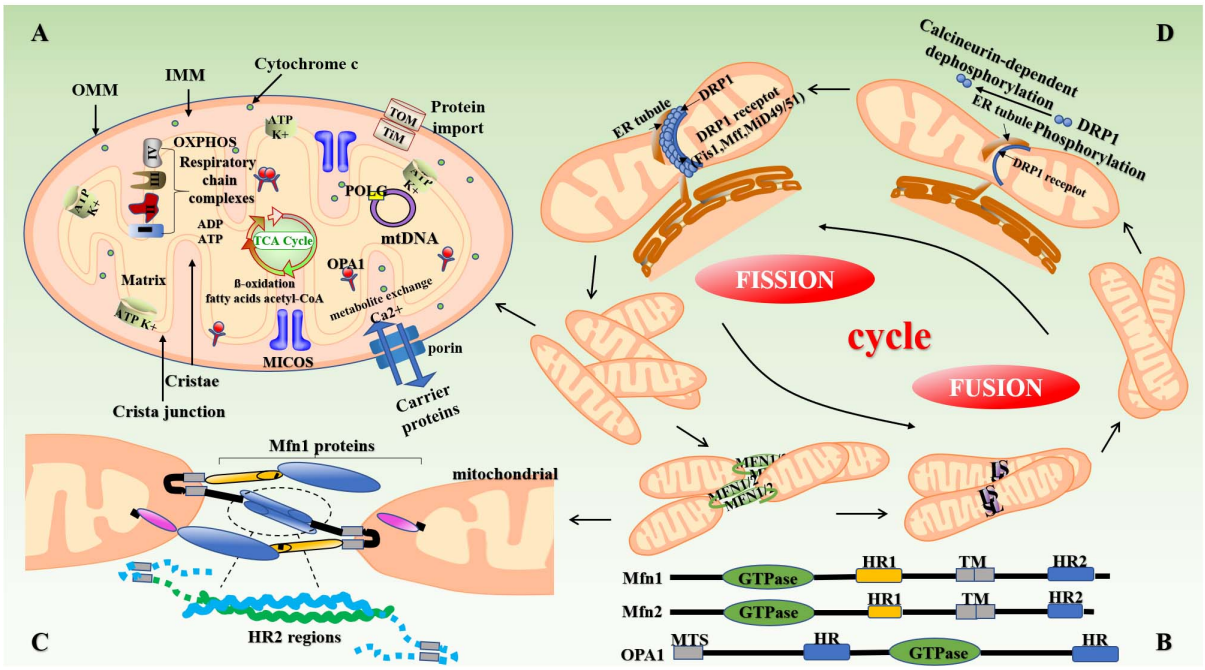

FIGURE 1 | Structure of mitochondria and mitochondrial dynamics. **(A)** The mitochondrion is mainly composed of OMM, mitochondrial membrane gap, IMM, and the mitochondrial matrix. The intima folds inward to form mitochondrial cristae perpendicular to the mitochondrial long axis. Mitochondria produce reduced nicotinamide adenine dinucleotide (NADH) through the Krebs cycle, which is then oxidized and phosphorylated to release ATP. **(B,C)** Mitochondrial fusion involves three types of dyneins, namely MFN (Mfn1 and Mfn2), OPA1, and MSTO1. First, the transmembrane GTPases on the mitochondrial outer membrane, namely Mfn1 and Mfn2, fuse through the HR structure. Subsequently, OPA1-mediated IMM fusion occurs in the mitochondrial inner membrane. OPA1 also includes L-OPA1 and the S-OPA1 formed after the removal of L-OPA1 via action of proteolytic enzymes OMA1 and YME1L1. Mitochondrial mitosis is mediated mainly by Drp1. Drp1 is recruited into mitochondria by several ligand proteins (MFF, MIEF1/Mid51, and MIEF2/Mid49) that assemble into spiral fragments around the OMM, induce mitochondrial fission, and complete division by the transport of microtubules and actin. **(D)** The fusion and fission of mitochondria is a cyclic process. IMM, inner mitochondrial membrane; OMM, outer mitochondrial membrane; OPA1, optic atrophy protein-1; Drp1, dynamin-related protein; NADH, nicotinamide adenine dinucleotide.

regulate mitochondrial fusion. When ROMO1 (ROS regulatory protein 1) is inactivated, OPA1 expression is reduced, resulting in the remodeling of mitochondrial cristae and fragmented mitochondria (Norton et al., 2014). Studies have shown that high glucose levels can increase the activity of Drp1 in the mitochondria of endothelial cells, leading to mitochondrial fission and production of mitoROS. Mdivi-1 can reduce high glucose induced oxidative stress and injury to aortic cells (Wang et al., 2017b).

Lipid accumulation is an important link in the formation of plaque during the early stages of atherosclerosis (Chistiakov et al., 2018), and increased ROS levels induce endothelial dysfunction, vascular inflammation, and accelerated accumulation of oxidized low density lipoprotein (ox-LDL) in the arterial wall, a phenomenon that promotes atherosclerosis (Naik and Dixit, 2011; Yu et al., 2017). As an activator of NLRP3, ox-LDL can induce alterations in MMP, which leads to the generation of mitoROS and activation of Ca^{2+} signals, calcium influx, and mitochondrial damage (Triantafilou et al., 2013). *In vitro* experiments have shown that lectin-type oxidized LDL receptor 1 (LOX-1), the main receptor for ox-LDL, expressed in response to lipopolysaccharide (LPS) induction, can lead to ROS production, mtDNA damage (**Figure 2B**), and the production of NLRP3 inflammasomes and play an important role in inflammatory diseases such as atherosclerosis (Ding et al., 2014). Studies have reported that ox-LDL and ROS can damage mitochondria, release mitoROS, induce the activation of NLRP3, elevate levels of IL-1β and IL-18, and cause inflammation (Huang et al., 2020; Markin et al., 2021). At the same time, ROS leads to endothelial nitric oxide synthase (eNOS) degradation by increasing the activity of mitochondrial arginase II (Suárez-Rivero et al., 2021). *In vivo* studies have found that Mfn2 inhibits ox-LDL-induced rabbit smooth muscle cell proliferation and reduces atherosclerotic plaques by regulating Akt and ERK phosphorylation (Guo et al., 2007b).

In addition to mitoROS produced by activity of the mitochondrial electron transport chain (ETC), NADPH oxidase (NOX), xanthine oxidase and cyclooxygenase can also release large amounts of ROS (Yeh et al., 2018). Various sources of ROS play an important role in angiogenesis (Fukai and Ushio-Fukai, 2020). Angiogenesis has a significant impact on the treatment of ischemic cardiovascular disease (CVD). Restoring intravascular perfusion by enhancing or inhibiting angiogenesis is an important means of treating peripheral arterial disease (PAD) caused by atherosclerosis (Simons et al., 2016). Mitochondria play a key role in angiogenic responses induced by growth factors such as VEGF (Guo et al., 2017) by regulating mitoROS-related activities (Wang et al., 2011). *In vivo* studies

have shown that in presence of high glucose, the consumption of PDIA1 in endothelial cells can induce Drp1 sulfenylation at Cys^{644}, promote mitochondrial fission, and increase ROS levels. Therefore, PDIA1 or the Cys oxidation-defective mutant Drp1 can promote angiogenesis in diabetic mice (Kim et al., 2018). Inhibition of Drp1 can result in the dysfunction of mitochondrial respiratory function (Ota et al., 2020).

mtDNA Damage in Atherosclerosis

The mitochondrial genome comprises naked, independently encoded, double-stranded DNA molecules that exist mainly as small loops (in yeast and mammals) or linear molecules (protozoa) (Suzuki et al., 2011). mtDNA is the only DNA molecule that exists in the human cytoplasm. It is 16,569-basepair long and includes the heavy chain of the outer ring (high molecular weight) and the light chain of the inner ring (low molecular weight). mtDNA encodes 37 genes, among them, 13 protein-coding regions have been identified to play a role in maintaining normal cellular OXPHOS (Tang et al., 2020). High levels of mitochondrial mutation represent an important factor that leads to dysfunction of oxidative phosphorylation and energy metabolism and endothelial injury (Ueda et al., 2015). As opposed to genomic DNA, mtDNA in the mitochondrial matrix or inner membrane does not contain any histones and is free of structural protection; this DNA is in a state of continuous synthesis throughout the cell cycle, with poor stability and is in close proximity to the site where the electron transport system—that continuously produces ROS—is located. Therefore, mtDNA is more easily and extensively damaged (Ahmed et al., 2015).

In humans, mtDNA damage has been confirmed in atherosclerotic diseases, and may be attributed to the damage of this DNA by ROS produced by the adjacent respiratory chains (Muñoz-Carvajal and Sanhueza, 2020; **Figure 2A**). As such, mitochondria are the site of activation of the NRLP3 inflammasome. When mitochondria are dysfunctional, changes in the production of ROS, mtDNA release, cardiolipin, and NAD/NADH can activate NLRP3. mtDNA damage may therefore result in mitochondrial dysfunction and increased IL-1β levels through the aforementioned mechanisms of promoting atherosclerosis (Freigang et al., 2013). Furthermore, mtDNA

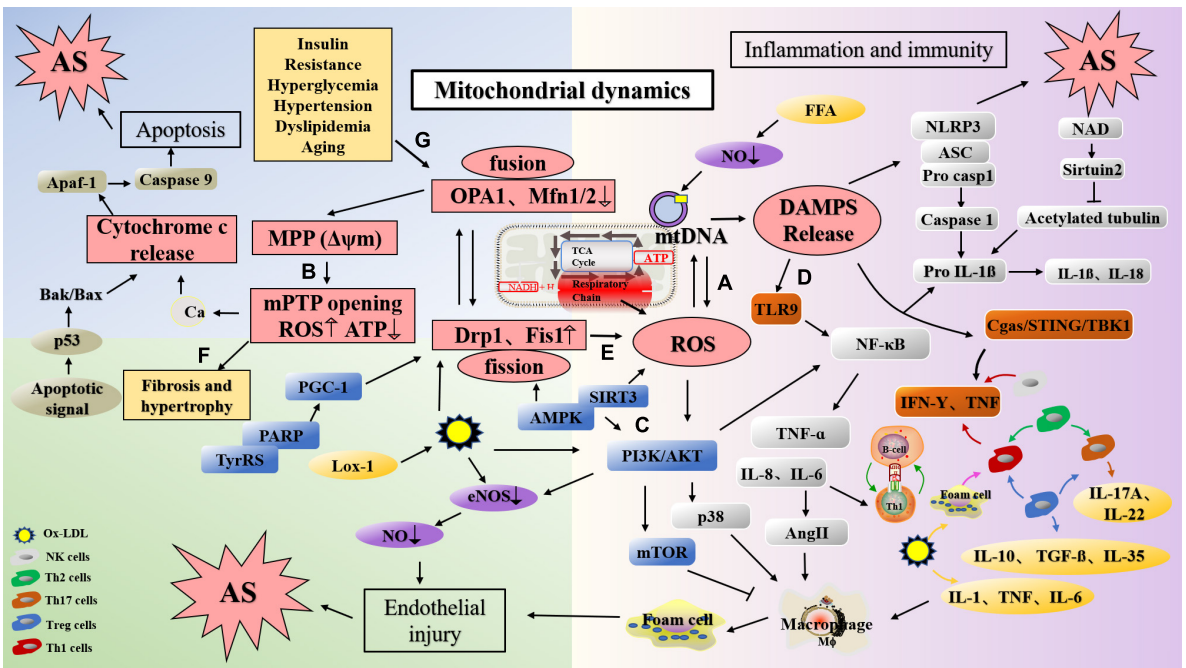

FIGURE 2 | The mechanism of atherosclerosis formation caused via dysfunction of mitochondrial function and dynamics. **(A)** ROS produced in the respiratory chains of mitochondria can cause damage to mtDNA. **(B)** Ox-LDL induced the change of MMP, lead to Ca^{2+} influx, ROS production and mitochondrial damage. In addition, the decrease of MFN and OPA1 levels can also lead to the change of MMP and damage of mitochondria. **(C)** *PPAR* deletion decreases Mfn2 expression and PGC-1 expression, and leading to mitochondrial dysfunction; AMPK activates endothelial cells through the phosphatidyl inositol 3 kinase protein kinase B (PI3Kb) pathway, stimulates eNOS activation, and generates NO to protect endothelial cells; Mfn2 can inhibit the PI3K/Akt pathway by activating the mitochondrial apoptotic pathway, resulting in VSMC apoptosis. **(D)** DAMP promotes inflammation by activating PRRs. mtDNA can activate NF-κB and trigger TLR9 signaling pathway to mediate p38 pathway. Mitochondrial damage induces NLRP3 activation, and NLRP3 amplify the production of ROS. **(E)** Silencing Drp1 can inhibit mitochondrion fission, decrease ROS levels and inhibits smooth muscle cell migration. **(F)** Mfn2 deficiency leads to the increase of Ca^{2+} expression in cardiomyocytes, mitochondrial swelling, and eventually leads to cardiac hypertrophy. **(G)** Diabetes mellitus, insulin resistance, dyslipidemia, obesity, hypertension and aging may damage mitochondrial function, and lead to the development of atherosclerosis. mtDNA, mitochondrial DNA; Drp1, dynamin-related protein; Mfn1, mitofusin 1; Mfn2, mitofusin 2; OPA1, optic atropy-1; Fis1, mitochondrial fission protein 1; MMP ($\Delta\psi$m), mitochondrial membrane potential; mPTP, mitochondrial permeability transition pore open; Cyt c, cytochrome C; ROS, reactive oxygen species; LOX-1, lectin-type oxidized LDL receptor 1; ox-LDL, oxidized low density lipoprotein; DAMP, damage-associated molecular pattern; PI3K, phosphatidyl inositol 3; NF-κB, nuclear factor-κB; TyrRS-PARP1, tyrosyl transfer- RNA synthetase (TyrRS) and poly (ADP-ribose) polymerase 1 (PARP1).

damage leads to mitochondrial dysfunction, resulting in the removal of abnormal mitochondria, which may be detrimental to cell function under conditions of oxidative stress. Altered membrane potential in cells lacking MFN or OPA1 may cause mitochondrial damage, which can be compensated by the dynamic cycle of mitochondrial fusion and fission (Chen et al., 2007; Weaver et al., 2014). Studies have reported that mitochondrial fusion possesses a dual function, and that it not only protects the integrity of mtDNA, but also maintains the mtDNA function under conditions of mutational pressure. Therefore, mitochondrial fusion may have some compensatory effects on mtDNA mutation (Chen et al., 2010). Liu et al. (2020) found that overexpression of Mfn2 can increase MMP, enhance mitochondrial fusion, reduce mitoROS accumulation, activate the AMPK/SIRT3 signaling pathway, and prevent cardio-cerebrovascular ischemia/reperfusion (I/R) damage.

Furthermore, somatic mutations in the human mitochondrial genome may play a role in the development of atherosclerosis (Sazonova et al., 2017; Volobueva et al., 2019). Investigations on 12 aorta samples from male have revealed that compared with non-atherosclerotic intima, lipofibrous plaques have a high frequency of *MT-RNR1* A1555G, *MT-TL1* C3256T, *MT-CYB* G12315A, and *MT-TL2* G15059A (Sobenin et al., 2013b). In addition, compared with healthy vascular tissue, atherosclerotic plaques exhibit significant differences in the frequency of C3256T, T3336C, G12315A, and G14459A mutations (Sazonova et al., 2009). The C5178A mutation is more common in normal vascular tissues than in atherosclerotic plaques (Matsunaga et al., 2001).

Pathways Related to Mitochondria in Atherosclerosis

Peroxisomal proliferator-activated receptor (PPAR) is a transcription factor activated by nuclear receptor superfamily ligands; it activates target genes and affects lipid metabolism, glucose homeostasis, cell proliferation, differentiation, apoptosis, and inflammatory responses (Teixeira et al., 2021). Previous studies have confirmed that PPARs are expressed in atherosclerotic plaques, suggesting that PPARs are closely related to atherosclerosis-related mechanisms such as transcriptional regulation of pro-inflammatory genes, e.g., cytokines, chemokines, vascular endothelial cell adhesion factors, and metallostromal proteases (Corona et al., 2014). Studies have shown that cardiac defects involving PPARs can also lead to abnormal mitochondrial morphology, excessive lipid deposition, and other phenotypic changes (Cheng et al., 2004). PPARα induces the downregulation of Mfn2 expression in high-fat or high-glucose treated cardiomyocytes by promoting mitochondrial fusion. Exogenous supply of Mfn2 in this background can restore MMP, inhibit mitochondrial oxidative stress, and improve mitochondrial function (Hu et al., 2019). Additionally, studies have revealed that *PPAR* deletion significantly decreases PGC-1 expression in C57BL/6J mice, thereby leading to mitochondrial dysfunction at the structural and functional levels (Zhou et al., 2016b). Yang et al. found that resveratrol could inhibit palmitic acid-induced damage to human umbilical vein endothelial cells (HUVECs), increase the expression of Mfn1, Mfn2, and OPA1, inhibit mitochondrial fragmentation, and reduce oxidative damage in endothelial cells by regulating mitochondrial fusion through the TyPRS-PARP1 signaling pathway (Yang et al., 2019; **Figure 2C**).

AMPK is a cellular energy receptor activated by AMP that affects sugar, fatty acid, and protein metabolism (Dehnavi et al., 2021). Importantly, AMPK activation can lead to inhibition of cell proliferation when cardiomyocytes and vascular smooth muscle cells (VSMCs) are in a state of ischemia and hypoxia, thus playing an important role in the regulation of cardiovascular diseases and in the prevention and treatment of atherosclerosis (Yan et al., 2018). Moreover, AMPK activates endothelial cells through the phosphatidyl inositol 3 kinase protein kinase B (PI3Kb) pathway, stimulates eNOS activation, and generates NO to further protect endothelial cells; these phenomenons play important roles in the prevention of atherosclerosis (Tousoulis et al., 2012; Xing et al., 2015; **Figure 2C**). Studies have shown that the AMPK-SIRT3 pathway also affects mitochondrial function (Karnewar et al., 2016). In addition to affecting cell function and metabolism, AMPK can also affect mitochondrial homeostasis by promoting mitochondrial fission. Antimycin A (complex I inhibitor) and antiretroviral drug antimycin A (complex III inhibitor) were discovered based on the theory that AMPK could induce mitochondrial fission (Toyama et al., 2016). Previous studies have shown that MFF is a new substrate of AMPK and plays an important role in AMPK-mediated regulation of mitochondrial morphology (Ducommun et al., 2015). Phosphorylation of AMPK-induced MFF by SAMP155 at Ser172, for example, is a potential mechanism used to explain mitochondrial fission due to diminished mitochondrial respiration. Additionally, MFF in human osteosarcoma cells has been shown to induce mitochondrial fission (Toyama et al., 2016). Notably, AMPK regulates mitochondrial fission through an autophagy-dependent Drp1 degradation mechanism. Observation of the aorta of PRKAA2/AMPKa2-deficient mice revealed that the number of autophagosomes in the aorta of PRKAA2/AMPKa2-deficient mice is significantly reduced, suggesting abnormal mitochondrial mitosis (Wang et al., 2017a).

The phosphoinositide 3-kinase/protein kinase B (PI3K/Akt) signaling pathway is known to regulate cell growth, differentiation, and proliferation (Shao et al., 2021). Studies have shown that knockout of a PI3Kγ subunit, i.e., P110γ can reduce the size of atherosclerotic plaques in $ApoE^{-/-}$ and $LDLr^{-/-}$ mice. Moreover, the Class IA PI3K signaling pathway can significantly reduce the levels of serum free fatty acids (FFA), cholesterol, and triglycerides in mice and inhibit the production of intracellular ROS (Wang et al., 2021b). Akt also plays an important role in glucose metabolism, apoptosis, cell proliferation, and other aspects of cell growth (Linton et al., 2019). Furthermore, Mfn2 can inhibit the PI3K/Akt pathway by activating the mitochondrial apoptotic pathway, resulting in increased mitochondrial outer membrane permeability and ultimately VSMC apoptosis (Guo et al., 2007a; **Figure 2C**). Fang et al. found that decreased Mfn2 expression might be related to pulmonary arterial smooth muscle cell (PASMC) proliferation under hypoxic conditions (Fang et al., 2016).

Role of Mitochondria in Inflammation and Immunity Related in Atherosclerosis

Inflammation and immunity are inseparable in atherosclerosis, as the two influence each other to accelerate the progression of atherosclerosis (Saigusa et al., 2020). Atherosclerosis is not only an inflammatory disease, but it is also an autoimmune disorder. Additionally, atheromatous plaques and phenotypic changes in vascular cells are the main manifestations of atherosclerosis, and most of these immune responses are can be attributed to Th-1 cells (Kuznetsova et al., 2019). Furthermore, ox-LDL, ROS, and advanced glycation end products (AGEs) further aggravate the occurrence of inflammatory reactions and vulnerable plaque rupture events.

Inflammation is related to innate defense and tissue damage. Pattern recognition receptors (PRRs) are located on the surface of cell membranes or inside cells. They recognize and bind to pathogen-associated molecular patterns (PAMPs) and damage-associated molecular patterns (DAMPs) to trigger the inflammatory cascade in innate immunity (Zhang et al., 2010). PRRs, LPS receptors, Toll-like receptors (TLRs), and Nod like receptors (NLRs) play important roles in the pathogenesis of atherosclerosis (Shimada et al., 2012). In contrast, mtDNA that functions as a DAMP plays an important role in the inflammatory response. DAMPs can accumulate when mtDNA is damaged or degraded, and these promote inflammation by binding to—and activating—PRRs (Mathew et al., 2012; Picca et al., 2017). Studies have shown that cytokines produced by mitochondrial DAMPs play a key role in the inflammatory signaling pathway in atherosclerosis (Goossens et al., 2010; Yu et al., 2013; Tumurkhuu et al., 2016). NLRs are scaffold proteins that play key roles in regulating innate immune responses by triggering the NF-κB and mitogen-activated protein kinase (MAPK) signaling pathways, and by controlling caspase activation (Zhang et al., 2014). Mitochondrial antiviral signaling protein (MAVS) is a key signaling protein activated by viral RNA sensors RIG-1 and MDA5, which can promote gene expression by activating the NF-κB pathways (Loo and Gale, 2011). In addition, MAVS associates with NLRP3 and promotes its oligomerization, which leads to the activation of caspase-1 (Mohanty et al., 2019). It has recently been demonstrated that the activation of NLRP3 caused by the synthetic TLR7 ligand imiquimod is the result of the production of mitoROS induced by complex I of the respiratory redox chain and the quinone oxidoreductase NQO2 (Groß et al., 2016).

In recent years, increasing numbers of studies have demonstrated that mtDNA regulates the development of inflammation in disease states by activating the immune system (West and Shadel, 2017). In mice, inflammatory arthritis was induced upon the intra-articular injection of mtDNA, which induced the secretion of TNF by spleen cells; this was the first report on the immunological potential of mtDNA (Kepp et al., 2011). mtDNA can induce the activation of the NF-κB pathway and the release of TNF-α and IL-6 after being sensed by TLR9 (Zhong et al., 2016). mtDNA accumulation also results in the activation of caspase-1 and promotes the secretion of IL-1β and IL-18 in macrophages, thereby participating in a series of inflammatory responses (Mottis et al., 2019). Further, mtDNA activates the p38 and p42-44 MAPK pathways and chemotaxis of neutrophils to endothelial injury sites by triggering TLR9 signaling (Zhang et al., 2010). This induces the development of a range of inflammatory diseases, including rheumatoid arthritis, atherosclerosis, and non-alcoholic steatohepatitis. NLRP3 inflammasome, whose formation is triggered by mitochondrial damage and IRF3-signaling-induced endothelial inflammation also contributes to the progression of atherosclerosis (Mao et al., 2017). In addition, mitochondrial dysfunction may also amplify the activation of NLRP3 through the production of mitoROS (**Figure 2D**).

Mitochondrial Associated Endothelial Injury and Smooth Muscle Proliferation in Atherosclerosis

Endothelial dysfunction leads to the development of atherosclerosis in patients with diabetes, and induces many changes in terms of mitochondrial dynamics and mitochondrial fission, and increases ROS production (Ago et al., 2010). Mitochondrial NOX4 promotes the production of ROS by mitochondria, which in turn can induce mitochondrial damage (Vendrov et al., 2015) and endothelial injury (Kim et al., 2016). Metformin can inhibit the expression of NOX4, reduce the production of ROS, and improve endothelial function (Cheng and Lanza-Jacoby, 2015; Victor et al., 2015). D-chiro inositol can inhibit the expression of Drp1, reduce the levels of NOX4, and enhance the production of NO in mouse aortic endothelial cells to protect against endothelial injury (Zhang et al., 2017). After hypoxia/reoxygenation (H/R) injury, ROS levels increase significantly, and ROS promote mitochondrial fission in myocardial endothelial cells through JNK-mediated phosphorylation of Drp1 (Chen et al., 2021b).

Epigenetic modifications induced in response to mtDNA damage have become a research hotspot in the domains of aging and atherosclerotic diseases (Schiano et al., 2015). *In vivo* studies have shown that even if ROS levels do not increase significantly, mtDNA damage can reduce mitochondrial respiration and ATP content in smooth muscle cells, promote apoptosis of VSMCs and aggravate atherosclerosis (Yu et al., 2014). After endothelial injury, proliferation, migration, and vascular remodeling of VSMCs are important for the rupture of atherosclerotic plaques, wherein the fission of mitochondria and deregulated secondary morphological functions play an important role (Wang et al., 2015; Hong et al., 2017). Once mitochondrion fission is inhibited by silencing Drp1, the protons leak across the mitochondrial inner membrane, resulting in decreased ROS levels in primary mouse smooth muscle cells, a phenomenon that inhibits smooth muscle cell migration (Wang et al., 2015; **Figure 2E**).

Mitochondria-Related Fibrosis and Hypertrophy in Atherosclerosis

Mitochondrial damage is involved in myocardial cell loss and myocardial fibrosis, both of which eventually manifest as cardiac ischemia (Bonnans et al., 2014; Humeres and Frangogiannis, 2019; Nielsen et al., 2019). Atherosclerosis is the pathological basis for a variety of cardiovascular and cerebrovascular diseases,

eventually leading to cardiac dysfunction (Jonsson and Bäckhed, 2017). Compared with cardiomyocytes, cardiac fibroblasts have lower mitochondrial respiratory function and expression of mitochondrial complexes I, II, III, IV, and V, and this is the main cause of cardiac fibrosis (Zhao et al., 2019). *In vivo* studies have found that mitochondrial respiratory chain complex dysfunction, mtDNA damage, increased ROS abundance, and secondary oxidative stress in myocardial infarction models lead to the activation of many protein kinases and transcription factors involved in hypertrophy signals (Rababa'h et al., 2018; Bugger and Pfeil, 2020).

STAT3 plays an important role in maintaining the physiological balance in the heart and protecting the heart from harm (Heusch et al., 2011; Gent et al., 2017; Kleinbongard et al., 2018). If myocardial cells are stimulated by H_2O_2 or treated with rotenone, mitochondrial function is impaired, and STAT3 signaling is inhibited. Cardiac fibroblasts also express STAT3. In cardiac fibroblasts, STAT3 activation promotes cardiac fibroblast proliferation (Haghikia et al., 2014) and hyaluronic acid accumulation during wound healing after acute myocardial infarction (Müller et al., 2014).

Mitochondrial dynamics play an important role in the development of cardiac hypertrophy (Jong et al., 2019). The MMP of cardiomyocytes in mice lacking Mfn2 is decreased and cells exhibit a certain degree of cardiac hypertrophy. The reason may be that the level of Ca^{2+} in mitochondria deficient in Mfn2 increases and the mitochondria swell. In addition, reduced cell death in cardiomyocytes lacking Mfn2 is related to the inhibition of mPTP (Qiu et al., 2020; **Figure 2F**). It has been reported that Drp1 expression is related to the pathogenesis of cardiac hypertrophy (Pennanen et al., 2014). In cardiomyocytes of hypertensive rats, high levels of ROS—associated with overexpression of Drp1—can activate calcineurin and CaMKII, and lead to aggravation of cardiac hypertrophy. Mdivi-1 can reduce the production of ROS and inhibit the expression of Drp1 (Hasan et al., 2018). L-2286 induced the translocation of mitochondrial Drp1, reduced Drp1 expression, inhibited mitochondrial fission, and reduced the number of mitochondrial cristae. At the same time, it increased the expression of OPA1 and Mfn2 to prevent the development of spontaneous left ventricular hypertrophy in rats (Ordog et al., 2021).

Mitochondrial Dynamics and Risk Factors for Atherosclerosis

Diabetes Mellitus, Insulin Resistance, and Mitochondrial Dynamics

Atherosclerosis is the most common macrovascular complication of diabetes. Imbalance between oxidative and antioxidant systems *in vivo* leads to increased levels of ROS, a phenomenon that results in linear DNA strand breaks, an important factor in progression of atherosclerosis and functional damage to endothelial cells (Fetterman et al., 2016). Hyperglycemia can trigger this mechanism through the ETC, leading to endothelial cell injury and dysfunction (Forrester et al., 2018). Patients with diabetes exhibit altered mitochondrial dynamics and endothelial cell morphology; for example, the mitochondria of the immortalized endothelial cell line Eahy926 will rupture in the presence of high glucose (Paltauf-Doburzynska et al., 2004). *In vivo* studies showed that mitochondrial debris and ROS production increased in endothelial cells isolated from coronary arteries of diabetic mice (Makino et al., 2010). Furthermore, the expression of Drp1 and Fis1 is increased and the production of ROS augmented in HUVECs under high glucose conditions; Silencing of Drp1 can prevent the damage caused by insulin, calcium ionophores, and eNOS phosphorylation (Shenouda et al., 2011; **Figure 2G**).

Studies have shown that activation of various pro-inflammatory factors and signaling pathways during the development of atherosclerosis is closely related to insulin resistance (Boudina et al., 2009; Watanabe et al., 2014). The increase in ROS levels after endothelial injury can lead to the activation of the AMPK pathway, increase the level of eNOS, trigger insulin resistance, and promote the development of atherosclerosis (Förstermann et al., 2017). Insulin resistance also alters lipid and protein metabolism. Increased ROS and pro-inflammatory cytokine levels impair insulin signaling, activate the NF-κB pathway, perpetuate the inflammatory and oxidative environment, prolong insulin resistance, and to some extent prolong atherosclerosis. Changes in mitochondrial activity caused by mitochondrial number and functional abnormalities induced by abnormal Mfn2 expression are some of the characteristic features associated with insulin resistance (Peyravi et al., 2020).

Dyslipidemia, Obesity, and Mitochondrial Dynamics

Inappropriate changes in lifestyle and dietary habits and alterations to metabolism are responsible for the globally increasing incidence of obesity, even in developed countries (Blüher, 2019). As an important mechanism associated with obesity development, deregulated lipid metabolism also results in the development of atherosclerosis and other diseases (Laslett et al., 2012). When various factors lead to substantial LDL deposition, enhanced HDL transport capacity and increased macrophage-mediated lipid phagocytosis occur, and finally, foam cell deposition occurs in damaged areas of blood vessels, thereby leading to the subcutaneous formation of atherosclerotic plaques (Everts et al., 2014; Cader et al., 2016). Excessive LDL deposition can induce vascular cell apoptosis through a mitochondria-dependent pathway after oxidative modification (Nazzal et al., 2006). Ox-LDL mediates the opening of mPTP through the activation of cysteine proteases, and then the mitochondria release cytochrome C and activated caspase-3, thereby releasing interleukins and other inflammatory factors (Vindis et al., 2005; **Figure 2G**).

Aortic mtDNA damage and protein nitrification are significantly increased in ApoE$^{-/-}$ mice exposed to secondhand smoke, suggesting that mtDNA damage caused by high cholesterol is one of the important mechanisms for the development of atherosclerosis. Additionally, Mfn2 is expressed at relatively low levels in the muscle tissues of obese people compared to those of lean individuals (Knight-Lozano et al., 2002). In some patients with extrahepatic cholestasis, Mfn2 expression in the liver is decreased, suggesting that Mfn2 plays an

important role in regulating lipid metabolism and mitochondrial function (Chen et al., 2013).

Hypertension and Mitochondrial Dynamics

Mitochondria play an important role in maintaining the stability of arterial blood pressure by regulating the superoxide content and energy metabolism (Vaka et al., 2018). Energy metabolism disorders involving myocardial mitochondria may be an important mechanism in hypertension (Marshall et al., 2018). For example, the arterial blood pressure of SOD2-deficient mice is significantly increased with age under conditions of a high-salt diet, and oxidative stress in SOD2-deficient mice might explain this increase; this leads to inflammatory cell infiltration and promotes sodium retention (Rodriguez-Iturbe et al., 2007). Additionally, studies have found that cholesterol and blood pressure are elevated in patients aged approximately 30 years, and that the degree of elevation is related to age; further, mitochondrial tRNA mutation and decline in mitochondrial function may be important factors leading to the onset of the disorder in these patients (Wilson et al., 2004; Bernal-Mizrachi et al., 2005). In pulmonary arterial hypertension, mdivi-1 inhibits the mitochondrial fragmentation of PASMCs isolated under hypoxic conditions and improves the function of these cells, while overexpression of Drp1 increases mitochondrial fragmentation (Zhuan et al., 2020). Dikalova et al. (2020) studied an animal hypertension model involving SIRT3$^{-/-}$ mice and found that decreased expression of mitochondrial deacetylase SIRT3 resulted in SOD2 inactivation and mitochondrial oxidative stress injury. Subsequently, mtDNA release activates inflammasomes and other inflammatory cells to stimulate accumulation of inflammatory cells, thereby damaging vascular endothelial cells and promoting the development of hypertension and vascular aging (Dikalova et al., 2020). Studies have shown that excessive ROS levels induced in response to altered mitochondrial morphology and apoptosis via dynein-mediated cytochrome C release are important mechanisms leading to the development of hypertension-associated left ventricular hypertrophy (López Farré and Casado, 2001; van Empel and De Windt, 2004; **Figure 2G**).

Abnormal mitochondrial function and changes in mtDNA are important factors affecting vasoconstriction (Zhou et al., 2016a). Liu et al. (2016) found that mitochondrial dynamics are closely related to the functional state of blood vessels. They also found that changes in arterial vascular state caused by changes in mitochondrial dynamics of smooth muscle cells caused changes in arterial blood pressure (Liu et al., 2016). Additionally, studies have shown that the mitochondria of pulmonary VSMCs affect respiratory function and oxidative metabolism by regulating intracellular calcium homeostasis and also affect pulmonary vascular contraction, which is a key factor in the pathogenesis of pulmonary hypertension (Tuder et al., 2012).

Aging and Mitochondrial Dynamics

A considerable number of studies have shown that the mechanisms involved in age-related cardiovascular dysfunction, such as mitochondrial fusion and fission disorder, mtDNA mutation, excessive ROS production, mitochondrial respiratory chain function, and metabolic dysfunction are closely related to mitochondrial functional homeostasis (Ames, 2004; Koltover, 2017). During cardiac aging, mitochondrial structures are destroyed and mitochondrial size increases (Duicu et al., 2013). Mitochondria promote fusion or inhibit fission to promote cell aging (Picca et al., 2018). MFN-1/2 and OPA1 modulate mitochondrial morphology in adult cardiomyocytes (Faelber et al., 2019). Sebastián et al. (2016) found that Mfn2 expression decreased with skeletal muscle aging and triggered increased numbers of damaged mitochondria. D'Amico et al. (2019) showed that MFF expression of RNA-binding protein Pumilio2 (PUM2) decreases with age, which further leads to reduced mitotic division and dysfunction.

The decline of mitochondrial energy metabolism in the heart is associated with aging, and aging leads to mtDNA damage, and ROS (Elorza and Soffia, 2021). Studies have shown that with age, mitochondrial volume increases, and a considerable amount of ROS is produced during oxidative phosphorylation (**Figure 2G**). mtDNA mutations are found in disease states in patients with age-related diseases, including chronic coronary artery disease (Phillips et al., 2014). Strutynska et al. (2016) found that the concentration of nitric oxide (NO) and hydrogen sulfide in the mitochondria of aged rats is decreased, while the level of ROS is increased, resulting in increased sensitivity of mPTP to calcium. Foote et al. (2018) observed aorta and carotid arteries in mice and found that at 44 weeks if age, carotid artery wall elasticity decreased, aortic collagen content and elastin fragmentation increased, arterial mtDNA copy number decreased, mitochondrial respiration decreased, and blood vessel aging accelerated.

ANTI-ATHEROSCLEROTIC TREATMENT TARGETING THROUGH MITOCHONDRIA

Mitochondria are considered to be one of the main targets for the design and development of new drugs in CVD and other diseases (including cancer and neurological diseases), and represent a promising strategy to treat atherosclerosis by modulating the mitochondria (Zielonka et al., 2017).

Diet and Lifestyle

Diet

Studies have shown that controlling cardiovascular risk factors by adjusting diet, correcting obesity and properly controlling blood sugar levels, can prevent mitochondrial stress and reduce mitochondrial damage (Stanzione et al., 2021). The increase in FFAs contributes to the activation of oxidative stress, mitochondrial stress and pro-inflammatory signals (Kaludercic and Di Lisa, 2020). *Trans*-fatty acids (TFAs), which are found in many fast foods and meats, are unsaturated fats. TFAs increase TG, LDL, and decrease LDL particle size and HDL levels. TFAs also increase pro-inflammatory cytokine abundance, inducing endothelial dysfunction and insulin resistance (Micha and Mozaffarian, 2009). Artificial TFAs are associated with an increased risk of atherosclerosis and CV events (Valenzuela et al., 2019). The level of plasma FFA was increased with carotid

atherosclerotic plaque in 320 patients with type 2 diabetes mellitus (T2DM) through carotid artery ultrasound examination and reporting, so reducing plasma FFA levels may be an effective way to reduce T2DM (Tibaut et al., 2019). Previous studies have reported that FFA can increase NO production, damage mtDNA and induce apoptosis (Li et al., 2015a).

Lifestyle

In addition, sedentary time is an independent risk factor for atherosclerosis and CVD, and at least one-third of deaths from coronary heart disease or T2DM are associated with sedentary time (Thijssen et al., 2010; Fletcher et al., 2018). In turn, exercise enhances endothelial function, protects against oxidative stress and inflammation, reduces the levels of TG, ApoB, and LDL, and increases HDL (Cai et al., 2018). Studies have shown that long-term aerobic exercise can reduce the formation of ROS and mitochondrial swelling in aortic endothelial cells of aged rats, increase the content of mtDNA, and reduce the vascular sclerosis and endothelial dysfunction caused by aging (Gu et al., 2014). However, it should be noted that excessive and overloaded exercise can also induce mitochondrial disorders, cause heart abnormalities, chronic fatigue syndrome and other diseases (Ostojic, 2016). Studies have confirmed that strenuous exercise can cause muscle dysfunction and increase mitochondrion fission (Pataky and Nair, 2021).

Anti-atherosclerotic Drugs Targeting Mitochondria

Antioxidants

Selective mitochondrial-targeting drugs such as mitochondrial antioxidants are being tested in preclinical and clinical trials (Kiyuna et al., 2018). Some natural Chinese medicine ingredients with antioxidant effects have also been gradually discovered (**Table 1**). For example, luteolin exhibits antioxidant properties in HUVECs that significantly reverse the symptoms of oxidative stress in atherosclerosis (Wu et al., 2018). Resveratrol has been shown to promote mitochondrial fusion and can improve endothelial cells by maintaining mitochondrial membrane proteins and reducing ROS, and may be used in the prevention of atherosclerosis (Yu et al., 2019). Studies have found that Ilexgenin A inhibits palmitate-induced Drp1 expression and mitochondrial fission by regulating proteases, reduces the production of ROS and inflammatory factors, improves endothelial dysfunction, and reduces atherosclerosis (Zhu et al., 2019). Salidroside is considered to be an antioxidant with anti-cardiovascular and vascular protective effects. It can inhibit VSMC proliferation, Drp1 expression and oxidative stress, and up-regulate Mfn2 expression, which may improve the proliferation of VSMCs induced by high glucose (Zhuang et al., 2017). Corylin, a flavonoid compound, inhibits the proliferation of VSMCs induced by platelet-derived growth factor-BB (PDGF-BB) by regulating mTOR/Drp1, and reduces atherosclerotic lesions in $ApoE^{-/-}$ mice (Chen et al., 2020).

Mitochondrial Homeostasis Regulator

Therapeutic strategies for maintaining mitochondrial homeostasis are already under study. MitoTEMPO, a mitochondrial-targeted SOD mimic, can reduce mitochondrial superoxide anions in high-fat diet mice, reduce the production of mitoROS, and prevent cardiomyocyte hypertrophy in the hearts of diabetic mice (Ni et al., 2016). Currently, specific inhibitors of mitochondrial fusion (*M*-hydrazone) and fission (MDIVI-1 and P110) are under investigation (Cassidy-Stone et al., 2008; Qi et al., 2013). mtDNA is an important cause of ROS production and mitochondrial damage. Mitochondrial miRNA is involved in the post-transcriptional regulation and metabolism of mitochondrial gene expression, ROS production and lipid metabolism, and can lead to abnormal mitochondrial function and increased oxidative stress, such as miR-484 inhibition of Fis1 expression. In addition, related research regarding mtDNA and mitochondrial miRNA may be a future direction for diagnosis and treatment of mitochondrial-related diseases (Song et al., 2019).

AMPK Regulator

Some drugs are aimed at regulating the levels of mitochondrial fusion and fission proteins by activating AMPK kinase, inhibiting ROS and inflammation and thereby improving endothelium, and prevent and treat atherosclerosis (Apostolova et al., 2020). For example, Coenzyme Q10 (CoQ10) is one of the components of the mitochondrial respiratory chain, which performs electron transfer, reduces oxidative stress damage and improves mitochondrial function. *In vivo* studies have shown that CoQ10 may negatively regulate YAP by activating AMPK and promote the expression of OPA1 to improve mitochondrial function, inhibit ROS production, and improve atherosclerosis (Xie et al., 2020). Thiazolidinediones such as pioglitazone as PPARγ inhibitors can activate AMPK and increase the expression of genes related to mitochondrial function. Studies have shown that AMPK activation regulates Drp1 phosphorylation to help inhibit the activation of mitochondrial ROS and TXNIP/NLRP3, thereby improving endothelial dysfunction (Li et al., 2015b).

NLRP3 Regulator

In atherosclerosis, oxidative stress and mitochondrial dysfunction are important mechanisms leading to NLRP3 activation. NLRP3 activation is closely related to mitochondrial damage (Ding et al., 2014). Fatty acid-mediated mitochondrial cartilage uncoupling promotes the release of NLRP3-dependent interleukin-1α (IL-1α) and aggravates the progression of atherosclerosis (Freigang et al., 2013). Both *in vivo* and *in vitro* studies have shown that Drp1-mediated mitochondrial fission is the cause of the activation of NADPH and NLRP3 inflammasomes in endothelial cells (Li et al., 2016). Statins mainly act by inhibiting 3-hydroxymethyl-3-glutaryl CoA (HMG-COA) reductase to reduce intracellular cholesterol biosynthesis. Approximately 40% of patients who fail to achieve their target levels after high doses of statins are treated with a combination of statins and other drugs (Boekholdt et al., 2014). In addition to lowering cholesterol, statins can also improve the endothelium through antioxidant activity to play an anti-atherosclerotic effect (Oesterle et al., 2017). *In vivo* studies found that mitochondrial ROS levels in mice treated with rosuvastatin are decreased, NLRP3, caspase-1 and IL-β levels decreased,

TABLE 1 | Natural compounds target mitochondrial to ameliorate atherosclerosis.

Natural compounds	Sources	Cell types	Changes to mitochondrial	Effects on mitochondria and atherosclerosis	References
Resveratrol	*Polygonum cuspidatum*	HUVECs	Mfn1, Mfn2 and OPA1↑, fission↓, ROS↓	Attenuated endothelial oxidative injury by regulating mitochondrial fusion, inhibiting mitochondrial fission via TyrRS-PARP1 signaling pathway.	Yang et al., 2019
Salidroside	Component of *Rhodiola rosea*	VSMCs isolated from aorta of male Sprague Dawley (SD) rats	Drp1↓,Mfn2↑, fission↓, ROS and NADPH↓	Inhibits high glucose induced proliferation of VSMCs by inhibiting mitochondrial fission and regulating oxidative stress	Zhuang et al., 2017
Corylin	*Psoralea corylifolia* L. (Fabaceae)	HUVECs A7r5 VSMC and RAW264.7 cells	Drp1 and Drp1 phosphorylation↓, fission↓, ROS↓	Inhibited the proliferation and migration of mammalian VSMC, in which rapamycin target protein (mTOR)/Dynamin-1 like protein 1 (Drp1) played an important role.	Chen et al., 2020
Ilexgenin A	*Ilex hainanensis Merr.*	RAECs and HUVECs	Drp1↓, fission↓ ROS↓, NO↑	Promote the expression of PSMB5, inhibit ROS production and Drp1 in a Nrf2 dependent manner, thereby inhibiting mitochondrial fission and improving endothelial dysfunction.	Zhu et al., 2019
Berberine	*Coptis chinensis* Franch	mouse podocytes	Drp1↓, MFF↓, Fis1, fission↓, ROS↓	Improve the mitochondrial damage of glomerular podocytes in DKD mice by inhibiting Drp1, Fis1 and mitochondrial fission.	Qin et al., 2019
Quercetin	Component of hawthorn	Calcifying VSMCs	Drp1↓, fission↓, ROS↓	Improve mitochondrial cristae rupture, inhibit mitochondrial fission, reduce ROS production, reduce apoptosis of VSMCs, thus alleviate adenine induced aortic calcification in rats.	Cui et al., 2017
Vitexin	Component of hawthorn	H9c2 cells	Mfn2↑, Drp1↓, fission↓, ROS↓, inhibited the release of Cyt-c, MMP($\Delta\psi$m)↑, ATP↑	Protects H9c2 cells from I/R-induced mitochondrial dysfunction and significantly reduces ROS level by alleviating myocardial I/R injury in rats.	Xue et al., 2020
Crocin	Ingredient of saffron	Cells from muscle tissue of rats	Mfn2↑, Drp1↓	Change insulin resistance index and glucose homeostasis in diabetes by improving mitochondrial fusion and fission indices.	Peyravi et al., 2020
Baicalin	*Baikal Skullcap*	Rat pheochromocytoma PC12 cells	Drp1↓, fission↓, Mfn2↑, Drp-1 Ser637 phosphorylation↑, MMP($\Delta\psi$m)↑, ROS↓,	Protected against hyperglycemia aggravated I/R injury by regulating mitochondrial functions in a manner dependent on AMPK.	Li et al., 2017

HUVECs, human umbilical vein endothelial cells; RAECs, rat aortic endothelial cells; VSMCs, vascular smooth muscle cells; Drp1, dynamin-related protein; Mfn1, mitofusin 1; Mfn2, mitofusin 2; OPA1, optic atropy-1; ROS, reactive oxygen species; NADPH, nicotinamide adenine dinucleotide phosphate; MFF, mitochondrial fission protein; Fis1, mitochondrial fission protein 1; Cyt c, cytochrome C; MMP ($\Delta\psi$m), mitochondrial membrane potential; DKD, diabetic kidney disease; I/R, ischemia/reperfusion.

mitochondrial damage was reduced, and myocardial fibrosis and infarct size were significantly reduced (Chen et al., 2021a).

CONCLUSION AND PERSPECTIVES

Atherosclerosis is a disease caused by multiple complex factors. A high-fat and high-calorie diet leads to the deposition of lipid particles, and ox-LDL produces a series of complex oxidative stress and inflammatory responses to endothelial stimulation, eventually forming foam cells and typical atheromatous plaques. In recent years, an increasing number of studies have shown that atherosclerosis may be related to mitochondrial fusion and fission. Cardiomyocytes consume substantial amounts of energy, and mitochondria produce ATP through oxidative phosphorylation. The dynamic homeostasis of mitochondria is essential to ensure normal functioning. Multiple studies have shown that mitochondrial dynamic dysfunction, such as mitochondrial over-division due to the absence of the fusion protein Mfn2 or overexpression of Drp1, can lead to CVD progression. The mechanisms involved in atherosclerosis may be closely related to mitochondrial fusion and fission.

In addition to lifestyle improvements and drugs such as statins, new types of antioxidants and mitochondrial regulators such as mdivi-1 have become research hotspots for the treatment of atherosclerosis. Exploration of treatment options for atherosclerosis is warranted; however, this is difficult because only a few classes of drugs are available for treatment, lipid-lowering therapy standards have not been agreed upon, and the cost of new drugs remains unaffordable. Moreover, the mechanisms involved in mitochondrial dynamics are relatively complex and their study is limited as the models are affected by many factors. Therefore, studies on the

role of mitochondrial dynamics in atherosclerosis are at the basic research stage and lacks validation based on large-scale clinical studies. While mitochondrial dynamic homeostasis may play a role in atherosclerotic therapy, this hypothesis needs further confirmation.

AUTHOR CONTRIBUTIONS

MW and LL designed and directed the manuscript. DL wrote the manuscript. LP and SY revised the manuscript. RZ searched the literature. YX and YZ aided in the design of the illustrations. All the authors approved the manuscript for publication.

FUNDING

This work was supported by the National Natural Science Foundation of China (Grant Nos. 81202805, 81973689, 81573821, and 82074254) and the Beijing Natural Science Foundation (Nos. 7172185 and 7202176).

REFERENCES

Ago, T., Kuroda, J., Pain, J., Fu, C., Li, H., and Sadoshima, J. (2010). Upregulation of Nox4 by hypertrophic stimuli promotes apoptosis and mitochondrial dysfunction in cardiac myocytes. *Circ. Res.* 106, 1253–1264. doi: 10.1161/circresaha.109.213116

Ahmed, N., Ronchi, D., and Comi, G. P. (2015). Genes and pathways involved in adult onset disorders featuring muscle mitochondrial DNA instability. *Int. J. Mol. Sci.* 16, 18054–18076. doi: 10.3390/ijms160818054

Ames, B. N. (2004). Delaying the mitochondrial decay of aging. *Ann. N. Y. Acad. Sci.* 1019, 406–411. doi: 10.1196/annals.1297.073

Apostolova, N., Iannantuoni, F., Gruevska, A., Muntane, J., Rocha, M., and Victor, V. M. (2020). Mechanisms of action of metformin in type 2 diabetes: Effects on mitochondria and leukocyte-endothelium interactions. *Redox Biol.* 34:101517. doi: 10.1016/j.redox.2020.101517

Bernal-Mizrachi, C., Gates, A. C., Weng, S., Imamura, T., Knutsen, R. H., DeSantis, P., et al. (2005). Vascular respiratory uncoupling increases blood pressure and atherosclerosis. *Nature* 435, 502–506. doi: 10.1038/nature03527

Blüher, M. (2019). Obesity: global epidemiology and pathogenesis. *Nat. Rev. Endocrinol.* 15, 288–298. doi: 10.1038/s41574-019-0176-8

Boekholdt, S. M., Hovingh, G. K., Mora, S., Arsenault, B. J., Amarenco, P., Pedersen, T. R., et al. (2014). Very low levels of atherogenic lipoproteins and the risk for cardiovascular events: a meta-analysis of statin trials. *J. Am. Coll. Cardiol.* 64, 485–494. doi: 10.1016/j.jacc.2014.02.615

Bonnans, C., Chou, J., and Werb, Z. (2014). Remodelling the extracellular matrix in development and disease. *Nat. Rev. Mol. Cell Biol.* 15, 786–801. doi: 10.1038/nrm3904

Boudina, S., Bugger, H., Sena, S., O'Neill, B. T., Zaha, V. G., Ilkun, O., et al. (2009). Contribution of impaired myocardial insulin signaling to mitochondrial dysfunction and oxidative stress in the heart. *Circulation* 119, 1272–1283. doi: 10.1161/circulationaha.108.792101

Breitzig, M. T., Alleyn, M. D., Lockey, R. F., and Kolliputi, N. (2018). A mitochondrial delicacy: dynamin-related protein 1 and mitochondrial dynamics. *Am. J. Physiol. Cell Physiol.* 315, C80–C90. doi: 10.1152/ajpcell.00042.2018

Bugger, H., and Pfeil, K. (2020). Mitochondrial ROS in myocardial ischemia reperfusion and remodeling. *Biochim. Biophys. Acta Mol. Basis Dis.* 1866:165768. doi: 10.1016/j.bbadis.2020.165768

Cader, M. Z., Boroviak, K., Zhang, Q., Assadi, G., Kempster, S. L., Sewell, G. W., et al. (2016). C13orf31 (FAMIN) is a central regulator of immunometabolic function. *Nat. Immunol.* 17, 1046–1056. doi: 10.1038/ni.3532

Cai, Y., Xie, K. L., Zheng, F., and Liu, S. X. (2018). Aerobic exercise prevents insulin resistance through the regulation of miR-492/Resistin axis in aortic endothelium. *J. Cardiovasc. Transl. Res.* 11, 450–458. doi: 10.1007/s12265-018-9828-7

Cassidy-Stone, A., Chipuk, J. E., Ingerman, E., Song, C., Yoo, C., Kuwana, T., et al. (2008). Chemical inhibition of the mitochondrial division dynamin reveals its role in Bax/Bak-dependent mitochondrial outer membrane permeabilization. *Dev. Cell* 14, 193–204. doi: 10.1016/j.devcel.2007.11.019

Chen, A., Chen, Z., Zhou, Y., Wu, Y., Xia, Y., Lu, D., et al. (2021a). Rosuvastatin protects against coronary microembolization-induced cardiac injury via inhibiting NLRP3 inflammasome activation. *Cell Death Dis.* 12:78. doi: 10.1038/s41419-021-03389-1

Chen, C. C., Li, H. Y., Leu, Y. L., Chen, Y. J., Wang, C. J., and Wang, S. H. (2020). Corylin Inhibits vascular cell inflammation, proliferation and migration and reduces atherosclerosis in ApoE-Deficient Mice. *Antioxidants (Basel)* 9:275. doi: 10.3390/antiox9040275

Chen, H., McCaffery, J. M., and Chan, D. C. (2007). Mitochondrial fusion protects against neurodegeneration in the cerebellum. *Cell* 130, 548–562. doi: 10.1016/j.cell.2007.06.026

Chen, H., Vermulst, M., Wang, Y. E., Chomyn, A., Prolla, T. A., McCaffery, J. M., et al. (2010). Mitochondrial fusion is required for mtDNA stability in skeletal muscle and tolerance of mtDNA mutations. *Cell* 141, 280–289. doi: 10.1016/j.cell.2010.02.026

Chen, Y., Liu, C., Zhou, P., Li, J., Zhao, X., Wang, Y., et al. (2021b). Coronary endothelium no-reflow injury is associated with ROS-modified mitochondrial fission through the JNK-Drp1 signaling pathway. *Oxid. Med. Cell Longev.* 2021:6699516. doi: 10.1155/2021/6699516

Chen, Y., Lv, L., Jiang, Z., Yang, H., Li, S., and Jiang, Y. (2013). Mitofusin 2 protects hepatocyte mitochondrial function from damage induced by GCDCA. *PLoS One* 8:e65455. doi: 10.1371/journal.pone.0065455

Cheng, G., and Lanza-Jacoby, S. (2015). Metformin decreases growth of pancreatic cancer cells by decreasing reactive oxygen species: role of NOX4. *Biochem. Biophys. Res. Commun.* 465, 41–46. doi: 10.1016/j.bbrc.2015.07.118

Cheng, L., Ding, G., Qin, Q., Huang, Y., Lewis, W., He, N., et al. (2004). Cardiomyocyte-restricted peroxisome proliferator-activated receptor-delta deletion perturbs myocardial fatty acid oxidation and leads to cardiomyopathy. *Nat. Med.* 10, 1245–1250. doi: 10.1038/nm1116

Chiong, M., Cartes-Saavedra, B., Norambuena-Soto, I., Mondaca-Ruff, D., Morales, P. E., García-Miguel, M., et al. (2014). Mitochondrial metabolism and the control of vascular smooth muscle cell proliferation. *Front. Cell Dev. Biol.* 2:72. doi: 10.3389/fcell.2014.00072

Chistiakov, D. A., Shkurat, T. P., Melnichenko, A. A., Grechko, A. V., and Orekhov, A. N. (2018). The role of mitochondrial dysfunction in cardiovascular disease: a brief review. *Ann. Med.* 50, 121–127. doi: 10.1080/07853890.2017.1417631

Cid-Castro, C., and Morán, J. (2021). Differential ROS-mediated phosphorylation of Drp1 in mitochondrial fragmentation induced by distinct cell death conditions in cerebellar granule neurons. *Oxid. Med. Cell Longev.* 2021:8832863. doi: 10.1155/2021/8832863

Commodore-Mensah, Y., Lazo, M., Tang, O., Echouffo-Tcheugui, J. B., Ndumele, C. E., Nambi, V., et al. (2021). High burden of subclinical and cardiovascular disease risk in adults with metabolically healthy obesity: the atherosclerosis risk in communities (ARIC) Study. *Diabetes Care* doi: 10.2337/dc20-2227 [Epub ahead of print].

Corona, J. C., de Souza, S. C., and Duchen, M. R. (2014). PPARγ activation rescues mitochondrial function from inhibition of complex I and loss of PINK1. *Exp. Neurol.* 253, 16–27. doi: 10.1016/j.expneurol.2013.12.012

Cui, L., Li, Z., Chang, X., Cong, G., and Hao, L. (2017). Quercetin attenuates vascular calcification by inhibiting oxidative stress and mitochondrial fission. *Vascul. Pharmacol.* 88, 21–29. doi: 10.1016/j.vph.2016.11.006

D'Amico, D., Mottis, A., Potenza, F., Sorrentino, V., Li, H., Romani, M., et al. (2019). The RNA-binding protein PUM2 impairs mitochondrial dynamics and mitophagy during aging. *Mol. Cell* 73, 775.e–787.e. doi: 10.1016/j.molcel.2018.11.034

Dehnavi, S., Kiani, A., Sadeghi, M., Biregani, A. F., Banach, M., Atkin, S. L., et al. (2021). Targeting AMPK by statins: a potential therapeutic approach. *Drugs* 81, 923–933. doi: 10.1007/s40265-021-01510-4

Dikalova, A. E., Pandey, A., Xiao, L., Arslanbaeva, L., Sidorova, T., Lopez, M. G., et al. (2020). Mitochondrial Deacetylase Sirt3 reduces vascular dysfunction and hypertension while Sirt3 depletion in essential hypertension is linked to vascular inflammation and oxidative stress. *Circ. Res.* 126, 439–452. doi: 10.1161/circresaha.119.315767

Ding, Z., Liu, S., Wang, X., Dai, Y., Khaidakov, M., Deng, X., et al. (2014). LOX-1, mtDNA damage, and NLRP3 inflammasome activation in macrophages: implications in atherogenesis. *Cardiovasc. Res.* 103, 619–628. doi: 10.1093/cvr/cvu114

Du, J., Song, D., Li, J., Li, Y., Li, B., and Li, L. (2021). Paeonol triggers apoptosis in HeLa cervical cancer cells: the role of mitochondria-related caspase pathway. *Psychopharmacology (Berl)* doi: 10.1007/s00213-021-05811-0 [Epub ahead of print].

Ducommun, S., Deak, M., Sumpton, D., Ford, R. J., Núñez Galindo, A., Kussmann, M., et al. (2015). Motif affinity and mass spectrometry proteomic approach for the discovery of cellular AMPK targets: identification of mitochondrial fission factor as a new AMPK substrate. *Cell Signal.* 27, 978–988. doi: 10.1016/j.cellsig.2015.02.008

Duicu, O. M., Mirica, S. N., Gheorgheosu, D. E., Privistirescu, A. I., Fira-Mladinescu, O., and Muntean, D. M. (2013). Ageing-induced decrease in cardiac mitochondrial function in healthy rats. *Can. J. Physiol. Pharmacol.* 91, 593–600. doi: 10.1139/cjpp-2012-0422

Elorza, A. A., and Soffia, J. P. (2021). mtDNA Heteroplasmy at the Core of aging-associated heart failure. an integrative view of OXPHOS and mitochondrial life cycle in cardiac mitochondrial physiology. *Front. Cell Dev. Biol.* 9:625020. doi: 10.3389/fcell.2021.625020

Everts, B., Amiel, E., Huang, S. C., Smith, A. M., Chang, C. H., Lam, W. Y., et al. (2014). TLR-driven early glycolytic reprogramming via the kinases TBK1-IKK? supports the anabolic demands of dendritic cell activation. *Nat. Immunol.* 15, 323–332. doi: 10.1038/ni.2833

Faelber, K., Dietrich, L., Noel, J. K., Wollweber, F., Pfitzner, A. K., Mühleip, A., et al. (2019). Structure and assembly of the mitochondrial membrane remodelling GTPase Mgm1. *Nature* 571, 429–433. doi: 10.1038/s41586-019-1372-3

Fang, X., Chen, X., Zhong, G., Chen, Q., and Hu, C. (2016). Mitofusin 2 downregulation triggers pulmonary artery smooth muscle cell proliferation and apoptosis imbalance in rats with hypoxic pulmonary hypertension via the PI3K/Akt and mitochondrial apoptosis pathways. *J. Cardiovasc. Pharmacol.* 67, 164–174. doi: 10.1097/fjc.0000000000000333

Fetterman, J. L., Holbrook, M., Westbrook, D. G., Brown, J. A., Feeley, K. P., Bretón-Romero, R., et al. (2016). Mitochondrial DNA damage and vascular function in patients with diabetes mellitus and atherosclerotic cardiovascular disease. *Cardiovasc. Diabetol.* 15, 53. doi: 10.1186/s12933-016-0372-y

Fletcher, E. A., McNaughton, S. A., Crawford, D., Cleland, V., Della Gatta, J., Hatt, J., et al. (2018). Associations between sedentary behaviours and dietary intakes among adolescents. *Public Health Nutr.* 21, 1115–1122. doi: 10.1017/s136898001700372x

Foote, K., Reinhold, J., Yu, E. P. K., Figg, N. L., Finigan, A., Murphy, M. P., et al. (2018). Restoring mitochondrial DNA copy number preserves mitochondrial function and delays vascular aging in mice. *Aging Cell* 17:e12773. doi: 10.1111/acel.12773

Forrester, S. J., Kikuchi, D. S., Hernandes, M. S., Xu, Q., and Griendling, K. K. (2018). Reactive oxygen species in metabolic and inflammatory signaling. *Circ. Res.* 122, 877–902. doi: 10.1161/circresaha.117.311401

Förstermann, U., Xia, N., and Li, H. (2017). Roles of vascular oxidative stress and nitric oxide in the pathogenesis of atherosclerosis. *Circ. Res.* 120, 713–735. doi: 10.1161/circresaha.116.309326

Forte, M., Palmerio, S., Bianchi, F., Volpe, M., and Rubattu, S. (2019). Mitochondrial complex I deficiency and cardiovascular diseases: current evidence and future directions. *J. Mol. Med. (Berl)* 97, 579–591. doi: 10.1007/s00109-019-01771-3

Freigang, S., Ampenberger, F., Weiss, A., Kanneganti, T. D., Iwakura, Y., Hersberger, M., et al. (2013). Fatty acid-induced mitochondrial uncoupling elicits inflammasome-independent IL-1α and sterile vascular inflammation in atherosclerosis. *Nat. Immunol.* 14, 1045–1053. doi: 10.1038/ni.2704

Fukai, T., and Ushio-Fukai, M. (2020). Cross-Talk between NADPH oxidase and mitochondria: role in ROS signaling and angiogenesis. *Cells* 9:1849. doi: 10.3390/cells9081849

Gao, P., Yan, Z., and Zhu, Z. (2020). Mitochondria-associated endoplasmic reticulum membranes in cardiovascular diseases. *Front. Cell Dev. Biol.* 8:604240. doi: 10.3389/fcell.2020.604240

Gent, S., Skyschally, A., Kleinbongard, P., and Heusch, G. (2017). Ischemic preconditioning in pigs: a causal role for signal transducer and activator of transcription 3. *Am. J. Physiol. Heart Circ. Physiol.* 312, H478–H484. doi: 10.1152/ajpheart.00749.2016

Gherardi, G., Monticelli, H., Rizzuto, R., and Mammucari, C. (2020). The Mitochondrial Ca(2+) uptake and the fine-tuning of aerobic metabolism. *Front. Physiol.* 11:554904. doi: 10.3389/fphys.2020.554904

Gisterå, A., and Ketelhuth, D. F. J. (2018). Lipid-driven immunometabolic responses in atherosclerosis. *Curr. Opin. Lipidol.* 29, 375–380. doi: 10.1097/mol.0000000000000540

Goossens, P., Gijbels, M. J., Zernecke, A., Eijgelaar, W., Vergouwe, M. N., van der Made, I., et al. (2010). Myeloid type I interferon signaling promotes atherosclerosis by stimulating macrophage recruitment to lesions. *Cell Metab.* 12, 142–153. doi: 10.1016/j.cmet.2010.06.008

Groß, C. J., Mishra, R., Schneider, K. S., Médard, G., Wettmarshausen, J., Dittlein, D. C., et al. (2016). K(+) efflux-independent NLRP3 inflammasome activation by small molecules targeting mitochondria. *Immunity* 45, 761–773. doi: 10.1016/j.immuni.2016.08.010

Gu, Q., Wang, B., Zhang, X. F., Ma, Y. P., Liu, J. D., and Wang, X. Z. (2014). Chronic aerobic exercise training attenuates aortic stiffening and endothelial dysfunction through preserving aortic mitochondrial function in aged rats. *Exp. Gerontol.* 56, 37–44. doi: 10.1016/j.exger.2014.02.014

Guo, D., Wang, Q., Li, C., Wang, Y., and Chen, X. (2017). VEGF stimulated the angiogenesis by promoting the mitochondrial functions. *Oncotarget* 8, 77020–77027. doi: 10.18632/oncotarget.20331

Guo, X., Chen, K. H., Guo, Y., Liao, H., Tang, J., and Xiao, R. P. (2007a). Mitofusin 2 triggers vascular smooth muscle cell apoptosis via mitochondrial death pathway. *Circ. Res.* 101, 1113–1122. doi: 10.1161/circresaha.107.157644

Guo, Y. H., Chen, K., Gao, W., Li, Q., Chen, L., Wang, G. S., et al. (2007b). Overexpression of Mitofusin 2 inhibited oxidized low-density lipoprotein induced vascular smooth muscle cell proliferation and reduced atherosclerotic lesion formation in rabbit. *Biochem. Biophys. Res. Commun.* 363, 411–417. doi: 10.1016/j.bbrc.2007.08.191

Haghikia, A., Ricke-Hoch, M., Stapel, B., Gorst, I., and Hilfiker-Kleiner, D. (2014). STAT3, a key regulator of cell-to-cell communication in the heart. *Cardiovasc. Res.* 102, 281–289. doi: 10.1093/cvr/cvu034

Hasan, P., Saotome, M., Ikoma, T., Iguchi, K., Kawasaki, H., Iwashita, T., et al. (2018). Mitochondrial fission protein, dynamin-related protein 1, contributes to the promotion of hypertensive cardiac hypertrophy and fibrosis in Dahl-salt sensitive rats. *J. Mol. Cell Cardiol.* 121, 103–106. doi: 10.1016/j.yjmcc.2018.07.004

Heusch, G., Musiolik, J., Gedik, N., and Skyschally, A. (2011). Mitochondrial STAT3 activation and cardioprotection by ischemic postconditioning in pigs with regional myocardial ischemia/reperfusion. *Circ. Res.* 109, 1302–1308. doi: 10.1161/circresaha.111.255604

Hong, S., Zhang, X., Zhang, X., Liu, W., Fu, Y., Liu, Y., et al. (2017). Role of the calcium sensing receptor in cardiomyocyte apoptosis via mitochondrial dynamics in compensatory hypertrophied myocardium of spontaneously hypertensive rat. *Biochem. Biophys. Res. Commun.* 487, 728–733. doi: 10.1016/j.bbrc.2017.04.126

Hu, C., Shu, L., Huang, X., Yu, J., Li, L., Gong, L., et al. (2020). OPA1 and MICOS Regulate mitochondrial crista dynamics and formation. *Cell Death Dis.* 11:940. doi: 10.1038/s41419-020-03152-y

Hu, L., Ding, M., Tang, D., Gao, E., Li, C., Wang, K., et al. (2019). Targeting mitochondrial dynamics by regulating Mfn2 for therapeutic intervention in diabetic cardiomyopathy. *Theranostics* 9, 3687–3706. doi: 10.7150/thno.33684

Huang, D., Gao, W., Zhong, X., and Ge, J. (2020). NLRP3 activation in endothelia promotes development of diabetes-associated atherosclerosis. *Aging (Albany NY)* 12, 18181–18191. doi: 10.18632/aging.103666

Hughes, W. E., Beyer, A. M., and Gutterman, D. D. (2020). Vascular autophagy in health and disease. *Basic Res. Cardiol.* 115:41. doi: 10.1007/s00395-020-0802-6

Humeres, C., and Frangogiannis, N. G. (2019). Fibroblasts in the infarcted, remodeling, and failing heart. *JACC Basic Transl. Sci.* 4, 449–467. doi: 10.1016/j.jacbts.2019.02.006

Ikeda, Y., Shirakabe, A., Maejima, Y., Zhai, P., Sciarretta, S., Toli, J., et al. (2015). Endogenous Drp1 mediates mitochondrial autophagy and protects the heart against energy stress. *Circ. Res.* 116, 264–278. doi: 10.1161/circresaha.116.303356

Jong, C. J., Yeung, J., Tseung, E., and Karmazyn, M. (2019). Leptin-induced cardiomyocyte hypertrophy is associated with enhanced mitochondrial fission. *Mol. Cell Biochem.* 454, 33–44. doi: 10.1007/s11010-018-3450-5

Jonsson, A. L., and Bäckhed, F. (2017). Role of gut microbiota in atherosclerosis. *Nat. Rev. Cardiol.* 14, 79–87. doi: 10.1038/nrcardio.2016.183

Kaludercic, N., and Di Lisa, F. (2020). Mitochondrial ROS formation in the pathogenesis of diabetic cardiomyopathy. *Front. Cardiovasc. Med.* 7:12. doi: 10.3389/fcvm.2020.00012

Karnewar, S., Vasamsetti, S. B., Gopoju, R., Kanugula, A. K., Ganji, S. K., Prabhakar, S., et al. (2016). Mitochondria-targeted esculetin alleviates mitochondrial dysfunction by AMPK-mediated nitric oxide and SIRT3 regulation in endothelial cells: potential implications in atherosclerosis. *Sci. Rep.* 6:24108. doi: 10.1038/srep24108

Kepp, O., Galluzzi, L., and Kroemer, G. (2011). Mitochondrial control of the NLRP3 inflammasome. *Nat. Immunol.* 12, 199–200. doi: 10.1038/ni0311-199

Kim, J., Seo, M., Kim, S. K., and Bae, Y. S. (2016). Flagellin-induced NADPH oxidase 4 activation is involved in atherosclerosis. *Sci. Rep.* 6:25437. doi: 10.1038/srep25437

Kim, Y. M., Youn, S. W., Sudhahar, V., Das, A., Chandhri, R., Cuervo Grajal, H., et al. (2018). Redox regulation of mitochondrial fission protein Drp1 by protein disulfide isomerase limits endothelial senescence. *Cell Rep.* 23, 3565–3578. doi: 10.1016/j.celrep.2018.05.054

Kiyuna, L. A., Albuquerque, R. P. E., Chen, C. H., Mochly-Rosen, D., and Ferreira, J. C. B. (2018). Targeting mitochondrial dysfunction and oxidative stress in heart failure: challenges and opportunities. *Free Radic. Biol. Med.* 129, 155–168. doi: 10.1016/j.freeradbiomed.2018.09.019

Kleinbongard, P., Skyschally, A., Gent, S., Pesch, M., and Heusch, G. (2018). STAT3 as a common signal of ischemic conditioning: a lesson on "rigor and reproducibility" in preclinical studies on cardioprotection. *Basic Res. Cardiol.* 113:3. doi: 10.1007/s00395-017-0660-z

Knight-Lozano, C. A., Young, C. G., Burow, D. L., Hu, Z. Y., Uyeminami, D., Pinkerton, K. E., et al. (2002). Cigarette smoke exposure and hypercholesterolemia increase mitochondrial damage in cardiovascular tissues. *Circulation* 105, 849–854. doi: 10.1161/hc0702.103977

Koltover, V. K. (2017). Free radical timer of aging: from chemistry of free radicals to systems theory of reliability. *Curr. Aging Sci.* 10, 12–17. doi: 10.2174/1874609809666161009220822

Kuznetsova, D. A., Gaynanova, G. A., Vasileva, L. A., Sibgatullina, G. V., Samigullin, D. V., Sapunova, A. S., et al. (2019). Mitochondria-targeted cationic liposomes modified with alkyltriphenylphosphonium bromides loaded with hydrophilic drugs: preparation, cytotoxicity and colocalization assay. *J. Mater. Chem. B* 7, 7351–7362. doi: 10.1039/c9tb01853k

Kyriakoudi, S., Drousiotou, A., and Petrou, P. P. (2021). When the balance tips: dysregulation of mitochondrial dynamics as a culprit in disease. *Int. J. Mol. Sci.* 22:4617. doi: 10.3390/ijms22094617

Lackner, L. L. (2019). The expanding and unexpected functions of mitochondria contact sites. *Trends Cell Biol.* 29, 580–590. doi: 10.1016/j.tcb.2019.02.009

Laslett, L. J., Alagona, P. Jr., Clark, B. A. III, Drozda, J. P. Jr., Saldivar, F., Wilson, S. R., et al. (2012). The worldwide environment of cardiovascular disease: prevalence, diagnosis, therapy, and policy issues: a report from the American College of Cardiology. *J. Am. Coll. Cardiol.* 60, S1–S49. doi: 10.1016/j.jacc.2012.11.002

Li, A., Zheng, N., and Ding, X. (2021). Mitochondrial abnormalities: a hub in metabolic syndrome-related cardiac dysfunction caused by oxidative stress. *Heart Fail Rev.* doi: 10.1007/s10741-021-10109-6 [Epub ahead of print].

Li, J., He, W., Liao, B., and Yang, J. (2015a). FFA-ROS-P53-mediated mitochondrial apoptosis contributes to reduction of osteoblastogenesis and bone mass in type 2 diabetes mellitus. *Sci. Rep.* 5:12724. doi: 10.1038/srep12724

Li, J., Wang, Y., Wang, Y., Wen, X., Ma, X. N., Chen, W., et al. (2015b). Pharmacological activation of AMPK prevents Drp1-mediated mitochondrial fission and alleviates endoplasmic reticulum stress-associated endothelial dysfunction. *J. Mol. Cell Cardiol.* 86, 62–74. doi: 10.1016/j.yjmcc.2015.07.010

Li, S., Sun, X., Xu, L., Sun, R., Ma, Z., Deng, X., et al. (2017). Baicalin attenuates in vivo and in vitro hyperglycemia-exacerbated ischemia/reperfusion injury by regulating mitochondrial function in a manner dependent on AMPK. *Eur. J. Pharmacol.* 815, 118–126. doi: 10.1016/j.ejphar.2017.07.041

Li, Y., Zhou, Z. H., Chen, M. H., Yang, J., Leng, J., Cao, G. S., et al. (2016). Inhibition of mitochondrial fission and NOX2 expression prevent NLRP3 inflammasome activation in the endothelium: the role of corosolic acid action in the amelioration of endothelial dysfunction. *Antioxid Redox Signal.* 24, 893–908. doi: 10.1089/ars.2015.6479

Linton, M. F., Moslehi, J. J., and Babaev, V. R. (2019). Akt signaling in macrophage polarization, survival, and atherosclerosis. *Int. J. Mol. Sci.* 20:2703. doi: 10.3390/ijms20112703

Liu, M., Li, X., and Huang, D. (2020). Mfn2 overexpression attenuates cardio-cerebrovascular ischemia-reperfusion injury through mitochondrial fusion and activation of the AMPK/Sirt3 Signaling. *Front. Cell Dev. Biol.* 8:598078. doi: 10.3389/fcell.2020.598078

Liu, M. Y., Jin, J., Li, S. L., Yan, J., Zhen, C. L., Gao, J. L., et al. (2016). Mitochondrial fission of smooth muscle cells is involved in artery constriction. *Hypertension* 68, 1245–1254. doi: 10.1161/hypertensionaha.116.07974

Loo, Y. M., and Gale, M. Jr. (2011). Immune signaling by RIG-I-like receptors. *Immunity* 34, 680–692. doi: 10.1016/j.immuni.2011.05.003

López Farré, A., and Casado, S. (2001). Heart failure, redox alterations, and endothelial dysfunction. *Hypertension* 38, 1400–1405. doi: 10.1161/hy1201.099612

Luptak, I., Qin, F., Sverdlov, A. L., Pimentel, D. R., Panagia, M., Croteau, D., et al. (2019). Energetic dysfunction is mediated by mitochondrial reactive oxygen species and precedes structural remodeling in metabolic heart disease. *Antioxid Redox Signal.* 31, 539–549. doi: 10.1089/ars.2018.7707

Makino, A., Scott, B. T., and Dillmann, W. H. (2010). Mitochondrial fragmentation and superoxide anion production in coronary endothelial cells from a mouse model of type 1 diabetes. *Diabetologia* 53, 1783–1794. doi: 10.1007/s00125-010-1770-4

Mao, Y., Luo, W., Zhang, L., Wu, W., Yuan, L., Xu, H., et al. (2017). STING-IRF3 triggers endothelial inflammation in response to free fatty acid-induced mitochondrial damage in diet-induced obesity. *Arterioscler. Thromb. Vasc. Biol.* 37, 920–929. doi: 10.1161/atvbaha.117.309017

Markin, A. M., Khotina, V. A., Zabudskaya, X. G., Bogatyreva, A. I., Starodubova, A. V., Ivanova, E., et al. (2021). Disturbance of mitochondrial dynamics and mitochondrial therapies in atherosclerosis. *Life (Basel)* 11:165. doi: 10.3390/life11020165

Marshall, J. D., Bazan, I., Zhang, Y., Fares, W. H., and Lee, P. J. (2018). Mitochondrial dysfunction and pulmonary hypertension: cause, effect, or both. *Am. J. Physiol. Lung Cell Mol. Physiol.* 314, L782–L796. doi: 10.1152/ajplung.00331.2017

Mathew, A., Lindsley, T. A., Sheridan, A., Bhoiwala, D. L., Hushmendy, S. F., Yager, E. J., et al. (2012). Degraded mitochondrial DNA is a newly identified subtype of the damage associated molecular pattern (DAMP) family and possible trigger of neurodegeneration. *J. Alzheimers Dis.* 30, 617–627. doi: 10.3233/jad-2012-120145

Matsunaga, H., Tanaka, Y., Tanaka, M., Gong, J. S., Zhang, J., Nomiyama, T., et al. (2001). Antiatherogenic mitochondrial genotype in patients with type 2 diabetes. *Diabetes Care* 24, 500–503. doi: 10.2337/diacare.24.3.500

Micha, R., and Mozaffarian, D. (2009). Trans fatty acids: effects on metabolic syndrome, heart disease and diabetes. *Nat. Rev. Endocrinol.* 5, 335–344. doi: 10.1038/nrendo.2009.79

Mohanty, A., Tiwari-Pandey, R., and Pandey, N. R. (2019). Mitochondria: the indispensable players in innate immunity and guardians of the inflammatory response. *J. Cell Commun. Signal.* 13, 303–318. doi: 10.1007/s12079-019-00507-9

Morales, P. E., Arias-Durán, C., Ávalos-Guajardo, Y., Aedo, G., Verdejo, H. E., Parra, V., et al. (2020). Emerging role of mitophagy in cardiovascular physiology and pathology. *Mol. Aspects Med.* 71:100822. doi: 10.1016/j.mam.2019.09.006

Mottis, A., Herzig, S., and Auwerx, J. (2019). Mitocellular communication: Shaping health and disease. *Science* 366, 827–832. doi: 10.1126/science.aax3768

Müller, J., Gorressen, S., Grandoch, M., Feldmann, K., Kretschmer, I., Lehr, S., et al. (2014). Interleukin-6-dependent phenotypic modulation of cardiac fibroblasts after acute myocardial infarction. *Basic Res. Cardiol.* 109:440. doi: 10.1007/s00395-014-0440-y

Muñoz-Carvajal, F., and Sanhueza, M. (2020). The mitochondrial unfolded protein response: a hinge between healthy and pathological aging. *Front. Aging Neurosci.* 12:581849. doi: 10.3389/fnagi.2020.581849

Naik, E., and Dixit, V. M. (2011). Mitochondrial reactive oxygen species drive proinflammatory cytokine production. *J. Exp. Med.* 208, 417–420. doi: 10.1084/jem.20110367

Navaratnarajah, T., Anand, R., Reichert, A. S., and Distelmaier, F. (2021). The relevance of mitochondrial morphology for human disease. *Int. J. Biochem. Cell Biol.* 134:105951. doi: 10.1016/j.biocel.2021.105951

Nazzal, D., Cantero, A. V., Therville, N., Segui, B., Negre-Salvayre, A., Thomsen, M., et al. (2006). Chlamydia pneumoniae alters mildly oxidized low-density lipoprotein-induced cell death in human endothelial cells, leading to necrosis rather than apoptosis. *J. Infect. Dis.* 193, 136–145. doi: 10.1086/498617

Ni, R., Cao, T., Xiong, S., Ma, J., Fan, G. C., Lacefield, J. C., et al. (2016). Therapeutic inhibition of mitochondrial reactive oxygen species with mito-TEMPO reduces diabetic cardiomyopathy. *Free Radic. Biol. Med.* 90, 12–23. doi: 10.1016/j.freeradbiomed.2015.11.013

Nielsen, S. H., Mouton, A. J., DeLeon-Pennell, K. Y., Genovese, F., Karsdal, M., and Lindsey, M. L. (2019). Understanding cardiac extracellular matrix remodeling to develop biomarkers of myocardial infarction outcomes. *Matrix Biol.* 7, 43–57. doi: 10.1016/j.matbio.2017.12.001

Norton, M., Ng, A. C., Baird, S., Dumoulin, A., Shutt, T., Mah, N., et al. (2014). ROMO1 is an essential redox-dependent regulator of mitochondrial dynamics. *Sci. Signal.* 7:ra10. doi: 10.1126/scisignal.2004374

Oesterle, A., Laufs, U., and Liao, J. K. (2017). Pleiotropic effects of statins on the cardiovascular system. *Circ. Res.* 120, 229–243. doi: 10.1161/circresaha.116.308537

Ordog, K., Horvath, O., Eros, K., Bruszt, K., Toth, S., Kovacs, D., et al. (2021). Mitochondrial protective effects of PARP-inhibition in hypertension-induced myocardial remodeling and in stressed cardiomyocytes. *Life Sci.* 268:118936. doi: 10.1016/j.lfs.2020.118936

Ostojic, S. M. (2016). Exercise-induced mitochondrial dysfunction: a myth or reality? *Clin. Sci. (Lond)* 130, 1407–1416. doi: 10.1042/cs20160200

Ota, A., Ishihara, T., and Ishihara, N. (2020). Mitochondrial nucleoid morphology and respiratory function are altered in Drp1-deficient HeLa cells. *J. Biochem.* 167, 287–294. doi: 10.1093/jb/mvz112

Paltauf-Doburzynska, J., Malli, R., and Graier, W. F. (2004). Hyperglycemic conditions affect shape and Ca2+ homeostasis of mitochondria in endothelial cells. *J. Cardiovasc. Pharmacol.* 44, 423–436. doi: 10.1097/01.fjc.0000139449.64337.1b

Pataky, M. W., and Nair, K. S. (2021). Too much of a good thing: excess exercise can harm mitochondria. *Cell Metab.* 33, 847–848. doi: 10.1016/j.cmet.2021.04.008

Pennanen, C., Parra, V., López-Crisosto, C., Morales, P. E., Del Campo, A., Gutierrez, T., et al. (2014). Mitochondrial fission is required for cardiomyocyte hypertrophy mediated by a Ca2+-calcineurin signaling pathway. *J. Cell Sci.* 127, 2659–2671. doi: 10.1242/jcs.139394

Peyravi, A., Yazdanpanahi, N., Nayeri, H., and Hosseini, S. A. (2020). The effect of endurance training with crocin consumption on the levels of MFN2 and DRP1 gene expression and glucose and insulin indices in the muscle tissue of diabetic rats. *J. Food Biochem.* 44:e13125. doi: 10.1111/jfbc.13125

Pham, L. M., Kim, E. C., Ou, W., Phung, C. D., Nguyen, T. T., Pham, T. T., et al. (2021). Targeting and clearance of senescent foamy macrophages and senescent endothelial cells by antibody-functionalized mesoporous silica nanoparticles for alleviating aorta atherosclerosis. *Biomaterials* 269:120677. doi: 10.1016/j.biomaterials.2021.120677

Phillips, N. R., Simpkins, J. W., and Roby, R. K. (2014). Mitochondrial DNA deletions in Alzheimer's brains: a review. *Alzheimers Dement* 10, 393–400. doi: 10.1016/j.jalz.2013.04.508

Picca, A., Lezza, A. M. S., Leeuwenburgh, C., Pesce, V., Calvani, R., Landi, F., et al. (2017). Fueling inflamm-aging through mitochondrial dysfunction: mechanisms and molecular targets. *Int. J. Mol. Sci.* 18:933. doi: 10.3390/ijms18050933

Picca, A., Mankowski, R. T., Burman, J. L., Donisi, L., Kim, J. S., Marzetti, E., et al. (2018). Mitochondrial quality control mechanisms as molecular targets in cardiac ageing. *Nat. Rev. Cardiol.* 15, 543–554. doi: 10.1038/s41569-018-0059-z

Qi, X., Qvit, N., Su, Y. C., and Mochly-Rosen, D. (2013). A novel Drp1 inhibitor diminishes aberrant mitochondrial fission and neurotoxicity. *J. Cell Sci.* 126, 789–802. doi: 10.1242/jcs.114439

Qin, X., Zhao, Y., Gong, J., Huang, W., Su, H., Yuan, F., et al. (2019). Berberine protects glomerular podocytes via inhibiting Drp1-mediated mitochondrial fission and dysfunction. *Theranostics* 9, 1698–1713. doi: 10.7150/thno.30640

Qiu, Y., Cheng, R., Liang, C., Yao, Y., Zhang, W., Zhang, J., et al. (2020). MicroRNA-20b promotes cardiac hypertrophy by the inhibition of mitofusin 2-Mediated Inter-organelle Ca(2+) Cross-Talk. *Mol. Ther. Nucleic Acids* 19, 1343–1356. doi: 10.1016/j.omtn.2020.01.017

Rababa'h, A. M., Guillory, A. N., Mustafa, R., and Hijjawi, T. (2018). Oxidative stress and cardiac remodeling: an updated edge. *Curr. Cardiol. Rev.* 14, 53–59. doi: 10.2174/1573403x14666180111145207

Rodriguez-Iturbe, B., Sepassi, L., Quiroz, Y., Ni, Z., Wallace, D. C., and Vaziri, N. D. (2007). Association of mitochondrial SOD deficiency with salt-sensitive hypertension and accelerated renal senescence. *J. Appl. Physiol. (1985)* 102, 255–260. doi: 10.1152/japplphysiol.00513.2006

Saigusa, R., Winkels, H., and Ley, K. (2020). T cell subsets and functions in atherosclerosis. *Nat. Rev. Cardiol.* 17, 387–401. doi: 10.1038/s41569-020-0352-5

Sazonova, M., Budnikov, E., Khasanova, Z., Sobenin, I., Postnov, A., and Orekhov, A. (2009). Studies of the human aortic intima by a direct quantitative assay of mutant alleles in the mitochondrial genome. *Atherosclerosis* 204, 184–190. doi: 10.1016/j.atherosclerosis.2008.09.001

Sazonova, M. A., Sinyov, V. V., Ryzhkova, A. I., Galitsyna, E. V., Khasanova, Z. B., Postnov, A. Y., et al. (2017). Role of mitochondrial genome mutations in pathogenesis of carotid atherosclerosis. *Oxid. Med. Cell Longev.* 2017:6934394. doi: 10.1155/2017/6934394

Schiano, C., Vietri, M. T., Grimaldi, V., Picascia, A., De Pascale, M. R., and Napoli, C. (2015). Epigenetic-related therapeutic challenges in cardiovascular disease. *Trends Pharmacol. Sci.* 36, 226–235. doi: 10.1016/j.tips.2015.02.005

Sebastián, D., Sorianello, E., Segalés, J., Irazoki, A., Ruiz-Bonilla, V., Sala, D., et al. (2016). Mfn2 deficiency links age-related sarcopenia and impaired autophagy to activation of an adaptive mitophagy pathway. *Embo J.* 35, 1677–1693. doi: 10.15252/embj.201593084

Shao, Z. Q., Dou, S. S., Zhu, J. G., Wang, H. Q., Wang, C. M., Cheng, B. H., et al. (2021). Apelin-13 inhibits apoptosis and excessive autophagy in cerebral ischemia/reperfusion injury. *Neural Regen. Res.* 16, 1044–1051. doi: 10.4103/1673-5374.300725

Sharp, W. W., and Archer, S. L. (2015). Mitochondrial dynamics in cardiovascular disease: fission and fusion foretell form and function. *J. Mol. Med. (Berl)* 93, 225–228. doi: 10.1007/s00109-015-1258-2

Shenouda, S. M., Widlansky, M. E., Chen, K., Xu, G., Holbrook, M., Tabit, C. E., et al. (2011). Altered mitochondrial dynamics contributes to endothelial dysfunction in diabetes mellitus. *Circulation* 124, 444–453. doi: 10.1161/circulationaha.110.014506

Shimada, K., Crother, T. R., Karlin, J., Dagvadorj, J., Chiba, N., Chen, S., et al. (2012). Oxidized mitochondrial DNA activates the NLRP3 inflammasome during apoptosis. *Immunity* 36, 401–414. doi: 10.1016/j.immuni.2012.01.009

Simons, M., Gordon, E., and Claesson-Welsh, L. (2016). Mechanisms and regulation of endothelial VEGF receptor signalling. *Nat. Rev. Mol. Cell Biol.* 17, 611–625. doi: 10.1038/nrm.2016.87

Sobenin, I. A., Chistiakov, D. A., Bobryshev, Y. V., Postnov, A. Y., and Orekhov, A. N. (2013a). Mitochondrial mutations in atherosclerosis: new solutions in research and possible clinical applications. *Curr. Pharm. Des.* 19, 5942–5953. doi: 10.2174/1381612811319330013

Sobenin, I. A., Sazonova, M. A., Postnov, A. Y., Bobryshev, Y. V., and Orekhov, A. N. (2013b). Changes of mitochondria in atherosclerosis: possible determinant in the pathogenesis of the disease. *Atherosclerosis* 227, 283–288. doi: 10.1016/j.atherosclerosis.2013.01.006

Song, R., Hu, X. Q., and Zhang, L. (2019). Mitochondrial MiRNA in cardiovascular function and disease. *Cells* 8:1475. doi: 10.3390/cells8121475

Stanzione, R., Forte, M., Cotugno, M., Bianchi, F., Marchitti, S., Busceti, C. L., et al. (2021). Uncoupling Protein 2 as a pathogenic determinant and therapeutic target in cardiovascular and metabolic diseases. *Curr. Neuropharmacol.* doi: 10.2174/1570159x19666210421094204 [Epub ahead of print].

Strutynska, N. A., Kotsiuruba, A. V., Budko, A. Y., Mys, L. A., and Sagach, V. F. (2016). Mitochondrial dysfunction in the aging heart is accompanied by constitutive no-synthases uncoupling on the background of oxidative and nitrosative stress. *Fiziol. Zh* 62, 3–11. doi: 10.15407/fz62.02.003

Suárez-Rivero, J. M., Pastor-Maldonado, C. J., Povea-Cabello, S., Álvarez-Córdoba, M., Villalón-García, I., Talaverón-Rey, M., et al. (2021). From mitochondria to atherosclerosis: the inflammation path. *Biomedicines* 9:258. doi: 10.3390/biomedicines9030258

Suzuki, T., Nagao, A., and Suzuki, T. (2011). Human mitochondrial tRNAs: biogenesis, function, structural aspects, and diseases. *Annu. Rev. Genet.* 45, 299–329. doi: 10.1146/annurev-genet-110410-132531

Tang, J. X., Thompson, K., Taylor, R. W., and Oláhová, M. (2020). Mitochondrial OXPHOS biogenesis: co-regulation of protein synthesis, import, and assembly pathways. *Int. J. Mol. Sci.* 21:3820. doi: 10.3390/ijms21113820

Teixeira, L. L., Pilon, G., Coutinho, C. P., Dudonné, S., Dube, P., Houde, V., et al. (2021). Purple grumixama anthocyanins (Eugenia brasiliensis Lam.) attenuate obesity and insulin resistance in high-fat diet mice. *Food Funct.* 12, 3680–3691. doi: 10.1039/d0fo03245j

Thijssen, D. H., Maiorana, A. J., O'Driscoll, G., Cable, N. T., Hopman, M. T., and Green, D. J. (2010). Impact of inactivity and exercise on the vasculature in humans. *Eur. J. Appl. Physiol.* 108, 845–875. doi: 10.1007/s00421-009-1260-x

Tibaut, M., Caprnda, M., Kubatka, P., Sinkoviè, A., Valentova, V., Filipova, S., et al. (2019). Markers of atherosclerosis: part 1 - serological markers. *Heart Lung Circ.* 28, 667–677. doi: 10.1016/j.hlc.2018.06.1057

Tousoulis, D., Kampoli, A. M., Tentolouris, C., Papageorgiou, N., and Stefanadis, C. (2012). The role of nitric oxide on endothelial function. *Curr. Vasc. Pharmacol.* 10, 4–18. doi: 10.2174/157016112798829760

Toyama, E. Q., Herzig, S., Courchet, J., Lewis, T. L. Jr., Losón, O. C., Hellberg, K., et al. (2016). Metabolism. AMP-activated protein kinase mediates mitochondrial fission in response to energy stress. *Science* 351, 275–281. doi: 10.1126/science.aab4138

Triantafilou, K., Hughes, T. R., Triantafilou, M., and Morgan, B. P. (2013). The complement membrane attack complex triggers intracellular Ca2+ fluxes leading to NLRP3 inflammasome activation. *J. Cell Sci.* 126, 2903–2913. doi: 10.1242/jcs.124388

Tuder, R. M., Davis, L. A., and Graham, B. B. (2012). Targeting energetic metabolism: a new frontier in the pathogenesis and treatment of pulmonary hypertension. *Am. J. Respir. Crit. Care Med.* 185, 260–266. doi: 10.1164/rccm.201108-1536PP

Tumurkhuu, G., Shimada, K., Dagvadorj, J., Crother, T. R., Zhang, W., Luthringer, D., et al. (2016). Ogg1-Dependent DNA repair regulates NLRP3 inflammasome and prevents atherosclerosis. *Circ. Res.* 119, e76–e90. doi: 10.1161/circresaha.116.308362

Ueda, S., Ozawa, S., Mori, K., Asanuma, K., Yanagita, M., Uchida, S., et al. (2015). ENOS deficiency causes podocyte injury with mitochondrial abnormality. *Free Radic. Biol. Med.* 87, 181–192. doi: 10.1016/j.freeradbiomed.2015.06.028

Vaka, V. R., McMaster, K. M., Cunningham, M. W. Jr., Ibrahim, T., Hazlewood, R., Usry, N., et al. (2018). Role of mitochondrial dysfunction and reactive oxygen species in mediating hypertension in the reduced uterine perfusion pressure rat model of preeclampsia. *Hypertension* 72, 703–711. doi: 10.1161/hypertensionaha.118.11290

Valenzuela, C. A., Baker, E. J., Miles, E. A., and Calder, P. C. (2019). Eighteen-carbon trans fatty acids and inflammation in the context of atherosclerosis. *Prog. Lipid Res.* 76:101009. doi: 10.1016/j.plipres.2019.101009

van Empel, V. P., and De Windt, L. J. (2004). Myocyte hypertrophy and apoptosis: a balancing act. *Cardiovasc. Res.* 63, 487–499. doi: 10.1016/j.cardiores.2004.02.013

Vendrov, A. E., Vendrov, K. C., Smith, A., Yuan, J., Sumida, A., Robidoux, J., et al. (2015). NOX4 NADPH Oxidase-dependent mitochondrial oxidative stress in aging-associated cardiovascular disease. *Antioxid Redox Signal.* 23, 1389–1409. doi: 10.1089/ars.2014.6221

Victor, V. M., Rovira-Llopis, S., Bañuls, C., Diaz-Morales, N., Lopez-Domenech, S., Escribano-López, I., et al. (2015). Metformin modulates human leukocyte/endothelial cell interactions and proinflammatory cytokines in polycystic ovary syndrome patients. *Atherosclerosis* 242, 167–173. doi: 10.1016/j.atherosclerosis.2015.07.017

Vindis, C., Elbaz, M., Escargueil-Blanc, I., Augé, N., Heniquez, A., Thiers, J. C., et al. (2005). Two distinct calcium-dependent mitochondrial pathways are involved in oxidized LDL-induced apoptosis. *Arterioscler. Thromb. Vasc. Biol.* 25, 639–645. doi: 10.1161/01.Atv.0000154359.60886.33

Volobueva, A., Grechko, A., Yet, S. F., Sobenin, I., and Orekhov, A. (2019). Changes in mitochondrial genome associated with predisposition to atherosclerosis and related disease. *Biomolecules* 9:377. doi: 10.3390/biom9080377

Wang, L., Yu, T., Lee, H., O'Brien, D. K., Sesaki, H., and Yoon, Y. (2015). Decreasing mitochondrial fission diminishes vascular smooth muscle cell migration and ameliorates intimal hyperplasia. *Cardiovasc. Res.* 106, 272–283. doi: 10.1093/cvr/cvv005

Wang, Q., Wu, S., Zhu, H., Ding, Y., Dai, X., Ouyang, C., et al. (2017a). Deletion of PRKAA triggers mitochondrial fission by inhibiting the autophagy-dependent degradation of DNM1L. *Autophagy* 13, 404–422. doi: 10.1080/15548627.2016.1263776

Wang, Q., Zhang, M., Torres, G., Wu, S., Ouyang, C., Xie, Z., et al. (2017b). Metformin suppresses diabetes-accelerated atherosclerosis via the inhibition of Drp1-mediated mitochondrial fission. *Diabetes* 66, 193–205. doi: 10.2337/db16-0915

Wang, R., Mishra, P., Garbis, S. D., Moradian, A., Sweredoski, M. J., and Chan, D. C. (2021a). Identification of new OPA1 cleavage site reveals that short isoforms regulate mitochondrial fusion. *Mol. Biol. Cell.* 32, 157–168. doi: 10.1091/mbc.E20-09-0605

Wang, S. S., Li, K., Liu, Z., Gui, S., Liu, N., and Liu, X. (2021b). Aerobic exercise ameliorates benign prostatic hyperplasia in obese mice through downregulating the AR/androgen/PI3K/AKT signaling pathway. *Exp. Gerontol.* 143:111152. doi: 10.1016/j.exger.2020.111152

Wang, Y., Zang, Q. S., Liu, Z., Wu, Q., Maass, D., Dulan, G., et al. (2011). Regulation of VEGF-induced endothelial cell migration by mitochondrial reactive oxygen species. *Am. J. Physiol. Cell Physiol.* 301, C695–C704. doi: 10.1152/ajpcell.00322.2010

Watanabe, T., Saotome, M., Nobuhara, M., Sakamoto, A., Urushida, T., Katoh, H., et al. (2014). Roles of mitochondrial fragmentation and reactive oxygen species in mitochondrial dysfunction and myocardial insulin resistance. *Exp. Cell Res.* 323, 314–325. doi: 10.1016/j.yexcr.2014.02.027

Weaver, D., Eisner, V., Liu, X., Várnai, P., Hunyady, L., Gross, A., et al. (2014). Distribution and apoptotic function of outer membrane proteins depend on mitochondrial fusion. *Mol. Cell* 54, 870–878. doi: 10.1016/j.molcel.2014.03.048

West, A. P., and Shadel, G. S. (2017). Mitochondrial DNA in innate immune responses and inflammatory pathology. *Nat. Rev. Immunol.* 17, 363–375. doi: 10.1038/nri.2017.21

Wilson, F. H., Hariri, A., Farhi, A., Zhao, H., Petersen, K. F., Toka, H. R., et al. (2004). A cluster of metabolic defects caused by mutation in a mitochondrial tRNA. *Science* 306, 1190–1194. doi: 10.1126/science.1102521

Wolf, C., López Del Amo, V., Arndt, S., Bueno, D., Tenzer, S., Hanschmann, E. M., et al. (2020). Redox modifications of proteins of the mitochondrial fusion and fission machinery. *Cells* 9:815. doi: 10.3390/cells9040815

Wu, Y., Wang, F., Fan, L., Zhang, W., Wang, T., Du, Y., et al. (2018). Baicalin alleviates atherosclerosis by relieving oxidative stress and inflammatory responses via inactivating the NF-κB and p38 MAPK signaling pathways. *Biomed. Pharmacother.* 97, 1673–1679. doi: 10.1016/j.biopha.2017.12.024

Xie, T., Wang, C., Jin, Y., Meng, Q., Liu, Q., Wu, J., et al. (2020). CoenzymeQ10-Induced Activation of AMPK-YAP-OPA1 pathway alleviates atherosclerosis by improving mitochondrial function, inhibiting oxidative stress and promoting energy metabolism. *Front. Pharmacol.* 11:1034. doi: 10.3389/fphar.2020.01034

Xin, Y., Li, J., Wu, W., and Liu, X. (2021). Mitofusin-2: a new mediator of pathological cell proliferation. *Front. Cell Dev. Biol.* 9:647631. doi: 10.3389/fcell.2021.647631

Xing, S. S., Yang, X. Y., Zheng, T., Li, W. J., Wu, D., Chi, J. Y., et al. (2015). Salidroside improves endothelial function and alleviates atherosclerosis by activating a mitochondria-related AMPK/PI3K/Akt/eNOS pathway. *Vascul. Pharmacol.* 72, 141–152. doi: 10.1016/j.vph.2015.07.004

Xue, W., Wang, X., Tang, H., Sun, F., Zhu, H., Huang, D., et al. (2020). Vitexin attenuates myocardial ischemia/reperfusion injury in rats by regulating mitochondrial dysfunction induced by mitochondrial dynamics imbalance. *Biomed. Pharmacother.* 124:109849. doi: 10.1016/j.biopha.2020.109849

Yan, Y., Zhou, X. E., Xu, H. E., and Melcher, K. (2018). Structure and physiological regulation of AMPK. *Int. J. Mol. Sci.* 19:3534. doi: 10.3390/ijms19113534

Yang, J., Zhou, X., Zeng, X., Hu, O., Yi, L., and Mi, M. (2019). Resveratrol attenuates oxidative injury in human umbilical vein endothelial cells through regulating mitochondrial fusion via TyrRS-PARP1 pathway. *Nutr. Metab. (Lond)* 16:9. doi: 10.1186/s12986-019-0338-7

Yapa, N. M. B., Lisnyak, V., Reljic, B., and Ryan, M. T. (2021). Mitochondrial dynamics in health and disease. *FEBS Lett.* 595, 1184–1204. doi: 10.1002/1873-3468.14077

Yeh, H. L., Kuo, L. T., Sung, F. C., and Yeh, C. C. (2018). Association between polymorphisms of antioxidant gene (MnSOD, CAT, and GPx1) and risk of

coronary artery disease. *Biomed. Res. Int.* 2018:5086869. doi: 10.1155/2018/5086869

Yu, E., Calvert, P. A., Mercer, J. R., Harrison, J., Baker, L., Figg, N. L., et al. (2013). Mitochondrial DNA damage can promote atherosclerosis independently of reactive oxygen species through effects on smooth muscle cells and monocytes and correlates with higher-risk plaques in humans. *Circulation* 128, 702–712. doi: 10.1161/circulationaha.113.002271

Yu, E., Calvert, P. A., Mercer, J. R., Harrison, J., Baker, L., Figg, N. L., et al. (2014). Response to letter regarding article, "Mitochondrial DNA damage can promote atherosclerosis independently of reactive oxygen species through effects on smooth muscle cells and monocytes and correlates with higher-risk plaques in humans". *Circulation* 129:e408. doi: 10.1161/circulationaha.113.008032

Yu, E. P. K., Reinhold, J., Yu, H., Starks, L., Uryga, A. K., Foote, K., et al. (2017). Mitochondrial respiration is reduced in atherosclerosis, promoting necrotic core formation and reducing relative fibrous cap thickness. *Arterioscler. Thromb. Vasc. Biol.* 37, 2322–2332. doi: 10.1161/atvbaha.117.310042

Yu, S., Zhang, L., Liu, C., Yang, J., Zhang, J., and Huang, L. (2019). PACS2 is required for ox-LDL-induced endothelial cell apoptosis by regulating mitochondria-associated ER membrane formation and mitochondrial Ca(2+) elevation. *Exp. Cell Res.* 379, 191–202. doi: 10.1016/j.yexcr.2019.04.002

Zhang, B., Guo, X., Li, Y., Peng, Q., Gao, J., Liu, B., et al. (2017). d-Chiro inositol ameliorates endothelial dysfunction via inhibition of oxidative stress and mitochondrial fission. *Mol. Nutr. Food Res.* 61:710. doi: 10.1002/mnfr.201600710

Zhang, J. Z., Liu, Z., Liu, J., Ren, J. X., and Sun, T. S. (2014). Mitochondrial DNA induces inflammation and increases TLR9/NF-κB expression in lung tissue. *Int. J. Mol. Med.* 33, 817–824. doi: 10.3892/ijmm.2014.1650

Zhang, Q., Raoof, M., Chen, Y., Sumi, Y., Sursal, T., Junger, W., et al. (2010). Circulating mitochondrial DAMPs cause inflammatory responses to injury. *Nature* 464, 104–107. doi: 10.1038/nature08780

Zhao, J., Gao, J. L., Zhu, J. X., Zhu, H. B., Peng, X., Jiang, M., et al. (2019). The different response of cardiomyocytes and cardiac fibroblasts to mitochondria inhibition and the underlying role of STAT3. *Basic Res. Cardiol.* 114:12. doi: 10.1007/s00395-019-0721-6

Zhong, Z., Umemura, A., Sanchez-Lopez, E., Liang, S., Shalapour, S., Wong, J., et al. (2016). NF-κB restricts inflammasome activation via elimination of damaged mitochondria. *Cell* 164, 896–910. doi: 10.1016/j.cell.2015.12.057

Zhou, J., Zhang, J., Lu, Y., Huang, S., Xiao, R., Zeng, X., et al. (2016a). Mitochondrial transplantation attenuates hypoxic pulmonary vasoconstriction. *Oncotarget* 7, 31284–31298. doi: 10.18632/oncotarget.8893

Zhou, Y., Zhang, M. J., Li, B. H., Chen, L., Pi, Y., Yin, Y. W., et al. (2016b). PPARγ Inhibits VSMC proliferation and migration via attenuating oxidative stress through upregulating UCP2. *PLoS One* 11:e0154720. doi: 10.1371/journal.pone.0154720

Zhu, Y., Li, M., Lu, Y., Li, J., Ke, Y., and Yang, J. (2019). Ilexgenin A inhibits mitochondrial fission and promote Drp1 degradation by Nrf2-induced PSMB5 in endothelial cells. *Drug Dev. Res.* 80, 481–489. doi: 10.1002/ddr.21521

Zhuan, B., Wang, X., Wang, M. D., Li, Z. C., Yuan, Q., Xie, J., et al. (2020). Hypoxia induces pulmonary artery smooth muscle dysfunction through mitochondrial fragmentation-mediated endoplasmic reticulum stress. *Aging (Albany NY)* 12, 23684–23697. doi: 10.18632/aging.103892

Zhuang, X., Maimaitijiang, A., Li, Y., Shi, H., and Jiang, X. (2017). Salidroside inhibits high-glucose induced proliferation of vascular smooth muscle cells via inhibiting mitochondrial fission and oxidative stress. *Exp. Ther. Med.* 14, 515–524. doi: 10.3892/etm.2017.4541

Zielonka, J., Joseph, J., Sikora, A., Hardy, M., Ouari, O., Vasquez-Vivar, J., et al. (2017). Mitochondria-Targeted Triphenylphosphonium-based compounds: syntheses, mechanisms of action, and therapeutic and diagnostic applications. *Chem. Rev.* 117, 10043–10120. doi: 10.1021/acs.chemrev.7b00042

Conflict of Interest: The authors declare that the research was conducted in the absence of any commercial or financial relationships that could be construed as a potential conflict of interest.

Advantages of publishing in Frontiers

OPEN ACCESS
Articles are free to read for greatest visibility and readership

FAST PUBLICATION
Around 90 days from submission to decision

HIGH QUALITY PEER-REVIEW
Rigorous, collaborative, and constructive peer-review

TRANSPARENT PEER-REVIEW
Editors and reviewers acknowledged by name on published articles

Frontiers
Avenue du Tribunal-Fédéral 34
1005 Lausanne | Switzerland

Visit us: www.frontiersin.org
Contact us: frontiersin.org/about/contact

REPRODUCIBILITY OF RESEARCH
Support open data and methods to enhance research reproducibility

DIGITAL PUBLISHING
Articles designed for optimal readership across devices

FOLLOW US
@frontiersin

IMPACT METRICS
Advanced article metrics track visibility across digital media

EXTENSIVE PROMOTION
Marketing and promotion of impactful research

LOOP RESEARCH NETWORK
Our network increases your article's readership